LBNL-60184

Assessing the Effectiveness of Shelter-in-Place as an Emergency Response to Large-Scale Outdoor Chemical Releases

Wanyu R. Chan

Environmental Energy Technologies Divison
Indoor Environment Department
Lawrence Berkeley National Laboratory
University of California
Berkeley, CA 94720

May 2006

This work was supported by the Office of Chemical Biological Countermeasures, of the Science and Technology Directorate of the Department of Homeland Security, and performed under US Department of Energy Contract No. DE-AC02-05CH11231.

Assessing the Effectiveness of Shelter-in-Place as an Emergency Response to Large-Scale Outdoor Chemical Releases

by

Wanyu Rengie Chan

B.S. (Carnegie Mellon University) 2001
M.S. (University of California, Berkeley) 2002

A dissertation submitted in partial satisfaction of the

requirements for the degree of

Doctor of Philosophy

in

Engineering – Civil and Environmental Engineering

in the

Graudate Division

of the

University of California, Berkeley

Committee in charge:

Professor William W Nazaroff, Chair
Professor Ashok J Gadgil
Professor Robert A Harley
Professor Robert C Spear

Spring 2006

Assessing the Effectiveness of Shelter-in-Place as an
Emergency Response to Large-Scale Outdoor Chemical Releases

Copyright 2006

by

Wanyu Rengie Chan

Abstract

Assessing the Effectiveness of Shelter-in-Place as an
Emergency Response to Large-Scale Outdoor Chemical Releases

by

Wanyu Rengie Chan

Doctor of Philosophy in Engineering – Civil and Environmental Engineering

University of California, Berkeley

Professor William W Nazaroff, Chair

Large-scale outdoor chemical releases can cause severe harm to people in nearby communities. Sheltering in buildings may be used as a temporary measure to reduce health risk from exposure to the toxic materials. Shelter-in-place (SIP) is relatively straightforward to implement because most people are already in buildings most of the time, and so exercising the emergency response simply means closing windows and doors, and turning off ventilation fans. However, air leakage variability in the building stock can lead to considerable differences in the effectiveness of buildings in protecting occupants against outdoor releases. The effectiveness of SIP for the community can also vary for different release conditions.

This dissertation identifies and assesses the key factors that affect community-scale SIP effectiveness. Large-scale airborne toxic chemical releases are simulated to assess the potential acute health effects for the exposed population. Modeling of the distribution of indoor concentrations is accomplished through detailed analysis of the air leakage of

residential and non-residential buildings and simulation of their air infiltration rates. The expected outcome for a population that shelter indoors is quantified by a community-based metric that captures the variability among buildings. Sensitivity of SIP effectiveness to model parameters is evaluated under different release scenarios by comparing changes in the casualty reduction estimates.

Aside from the physical, biological, and chemical factors that influence SIP effectiveness – such as the building air exchange rate, the degree of nonlinearity of the dose-response relationship, and the extent of chemical sorption onto indoor surfaces – human factors, such as community response time in emergencies are also important factors that govern whether SIP can provide adequate protection for an exposed population. After the plume has dispersed, SIP should be terminated by means of exiting or deliberately ventilating the buildings. In most situations, however, it is found that a short delay in terminating SIP would not significantly degrade the overall effectiveness of the strategy. On the other hand, a potentially large enhancement of SIP effectiveness can be realized by reducing the time delay for SIP initiation. The understanding gained from these analyses can guide decisions in emergency response and pre-event planning.

Table of Contents

Abstract 1
Table of Contents i
List of Tables vi
List of Figures x
Acknowledgements xxi

1 Introduction 1
1.1 Background 1
1.2 Current State of Knowledge 3
1.3 Overview of the Research 6
1.4 Outline of the Dissertation Contents 7
1.5 References 10
2 Exploring the Effectiveness of Shelter-in-Place 13
2.1 Introduction 13
2.2 Methods 14
2.2.1 Outdoor and Indoor Concentrations 15
2.2.2 Health Effects 18
2.2.3 Measures of Shelter-in-Place Effectiveness 20
2.3 Model Parameter Selection 23
2.4 Results and Discussion 27
2.4.1 Illustrative Example 27
2.4.2 The Effect of Toxic Load Exponent 29
2.4.3 The Effect of System Time Scales 31
2.4.4 The Effect of Release Scale 33
2.4.5 Terminating Shelter-in-Place 35
2.5 Conclusions 40
2.6 References 42
2.7 Tables 44
2.8 Figures 46

3 Air Infiltration Rates of Residential Buildings 54
3.1 Introduction 54
3.2 Analysis of US Residential Air Leakage Database 56
3.2.1 Measurements of Air Leakage 57
3.2.2 Exploratory Analysis of Dataset 60
3.2.2.1 Data Collection 60
3.2.2.2 Data Processing 60
3.2.2.3 Data Summary 61
3.2.3 Analysis and Discussion 64
3.2.3.1 Categorical Approach 64
3.2.3.2 Multivariate Regression Approach 66
3.2.3.3 Data Aggregation 71
3.2.4 Summary 75
3.3 Air Infiltration Model 76
3.3.1 LBL Infiltration Model 77
3.3.1.1 Wind Effect 78
3.3.1.2 Stack Effect 80
3.3.1.3 Combined Air Infiltration Rate 83
3.3.1.4 Model Comparison with Measurements 85
3.4 Air Infiltration Rate Predictions 87
3.4.1 Albuquerque, NM – A Case Study 87
3.4.2 Housing Characteristics – Census-Tract Based Approach 90
3.4.2.1 Year Built Distribution 91
3.4.2.2 Floor Area Distribution 94
3.4.2.3 Joint Distribution of Year Built and Floor Area 97
3.4.2.4 Normalized Air Leakage Distribution 100
3.4.3 LBL Infiltration Model Input Parameters 102
3.4.4 Results and Discussion 103
3.4.5 Air-Exchange Rates under Normal Operating Conditions 106
3.5 Conclusions 110
3.6 References 113

3.7 Tables 118
3.8 Figures 125
4 Assessing Shelter-in-Place Effectiveness in a Residential Community 151
4.1 Introduction 151
4.2 Methods 153
4.2.1 Albuquerque, NM – A Case Study 153
4.2.2 Sorption and Decomposition on Indoor Surfaces 157
4.2.2.1 Model Formulation 158
4.2.2.2 Experimental Data 162
4.2.2.3 Implications for Indoor Concentrations 166
4.2.3 Shelter-in-Place Response Time 171
4.2.4 Summary of Model Parameters 179
4.3 Results and Discussion 181
4.3.1 Effects of Air Leakage Variability Among Residences 185
4.3.2 Effects of Sorption on Indoor Surfaces 187
4.3.3 Effects of Shelter-in-Place Initiation Delay 189
4.3.4 Model Limitations 195
4.4 Conclusions 199
4.5 References 203
4.6 Tables 207
4.7 Figures 216
5 Air Infiltration and Ventilation in Commercial Buildings 237
5.1 Introduction 237
5.2 Analysis of the Commercial Building Air Leakage Database 239
5.2.1 Data Description 239
5.2.2 Exploratory Analysis 243
5.2.3 Regression Analysis 246
5.2.4 Regression Model Assessment 250
5.3 Air Infiltration Model of Large Buildings 251
5.3.1 Driving Forces for Air Infiltration 251
5.3.2 Shaw-Tamura Infiltration Model 253

5.3.2.1 Stack Effect 253
5.3.2.2 Wind Effect 255
5.3.2.3 Combined Stack and Wind Effects 258
5.3.3 Air Infiltration Model Parameters and Uncertainties 261
5.3.3.1 Neutral Pressure Level and Thermal Draft Coefficient 262
5.3.3.2 Wind Angle Correction Factor and Wind-Pressure Coefficient 262
5.4 Air Infiltration Model Predictions and Measurements 265
5.4.1 Model Comparisons against Existing Air Infiltration Rate Measurements 265
5.4.1.1 Office Building Measurements 265
5.4.1.2 Small Commercial Buildings 271
5.4.2 Air Infiltration Rate Distribution of the US Commercial Building Stock .. 274
5.4.2.1 Characteristics of US Commercial Buildings 276
5.4.2.2 Modeling of Air Infiltration Rates of US Commercial Buildings 279
5.4.2.3 Implications for Shelter-in-Place in Commercial Buildings 283
5.5 Conclusions 286
5.6 References 289
5.7 Tables 294
5.8 Figures 301
6 Shelter-in-Place Effectiveness in Commercial Buildings 325
6.1 Introduction 325
6.2 Description of the Case Study 326
6.3 Commercial Building Characteristics in Oklahoma City 329
6.3.1 Description of Buildings 329
6.3.2 Identifying Commercial Buildings by Floor Area Distribution 331
6.3.3 Building Occupancy Estimates 334
6.3.4 Grouping Small Commercial Buildings to Reduce Model Runs 339
6.4 Modeling Approach 343
6.4.1 Distributions of Air Infiltration Rate 345
6.4.2 Distributions of Indoor Concentrations 348
6.4.3 Adverse Health Effects from Exposure 348
6.5 Results and Discussion 350

6.5.1 Air Infiltration Rate Predictions 350
6.5.2 Indoor Concentration Predictions 352
6.5.3 Shelter-in-Place Characteristics of Commercial Buildings 355
6.5.4 Normal Operating Conditions 359
6.5.5 Sorption to Indoor Surfaces 361
6.5.6 Shelter-in-Place Initiation Time Delay 363
6.5.7 Summary 365
6.6 Model Evaluation and Limitations 366
6.6.1 Air Leakage Characterization of Commercial Buildings 368
6.6.2 Air Infiltration Rate Predictions 369
6.6.3 Indoor Concentration Predictions 372
6.6.4 Exposure Assessment 376
6.7 Conclusions 377
6.8 References 380
6.9 Tables 383
6.10 Figures 389
7 Summary and Conclusions 421
7.1 Summary of Results 421
7.1.1 Community-Based Modeling of Shelter-in-Place 422
7.1.2 Key Factors Affecting Shelter-in-Place Effectiveness 423
7.2 Recommendations for Future Research 428
7.2.1 Model Refinements 428
7.2.2 Model Uncertainty Assessment 430
7.2.3 Characterize Variability in Model Predictions 432
7.2.4 Other Opportunities for Shelter-in-Place Modeling 433
7.2.5 Emergency Response Tools 435
7.3 References 438

List of Tables

Table 2.1 List of model parameters. 44

Table 2.2 Correlations for σ_x, σ_y, and σ_z based on Pasquill-Gifford stability class used in Gaussian plume dispersion modeling. 44

Table 2.3 Time when SIP should be terminated after the end of the release. 45

Table 3.1 Multivariable regression parameters for the normalized leakage of all valid data points, using indicator variables to identify low-income and energy-efficient houses 118

Table 3.2 Multivariable regression parameters for the normalized leakage of low-income, conventional, and energy-efficient houses 118

Table 3.3 Statistics of estimated normalized leakage distribution weighted for all single-family dwellings in US. 119

Table 3.4 LBL Infiltration Model shielding parameters. 119

Table 3.5 LBL Infiltration Model terrain parameters. 119

Table 3.6 Year built distributions of housing units in a census tract in Albuquerque 120

Table 3.7 Fraction of US housing units that are single-family detached units when grouped by year-built, owner versus renter occupied, and occupant poverty status 120

Table 3.8 Distribution of house floor area conditioned on the number of rooms in US single-family detached units 121

Table 3.9 Estimated house floor area distribution of single-family detached units in a census tract in Albuquerque 121

Table 3.10 Estimated house floor area distributions of the single-family detached units in a census tract in Albuquerque that are low-income and not low-income. 122

Table 3.11 House year built and floor area joint distribution of not low-income single-family detached units, based on analysis of national data from the American Housing Survey 123

Table 3.12 House year built and floor area joint distribution of low-income single-family detached units, based on analysis of national data from the American Housing Survey 123

Table 3.13 Geometric mean of the normalized leakage estimated for not low-income single-family detached units, as a function of their year built and floor area 124

Table 3.14 Geometric mean of the normalized leakage estimated for low-income single-family detached units, as a function of their year built and floor area 124

Table 4.1 Measured deposition velocity to indoor materials of some toxic industrial chemicals and a chemical warfare agent simulant 207

Table 4.2 Measured one-sink sorption and desorption rate coefficients of some toxic industrial chemicals and chemical warfare agents 207

Table 4.3 Measured sorption rate coefficients of three surrogates of G-series chemical warfare agents obtained from two sets of experiments 208

Table 4.4 List of sorption/desorption models and rate coefficients used to assess SIP effectiveness 209

Table 4.5 Approximate SIP initiation time delays estimated for a community 210

Table 4.6 Summary of model parameters used to assess SIP effectiveness 210

Table 4.7 List of simulations and their assigned codes 211

Table 4.8 List of simulations, as indicated by their designated codes, for which results are plotted in selected figures 213

Table 4.9 Casualty reduction factor (CRF) for SIP under base-case simulation conditions, without sorption..... 214

Table 4.10 Casualty reduction factor (CRF) when toxic load exponent = 1 under various pre-sheltering air exchange distributions and shelter-in-place initiation time, without sorption..... 214

Table 4.11 Casualty reduction factor (CRF) when toxic load exponent = 2 under various pre-sheltering air exchange distributions and shelter-in-place initiation time, without sorption..... 215

Table 4.12 Casualty reduction factor (CRF) when toxic load exponent = 3 under various pre-sheltering air exchange distributions and shelter-in-place initiation time, without sorption..... 215

Table 5.1 Types of data in the commercial building air leakage database. 294

Table 5.2 Buildings in the commercial air leakage database categorized by their usage and construction types 295

Table 5.3 Regression results of log-transformed air-leakage coefficient using the physical dimensions of the building as explanatory parameters..... 296

Table 5.4 Regression results of log-transformed air-leakage coefficient using the building floor area and height as the explanatory variables 297

Table 5.5 Neutral pressure level and thermal draft coefficient from pressure differential measurements on various high-rise buildings..... 298

Table 5.6 Descriptions of seven US federal office buildings pressure tested for their air leakage characteristics..... 299

Table 5.7 Assumed input parameter distributions of Shaw-Tamura and LBL Infiltration Model used in this analysis to predict distributions of air infiltration rates..... 300

Table 6.1 Two-step method to estimate the floor area distribution of commercial buildings in census tract 102600 in Oklahoma City 383

Table 6.2 Fraction of commercial buildings as a function of building floor area as estimated from US national data 383

Table 6.3 Building occupancy regression model results, estimated by summing number of employees and 25% of the building capacity 384

Table 6.4 Statistics of the predicted air leakage coefficient of buildings surveyed by the CBECB 384

Table 6.5 List of simulations and their assigned codes 385

Table 6.6 List of simulations, as indicated by their designated codes, for which the estimated number of casualties are plotted in selected figures 385

Table 6.7 SIP effectiveness of commercial buildings estimated in the 0.5-h release simulation in terms of casualty reduction factor. 386

Table 6.8 SIP effectiveness of commercial buildings estimated in the 0.5-h release in terms of casualty reduction factor, with additional air exchange to represent the mechanical ventilation system running in all buildings during the entire simulation 386

Table 6.9 SIP effectiveness of commercial buildings measured in terms of casualty reduction factor in the 0.5-h release, including effects of sorption and initiation delay 387

Table 6.10 Modeling parameters for the two-zone analysis of the commercial buildings in two grid cells in the simulation 388

List of Figures

Figure 2.1 Predicted outdoor and indoor concentrations at different downwind locations from the release source. 46

Figure 2.2 Predicted toxic loads at 0.5 km downwind from the release source if one were exposed to the outdoor and indoor contaminant levels 47

Figure 2.3 Community-based SIP effectiveness measured in terms of casualty reduction factor (CRF) and toxic load reduction factor (TLRF) as the 0.5-h release progresses in time. 48

Figure 2.4 SIP effectiveness measured in terms of casualty reduction factor (CRF) and toxic load reduction factor (TLRF) as a function of ξ. 49

Figure 2.5 SIP effectiveness measured in terms of casualty reduction factor (CRF) and toxic load reduction factor (TLRF) as function of ξ from 15 runs (3 release durations with indoor concentrations evaluated at 5 air-exchange rates)..... 50

Figure 2.6 Predicted SIP effectiveness measured in terms of casualty reduction factor and toxic load reduction factor versus release amount over a duration of 0.5-h..... 51

Figure 2.7 Dependence of CRF on delay in SIP termination 52

Figure 2.8 SIP effectiveness under linear dose-response as a function of ξ from 15 runs (3 release durations with indoor concentrations evaluated at 5 air-exchange rates) assuming SIP is terminated at 0.5, 1, and 3-h 53

Figure 3.1 Number of valid blower-door measurements from each state..... 125

Figure 3.2 (a) Comparison of the cumulative distribution function of the floor area of houses in the leakage database to the 1999 American Housing Survey. (b) Floor area of houses in the air leakage database grouped by number of measurements taken in each state..... 126

Figure 3.3 (a) Comparison of the cumulative distribution function of the year built of houses in the leakage database to the American Housing Survey. (b) Year built of houses in the air leakage database grouped by number of measurements taken in each state 127

Figure 3.4 Effects of year built and floor area on normalized leakage based on multiple linear regression models 128

Figure 3.5 Scatter plots of the observed geometric mean of normalized leakage as categorized by year built, floor area, and house type, against the predicted values based on multiple linear regression models 129

Figure 3.6 Estimated distribution of year built and floor area of low income and conventional houses based on the 1999 American Housing Survey 130

Figure 3.7 Estimated US nationwide distribution of normalized leakage for low income and conventional single-family houses, and their composite..... 131

Figure 3.8 Comparison of best-fit air-exchange rates estimated from linear regression models obtained in this analysis, and values found in EPA Exposure Factors Handbook 132

Figure 3.9 Outdoor temperature time profile in Albuquerque, NM dated February 24, 2003 at the time of the simulated hypothetical release. 133

Figure 3.10 Wind speed estimated at 10 m height in Albuquerque, NM dated February 24, 2003 at the time of the simulated hypothetical release..... 134

Figure 3.11 Wind speed estimated at 10 m height at various downwind distances from the release source. 135

Figure 3.12 Map of Albuquerque, NM, illustrating the census tract boundaries in Bernalillo County, and the release location 136

Figure 3.13 Distributions of house year built in 3 census tracts close to the release source 137

Figure 3.14 Fraction of US housing units that are single-family detached units versus other types according to national data from the American Housing Survey 138

Figure 3.15 Predicted house year-built distribution for single-family detached units in census tract 2700 in Albuquerque, NM. 139

Figure 3.16 Relationship between the number of rooms and house floor area of the 27,400 single-family detached units investigated by the American Housing Survey. 140

Figure 3.17 Cumulative distribution of number of rooms in renter and owner occupied housing units, as well as single-family detached units assessed by the American Housing Survey. 141

Figure 3.18 Distribution of number of rooms in owner-occupied housing units located in 3 census tracts close to the hypothetical release site in Albuquerque, NM. 142

Figure 3.19 Estimated floor area distribution of single-family detached units for the same 3 census tracts in Albuquerque, NM, as shown in Figure 3.18 142

Figure 3.20 Cumulative floor area distributions of single-family detached units and those that are classified as low-income as surveyed by the American Housing Survey 143

Figure 3.21 Relationship between the floor area cumulative distributions of all single-family detached units and that of the low-income subgroup 144

Figure 3.22 Floor area cumulative distributions of single-family detached units that were built in four different time periods. 145

Figure 3.23 Predicted house year built and floor area joint distributions of not low-income and low-income single-family detached units located in three census tracts close to the hypothetical release site in Albuquerque, NM. 146

Figure 3.24 Predicted normalized leakage distribution of houses in Bernalillo County of Albuquerque 147

Figure 3.25 Predicted median normalized leakage of houses in a census tract plotted against three house characteristics 148

Figure 3.26 Predicted median air infiltration rates at various downwind distances from the release source 149

Figure 3.27 Predicted distribution of air infiltration rates at two downwind locations from the release source 150

Figure 4.1 Outdoor concentrations of the 2-h contaminant release in Albuquerque. 216

Figure 4.2 Schematic of a two-sink sorption model 217

Figure 4.3 Predicted indoor concentrations for a well-mixed space exposed to constant outdoor concentration of 1 mg/m^3 for 1 h 218

Figure 4.4 The predicted total mass in a room when subjected to ambient Cl_2 at a constant concentration of 1 mg/m^3 for 1-h. 219

Figure 4.5 Predicted mass in a room when subjected to sarin at constant ambient concentration of 1 mg/m^3 for 1-h 220

Figure 4.6 Three emergency warning diffusion curves showing the expected time needed to inform the community about an emergency using different warning methods 221

Figure 4.7 Predicted number of potential casualties in three releases of various durations (0.5-h, 1-h, and 2-h) if people were outdoors, and if people were to take shelter in buildings. 222

Figure 4.8 Predicted cumulative toxic load in three releases of various durations (0.5-h, 1-h, and 2-h) if people were outdoors, and if people were to take shelter in buildings 223

Figure 4.9 The normalized number of potential casualties estimated for 4 release amounts: base case, 0.04×, 0.4×, and 4× of the base case amount 224

Figure 4.10 Differences in the potential casualty estimates if the distribution of air-exchange rate is captured, or if all houses in a census tract are assumed to have the median normalized air-leakage value 225

Figure 4.11 Predicted areas where indoor exposure is expected to exceed the toxic load limit for a 1-h release under linear dose-response conditions..... 226

Figure 4.12 Predicted time when the toxic load limit is exceeded for houses at the tightest and leakiest 10th percentiles, and houses that are at the median of the air-leakage distribution 227

Figure 4.13 Indoor concentration predictions at a nearby location to the release site under various sorption rates. 228

Figure 4.14 Predicted number of potential casualties if people were to take shelter indoors under various sorption conditions. 229

Figure 4.15 Air-exchange rate distribution of houses at two locations downwind of the release site before and after SIP is implemented. 230

Figure 4.16 Indoor concentrations predicted at two locations close to the release source under various SIP initiation time delays: 1, 0.5, and 0.25 h. The no delay case (0 h) is also presented for comparison..... 231

Figure 4.17 Ratio of peak indoor concentrations modeled under various SIP initiation time delay (0.25, 0.5, and 1 h) relative to the no-delay case. 232

Figure 4.18 Change in estimates of potential casualties subject to the pre-sheltering air-exchange rate distributions and the time delay in initiating shelter-in-place. All simulations assumed linear dose-response (i.e. toxic load exponent = 1) and no sorption. 233

Figure 4.19 Change in estimates of potential casualties subject to the pre-sheltering air-exchange rate distributions and the time delay in initiating shelter-in-place. All simulations assumed toxic load exponent = 2 and no sorption. 234

Figure 4.20 Change in estimates of potential casualties subject to the pre-sheltering air-exchange rate distributions and the time delay in initiating shelter-in-place. All simulations assumed toxic load exponent = 3 and no sorption. 235

Figure 4.21 Potential casualty estimates subject to various sorption rates to indoor surfaces, and delay in SIP initiation time. All simulations assumed linear dose response (toxic load exponent = 1) and summertime pre-sheltering conditions 236

Figure 5.1 Number of buildings in the commercial building air leakage database as a function of year built, floor area, and number of floors 301

Figure 5.2 Histogram of the air-leakage coefficient and flow exponent in the commercial building air leakage database. 302

Figure 5.3 Scatter plots of air-leakage coefficients of buildings in the commercial air leakage database against building year built, floor area, and height. 303

Figure 5.4 Boxplots of air-leakage coefficients of buildings in the commercial air leakage database grouped by their usage and construction types, and country where measurements were made. 304

Figure 5.5 Comparison of the prevalence of various building types in the commercial air leakage database and the US national estimates from CBECS 305

Figure 5.6 Year built of the buildings in the commercial air leakage database sorted by their construction types. 306

Figure 5.7 Regression results of the two models detailed in Table 5.4. 307

Figure 5.8 Comparison of observed and predicted air-leakage coefficients *C* presented in 1-to-1 scatter plot, and in terms of their cumulative distribution 308

Figure 5.9 Various methods to combine stack and wind induced air infiltration rates to give the total air infiltration rate proposed for the Shaw-Tamura Infiltration Model. 309

Figure 5.10 Comparison of measured and predicted air infiltration rates under meteorology conditions..... 310

Figure 5.11 Predicted air infiltration rates of the seven US federal buildings..... 311

Figure 5.12 Measured and predicted air infiltration rates of seven US federal office buildings 313

Figure 5.13 Air infiltration rates measured in 56 small commercial buildings 314

Figure 5.14 Comparison of air infiltration rate model predictions and observed values for the 56 small commercial buildings 315

Figure 5.15 Differences in the median air infiltration rate for each of the 56 small commercial buildings in Florida predicted using the Shaw-Tamura Infiltration Model and the LBL Infiltration Model..... 316

Figure 5.16 Air infiltration rates measured in 40 California buildings including schools, retail buildings, and offices, and 25 US office buildings..... 317

Figure 5.17 Building floor area of US commercial buildings surveyed in CBECS. Building height distribution is estimated from the number of floors, which is reported in the CBECS 318

Figure 5.18 Histogram of the estimated number of stories of buildings surveyed in CBECS 319

Figure 5.19 Scatter plot of flow exponent and air-leakage coefficient..... 320

Figure 5.20 Distribution of building aspect ratio, defined as the ratio of the length to width of the footprint area, of 1552 buildings in Oklahoma City..... 321

Figure 5.21 The monthly average temperature and wind speed in the 45 most populous cities in the US. 321

Figure 5.22 Predicted air infiltration rates of US commercial buildings..... 322

Figure 5.23 Ratio of monthly averaged stack-effect driven air infiltration rate to wind-effect driven air infiltration rate predicted in the US commercial building stock 323

Figure 5.24 Ratio of measured air infiltration rate and air-exchange rate from two datasets made by tracer-gas decay method with mechanical ventilation on, and with mechanical ventilation off. 324

Figure 6.1 Outdoor concentrations predicted at 5, 15, 25, and 35 minutes from the onset of a 0.5-h release 389

Figure 6.2 Outdoor concentration grid (gray) on the footprint of 6334 buildings in Oklahoma City contained within a 5.4 km × 5.4 km area. 390

Figure 6.3 Distribution of height (left) and floor area (right) of all buildings contained in the Oklahoma City 5.4 km × 5.4 km study area 391

Figure 6.4 Estimated fraction of residential and commercial buildings in 17 census tracts in Oklahoma City 391

Figure 6.5 Cumulative floor area distribution of single-family detached units in census tract 101600 in Oklahoma County, and the combined distribution that includes commercial buildings 392

Figure 6.6 Estimated number of residential and commercial buildings as a function of floor area 392

Figure 6.7 Estimated floor area and height of single-family detached units and commercial buildings in the 5.4 km × 5.4 km study area of Oklahoma City 393

Figure 6.8 Cumulative distribution of building occupancy per floor area estimated by two methods, which differ by whether the occupant capacity reported in CBECS is counted at 100% or at 25% when computing the building occupancy per floor area 394

Figure 6.9 Estimated occupancy per building floor area in buildings that were surveyed by the CBECS 395

Figure 6.10 Estimated building occupancy in 1997 commercial buildings that are located in the 5.4 km × 5.4 km study area of Oklahoma City 396

Figure 6.11 LANL daytime population estimates in Oklahoma City on a 250 m grid 397

Figure 6.12 Estimated commercial building occupancy in Oklahoma City projected on the same grid used in the LANL database. 397

Figure 6.13 Building floor area and number of story splits identified by the classification tree method to minimize the variance of air leakage coefficient estimated for buildings in the CBECS 398

Figure 6.14 Classification tree analysis for 1-story commercial buildings surveyed in the CBECS 399

Figure 6.15 Classification tree analysis for 2-story buildings surveyed in the CBECS 400

Figure 6.16 Classification tree analysis for 3 to 5-story buildings surveyed in the CBECS 400

Figure 6.17 Predicted air leakage coefficient distributions of buildings surveyed in CBECS partitioned into 9 groups by their number of floors and floor area 401

Figure 6.18 Predicted areas where exposure to the outdoor concentrations are expected to exceed the toxic load limit for the modeled 0.5-h release event. 402

Figure 6.19 Predicted air infiltration rates of commercial buildings in 17 census tracts selected from the 5.4 km × 5.4 km study area in Oklahoma City 403

Figure 6.20 Comparison of two methods used to predict the air infiltration rate distribution of commercial buildings in 5 randomly selected census tracts in Oklahoma City 404

Figure 6.21 Predicted air infiltration rate distributions of commercial buildings in 17 census tracts selected from the 5.4 km × 5.4 km study area in Oklahoma City 405

Figure 6.22 Air infiltration rates predicted for single-family detached units and commercial buildings in the 17 census tracts in the Oklahoma City study area 406

Figure 6.23 Median indoor concentrations (y-axis) predicted at each grid cell in the two classes of buildings: commercial and residential 407

Figure 6.24 Predicted indoor concentrations in commercial buildings at two locations 408

Figure 6.25 Predicted indoor concentration distributions in commercial and residential buildings at 3 locations in Oklahoma City 409

Figure 6.26 Predicted areas with various fractions of buildings having indoor concentrations toxic enough to exceed the toxic load limit for the modeled 0.5-h release event 410

Figure 6.27 Predicted population for which toxic load exceeds the toxic load limit for the simulated 0.5-h release event in Oklahoma City 411

Figure 6.28 Predicted potential casualties if people were to shelter in commercial buildings and in residences (single-family detached units) 412

Figure 6.29 Effect of additional air exchange induced by mechanical ventilation systems on SIP effectiveness of commercial buildings 413

Figure 6.30 Effect of chemical sorption on indoor surfaces on the SIP effectiveness of commercial buildings 414

Figure 6.31 Effect of chemical sorption on indoor surfaces on the SIP effectiveness of commercial buildings under normal operating conditions 415

Figure 6.32 Effects of initiation delay on the SIP effectiveness of commercial buildings in reducing potential casualties among the exposed population. Adverse health effects are assessed using toxic load exponent $m = 1$ in all simulations. 416

Figure 6.33 Effects of delay in initiating SIP on the effectiveness of commercial buildings in reducing potential casualties among the exposed population. Adverse health effects are assessed using toxic load exponent $m = 2$ in all simulations 417

Figure 6.34 Effects of delay in initiating SIP on the effectiveness of commercial buildings in reducing potential casualties among the exposed population. Adverse health effects are assessed using toxic load exponent $m = 3$ in all simulations 418

Figure 6.35 Plan view of a building illustrating the two-zone configuration used to model the indoor concentrations in the perimeter and core zone 419

Figure 6.36 Predicted two-zone indoor concentrations in commercial buildings in two census tracts 420

Acknowledgements

Phillip Price at Lawrence Berkeley National Laboratory (LBNL) oversaw much of the research presented in this dissertation. I greatly appreciate his insightful inputs and continuous support throughout the development of this work. Especially in the area of statistical analysis, I have benefited immensely from his guidance.

Throughout my residence at LBNL, I have also grown intellectually through interactions with other members of the Airflow and Pollutant Transport Group. Being part of such a wonderful team has allowed me to gain an understanding of aspects of research.

Special thanks must also be given to our collaborators at the National Atmospheric Release Advisory Center for providing me with the opportunity to apply my research operationally to improve public safety.

Finally, I want to express my gratitude to my advisors, Professor William Nazaroff and Professor Ashok Gadgil, for their mentorship and high standards of scientific excellence. Their contributions to my professional development are most invaluable, and will benefit me throughout my career.

This work was supported by the Office of Chemical Biological Countermeasures, of the Science and Technology Directorate of the Department of Homeland Security, and performed under US Department of Energy Contract No. DE-AC02-05CH11231.

1 Introduction

1.1 Background

Large-scale outdoor chemical releases can cause severe harm to nearby communities. In addition to the possible terrorist attack scenarios that have received much attention owing to recent events, chemical accidents at production facilities and during transportation have been and will continue to pose significant threats to public safety. Numerous catastrophic chemical releases worldwide - whether naturally occurring, industrial/transportation related, or deliberate incidents - have led to mass casualties in surrounding communities (Murray and Goodfellow, 2002). In the US, major chemical releases that require emergency operations involving community decisions and public responses occur at a rate of roughly 100 per year (Rogers, 1994; Elliott et al., 2004). Between 1994 and 1999, a preliminary analysis on a risk management database by the US EPA recorded 97 industrial accidents that led to off-site consequences involving a shelter-in-place response (Kleindorfer et al., 2003). Aside from these accidents that occurred at industrial facilities, the occurrence of accidents in transporting hazardous materials has increased over time (Vílchez et al., 1995; Orr et al., 2001; Horton et al., 2003). A high percentage of these transport accidents occurred in densely populated areas. Off-site emergency protective action plans are therefore essential to manage the public-health risk and to prepare officials and the public to respond quickly in such situations.

The sudden and unanticipated nature of these releases means that evacuation is often not an option for the nearby communities. In such cases, sheltering in buildings may be used as a temporary measure aimed at reducing health risk from exposure to the toxic materials. Shelter-in-place (SIP) is relatively straightforward to implement because most people are already in buildings most of the time, and so exercising the emergency response simply means closing windows and doors, and turning off ventilation fans. In such cases, the air exchange between the indoors and the outdoors will be at its lowest rate, which means that the rise in indoor concentration of toxic contaminants will be delayed compared with outdoors. The maximum concentration indoors will only reach a fraction of the concentration outdoors. Indoor removal mechanisms, such as sorption on surfaces and filtration by building envelopes, can further lower the indoor concentration of the toxic contaminants.

Some successful examples of SIP where injuries and fatalities were prevented have been documented (Mannan and Kilpatrick, 2000; NICS, 2001). Despite such successes, emergency responders often view SIP as effective only in areas that are far away from the source of the release, or when the perceived health risk is low (Rogers et al., 1990). In situations where the large-scale release subjected the public to high risk of exposure, emergency responders are much more inclined to evacuate the area instead. This reluctance in advising the public to shelter-in-place occurs because taking shelter in buildings does not completely eliminate contact with the toxic chemicals. Since building envelopes are not airtight, some toxic chemicals will infiltrate indoors. At times emergency responders might prefer to risk exposing the population to the outdoor

concentrations during evacuation, rather than instructing the public to shelter indoors. Relative to evacuation, which can be very time consuming, SIP can be implemented rather quickly. As people spend a majority of their time indoors, many can avoid direct exposure to the toxic contaminants outdoors entirely if SIP were instructed. Since both protective actions - evacuation and SIP - have their advantages and disadvantages, carefully considering the performance of each alternative in a given situation is important to minimize adverse health effects in the exposed population.

1.2 Current State of Knowledge

Past studies on sheltering often focused on characterizing the effectiveness of a single building (Engelmann, 1992; Siren, 1993; Casal et al., 1999). While some have acknowledged the dependence of air-exchange rate on weather parameters, very few have captured the variability among buildings in the analysis. Vogt et al. (1999) recommended special consideration for the proportion of residences constructed before 1950 and during 1950–1970 when assessing the suitability of the residential housing stock to function as shelters. Readily available software that makes a rough assessment of indoor concentrations during an atmospheric release event, such as the US EPA's ALOHA (Areal Locations of Hazardous Atmospheres), has pre-defined building parameters for only a few types of buildings. Previous studies on the air leakage of residential (Orme et al., 1994; Sherman and Dickerhoff, 1998) and non-residential (Persily, 1999) buildings found substantial variability among the different buildings tested. This variability, together with other building characteristics that affect the rate of air exchange with the

outdoors, can lead to considerable differences in their ability to protect building occupants against outdoor releases.

As toxic chemicals penetrate through building envelopes, some fraction might be lost to surfaces of the unintentional openings. This can potentially lower the exposure of building occupants in some circumstances, but preliminary assessment suggests that penetration of gaseous pollutants into the indoors is likely to be high under many conditions (Liu and Nazaroff, 2001). Another means of chemical loss indoors is a process known as sorption, which collectively describes the many modes of binding of the chemical with indoor materials (Karlsson and Huber, 1996; Blewett and Arca, 1999; Singer et al., 2005). This process can be fast relative to the air-exchange rate, meaning that it can effectively lower the concentration indoors. In a building stock, however, some variability in the efficiency of this process is expected. The specifics of the release scenario can also affect the importance of sorption on indoor surfaces for the protectiveness of SIP.

The benefit of sheltering has been quantified in past studies with a metric known as dosage reduction. However, this metric can underestimate the SIP effectiveness in some situations. Health effects, unlike dose, do not necessarily vary linearly with concentration. Analysis of inhalation toxicity experiments on chemicals like Cl_2 and NH_3 reveals that $C^m \times t$, where C is the concentration, t is the exposure duration, and $m \neq 1$, often predicts response better than dose (ten Berge, 1986). A similar conclusion has been reached for organophosphate-based nerve agents such as sarin (Hartmann, 2002). As the

goal of sheltering is to minimize health consequences caused by the release, it is imperative to consider the dose-response relationship for the toxic materials. Controversies remain, however, on how to predict the response from exposure to concentrations that vary rapidly with time (Ride, 1995; Stage, 2004).

A few experimental studies have investigated the performance of some forms of proactive measures, such as active filters (Blewett and Arca, 1999; Ward et al., 2005) and duct tape and plastic sheets (Sorensen and Vogt, 2001; Jetter and Whitfield, 2005). Results obtained under certain experimental conditions show that these strategies can be effective, but the effectiveness is likely to vary in different release scenarios and among different houses in a community. Members of one community have been supplied with active filters in case of emergency at the nearby stockpile of chemical warfare agents (NICS, 2003). However, this is far above the level of protection typical in residences. Application of duct tape and plastic sheets is less costly, but the effectiveness of this measure depends on properly sealing the room before the toxic plume arrives. Past survey studies (Rogers and Sorensen, 1991; Rogers, 1994) have found that the public can take a long time to respond in emergencies. As a result, it is questionable whether these additional SIP measures can be implemented successfully before the toxic contaminants infiltrate indoors. Another time constraint on SIP effectiveness is when SIP should be terminated. Concerns for post-event exposure to the toxic residuals left in indoor air suggest that SIP needs to be terminated as soon as possible to maximize its effectiveness (Yantosik et al., 2001). In practice, however, the decision to terminate must also consider the variability among buildings in a community. Another serious concern is the risk of

exposing some in the community to lingering puffs of outdoor contaminants, which can be highly concentrated and dangerous if exit from shelters too soon. A balance is needed in deciding when to terminate SIP so as to minimize the risk of adverse health effects imposed on the exposed community.

1.3 Overview of the Research

The main objectives of this research are to identify and assess key factors that affect SIP effectiveness, and to demonstrate through case studies the methodology of predicting the variability in a building stock. Understanding how the various factors can affect SIP effectiveness is essential to predict situations where SIP might fail to provide adequate protection to the exposed community, and when SIP is expected to be reliable. Such knowledge can also help identify opportunities where the effectiveness of SIP can be improved. This research focuses on the acute adverse health effects caused by exposure to toxic chemicals released to the atmosphere. Modeling the variability of the protection offered by different buildings in a community is crucial to this work. Since SIP is a community emergency response strategy, it is imperative that the assessment captures the range of indoor concentrations to which the community is exposed. To address this issue, a detailed analysis of the variability in building air leakage is performed. Realistic modeling of SIP in a community, one that considers how fast a community can respond to a release, and what the implications are from post-release exposure, is undertaken to assess the effectiveness of the response strategy in practice.

Large-scale airborne toxic chemical releases are simulated to assess the SIP effectiveness in reducing acute health effects in the exposed population. Three types of models are used to evaluate the effectiveness of SIP: an atmospheric dispersion model to predict the outdoor concentration, an air infiltration model and mass balance on the infiltrating toxic contaminants to predict the indoor concentration in buildings, and a dose-response model to predict the consequent health effects. The metric for evaluating the effectiveness of sheltering is defined by comparing the health consequences if people were to take shelter, relative to the case where people were exposed to outdoor concentrations. The protectiveness of both residential and non-residential buildings is examined. Detailed analysis of the air leakage of buildings and modeling of air infiltration rates are performed to estimate the distribution of indoor concentrations in buildings. Sensitivity of SIP effectiveness to the various model parameters is investigated under realistic conditions. Since it is likely that at least some fraction of the community will not receive sufficient advance notice to complete SIP before the toxic plume arrives, the protection offered by buildings under normal operating conditions is also assessed.

1.4 Outline of the Dissertation Contents

This dissertation starts with a systematic exploration of the key factors affecting SIP effectiveness (Chapter 2). Using simple models to simulate the outdoor and indoor concentrations, and the consequent health effects, SIP effectiveness is predicted under a full range of release conditions and building air leakage characteristics. A metric to measure SIP effectiveness in a community is introduced. Even though results from this

analysis are subject to a number of simplifying assumptions, they serve as a basis for selecting parameters that merit more careful investigation in the later chapters.

Chapters 3 and 4 present a detailed assessment of the SIP effectiveness of houses in an urban area. Because air exchange is a key determinant of the effectiveness of SIP, available data on air leakage of US houses is analyzed. A method is developed to make use of such findings to predict the air infiltration rate distribution of houses during SIP. To prepare for the assessment of indoor exposure to the toxic chemical before people successfully taken shelter, estimates of air-exchange rate with natural and mechanical ventilation typically found in residences are summarized. Chapter 4 starts by describing the outdoor concentration predictions for select hypothetical chemical releases in Albuquerque, NM. To more realistically model the indoor concentrations experienced by residents, sorption on indoor surfaces and delay in implementing SIP are included in the analysis. Existing experimental data on sorption to indoor surfaces, and survey data on response time of affected parties in emergency situations are reviewed. Simulations of SIP effectiveness are modeled using the parameters derived from these studies.

Chapters 5 and 6 assess the effectiveness of SIP in commercial buildings. While the overall structure of the analysis is similar to that of residential buildings, assessment of the air leakage distribution of commercial buildings requires a completely different set of data. Chapter 5 details the findings from such analysis, and outlines a different method to predict the air infiltration rates of commercial buildings. Unlike for residential buildings, mechanical ventilation is the predominant mode of fresh air entry in commercial

buildings before SIP is implemented. A brief summary on the air-exchange rates of buildings under normal operating conditions is included. A different set of hypothetical releases, one that is situated in Oklahoma City, OK, is used to compare the difference in SIP effectiveness of residential and commercial buildings. Examination of SIP effectiveness in the modeled scenarios includes sorption of chemicals on indoor surfaces. Casualty estimates are also derived in cases where buildings have left their mechanical ventilation systems running during SIP. Finally, the range of indoor concentrations under non-well mixed conditions is estimated using a simple two-zone model.

A summary of the research findings is given in Chapter 7 and opportunities for further research in this field are discussed.

1.5 References

Blewett, W.K., Arca, V.J., 1999. Experiments in sheltering in place: how filtering affects protection against sarin and mustard vapor. Edgewood Chemical Biological Center, ECBC-TR-034, Aberdeen Proving Ground, MD.

Casal, J., Planas-Cuchi, E., Casal, J., 1999. Sheltering as a protective measure against airborne virus spread. Journal of Hazardous Materials A68, 179–189.

Elliott, M.R., Wang, Y., Lowe, R.A., Kleindorfer, P.R., 2004. Environmental justice: frequency and severity of US chemical industry accidents and the socioeconomic status of surrounding communities. Journal of Epidemiology & Community Health 58, 24–27.

Engelmann, R.J., 1992. Sheltering effectiveness against plutonium provided by buildings. Atmospheric Environment 26A, 2037–2044.

Hartmann, H.M., 2002. Evaluation of risk assessment guideline levels for the chemical warfare agents mustard, GB, and VX. Regulatory Toxicology and Pharmacology 35, 347–356.

Horton, D.K., Berkowitz, Z., Haugh, G.S., Orr, M.F., Kaye, W.E., 2003. Acute public health consequences associated with hazardous substances released during transit, 1993-2000. Journal of Hazardous Materials B 98, 161–175.

Jetter, J.J., Whitfield, C., 2005. Effectiveness of expedient sheltering in place in a residence. Journal of Hazardous Materials A119, 31–40.

Karlsson, E., Huber, U., 1996. Influence of desoprtion on the indoor concentration of toxic gases. Journal of Hazardous Materials 49, 15-27.

Kleindorfer, P.R., Belke, J.C., Elliott, M.R., Lee K., Lowe, R.A., Feldman, H.I., 2003. Accident epidemiology and US chemical industry: accident history and worst-case data from RMP*Info. Risk Analysis 23 (5), 865–881.

Liu, D.L., Nazaroff, W.W., 2001. Modeling pollutant penetration across building envelopes. Atmospheric Environment 35, 4451–4462.

Mannan, M.S., Kilpatrick, D.L., 2000. The pros and cons of shelter-in-place. Process Safety Progress 19 (4), 210–218.

Murray, V., Goodfellow, F., 2002. Mass casualty chemical incidents – towards guidance for public health management. Public Health 116, 2–14.

NICS, 2001. Sheltering in place as a public protection action. National Institute for Chemical Studies, Charleston, WV.

NICS, 2003. National Institute for Chemical Studies News 12, Charleston, WV. http://www.nicsinfo.org/nm0203.pdf

Orme, M., Liddament, M., Wilson, A., 1994. An analysis and data summary of the AIVC's numerical database. Air Infiltration and Ventilation Centre, Coventry, UK.

Orr, M.F., Kaye, W.E., Zeitz, P., Powers, M.E., Rosenthal, L., 2001. Public health risks of railroad hazardous substance emergency events. Journal of Occupational and Environmental Medicine 43, 94–100.

Persily, A.K., 1999. Myths about building envelopes. ASHRAE Journal 41 (3), 39–47.

Ride, D.J., 1995. A practical method of estimating toxic loads in the presence of concentration fluctuations. Environmetrics 6, 643–650.

Rogers, G.O., Watson, A.P., Sorensen, J.H., Sharp, R.D., Carnes, S.A., 1990. Evaluating protective actions for chemical agent emergencies. ORNL-6615, Oak Ridge National Laboratory, Oak Ridge, TN.

Rogers, G.O., Sorensen, J.H., 1991. Diffusion of emergency warning: comparing empirical and simulation results. Risk Analysis Prospects and Opportunities, Zerros C., et al., Eds., Plenum Press, New York, NY, 117–134.

Rogers, G.O., 1994. The timing of emergency decisions: modeling decisions by community officials during chemical accidents. Journal of Hazardous Materials 37, 353–373.

Sherman, M.H., Dickerhoff, D.J., 1998. Airtightness of US dwellings. ASHRAE Transactions 104 (2), 1359–1367.

Singer, B.C., Hodgson, A.T., Destaillats, H., Hotchi, T., Revzan, K.L., Sextro, R.G., 2005. Indoor sorption of surrogates for sarin and related nerve agents. Environmental Science & Technology 39, 3203–3214.

Siren, K., 1993. The protection ability of the building shell against sudden outdoor air contamination. Building and Environment 28 (3), 255–269.

Sorensen, J.H., Vogt, B.M., 2001. Will duct tape and plastic really work? Issues related to expedient shelter-in-place. ORNL/TM-13742, Oak Ridge National Laboratory, Oak Ridge, TN.

Stage, S.A., 2004. Determination of acute exposure guideline levels in a dispersion model. Journal of Air & Waste Management Association 54, 49–59.

ten Berge, W.F., 1986. Concentration-time mortality response relationship of irritant and systemically acting vapors and gases. Journal of Hazardous Materials 13, 301–309.

Ward, M., Siegel, J.A., Corsi, R.L., 2005. The effectiveness of stand alone air cleaners for shelter-in-place. Indoor Air 15, 127–134.

Vílchez, J.A., Sevilla, S., Montiel, H., Casal, J., 1995. Historical analysis of accidents in chemical plants and in the transportation of hazardous materials. Journal of Loss Prevention in the Process Industries 8 (2), 87–96.

Vogt, B.M., Hardee, H.K., Sorensen, J.H., Shumpert, B.L., 1999. Assessment of housing stock age in the vicinity of chemical stockpile sites. ORNL-13742, Oak Ridge National Laboratory, Oak Ridge, TN.

Yantosik, G.D., Lerner, K., Maloney, D., Wasmer, F., 2001. When and how to end shelter-in-place protection from a release of airborne hazardous material: report on a decision-making concept and methodology. Argonne National Laboratory, IL.

2 Exploring the Effectiveness of Shelter-in-Place

2.1 Introduction

A systematic exploration of the key factors affecting shelter-in-place (SIP) effectiveness is presented. One difficulty in quantifying SIP effectiveness is a lack of simple yet informative metrics. Early studies on SIP effectiveness focused on the indoor-outdoor dose reduction when SIP is practiced (Engelmann, 1992; Blewett et al., 1996). However, community-scale SIP effectiveness is not easily related to the dosage reduction computed for one dwelling. In this chapter, the community SIP effectiveness is measured in terms of the expected reduction in adverse health consequences for an exposed community as a toxic plume disperses and travels downwind. The modeling approach emphasizes release scenario (duration and amount), chemical characteristics (toxicity and dose-response relationship), and features of residential shelters that influence protectiveness. Finally, the issue of when and how to end SIP is discussed. In this analysis, the emphasis is not on the optimization of SIP termination time, but rather to illustrate how SIP effectiveness might be affected under various scenarios by delays in termination.

This analysis will establish the groundwork for the case studies to follow, which seek to assess the SIP effectiveness of the residential and commercial building stock in the US. In this analysis, aspects associated with human factors, such as the time needed for decision-making or the effectiveness of communicating with the public, are not modeled

explicitly. Instead, it is assumed that the population would carry out SIP exactly as prescribed. Despite these simplifications, the model results provide useful information about the behavior of buildings as shelters that is a foundation to understanding how the full set of complex issues affect SIP effectiveness under various scenarios.

2.2 Methods

To quantify community-scale SIP effectiveness, the predicted health consequences associated with an SIP scenario is compared to a reference case for a large-scale toxic release. In the reference case, exposures occur at the outdoor concentration level. In the SIP case, exposures occur at the concentration predicted indoors, resulting from contaminant infiltration from the time-dependent passage of the outdoor plume. To address both cases, three types of model calculation are needed: an atmospheric dispersion model to predict the outdoor concentrations resulting from a hypothetical release; a building model to predict the indoor concentrations that result from temporally and spatially varying outdoor concentrations; and a dose-response model to predict the health effects resulting from exposure to time-varying outdoor or indoor concentrations. To emphasize the dependence of SIP effectiveness on key controlling variables, simple forms of these models are chosen: a Gaussian atmospheric dispersion model to predict outdoor concentrations; a well-mixed box model to predict indoor concentrations; and a toxic-load model to predict the health consequences of exposure.

2.2.1 Outdoor and Indoor Concentrations

The outdoor concentration field resulting from a short-term release is related to the well-known Gaussian atmospheric diffusion model as follows (Palazzi et al., 1982; Overcamp, 1990):

$$C_{out}(x,y,t) = C_G(x,y)\cdot\frac{1}{2}\left[erf\left(\frac{x}{\sigma_x\sqrt{2}}\right) - erf\left(\frac{x-\overline{U}t}{\sigma_x\sqrt{2}}\right)\right] \quad \text{for} \quad t \le T_r$$

$$C_{out}(x,y,t) = C_G(x,y)\cdot\frac{1}{2}\left[erf\left(\frac{x-\overline{U}(t-T_r)}{\sigma_x\sqrt{2}}\right) - erf\left(\frac{x-\overline{U}t}{\sigma_x\sqrt{2}}\right)\right] \quad \text{for} \quad t \ge T_r$$

$$\text{where} \quad C_G(x,y) = \frac{M}{2\pi\sigma_y\sigma_z\overline{U}}\cdot\exp\left(-\frac{y^2}{2\sigma_y}\right)\cdot\left[\begin{array}{l}\sum_{i=-\infty}^{\infty}\exp\left(-\frac{(z-2iH^*-H)^2}{2\sigma_z}\right)\\ +\sum_{i=-\infty}^{\infty}\exp\left(-\frac{(z+2iH^*+H)^2}{2\sigma_z}\right)\end{array}\right]$$

Eqn 2.1

C_G (g/m^3) represents the steady-state concentration resulting from a point source released at a constant mass rate M (g/s). H (m) is the height of the release, which is set to zero to represent a ground level release. H^* (m) is the height of the inversion layer that establishes an upper boundary for vertical pollutant dispersion. By assuming the no flux boundary condition at the ground and the inversion height, the concentration is expressed as an infinite series of contributions from images. The coordinates of the grid are arranged such that the point source is placed at the origin (x, y, z) = (0, 0, 0). The windward direction is aligned with the x-coordinate. The dispersion coefficients (σ_x, σ_y, and σ_z [m]) are based on curve fits to the standard Pasquill-Gifford data, which depend on the downwind distance, x, in a manner that varies with stability class (Seinfeld and Pandis, 1998).

C_{out} (g/m^3) is the time-dependent outdoor concentration resulting from a short-term release of duration T_r (h), beginning at $t = 0$. It is assumed that the mass release rate M is constant throughout the release duration. The solutions shown in Eqn 2.1 invoke the slender-plume approximation, which requires that the transverse spread of the contaminant is small compared to the downwind distance it has traveled. This assumption is typically valid unless the mean wind speed $\overline{U}$ (m/s) is very slow such that the condition $\sigma_x(x/\overline{U})/x << 1$ is no longer satisfied. In the scenarios modeled, the minimum wind speed used is 3 m/s.

A uniform model grid is employed, and the results were tested to ensure grid-size independence. The release source is assumed to occur at ground level. Outdoor concentrations are evaluated at the 2-m plane to represent the height of the breathing-zone. In addition, perfect reflection at the ground is incorporated. Also, in the expression for C_G, reflection at the base of an inversion layer is also assumed. The inversion base height is modeled to occur at $H^* = 750$ m for moderately unstable (stability class B) and neutral stability (class D) atmosphere, and 100 m for moderately stable (class E) atmosphere. The Gaussian model represented in Eqn 2.1 produces outdoor concentrations that exhibit a near square-wave profile close to the source (Figure 2.1). The concentrations are gradually transformed into a bell-shaped profile as the plume advects downwind. To model the effects of perfect reflection from the ground and the elevated inversion base, several image sources might be needed. However, it is found sufficient in this analysis to model just one set of image sources by including $i = -1$, 0, and 1 in Eqn 2.1. This is because in acute toxic releases of reasonable scale, adverse health effects are

predicted to occur in the vicinity of the release source. Relative to the height of the inversion layer used in the different stability classes, the estimated vertical dispersion of the plume remains narrow in the areas that are most affected by the toxic plume. Small changes in the outdoor concentrations, as captured by the multiple image sources, in areas that are further downwind of the release site therefore do not affect the overall SIP effectiveness predicted in the community.

The predicted outdoor concentrations are input into a well-mixed-box model to predict indoor concentrations, where the contaminant is assumed to be conserved indoors.

$$\frac{dC_{in}(t)}{dt} = \frac{Q}{V}\left(C_{out}(t) - C_{in}(t)\right)$$

Eqn 2.2

For small time steps, the time-dependent outdoor concentration $C_{out}(t)$ in Eqn 2.2 can be assumed to vary linearly during a time step from an initial concentration $C_{out}(t_o)$ (g/m^3) at a time rate of change of C'_{out} [g/(m^3·s)]:

$$C_{out}(t) = C_{out}(t_o) + C'_{out} \times (t - t_o)$$

Eqn 2.3

At an air-exchange rate of Q/V (h^{-1}) with the outdoors, the time-dependent indoor concentration is therefore:

$$\frac{dC_{in}(t)}{dt} = \frac{Q}{V}\left[\left(C_{out}(t_o) + C'_{out} \times (t - t_o)\right) - C_{in}(t)\right]$$

$$C_{in}(t) = \left(C_{out}(t_o) - C'_{out}\frac{V}{Q}\right) + \left[C_{in}(t_o) - \left(C_{out}(t_o) - C'_{out}\frac{V}{Q}\right)\right] \times \exp\left[-\frac{Q}{V} \times (t - t_o)\right] + C'_{out} \times (t - t_o)$$

Eqn 2.4

For all simulations, the outdoor and indoor concentrations were evaluated at one-minute intervals. Phenomena such as decay in ambient air, sorption on indoor surfaces (Karlsson, 1994), and filtration by building envelopes (Liu and Nazaroff, 2001) were not considered in this analysis, although they are recognized to be important under some circumstances and will be considered in the chapters to follow.

2.2.2 Health Effects

The time-integrated exposure, E [(mg/m^3)·h], is considered to be a good indicator of health risk for chronic low-level exposure to many toxic air contaminants.

$$\mathrm{E}(t) = \int_0^t C(t')\,dt'$$

Eqn 2.5

E(t) represents the time-integrated inhalation exposure for the period 0 to t, and $C(t')$ is the time-dependent concentration in the breathing zone of the person exposed. For acute effects owing to short-term exposures, ten Berge et al. (1986) analyzed data from inhalation toxicity studies for many chemicals and concluded that E is not always a good indicator for predicting mortality. Instead, evidence for some chemicals suggests that exposure to extremely high concentrations for a short duration can be much more dangerous than exposure to lower concentrations for a proportionally longer period. The rationale is that at low concentration the human body may be able to counteract adverse effects, but these defense mechanisms can be overwhelmed at higher concentrations. Instead of exposure, a metric known as the toxic load (TL) is used to estimate the adverse health consequences owing to acute exposures:

$$\mathrm{TL}(t) = \int_0^t \left[C(t')\right]^m dt'$$

Eqn 2.6

where *m* is an empirical parameter that varies among pollutants. Many of the toxic gases analyzed by ten Berge et al. (1986) have *m* between 1 and 3.

For the simulations considered here, the reported time-dependent toxic load as defined in Eqn 2.6 is computed at each grid point for both indoor and outdoor concentrations. The impact of the release to the exposed community is evaluated as the number of grid cells in which the toxic load exceeds certain limits at each time step. The limits reflect the toxicity of the chemical and are referred to as toxic load limits (TLL). The US National Research Council has used the toxic load model to derive acute exposure guideline levels (AEGLs) for many industrial toxic chemicals and warfare agents (NRC, 2003). AEGLs are designed to assess the consequences of emergency exposures ranging in duration from 10 min to 8 h. An AEGL represents a threshold below which specified adverse health effects are unlikely to occur in the general public. For example, the AEGL for chlorine with respect to life threatening conditions is 58 mg/m^3 (20 ppm) for 1-h exposure based on animal studies. From animal studies, the toxic load exponent for chlorine is estimated to be *m* = 2. Thus, the estimated toxic load limit for life threatening exposure to chlorine is:

$$\mathrm{TLL} = \mathrm{C}^2 \times \mathrm{T} = \left(58\left[\frac{\mathrm{mg}}{\mathrm{m}^3}\right]\right)^2 \times 1[\mathrm{h}] = 3300\left[\left(\frac{\mathrm{mg}}{\mathrm{m}^3}\right)^2 \mathrm{h}\right]$$

Eqn 2.7

Consequently, one would conclude that the exposure to chlorine is potentially life-threatening if the toxic load, computed according to Eqn 2.6, exceeds this TLL.

2.2.3 Measures of Shelter-in-Place Effectiveness

In past research, some have advocated measuring a building's SIP efficacy by the "dose reduction factor (DRF)" (Kocher, 1980; Engelmann, 1992; Yuan, 2000). DRF is defined as the ratio of indoor to outdoor time-integrated concentration. Unfortunately, for assessing *efficacy*, this definition is counterintuitive. A DRF that approaches 1 means that the building is *ineffective* in protecting its occupants, whereas a DRF approaching 0 means that the building is very effective in reducing exposure. Other researchers have preferred the use of the "protection factor (PF)" (Blewett et al., 1996; Jetter and Whitfield, 2005), which is the reciprocal of DRF. PF varies from a nominal minimum of one (no improvement from SIP) to high values for highly efficacious protection, with no upper limit.

Two alternative metrics for quantifying SIP effectiveness are used in this analysis. One is similar to the concept of PF, but instead of comparing the difference in exposure, Eqn 2.6 is used to include the potentially nonlinear dose-response effect. The toxic load reduction factor, TLRF, compares the total toxic load of the community if everyone were exposed to outdoor concentrations ($TL_{outdoor}$), versus the case if everyone took shelter indoors (TL_{indoor}).

$$TLRF = 1 - \frac{TL_{indoors}}{TL_{outdoors}}$$

Eqn 2.8

TLRF is scaled to vary from zero[1] (ineffective SIP) to one (perfect protection). At the individual building level, the TLRF only depends on the air-exchange rate and on the time-dependent outdoor concentration profile. If both of these factors are the same across the community, then all buildings will have the same TLRF. In practice, buildings have different air-exchange rates and would be exposed to different time profiles of outdoor concentration owing to deterministic and stochastic mechanisms of advection and dispersion. Consequently, a distribution of TLRF can occur in the community building stock. In the simple analysis presented in this chapter, however, since all buildings are assumed to have the same air-exchange rate, the difference in TLRF among buildings is quite small. The reported TLRF at the community level is therefore very similar in value to the TLRF found in a given building. This will be illustrated by an example in the discussion to follow.

TLRF is a simple measure of SIP effectiveness because it is insensitive to many aspects of the release scenario. However, a certain reduction in toxic load in a community does not imply the same level of reduction in adverse health effects, which is the primary goal of SIP. To measure SIP effectiveness in terms of the associated reduction in adverse health effects, the casualty reduction factor (CRF) is defined as follows:

[1] TLRF can become negative if the indoor-outdoor air-exchange rate is non-steady. This issue will be considered in the chapters to follow.

$$CRF = 1 - \frac{\text{Population}\,(TL_{indoors} > TLL)}{\text{Population}\,(TL_{outdoors} > TLL)}$$

Eqn 2.9

In computing the CRF, one compares the population for which the toxic load exceeds the TLL if exposed at the indoor concentration as compared to that if exposed at the outdoor concentration. This comparison indicates the fraction of the population that would avoid potential adverse health effects because of SIP. In the present analysis, land area is used as a proxy for population. This is the same as assuming that population density in the vicinity of the release is uniform. In future chapters, spatially varying population density will be considered.

At the community scale, the CRF represents the fractional reduction in the population whose toxic load exceeds the toxic load limit owing to the protectiveness of SIP. At a building, CRF = 1 if the reduction in toxic load owing to SIP is sufficient for all occupants in the building to avoid the adverse health effects. If the reduction in toxic load is insufficient and all occupants in the building would still accumulate toxic load that exceeds the limit, then CRF = 0. In contrast to the TLRF, the community-scale CRF depends on the severity of the release. In the event of a release that is just large enough to generate potential adverse health effects for an unsheltered population, CRF can be quite high because the reduction in toxic load owing to the protective effect of sheltering may be sufficient for most occupants to avoid adverse health consequences. Conversely, if the release is very large such that the toxic load limit is exceeded outdoors by a large factor, then CRF will tend to be lower because few buildings can ensure a safe indoor toxic load. In minor releases, CRF can be undefined because the denominator in Eqn 2.9

is zero. This can occur when no one in the community is expected to exceed the TLL even if all were exposed to the outdoor concentrations for the entire release event. All the scenarios modeled in this work are expected to generate potential adverse health effects in an unsheltered population, thus the effectiveness of SIP can be meaningfully measured in terms of CRF.

2.3 Model Parameter Selection

Table 2.1 lists the various parameter values modeled for evaluating TLRF and CRF. The goal of this analysis is to explore the dependence of SIP effectiveness on these potentially important factors. Parameter values were selected to vary within realistic ranges.

The severity of damage from an acute release depends on the nature of the chemical, especially its toxicity, and on the amount released. Intuitively, the more toxic the chemical, the less exposure is needed to generate the same severity of health effect relative to a chemical that is less toxic. One interpretation of toxicity of a chemical is therefore the quantity needed to cause certain level of potential health effects in a given exposure time. Three limits of exposure are modeled: 0.1, 1, and 10 mg/m^3 at the duration of 1 h. For $m = 1$, the corresponding toxic load limits are 0.1, 1, and 10 $mg/m^3 \cdot h$. However, there is no fundamental relationship that can relate such exposure limits to the toxic load limits at higher toxic load exponents. Based on the above definition of toxicity, it is possible to determine empirically what must the toxic load limits be at the different m in order for the same amount of chemical being released to cause an equivalent extent of

adverse health effects under the same conditions. To keep the input model parameters explicit, however, the toxic load limits at higher toxic load exponents are simply modeled as $(0.1)^m$, $(1)^m$, and $(10)^m$ $(mg/m^3)^m \cdot h$ respectively. In other words, the selected TLL for $m = 2$ are 10^{-2}, 1, and 10^2 $(mg/m^3)^2 \cdot h$; and for $m = 3$ are 10^{-3}, 1, and 10^3 $(mg/m^3)^3 \cdot h$. With one exception[2], all chemicals reviewed by NRC when finalizing the AEGLs have toxic load exponents between 1 and 3. Many of the toxic industrial chemicals have toxicity measured in terms of exposure on the order of 0.1–10 $(mg/m^3) \cdot h$. For example, severe health effects might occur if a population were exposed for 1 h to methyl isocyanate at 0.16 mg/m^3, chlorine at 5.8 mg/m^3, or hydrogen sulfide at 38 mg/m^3.

The release duration and amount considered are selected to represent a range of events that are potentially serious or severe. Releases of 0.1 and 10 tonnes over durations of 0.1, 0.5, and 5 h are modeled. Past major accidental chemical releases have occurred at scales even greater than those modeled here. For example, the 1984 accident in Bhopal, India, involved the release of 30 tonnes of methyl isocyanate (NRC, 2003). A 1996 train derailment near Alberton (MT), USA, led to the release of 59 tonnes of Cl_2 and 64 tonnes of potassium hydroxide (UNEP, 2005).

The dispersion of the toxic plume was modeled under 3 stability classes, ranging from moderately unstable (class B) to moderately stable (class E). A stable atmosphere, typical of nighttime, clear-sky, relatively calm conditions suppresses dispersion. Atmospheric mixing height tends to be at its lowest under stable conditions, thus

[2] The one chemical that does not follow this pattern is hydrogen sulfide (H_2S), for which the interim AEGLs imply a toxic load exponent of 4.4.

increasing the downwind exposure impact of a toxic release. On the other hand, the heating of the ground during a sunny day promotes vertical mixing, increasing the mixing height and the rate of vertical dispersion. In between these two cases, a neutral stability class D is also modeled to represent overcast conditions where the atmosphere is adiabatic. For each of the stability class, a different set of correlations (see Table 2.2) is used to estimate the dispersion coefficients σ_x, σ_y, and σ_z needed by Eqn 2.1.

A few modeling concerns required that the results from the worst-case scenario (10 tonnes release at toxicity of 0.1 mg/m^3·h) and the least-severe scenario (0.1 tonnes release at toxicity of 10 mg/m^3·h) be removed from the analysis. There are several reasons for discarding these simulations. First, the dispersion coefficients are developed for a finite distance only. Outdoor concentration predictions based on the Gaussian plume model are unreliable at distance less than 0.1 km or far greater than 10 km from the source. Second, the model equations assume that the meteorological conditions are constant with time. This assumption may not hold for times much longer than a few hours. At a wind speed of 3 m/s, the plume cannot travel far beyond a distance of 50 km within this time frame. Finally, the health assessment assumed that the exposed population density is spatially uniform. According to the US Office of Management and Budget, large US cities typically cover land area on the order of a few thousand square miles. This corresponds to a distance on the order of 50 to 100 km from one end of the city to the other[3]. After excluding the scenarios unsuitable for the simple modeling approach used here, the predicted adverse health effects outdoors extend over distances that range from 0.4 to 40

[3] Similar estimates of the extent of urban land areas are also obtained by Marshall et al. (2005) by using 2002 Highway Statistics from the US Department of Transportation.

km from the release location in the remaining scenarios. The majority of these scenarios caused adverse health effects up to a distance of a few kilometers outdoors.

The leakiness of residential structures influences the effectiveness of SIP. Analysis of a US air leakage database (see Chapter 3) indicates order of magnitude variability in the air tightness among single-family detached houses. Most houses are estimated to have an air-exchange rate between 0.2 and 2 h^{-1} under typical operating conditions. With windows and doors shut, and heating/cooling fans turned off, air-exchange rates are expected to be at the lower end of this range during SIP. On the other hand, high wind speeds and large indoor-outdoor temperature differences can increase air-exchange rates to higher levels. In this study, a community of buildings each having the same air-exchange rate that varied between 0.1 and 5 h^{-1} (see Table 2.1) is modeled.

SIP is an emergency response strategy that should be appropriately terminated after the release event. The decision of when to terminate SIP needs to balance the risk of being exposed to lingering toxics that have not yet dispersed from outdoor air versus the risk of prolonging exposure to residual contamination indoors. This decision also needs to take into account the variability and spatial distribution in a community of houses. However, as will be illustrated in the following discussion and subsequent chapters, termination time only significantly influences SIP effectiveness under certain conditions. In this analysis, the earliest that SIP can be safely terminated is set at the time when additional casualties outdoors are no longer expected. The effects of delaying SIP termination by 0.5, 1, and 3 h beyond this specific point in time are investigated.

2.4 Results and Discussion

2.4.1 Illustrative Example

For a release whose duration is short relative to the time constant associated with residential air-exchange, the peak indoor concentration is only a fraction of the peak outdoor concentration (Figure 2.1). After the plume has passed, the indoor concentration declines as controlled by the air-exchange rate. Using these outdoor and indoor concentration predictions, the outdoor and indoor toxic loads are computed at each grid cell. Figure 2.2 shows the predicted toxic loads at a downwind location for a specific release. When $m = 1$, there is ultimately no benefit of persistent sheltering in place with respect to a conserved pollutant. The reduced peak concentration indoors is compensated by much longer exposure to residual indoor contamination after the plume has passed, such that the ultimate time-integrated exposure (Figure 2.2, upper left frame) is the same indoors or outdoors. When $m = 2$ or 3, however, the predicted indoor toxic load is significantly lower than the outdoor levels at all air-exchange rates modeled.

Assuming that the entire population maintains SIP from the onset of the event ($t = 0$) until the end of the simulation, Figure 2.3 shows the resulting toxic-load reduction factor (TLRF) and the casualty reduction factor (CRF) for the exposed community in that same release. Initially, the CRF is close to 1 (indicating a high degree of SIP effectiveness) because concentrations indoors increase much more slowly than they do outdoors. Early in the event, the number of people in a sheltered population that exceeds the TLL is much smaller than it would be if the population did not take shelter. As the release progresses

and the contaminant continues to infiltrate indoors, the CRF decreases because more people are exposed to levels high enough to potentially cause adverse health effects, even among those who shelter in place. For the case $m = 1$, the CRF decreases markedly as time increases. This is a consequence of the persistent accumulation of an indoor dose in the event that SIP is not terminated quickly after the plume has passed. However, when $m = 2$ or 3, most of the potential health effects for a sheltered population occur as a consequence of peak exposures early in the event. In such cases, the casualty reduction factor remains at least moderately high, even if SIP is not promptly terminated.

The dashed lines in Figure 2.3 show the TLRF for the exposed population. Since the outdoor concentration predicted by the Gaussian model as a function of time resembles a square wave[4] in the most heavily exposed area, the TLRF in Figure 2.3 is well predicted by Eqn 2.10, which describes the TLRF for a building having an fixed exchange rate Q/V (h^{-1}) under a constant outdoor concentration C_o for T_r (h) duration:

$$\text{TLRF*}(t) = \begin{cases} \dfrac{\int_0^t \left[C_o \left(1 - e^{-Q/V \cdot t} \right) \right]^m dt}{Q/V \cdot t} & \text{for } t \le T_r \\ \dfrac{\int_0^{T_r} \left[C_o \left(1 - e^{-Q/V \cdot t} \right) \right]^m dt + \int_{T_r}^{t} \left[C_o \left(1 - e^{-Q/V \cdot T_r} \right) \cdot e^{-Q/V \cdot t} \right]^m dt}{Q/V \cdot T_r} & \text{for } t > T_r \end{cases}$$

Eqn 2.10

In the case of $m = 1$, the estimated TLRF is very close to the estimated CRF. However, there are significant differences between CRF and TLRF at higher values of the toxic

[4] Outdoor concentration sustains at a constant level for a duration of time, and declines quickly to zero after the plume has passed. See Figure 2.1.

load exponent. Even though SIP can reduce the ultimate toxic load for the exposed population by 89% (m = 2) and 98% (m = 3) for the 0.5-h release, some of these dosage reductions do not reduce the number of people with toxic load that exceeds the limits. Instead, for the particular parameters simulated in this case, SIP is expected to reduce potential casualties by 68% (m = 2), or 76% (m = 3). The difference is attributable to the fact that some population is exposed to such high outdoor concentration that even with significant reduction in toxic load by SIP, adverse health effects cannot be avoided. Consequently, SIP effectiveness as measured by CRF is lower than the TLRF.

The values of CRF and TLRF predicted here are specific to the release scenario modeled. Changing some of the model parameters might shift the curves presented in Figure 2.3. The discussion to follow will provide a broader look at the different parameters that can affect SIP effectiveness, both in terms of CRF and TLRF.

2.4.2 The Effect of Toxic Load Exponent

Both TLRF and CRF are strongly influenced by the toxic load exponent of the chemical. For a nonreactive contaminant, when the toxic load exponent equals one, the health effects for a population exposed indoors eventually reaches the same value as that for a population exposed outdoors, regardless of the outdoor concentration time profile. On the other hand, removal mechanisms such as filtration and sorption to indoor surfaces are likely to reduce the time-integrated concentration indoors with respect to the outdoors.

The equality of indoor and outdoor integrated exposures for nonreactive contaminants is true only if the building air-exchange rate remains constant. If the air-exchange rate is lower while the plume is passing and higher afterwards, then the time-integrated exposure is lower for SIP than if outdoors. This condition can be beneficially exploited by effective termination of SIP after the event. Conversely, if the air-exchange rate is higher for some reason during plume passage than afterwards, the overall exposure can be higher indoors than the outdoors. Residential air-exchange rates can be influenced by meteorology (higher values occurring with larger temperature differences and higher wind speeds) and by the tightness of the building envelope. Opening doors and windows, and operating exhaust fans or the forced-air heating or cooling system can also significantly increase residential air-exchange rates (Wallace et al., 2002; Johnson et al., 2004).

When the toxic load exponent exceeds 1, there can be significant benefit of staying indoors in case of an outdoor release owing to the reduction in peak exposure concentrations. Unlike the case for $m = 1$, this benefit does not continue to diminish with time once the peak concentrations have passed. Furthermore, the exponent m amplifies the significance of the difference between peak outdoor and peak indoor concentrations. As a result, SIP is relatively more effective in protecting the exposed population for $m = 2$, and for $m = 3$, than for $m = 1$. The difference in CRF when the toxic load exponent changes from 1 to 2 is much larger than when the toxic load exponent changes from 2 to 3. This diminishing effect on the CRF is expected as the toxic load exponent continues to increase.

In further analyses presented in this chapter, instead of evaluating TLRF and CRF as functions of time as the release progresses, they are evaluated at specific times. For $m \geq 2$, both TLRF and CRF cease to decrease within a few hours after the release has stopped. But for $m = 1$, both TLRF and CRF always approach zero as time increases, given the analysis approach and assumptions (constant air-exchange rate, nonreactive chemical) used in this analysis. In other words, SIP effectiveness depends more strongly on the termination time when $m = 1$ than when $m = 2$ or 3. Figures 2.4 and 2.5 show the dependence of SIP effectiveness on air-exchange rate, release duration, release amount, chemical toxicity, and stability class, for the cases of $m = 2$ and 3 respectively. The TLRF and CRF are evaluated sufficiently long after the release has stopped such that their values no longer change with time.

2.4.3 The Effect of System Time Scales

The release duration and the reciprocal of the building air-exchange rate are the time scales that determine SIP effectiveness. The higher the air-exchange rate, the faster the toxic materials will penetrate indoors, and the higher the ratio of peak indoor to outdoor concentrations. In terms of time-averaged indoor exposures, the higher rate of accumulation of toxic materials is ultimately balanced by the higher rate of removal of the toxic materials after the outdoor plume has passed. But in terms of toxic load, the adverse health effects caused by high indoor concentrations during the accumulation period dominate when $m > 1$. As a result, SIP effectiveness decreases with increasing air-exchange rates for many contaminants. The duration of a release dictates the length of

time during which indoor concentration rises. The longer this accumulation period, the closer the peak indoor concentrations will match those in outdoor air. Thus SIP effectiveness decreases with increasing duration of release.

When the outdoor concentration is constant for a period T_r, and the air-exchange rate Q/V is also constant, the ratio of the indoor to outdoor toxic load is governed by a dimensionless parameter equal to their product:

$$\xi = Q/V\ (\mathrm{h}^{-1}) \times T_r\ (\mathrm{h})$$

Eqn 2.11

This dependence can be easily demonstrated by evaluating the integral of TLRF* in Eqn 2.10 for the case when $T >> T_r$. As shown in Figures 2.4 and 2.5, the predicted toxic load reduction factor (TLRF) is also well characterized in terms of ξ, regardless of other factors. However, this simple scaling does not generally apply to the casualty reduction factor (CRF), which is also influenced by release scale relative to the toxicity. In extreme catastrophes, e.g. a large release of highly toxic materials under a stable atmospheric condition, SIP may not protect against adverse health consequences even in cases where the release duration is short. Furthermore, air-exchange rate and release duration can no longer compensate for one another as in a case when the release is less severe. Instead, air-exchange rates become exceedingly important to ensure SIP effectiveness in large-scale releases.

In the US, residential air leakage varies by approximately a factor of 10 from the leakiest 5% of the houses to the tightest 5% (see Chapter 3). This variation translates into substantial variability in the SIP effectiveness among residences in a community. Taking

steps to reduce air leakage in the building stock can therefore significantly improve SIP effectiveness.

2.4.4 The Effect of Release Scale

Severity of the release is largely dictated by the ratio between the amount of toxic material released and the toxicity of the material. As expected, the predictions show that the extent of adverse health effects caused by a release is determined by the ratio between the amount released and the toxicity (TLL), given that other parameters are unchanged. This result is a consequence of the linearity of the Gaussian plume model (Eqn 2.1) relating concentrations to the amount released. For example, SIP effectiveness caused by the release of 0.1 tonnes of a chemical with a TLL of 0.1^2 $(mg/m^3)^2 \cdot h$ is the same as that caused by the release of 10 tonnes with a TLL of 10^2 $(mg/m^3)^2 \cdot h$ (compare rows 2 and 3 in Figure 2.4).

Stability class also affects the severity of the release, as it determines the rate at which the plume disperses. The damage caused under stable atmospheric conditions can be much higher than if under unstable conditions, which promote more rapid dispersion. The sensitivity of CRF with respect to release amount to toxicity ratio is maximized under stable conditions and particularly for leaky buildings and short release durations (Figures 2.4 and 2.5). On the other hand, TLRF is largely unaffected by release scale or stability class. This means that while SIP effectiveness on a community level is affected by these two factors, SIP effectiveness on an individual building level is not. Nonetheless, the

dependence of CRF on both the scale of the release and the stability class is limited unless the release scale is extremely large or small. This is indicated in Figure 2.6 where the predicted CRF and TLRF are plotted as function of the release amount for a selected set of release conditions. Between the scales of 10 kg to 10 tonnes being released over the same duration (0.5 h), the predicted CRF remains essentially unchanged. The adverse health effects predicted in these simulations are evaluated at a fixed toxic load limit that is roughly comparable to the level of chlorine exposure that causes severe health effects. For a release of a chemical with a different toxicity and under a different stability class, the range over which CRF remains insensitive to the release amount would vary.

To summarize for a given toxic load exponent, SIP effectiveness measured by TLRF is only substantially affected by the release duration T_r and air-exchange rate Q/V of a building. The smaller the product is of these two parameters (ξ), the higher the TLRF. However, the severity of the release can also affect CRF, such as when the scale of the release is very large, or when the release occurs under stable atmospheric conditions. The larger the release extent or the more stable the atmosphere is, the less effective is SIP. But for most other conditions, the dependence of SIP effectiveness on release scale is weak, relative to other factors that affect time scales of the event, namely the release duration and air-exchange rates of buildings. The toxic load exponent affects both TLRF and CRF in a similar manner. The analysis so far has only considered cases where the dose-response curve is nonlinear with $m > 1$. In the next section, release of chemicals with a linear dose-response relationship ($m = 1$) is examined, in which SIP effectiveness is much more sensitive to termination time.

2.4.5 Terminating Shelter-in-Place

After the outdoor plume has dispersed, people should exit or deliberately ventilate their shelters to minimize exposure to indoor residual contamination. Theoretically, the optimal time to terminate SIP is when the indoor concentration reliably exceeds the outdoor concentration. However, this optimal time will vary among buildings in an exposed community. For example, once SIP is initiated, buildings that are located closer to the release source should terminate SIP sooner than those further downwind because the outdoor plume will leave the nearby area at an earlier time. Furthermore, owing to the stochastic nature of plume transport and dispersion not captured by the Gaussian model, the precise optimal time is practically unpredictable. Model predictions of indoor and outdoor concentrations possess significant uncertainties, and the risk of terminating SIP too early might be much worse than the penalty of terminating SIP too late. For example, exposure to a puff of concentrated toxic materials that lingers outdoors because of complex topography (e.g., in an urban street canyon) could cause more harm than some increased duration of exposure to the lower contaminant concentrations indoors. The optimal time to terminate SIP should be based on minimizing adverse health risks to the exposed population, taking into account uncertainty, rather than minimizing exposure. Further practical considerations, such as the time it takes to inform the exposed population and for them to take action, will also affect practical strategies for SIP termination.

In this exploratory analysis, the optimal SIP termination time is defined as when additional potential adverse health effects are no longer predicted for outdoor exposure.

This is a simple and reasonable basis for assessing the importance of termination delay on SIP effectiveness. Table 2.3 shows the time when SIP termination should occur after the release has stopped, according to above termination condition. In this treatment, optimal SIP termination time depends on how long the plume takes to disperse and be diluted to concentrations that will no longer cause adverse health effects outdoors. The smaller the release, or the more unstable the atmosphere, the sooner SIP should be terminated. On the other hand, larger releases under stable atmospheric conditions can cause more extensive damage as the contamination is advected downwind. Therefore SIP would need to be maintained for a longer duration in such cases. Among the scenarios modeled, the length of time adverse health effects continue to occur after the release has stopped varies from a few minutes to many hours. These time estimates also depend slightly on the release duration, as indicated by the range of values presented in Table 2.3.

By definition, outdoor exposure no longer causes additional adverse health effects when SIP is terminated at or after the times listed in Table 2.3. It is also assumed that when the community terminates SIP, no additional adverse health effects are expected owing to exposure indoors. It would be possible to achieve this result if residents were to step outside from their shelters, or if they could quickly ventilate their shelters to remove the residual contaminants that linger indoors. In reality, both of these actions might take some time to accomplish. Some community members might also refuse to follow the termination advice, or might not be aware of the advice. Consequently, the assumption that there is no additional adverse health effects both outdoors and indoors the moment SIP termination is invoked might be somewhat unrealistic. To address these concerns

would require an understanding of human reaction and response time in emergencies, an issue that lies beyond the scope of this chapter.

The CRF is recalculated at the instant SIP is terminated according to the times listed in Table 2.3. The denominator in Eqn 2.9 remains unchanged regardless of the termination time, as the final estimates of the populated being exposed to levels exceeding the TLL has already been reached by the time SIP is terminated. Only the numerator in Eqn 2.9 is affected by the SIP termination time. The highest CRF values are achieved when SIP is promptly terminated according to the times listed in Table 2.3. As SIP termination is delayed, the indoor exposure of the community would continue to accumulate from breathing the residual chemicals left indoors, thus the CRF would decrease. Figure 2.7 shows the sensitivity of CRF to this time delay for a subset of the scenarios modeled.

The significance of punctual SIP termination for preserving SIP effectiveness can be interpreted by how rapidly the CRF decreases with increasing termination delay. Punctual SIP termination is much more important for $m = 1$ than for $m = 2$, across all modeled scenarios. As shown in Figure 2.3, most of the adverse health effects are realized soon after the release onset when the toxic load exponent is $m = 2$ or 3. Consequently, there is very little loss in SIP effectiveness (< 20% in terms of CRF) by staying indoors for longer than needed. However, when $m = 1$, SIP can rapidly lose its effectiveness if termination does not occur within a few hours after the release has ended.

Figure 2.7 shows that the importance of punctual SIP termination varies with the building air-exchange rate and the release duration for the case of $m = 1$. Buildings with lower air-exchange rates are most effective in restricting infiltration of toxic materials. For relatively airtight buildings, SIP effectiveness decreases more gradually than in buildings with higher air-exchange rates. Conversely, SIP effectiveness among buildings with high air-exchange rates decreases rapidly with termination delay. However, because buildings with high air-exchange rates are relatively ineffective shelters anyway, this decrease in effectiveness does not appear to be as important as for buildings with moderate air-exchange rates, such as in the range of 0.5 to 1 h^{-1}. Incidentally, this range includes the air-exchange rates most typically found in residences in the US, which means that SIP termination time is potentially an important issue for nonreactive toxic materials that have a toxic load exponent close to 1. The dependence of SIP effectiveness on termination time is especially important when the release duration is on the order of an hour or less. As release duration lengthens, termination time becomes less significant because by the time the outdoor concentrations decline, indoor concentrations have already risen to values close to outdoor levels even among buildings with moderate air-exchange rates.

Figure 2.8 shows the SIP effectiveness for the case of $m = 1$ under the various release scenarios. The CRFs are evaluated at 0.5, 1, and 3 h from the time when additional health effects are no longer expected outdoors (see Table 2.3). The sensitivity of SIP effectiveness to termination time can be interpreted as the vertical distance between the CRFs evaluated at the different termination time. The further apart these three points are

in a given release scenario, the more important it is for the community to quickly terminate SIP when it is safe to do so. For relatively short releases (duration lasting 0.5 h and less), a 3-h delay in SIP termination time can cause a reduction by 2× to 3× in CRF for buildings with air-exchange rates typical of residential buildings in the US. The reduction in CRF by delaying termination from 0.5 h to 1 h is roughly the same as from 1 h to 3 h, meaning that the incremental importance of SIP termination slowly diminishes with time. This sharp initial decrease in SIP effectiveness shortly after it is safe to exit from the shelters will pose a challenge in taking full advantage of the benefit of punctual termination in practice.

Cross comparison of CRF resulting from simulations that used different toxic load exponents shows that even with punctual termination, SIP effectiveness when $m = 1$ is lower than in the case when $m = 2$ or 3. The differences are greatest for leaky buildings and for short release durations. Unlike the cases when $m = 2$ or 3, a reduction in peak indoor concentrations no longer translates into substantial protection when $m = 1$. In addition, exposure to the residual indoor contaminants after the plume has passed greatly lowers SIP effectiveness. Consequently, achieving low air-exchange rates in buildings becomes even more important in ensuring SIP effectiveness when $m = 1$. This explains why short release duration no longer compensates for the loss in effectiveness from high air-exchange rates, as in the cases when $m = 2$ or 3.

2.5 Conclusions

Two community-scale metrics for assessing SIP effectiveness are proposed to quantify the dependence of SIP effectiveness on release quantity, duration, meteorology, toxicity, and leakage properties of the shelters. Using well-established models and reasonable parameters, results show that changes in the release amount, meteorology, or toxicity can affect SIP effectiveness. The product of release duration and air-exchange rate also affects SIP effectiveness substantially. The toxic load exponent, a parameter that characterizes the exposure-response relationship, determines the significance of termination time for determining SIP effectiveness. Only for cases in which the dose-response relationship is nearly linear ($m \sim 1$) is prompt termination critical. Otherwise (i.e., when $m = 2$ or 3), the strategy can be simplified to take shelter until the outdoor level is undoubtedly safe enough to exit.

When a release occurs, few of the parameters considered in this analysis are subject to control. An exception is the air-exchange rates of buildings, which can be minimized by closing doors and windows, and by shutting off heating/cooling and exhaust fans. There can be considerable variability and uncertainty among the influencing parameters. The analyses presented here provide insight into the relative importance among these parameters on SIP effectiveness. The results support a view that variability in air-exchange rates among buildings should be carefully considered when evaluating SIP protectiveness for a release condition. Other parameters not modeled, such as pollutant dynamics in outdoor air (e.g. photochemical reactions) and indoor air (e.g. sorption on indoor surfaces), can also affect SIP effectiveness, including optimal SIP termination

time. Since the former affects the scale of the release, and the latter affects the time scale of SIP, the latter is expected to be more important in affecting SIP effectiveness. Delay in SIP initiation can also affect the results presented here. SIP effectiveness can be diminished dramatically if toxic chemicals have already entered a building before it is closed. Further analyses are warranted to consider the importance of these factors affecting the overall SIP effectiveness in a community.

2.6 References

Blewett, W.K., Reeves, D.W., Arac, V.J., Fatkin, D.P., Cannon, B.D., 1996. Expedient sheltering in place: an evaluation for the chemical stockpile emergency preparedness program. Chemical Research, Development & Engineering Center, ERDEC-TR-336, Aberdeen Proving Ground, MD.

Engelmann, R.J., 1992. Sheltering effectiveness against plutonium provided by buildings. Atmospheric Environment 26A, 2037–2044.

Irwin, J.S. A theoretical variation of the wind profile power-law exponent as a function of surface roughness and stability. Atmospheric Environment 13, 191–194.

Jetter, J., Whitfield, C., 2005. Effectiveness of expedient sheltering in place in a residence. Journal of Hazardous Materials A119, 31–40.

Johnson, T., Myers, J., Kelly, T., Wisbith, A., Ollison, W., 2004. A pilot study using scripted ventilation conditions to identify key factors affecting indoor pollutant concentration and air exchange rate in a residence. Journal of Exposure Analysis and Environmental Epidemiology 14, 1-22.

Karlsson, E., 1994. Indoor deposition reducing the effect of toxic gas clouds in ordinary buildings. Journal of Hazardous Materials 38, 313–327.

Kocher, D.C., 1980. Effects of indoor residence on radiation doses from routine releases of radionuclides to the atmosphere. Nuclear Technology 48, 171–179.

Liu, D.L., Nazaroff, W.W., 2001. Modeling pollutant penetration across building envelopes. Atmospheric Environment 35, 4451–4462.

Marshall, J.D., Teoh, S.K., Nazaroff, W.W., 2005. Intake fraction of nonreactive vehicle emissions in US urban areas. Atmospheric Environment 39, 1363–1371.

NRC, 2003. Acute Exposure Guideline Levels for Selected Airborne Chemicals: Volume 3. Subcommitte on Acute Exposure Guideline Levels, Committee on Toxicology, National Research Council, The National Academies Press, Washington DC.

Overcamp, T.J., 1990. Diffusion models for transient releases. Journal of Applied Meteorology 29, 1307–1312.

Palazzi, E., De Faveri, M., Fumarola, G., Ferraiolo, G., 1982. Diffusion from a steady source of short duration. Atmospheric Environment 16, 2785–2790.

Seinfeld, J.H., Pandis, S.N., 1998. Atmospheric Chemistry and Physics: From Air Pollution to Climate Change. Wiley-Interscience Publication, New York, NY, 926–931.

ten Berge, W.F., Zwart, A., Appleman, L.M., 1986. Concentration-time mortality response relationship of irritant and systemically acting vapours and gases. Journal of Hazardous Materials 13, 301–309.

UNEP, 2005. United Nations Environment Programme (UNEP), Awareness and Preparedness for Emergencies at a Local Level, Transport Disasters. http://www.uneptie.org/pc/apell/disasters/lists/cstransport.html

Wallace L., Emmerich S., and Howard-Reed C., 2002. Continuous measurements of air exchange rates in an occupied house for 1 year: the effect of temperature, wind, fans, and windows. Journal of Exposure Analysis and Environmental Epidemiology 12, 296–306.

Wilson, D.J., 1981. Along-wind diffusion of source transients. Atmospheric Environment 15, 489–495.

Yuan, L.L., 2000. Sheltering effects of buildings from biological weapons. Science & Global Security 8, 329–355.

2.7 Tables

Table 2.1 List of model parameters.

	Model Parameter	Model Values
Release Characteristics	Release Duration (h)	0.1 0.5 5
	Release Amount (kg)	10^2 10^4
Chemical Toxicity	Toxic Load Limit [(mg/m^3)·h]	0.1 1 10
	Toxic Load Exponent (-)	1 2 3
Meteorology	Stability Class (-)	B (unstable, 3 m/s wind) D (neutral, 6 m/s wind) E (stable, 3 m/s wind)
SIP Strategy	Air-Exchange Rate (h^{-1})	0.1 0.2 0.5 1 5
	Termination Time (h)	0.5 1 3 Inf.

Table 2.2 Correlations for σ_x, σ_y, and σ_z based on Pasquill-Gifford stability class used in Gaussian plume dispersion modeling (Seinfeld and Pandis, 1998).

	Stability Class		
	Unstable (Class B)	Neutral (Class D)	Stable (Class E)
Cross-wind dispersion: $\sigma_x(x) = \exp[I_y + J_y (\ln x) + K_y (\ln x)^2]$			
I_y	-1.634	-2.555	-2.754
J_y	1.0350	1.0423	1.0106
K_y	-0.0096	-0.0087	-0.0064
Vertical dispersion: $\sigma_z(x) = \exp[I_z + J_z (\ln x) + K_z (\ln x)^2]$			
I_z	-1.999	-3.186	-3.783
J_z	0.8752	1.1737	1.3010
K_z	0.0136	-0.0316	-0.0450
Along-wind dispersion*: $\sigma_x(x) = \left(\sigma_y^2 + 0.09\left(\frac{h+0.50\sigma_z}{h+0.17\sigma_z}\right)^{2p}\left(\frac{p\,x}{h+0.5\sigma_z}\right)^2\sigma_z^2\right)^{0.5}$ where h (m) is the release height			
p	0.28	0.37	0.47

* Formula for the along-wind dispersion coefficient approximation is obtained from the analysis by Wilson (1981). The wind profile power-law exponent p listed above refers to the case when the roughness height is 1 m (Irwin, 1979).

Table 2.3 Time when SIP should be terminated[#] after the end of the release.

			SIP Termination Time after Release has Stopped (h)		
Release Amount	Toxicity	Toxic Load Exponent	Unstable (Class B)	Neutral (Class D)	Stable (Class E)
10^2 (kg)	1 $(mg/m^3)\cdot h$	$m = 1$	0.07	0.07	0.3 – 0.4
		$m = 2$	0.03 – 0.1	0.03 – 0.1	0.1 – 0.5
		$m = 3$	0.03 – 0.1	0.03 – 0.1	0.1 – 0.4
	0.1 $(mg/m^3)\cdot h$	$m = 1$	0.2	0.2	1.5 – 1.8
		$m = 2$	0.1 – 0.3	0.1 – 0.4	0.7 – 1.6
		$m = 3$	0.1 – 0.3	0.1 – 0.4	0.5 – 1.5
10^4 (kg)	1 $(mg/m^3)\cdot h$	$m = 1$	0.6	1.0 – 1.1	14 – 15
		$m = 2$	0.4 – 0.8	0.5 – 1.3	4.8 – 6.8
		$m = 3$	0.3 – 0.8	1.4 – 1.3	3.2 – 5.5

[#] The condition for termination is when adverse health effects are no longer predicted for outdoor exposure. The range of values included results from 3 release durations: 0.1, 0.5, and 5.0 h.

2.8 Figures

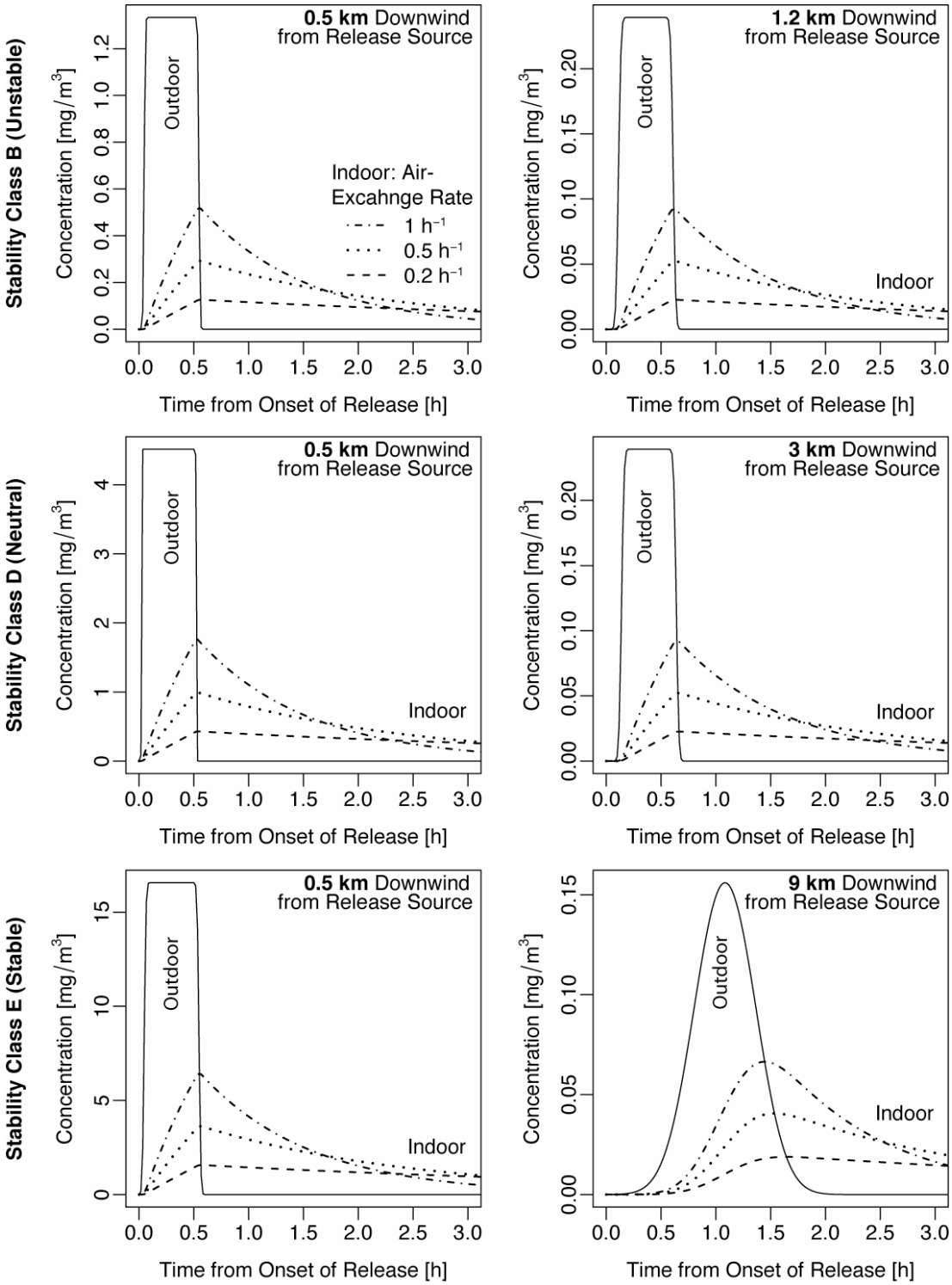

Figure 2.1 Predicted outdoor and indoor concentrations at different downwind locations from the release source. Three simulations are modeled under different stability classes, but the release duration (0.5-h) and amount (0.1 tonnes) are the same.

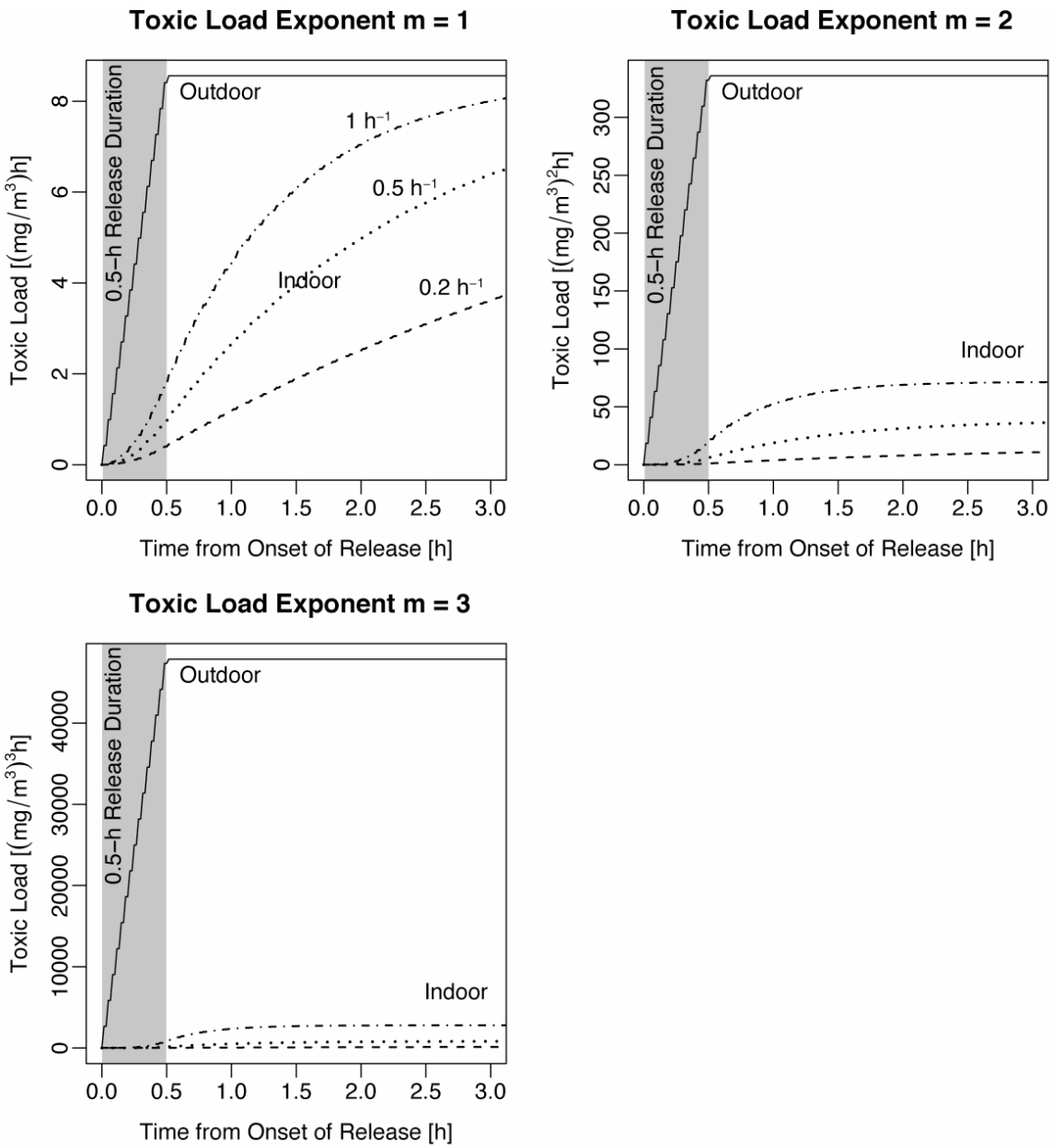

Figure 2.2 Predicted toxic loads at 0.5 km downwind from the release source if one were exposed to the outdoor and indoor contaminant levels. Toxic loads are evaluated at three toxic load exponents m = 1, 2, and 3 (Eqn 2.6). The results shown here are for the same 0.1 tonnes release over a duration of 0.5-h modeled under neutral atmospheric stability (class D) as shown in Figure 2.1 (middle left plot). The indoor toxic loads are evaluated using indoor concentrations predicted at three air-exchange rates: 0.2, 0.5, and 1 h^{-1}.

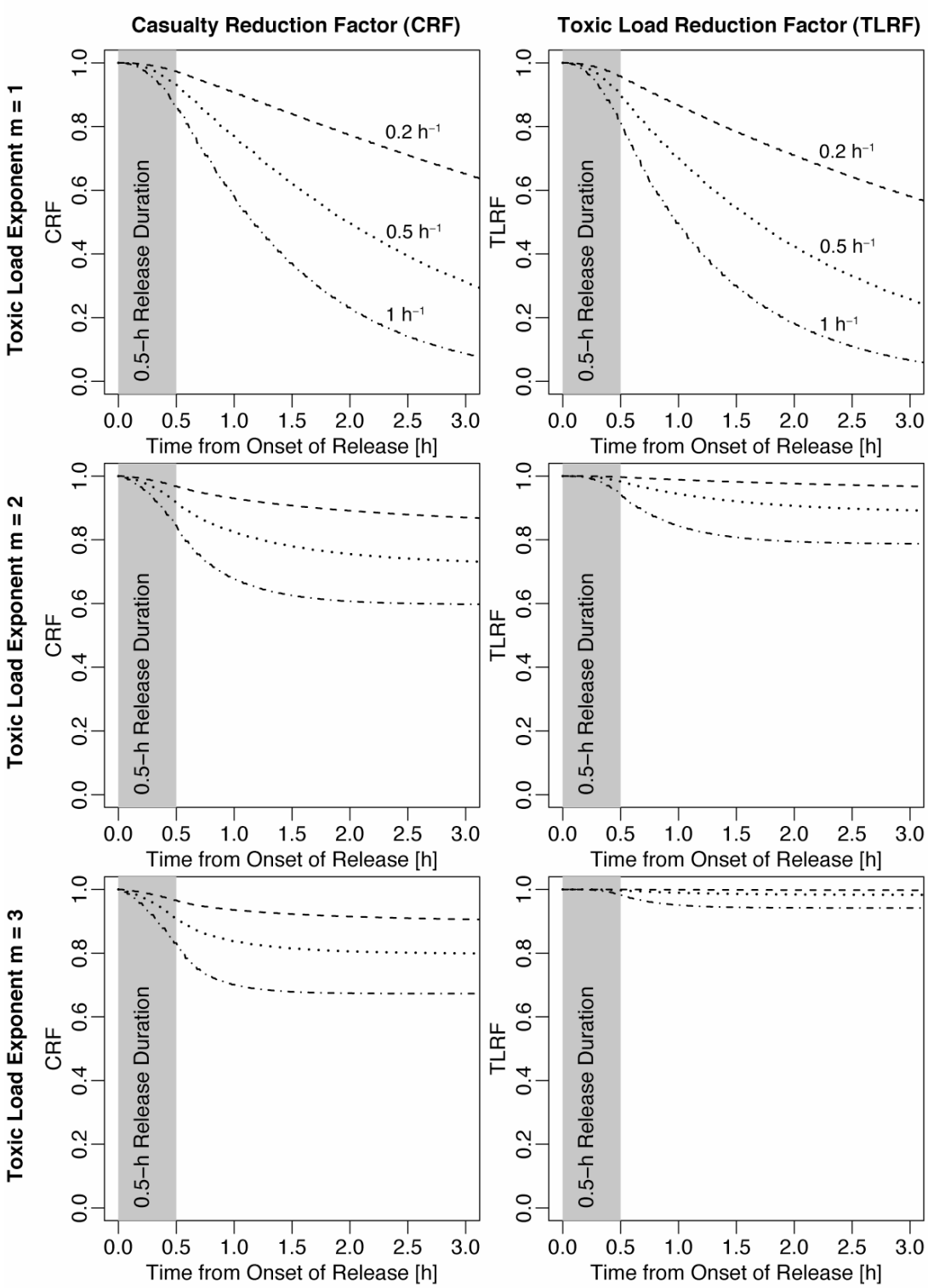

Figure 2.3 Community-based SIP effectiveness measured in terms of casualty reduction factor (CRF, left column) and toxic load reduction factor (TLRF, right column) as the 0.5-h release progresses in time. The 0.1 tonnes release is modeled under stability class D (same conditions as in Figure 2.2). The toxic load limits used to evaluate the CRF are 0.1 $(mg/m^3)\cdot h$, 0.1^2 $(mg/m^3)^2\cdot h$, and 0.1^3 $(mg/m^3)^3\cdot h$ for m = 1, 2, and 3 respectively.

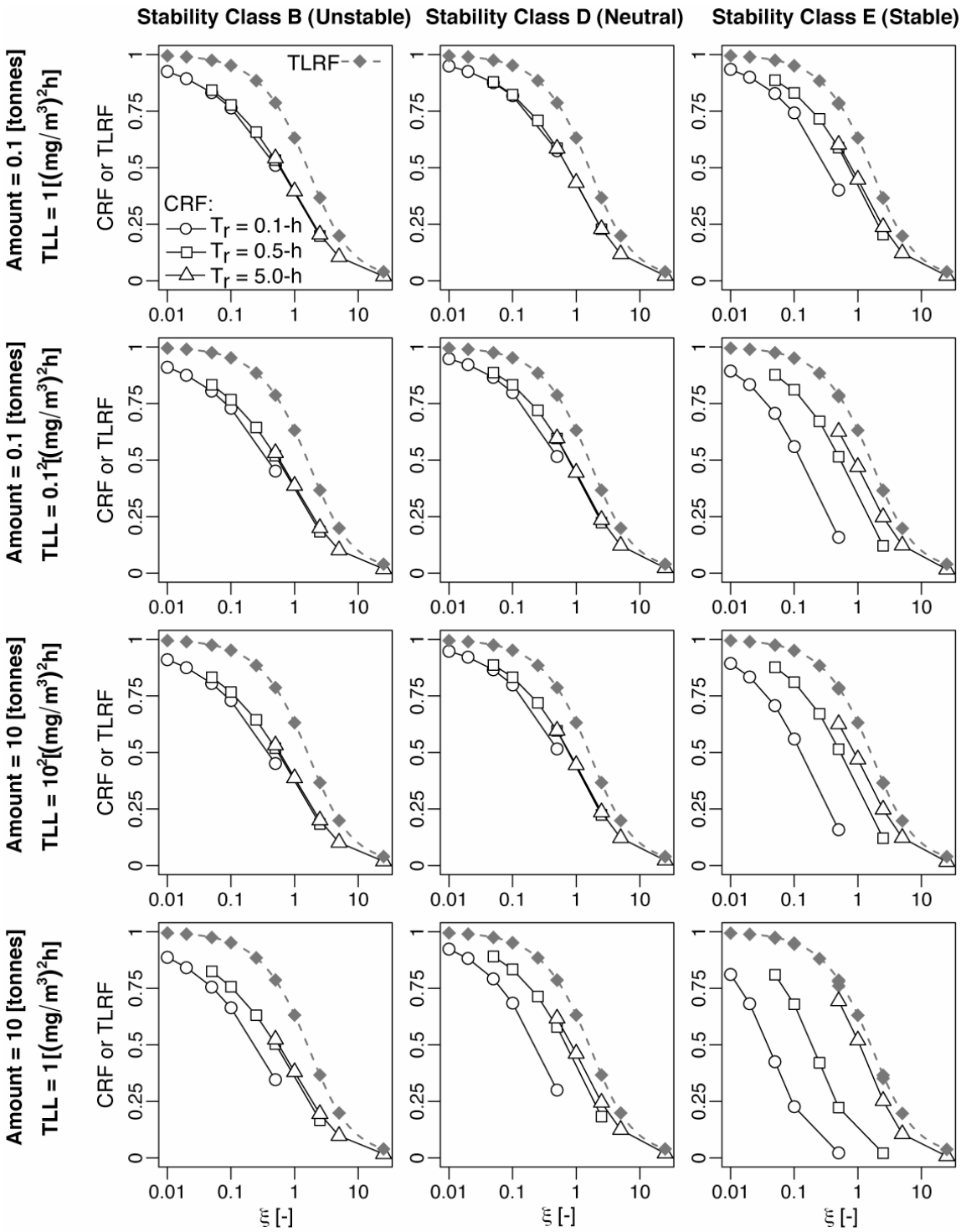

Figure 2.4 SIP effectiveness measured in terms of casualty reduction factor (CRF, open symbols and solid lines) and toxic load reduction factor (TLRF, solid diamond symbol and dashed line) as a function of ξ, which is a dimensionless number defined by the product of air-exchange rate Q/V (h^{-1}) and release duration T_r (h). Results from 15 runs (3 release durations with indoor concentrations evaluated at 5 air-exchange rates) are presented for simulations at 3 stability classes (columns) and 4 sets of release amount and toxicity (rows). All simulations are evaluated at toxic load exponent $m = 2$.

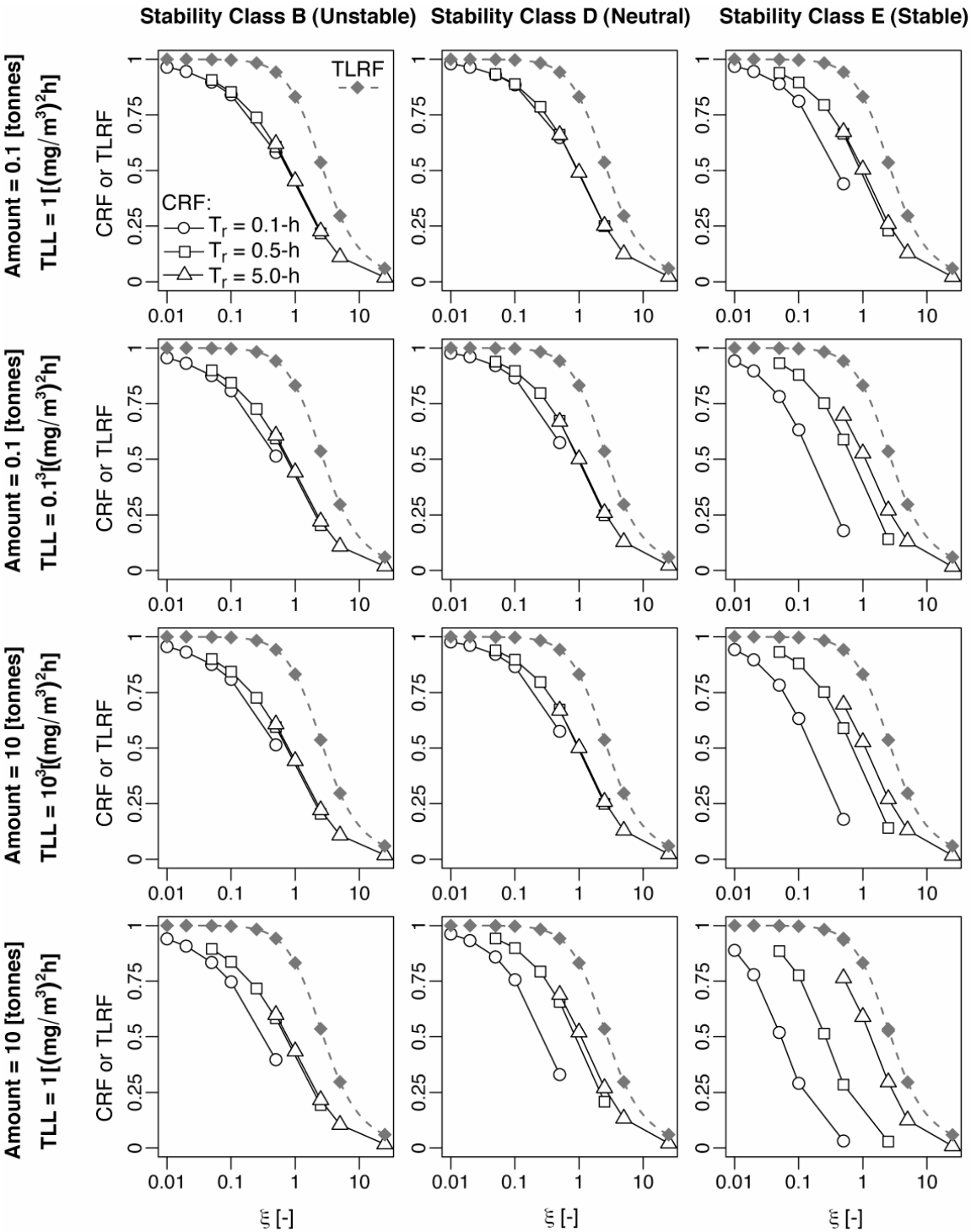

Figure 2.5 SIP effectiveness measured in terms of casualty reduction factor (CRF, open symbols and solid lines) and toxic load reduction factor (TLRF, solid diamond symbol and dashed line) as function of ξ, which is a dimensionless number defined by the product of air-exchange rate Q/V (h^{-1}) and release duration T_r (h). Results from 15 runs (3 release durations with indoor concentrations evaluated at 5 air-exchange rates) are presented for simulations at 3 stability classes (columns) and 4 sets of release amount and toxicity (rows). All simulations are evaluated at toxic load exponent $m = 3$.

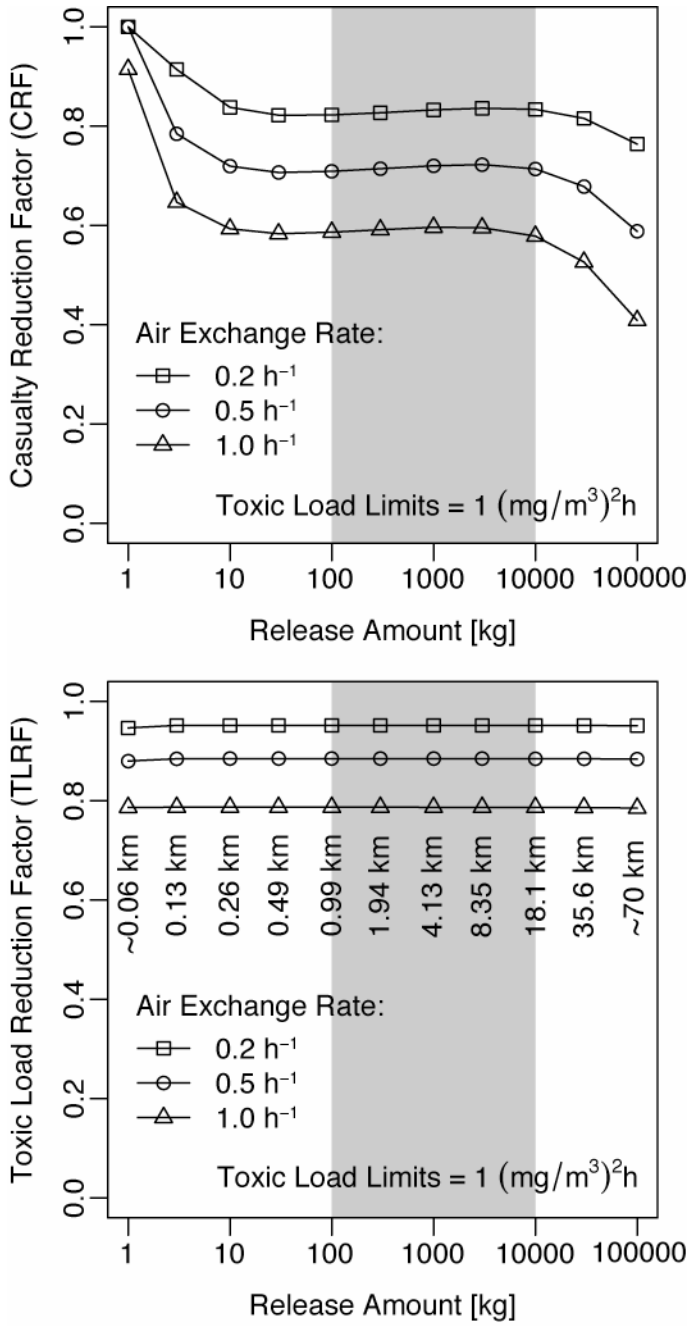

Figure 2.6 Predicted SIP effectiveness measured in terms of casualty reduction factor (top) and toxic load reduction factor (bottom) versus release amount over a duration of 0.5-h. Adverse health effects are evaluated at the toxic load limit as indicated in the plots with toxic load exponent $m = 2$. The distances labeled in the bottom plot are the furthest distance downwind from the release site where adverse health effects are predicted if people were exposed outdoors. When the release scale is very small (1 kg release) or very large (100 tonnes), the Gaussian plume model might not give reliable predictions. Model results from these simulations should therefore be interpreted as rough estimates only. The gray area highlights the order of release scales considered in this chapter.

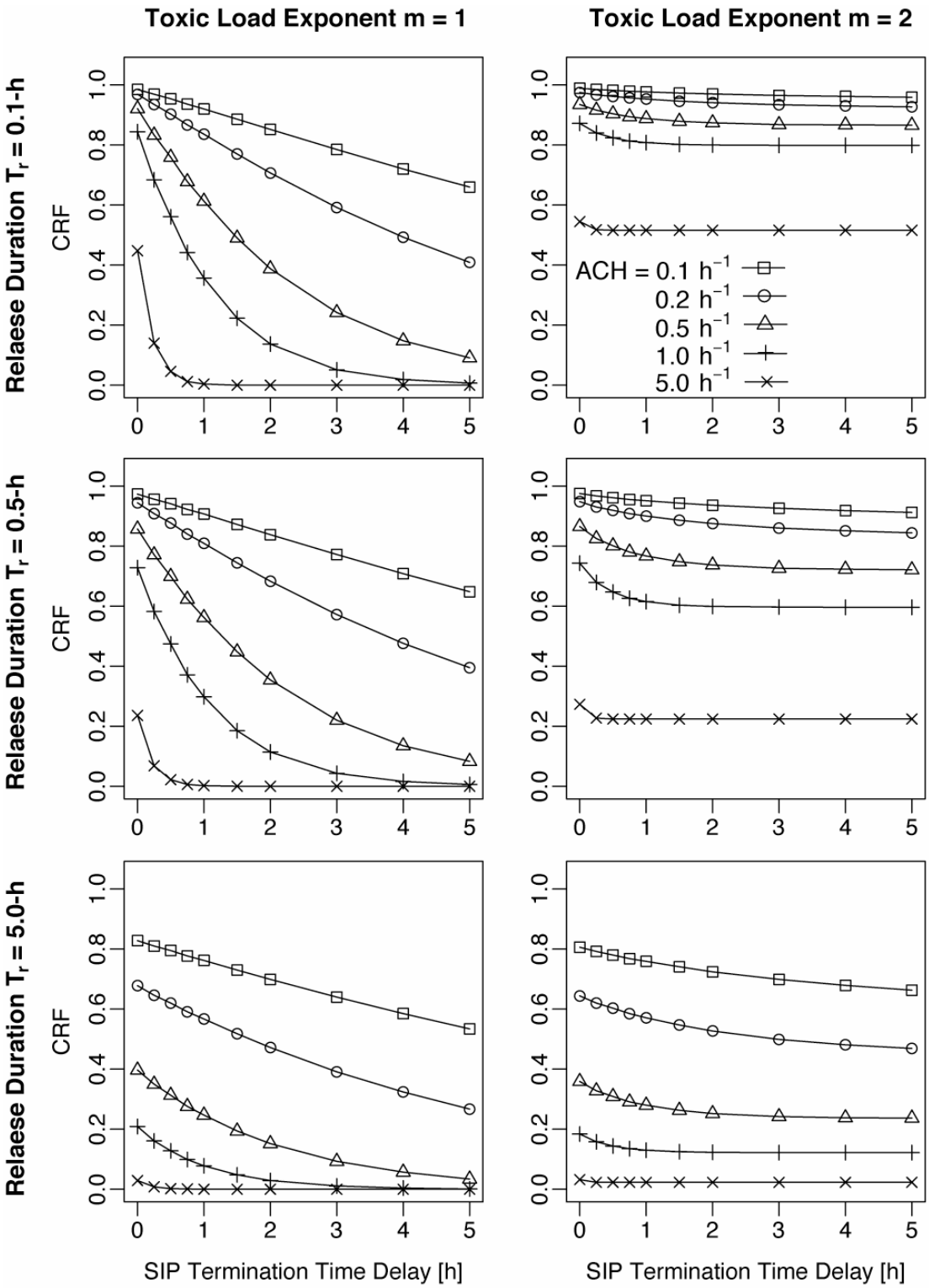

Figure 2.7 Dependence of CRF on delay in SIP termination. Time = 0 refers to the case where SIP is terminated at optimal times as indicated in Table 2.3. Presented are the model results for 0.1 tonnes released under neutral atmospheric stability. Adverse health effects are evaluated at TLL = 0.1 [(mg/m^3)·h] for m = 1, and TLL = 0.01 [(mg/m^3)^2 ·h] for m = 2.

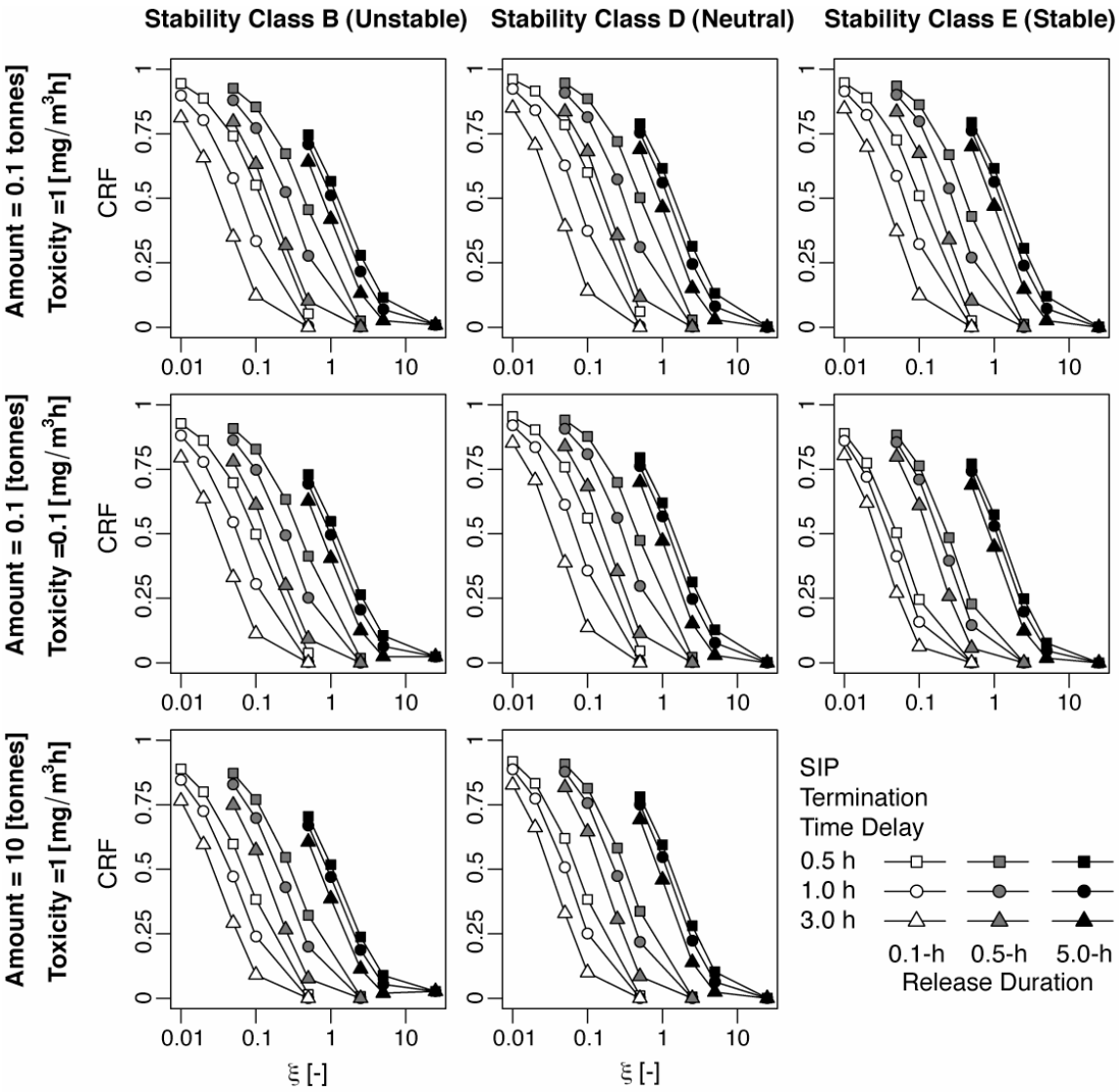

Figure 2.8 SIP effectiveness under linear dose-response (i.e. $m = 1$) as a function of ξ, which is the dimensionless number defined by the product of air-exchange rate Q/V (h^{-1}) and release duration T_r (h). Results from 15 runs (3 release durations with indoor concentrations evaluated at 5 air-exchange rates) are presented for simulations at 3 stability classes (columns) and 3 sets of release amount and toxicity (rows). Unlike in Figures 2.4 and 2.5 where SIP effectiveness is plotted without consideration of termination time, the SIP effectiveness plotted here assumes SIP is terminated at 0.5, 1, and 3-h after the time when additional adverse health effect is no longer expected outdoors (see Table 2.3).

3 Air Infiltration Rates of Residential Buildings

3.1 Introduction

This chapter presents a method to estimate the air infiltration rate distribution of houses in a community under shelter-in-place (SIP) scenarios. Most single-family dwellings in the United States are not equipped with mechanical ventilation systems. During shelter-in-place, assuming that doors and windows are kept closed, air exchange occurs mainly by uncontrolled air leakage across the building envelope, a phenomenon known as air infiltration. In this chapter, analysis of existing air leakage measurements of houses in the US[5] is detailed. Earlier versions of the same air leakage database have previously been analyzed by Sherman and Dickerhoff (1998), and Sherman and Matson (1997) for assessing residential energy use. Here, the database is re-analyzed with the addition of new data, and a change of focus to quantify the variability of air leakage among houses in the US. Readily available housing characteristics such as building size, year built, geographic region, and various construction characteristics are examined to determine the degree to which they can explain some of the variability observed in the air leakage data.

Following the analysis of air leakage data, a simple air infiltration model, known as the LBL Infiltration Model (Sherman, 1980), is described. The amount of air infiltration

[5] This part of the material has been published in Chan, W.R., Nazaroff, W.W., Price, P.N., Sohn, M.D., Gadgil, A.J., 2005. Analyzing a database of residential air leakage in the United States. Atmospheric Environment 39, 3445–3455.

through leaks, cracks, and other unintentional openings that together make up the leakage area of the house depends on the pressure difference across the building envelope. Wind and outdoor-indoor temperature difference are the two main driving forces of air infiltration. Formulation of the LBL Infiltration Model on these driving forces is described briefly. The purpose of the discussion is to point out the strengths and limitations of the model, as well as to summarize key findings of validation experiments (Sherman and Grimsrud, 1980; Modera et al., 1982, 1983; Sherman and Modera, 1986). This discussion provides the basis for assessing the reliability of the model predictions of air infiltration rates, which in turn affect the indoor concentrations in houses exposed to an outdoor release for SIP conditions.

Finally, a method is developed that utilizes the results from the air leakage analysis and the LBL Infiltration Model to predict air infiltration rates of houses during SIP. The city of Albuquerque, NM, is used as a test case to illustrate the variability in air infiltration rates predicted among houses. The distribution obtained will be used in Chapter 4 to assess the SIP effectiveness from some hypothetical releases in Albuquerque. Housing data from the US Census Survey and American Housing Survey are the key inputs needed to predict the air infiltration rates. Even though the focus here is on SIP, the air infiltration rates obtained can also be used to address residential energy use and indoor air quality concerns.

This chapter closes with a brief assessment of the air-exchange rates in houses induced by natural and mechanical ventilation. These estimates are needed to assess the indoor

concentrations in houses before SIP is implemented. As will be discussed in the following chapter, the time delay for people to respond to the emergency and carry out appropriate protective action can be significant. This can potentially lead to substantial loss in SIP effectiveness, which is a serious concern especially if the community is ill prepared for the emergency.

3.2 Analysis of US Residential Air Leakage Database

Most air leakage measurements in the US have been carried out in association with weatherization and energy efficiency programs, which aim to improve the air tightness of buildings, and therefore better control air infiltration. Air infiltration plays an important role in energy consumption. High infiltration rates can cause excessive energy demand because of the need to condition the infiltrating air. Air infiltration also affects indoor air quality because it causes the transport of outdoor pollutants to indoors, which can be an important exposure pathway for pollutants of outdoor origin. Conversely, insufficient air exchange with the outdoors can lead to high exposure to pollutants of indoor origin, such as environmental tobacco smoke, and emissions from building materials, cooking or cleaning activities.

Air leakage datasets often only include measurements from certain types of houses located in certain areas (e.g., Grot and Clark, 1979; Matson et al., 1994, Sherman and Matson, 2001). Such measurements do not capture the air leakage distribution of the whole US housing stock. The goal of this analysis is to characterize the leakage area

distribution of the US housing stock. The housing characteristics that are most predictive of the leakage area are identified using multivariate regression. Sherman and Matson (2001) analyzed a subset of the air leakage data for newly constructed houses and found that new houses are significantly tighter than is believed to be typical for the general US housing stock. Similar correlations between air leakage and other housing characteristics will be analyzed.

3.2.1 Measurements of Air Leakage

Blower door tests are commonly used to measure the air leakage of buildings. The test measures the amounts of airflow needed to pressurize a building to various indoor-outdoor pressure differences. Leakier buildings will require higher airflow rates to pressurize the building to a certain level, whereas tighter buildings will require lower flow rates. The general test method described in ASTM Standard E779 (ASTM, 1999) is appropriate for determining the air leakage of single-family dwellings that can be treated as single-zoned. There are other standards that specify test protocols for various applications in greater detail. Only the basics of using blower door measurements to determine leakage area of a residential building are summarized here; see Sherman (1995) for a thorough review and history.

In the case that air leakage is limited by the flow resistances at the entrance and the exit of cracks (i.e. the flow resistance by viscous drag is negligible), the Bernoulli equation from basic fluid mechanics reduces to the orifice equation:

$$Q_f = \text{ELA}\sqrt{\frac{2 \cdot P_f}{\rho}}$$

Eqn 3.1

where Q_f is the airflow rate, P_f is the pressure difference, ρ is the air density at standard temperature and pressure, and ELA is the effective leakage area of the building. For dwellings, viscous interactions also contribute to airflow resistance, so that Eqn 3.1 does not hold over a large range of pressure differences. However, it has proven useful to define the effective leakage area of a building as that value of ELA which provides the observed (or inferred) flowrate, Q_f, when the pressure difference takes on a reference value (i.e., when $P_f = P_r$). In the US, the reference pressure commonly used is 4 Pa. Single-family dwellings in the US typically have ELA at 4 Pa in the range of 0.04 m^2 (tight) to 0.3 m^2 (leaky).

In practice, blower door tests are often carried out at higher indoor-outdoor pressure differences to minimize measurement error. ELA depends on the indoor-outdoor pressure difference, so it is necessary to extrapolate experimental results to determine the ELA at the reference pressure. An empirical power-law relationship is widely used for this purpose:

$$Q_f = \kappa \cdot P_f^n$$

Eqn 3.2

where κ and n are the leakage coefficient and power law flow exponent respectively. Multipoint measurements of Q_f and P_f from blower door experiments permit κ and n to be determined. In general, n is observed to vary between 0.6 and 0.7 in houses (Orme et al., 1994).

Eqn 3.1 and Eqn 3.2 can be combined and rearranged to permit evaluation of the ELA at the reference pressure difference P_r, based on blower-door test measurements of κ and n:

$$\mathrm{ELA} = \sqrt{\frac{\rho}{2}} \cdot \kappa \cdot P_r^{(n-0.5)}$$

Eqn 3.3

Effective leakage area is used in infiltration models to predict the air-exchange rate as a function of wind speed and indoor-outdoor temperature difference. The LBL Infiltration Model (Sherman and Grimsrud, 1980) describes airflow as follows:

$$Q_f = \mathrm{ELA} \cdot s$$
$$s = \sqrt{f_s^2 \cdot \Delta T + f_w^2 \cdot v^2}$$

Eqn 3.4

where s is known as the specific infiltration rate, which is a function of indoor-outdoor temperature difference, ΔT, and wind speed, v. The parameters f_s and f_w are the stack-effect factor and the wind-effect factor, respectively, and their values depend on the geometry and air leakage distribution of the building. More details on the LBL Infiltration Model will be presented in the subsequent sections of this chapter.

In the discussion to follow, the effective leakage area ELA (m^2) is normalized with the building floor area A_f (m^2) and a correction factor for the building height H (m).

$$\mathrm{NL} = 1000 \frac{\mathrm{ELA}}{A_f} \left(\frac{H}{2.5} \right)^{0.3}$$

Eqn 3.5

Normalized leakage (NL) helps to describe the relative leakage for a wide range of building sizes. Other airtightness parameters commonly used in the literature include airflow rate normalized by building volume or envelope surface area. NL is used in this

study so as to be consistent with earlier analyses of this air leakage database (Sherman and Dickerhoff, 1998; Sherman and Matson, 2001). Normalized leakage is also the parameter used for verification when the data were collected and compiled. Most single-family dwellings in the US have normalized leakage in the range 0.2 to 2.

3.2.2 Exploratory Analysis of Dataset

3.2.2.1 Data Collection

The goal of this analysis is to characterize the air-leakage area distribution of the US housing stock. The housing characteristics that are most predictive of the air-leakage area are identified using multivariate regression. Sherman and Matson (2001) compiled approximately 70,000 entries in the air leakage database. The database should continue to expand since data collection efforts remain active. The three largest contributors to the database are the Ohio Weatherization Program (77% or 51,300 pre-weatherization measurements); an energy-efficiency program in Alaska, AKWarm (11% or 7,200 measurements); and the Wisconsin Energy Conservation Corporation (3% or 2,200 measurements). Thirty-one other organizations contributed the remaining 5,700 measurements from 30 states.

3.2.2.2 Data Processing

Several validation and verification tests were performed on the normalized leakage data. Most measurements reported the amount of airflow needed to pressurize the house to 50 Pa (i.e., Q_{50}). Referring to Eqn 3.2 and Eqn 3.3, ELA was estimated from measured Q_f =

Q_{50} (at P_f = 50 Pa) by assigning the reference pressure, P_r = 4 Pa. Most power law flow exponents, n, in the database were not reported but assumed to be 0.65. There are about 1,300 data points with reported Q_{50} less than 100 cfm (or 170 m^3/h); all of these data are from the Ohio Weatherization Program. These data were marked as invalid and are excluded from further analysis because they correspond to unrealistically low air-exchange rates even for very small houses. This left approximately 66,500 data points for further data analysis.

Normalizing from ELA to NL requires knowledge of the floor area and the height of each house. Almost all data entries include the floor area of the house. However, building height is often not reported. Instead, it is estimated by assuming that houses with floor areas less than 1000 ft^2 (or 92 m^2) were single story, and that the rest were one and a half story. Even though two-story dwellings are more common than split-level or bi-level houses in some areas, this uncertainty does not constitute a large source of error in estimating NL, because NL only varies in proportion to $H^{0.3}$ as shown in Eqn 3.5. Further, the building height is approximated by assuming each story is 2.5 m and adding 0.5 m for roof space.

3.2.2.3 Data Summary

Most of the measurements are from houses located in Ohio, Alaska and Wisconsin (Figure 3.1). The most sampled region is the Midwest. Arizona, California, and Washington together make up the second-most-sampled region (West region). This is

followed by the South region, which consists of data from Florida, North Carolina, Arkansas, and Oklahoma. Data in the Northeast region are mostly from houses in Vermont and Rhode Island. Over 94% of the data also included zip codes and city names.

Selected characteristics of the houses in the database were analyzed to test how well they represent the overall US housing stock. The primary housing database used is from the American Housing Survey (AHS), conducted by the US Census Bureau. The 1999 national survey (US HUD, 2000) is a sample resulting from 58,400 interviews of homeowners. The raw numbers are reported as scaled estimates according to the total number of homes reported by the 1990 Census Decennial Survey for a given region.

Houses in the leakage database are generally smaller and older than those reported in the 1999 AHS (Figures 3.2 and 3.3), owing to the dominance of measurements from the Ohio Weatherization Program. This program only included residences with household incomes lower than 125% of the poverty guideline. Since floor area and house age affect the price of the property, houses occupied by low-income households tend to be smaller and older. On the other hand, there are also a disproportionate number of recently built energy-efficient homes in the air leakage database, such as those in Alaska, Vermont, Arizona and Kansas.

The presence of a duct system for thermal conditioning can be a significant determinant of air leakage, especially when the ducts traverse unconditioned spaces. Sherman and Dickerhoff (1998) report that duct systems typically account for almost 30% of the total

leakage area of the house. The air leakage database contains about 2,000 data points that record the presence or absence of duct systems. Of these 2,000 houses, 76% have a duct system. In contrast, the 1999 AHS classifies heating equipment into several types, but the two that use ducts as part of the system are warm-air furnaces and electric heat pumps. They represent 60% and 10% of the total US housing stock, respectively.

Sherman and Dickerhoff (1998) point out that the normalized leakage of houses with a slab-on-grade foundation is significantly less than for houses with a crawlspace or an unconditioned basement. The underfloor construction was recorded in fewer than 10% of the houses in the database. Among those reported, 8%, 45%, and 41% of the houses have a slab, basement, or crawlspace respectively. In comparison, the 1999 AHS recorded the presence of a slab, basement, or crawlspace to be about 29%, 43%, and 27%, respectively, among single-unit buildings in the US housing stock. The AHS did not differentiate between conditioned and unconditioned basements.

Lastly, houses that are participants of energy-efficiency programs are designed to be especially air tight to save thermal conditioning costs. Thus, these houses may have very different leakage distributions and are therefore treated as a separate group in this analysis. Thirteen percent of the database measurements are from energy-efficiency programs in 24 different states, with the majority from Alaska. The fraction of houses in an energy-efficiency program in the database is much higher in the total national housing stock, which is to be expected since blower-door measurements are often used for the energy analysis that is commonly performed on participating energy-efficiency houses.

3.2.3 Analysis and Discussion

The database does not statistically represent the characteristics of houses in the US as a whole for two main reasons: (1) data were contributed voluntarily by home weatherization contractors (and others) from around the country, and some contractors contributed much more data than others; and (2) most of the data were gathered in programs to target particular classes of homes, primarily low-income households that were tested as part of a weatherization program, and energy-efficient homes that were tested to check compliance with air-tightness targets. Adjustments for these effects are desired so that an unbiased estimate of leakage distribution can be obtained for any given geographic region. The approach taken is to determine the relationship between home characteristics and air leakage, so that one can adjust for different distributions of home types in different communities. This approach is known as "post-stratification" in statistical terminology.

Houses are divided into three broad classes: conventional, energy-efficient, and those that are occupied by low-income households. A limitation of the present data set is that all of the known low-income homes are from Ohio; data from the other states include some low-income homes, but these are not identified in the data. This issue is discussed further below.

3.2.3.1 Categorical Approach

The classification tree analysis (Breiman et al., 1984) is used to find the important building factors that are related to normalized leakage. Given a list of possible factors, the

method identifies those that can best subdivide the data such that the variance within each subgroup is minimized. The most important factors associated with normalized leakage were determined to be the year of construction, the size of the dwelling, and whether the dwelling is either energy-efficient or occupied by a low-income family.

The normalized leakage of houses can be categorized effectively according to their year built: before 1950, 1950–1980, 1980–1995, and after 1995. These four categories partitioned the data into groups of houses such that the difference in the normalized leakage of houses within each category is minimized. The exact years at which the splits occurred are somewhat affected by clustering of the house year-built in the database. Sherman and Dickerhoff (1998) observed substantially smaller leakage in homes built after 1980 than in homes built earlier. Some reasons why newer dwellings might tend to be tighter than older ones include improved materials (e.g. weatherstripped windows), better building techniques (e.g. air barriers) and lesser degrees of age-induced deterioration (e.g. settling of foundation).

Normalized leakage is also a function of floor area among houses that were built before 1995: larger homes have smaller normalized leakage. One explanation is that larger (more expensive) homes are likely to have tighter envelopes because they are better built and maintained. However, it is also possible that the dependence of normalized leakage on floor area is merely an artifact of the normalization method used in converting effective leakage area to normalized leakage (Eqn 3.5).

The geometric mean (GM) of the normalized leakage of subgroups of conventional houses varies between 0.18 and 1.1. The lower limit applies to houses that were built after 1995 and are larger than 232 m^2 in floor area, and the upper limit applies to those that were built before 1950 and are smaller than 93 m^2 in floor area. The GMs of subgroups of low-income houses are higher than those of the conventional ones, ranging from 0.28 to 1.5. The GMs of subgroups of energy-efficient houses are generally the lowest among the three house types, ranging from 0.22 to 0.85.

The geometric standard deviation (GSD) of normalized leakage quantifies the variation in leakiness among houses. When normalized leakage data are categorized by the house year built and floor area according to the classification tree method, the observed GSD in each category varies between 1.4 and 2.1, with an average of 1.7. Despite the modest variability in observed GSDs, the actual variability in GSDs is still likely to be overstated because it includes the effect of small-sample variability. House categories with large numbers of observations have measured GSDs that are close to 1.7. The magnitude of variation within a category, as measured by the GSD, does not appear to be systematically related to year built, area, geometric mean of leakage, or house type.

3.2.3.2 Multivariate Regression Approach

An alternative to the categorical approach is to use a regression method to establish a relationship between the observations and the explanatory variables. This method allows the study of multiple variables without having to divide data points into smaller sample

sizes. A quantile-quantile plot indicates that normalized leakage within each year-built and floor area subgroup is approximately lognormal. The use of a linear regression model is therefore appropriate to describe the relationship between the logarithm of normalized leakage and the explanatory variables. The first analysis incorporated the entire data set, using indicator variables I_E and I_L, where I_E takes value of 1 if the house is energy efficient and 0 otherwise, and I_L takes value of 1 if the house is occupied by low-income household and 0 otherwise. After transforming from log space, this description corresponds to the following model:

$$\mathrm{NL} = \exp\left(\beta_0 + \beta_1 \cdot \text{Year Built} + \beta_2 \cdot \text{Floor Area} + \beta_3 \cdot I_E + \beta_4 \cdot I_L + \varepsilon\right) \qquad \text{Eqn 3.6}$$

where ε is the residual term between the model prediction and observed value.

This approach yields a reasonably good model fit (R^2=0.56); regression coefficients are shown in Table 3.1. Much of the predictive value of the model is due to the substantial effects associated with energy-efficient homes, which are much tighter than conventional homes, and those associated with low-income homes, which are much leakier.

All of the known low-income homes in the data set are from the Ohio Weatherization Program. It is expected that the quantitative results for these homes should apply reasonably well to the Midwest in general, but their applicability to other parts of the country is unknown. If the lack of regional effect observed among conventional houses is also true for low-income homes, then low-income homes nationwide would tend to be leakier than conventional homes. However, the exact magnitude of this effect might vary with the region of the country.

The issue is further complicated by two facts. First, some of the conventional and energy-efficiency program houses in the database are occupied by families with low incomes. Incomplete identification of houses with families having low incomes compromises the analysis of the effect of income on the leakage statistics of all house types. Second, there are some recent efforts that are specifically designed to promote energy efficiency in houses occupied by low-income families. As a result, some low-income homes are unlikely to be any leakier than houses occupied by higher income families. Collection of additional leakage data on low-income houses from other parts of the country would be required to confirm and refine the finding that low-income houses tend to be leakier than conventional houses.

Using a single model for the entire data set assumes that floor area and year built have the same influence on all homes regardless of their house types. However, categorical analysis indicated otherwise. It is therefore appropriate to perform a separate analysis for each house type using this model:

$$\mathrm{NL} = \exp\left(\beta_0 + \beta_1 \cdot \text{Year Built} + \beta_2 \cdot \text{Floor Area} + \varepsilon\right)$$

Eqn 3.7

Table 3.2 shows the resulting coefficient estimates. The low R^2 values are due to the inherent large variability in leakage even among houses of similar characteristics, as denoted by ε. The relevance of Eqn 3.7 in explaining systematic differences in leakage among houses can be examined by comparing the central tendency of the data and the predictions. Figure 3.4 shows the expected value of the geometric mean of normalized leakage with respect to year built and floor area predicted by Eqn 3.7 when ε is set to zero. The low-income houses have greater leakage than conventional and energy-efficient

houses, regardless of year built and floor area. Their normalized leakage areas vary more substantially with floor area than with year built. The opposite is true for conventional and energy-efficiency program houses, where normalized leakage is almost independent of floor area, which is the intended effect of normalization. For energy-efficient houses, the regression is shown only from 1960 onwards because there are too few data points to provide leakage information for this class of houses built before 1960.

To demonstrate the goodness of fit of the regression models, the observed categorical geometric means (GMs) are plotted against the predicted values. The data are first categorized by their house types: low income, conventional, or energy efficient. They are then further divided into groups according to their year built and floor area. As shown in Figure 3.5, the regression models predict the GMs of normalized leakage with high fidelity (R^2 ranges from 0.86 to 0.92). This suggests that the model has adequately captured the deterministic factors that affect the normalized leakage of houses. The largest discrepancies came from groups that have relatively few observations. Except for these outliers, the rest of the residuals (ε) appear to be well behaved and follow an approximately normal distribution $N(\mu, \sigma^2)$: $N(0.00, 0.26)$ for the low-income group, $N(0.00, 0.27)$ for conventional, and $N(0.00, 0.27)$ for energy efficient. Regression analysis shows that these residual terms are not a function of year built or floor area. Based on these results, the random errors satisfy the least-squares estimation assumptions of the regression models.

Additional variables were tested to see if they should be included when trying to predict the leakage distribution of a population of houses. Four binary variables were created, each indicating whether the data point was collected from a corresponding US Census Region (Northeast, South, Midwest, and West). None of the binary variables improved the fit of the model. There is also no relationship between the nine US Census divisions where the data were obtained and the normalized leakage. Another parameter of interest is the presence of ducts, since studies have shown that they can be a major source of leaks. The binary variable (1 = ducts, 0 = no ducts) introduced to indicate the presence of ducts again did not improve the fit of the model. It is plausible that the determining factor is whether the ducts run through unconditioned spaces. However, such information is not available in the database for analysis.

The only remaining available factor that improves the fit of the model is a binary variable indicating the presence of direct leaks through a crawlspace or unconditioned basement. The revised regression model is as follows:

$$\mathrm{NL} = \exp\left(\beta_0 + \beta_1 \cdot \text{Year Built} + \beta_2 \cdot \text{Floor Area} + \beta_3 \cdot I_F + \varepsilon\right) \qquad \text{Eqn 3.8}$$

where I_F is the binary variable used to indicate the presence of floor leaks (i.e. I_F takes value of 1 if the house has direct floor leaks, and 0 otherwise). Houses with a slab or a conditioned basement are considered to have no direct floor leaks to the outside. Using only these data points, we obtained new linear regression models using Eqn 3.8. The difference in the estimated normalized leakage due to the presence of floor leaks can be calculated as follows:

$$\Delta NL = \frac{NL_{\text{With Leaks}} - NL_{\text{No Leaks}}}{NL_{\text{No Leaks}}} = \exp(\beta_3) - 1$$

Eqn 3.9

Using this approach, conventional houses with direct floor leaks are found to be 56% leakier than those without, but the difference is only 7% among energy-efficient houses. However, owing to the small number of homes known to have leaky floors, the fit of the model improves only slightly by incorporating this additional building characteristic (conventional: ΔR^2 = +0.025; energy-efficiency program: ΔR^2 = +0.005). Consequently, in the following analysis, Eqn 3.7 is used rather than Eqn 3.8.

3.2.3.3 Data Aggregation

To illustrate how to compute the distribution of normalized leakage for houses in a specific area of interest, the 1999 National AHS microdata, which contains the individual household responses to the survey questions, is used to predict such a distribution for the entire US. Figure 3.6 shows the difference in cumulative distribution of year built and floor area between low income and conventional houses for the US stock of single-family dwellings. It is evident that low-income houses tend to be older and smaller than conventional ones.

Houses are first separated into 2 groups: low income and conventional. Each group is then further divided into 42 groups: 7 year-built categories and 6 floor-area categories. The geometric mean of the normalized leakage area for each group of houses is computed using the regression model presented in Eqn 3.7. Using a constant geometric standard

deviation of 1.7 as determined from the distribution of ε, the distribution of normalized leakage for each group of houses is defined. Finally, the composite distribution is obtained as the weighted sum of the individual distributions.

The predicted leakage distributions are displayed in Figure 3.7 for conventional houses, low-income houses and the composite of the two distributions for the entire US. Most of the houses have normalized leakage areas below 1.5, with a median of about 0.5. The statistics of the distributions are summarized in Table 3.3.

In the present analysis, low-income homes are those that qualified for Ohio's weatherization program; homes were eligible if their residents earned below 125% of the poverty guideline (which varies with the number of members in the household). Based on the 1999 AHS microdata, about 13.4% of the households nationwide are considered as low income. According to the joint HUD-Census report (US HUD, 2000) detailing the results of the AHS, it is noted that the AHS historically underestimates income and overestimates poverty when compared to the Current Population Survey (US BLS, 2000). However, it is believed that the housing characteristics of low-income households remain accurate.

Weatherized homes usually have some reduction in air infiltration, but the magnitude of improvement varies greatly. In addition, the number of houses that have been weatherized in the US remains small. In 2000, the DOE's Weatherization Assistance Program estimated that only 16% of currently eligible low-income households have

received weatherization services (US EERE, 2006). This corresponds to about 5.2 million low-income households, which is 4% of the total housing units in the US. Since the number of weatherized houses is not large enough to strongly affect the overall air leakage distribution of low-income houses, no adjustment is made in the analysis to follow. Similarly, the presence of energy-efficiency program houses is also ignored because their prevalence in the current US housing stock is small. As of July 2001, there were 34,642 EPA ENERGY STAR[6] rated homes in the US, which constitute only 0.05% of the housing stock (US EPA, 2003).

In 1997, the US Environmental Protection Agency published the Exposure Factors Handbook (US EPA, 1997) to provide a summary of the available statistical data on parameters commonly used in human exposure assessments. Chapter 17, entitled "Residential Building Characteristics", includes a section on air-exchange rates and other factors that are also of interest, such as volumes and surface areas of rooms, presence of mechanical ventilation system, foundation types, filtration, inter-zonal airflows, and so on. The Handbook reports on several studies that analyze data from the perfluorocarbon tracer (PFT) technique to estimate air-exchange rates in dwellings, which includes not only air infiltration, but also natural and mechanical ventilation.

[6] ENERGY STAR labeled homes are typically at least 30% more energy-efficient than standard homes. The following technologies and building practices are used to achieve this improved performance: tight construction and ducts, improved insulation, high performance windows, and energy-efficient heating and cooling equipment.

To compare the model predictions against published values of air-exchange rates in the EPA Exposure Factors Handbook, normalized leakage is converted to air-exchange rate (ACH) as follows:

$$\mathrm{ACH} = \frac{\mathrm{ACH}_{50}}{F}$$

Eqn 3.10

where F is a factor used to relate the air-exchange rate under typical conditions with the air-exchange rate at 50 Pa. Assuming that the volume of a house V [m^3] is approximately equal to the floor area A_f [m^2] (not the footprint area) multiplied by an equivalent height H [m] (typically about 3 m), Eqn 3.10 can be rewritten as a function of normalized leakage, height H [m] and the parameter F only:

$$\begin{aligned}\mathrm{ACH} &\approx \frac{Q_{50}/V}{F} \\ &= \frac{\mathrm{NL}\dfrac{A_f}{1000}\left(\dfrac{2.5}{H}\right)^{0.3}\sqrt{\dfrac{2\cdot(4\,\mathrm{Pa})}{\rho}}\left(\dfrac{50\,\mathrm{Pa}}{4\,\mathrm{Pa}}\right)^{0.65}}{V\cdot F}[\mathrm{s}^{-1}] \\ &= 48\left(\frac{2.5\,\mathrm{m}}{H}\right)^{0.3}\frac{\mathrm{NL}}{H\cdot F}[\mathrm{h}^{-1}]\end{aligned}$$

Eqn 3.11

where NL and F are dimensionless, and H is in units of m.

The use of a scaling factor to relate NL to ACH is a simplified treatment of a complex reality, which might be inappropriate for detailed analysis of an individual house. Normalized leakage describes only the tightness of a building, whereas the air-exchange rate also includes operational contributions such as natural ventilation from opening windows, mechanical ventilation from exhaust fans, as well as the influence of weather. The scaling factor F is an attempt to connect the two concepts. This factor typically

varies from 10 to 30 in residences[7]. Best fit for the national data shown in Figure 3.8 is obtained when F = 16. The spread of the distribution predicted from the leakage database is in good agreement with those of the PFT measurements. Given the measurement uncertainties in the PFT data and the theoretical limitations of Eqn 3.10, the comparison shows that the estimates of air-exchange based on the air leakage database are reasonable with respect to other published values based on tracer-gas measurements.

3.2.4 Summary

Analyses have shown significant variation in the air leakage of houses with similar characteristics. As a result, it is important to capture this variability when carrying out community-based assessment. A key uncertainty in the regression model is that the analysis of low-income houses is based solely on data collected by the Ohio Weatherization Program. While it is reasonable to assume that low-income houses in other parts of the country have similar leakage characteristics, only additional data can substantiate this assumption. It is also important to note that the results here are empirical findings based on samples of the existing US housing stock. Application of the results is therefore intended to be restricted to single-family detached dwellings located within the US.

[7] As an example, EPA ENERGY STAR Home Sealing Specification (US EPA, 2002) defined an "LBL Factor" based on climate region, number of stories, and amount of sheltering from wind, to convert ACH_{50} to ACH. The value of the "LBL Factor" ranges between 9.8 for a 3-story building with no shielding in cold climate zone 1, to 29.4 for well-shielded, 1-story building in warm climate zone 4.

3.3 Air Infiltration Model

Air infiltration is driven by the pressure difference across the building envelope. In general, the internal airflow in a small building is relatively weak and does not affect the pressure differences generated by the wind and the buoyancy differences of the internal and external air (Feustel and Dieris, 1992). Single-zone air infiltration models make use of this simplification and consider only wind and buoyancy driven airflow into and out of the building as a whole. On the other hand, more complex multi-zone airflow models take into account internal airflow and pressures while solving for the air infiltration through the building envelope. Such models can predict airflow patterns in the different zones of a building, but they also require detailed information on the geometry and position of the openings, and the connectivity between different zones. The numerical algorithms necessary to solve these coupled mass-balance equations also become much more involved. A survey by Feustel and Dieris (1992) detailed many of the existing multi-zone models. For the purpose of predicting air infiltration rates for a community of houses, however, the use of single-zone air infiltration model is generally considered sufficient.

Four basic types of information are needed by single-zone models to predict air infiltration. The first two are the driving forces for infiltration, namely the surface pressure differences generated by wind and the surface pressure differences generated by buoyancy. The latter two are characteristics of the cracks and leaks in the building envelope, namely the geometry and the position of these openings. Much of the differences among single-zone air infiltration models emerge from whether the pressure and leakage information is required as input parameters to the model, or is incorporated

in the model as assumptions. Etheridge (1988) and Lyberg (1997) reviewed the performance of a number of model formulations and critiqued their limitations. The LBL Infiltration Model is among the simpler models that has been validated with experimental data.

3.3.1 LBL Infiltration Model

The LBL Infiltration Model (Sherman and Grimsrud, 1980) uses a power-law formulation (Eqn 3.2) to describe airflow through building envelopes. Like other infiltration models, the LBL Infiltration Model first considers the effect of wind and buoyancy separately. It then combines the two effects to give the overall air infiltration rate. Key components of the model are summarized below to explain the underlying principles on which the model is based. The purpose here is not to show the derivation of the model, as is detailed in Sherman (1980), but to state explicitly the assumptions and limitations of the model. These are important when the model is used to predict the amount of toxic materials that will infiltrate into houses in the event of a large-scale release.

An alternative approach to the power-law formulation to describe airflow is the so-called quadratic form, which describes the pressure-flow relationship by a linear sum of the inertial ($Q = \kappa \cdot \Delta P^{0.5}$) and viscous ($Q = \kappa \cdot \Delta P$) components. Walker et al. (1998) considered the validity of the two formulations by examining both the theoretical and

experimental evidence. They concluded that the power-law formulation works better in describing typical airflow rates through building envelopes.

3.3.1.1 Wind Effect

As wind flows around a building, it induces a field of positive and negative pressures across the building envelope relative to the internal pressure. The wind pressure P_w (Pa) exerted on the exterior surface of the building can be expressed as:

$$P_w = C_p \cdot \frac{1}{2} \cdot \rho_o \cdot U^2$$

Eqn 3.12

where C_p (-) is the pressure coefficient, ρ_o (kg/m^3) is the air density, and U (m/s) is the free stream wind speed. The pressures induced on the building envelope typically differ by façade, with the windward side likely pressurized, and the adjacent sides likely depressurized. For simplicity, single-zone models often compute the overall amount of wind-driven airflow into the building by adjusting the wind pressure coefficient instead of modeling each side of the building envelope separately.

Both building geometry and local shielding affect the wind flow patterns around a building. Sherman (1980) used wind tunnel data to find the generalized shielding coefficient for the case where there are no significant obstructions in the vicinity of the structure. As a building becomes more obstructed from the wind, the wind pressure on the building envelope decreases. Five shielding classes are defined for use in the LBL Infiltration Model (Table 3.4). These shielding parameters are loosely based on wind

tunnel experiments. For ease of use in practice, they are obtained by simple scaling from the no obstruction case.

The LBL Infiltration Model does not adjust for the effect of building geometry on wind pressure coefficient. However, the model does assume that the floor and ceiling are shielded from the influence of the wind. The model requires knowledge on the fraction of the total air leakage attributable to the vertical walls (1-*R*), and the fraction attributable to the floor and ceiling *R* (Eqn 3.13). The wind pressure coefficient scales with the fraction (1-*R*).

$$R = \frac{\text{Leakage Area}_{\text{Ceiling}} + \text{Leakage Area}_{\text{Floor}}}{\text{Leakage Area}_{\text{Total}}}$$

Eqn 3.13

The final adjustment in computing the pressure coefficient is the terrain effect. Again, five classes are defined for practical use in the LBL Infiltration Model (Table 3.5). This adjustment is needed to convert wind speed measured at 10 m at a distant weather station to the local wind speed at the building site. A power-law coefficient is used to adjust for the vertical profile of wind speed. Terrain effect is also needed to adjust for the intensity of wind turbulence on building walls. High turbulence implies that the wind pressure is less consistently sustained on the building walls, leading to lower air infiltration. These two terrain parameters are inversely related to each other, since the wind power-law coefficient tends to decrease with surface roughness while turbulence intensity tends to increase with surface roughness.

The LBL Infiltration Model lumps the shielding and terrain adjustment factors into a factor known as the wind-effect factor f_w (-). By assuming $n = 0.5$ (i.e. flow resistance dominated by inertia) in the power-law relationship that relates airflow rate and pressure difference (see Eqn 3.1), the LBL Infiltration Model estimates the wind induced air infiltration rate Q_w (m^3/s) as follows:

$$\begin{aligned} Q_w &= \mathrm{ELA} \cdot \sqrt{\frac{2 \cdot \Delta P_w}{\rho}} \\ &= \mathrm{ELA} \cdot f_w \cdot U \\ &= \mathrm{ELA} \cdot \left[C \cdot (1-R)^{\frac{1}{3}} \cdot \frac{A \cdot \left(\frac{H}{10\ \mathrm{m}}\right)^{B}}{A^{*} \cdot \left(\frac{H^{*}}{10\ \mathrm{m}}\right)^{B^{*}}} \right] \cdot U \end{aligned}$$

Eqn 3.14

where A and B are the terrain parameters (Table 3.5), C is the shielding parameter (Table 3.4), H (m) and H^* (m) is the height of the building and the wind speed measurement height respectively. A^* and B^* represent the terrain parameters at the weather station. The effective leakage area (ELA) of the building envelope is related to normalized leakage (NL) analyzed in Section 3.2 in manner as shown in Eqn 3.5. Assuming that half of the total leakage area is attributable to the vertical walls ($R = 0.5$), and the terrain and shielding both vary between class 3 and class 5, then the resulting f_w varies between 0.05 and 0.20, with a mean at 0.11.

3.3.1.2 Stack Effect

Stack effect is driven by the difference in vertical rate of change in pressure (dP_s/dh in Eqn 3.15) in the indoor and outdoor air. This is caused by a difference in the air density

indoors ρ_i (kg/m^3) and outdoors ρ_o (kg/m^3), which is a result of the difference in their temperature (T_i and T_o [K]). In the case that the outdoor air is cooler than the indoor air, the denser outdoor air causes the vertical rate of change in pressure to be faster than that indoors. Near the ceiling of the building, the relatively lower outdoor pressure drives air to exfiltrate from the indoors through the building envelope. Air infiltrates through the lower parts of the building to replace the exfiltrating air mass. In the case that the indoor air is cooler than the outdoor air, the airflow direction will be reversed and air will infiltrate through the building envelope near the ceiling due to the relatively lower indoor pressure there. Given that the mass of air entering the building must be equal to the mass of air leaving it, there must be a certain height, H''(m), within the building at which the pressure indoors equals the pressure outdoors. At that location, known as the neutral pressure level, $\Delta P_s(H'') = 0$. The LBL Infiltration Model uses this condition to solve for the stack effect pressure:

$$\begin{aligned}
\frac{dP_s(h)}{dh} &= -\rho \cdot g \\
\frac{dP_s(h)}{dh}\Big|_{outdoor} - \frac{dP_s(h)}{dh}\Big|_{indoor} &= -\left(\rho_o - \rho_i\right) \cdot g \\
\frac{d\left(\Delta P_s(h)\right)}{dh} &= -\rho_o \cdot g \cdot \left(1 - \frac{\rho_i}{\rho_o}\right) \\
&= -\rho_o \cdot g \cdot \left(1 - \frac{T_o}{T_i}\right) \\
\int_{\Delta P_s(H'')}^{\Delta P_s(h)} \Delta P_s(h) &= -\rho_o \cdot g \cdot \left(1 - \frac{T_o}{T_i}\right) \cdot \int_{H''}^{h} dh \\
\Delta P_s(h) &= 0 - \rho_o \cdot g \cdot \left(1 - \frac{T_o}{T_i}\right) \cdot \left(h - H''\right) \\
&= \rho_o \cdot g \cdot H \cdot \frac{\Delta T}{T_i} \cdot \left(\frac{H''}{H} - \frac{h}{H}\right)
\end{aligned}$$

Eqn 3.15

where g = 9.8 (m/s^2), and H (m) is the height of the building. The location of the neutral plane depends on the distribution of the leaks and other openings in the building envelope. To account for this, the LBL Infiltration Model defines the difference between the air leakage associated with the ceiling and the floor of the buildings as follows:

$$X = \frac{\text{Leakage Area}_{\text{Ceiling}} - \text{Leakage Area}_{\text{Floor}}}{\text{Leakage Area}_{\text{Total}}}$$

Eqn 3.16

$X = 0$ means that there is no difference between the air leakage associated with the ceiling and the floor of the building. For X to approach 1, all of the air leakage needs to be associated with the ceiling of the building, and none with either the floor or the walls of the building. This is unlikely in most residential buildings, since features like windows and doors on the vertical façades of the buildings are not airtight (Proskiw, 1995). The foundation of houses is also a known source of air leakage, especially in houses with unconditioned crawlspaces and basements (Brennan et al., 1990; Sherman and Dickerhoff, 1998). In the case that the floor of the building is much more leaky than the ceiling, the neutral pressure level will be pulled towards the floor. The extent to which this difference affects H'' depends on the fraction of air leakage that is attributable to the flooring and ceiling. The LBL Infiltration Model takes account of these dependencies by the stack-effect factor f_s [(m/s)/K$^{0.5}$]:

$$\begin{aligned} Q_s &= \text{ELA} \cdot \sqrt{\frac{2 \cdot \Delta P_s}{\rho}} \\ &= \text{ELA} \cdot f_s \cdot \Delta T^{0.5} \\ &= \text{ELA} \cdot \left[\left(\frac{1 + R/2}{3} \right) \cdot \left(1 - \frac{X^2}{(2-R)^2} \right)^{\frac{3}{2}} \cdot \left(\frac{g \cdot H}{T_i} \right)^{\frac{1}{2}} \right] \cdot \Delta T^{0.5} \end{aligned}$$

Eqn 3.17

where Q_s (m^3/s) is the stack driven air infiltration rate, and ΔT (K) is the indoor-outdoor temperature difference.

Consider the case where the fraction of air leakage attributable to the floor and ceiling (R) ranges between 0.3 and 0.7, and the difference in fraction of these two sources of air leakage (X) ranges between 0 and 0.2, then the resulting f_s varies between 0.14 and 0.18 for a single-story house under typical outdoor temperature conditions. The values of f_s are comparable in magnitude to the values of the wind-effect factor f_w. This means that the contributions of wind and stack effects are also likely to be comparable, given that the numerical values of ΔT (K) and U^2 [$(m/s)^2$] are similar. With typical wind speeds in the range of 2 to 4 m/s, the stack effect will only completely dominate the overall air infiltration rate when the indoor-outdoor temperature difference exceeds 20 K. Conversely, the wind effect can dominate when the indoor-outdoor temperature difference drops below 5 K in absolute value, or when the wind speed is much higher than usual. For U ~ 2-4 m/s and ΔT ~ 5-20 K, both effects are important to consider.

3.3.1.3 Combined Air Infiltration Rate

The LBL Infiltration Model combines the stack Q_s (m^3/s) and wind Q_w (m^3/s) driven air infiltration rate by adding the two flows in quadrature:

$$Q = \sqrt{Q_s^2 + Q_w^2}$$

Eqn 3.18

In effect, the model assumes that the pressure differences induced by stack and wind effects are independent of one another. Since the LBL Infiltration Model assumes that

resistance to flow through cracks in the building envelope is dominated by the inertia of air, this independence can be illustrated mathematically as follows:

$$Q^2 = Q_s^2 + Q_w^2$$
$$\left(\kappa \cdot \Delta P^{0.5}\right)^2 = \left(\kappa \cdot \Delta P_s^{0.5}\right)^2 + \left(\kappa \cdot \Delta P_w^{0.5}\right)^2$$
$$\Delta P = \Delta P_s + \Delta P_w$$

Eqn 3.19

The assumption of $n = 0.5$ is invoked in the LBL Infiltration Model to keep the form and the derivation of the model simple. Air leakage measurements in houses show that the exponent in the pressure-flow equation is around 0.65 (Orme et al., 1994). This means that the flow regime in buildings is typically closer to inertial ($n = 0.5$) than viscous ($n = 1$). Conceptually, this notion of independence between the two driving forces of air infiltration is still approximately valid even in cases when $n \neq 0.5$. This is because stack and wind driven air infiltration generally occurs at different parts of the building envelope. While wind acts on the vertical facades of the building, stack effect drives air infiltration through the floor and ceiling. As a result, the overall air infiltration rate can be approximated by summing the pressure differences caused by the two effects.

A related assumption used in the LBL Infiltration Model to combine the stack and wind effect is that there is no interaction term between the two. Sherman (1980) cited an experimental study showing that the first-order interaction term is only important when the wind and stack-driven air infiltration rates are comparable in magnitude. Walker and Wilson (1990) chose to include this interaction term in their revision of the LBL Infiltration Model for houses in Canada. They too found the interaction term to be relatively small, especially when neither one of the terms dominates.

3.3.1.4 Model Comparison with Measurements

A key difference between the LBL Infiltration Model and its revision by Walker and Wilson (1990) is that the latter considers air leakage through the furnace flue of the house. The furnace flue is likely to experience a pressure difference that differs from the rest of the building envelope because it goes through the ceiling of the structure and is designed to protrude into the free-stream wind. Walker and Wilson (1990) found that their model predictions fit infiltration measurements with a bias only 1/3 that of the LBL Model. Both models underpredict air infiltration rates on average. This added level of model detail is not included in the analysis to follow because the air leakage characteristics of furnace flues in US houses have not been well characterized. In parts of the country where furnace flues are present in the majority of houses, the use of this alternative model, known as AIM-2, should be considered.

Sherman and Grimsrud (1980) carried out air infiltration measurements to evaluate the LBL Infiltration Model. They first used a fan pressurization method to determine the leakage areas of 15 houses. The air infiltration rates were then measured using a tracer gas decay technique over a period of 1 h. They found that model predictions were within the measurement error 75% of the time, and thus concluded that the model provided good agreement with observations. The key limitation of using the LBL Model to predict short-term air infiltration rate is not accounting for the directional effect of wind. Building orientation, air leakage distribution over the building envelope, and uneven shielding can all contribute to the dependence of air infiltration rate on wind direction. Unlike the study by Walker and Wilson (1990), no systematic bias between measurements and predictions

was observed. Among the 15 buildings measured, estimated values of f_s ranged from 0.09 to 0.16 [(m/s)/$K^{0.5}$], with a mean of 0.15 [(m/s)/$K^{0.5}$]. Estimated values of f_w ranged from 0.07 to 0.22, with the mean of 0.12. These ranges are similar to those estimated earlier. The variability of the wind-effect factor f_w is also slightly larger than the stack-effect factor f_s as predicted.

Modera et al. (1982) compared model predictions against long-term measurements made in an experimental trailer and three test houses. The authors found reasonable agreement between predictions and measurements made in the trailer. The ratio of the predicted and measured half-hour averaged air infiltration rate had a geometric mean of 1.2. Over the period of 34 days, most ratios fell between 0.7 and 2. The performance of the model in predicting 1-h averaged air infiltration rates of the 3 houses was somewhat less satisfactory. There was evidence of underprediction by the model, some of which can be explained by experimental artifact. Loss of tracer gas to the unconditioned space of the house immediately following injection caused air infiltration rates to appear higher than actual values. Nonetheless, no significant bias was observed in any of these houses. The mean ratios were within 15% of unity.

Modera et al. (1983) refined some of the input parameters and revised the formulation of the LBL Infiltration Model to test if such changes would improve the agreement between model and measurement. Three factors were found to contribute almost equally to bias in the model predictions: (1) the assumption of orifice flow to describe flow through cracks in the building envelope; (2) the assumption of adding wind and stack driven air

infiltration rate in quadrature; and (3) the use of wind pressure coefficients that are not specific to the aspect ratio of the test houses. In terms of factors leading to variability between predictions and measurements, neglecting wind direction together with factor (1) and (3) are the main causes. These comparisons show that while improvements of the LBL Infiltration Model are possible, predictions from the model are reasonably reliable when compared to measurements. For the sake of keeping the requirements for input parameters manageable when modeling a large number of dwellings, the LBL Infiltration Model is an appropriate choice. Relative to other components of modeling SIP effectiveness, uncertainty introduced by predicting the distribution of air infiltration rates is likely to be minor.

3.4 Air Infiltration Rate Predictions

3.4.1 Albuquerque, NM – A Case Study

In case of a large-scale outdoor release, characteristics of the houses being exposed to the toxic plume are needed to predict air-exchange rates and, subsequently, the range of indoor concentrations to which residents are exposed. The local meteorology is also needed to estimate the forces that drive air infiltration. In Chapter 4, hypothetical releases situated in the city of Albuquerque, NM, modeled under different durations and source strengths are used as case studies for assessing SIP effectiveness. This location was chosen because of the availability of outdoor plume predictions made by the National Atmospheric Release Advisory Center at Lawrence Livermore National Laboratory. Part of the work described here is intended for integration with their real-time modeling

capability to assess health consequences in an exposed population that shelters indoors as the emergency response to an outdoor release event. Because the modeling system is intended for use throughout the US, the method developed here relies only on input parameters that are available with nationwide coverage. A specialized, opportunistic dataset tailored to the types of residences present in Albuquerque is not utilized. The atmospheric dispersion model used and the predicted outdoor concentration fields are discussed in Chapter 4.

The outdoor plume only affected one county, which encompasses the city of Albuquerque – Bernalillo County. There are 3 adjacent counties that make up the metropolitan statistical area of Albuquerque, but population in these adjacent counties is not significantly exposed. Bernalillo County extends roughly 40 km in the north-south direction, and 80 km in the east-west direction. The Albuquerque metropolitan area is located at the center north of the county covering an area of 25 km × 30 km. The county has a reported population of 557,000 in 2000 (US Census, 2000). There are 239,000 housing units in the county, of which 60% are single-family detached units. The remaining housing units are made up of multi-unit dwellings, as well as some single-unit attached dwellings and mobile homes.

The driving forces for air infiltration, namely the wind and indoor-outdoor temperature difference, are based on the same meteorology used to predict the outdoor concentrations. The surface level outdoor air temperature (Figure 3.9) is assumed to be uniform throughout the entire 48 km × 48 km model domain. On the winter evening modeled

using the meteorology dated February 24, 2003 in Albuquerque, the indoor-outdoor temperature differences in houses are fairly large. The meteorology module used to predict the wind field includes a complex vertical temperature gradient of the atmosphere. Due to difficulty in extracting this intermediate parameter from the module, the spatial resolution of outdoor temperature is not used in modeling the air infiltration rates. The indoor temperature in houses is assumed to be uniform at 20 ^{o}C. This is a reasonable assumption because according to the 2001 Residential Energy Consumption Survey by the US Energy Information Administration, the vast majority (70%) of single-family homes have their heat regulators set to between 19.4 and 22.8 ^{o}C during daytime in winter months.

Relative to the outdoor temperature, wind speed is more spatially variable across the model domain. Figure 3.10 shows the estimated wind speed at 10 m height projected onto a variable-resolution grid used to predict outdoor concentrations. The origin of the grid is centered at the release source, which is located just a few blocks west of the city's downtown core. Most locations are estimated to have a wind speed between 2 and 4 m/s, but there are also areas of high wind reaching 7 m/s. Areas of high and low wind changed during the 4-h simulation. Situated in a valley with the Sandia/Manzano mountain ridge to the east of the city, strong east winds are common in Albuquerque (Ford, 2004). During this particular hypothetical release, the wind direction is also predominantly from the east. Consequently, population on the west of the city is the most exposed to the advecting toxic plume. The time-varying wind profiles at selected locations downwind

from the source are shown in Figure 3.11. The wind speeds are milder at these locations than in other areas in the model domain.

3.4.2 Housing Characteristics – Census-Tract Based Approach

The US Census provides spatially resolved data on housing characteristics that can be used to estimate the air leakage distribution of houses in an area. The data needed to predict the air leakage of houses are the joint distribution of year built and floor area of houses occupied by low-income and not low-income households. These data are the input to the regression model (Eqn 3.7 and Table 3.2), which describe the dependency of normalized leakage on year built and floor area in houses occupied by low-income and not low-income households. Census tract is chosen as the geographical unit of analysis because when first delineated, boundaries of census tracts are designed to contain between 1500 to 8000 people. This ensures that a sizeable residential community is present in most census tracts. Bernalillo County in Albuquerque is composed of 141 census tracts (Figure 3.12). Most census tracts have roughly 1000 houses each. However, there are also some census tracts with only a few tens of houses, and some with as many as 2500.

The analysis here only considers the air infiltration rate of single-family detached units. Thus, the SIP effectiveness assessment is specific to this type of residences. Air leakage measurements in multi-family housing units reveal pathways that are distinct in these types of residences, e.g. between adjacent units, through stairwell doors, into garbage

chutes, with elevator shafts, etc. A review by Sherman and Chan (2004) summarized the major studies that measured component, unit-by-unit, and whole-building air leakage in various types of buildings, including multi-family housing units. Multi-family housing units not only have different air leakage characteristics, their structural complexities also require more careful modeling of their air infiltration rates. Future work should consider the SIP effectiveness of these residences because in many urban areas in the US, a significant fraction of the population resides in these types of units. For now, the spatial distribution of population used when assessing residential SIP effectiveness in the community is based on the total number of residents residing in single-family detached units only.

3.4.2.1 Year Built Distribution

Air leakage of houses is found to be correlated with the year built (Section 3.2.3): the older the house, the more leaky it tends to be. The US Census Survey reports the number of houses that belong to each of 9 year built categories: <1939, 1940 to 1949, …, 1980 to 1989, 1990 to 1994, 1995 to 1998, and 1999 to March 2000. In Albuquerque, among the census tracts closest to the source of the release, variability in house year built is evident (Figure 3.13). This variability translates to differences in the normalized leakage distribution of houses. Recall also from analysis in Section 3.2.3 that significant difference in the air leakage characteristics of houses occupied by low-income and not low-income households is observed. Thus, the next step is to split the year built distribution of houses in each census tract into two: one for low-income households, and

the other for not low-income households. This is necessary because data from the American Housing Survey show that low-income households tend to live in older houses. This makes intuitive sense since house age often plays a role in determining the price of the property. Poverty status is determined in the Census Survey according to the federal government's official poverty definition. These poverty thresholds are functions of both the family size and the number of family members under 18 years old. However, the Census Survey does not report house year built as function of the poverty status of the occupied household directly in their sample data intended for public use. Instead, the survey reports year built in terms of whether the housing unit is renter or owner occupied, and if the occupied household is above or below poverty line. These year built distributions are, however, non-specific to single-family detached houses. This incompleteness in the available data poses a problem because the year built distribution of multi-family housing units can be quite different from that of single-family houses. In some cases, simple logic and reasonable assumptions are sufficient to deduce the needed house year built distributions for low-income and not low-income households. In other cases, national data from the American Housing Survey (AHS) are needed to extract these two distributions. Figure 3.14 shows that owner-occupied housing units are more likely to be single-family detached units than units that are renter occupied. Housing units that are occupied by above poverty line households are also slightly more likely to be houses than units that are occupied by below poverty line households.

Table 3.6 illustrates the method used to obtain the needed year built distributions using an example. This census tract is located immediately downwind of the release source. Of the

1366 houses, 66% are owner occupied. It is not difficult to identify above poverty houses from below poverty houses by comparing column (a) with (b) and (c). For example, since there are no below poverty housing units built between 1970 and 2000, all single-family detached units built between these periods must be above poverty. When the above and below poverty housing units sum to give the number of single-family detached units built between certain years, such as in the case of row (4), (6), and (7), then all the housing units identified as above and below must be single-family detached units. Only the housing units that are built between 1950 and 1959 (row (5)) require the use of the AHS data to estimate the number of above and below poverty housing units that are single-family detached units. The fractions of single-family detached units given that the units are owner occupied are 0.957 and 0.946 for above and below poverty, respectively (Table 3.7; also see Figure 3.14). Thus, the number of above and below poverty single-family houses built between 1950 and 1959 are estimated as:

$$\begin{aligned}
\text{Number of above poverty 1-family detached units} &= 73 \cdot \frac{73 \times 0.957 + 9 \times 0.946}{73 + 9} \\
&= 70 \\
\text{Number of below poverty 1-family detached units} &= 73 - 70 \\
&= 3
\end{aligned}$$

Eqn 3.20

This same method is used to determine the poverty status of the renter occupied single-family housing units. The resulting year built distributions of houses in this census tract are shown in Figure 3.15. Roughly 15% of the single-family detached units are set to be below poverty line in this census tract. It worth mentioning here that there is a minor difference between the definitions of “low income” used in the air leakage database, and “below poverty” used in the Census Survey. “Low income” houses analyzed in Section

3.2.3 are participants of a weatherization assistance program in the state of Ohio. Participation eligibility requires that household income must be below 125% of the poverty guidelines. On the other hand, a household is classified as "below poverty" if its income is less than the poverty thresholds. There is also a slight difference between the poverty guidelines and poverty thresholds. Poverty guidelines do not adjust for family size by the age of family members, but poverty thresholds do. These differences are not accounted for in the analysis because they are expected to be of minor consequence.

3.4.2.2 Floor Area Distribution

The Census Survey does not provide data on the floor area of the housing units surveyed, which is needed in the air leakage regression model. The approach here is to use some other characteristics of houses reported in the sample data to approximate the floor area distribution. Analysis of the AHS national data shows meaningful correlation between the number of rooms in a house and its floor area (Figure 3.16). In each housing unit, the Census Survey counts the number of rooms including living rooms, dining rooms, kitchens, bedrooms, finished recreation rooms, enclosed porches suitable for year-round use, and lodgers' rooms. Excluded are strip or pullman kitchens, bathrooms, open porches, balconies, halls or foyers, half-rooms, utility rooms, unfinished attics or basements, or other unfinished space used for storage.

The Census Survey provides sample data on the number of rooms for both owner and renter occupied housing units. However, data specific to single-family detached units are

not available. To approximate the needed floor area distribution, the owner occupied data are used. This choice is reasonable because the majority of owner-occupied housing units are single-family houses, as shown in Figure 3.14. Consequently, the owner occupied housing units surveyed by AHS have a number of rooms distribution very close to that of the single-family detached units (Figure 3.17). On the other hand, the renter occupied distribution is distinctly shifted to the left, meaning that these housing units tend to have fewer rooms. The number of rooms distributions shown in Figure 3.17 are generated using the AHS national data, which included 26,000 housing units. In census tracts where the number of housing units is far fewer, owner-occupied data might not reliably approximate the number of rooms distribution in single-family detached units. This can occur in some neighborhoods of densely populated cities, where many of the owner-occupied units are multi-family dwellings instead of single-family houses.

To demonstrate that there is reasonable variability worth modeling in the number of rooms among houses in different census tracts, Figure 3.18 shows such distributions in 3 selected census tracts surrounding the hypothetical release site. These distributions are meant to represent single-family detached units only. Most of these housing units have 4 to 6 rooms. The variability in the number of rooms distributions among census tracts is less than the year built distributions, yet it is clear that houses in some census tracts tend to have more rooms than others.

A method is needed to translate the number of rooms distributions to floor area distributions. For this, data from the American Housing Survey is used. Table 3.8 shows

the floor area distributions of single-family detached units surveyed by AHS, conditioned on the number of rooms in the dwelling. In other words, the table shows the frequency that the floor area of a house is described by one of the six floor area categories given that it has a certain number of rooms. Assuming that these conditional probabilities apply to the single-family detached houses in Albuquerque, floor area distribution can be predicted by multiplying these conditional probabilities with the number of rooms distribution. Table 3.9 shows the step-by-step algebra of this method using the same census tract discussed earlier as an example. Using the method outlined there, the floor area distributions are predicted for the 3 selected census tracts close to the release source (Figure 3.19). These distributions are more similar to one another compared to their year built distributions, but they are distinct enough to cause some differences in the predicted air leakage distribution.

Like the year built distribution, the floor area distribution is further divided into two: one that describes the low-income single-family detached units and another that describes the not low-income units. Again, national data from AHS is used to distinguish between the two. As expected, low-income housing units tend to be smaller in floor area than not low-income ones (Figure 3.20). The relationship between these two floor area cumulative distributions is modeled by an empirical formula, as shown in Figure 3.21. This allows the floor area cumulative distribution of low-income housing units be determined, while using the floor area cumulative distribution of all single-family detached units as the predictor. Table 3.10 illustrates how the floor area distribution obtained earlier is split into a low-income and a not low-income part. This method systematically associates low-

income houses with smaller floor area, which is an important relationship to capture because low-income houses that are also small in floor area have especially high air leakages (Section 3.2.3). Consequently, occupants in these dwellings are likely to be the most at risk when sheltering from an outdoor release.

3.4.2.3 Joint Distribution of Year Built and Floor Area

Up to this point, two sets of distributions are obtained: one for the low-income single-family detached units, and the other for the not low-income units. Each set is made up of a year built distribution and a floor area distribution. The year built distribution describes the year during which the housing units were built at 10-year intervals. The floor area distribution describes the floor area of the housing units at 46-m^2 (500 ft^2) intervals. A method is now needed to combine the year built and floor area distribution in each set to form a joint distribution, such that the air leakage of houses in a census tract can be predicted using the multiple linear regression as shown in Table 3.2.

One method to obtain the joint distribution is to assume independence between year built and floor area of houses. In this case, the joint distribution is simply the product of the two distributions. However, analysis of the AHS national data shows that this assumption is not justified. Correlation test shows a positive association between the year built and floor area of houses. Even though the strength of the correlation is not strong (the measure of association is 0.21, with 95% confidence interval between 0.20 and 0.22), this correlation between year built and floor area is still important to capture because together,

they affect air leakage in a nonlinear manner. This positive correlation is also illustrated in Figure 3.22. In both the low-income and not low-income single-family detached units surveyed by the AHS, newly constructed houses are consistently larger in floor area than the others. Since low normalized air-leakage is associated with both newly constructed houses (built between 1990 and 2000) and houses that are larger in size, this group of houses are particularly airtight. On the other hand, older houses built in the 1950s have particularly high normalized air-leakage because these houses also tend to be smaller in size.

An alternative method is needed to compute the joint distribution that does not assume independence. The Algebraic Reconstruction Technique (ART) is an iterative method where each projected density is thrown back across the reconstruction space in order to bring each reconstructed projection into agreement with the measured projection (Raparia et al., 1997). It is often used in computed tomography to produce, for example, medical imagery. ART has also been used in other applications. For example, Drescher et al. (1996) used the technique to model the spatial distribution of gaseous pollutant concentrations in an experimental chamber. In the present case, the measured projections are the year built distribution and floor area distribution, and the sought reconstruction is the year built and floor area joint distribution. The method requires an initial estimate of the matrix. A reasonable initial guess is the year built and floor area joint distribution of single-family detached units from the AHS (Tables 3.11 and 3.12). These joint distributions can be interpreted simply as the allocation of housing units to the different combinations of year built and floor area characteristics.

The key steps of the ART algorithm are outlined as follows:

Step I. Obtain the initial matrix by multiplying the appropriate AHS joint distribution with the total number of single-family detached units in the census tract.

Step II. Compute the marginal distributions by summing over rows (i.e. sum over floor area as function of year built) and over columns (i.e. sum over year built as function of floor area).

Step III. Compare the marginal distributions with the year built and floor area distributions of the census tract. Select the row or column with the most difference. Add or subtract the difference equally from all the cells in that row or column.

Step IV. Redistribute the amount added or subtracted from the previous step to the remaining cells in the matrix. Exclude cells that would result in negative number of houses from the redistribution.

Step V. Check for convergence. Loop back to Step III if not converged.

A reconstruction is considered converged when the difference between the marginal distribution and the year built and floor area distribution are no more than 1% of the total number of houses in the census tract. Any year built and floor area categories with less than one house are excluded from this criterion. At each iteration, the maximum number of houses to be allocated is restricted to five houses to avoid overshoot. These parameter choices have been tested using census tracts in Albuquerque to ensure that reasonable joint distributions are obtained without an excessive number of iterations. It is also observed that the method is not very sensitive to the initial matrix used in the reconstruction.

Figure 3.23 shows the joint distributions obtained using ART in three census tracts close to the release source in Albuquerque. In all three cases, low-income houses are predicted

to be older in age and smaller in size. Most of the low-income houses were built before 1960 and have a floor area less than 150 m^2. There are only a small number of low-income houses that were built after 1980 and are larger than 200 m^2. Not low-income houses are relatively larger in size. In two of the census tracts, there is evidence of some new housing developments that are relatively large in floor area. Overall, this neighborhood is dominated by houses that were built before 1950. But even among the three census tracts that are adjacent to each other, there are significant differences in their year built and floor area joint distributions that would lead to differences in their normalized air-leakage distributions.

3.4.2.4 Normalized Air Leakage Distribution

The procedure used to predict the normalized air leakage distribution of the houses in a census tract is as follows. Houses in each census tract are first divided into 2 sets: low-income and not low-income. Each set is further divided into 42 groups: 7 year-built categories by 6 floor-area categories. The geometric mean of the normalized air leakage area for each group of houses is tabulated in Tables 3.13 and 3.14. These values are computed using the linear regression model presented in Eqn 3.7. Analysis of the air leakage database suggests the use of a constant geometric standard deviation of 1.7 when computing the distribution. Finally, individual distributions, all 84 of them, are summed according to the number of houses each distribution represents to give the composite distribution. The number of houses each distribution represents are determined by manipulation of the Census Survey and AHS data by methods as described in the prior

sections. The end result is a predicted normalized leakage distribution that describes the air leakage of houses in each census tract.

Figure 3.24 shows the predicted normalized leakage distributions of houses in each of the census tracts in Bernalillo County in Albuquerque. A factor of ten variability is predicted among houses in most of the census tracts. Houses in the residential neighborhoods surrounding the release source are predicted to be more leaky than others in the county. Located just west of the downtown area, the poverty rate among households in these neighborhoods ranges from 0.1 to 0.25, which is high relative to other census tracts in the city. Being close to downtown, these neighborhoods were also developed earlier than more distant parts of the city. Many of the houses are old, with the mean year built in a census tract before 1970. Houses are also smaller in size in these neighborhoods, with the mean floor area ranging from 120 to 160 m^2. Figure 3.25 shows the contribution of each of the three factors considered: poverty rate, year built, and floor area, to the median predicted normalized leakage in each census tract. Reasonable trends are identifiable in all three plots, which means that no single factor dominates over the others in its influence on the air leakage distribution of houses.

At the moment, a large dataset of house air leakage that is independent of the database analyzed in Section 3.2 does not exist. Consequently, it is not yet possible to validate the method developed here. Theoretically, statistical resampling techniques such as bootstrapping could be used to test model performance using the same data from which the regression is based. However, this would require geo-coding of each data entry to a

census tract, which is a labor-intensive task beyond the scope of this work. In the future, when an air-leakage dataset with well-documented housing characteristics becomes available, then model predictions could be compared with measurements. To compare against the variability predicted in houses both within and between census tracts, the measurements must also cover a wide spatial area. Lacking such a dataset, there is no simple way to validate the method developed here. However, based on the fact that all three factors considered in the analysis affect the normalized leakage predictions in a reasonable manner, the approach outlined is at least useful in explaining some of the variability known to exist among houses.

3.4.3 LBL Infiltration Model Input Parameters

For the Albuquerque case study, the areas that are affected by the release as it advects downwind can be characterized as mostly residential neighborhoods with some low-rise commercial buildings. A terrain class 3 to 4 (Table 3.5) is reasonable to characterize the areas that are most exposed to the plume. Other types of land use are also present along the path of the moving plume, such as a state park and a golf course, but they are located more downwind and are assumed not to affect the overall wind profile of the area in this analysis. The population density in the city of Albuquerque is not very high. Most census tracts have 10 to 100 houses per km^2 of area. However, other types of buildings besides neighboring houses and vegetation planted in close proximity can also shield the house from wind-driven air infiltration. In this mid-size metropolitan area, shielding class 3 and

4 described in Table 3.4 are reasonable choices for parameters to use in the LBL Infiltration Model.

The LBL Infiltration Model also requires some knowledge of the air leakage distribution in houses. In principle, R (Eqn 3.13) and X (Eqn 3.16) could be measured experimentally by determining the component leakage area of the walls, floor, and ceiling. However, Reinhold and Sonderegger (1983) showed that a rigorous measurement procedure is not required because model predictions are only weakly dependent on these parameters. Their study aims to predict the total house leakage area by summing over each leakage component based on descriptions and drawings of the dwelling. To do so, components of air leakage were assigned to the floor, ceiling, and walls. The R and X values inferred from these estimates are 0.6 and 0.2, respectively, with a standard deviation of about 0.1 for both parameters. The convention is to assume $R = 0.5$ and $X = 0$ (Sherman, 1980), which tends to give conservative (higher) estimates of the air infiltration rates. This assumption implies that half of the total air-leakage area is from the walls, with the remaining equally distributed between the floor and the ceiling.

3.4.4 Results and Discussion

Figure 3.26 shows the predicted air infiltration rates at different downwind distances directly west of the release source. The predicted rates vary with time following a pattern similar to the change of wind speed with time (Figure 3.11). The influence on the air infiltration rate predictions of the change in outdoor temperature (Figure 3.9) is less

obvious because the time rate of change is small relative to the magnitude of the indoor-outdoor temperature difference. The median air infiltration rates in census tracts that are closest to the source are twice as high as in locations that are further away. As noted earlier, this is because each census tract has a different mix of houses, which leads to differences in their air leakage. However, the extent to which the air infiltration rates in one census tract differ from the others depends also on the driving forces for air infiltration. Initially, the median predicted air infiltration rates only vary between 0.3 to 0.55 h^{-1}. As the outdoor temperature continues to drop in the evening causing stack-driven infiltration to increase, the range of predicted values widens to 0.3 to 0.7 h^{-1}. The analysis here assumed that the indoor temperature stayed at 20 ^{o}C throughout the 4-h duration. In reality, infiltrating cold outdoor air will bring down the indoor temperature if heaters are turned off. Consequently, the stack-effect driving force might diminish somewhat with time compared with these predictions.

The above comparison is based on the median air infiltration rate predictions only. At each location, a distribution of air infiltration rates is also computed. Figure 3.27 shows the variability predicted at two of the locations compared in the previous figure. The upper plot shows the predictions made at a location fairly close to the release source with houses that are quite leaky. The most leaky 5% of the houses are predicted to have air infiltration rates exceeding 1.5 h^{-1}, whereas the tightest 5% of the houses are predicted to have air infiltration rates of only 0.25 h^{-1}. Because air leakage of houses is roughly lognormally distributed (Section 3.2.3), leaky houses can have air infiltration rates far higher than the median (0.6 h^{-1}). Similar variability in the predicted air infiltration rates is

observed at the other location. But because the houses there are on average more air tight, the maximum predicted air infiltration rates are only 1.0 h^{-1}. Slower wind speed also contributed to lower predicted rates relative to the other location.

The results shown so far assumed moderate shielding (class 3 in Table 3.4) from the surroundings, and also urban terrain (class 4 in Table 3.5) at all locations. Changing the shielding class from moderate to heavy (class 4) causes the predicted air infiltration rates to decrease by about 8%. Changing the terrain class from urban to rural (class 3) causes the predictions to increase by 3%. In reality, a mix of shielding conditions is expected in a community. The terrain is also not uniform in different parts of the city. These factors can introduce even more variability in the air infiltration rates among houses than what is already predicted. Currently, houses at the same percentile on the respective air leakage distribution in different census tracts are predicted to have air infiltration rates that differ by factors of 2 to 6. When making predictions for a community of houses, it is unrealistic to expect the shielding and terrain class chosen to describe the local conditions at each grid cell perfectly. Future work should consider implications of the uncertainty of these parameters on SIP effectiveness.

Unfortunately, there is a lack of air infiltration rate measurements appropriate for comparison with the predictions. None of the air-exchange rates measurements cited in the earlier comparison (Figure 3.8) included houses in the state of New Mexico. Houses in this state are also absent from the air leakage database. Nonetheless, the predicted air infiltration rates are similar in magnitude to the air-exchange rates reviewed. For

example, Panadian et al. (1998) estimated that the 5th, 50th, and 95th percentile air-exchange rates of US houses in winter months (December to February) are 0.15, 0.42, and 1.3 h^{-1} respectively. In Albuquerque, the population-weighted air infiltration rates evaluated at the same three percentiles (5th, 50th, and 95th) are 0.15, 0.40, and 1.2 h^{-1} respectively. These air infiltration rates are predicted using the wind speed and outdoor temperature at the start of the 4-h simulation. In winter months when windows are usually kept closed, uncontrolled air infiltration is likely to be the key source of air exchange. It is therefore reassuring that similar range of air infiltration rates are predicted by the method described here.

3.4.5 Air-Exchange Rates under Normal Operating Conditions

Studies that measured air-exchange rate have pointed out many other factors that may influence the amount of air exchange in dwellings aside from wind and indoor-outdoor temperature difference. Findings from these studies are relevant even in SIP scenarios. Non-compliance with SIP instructions is certainly possible for some in a community, especially if the population is not well prepared to respond in emergencies. The community can also be unaware that an event has occurred, and SIP instruction may not be given out in a timely manner to the exposed population. Under these circumstances, most people are still likely to be indoors. However, the amount of air exchange might be significantly higher than the predicted air infiltration rates. Analyses in the next chapter will include assessment of SIP effectiveness both with and without some fraction of residences having windows opened and engaged in other activities that might induce

additional air exchange with the outdoors. To facilitate such analysis, assessment of the key factors other than infiltration that affect air-exchange rates are discussed here.

When open, airflows through windows, doors, and other designed openings in the building envelope, collectively known as natural ventilation, can dominate the air-exchange rates in residences. Howard-Reed et al. (2002) measured the air-exchange rates in two residences and found that opening one window increased the air-exchange rates by 0.1 to 2.8 h^{-1} in one residence, and by 0.5 to 1.7 h^{-1} in the other residence. These are substantial increases relative to the average air-exchange rates measured, which were 0.37 h^{-1} and 0.41 h^{-1} for the two residences respectively. Similar long-term measurements of air-exchange rates also show strong influence by opening windows (Johnson et al., 2004). In other studies of air-exchange rate measurements taken from a larger number of residences at different time of the year, summer seasons are almost always correlated with high air-exchange rates (Murray and Burmaster, 1995; Panadian et al., 1998; Wilson et al., 1996). The estimated median air-exchange rate varies by 2× from its summer high (~1 h^{-1}) to its winter low (~0.5 h^{-1}). These observations imply that window openings are prevalent in communities when the weather is comfortable. In a pilot survey study carried out in North Carolina, Johnson and Long (2005) observed that roughly 35% of houses have at least one window or door open in the spring season. At times when the outdoor temperature is less comfortable (<60 ^{o}F or >100 ^{o}F), only 20% or so of the residences have at least one window or door open. A large sample survey by Price and Sherman (2006) on the ventilation behavior in new California houses (all built in 2003) also found similar seasonal dependence in the percentage of residences with open windows. In

summer and spring, the survey shows that roughly 40% of homes have at least one window open for >2 h between 6 am to 6 pm weekdays. In winter, only 15% of homes have at least one window open for >2 h during the same time period.

Mechanical ventilation affects the air-exchange rate by intentionally drawing air in and out of residences. Internal fans can also induce some additional air exchange by changing the distribution of indoor pressures throughout a building. Operation of an attic fan caused air-exchange rates to increase by 0.8 h^{-1} in one residence measured by Wallace et al. (2002). The authors found that the use of the furnace fan (flue closed) had no effect on air-exchange rates. However, operating a fireplace with large rate of airflow out of the chimney can induce significant air-exchange. For example, during a 15-week monitoring period in a house, Nazaroff et al. (1985) found +0.4 to +0.6 h^{-1} when the fireplace was in operation. A study by Wilson et al. (1996) also found that houses in California with a particular type of furnace that has an exhaust stack for venting have +0.2 h^{-1} air-exchange rates on average. On the other hand, houses with gas forced-air furnace were found not to be statistically different from houses that have electric heater. However, the authors did not specify the number of California residences that had operated their gas-forced furnaces when the measurements were taken during a two-day sampling period in winter.

Duct leaks are common because most residential thermal distribution systems are installed outside the heated or cooled part of the house. Leaks can occur at all connections within a system. Practical testing and sealing methods have therefore been developed to guide commission efforts (LBNL, 2003; Modera, 2005). Cummings et al.

(1990) found that most infiltration rates measured in 91 Florida homes ranged between 0.25 and 1.5 h^{-1} (mean = 0.93 h^{-1}) when the system was in operation. When the systems were turned off, most measured infiltration rates were below 0.5 h^{-1} (mean = 0.21 h^{-1}). Gammage et al. (1986) found the mean air infiltration rate in 31 Tennessee homes to be 0.78 and 0.41 h^{-1} when measurements were made with the central duct fan on and off, respectively. Significant air leakage contributions from the thermal distribution system were also observed among houses in the Pacific Northwest. One-time measurements in 20 conventional homes (Robinson and Lambert, 1989) show that the mean infiltration rate was 0.82 and 0.28 h^{-1} measured with fan on and off, respectively. Based on long-term measurements taken over 4 months in a related study (Parker, 1989), the mean air-exchange rates among houses having a forced-air heating system was about 0.2 h^{-1} higher than the non-forced system group.

The evidence so far suggests that both natural and mechanical ventilation can significantly induce additional air exchange on top of air infiltration under many circumstances. It has even been observed in some studies that the influence of these factors overpowers the dependence of the measured air-exchange rates on wind speed (Johnson et al., 2004) and on indoor-outdoor temperature difference (Wallace et al., 2002). While only few dwellings have been extensively studied and analyzed in such detailed manner, it is conceivable that airflow through some large openings can outweigh the contribution from air infiltration. In fact, large openings are of such importance to the airflow patterns in buildings that they are modeled differently from the usual cracks and leaks on the building envelope (Feustel and Dieris, 1992). Their presence can change the

functional dependence of air infiltration rate on wind and indoor-outdoor temperature difference altogether. In Chapter 4, before the community implements SIP, a fixed amount of air-exchange is added to all houses to model the indoor concentrations before windows are shut, and exhaust fans turned off. The additional amount of air exchange is likely to be somewhat less in wintertime than in summertime, with reasonable values in the range of 0.2 to 1.0 h^{-1}.

3.5 Conclusions

To assess the shelter-in-place (SIP) effectiveness in a community requires quantification of the range of air infiltration rates in houses. Two sets of parameters are required to predict the needed distributions for a community of houses: leakage characteristics of the housing stock and driving forces for air infiltration. Pressurization measurements have been analyzed to quantify the variability in the air leakage of houses, both in terms of central tendency and variability. The relationship between leakage area of the building envelope and the house characteristics is identified by the method of regression. House year built, floor area and household poverty status are useful parameters that can explain some of the variability observed in the normalized leakage areas of the housing stock. Regression results show that older and smaller houses, and houses that are occupied by low-income households tend to be more leaky than the average.

Air infiltration is the result of pressure difference imposed on the building envelope. To predict air infiltration rate, which is the dominant mode of air exchange during well-executed SIP, one needs to know not only how leaky the building envelope is, but also

the driving forces. A mathematical model, known as the LBL Infiltration Model, describes how wind and indoor-outdoor temperature difference induce pressures that cause air infiltration to occur. The model formulation and the choice of input parameters have been presented and discussed. Past validation experiments show reasonable agreement between model predictions and measured air infiltration rates in houses and test facilities. For the purpose of predicting the air infiltration rate distributions in a community of single-family homes, performance of the LBL Infiltration Model appears suitable.

Finally, this chapter illustrates a method that makes use of results of the air leakage analysis and the LBL Infiltration Model to predict the air infiltration rate distribution in a portion of a community. The case study location, Albuquerque, NM, is chosen to prepare for the SIP assessment in Chapter 4. Detailed discussions on how US Census Survey data are manipulated to generate the needed housing characteristics for air leakage predictions are presented. Significant variability in predicted air infiltration rates is observed among houses, both within and between census tracts. Even though no direct measurement of air infiltration rates is available from this area to compare with the model predictions, comparison with air-exchange rates measured in the winter seasons from other parts of the US shows reasonable agreement. All factors considered in this analysis, namely the various housing characteristics and the driving forces for air infiltration, affect the air infiltration rate distribution without one being the clearly dominant cause. At least as illustrated in this case study, all the parameters discussed are needed for the proper characterization of the air infiltration rate distribution in a community of houses under

SIP conditions. The resulting distributions will be used in Chapter 4 to assess the SIP effectiveness of the community against hypothetical large-scale outdoor releases.

3.6 References

ASTM, 1999. ASTM Standard E779. Standard test method for determining air leakage by fan pressurization. American Society of Testing and Materials, Philadelphia, PA.

Breiman, L., Friedman, J.H., Olshen, R.A., Stone, C.J., 1984. Classification and Regression Trees, Wadsworth International Group, Belmont, CA.

Brennan, T., Pyle, B., Williamson, A., Balzer, F., Osborne M., 1990. Fan door testing on crawl space buildings. Air Change Rate and Airtightness in Buildings, ASTM STP 1067, American Society of Testing and Materials, Philadelphia, PA, 146–150.

Cummings, J.B., Tooley, J.J., Moyer, N.A., Dunsmore, R., 1990. Impacts of duct leakage on infiltration rates, space conditioning energy use, and peak electrical demand in Florida homes. Proceedings, ACEEE Summer Study, American Council for an Energy-Efficient Economy, Washington, DC.

Drescher, A.C., Gadgil, A.J., Price, P.N., Nazaroff, W.W., 1996. Novel approach for tomographic reconstruction of gas concentration distributions in air: use of smooth basis functions and simulated annealing. Atmospheric Environment 30, 929–940.

Etheridge, D.W., 1988. Modeling of air infiltration in single- and multi-cell buildings. Energy and Buildings 10, 185–192.

Feustel H.E., Dieris J., 1992. A survey of airflow models for multizone structures. Energy and Buildings 18, 79–100.

Ford, M.J., 2004. East wind storms at Albuquerque, NM. March Monthly Report, Weather Forecast Office, National Weather Service. http://www.srh.noaa.gov/abq/climate/Monthlyreports/March/eastwinds_mf.pdf

Gammage, R.B., Hawthorne, A.R., White, D.A., 1986. Parameters affecting air infiltration and airtightness in thirty one east Tennessee homes. Measured Air Leakage of Buildings, ASTM STP 904, Trechsel, H.R., Lagus, P.L., Eds., American Society of Testing and Materials, Philadelphia, PA, 61–69.

Grot, R.A., Clark, R.E., 1979. Air leakage characteristics and weatherization techniques for low-income housing. Proceedings, ASHRAE/DOE Conference, Thermal performance of the exterior envelopes of buildings, Kissimmee, FL.

Howard-Reed, C., Wallace, L.A., Ott, W.R., 2002. The effect of opening windows on air change rates in two homes. Journal of the Air and Waste Mangement Association 52 (2), 147–159.

Johnson T., Myers J., Kelly, T., Wisbith, A., Ollison, W., 2004. A pilot study using scripted ventilation conditions to identify key factors affecting indoor pollutant concentration and air exchange rate in a residence. Journal of Exposure Analysis and Environmental Epidemiology 14, 1–22.

Johnson T., Long, T., 2005. Determining the frequency of open windows in residences: a pilot study in Durham, North Carolina during varying temperature conditions. Journal of Exposure Analysis and Environmental Epidemiology 15, 329–349.

Koontz, M.D., Rector, H.E., 1995. Estimation of distributions for residential air exchange rates, Technical report, Technologies Division, Office of Pollution Prevention and Toxics, United States Environmental Protection Agency.

LBNL, 2003. Thermal Energy Distribution. Energy Performance of Buildings Group, Environmental Energy Technologies Division, Lawrence Berkeley National Laboratory, Berkeley, CA. http://ducts.lbl.gov/

Lyberg, M.D., 1997. Basic air infiltration. Building and Environment 12 (2), 95–100.

Matson, N.E., Feustel, H.F., Warner, J.L., 1994. Climate-based analysis of residential ventilation options: New York analysis. Proceedings, 15th Air Infiltration and Ventilation Centre Conference, Buxton, UK.

Modera, M.P., Sherman, M.H., Grimsrud, D.T., 1982. A predictive air infiltration model – long-term field test validation. Proceedings, ASHRAE Semi-Annual Meeting, Houston, TX.

Modera, M.P., Sherman, M.H., Levin, P.A., 1983. A detailed examination of the LBL infiltration model using the mobile infiltration test unit. Proceedings, ASHRAE Annual Meeting, Washington, DC.

Modera, M.P., 2005. ASHRAE Standard 152 & duct leaks in houses. ASHRAE Journal, March, 29–33.

Murray, D.M., Burmaster, D.E., 1995. Residential air exchange rates in the United States: Empirical and estimated parametric distributions by season and climatic region. Risk Analysis 15 (4), 459–465.

Nazaroff, W.W., Feustel, H., Nero, A.V., Revzan, K.L., Grimsrud, D.T., Essling, M.A., Toohey, R.E., 1985. Radon transport into a detached one-story house with a basement. Atmospheric Environment 19, 31–46.

Orme, M., Liddament, M., Wilson, A., 1994. An analysis and data summary of the AIVC's numerical database, Air Infiltration and Ventilation Centre, Coventry, UK.

Pandian, M.D., Behar, J.V., Ott, W.R., Wallace, L.A., Wilson, A.L., Colome, S.D., Koontz, M.D., 1998. Correcting errors in the nationwide data base of residential air exchange rates. Journal of Exposure Analysis and Environmental Epidemiology 8 (4), 577–586.

Parker, D.S., 1989. Thermal performance monitoring results from the residential standards demonstration program. Energy and Buildings 13 (3), 231–248.

Price, P.N., Sherman, M.H., 2006. Ventilation behavior and household characteristics in new California houses. LBNL-59620, Lawrence Berkeley National Laboratory, Berkeley, CA.

Proskiw, G., 1995. Air leakage characteristics of various rough-opening sealing methods for windows and doors. Airflow Performance of Building Envelopes, Components, and Systems, ASTM STP 1255, American Society for Testing and Materials, Philadelphia, PA.

Raparia, D., Alessi, J., Kponou, A., 1997. The algebraic reconstruction technique (ART). Proceedings, IEEE Practice Accelerator Conference 2, Piscataway, NJ, 2023–2025.

Reinhold C., Sonderegger, R., 1983. Component leakage areas in residential buildings. Proceedings, 4th Air Infiltration Centre Conference, Elm, Switzerland.

Robinson, D.H., Lambert L.A.,1989. Field investigation of residential infiltration and heating duct leakage. ASHRAE Transactions 95 (2), 542–550.

Sherman, M.H., 1980. Air Infiltration in Buildings. PhD Thesis, University of California, Berkeley, CA.

Sherman, M.H., Grimsrud, D.T., 1980. Measurement of infiltration using fan pressurization and weather data. LBNL-10852, Lawrence Berkeley National Laboratory Report, Berkeley, CA.

Sherman, M.H., Modera, M.P., 1986. Comparison of measured and predicted infiltration using the LBL infiltration model. Measured Air Leakage of Buildings, ASTM STP 904, Trechsel, H.R., Lagus, P.L., Eds., American Society of Testing and Materials, Philadelphia, PA, 349–364.

Sherman, M.H., 1995. The use of blower-door data. Indoor Air 5 (3), 215–224.

Sherman, M.H., Matson, N.E., 1997. Residential ventilation and energy characteristics. LBNL-39036, Lawrence Berkeley National Laboratory, Berkeley, CA.

Sherman, M.H., Dickerhoff, D.J., 1998. Airtightness of US dwellings. ASHRAE Transactions 104 (2), 1359–1367.

Sherman, M.H., Matson, N.E., 2001. Air tightness of new houses in the US. Proceedings, 22nd Air Infiltration and Ventilation Centre Conference, Bath, UK.

Sherman, M.H., Chan, W.R., 2004. Building airtightness: research and practice. LBNL-53356, Lawrence Berkeley National Laboratory, Berkeley, CA.

US BLS, 2000. Current Population Survey: Annual Demographic Survey, March Supplement, Detailed Poverty Table. The Bureau of Labor Statistics and The Bureau of the Census. http://www.bls.census.gov/cps/ads/2000/sdata.htm

US Census, 2000. Census 2000 Summary File 3 Data on Bernalillo County, NM. Sample data accessed on American FactFinder, The Bureau of the Census. http://factfinder.census.gov/home/

US EERE, 2006. Weatherization Assistance Program. Energy Efficiency and Renewable Energy, United States Department of Energy. http://www.eere.energy.gov/wip/program/weatherizationassitance.html

US EPA, 1997. Exposure Factors Handbook, Vol. III, Ch. 17: Residential Building Characteristics, National Center for Environmental Assessment, United States Environmental Protection Agency. http://cfpub.epa.gov/ncea/

US EPA, 2002. Energy Star Home Sealing Specification. United States Environmental Protection Agency. http://yosemite1.epa.gov

US EPA, 2003. Energy Star Program Snapshot. United States Environmental Protection Agency. http://www.energystar.gov

US HUD, 2000. American Housing Survey for the United States 1999: Current Housing Reports. United States Department of Housing and Urban Development and United States Census Bureau. http://www.census.gov/hhes/www/housing/ahs/nationaldata.html

Wallace, L.A., Emmerich, S.J., Howard-Reed, C., 2002. Continuous measurements of air change rates in an occupied house for 1 year: The effect of temperature, wind, fans, and windows. Journal of Exposure Analysis and Environmental Epidemiology 12, 296–306.

Walker, I.S., Wilson, D.J., 1990. The Alberta air infiltration model. Technical Report 71, Department of Mechanical Engineering, The University of Alberta, Canada.

Walker, I.S., Wilson, D.J., Sherman, M.H., 1998. A comparison of the power law to quadratic formulations for air infiltration calculations. Energy and Buildings 27, 293–299.

Wilson, A.L., Colome, S.D., Tian, Y., Beck, E.W., Baker, P.E., Behrens, D.W., Billick, I.H., Garrison, C.A., 1996. California residential air exchange rates and residential volumes. Journal of Exposure Analysis and Environmental Epidemiology 6 (3), 311–326.

3.7 Tables

Table 3.1 Multivariable regression parameters for the normalized leakage of all valid data points, using indicator variables I_E and I_L to identify low-income and energy-efficient houses[§].

	Coefficients	Estimate	Std. Error	t-value	R^2
β_0	(Intercept)	9.63	0.17	60	
β_1	YearBuilt	-5.03×10^{-3}	8.1×10^{-5}	-62	
β_2[*]	FloorArea	-2.69×10^{-3}	3.2×10^{-5}	-85	0.56
β_3	I_E[#]	-0.48	0.011	-43	
β_4	I_L[#]	0.61	0.010	59	

[§] See Eqn 3.6.
[*] Expressed in units of m^{-2}.
[#] I_E takes the value of 1 if the house is energy-efficient and 0 otherwise; I_L takes the value of 1 if the occupied household is low income and 0 otherwise.

Table 3.2 Multivariable regression parameters for the normalized leakage of low-income, conventional, and energy-efficient houses[§].

House Types		Coefficients	Estimate	Std. Error	t-value	R^2
Low-Income	β_0	(Intercept)	11.1	0.17	67	
	β_1	YearBuilt	-5.37×10^{-3}	8.4×10^{-5}	-64	0.17
	β_2[*]	FloorArea	-4.18×10^{-3}	4.3×10^{-5}	-97	
Conventional	β_0	(Intercept)	20.7	0.58	36	
	β_1	YearBuilt	-1.07×10^{-2}	3.0×10^{-4}	-36	0.41
	β_2[*]	FloorArea	-2.20×10^{-3}	7.5×10^{-5}	-29	
Energy-Efficient	β_0	(Intercept)	34.3	2.1	17	
	β_1	YearBuilt	-1.79×10^{-2}	1.0×10^{-3}	-17	0.04
	β_2[*]	FloorArea	-1.83×10^{-4}	5.7×10^{-5}	-3.2	

[§] See Eqn 3.7.
[*] Expressed in units of m^{-2}.

Table 3.3 Statistics of estimated normalized leakage distribution weighted for all single-family dwellings in US.

House Type	Estimated Normalized Leakage Percentiles							Estimated	
	5th	10th	25th	50th	75th	90th	95th	GM	GSD
Low Income	0.30	0.39	0.62	0.98	1.5	2.2	2.7	0.92	1.9
Conventional	0.17	0.21	0.31	0.48	0.75	1.1	1.4	0.49	1.9
Whole US	0.17	0.22	0.33	0.52	0.84	1.3	1.7	0.54	2.0

Table 3.4 LBL Infiltration Model shielding parameters[#].

Shielding Class	Description	C
1	No obstructions, including trees, fences, and nearby houses	0.34
2	Few obstructions; light local shielding	0.30
3	Some obstructions within two house heights	0.25
4	Obstructions around most of house perimeter	0.19
5	Large obstructions surrounding perimeter	0.11

[#] Source: Sherman and Grimsrud (1980)

Table 3.5 LBL Infiltration Model terrain parameters[#].

Terrain Class	Description	A	B
1	Ocean or other body of water	1.30	0.10
2	Flat terrain with some isolated obstacles	1.00	0.15
3	Rural areas with low buildings, trees, etc.	0.85	0.20
4	Urban, industrial, or forest areas	0.67	0.25
5	Center of a large city	0.47	0.35

[#] Source: Sherman and Grimsrud (1980)

Table 3.6 Year built distributions of housing units in a census tract[#] in Albuquerque.

Year Built		Number of Housing Units					
		Owner Occupied			Renter Occupied		
		Single-Family Detached Units	All Housing Units		Single-Family Detached Units	All Housing Units	
			Above Poverty	Below Poverty		Above Poverty	Below Poverty
	Row/ Col	(a)	(b)	(c)	(d)	(e)	(f)
1990-2000	(1)	48	48	0	7	21	9
1980-1989	(2)	39	39	0	5	12	3
1970-1979	(3)	30	30	0	15	56	22
1960-1969	(4)	42	35	7	29	62	32
1950-1959	(5)	73	73	9	83	126	14
1940-1949	(6)	118	97	21	118	126	73
<1939	(7)	561	534	48	208	293	144

[#] Census tract ID 2700 in Bernalillo County.

Table 3.7 Fraction of US housing units that are single-family detached units when grouped by year-built, owner versus renter occupied, and occupant poverty status[#].

Year Built	Fraction of Single-Family Detached Housing Units			
	Owner Occupied		Renter Occupied	
	Above Poverty	Below Poverty	Above Poverty	Below Poverty
1990-2000	0.753	0.595	0.146	0.141
1980-1989	0.731	0.573	0.116	0.100
1970-1979	0.797	0.577	0.162	0.120
1960-1969	0.901	0.787	0.230	0.188
1950-1959	0.957	0.946	0.434	0.344
1940-1949	0.943	0.912	0.425	0.334
<1939	0.867	0.868	0.330	0.340

[#] Statistics are based on analysis of the national data from American Housing Survey (AHS). Remaining fraction of the housing units (not shown) are non single-family detached units, which might include multi-family housing units, as well as single-family attached units and mobile homes.

Table 3.8 Distribution of house floor area conditioned on the number of rooms in US single-family detached units[#].

Number of Rooms		Floor Area (m^2)					
		<46 m^2	46 to 93 m^2	93 to 139 m^2	139 to 186 m^2	186 to 232 m^2	>232 m^2
	Col.	(a)	(b)	(c)	(d)	(e)	(f)
1		0.388	0.441	0.085	0.034	0	0.051
2		0.388	0.368	0.175	0.023	0.023	0.023
3		0.185	0.526	0.202	0.037	0.027	0.023
4		0.032	0.370	0.366	0.148	0.048	0.037
5		0.007	0.136	0.427	0.259	0.101	0.071
6		0.004	0.052	0.302	0.345	0.169	0.127
7		0.002	0.019	0.154	0.321	0.263	0.241
8		0.003	0.012	0.059	0.177	0.315	0.436
>9		0.001	0.011	0.043	0.096	0.186	0.662

[#] Statistics are based on analysis of the national data from American Housing Survey (AHS). Each cell represents the fraction of housing units having the floor area given that they have certain number of rooms (i.e. each row sums to 1).

Table 3.9 Estimated house floor area distribution[#] of single-family detached units in a census tract in Albuquerque (census tract ID 2700).

Number of Rooms		Number of Single-Family Detached Units					
		Floor Area (m^2)					
		<46 m^2	46 to 93 m^2	93 to 139 m^2	139 to 186 m^2	186 to 232 m^2	>232 m^2
	Col. (n)	(n) × (a)	(n) × (b)	(n) × (c)	(n) × (d)	(n) × (e)	(n) × (f)
1	0	0	0	0	0	0	0
2	62	24	23	11	1	1	1
3	115	21	60	23	4	3	3
4	308	10	114	113	45	15	11
5	334	2	45	143	86	34	24
6	257	1	13	78	89	44	33
7	138	0	3	21	44	36	33
8	62	0	1	4	11	20	27
>9	90	0	1	4	9	17	60
	Row (1)	Σ = 58	Σ = 260	Σ = 397	Σ = 289	Σ = 170	Σ = 192

[#] The floor area distribution, Row (1), is obtained by first multiplying the number of rooms distributions, Col. (n), by the conditional probability shown in Table 3.8 (Col. (a) to (f)) to obtain the number of housing units given the number of rooms. The estimated number of housing units having certain floor area is summed by column to give Row (1).

Table 3.10 Estimated house floor area distributions of the single-family detached units in a census tract in Albuquerque (census tract ID 2700) that are low-income (Col. (d)) and not low-income (Col. (e)).

		Single-Family Detached Housing Units				
		All Units		Low-Income Units		Not Low-Income Units
		Unit Count	Cumulative Distribution (f_a)	Cumulative Distribution (f_l)	Unit Count $\Sigma = 207$	Unit Count
Floor Area	Col.	(a)[§]	(b)[*]	(c)[◊]	(d)[#]	(e)[‡]
<46 m^2		58	0.042	0.095	20	38
46 to 93 m^2		260	0.233	0.368	56	204
93 to 139 m^2		397	0.523	0.692	67	330
139 to 186 m^2		289	0.735	0.859	35	254
186 to 232 m^2		170	0.859	0.930	14	156
>232 m^2		192	1.0	1.0	15	177

[§] Col. (a) is the floor area distribution of all single-family detached units, as obtained in Table 3.9.

[*] Col. (b), referred to as f_a, is the cumulative distribution representation of Col. (a).

[◊] Col. (c), referred to as f_l, is the cumulative house floor area distribution of low-income single-family detached units. Based on the best-fit regression relationship as described in Figure 3.21, f_l is estimated using f_a as the input.

[#] Col. (d) is obtained by multiplying the cumulative distribution f_l and the total number of low-income houses in the census tract, which is 207 in this case.

[‡] Col. (e) is computed by subtracting Col. (d) from Col. (a).

Table 3.11 House year built and floor area joint distribution of not low-income single-family detached units, based on analysis of national data from American Housing Survey (AHS).

Year Built	Floor Area					
	<46 m^2	46 to 93 m^2	93 to 139 m^2	139 to 186 m^2	186 to 232 m^2	>232 m^2
1990-2000	3.69×10^{-4}	2.55×10^{-3}	2.39×10^{-2}	4.20×10^{-2}	3.66×10^{-2}	6.08×10^{-2}
1980-1989	2.11×10^{-4}	3.28×10^{-3}	2.37×10^{-2}	3.34×10^{-2}	2.36×10^{-2}	3.36×10^{-2}
1970-1979	9.63×10^{-4}	6.26×10^{-3}	3.97×10^{-2}	5.18×10^{-2}	4.14×10^{-2}	4.20×10^{-2}
1960-1969	8.17×10^{-4}	9.64×10^{-3}	3.93×10^{-2}	4.21×10^{-2}	2.80×10^{-2}	2.59×10^{-2}
1950-1959	7.52×10^{-4}	1.64×10^{-2}	4.78×10^{-2}	3.85×10^{-2}	2.10×10^{-2}	2.05×10^{-2}
1940-1949	1.03×10^{-3}	1.26×10^{-2}	2.32×10^{-2}	1.83×10^{-2}	1.05×10^{-2}	9.78×10^{-2}
<1939	2.18×10^{-3}	1.71×10^{-2}	4.12×10^{-2}	4.03×10^{-2}	2.80×10^{-2}	3.89×10^{-2}

Table 3.12 House year built and floor area joint distribution of low-income single-family detached units, based on analysis of national data from American Housing Survey (AHS).

Year Built	Floor Area					
	<46 m^2	46 to 93 m^2	93 to 139 m^2	139 to 186 m^2	186 to 232 m^2	>232 m^2
1990-2000	9.79×10^{-4}	5.01×10^{-3}	1.37×10^{-2}	2.10×10^{-2}	1.40×10^{-2}	1.62×10^{-2}
1980-1989	1.06×10^{-3}	6.51×10^{-3}	2.56×10^{-2}	2.07×10^{-2}	1.07×10^{-2}	1.04×10^{-2}
1970-1979	1.70×10^{-3}	1.96×10^{-2}	4.86×10^{-2}	3.27×10^{-2}	2.06×10^{-2}	1.79×10^{-2}
1960-1969	1.53×10^{-3}	2.44×10^{-2}	5.27×10^{-2}	2.93×10^{-2}	2.31×10^{-2}	1.98×10^{-2}
1950-1959	2.78×10^{-3}	3.61×10^{-2}	7.15×10^{-2}	3.83×10^{-2}	1.61×10^{-2}	1.44×10^{-2}
1940-1949	1.97×10^{-3}	3.02×10^{-2}	4.34×10^{-2}	2.24×10^{-2}	1.02×10^{-2}	6.49×10^{-3}
<1939	6.67×10^{-3}	4.38×10^{-2}	8.46×10^{-2}	5.35×10^{-2}	3.37×10^{-2}	4.61×10^{-2}

Table 3.13 Geometric mean of the normalized leakage estimated for not low-income single-family detached units, as a function of their year built and floor area.

Year Built	Floor Area					
	<46 m^2	46 to 93 m^2	93 to 139 m^2	139 to 186 m^2	186 to 232 m^2	>232 m^2
1990-2000	0.48	0.45	0.41	0.37	0.33	0.28
1980-1989	0.54	0.50	0.45	0.41	0.37	0.32
1970-1979	0.60	0.56	0.50	0.45	0.41	0.35
1960-1969	0.64	0.59	0.54	0.48	0.44	0.38
1950-1959	0.74	0.69	0.62	0.56	0.51	0.44
1940-1949	0.82	0.77	0.69	0.63	0.57	0.48
<1939	1.02	0.95	0.86	0.78	0.70	0.60

Table 3.14 Geometric mean of the normalized leakage estimated for low-income single-family detached units, as a function of their year built and floor area.

Year Built	Floor Area					
	<46 m^2	46 to 93 m^2	93 to 139 m^2	139 to 186 m^2	186 to 232 m^2	>232 m^2
1990-2000	1.26	1.10	0.91	0.75	0.62	0.46
1980-1989	1.33	1.16	0.96	0.79	0.65	0.49
1970-1979	1.40	1.23	1.01	0.83	0.68	0.51
1960-1969	1.45	1.27	1.04	0.86	0.71	0.53
1950-1959	1.56	1.36	1.12	0.93	0.76	0.57
1940-1949	1.65	1.44	1.19	0.98	0.80	0.60
<1939	1.84	1.60	1.32	1.09	0.90	0.67

3.8 Figures

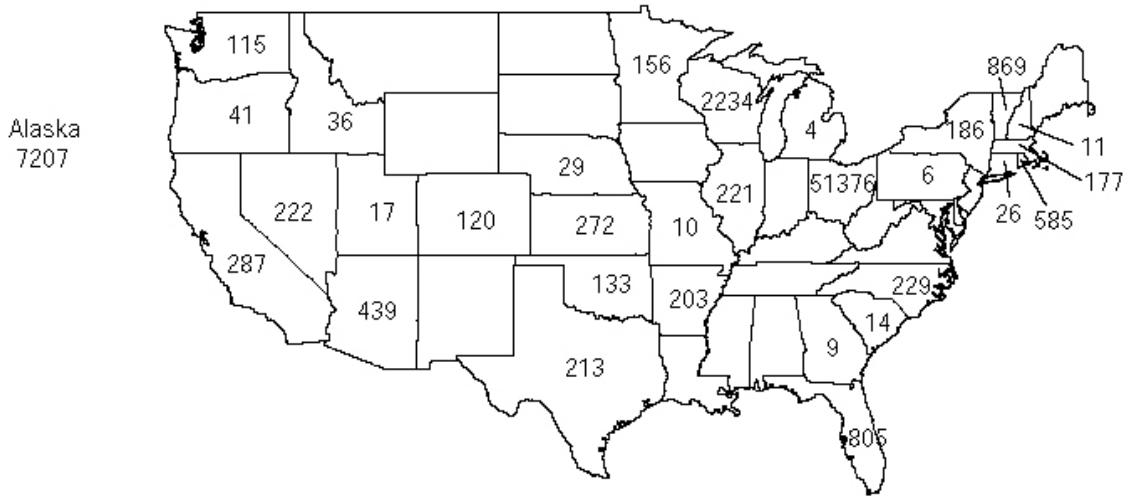

Figure 3.1 Number of valid blower-door measurements from each state.

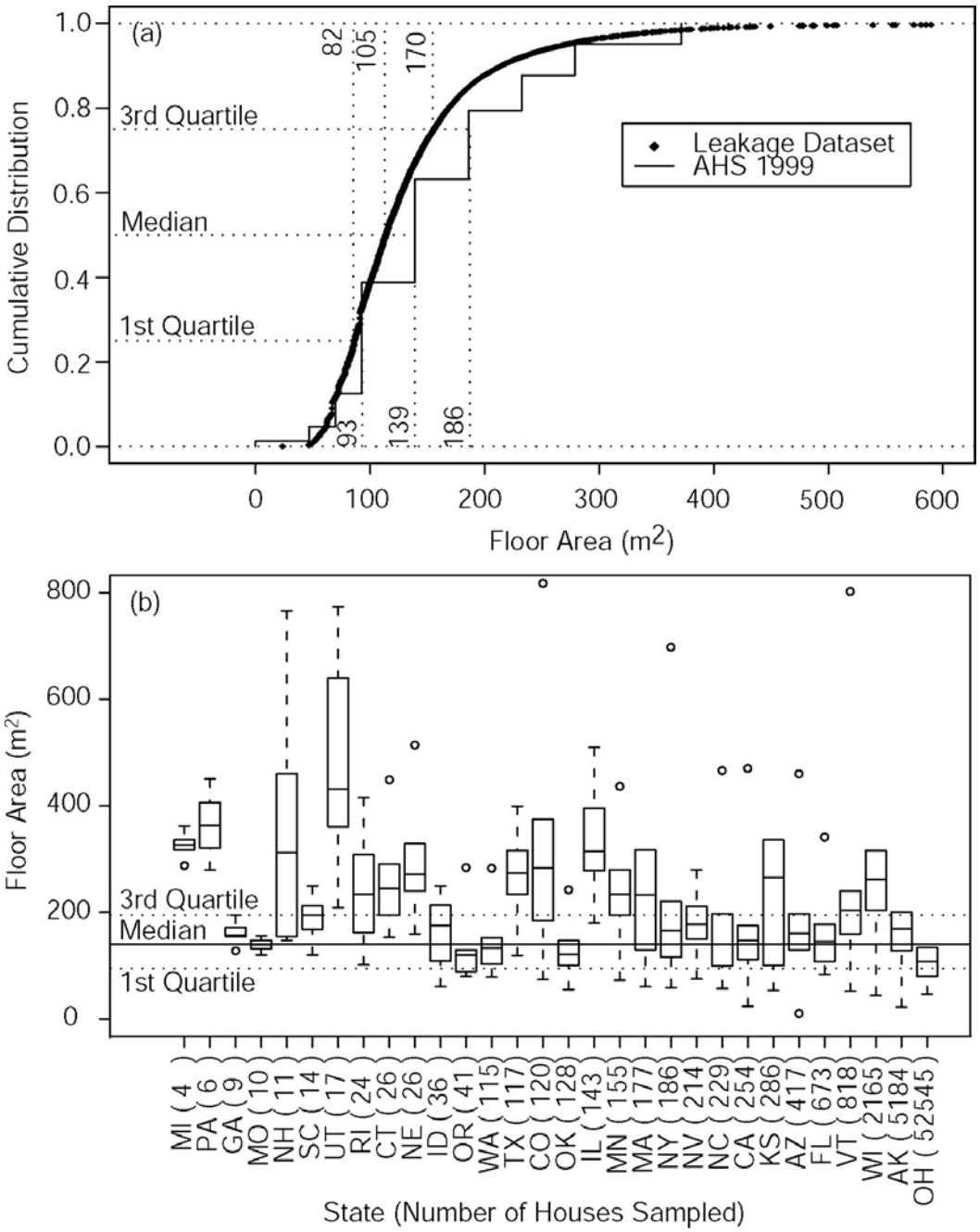

Figure 3.2 (a) Comparison of the cumulative distribution function of the floor area of houses in the leakage database to the 1999 American Housing Survey (AHS; US HUD, 2000). Highlighted for each distribution are the 1st and 3rd quartiles (i.e., 25th and 75th percentiles), and the median. (b) Floor area of houses in the air leakage database grouped by number of measurements taken in each state. The solid line represents the median floor area from the 1999 AHS, and the two dotted lines indicate the 1st and 3rd quartiles. In parentheses are the numbers of data points collected from each state.

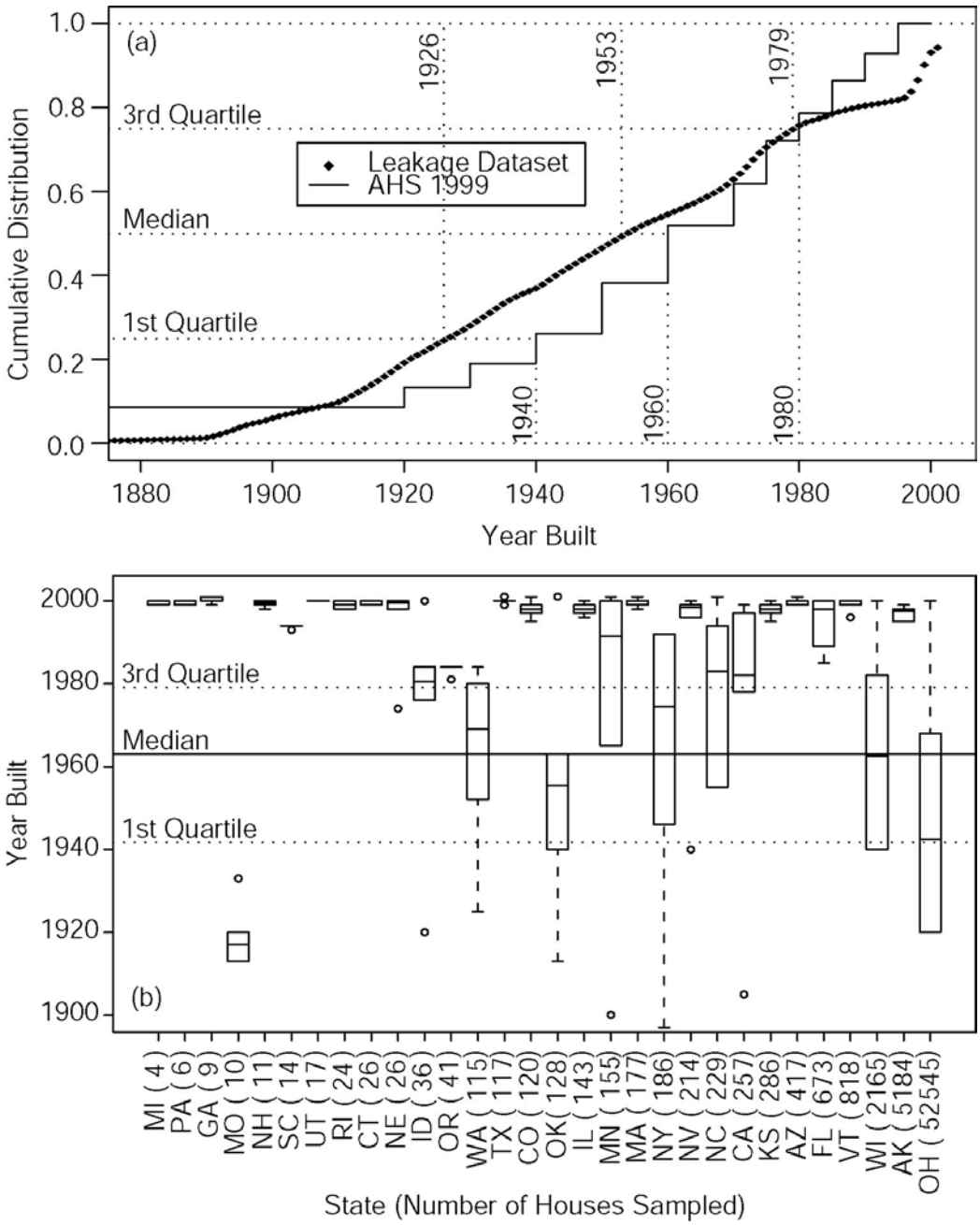

Figure 3.3 (a) Comparison of the cumulative distribution function of the year built of houses in the leakage database to the American Housing Survey (AHS; US HUD, 2000). Highlighted for each distribution are the 1st and 3rd quartiles (i.e., 25th and 75th percentiles), and the median. (b) Year built of houses in the air leakage database grouped by number of measurements taken in each state. The solid line indicates the median year built from the 1999 AHS, and the two dotted lines represent the 1st and 3rd quartiles. In parentheses are the number of data points collected from each state.

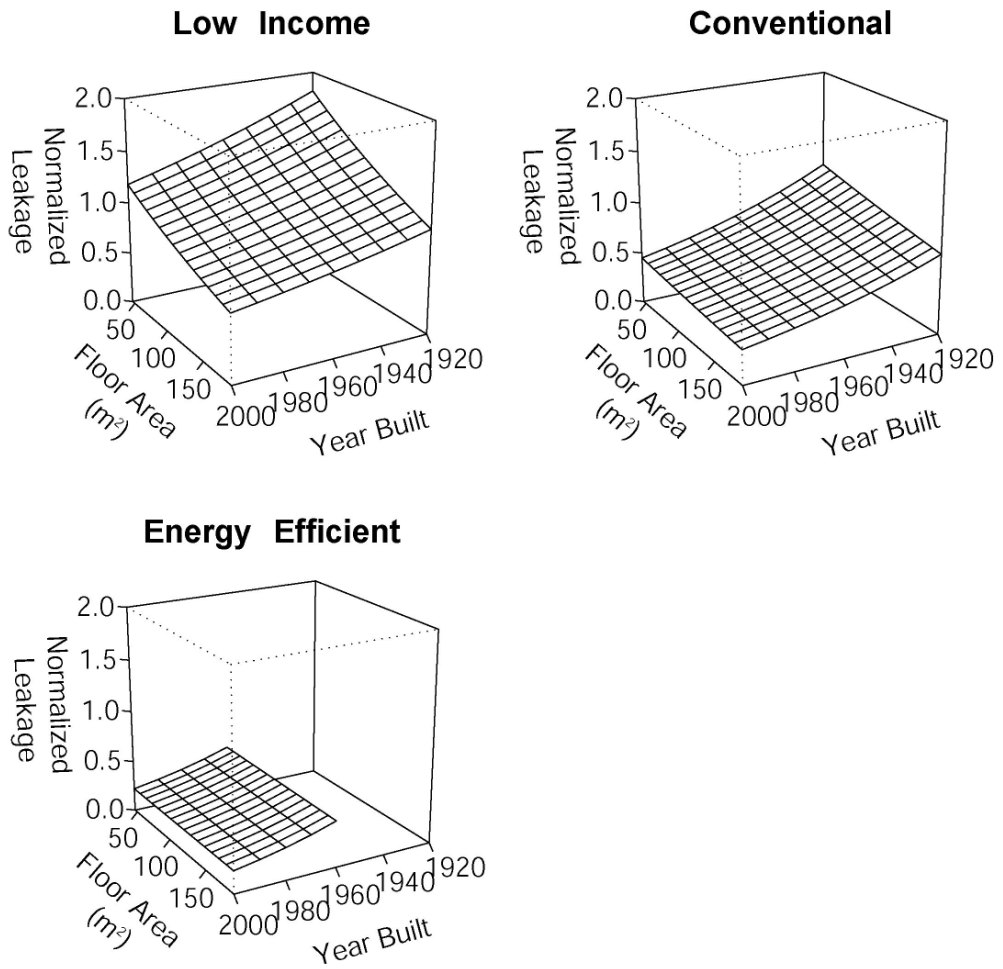

Figure 3.4 Effects of year built and floor area on normalized leakage, based on multiple linear regression models described in Table 3.2. Plotted results (y-axis) are the predicted geometric mean of normalized leakage in each case.

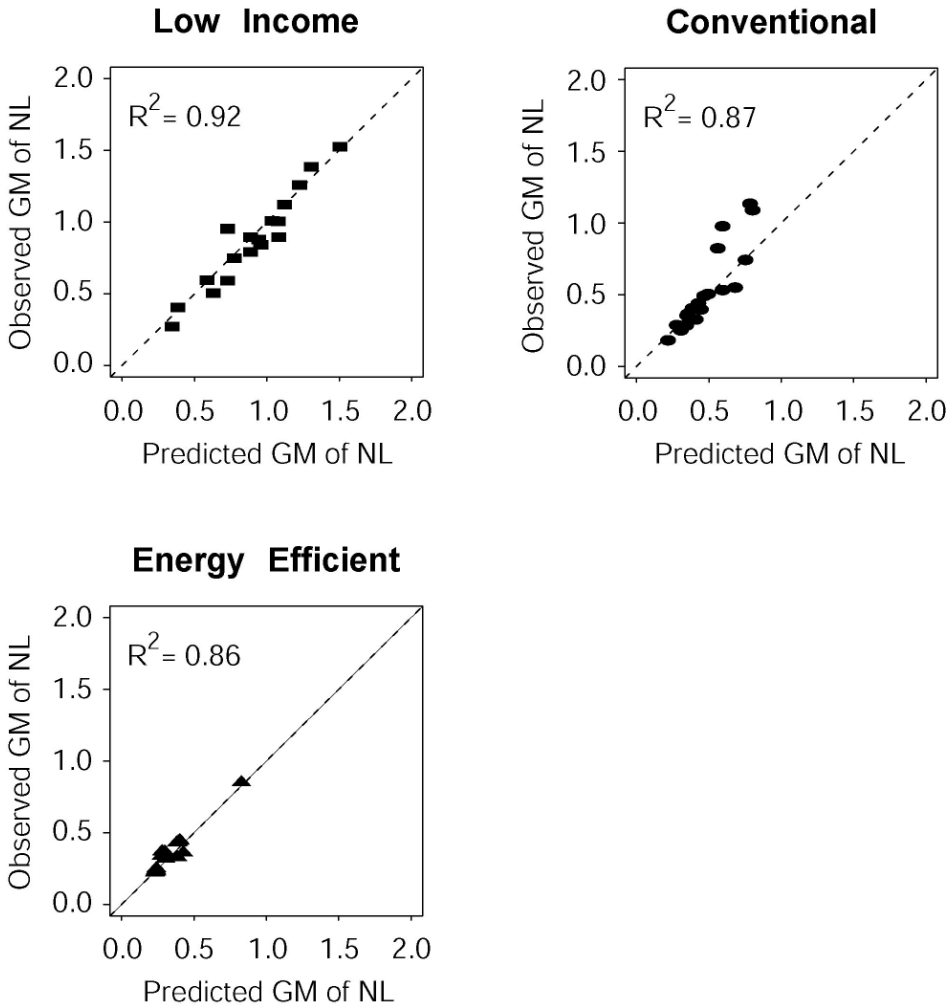

Figure 3.5 Scatter plots of the observed geometric mean (GM) of normalized leakage (NL) as categorized by year built, floor area, and house type, against the predicted values based on multiple linear regression models described in Table 3.2. The high R^2 values shown here indicate that the regression model describes the deterministic relationship between NL and the housing characteristics quite well. However, even among houses with similar characteristics, the variability in NL remains large. Because of this inherently large variability that cannot be explained by the differences in housing characteristics alone, the R^2 values shown in Table 3.2 are much lower.

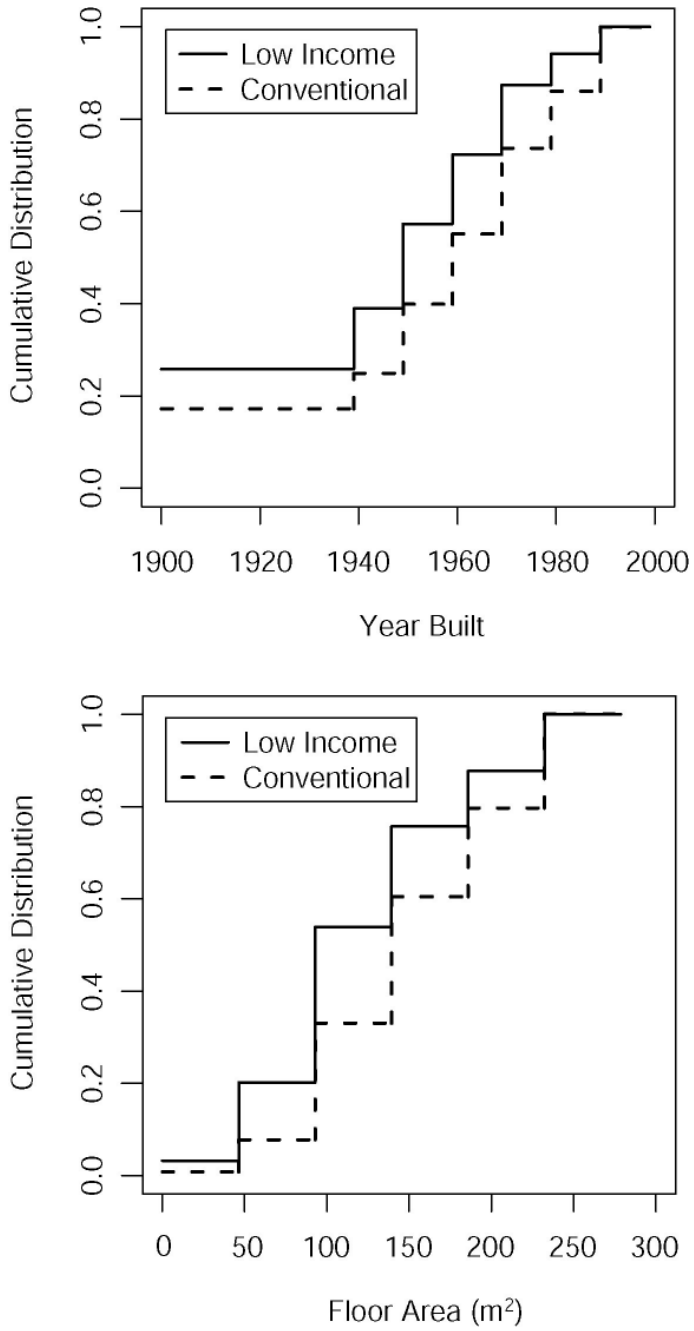

Figure 3.6 Estimated distribution of year built and floor area of low income and conventional houses based on the 1999 American Housing Survey (US HUD, 2000).

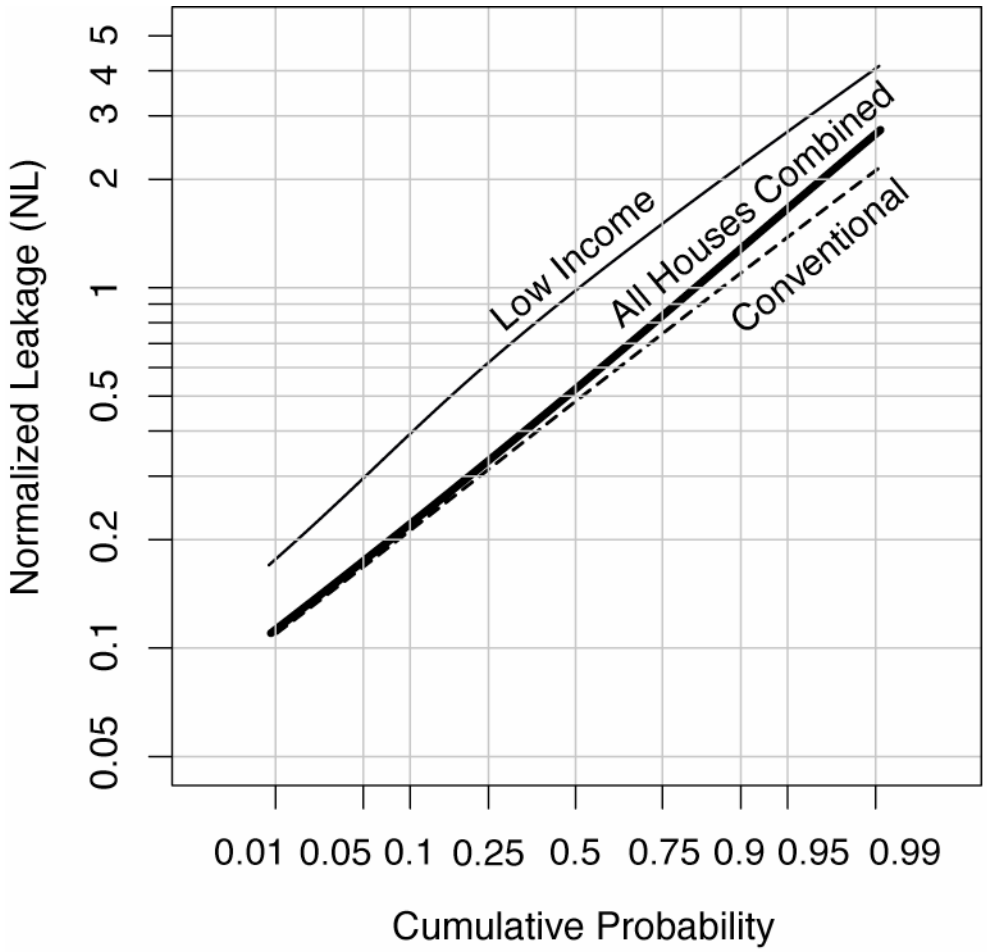

Figure 3.7 Estimated US nationwide distribution of normalized leakage for low income and conventional single-family houses, and their composite. Characteristics of the housing stock are based on the 1999 American Housing Survey (US HUD, 2000).

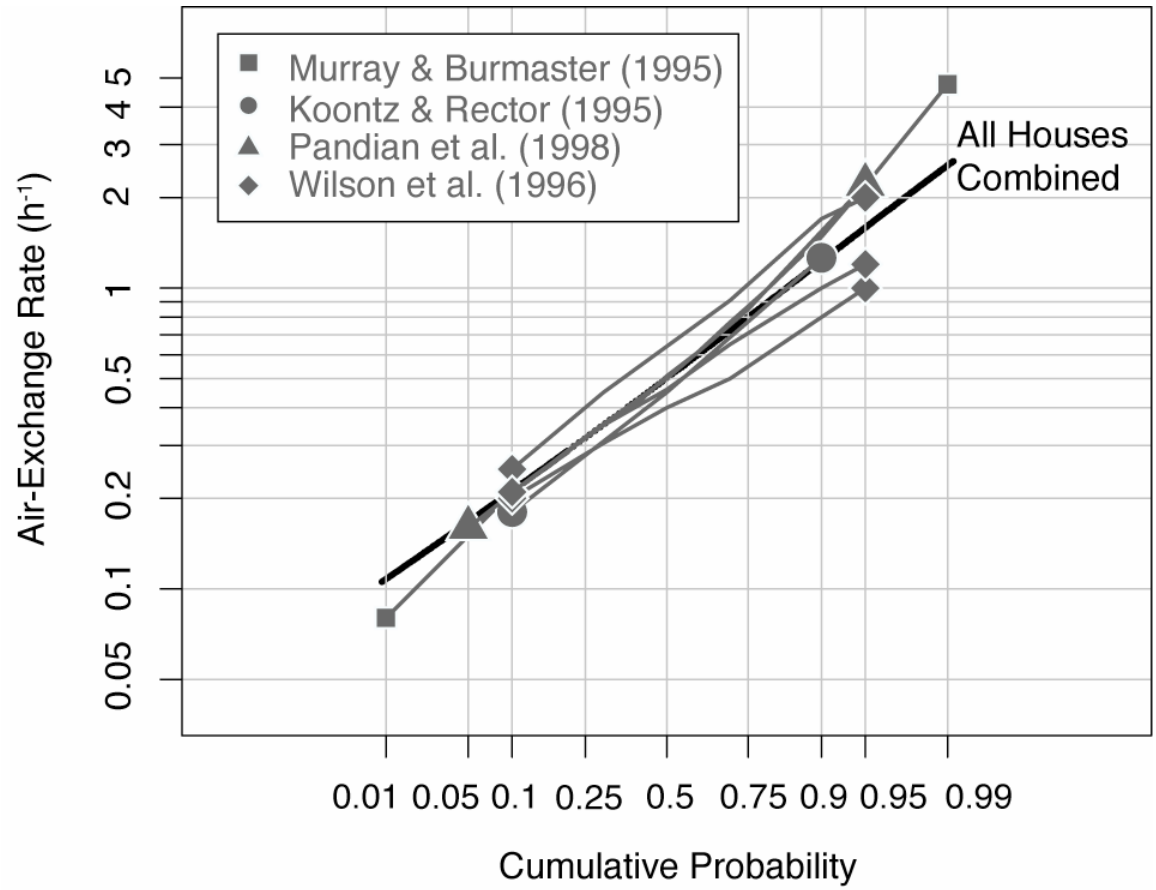

Figure 3.8 Comparison of best-fit air-exchange rates estimated from linear regression models obtained in this analysis, and values found in EPA Exposure Factors Handbook (US EPA, 1997). The distributions reported by Pandian et al. (1998) are inclusive of all the studies listed. In Wilson et al. (1996) all residences measured are located in California (3 distributions are shown: measurements from Los Angeles being most leaky, followed by San Diego and Northern California). The other references analyze collections of multiple projects. Koontz and Rector (1995) assigned weights to the results to compensate for geographic imbalance of measurements. Murray and Burmaster (1995) presented results as functions of weather using the degree-day metric.

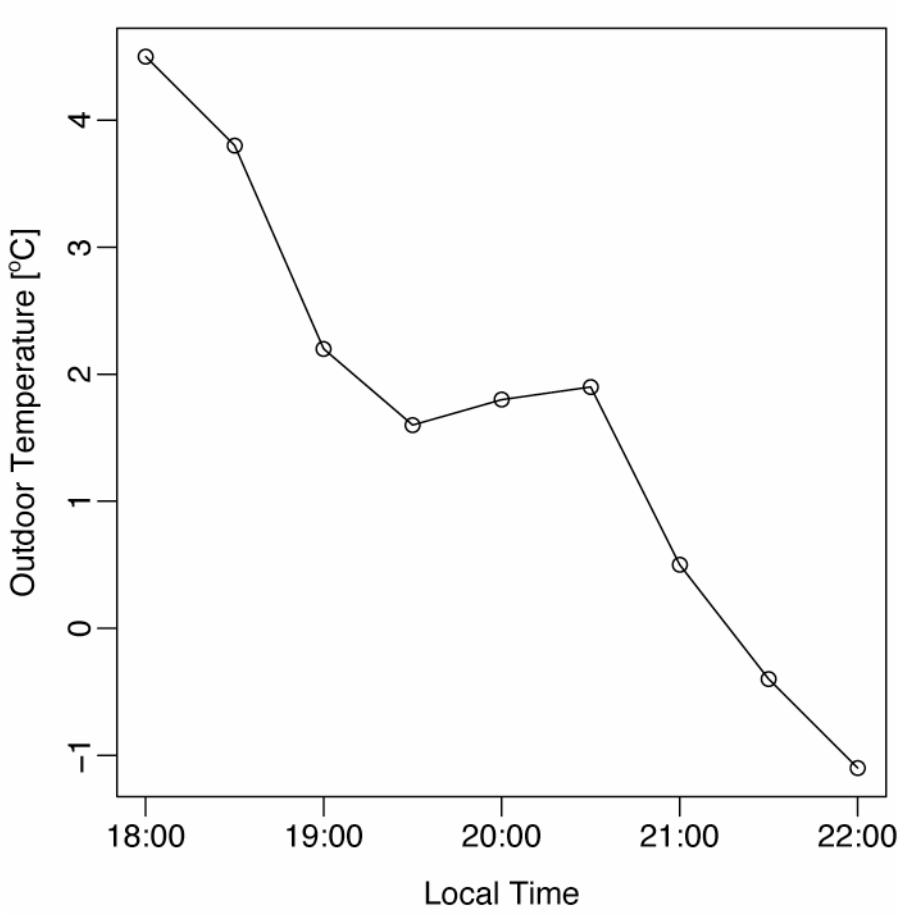

Figure 3.9 Outdoor temperature time profile in Albuquerque, NM dated February 24, 2003 at the time of the simulated hypothetical release.

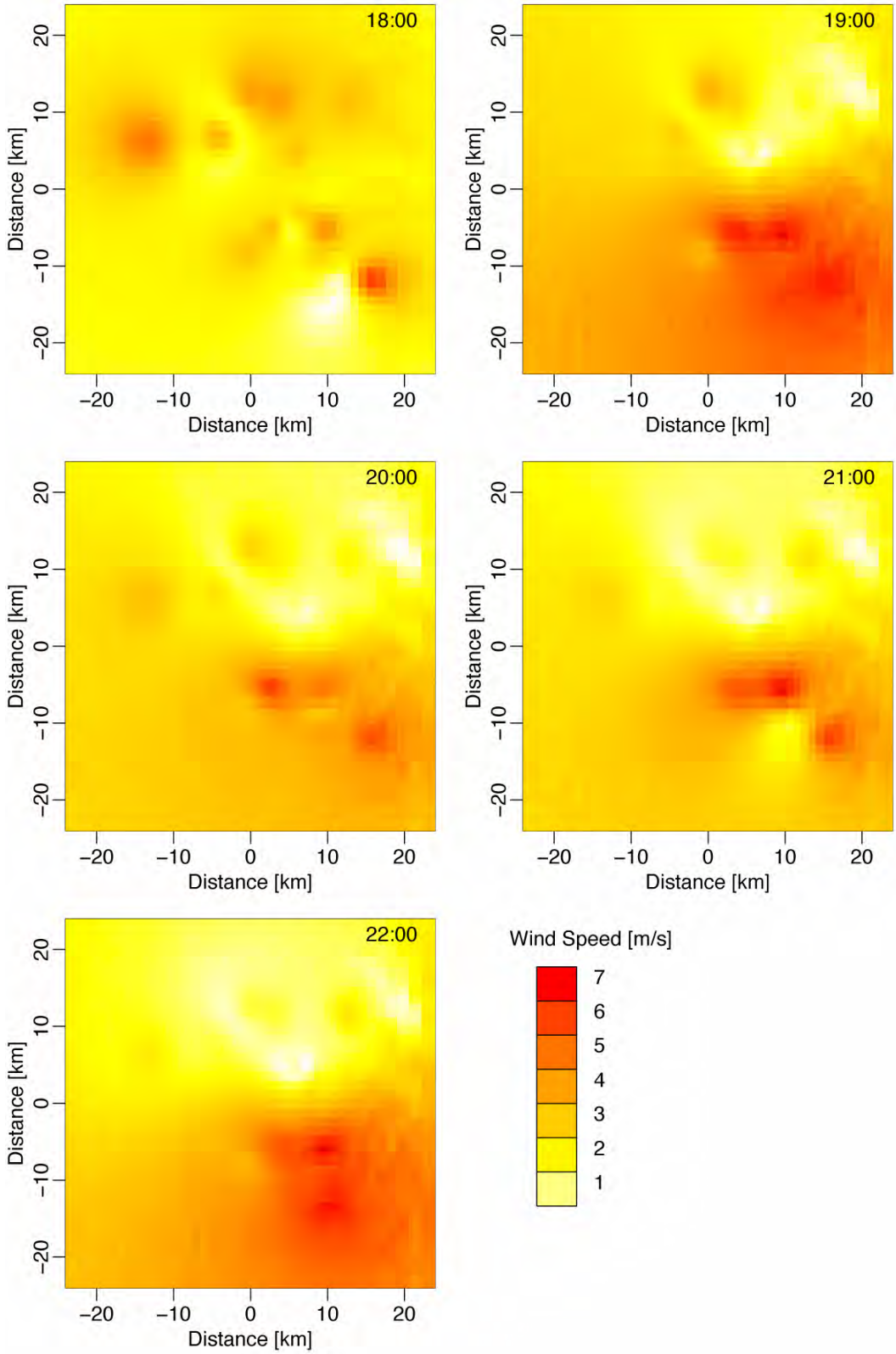

Figure 3.10 Wind speed estimated at 10 m height in Albuquerque, NM dated February 24, 2003 at the time of the simulated hypothetical release.

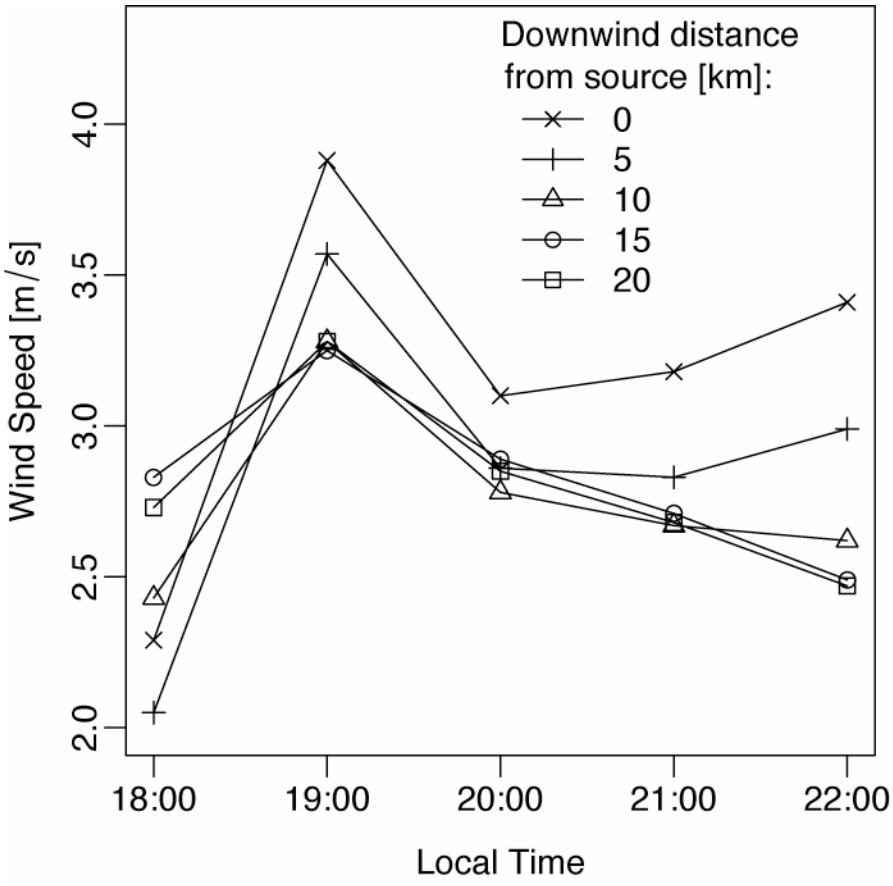

Figure 3.11 Wind speed estimated at 10 m height at various downwind distances from the release source. All five locations are aligned along the same predominant wind direction as the advecting plume.

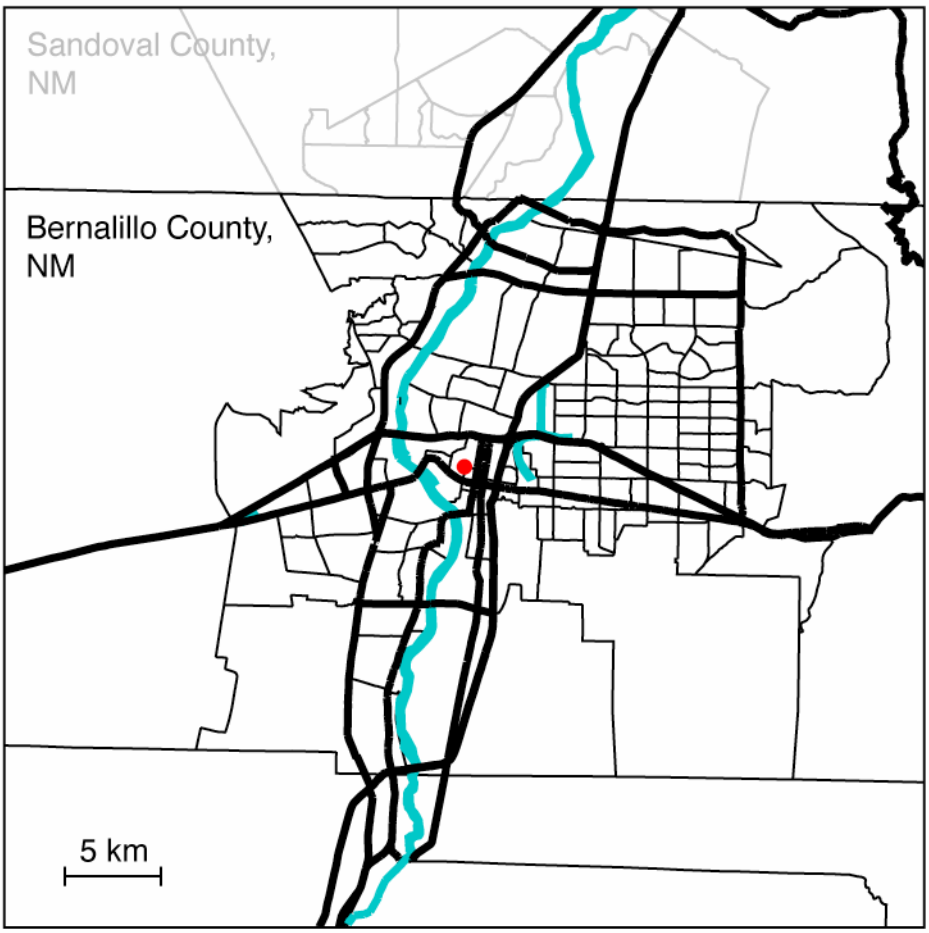

Figure 3.12 Map of Albuquerque, NM, illustrating the census tract boundaries in Bernalillo County, and the release location (red circle). Heavy lines represent are the main roadways and river that run through the city.

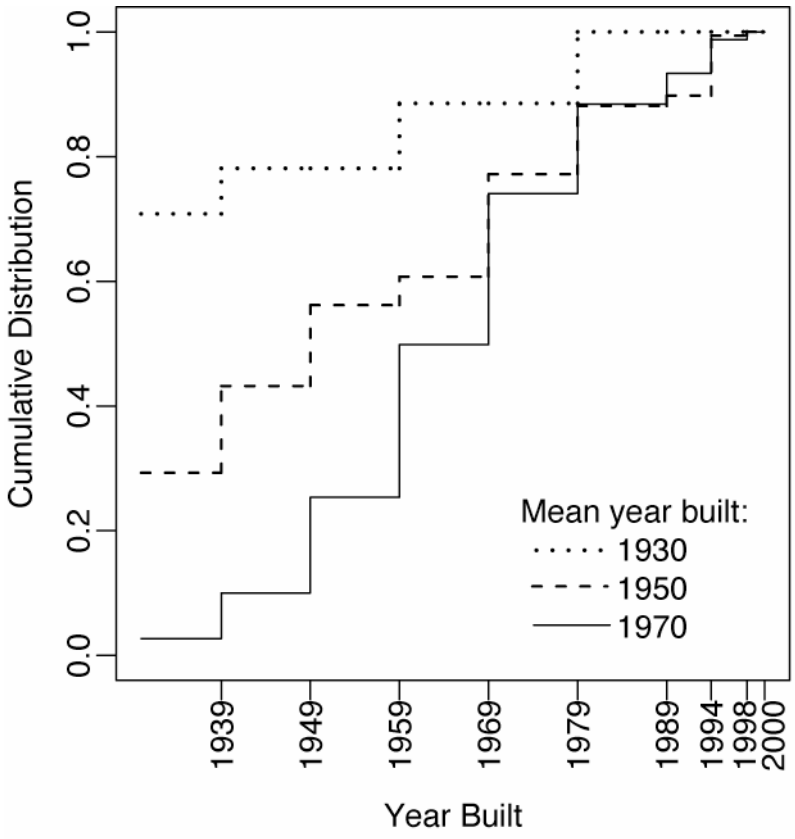

Figure 3.13 Distributions of house year built in 3 census tracts close to the release source. Each discrete curve represents the fraction of single-family detached units built before the corresponding year. These census tracts are selected by their mean year built to represent the oldest (~1930), the newest (~1970), and a median (~1950) group of houses among the 11 census tracts that are most affected by the hypothetical toxic release.

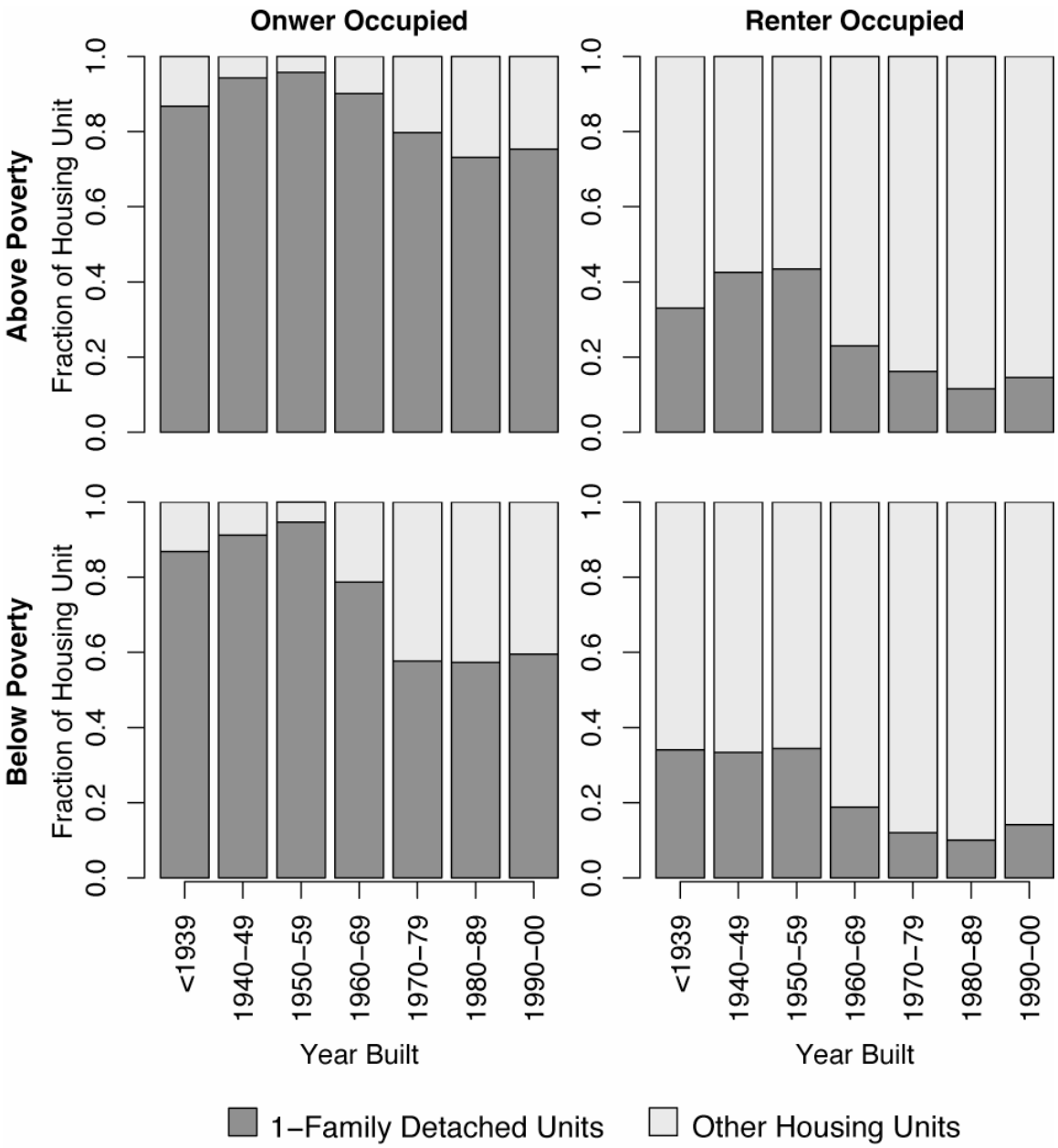

Figure 3.14 Fraction of US housing units that are single-family detached units versus other types according to national data from the American Housing Survey (AHS). These fractions are presented as a function of their tenure and household income levels: occupied by owners that are above and below poverty levels, and occupied by renters that are above and below poverty levels. See Table 3.7 for the numerical values of these fractions presented here.

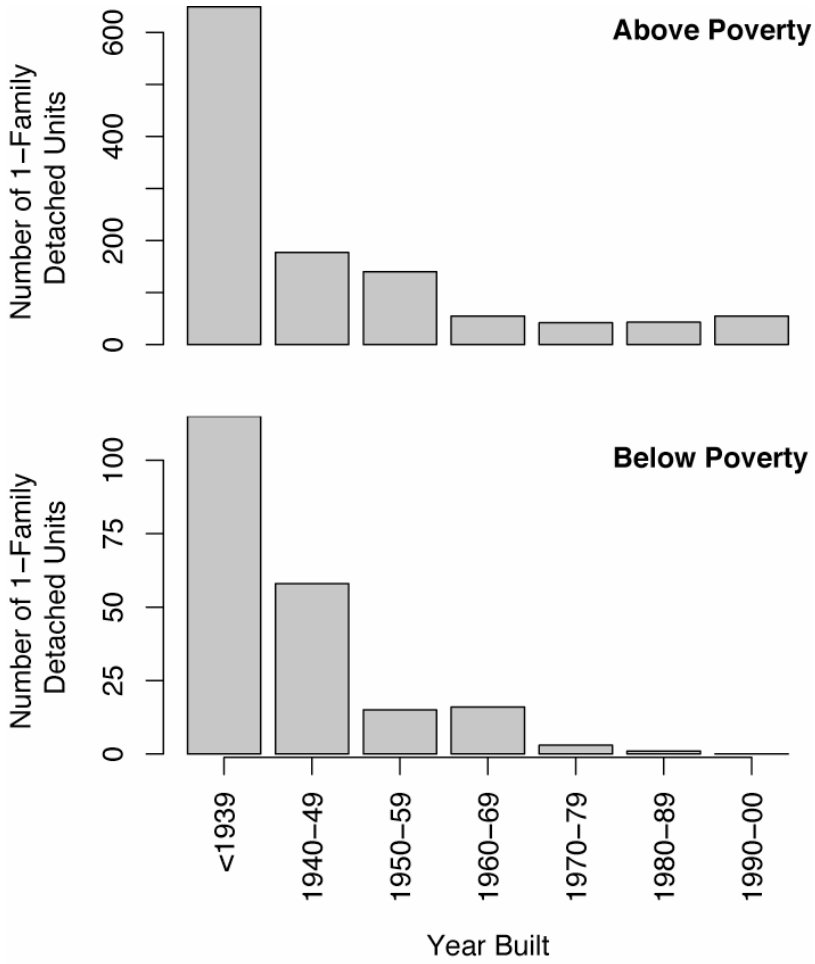

Figure 3.15 Predicted house year-built distribution for single-family detached units in census tract 2700 in Albuquerque, NM.

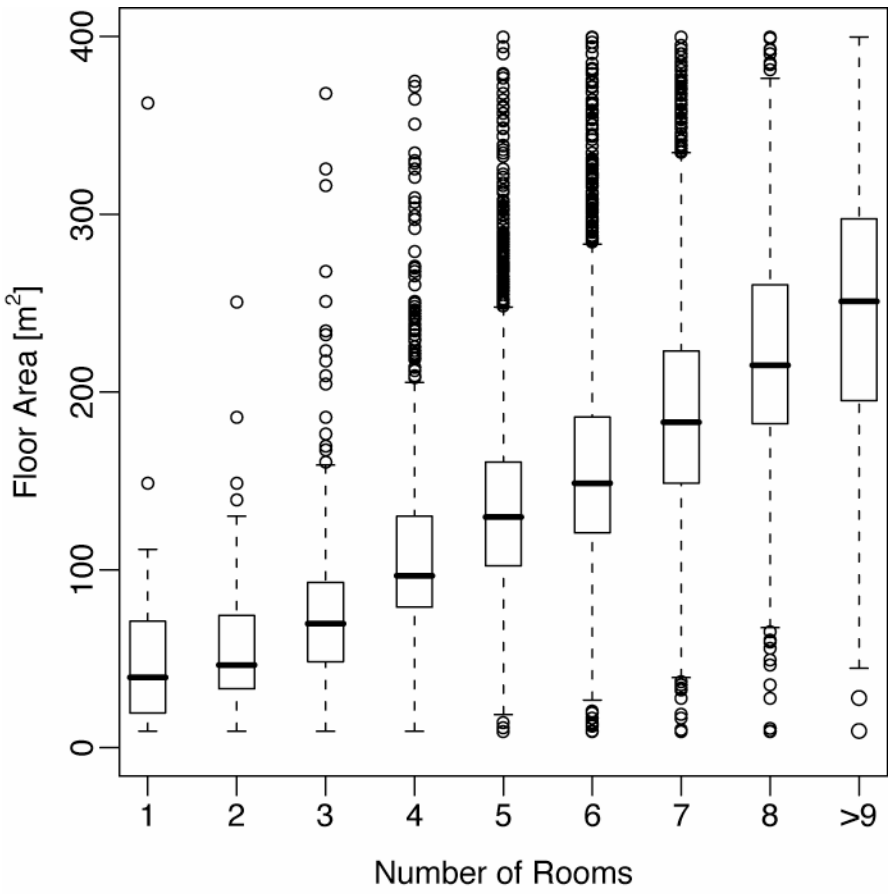

Figure 3.16 Relationship between the number of rooms and house floor area of the 27,400 single-family detached units investigated by the American Housing Survey. Each box-and-whisker plot shows the lower and upper quartile (box) of the floor area among the houses with certain number of rooms. The whiskers extend to include houses with floor area within 1.5 times the inter-quartile range. Houses with floor area more extreme than this range are plotted as open circles.

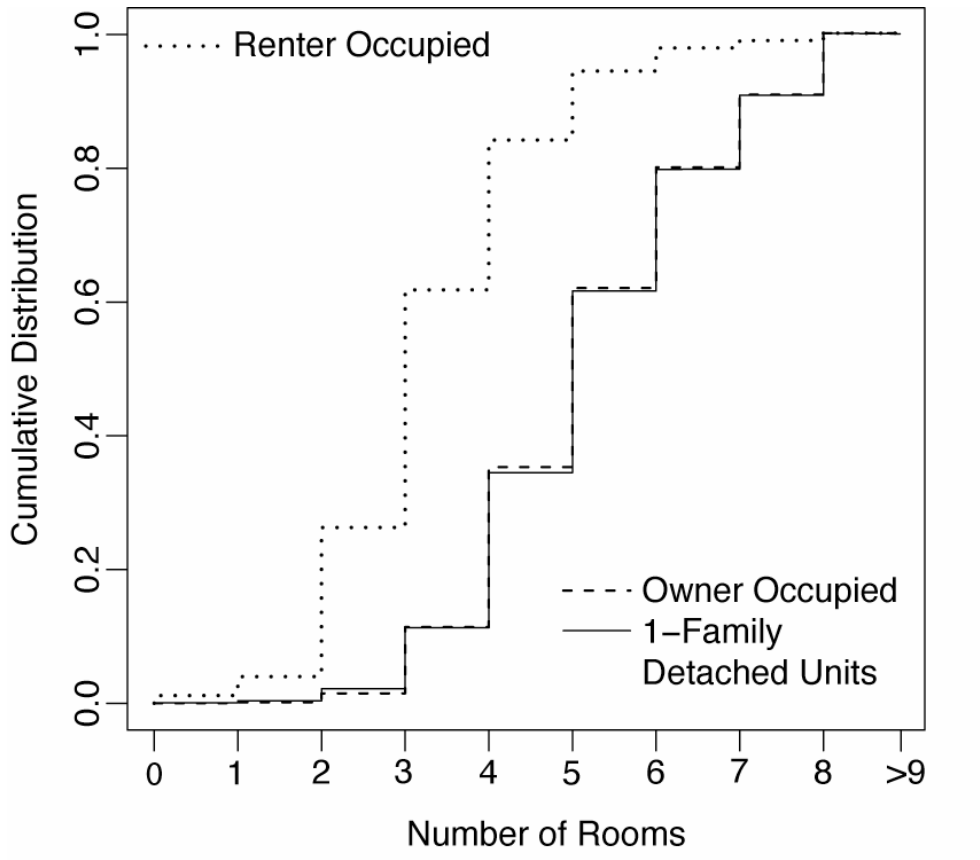

Figure 3.17 Cumulative distribution of number of rooms in renter and owner occupied housing units, as well as single-family detached units assessed by the American Housing Survey.

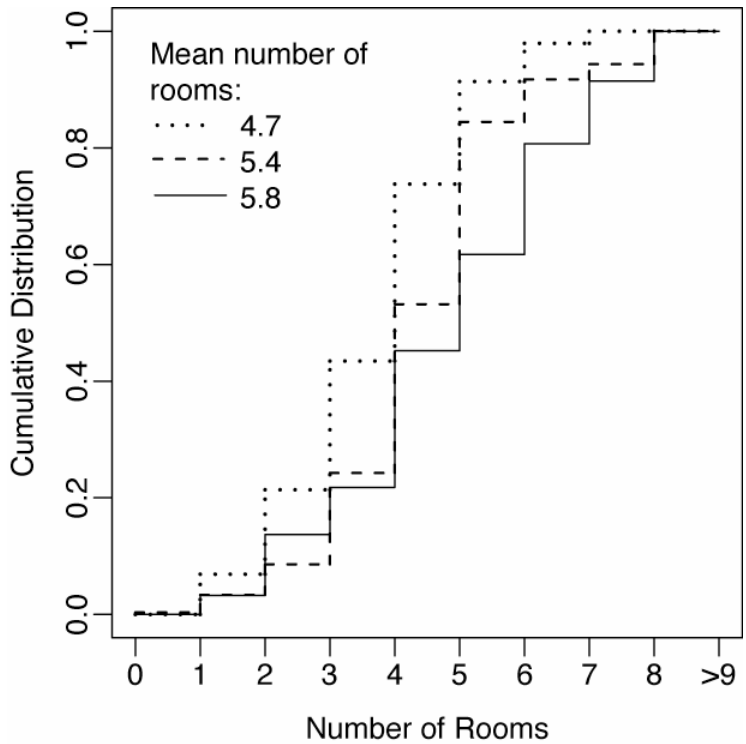

Figure 3.18 Distribution of number of rooms in owner-occupied housing units located in 3 census tracts close to the hypothetical release site in Albuquerque, NM.

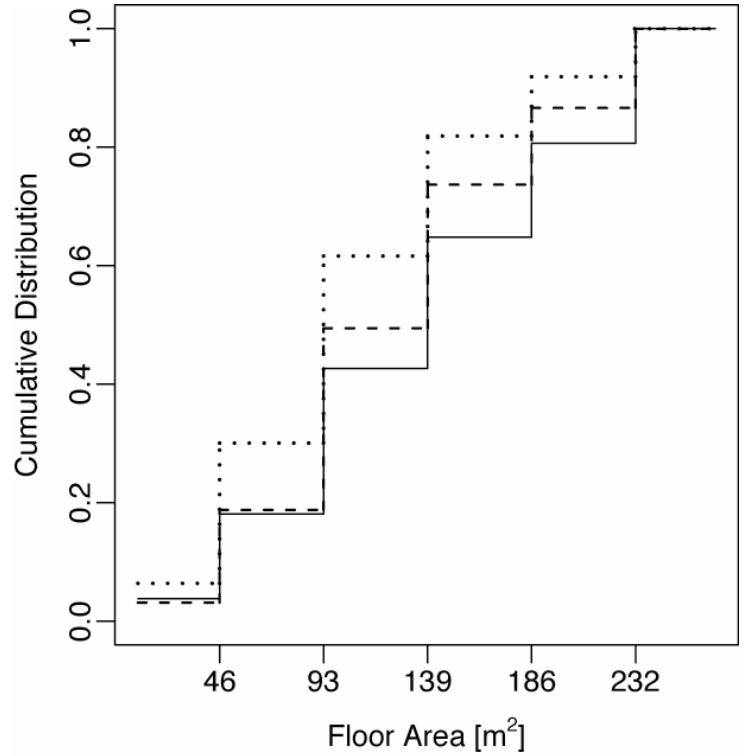

Figure 3.19 Estimated floor area distribution of single-family detached units for the same 3 census tracts in Albuquerque, NM, as shown in Figure 3.18.

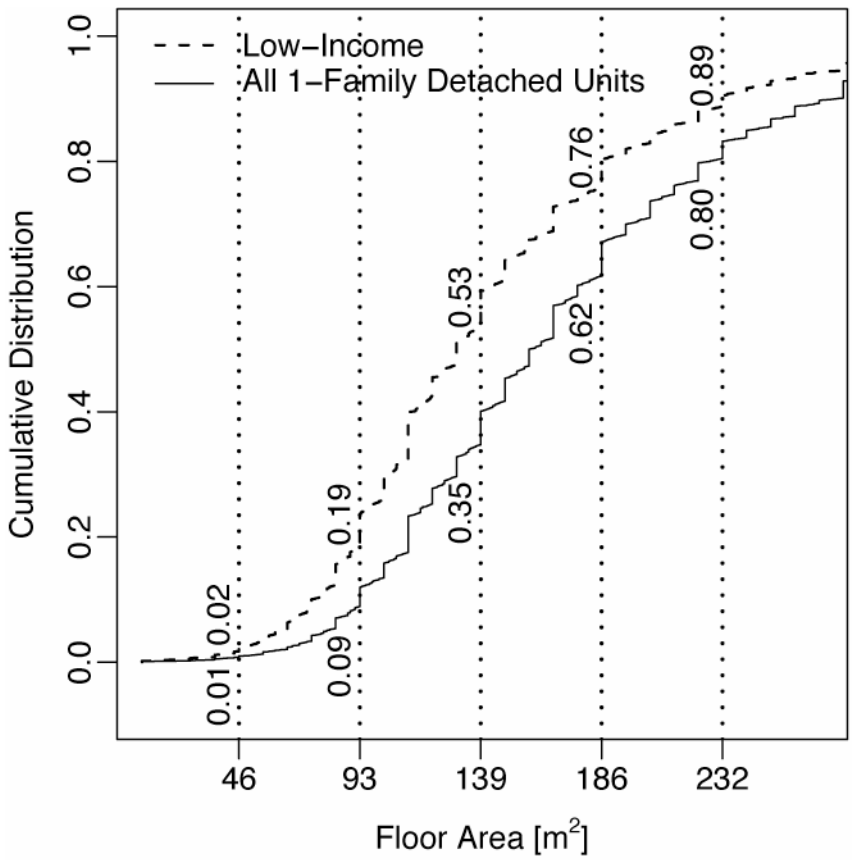

Figure 3.20 Cumulative floor area distributions of single-family detached units and those that are classified as low-income as surveyed by the American Housing Survey (AHS). Households are classified as low-income when the occupants' reported income is below 125% of the poverty guidelines, which is the same classification used by low-income weatherization program in the air leakage database. The numbers labeled on the plot represent the fractions of houses that have less than the corresponding floor area. For example, 89% of low-income single-family detached units have floor area less than 232 m^2 (or 2500 ft^2).

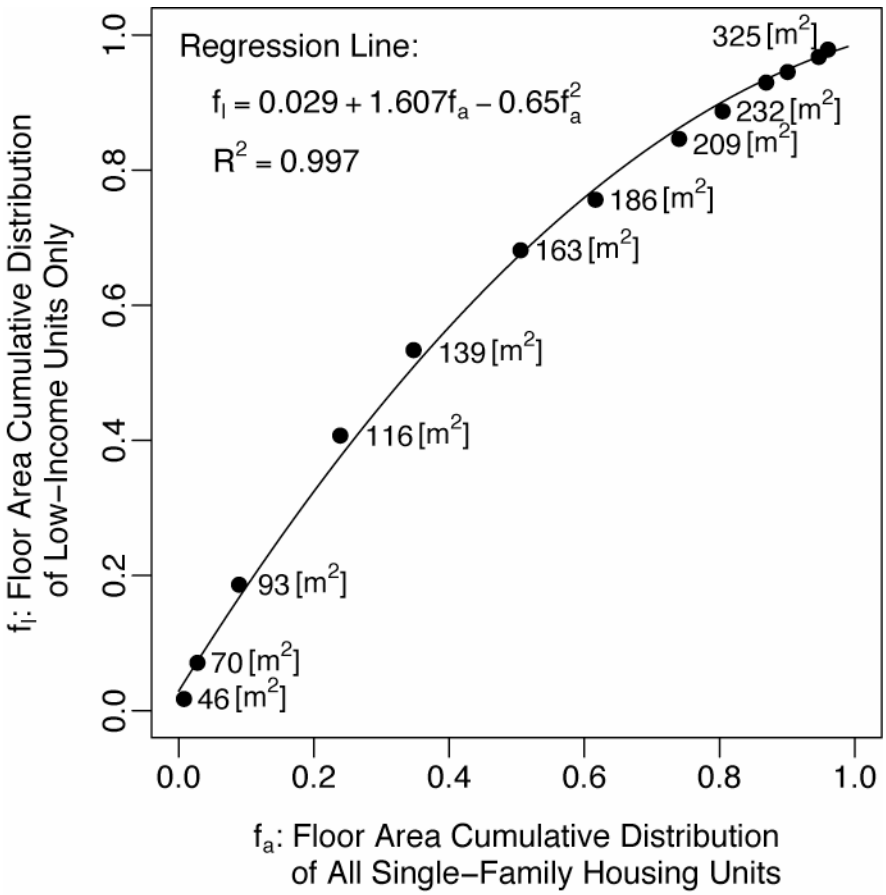

Figure 3.21 Relationship between the floor area cumulative distributions of all single-family detached units (f_a) and that of the low-income subgroup (f_l). The floor area cumulative distributions, as shown in Figure 3.20, of both sets of housing units are evaluated between 500 m^2 and 3500 m^2 at every 250-m^2 interval. The best-fit regression line shows good empirical fit to the relationship between f_a and f_l by using a second order polynomial.

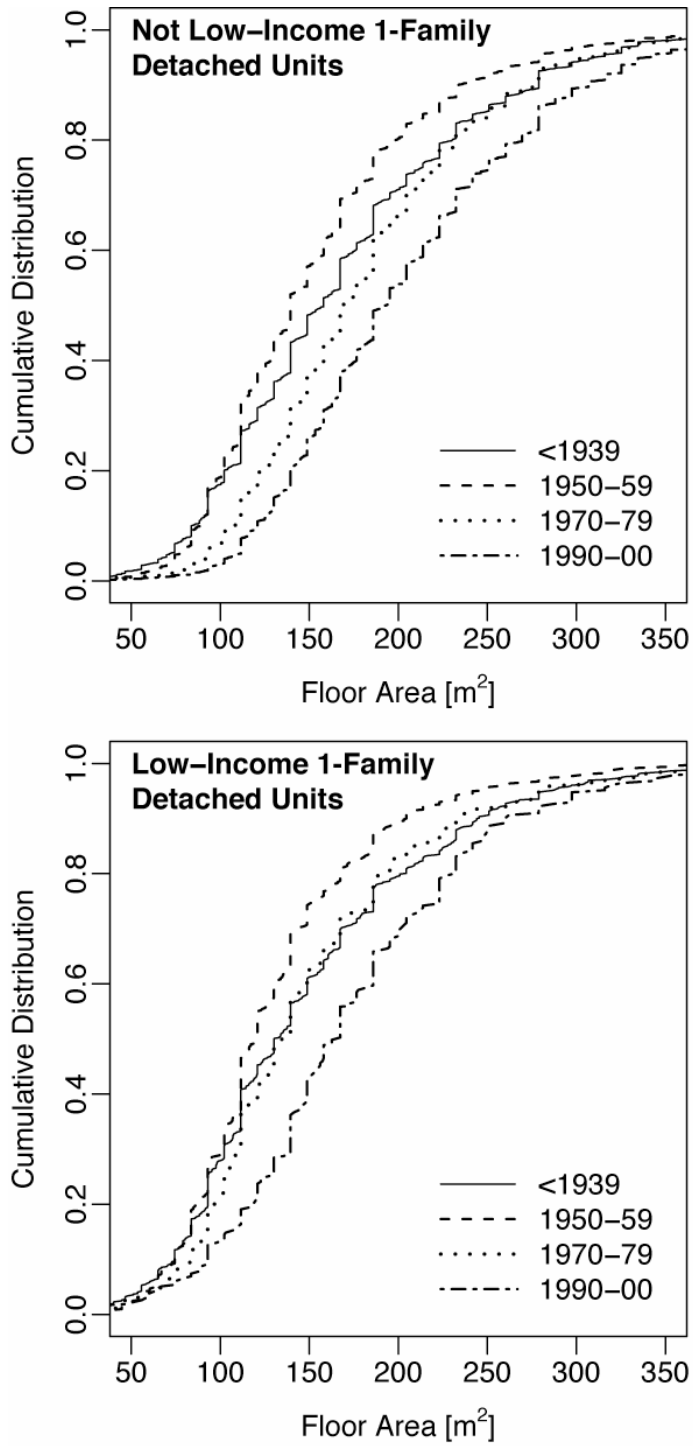

Figure 3.22 Floor area cumulative distributions of single-family detached units that were built in four different time periods. These cumulative distributions are based on analysis of the national data in the American Housing Survey (AHS). The upper plot contains only houses that are occupied by not low-income households. The lower plot contains only houses that are occupied by low-income households. These curves show a trend of increasing house floor area with more recent construction, except for houses that were built in 1950's, which appear to be the smallest in floor area.

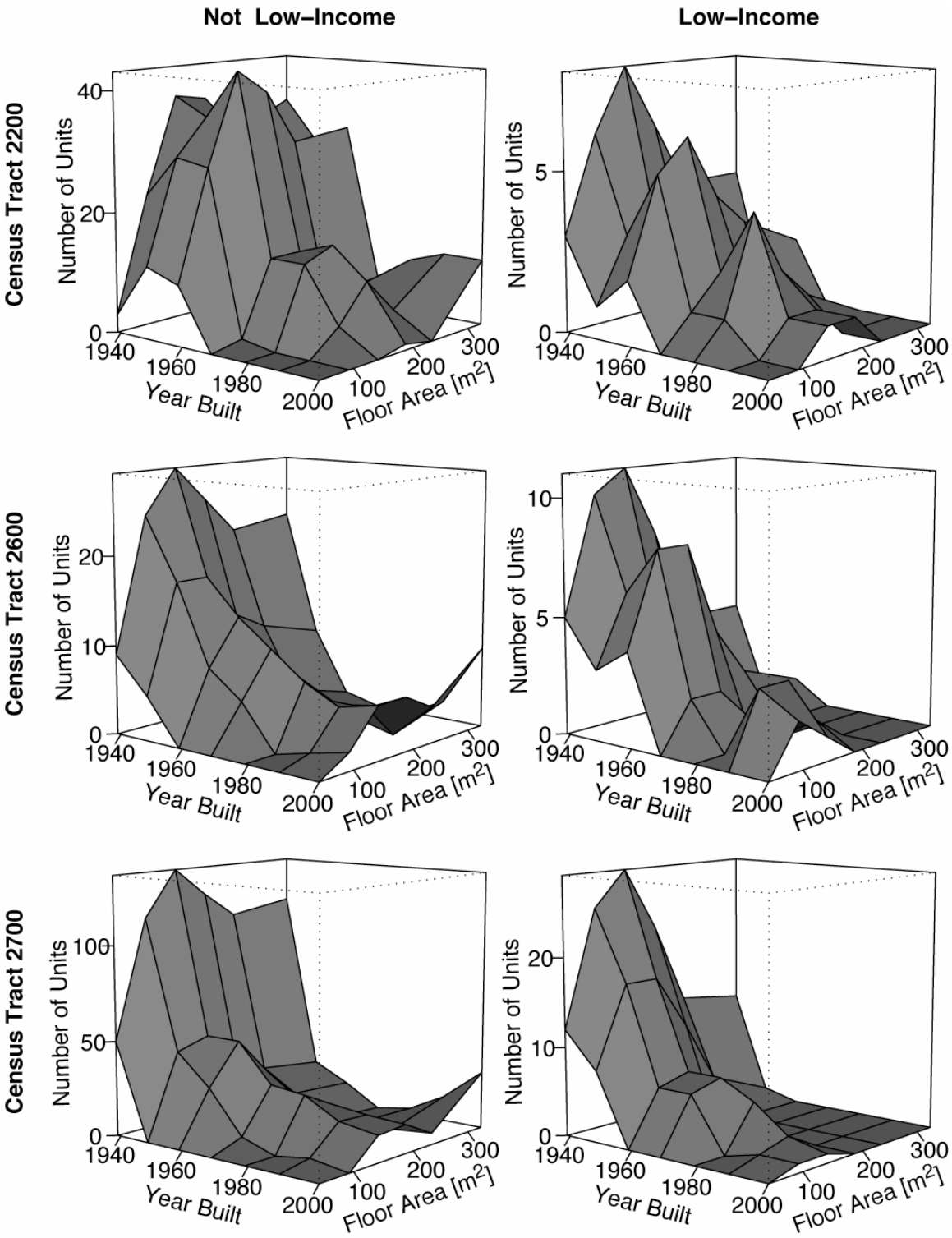

Figure 3.23 Predicted house year built and floor area joint distributions of not low-income (left column) and low-income (right column) single-family detached units located in three census tracts close to the hypothetical release site in Albuquerque, NM.

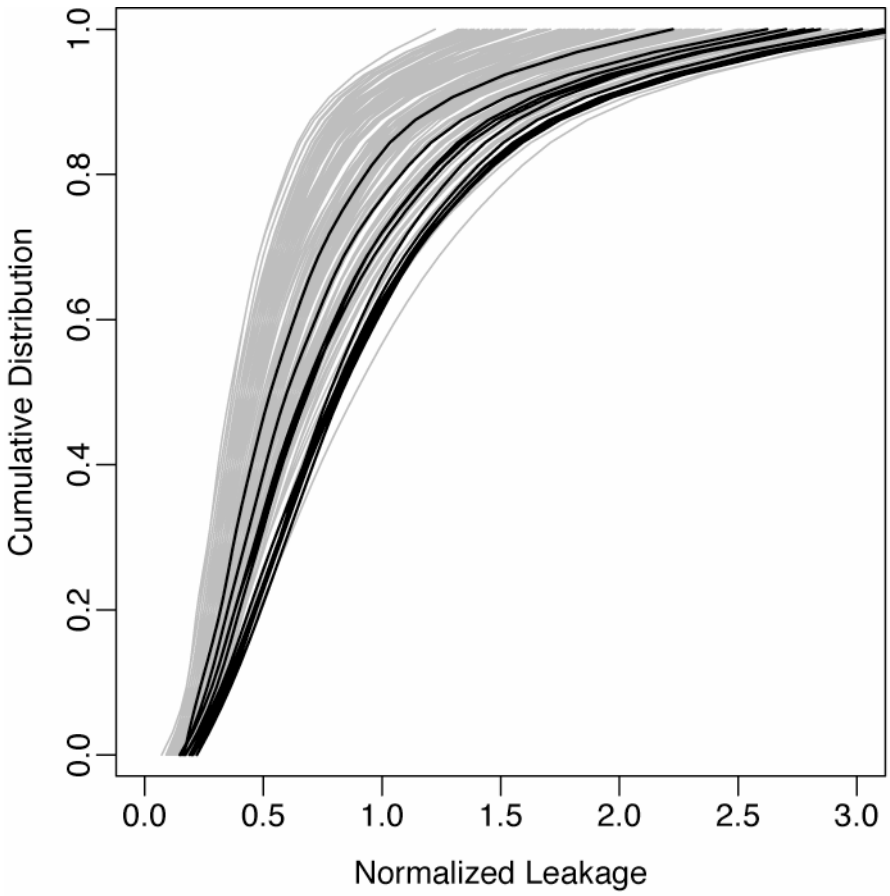

Figure 3.24 Predicted normalized leakage distribution of houses in Bernalillo County of Albuquerque. Each line represents the cumulative distribution predicted for the houses in a census tract. There are 141 census tracts in this county. Highlighted in black lines are the 11 census tracts closest to the release source.

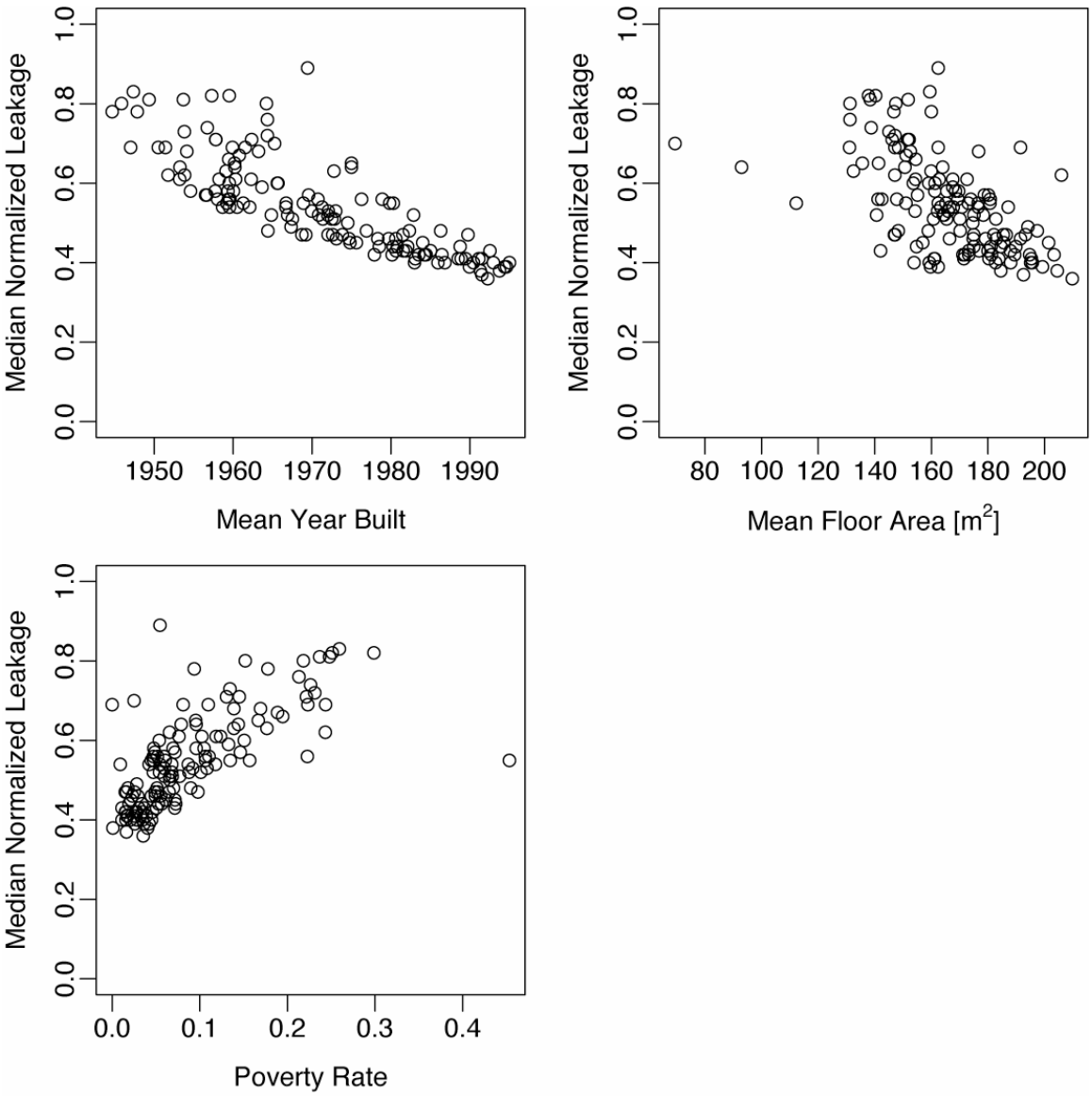

Figure 3.25 Predicted median normalized leakage of houses in a census tract plotted against three house characteristics: (1) mean year built, (2), mean floor area, and (3) poverty rate of households in the census tract. Each plot contains the results of 141 census tracts in Bernalillo County.

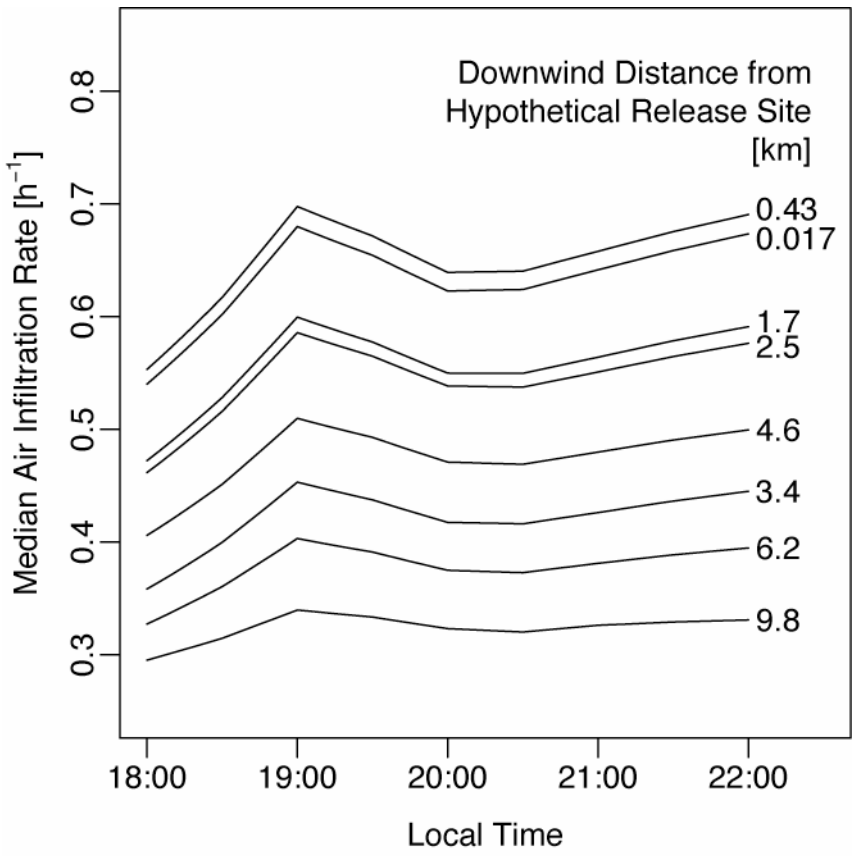

Figure 3.26 Predicted median air infiltration rates at various downwind distances from the release source. Each location falls into a different census tract with different mixes of houses, which explains the variation in the air infiltration rates predicted.

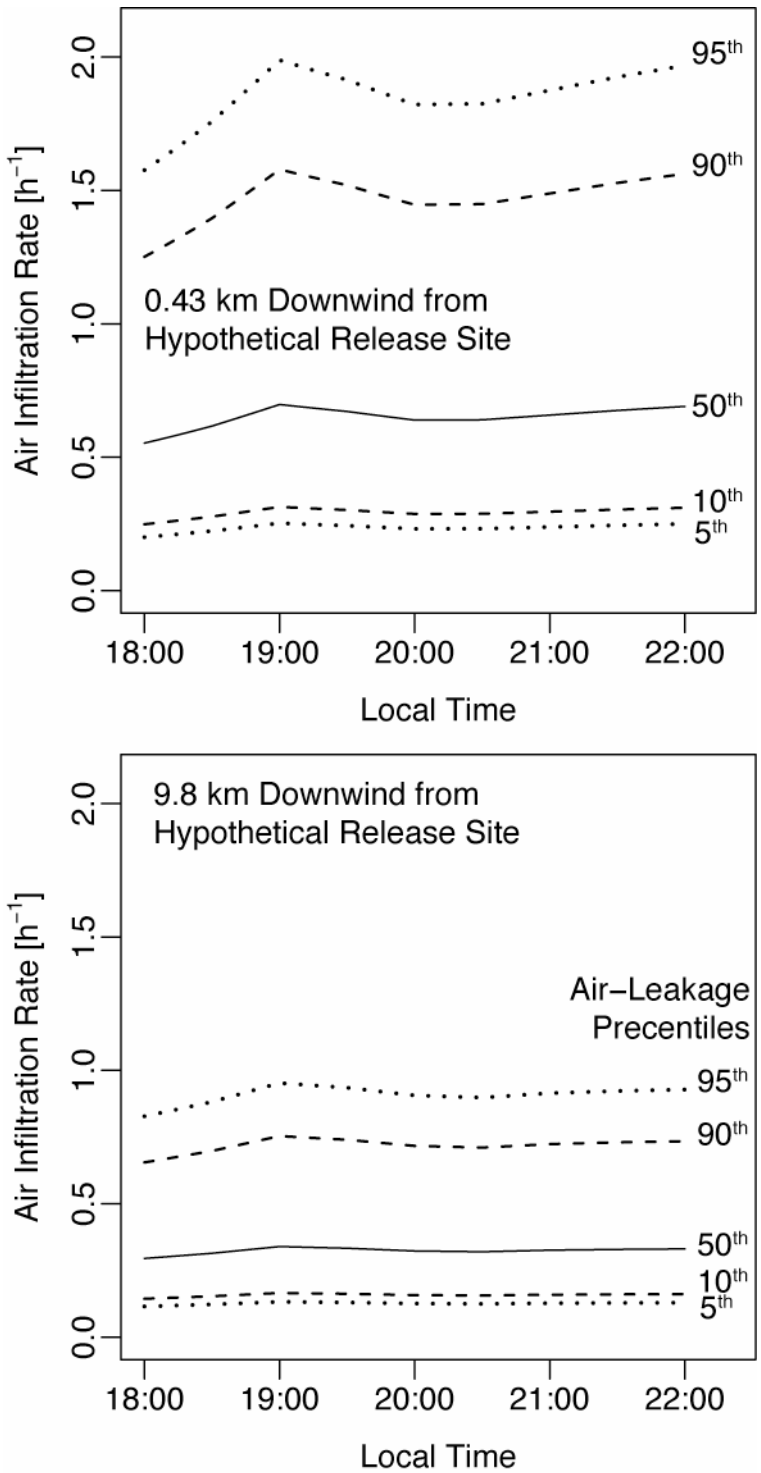

Figure 3.27 Predicted distribution of air infiltration rates at two downwind locations from the release source. The labeled percentiles refer to the fraction of houses that are predicted to have air infiltration rates equal to or less than the values plotted. For example, 95% of the houses located in the respective grid cells are expected to have air infiltration rates below the highest values predicted here.

4 Assessing Shelter-in-Place Effectiveness in a Residential Community

4.1 Introduction

Chapter 2 assessed shelter-in-place (SIP) effectiveness in a community of buildings using simple models. Hypothetical releases of various amount and duration were simulated under different meteorology. Some key parameters affecting SIP effectiveness were identified. Of foremost importance are the toxic load exponent of the chemical released and time-scale parameters, namely the release duration, the air-exchange rate of buildings, and the SIP termination time. Release amount and atmospheric dispersion affect the intensity and extent of the hazardous exposure, but these factors affect SIP effectiveness to a lesser degree. The analysis performed there assumed fixed air-exchange rates in a community. As demonstrated in Chapter 3, this assumption is not justified in practice. Not only is there considerable variability in building air-exchange rates in a community, the distribution might actually change over time in response to local meteorology, which drives air infiltration. Furthermore, in situations where the community is unaware of the outdoor release, natural or mechanical ventilation might induce additional air exchange with the outdoors in advance of SIP implementation. In the case of a long time delay between the time of release and when a community takes shelter, SIP effectiveness can be compromised by the pre-sheltering elevated air-exchange rates in houses.

The goal of this chapter is to assess SIP effectiveness in a residential community using more realistic models and parameters. As contrasted with the Gaussian model used in Chapter 2, outdoor concentrations are obtained from a more complex atmospheric dispersion model. Distributions of air infiltration rates obtained in Chapter 3 are used, which includes the variability in air leakage among dwellings and predictions using the LBL Infiltration Model. SIP termination time and delays in initiating SIP are investigated. One issue that has not been discussed in previous chapters is the interaction of chemicals with indoor surfaces. Many toxic chemicals can sorb onto indoor surfaces. In such cases, sheltering indoors has the added advantage that the peak indoor concentrations will be lowered. Several experimental studies on sorption of toxic chemicals are reviewed. Mathematical descriptions of the process are integrated into the mass balance that is used to model indoor concentrations.

The modeling approach taken here is deterministic instead of probabilistic sampling. Relatively large-scale release scenarios are modeled such that the affected population is large enough to allow for some averaging in factors that are inherently probabilistic. This analysis only encompasses releases taking placed at one location, the city of Albuquerque, NM, under one set of meteorological conditions. Inevitably, some aspects of the results are case specific. However, many of the findings discussed here should apply to other residential communities taking shelter from large-scale outdoor releases.

There have been a few experimental studies on the performance of some forms of proactive measures to enhance SIP protectiveness. Some studies have investigated the

effectiveness of stand-alone air cleaners to actively remove toxic chemicals and particles from the air (Blewett and Arca, 1999; Ward et al., 2005). Others measured the effectiveness of using duct tape and plastic sheets to reduce the air-exchange rate with the outdoors (Sorensen and Vogt, 2001; Jetter and Whitfield, 2005). Strategies such as these might be effective, but results are likely to vary in different scenarios and among houses. For example, high air-exchange rates diminish the relative effectiveness of portable air cleaners. The cost of purchasing and properly maintaining high efficiency portable air cleaners can also be substantial at the community scale. Proper sealing can reduce air exchange through the building envelope, but the time required to seal even a single room can be significant. For example, the average time to seal up a bathroom with duct tape and plastic sheets among 12 participants was found to be 35 minutes (Jetter and Whitfield, 2005). Unless advance notice is given to the public, it is unlikely that many would be able to complete the task before arrival of a toxic plume. The analyses presented in this chapter do not include the use of any of these devices or actions taken to enhance SIP effectiveness other than simply closing doors and windows, and turning off heating, cooling, and mechanical ventilation systems. The predicted SIP effectiveness should therefore be easily achievable in typical residences.

4.2 Methods

4.2.1 Albuquerque, NM – A Case Study

In this analysis, three hypothetical releases of different durations are modeled in Albuquerque, NM, using consistent meteorology conditions as determined for February

24, 2003 from 18:00 to 22:00 local time. This location was chosen because of the availability of outdoor plume predictions made by the National Atmospheric Release Advisory Center at Lawrence Livermore National Laboratory. The computer simulations were generated using an atmospheric dispersion model known as the Lagrangian Operation Dispersion Integrator (LODI). The model solves the 3-D advection-diffusion equation using a Lagrangian stochastic, Monte Carlo approach (Ermak and Nasstrom, 2000). LODI includes methods for simulating the processes of mean wind advection, turbulent diffusion, buoyant plume rise, and other pollutant dynamics such as first-order chemical reactions and wet and dry deposition. However, to keep the simulations independent of the chemical being modeled such that the same simulation outputs can be used to represent different hypothetical releases, pollutant dynamics are not included. As a result, outdoor concentrations are linear with respect to the release amount.

Figure 4.1 shows the predicted outdoor concentration of the hypothetical 2-h release sited just west of the downtown core of the city. The concentrations are 5-minute averaged values predicted at a grid cell resolution that varies from 34 m near the source to 1.8 km at the most distant location. The release source is modeled to occur at 5 m above ground to represent a slightly elevated point source (e.g. top of a tank car). The outdoor concentrations used in this analysis are all evaluated at 10 m height. The two other release durations modeled are 0.5-h and 1-h. The mass release rate is assumed to be constant throughout the release duration. In all cases, the outdoor concentrations were simulated for 4 h beginning from the start of the release.

The predominantly east wind causes the plume to pass through the western part of Albuquerque. Since the meteorology used is the same in all three cases, the outdoor concentrations per unit rate of emission duing the release is similar. However, as the wind direction rotated slightly (from northeast to east wind) during the first hour of the simulation, the concentration fields vary between the different release simulations at sites that are more downwind of the source. From the second hour of the simulation onwards, the plume is consistently blown towards the west. The outdoor concentrations vary by 3 to 4 orders of magnitude over a downwind distance of 10 km. The width of the plume remains fairly narrow (~2 km) within this distance.

The gray lines in the background of Figure 4.1 outline the boundaries of census tracts. The size of the census tract is inversely related to the residential population density in that tract. The last census tract on the west of the city is largely uninhabited, containing a national park and a municipal airport north of the interstate highway. In assessing the exposure of the population and the health consequences, the population density is assumed to be uniform within a census tract. Finer spatial resolution of residential population density is available from the US Census Survey, known as the census block group. Census block groups generally contain between 600 and 3000 people, which is roughly half the target size of census tracts. Using more spatially refined population data might affect the assessment of SIP effectiveness somewhat. For example, if the number of people exposed in areas with high contaminant concentration is relatively fewer, then the apparent SIP effectiveness measured in terms of casualty reduction with respect to the outdoors will increase. However, because the ratio of the targeted number of people in

census block groups to those in census tracts is only one-half, the change in the predicted SIP effectiveness with such improved spatial resolution is expected to be small.

The choice of using residential population density is reasonable if most people are at home at the time of the release. The release simulations considered here started at the end of a workday (18:00 local time), so many people are likely to be on the road commuting from work to home. Effectiveness of in-vehicle sheltering is an important issue to consider in practice (Engelmann et al., 1992), but will not be covered in this dissertation. The analysis in this chapter also does not consider those who are exposed in buildings other than the single-family detached units in which they reside. The SIP effectiveness of non-residential buildings will be examined in Chapters 5 and 6.

The three sets of outdoor concentration predictions are used to predict hypothetical levels of chemicals with different pollutant dynamics in the indoor space. Models used to describe the sorptive interactions of chemicals with indoor surfaces are detailed in Section 4.2.2. Similar to the approach used in Chapter 2, SIP effectiveness is measured in terms of the estimated reduction in potential casualties. This estimate is relative to the case of everyone being exposed to outdoor concentrations. Unlike in Chapter 2, spatially and temporally varying distributions of air-exchange rates are included in the simulation. In addition to SIP termination time, the time delay between the start of the release event and the initiation of shelter-in-place is also considered. Section 4.2.3 will discuss the processes that contribute to this time delay. Findings from survey data gathered from officials and communities affected by past emergency events are reviewed. Before SIP is

initiated, a certain fraction of households is assumed to have their windows opened, or, in another case, their heaters on. Consequently, air-exchange rates are expected to be larger than from air infiltration alone. On the other hand, the presence of contaminant removal mechanisms might offset some loss in effectiveness due to a late start. The analysis presented here aims to assess SIP effectiveness under these realistic conditions in a community of single-family detached dwellings.

4.2.2 Sorption and Decomposition on Indoor Surfaces

Sorption encompasses a class of processes by which gas-phase chemicals interact with surface materials. Depending on the properties of the chemical, sorption may include physical binding at the exposed surface, absorption into the bulk of the material, or chemical reaction with the material. Collectively, these processes are often modeled as first-order loss mechanisms with the potential for partial or complete reversibility. In an indoor environment where the gas-phase chemical is assumed to be well-mixed, the loss rate of the chemical to surface materials is modeled as being proportional to the well-mixed concentration. Many models also account for desorption of a chemical from surfaces back into the gas-phase. Sorption can reduce indoor inhalation exposures from an outdoor release, but desorption can lead to low-level exposure long after the release. A search of the literature revealed that only a few sets of sorption and decomposition data exist on chemical warfare agents and toxic industrial chemicals with respect to indoor materials: G-series agents, VX simulant, mustard gas (HD), chlorine (Cl_2), ammonia (NH_3), and sulfur dioxide (SO_2). More commonly measured are the interactions between

typical indoor surfaces and conventional air pollutants, such as ozone (Morrison and Nazaroff, 2002), volatile organic compounds (Singer et al., 2004) and constituents of environmental tobacco smoke (Singer et al., 2002).

In this section, experimental data on the sorptive and decomposition characteristics of toxic industrial chemicals and chemical warfare agents are reviewed. Mathematical models that had been developed to describe their interactions with indoor surfaces are discussed. These models are then integrated into the mass-balance model used to predict the indoor concentrations in residences of the exposed community. Most of the experimental data are obtained from room-scale experiments where a certain amount of the chemical is released indoors, and the airborne concentrations are measured over time. The sorption (and desorption) rate coefficients are then deduced by curve fitting while accounting for other losses of the chemical, such as by exfiltration to the outdoors. Many environmental factors are known or suspected to affect the experimental results: types and amount of surface materials present, effect of moisture and temperature, aging of surfaces, etc. As the ability to model these influences remains limited, most sorption or decomposition experiments, including the ones reviewed here, aimed to mimic typical indoor conditions such that the observed rates are applicable without further adjustments.

4.2.2.1 Model Formulation

Jørgensen et al. (2000) summarized the different types of mathematical model used to describe the interaction between volatile organic compounds in the indoor air and

material surfaces. The two models reviewed in the paper are the one-sink model and the two-sink and diffusion model. Others have also used these models to describe the interactions between toxic chemicals and indoor surfaces. Both models assume that sorption is a fully reversible process, meaning that the sorbed mass will eventually be desorbed to the room air when the concentration in the room air is lower. This can lead to post-event exposure and decontamination concerns in SIP scenarios. Before going into details of the formulations of these two models, a simpler irreversible uptake model is first discussed here. The irreversible uptake model is relevant for certain classes of pollutant-surface interactions such as reduction-oxidation reactions.

For chemical species that readily react with indoor surfaces, such as O_3 and SO_2 (Grøntoft and Raychaudhuri, 2004), deposition velocities v_d (m/s) are used to describe the irreversible loss of chemicals from gas-phase to indoor surfaces. This type of model involves only one additional loss term in the mass balance of the test room or chamber. In a case where the source of the chemical is from the outdoors at a constant concentration C_{out} (g/m^3), the mass balance on the amount of chemical in the gas-phase yields:

$$V \cdot \frac{dC(t)}{dt} = Q \cdot \left(C_{out} - C(t)\right) - v_d \cdot S \cdot C(t)$$

Eqn 4.1

where S (m^2) is the surface area of materials in the room, V (m^3) is the room volume, Q (m^3/s) is the volumetric ventilation rate, and C (g/m^3) is the indoor concentration of the chemical. This equation can be easily solved by direct integration following rearrangement.

The one-sink reversible sorption model is theoretically derived from the Langmuir isotherm at a low surface loading level. The Langmuir model postulates a monolayer of sorption sites with all sites possessing equal affinity for the sorbing chemical and being mutually independent. Based on these assumptions, the equilibrium concentration in the sorbed-phase is linearly dependent on the gas-phase concentration at low fractional loadings of surface sites. The rate of sorptive uptake on the surface materials (sink) is proportional to the concentration in the test chamber or room, C (g/m^3), multiplied by the sorption rate constant, k_a (m/s). Desorption from the surface is proportional to the mass in the surface sink, M (g/m^2), multiplied by the desorption rate constant, k_d (s^{-1}). A mass balance on the indoor air yields this equation (Dunn and Tichenor, 1988):

$$V \cdot \frac{dC(t)}{dt} = Q \cdot \left(C_{out} - C(t)\right) - k_a \cdot S \cdot C(t) + k_d \cdot S \cdot M(t)$$

Eqn 4.2

where C_{out} (g/m^3), S (m^2), V (m^3), and Q (m^3/s) are the same as defined for Eqn 4.1. The mass balance on the amount of chemical sorbed on the surface sink gives:

$$S \cdot \frac{dM(t)}{dt} = k_a \cdot S \cdot C(t) - k_d \cdot S \cdot M(t)$$

Eqn 4.3

The solution to this pair of coupled first-order ordinary differential equations is detailed in Jørgensen et al. (2000). The solution technique involves first obtaining the eigenvalues and the corresponding eigenvectors of the general solution. Then, the particular solution is obtained by using the initial mass in the gas-phase and sorbed-phase. In the case that the outdoor concentration varies with time in a simple, analytical manner, the method of undetermined coefficients can be used to obtain the solution. In this case study, the

outdoor concentration predictions are available at 5-minute averages. When solving Eqn 4.2 and Eqn 4.3, C_{out} is modeled as piecewise constant during each 5-minute time step.

The two-sink and diffusion model by Singer et al. (2004) consolidates the partitioning of chemicals in a room to three compartments (Figure 4.2): the room air, the surface material in contact with the room air, and an embedded sink in contact with the surface sink. Chemicals in the room air first sorb onto the surface sink, then diffuse into the bulk of the material or down to subsurface pores, which are collectively modeled as the embedded sink. Both processes are potentially reversible. The embedded sink interacts with the surface layer only, and not directly with the room air. Experiments show that the interaction between the surface sink and the embedded sink in some cases can be approximated by the Fickian one-dimensional mass diffusion equation:

$$\text{Mass flux}\left(\frac{\text{g}}{\text{s}\cdot\text{m}^2}\right) = -D\cdot\frac{dM}{dx} \approx k_{diff}\cdot(M_1 - M_2)$$

Eqn 4.4

where M_1 (g/m^2) is the mass density sorbed in the surface sink, and M_2 (g/m^2) is the mass density sorbed onto the embedded sink. In Fick's law, D (m^2/s) is the diffusion coefficient of the chemical species in the bulk indoor material. In modeling sorption, however, the parameter k_{diff} (s^{-1}) is not the true diffusion coefficient, but rather it describes the effective mass movement of the chemical species between the surface and embedded sinks. This mass flux drives the mass of the sorbed material to change over time in the embedded sink.

$$S \cdot \frac{dM_2(t)}{dt} = S \cdot k_{diff} \cdot \left(M_1(t) - M_2(t)\right)$$

Eqn 4.5

The mass balances on the surface sink (M_1) and the room air (C) yield these equations:

$$S \cdot \frac{dM_1(t)}{dt} = S \cdot k_a \cdot C(t) - S \cdot k_d \cdot M_1(t) - S \cdot k_{diff} \cdot \left(M_1(t) - M_2(t)\right)$$

Eqn 4.6

$$V \cdot \frac{dC(t)}{dt} = Q \cdot \left(C_{out} - C(t)\right) - k_a \cdot S \cdot C(t) + k_d \cdot S \cdot M_1(t)$$

Eqn 4.7

Some experiments suggest that the introduction of another rate coefficient seems to improve the model fit to data (see Figure 4.2). Instead of using k_{diff} to describe the rate of movement of chemical between the surface and embedded sink in both directions, the refined model uses two different rate coefficients, k_1 (s^{-1}) and k_2 (s^{-1}) instead. Singer et al. (2004) found that this model refinement gives substantially better fits for strongly sorbing compounds. For these compounds, the rate of sorption into the embedded sink, k_1, has been found to be as much as 3 to 8 times higher than the rate of desorption from the embedded sink, k_2. This suggests a higher affinity for the sorbed chemicals in the embedded sink, which leads to tighter binding than that occurring with the initial surface sorption. Among moderately sorptive chemicals, however, the three-parameter model (k_a, k_d, and k_{diff}) is sufficient to describe the observed change in the gas-phase concentration.

4.2.2.2 Experimental Data

Grøntoft and Raychaudhuri (2004) summarized various deposition measurements of SO_2 onto materials commonly found indoors including different types of wood, carpet, fabric, wallpaper, glass, metal, and stone. The experimental data are reported in terms of

deposition velocity, v_d (m/s), which is defined as the net mass flux [g/(s·m^2)] of a species to a surface normalized by the gas-phase concentration (g/m^3). Since SO_2 is an acidic gas, the highest deposition rates were measured for basic indoor surfaces like concrete panels, plaster walls, and gypsum wallboard. Lower deposition rates were observed when surfaces such as wood, cloth, metal, brick and glass were tested. The highest deposition rate measured was 0.27×10^{-2} m/s on surface treated gypsum wallboard at 90% relative humidity. At 50% relative humidity, the measured deposition velocity was approximately 0.15×10^{-2} m/s for the more reactive surfaces, and 0.03×10^{-2} m/s for the less reactive surfaces.

Karlsson (1994) summarized the measured deposition velocities of NH_3, Cl_2, and trialkylphosphonoacetate, which is a surrogate for the chemical warfare agent VX (Table 4.1). The experiments involved first injecting a certain amount of the test chemicals into a chamber, and then measuring the decaying concentrations over time. A fan was used to keep the concentration uniform throughout the test chamber. The air-exchange rate between the test chamber and the outdoors was characterized by the change in N_2O concentration. The sorption experiments were conducted in similar rooms and under similar environmental conditions (15 to 20 $^{\circ}$C, <30% to <50% RH). The surface-to-volume ratios (*S/V*) of the test rooms ranged from 2.1 to 3.4 (m^2/m^3). The test chamber was furnished with painted walls, roof, and synthetic carpet. Further details on experimental conditions are described in Karlsson et al. (1992). The VX simulant was found to be the most sorptive among the three chemicals tested. This is not surprising, since VX is deliberately formulated to possess a low volatility. It is used as a persistent,

“terrain denial” military compound with the potential to off-gas toxic vapor for days following surface application (NRC, 2003). On the other hand, NH_3 was found to the least sorptive. NH_3 is a basic gas and is expected to sorb onto acidic surfaces such as wood and paper, which are generally present in lesser quantity indoors relative to basic surfaces.

Karlsson and Huber (1996) reanalyzed the same sorption/desorption experiments using the one-sink model (Table 4.2). The authors also carried out additional experiments using another chemical agent, sarin (GB), in a larger room that had old chalking paint on concrete. Results showed that sarin sorbs on indoor surfaces at rates in between VX and Cl_2. The desorption rate of sarin from the sorbed-phase back into the room air is considerably slower than for the other three chemicals. However, cross-experiment comparison is complicated by the fact that the types of indoor surfaces present in the test rooms are different. A similar sarin experiment that was conducted in a room with alkyd/plastic paint on the walls and ceiling and synthetic carpet showed no loss by sorption. Unfortunately, the authors did not comment on the reliability of these sarin experiments nor provide an interpretation of their conflicting findings.

Singer et al. (2005a) measured the sorption rates of three organophosphorus (OP) compounds that are used as surrogates for the G-type nerve agents, including sarin. Experiments were carried out in a test chamber finished with painted wallboard. Results from two levels of furnishing were compared. Faster sorption rates were observed in the presence of plush surfaces, including carpet, cushion, draperies, and upholstered

furniture, than with hard surface materials alone. Faster sorption rates were also observed with new wallboard instead of aged wallboard. The authors compared the model fit using three types of mathematical model: (1) one-sink model, (2) two-sink diffusion model (k_{diff}), and (3) two-sink four-parameter model (k_1 and k_2). The authors found that the two-sink four-parameter model is needed in many cases to a produce satisfactory fit to the experimental data. The rate coefficients obtained from these sorption experiments are all reported in units of inverse time. The model formulations used by Singer et al. (2005a) are consistent with those described in Eqn 4.4 to 4.7. The only difference is that Singer et al. report the sorption rate k'_a in units of s^{-1}, which needs to be divided by the surface-to-volume ratio S/V (m^2/m^3) to convert to units of m/s (k_a) used in Eqn 4.4 to 4.7.

Using similar experimental techniques, Singer et al. (2005b) measured the sorption rates of these same chemicals in single rooms (four bedrooms and two bathrooms) of real residences. Experiments were carried out in these rooms with material surfaces and furnishings unaltered. The surface-to-volume ratios of the rooms were characterized by visual inspection, and found to range from 2.5 to 5.5 m^2/m^3. Wood, plastic, laminate, and painted wallboard/plaster are the types of surfaces that made up most of the apparent surface area in the rooms studied. It was found that sorption rates did not vary widely by room type or across rooms of varying size and furnishing level. Similar rate coefficients were obtained relative to the experiments carried out in a test chamber (Singer et al., 2005a). Table 4.3 summaries the available rate coefficients from both sets of experiments fitted to the three sorption models. It is apparent that all three surrogates have similar sorption behavior. Even though the initial sorption rate coefficient is somewhat higher

among the experiments carried out in residences than in the test chamber, results from the two sets of experiments agree reasonably well.

Blewett and Arca (1999) carried out experiments to measure the change in indoor concentrations in a test cottage while its envelope was exposed to known amount of chemical agents and a surrogate. Most of the experiments were performed using methyl salicylate (MS), a simulant for the blister chemical agent mustard gas (HD). A few experiments were carried out using the actual chemical agents GB and HD. It was observed that more of the MS and HD agents were lost to the building envelope than GB, presumably because MS and HD have lower volatility than GB. The authors did not quantify separately the loss to filtration by the building envelope from the loss by sorption on indoor surfaces. The authors also did not analyze the experimental data in terms of rate coefficients, but rather the reduction in exposure (time-integrated concentration) level relative to outdoors. Two aspects of this dataset make it difficult to extract the implied sorption rate coefficients: (1) lack of time resolution from the time-integrated sample measurements, and (2) lack of concurrent measurements of building air-exchange rate. Consequently, data from these experiments are not used in this dissertation.

4.2.2.3 Implications for Indoor Concentrations

In the case that a toxic chemical is irreversibly lost on surfaces, the time-integrated airborne concentration would clearly be lower than if the chemical were inert. Even though many of the chemicals examined above sorb reversibly to indoor surfaces, the

slow desorption rates mean that the time-integrated concentration would take a very long time to reach that of the nonreactive case. As a result, there would be a net reduction in the acute exposure to the toxic chemicals if SIP were to terminate after the toxic plume has passed. Furthermore, if the dose-response effect of the chemical is nonlinear with toxic load exponent $m > 1$, significant health protection benefit will be realized through sorption by reducing the short-term peak concentration. Figure 4.3 shows the indoor concentrations predicted in a simple well-mixed room when subjected to various toxic chemicals at a constant level for 1-h. In the event of surface interactions, the predicted indoor concentrations are lower than the nonreactive case at all times. Desorption from the sorbed-phase, as represented by the change in mass per surface area over time, is gradual for the contaminants considered. The surface-to-volume ratio used in these predictions is 3.5 m^2/m^3, which is typical of those observed in real rooms (Nazaroff et al., 1993; Singer et al., 2005b).

Using Cl_2 as an example, Figure 4.4 shows that the mass sorbed onto indoor surfaces far exceeds the mass in the room-air. In fact, because indoor surfaces represent such effective storage sites for the chemical, the total mass accumulated in the room is higher than in the nonreactive case. This sorbed mass raises significant decontamination concerns; however, these will not be addressed here. In the case when a two-sink model is applied, the partitioning of the chemical to indoor surfaces can be even more profound. Figure 4.5 shows the predictions using two variations of the two-sink model. Model (2) refers to the two-sink model in which the interactions between the surface and the embedded sink are modeled with a symmetric rate constant (k_{diff}). Model (3) refers to the

two-sink model in which the soption to and desorption from the embedded sink are modeled using different rate coefficients. Using the rate coefficients obtained from one set of experiments carried out in the bedrooms and bathrooms in residences (for chemical species DMMP in Table 4.3), model (3) gives slightly lower peak indoor concentrations than model (2). Model (3) also gives indoor concentrations that are slightly more persistent after the plume has passed. However, the key difference between the two models is in the distribution of the sorbed mass between the two conceptual sinks. For the purpose of modeling SIP effectiveness against acute health effects, the indoor air concentrations are the most important to consider. In this regard, both two-sink models are expected to produce similar results.

The key benefit identified by researchers who have studied the sorptive behavior of toxic chemicals (Karlsson and Huber, 1996; Singer et al., 2005a) is a reduction of the peak indoor air concentration. Reversible sorption lowers the concentration in the air when it is high, and slowly remits the sorbed mass back into the air when the concentration is low. This change in the indoor concentration time-profile can lead to a substantial reduction in the adverse health effects suffered by occupants. On the other hand, a high air-exchange rate can compete with the kinetics of sorption, causing it to be less effective in lowering indoor concentrations. For example, for the conditions in Figure 4.5, increasing the air-exchange rate from 0.5 h^{-1} to 2 h^{-1} while holding all remaining parameters the same would increase the ratio between the peak indoor to outdoor concentration from 0.31:1 to 0.43:1. Under certain conditions, it is possible for some residences to have air-exchange rates reaching such high level. The effect of sorption can also be influenced by the times

when SIP is initiated and terminated in the community. Before SIP is implemented, some residences can have air-exchange rates far exceeding the amount caused by air infiltration alone. During these times, the efficiency of sorption will also be lower than otherwise. Finally, the efficiency of sorption to reduce the number of potential casualties for those who took shelter would depend on the extent to which the toxic load limits are exceeded in residences. Therefore, it is only through a community-based analysis that the efficiency of the sorption process can be properly determined.

Three levels of sorption will be modeled in the case studies. Parameters for DMMP, a surrogate for sarin, will be used to model chemicals that sorb strongly onto surfaces. Its sorption rate, roughly 5 h^{-1} (Table 4.3), is much faster than typical air-exchange rates in residences. Parameters for NH_3, which has a measured sorption coefficient of 0.7×10^{-4} m/s as a lower estimate (Table 4.2), are used to model moderately sorptive chemicals. Assuming a surface-to-volume ratio of 3.5 m^2/m^3, a value of $k_a = 0.7\times10^{-4}$ m/s corresponds to a sorption rate coefficient of 0.9 h^{-1}. This rate is within the range of typical air-exchange rates in residences. As the process of sorption can be sensitive to the quantities and qualities of the materials present indoors, an upper and lower estimate of the indoor concentrations will be considered based on the range of sorptive rate coefficients observed in experiments. The upper indoor concentration estimates will be computed by combination of a slower sorption rate and a faster desorption rate, and the reverse combination will be used to obtain the lower indoor concentration estimates. In general, the sorption rates of toxic gases are relatively fast compared to the range of

values measured among various organic gases (Singer et al., 2004). A non-sorbing case is included for comparison.

Analogous to the process of sorption to indoor surface materials, dry deposition can remove chemicals from the atmosphere, thereby lowering the outdoor concentrations resulting from a release. Jonsson et al. (2005) used a modeling approach to examine the extent to which dry deposition would impact the outdoor concentrations estimated for toxic releases. The dry deposition rates of the few toxic chemicals studied (Cl_2, HF, SO_2, VX) are quite fast. Dry deposition could dramatically lower outdoor concentrations, especially if the plume passes over wet surfaces. The absolute reduction in outdoor concentration is most dramatic close to the release source, as the loss rate is proportional to the concentration. A change in the spatial distribution of ground level outdoor concentration could affect SIP effectiveness. The extent of influence would depend on the measure of SIP effectiveness chosen, and on the scale of the release (i.e. the mass released in relation to its chemical toxicity). The spatial distribution of the exposed population can also affect how sensitive the potential casualty estimates would be in relation to the change in outdoor concentrations owing to dry deposition. In the analysis presented in this dissertation, atmospheric dry deposition is not modeled.

Another simplification in the modeling approach is the restriction of considering only the transport and health effects of the primary toxic chemical. For example, catastrophic releases of toxic chemicals stored under pressure (Deaves et al., 2001) can result in droplet and aerosol formation. The fate and transport of contaminants in these physical

forms can differ from the gaseous state considered in this analysis. In the event of a massive release of ammonia, formation of ammonium salt aerosols from reaction with acidic air pollutants, such as sulfur and nitrogen oxides (Renard et al., 2004), can be transported over long distances and pose additional health concerns beyond those associated with acute exposure to the gaseous plume. These are some of the complications not covered in this analysis, but their impacts might be worthy of further studies.

4.2.3 Shelter-in-Place Response Time

As discussed in Chapter 2, SIP effectiveness is sensitive to time-scale parameters. One major consideration in responding to an emergency is the time required to warn the public and the time required for them to implement protective actions. Rogers (1994) compiled data on the timing of emergency decisions made by officials during recent airborne chemical releases. Key community officials were interviewed about when decisions were made to warn the public after the occurrence of a release event. Activities taken within this time can include identifying, locating, and assessing the hazard by emergency responders. It was found that the selection of an appropriate protective action was often included in this step, which typically involved making a group decision from among several alternative responses. The median time officials took to warn the public of an impending hazard was about 30 minutes. In 30% of the 51 events studied, this step to warn the public was completed within 10 minutes. These statistics are specific to evacuation type events. In a more recent study by NICS (2001), the incident timeline was

reported for 6 past accidents that involved SIP. Officials gave instructions to shelter at 6, 10, 15, 17, 35, and 45 minutes respectively, from the estimated time when the release started. From these data, it is clear that SIP initiation requires time. Consequently, some people might be exposed to high outdoor concentrations before they are instructed to take shelter in buildings.

Even after officials have decided to give a warning, there can be another time delay until people receive the warning that a release has occurred. Post-event surveys were conducted in two communities affected by train derailment accidents that occurred in Pennsylvania in 1987 (Rogers and Sorensen 1989, 1991). In both events, multiple methods were used to notify the public to evacuate, including door-to-door visits by officials and use of loudspeakers. The times at which people first received the warning to evacuate were plotted. In these two accidents, half of the public reported that they received warning at 40 and 90 minutes, respectively, after the start of the event. Although various methods were used to notify the public, the shape of the observed warning-receipt curve is best described by a media-based model, in which notification is given out through television or radio.

Different emergency warning diffusion models are discussed in Rogers and Sorensen (1991). There are two processes involved in the spread of an emergency warning. First is the alert process, whereby a certain fraction of the population receives the emergency message broadcast and recognizes the meaning of the alert signal. Then, people who have heard the event will sequentially tell others they know, which is referred to as the

contagion process. The fraction of people who become aware of the event (n_t) within a period of Δt reflects the sum of the effects of the alert process and the contagion process.

$$n_{t+1} = \left[k \cdot f_a \cdot \Delta t \cdot \left(N_t - n_t\right)\right] + \left[\left(1-k\right) \cdot f_c \cdot \Delta t \cdot n_t \cdot \left(N_t - n_t\right)\right]$$
$$N_{t+1} = N_t - n_{t+1}$$
$$\text{Initial Conditions}: \; n_0 = 0, \; N_0 = 1$$

Eqn 4.8

Here, k is the fraction of the population notified by the alert process, and the remaining fraction of the population (1-k) has to be notified by contagion. In a given period of time, f_a is the fraction of population that will be successfully notified through the alert process, and f_c is the fraction of the population that will be notified by talking to others who are already aware of the event. N_t is the fraction of people who are still unaware of the event occurrence at time t. Initially, no one in the community is aware of the event, i.e. $N_0 = 1$. The fraction of the people who have become aware of the event in the beginning of time is also zero (i.e. $n_0 = 0$). In the next time step, Eqn 4.8 predicts that all the people who will become aware of the event must be those who have heard the alert, i.e. $n_1 = k \cdot f_a \cdot \Delta t$. At the end of this time step, the fraction of people who are yet to be notified by either process is $N_1 = 1 - n_1$. In the following time steps, n_t and N_t are used to predict values of n_{t+1} and N_{t+1} iteratively as described in Eqn 4.8. The so-called emergency warning diffusive curve is the fraction of people notified of the event (1- N_t) plotted as function of time t. Examples of diffusion curves of three types of emergency warning systems are shown in Figure 4.6. These curves are the direct reproduction of a selected set of systems considered by Rogers and Sorensen (1991).

The three different emergency warning systems plotted include both the most effective (sirens plus telephone ring-down system) and the least effective (media) systems. Sirens alone can give warnings that are moderately effective. Among these three types of warning systems, sirens plus telephone has the highest k value because this method can clearly communicate the nature of the warning and immediately give appropriate guidance. As a result, a higher fraction of people is likely to be successfully notified of the occurrence of the release by this alert process. In contrast, sirens alone have a low k value because this warning method requires the recipient to acquire information on the meaning of the warning and how to act accordingly. This means that a larger fraction of the population will need to talk to one another (contagion process) before they can fully comprehend what had happened. Media-based systems are classified as having a k value that is somewhere in between sirens alone and sirens plus telephone. This means that a lesser fraction of those who receive the warning through the media is expected to understand the warning completely, relative to the use of telephone ring-down system.

The alert efficiency f_a reflects the ability of the warning system to reach and successfully notify the population. Media-based systems work only if the recipient happens to be listening at the time of the warning. On the other hand, people are much more likely to be reachable by telephone. They are also more likely to pay attention to the message if it clearly indicates that there is an emergency. The alert efficiency is a function of where people are and what activities they are engaged in at that time. For example, during night hours, when most people are asleep, the value of f_a depends on the fraction of people who can be woken up by sirens or telephone calls. During the evening, when more people are

possibly watching television, the chance that they receive a broadcast of an emergency message can be higher. Rogers and Sorensen (1991) reviewed these dependencies and also the time-activity patterns of the general population to derive the diffusion curves shown in Figure 4.6.

In emergencies, people are likely to contact neighbors or families and friends to exchange information about what to do. The efficiency of this contagion process, f_c, depends on how receptive people are when they receive knowledge about the event from others. For example, recall that the siren system alone is expected to have a low k value. This means that there would be a large fraction of people who have heard the siren but not yet understood its meaning. Presumably, these people will actively seek further information regarding the siren. Because they are actively seeking more information, they are also likely to be more receptive to incoming sources of information. Consequently, a higher f_c is expected. On the other hand, using a telephone ring-down system alone is expected to have a somewhat low f_c value. This is because such a warning system can provide information to a limited number of people at a time.

Overall, a telephone ring-down system can be very effective at giving emergency warnings, especially if it is combined with a siren to alert the community. It is estimated that most of the population in a warning area could have received the notification within 15 minutes using this method (Figure 4.6). On the other hand, if a siren alone is used, only half of the population is expected to have received the warning after 15 minutes. Based on some empirical observations, Rogers and Sorensen (1991) further limit the

fraction of people warned by a siren alone and by media at 30 minutes from the start of the process to 0.75 and 0.5 respectively. These limits are set based on survey results for the time when residents first received warnings in four communities that had faced either sudden flooding or a train derailment. In Figure 4.6, the fraction of people notified by 30 minutes is slightly different from these limiting fractions because of the adjustment made to account for the dependency of the warning system effectiveness on time of day.

Once the public receives a warning, there is another time delay for people to take action to avoid harm. People do not respond instantly to a warning. Rather, people tend to seek additional information from multiple sources including friends, relatives, and the media. Rogers and Sorensen (1989) found that both the social dynamics at the time of the incident and the perception of risk affect the response time of the public. In one of the two past events studied where the event started at a time when most families were together and the perceived risk of exposure was immense, most people evacuated within 25 minutes after they were first advised to do so. In an SIP scenario, the response actions required are considerably simpler: closing windows and doors, and turning off heating and cooling fans, and ventilation devices. There is also less risk involved with undertaking these actions, relative to that of evacuation[8]. Consequently, a quicker response time might be expected. There is, however, a lack of survey data to verify this expectation.

[8] A report on a large-scale Cl_2 release at Henderson, NV (Routley, 1991) found that there is considerable risk of exposure associated with evacuation. While residents were waiting for busses to pick them up from their home to a safe location, many were exposed to the toxic cloud. The report also concluded that the risk of exposure during evacuation might have been greater than the risk if they had remained indoors.

Some assumptions have to be made due to the lack of data on response time and compliance in response to SIP advice. Based on the observation that the mean time for evacuation was 25 minutes in one of the two accidents previously analyzed (Rogers and Sorensen 1989, 1991), Rogers et al. (1990) assumed that the public would respond 25% faster if they were instructed to shelter-in-place instead. It seems plausible that the time needed for a family to decide on and complete SIP should take not much longer than 20 minutes. This is roughly the same amount of time needed to inform the public by telephone. The response time might depend also on time of day and on weather conditions. For example, during cold winter nights, most families would already be in their homes with windows and doors closed. While it is methodologically easier and also poses fewer risks to shelter-in-place than to evacuate, a higher rate of compliance is not always guaranteed in practice (Vogt and Sorensen, 1999; Lasker, 2004). This is because a determining factor for compliance is how the public perceives the risk from the release, and if people can communicate with loved ones and be certain of their safety. Relative to evacuation, SIP is often perceived as the less-active response measure, and might therefore be associated with less serious releases. With such impressions, people might be less inclined to follow instructions from emergency responders to take protective action (Rogers and Sorensen, 1989). Lack of confidence in their community's preparedness plans can be another reason why people might not shelter-in-place when instructed to do so.

In summary, there are three key steps involved in the initiation of SIP: (1) the time required for officials to identify the hazard and decide to issue a warning to the public,

(2) the time required for the population to receive the instruction to shelter in-place, and (3) the time required for people to implement SIP. The time requirement of each of these steps can vary considerably depending on the release scenarios. Table 4.5 lists the range and typical time requirements of each step based on the studies reviewed. Values chosen for step (1) span the range reported in the NICS (2001) study. The fast, typical, and slow timing represent also the 10th, 40th, and 65th percentile among the 51 evacuation case studies surveyed by Rogers (1994). Values chosen for step (2) represent the time needed for 50% of the population to receive a warning given out by the three methods reviewed: sirens plus telephones, sirens only, and broadcast media. As a first attempt, this analysis will assume that all households react the same to the warning message. In future work, diffusion curves such as shown in Figure 4.6 could be used to perform analysis where each household is assigned a different notification time according to the probability functions. Values chosen for step (3) are based on the analysis by Rogers et al. (1990) on protective actions in response to chemical agent emergencies in communities located close to a chemical stockpile. These time estimates were derived from survey data on an evacuation event described earlier. To further reduce the number of model runs, instead of considering all combinations of time delays detailed in Table 4.5, only three initiation time delays are modeled: 0.25, 0.5, and 1 h from the start time of the release.

In the discussion of air-exchange rates measurement (Chapter 3), it was shown that the prevalence of window opening in a community depends on the weather. Under comfortable outdoor conditions, as much as 35% of households are reported to have some of their windows opened. Operation of exhaust fans or heating and cooling systems can

also increase air-exchange rates, but likely to a lesser extent. In this analysis, three cases are considered: (1) air infiltration rates only, (2) 40% of households with an additional 1 h^{-1} air-exchange rate to represent summertime conditions with some residences having windows opened, and (3) 80% of households with an additional 0.3 h^{-1} air-exchange rates to represent wintertime conditions with many residences having a heater on or some other minor source of induced air exchange. As discussed in the last chapter, not all types of heaters induce additional air exchange to the same extent. Variability is also expected in the number and the extent to which windows are opened in residences. Nonetheless, the cases chosen here are loosely based on measurements of air-exchange rates in residences. It is also assumed in this analysis that the additional air exchange does not significantly alter the amount of unavoidable air infiltration in residences.

4.2.4 Summary of Model Parameters

Table 4.6 lists the model parameters considered in this analysis. A number of simulations were performed (Table 4.7) and their results analyzed in terms of various metrics (Table 4.8). In all the simulations modeled, the outdoor concentrations are scaled such that the number of potential casualties estimated for outdoor exposure are the same. The releases modeled are approximately equivalent in scale to a large-scale chlorine gas release, with the release amount on the order of 1 to 10 tonnes. These are large-scale events, but are not unprecedented in comparison with the history of past chemical accidents in the US and other countries (Murray and Goodfellow, 2002). Three sets of releases of different durations (0.5-h, 1-h, and 2-h) are modeled using the same meteorology. Acute adverse

health effects are predicted to occur up to a distance of 5 to 7 km downwind from the release source if people were exposed to the outdoor concentrations. The crosswind extent of the plume ranges from 1 to 3 km. Even though the simulations are scaled to give the same number of potential casualties, the locations where the casualties occur might slightly differ among the cases. This is a result of changes in wind direction as the plume moves across the model domain.

The remaining parameters considered in this analysis affect indoor concentrations only. These include the effect of sorption on indoor surfaces, the air-exchange rate distribution of houses before and after SIP is implemented, and the times when SIP is implemented and terminated. The analysis starts with investigating the implications of the air infiltration rate distribution on the SIP effectiveness of houses. The base-case simulations[9] ignore sorption effects and assume that all houses have initiated SIP before the release has started. Consequently, air infiltration is the only mechanism that brings about air exchange with the outdoors.

As in Chapter 2, the main measure of SIP effectiveness considered is the casualty reduction factor. Potential health effects are evaluated at one intensity level only, which is referred as the toxic load limit. In responding to emergencies, it is informative to present model results evaluated at different severities of health effects. For example, the US EPA provided acute exposure guidelines at three levels of severity: minor/reversible effects, serious/permanent impairment, and lethal level. In some cases, SIP reduces

[9] The base-case simulations are referred to as 6Ai, ii, iii; 6Bi, ii, iii; 6Ci, ii, iii in Table 4.7.

exposure enough to eliminate all possible health effects. In other cases, SIP can only reduce the severity of health effects among those exposed. From the reports of past events (NRC, 2001), situations where a small fraction of those who took shelter were treated for minor injuries are common. Since the injured are likely to have suffered even more severe health effects if they did not take shelter in buildings, SIP should still be credited as effective. On the other hand, because adverse health effects are not eliminated completely, simple SIP alone can be evaluated as an inadequate response. To incorporate this level of complexity, future work should consider alternative measures of community-based SIP effectiveness that accounts for varying degrees of adverse health effects. However, in evaluating such measures, even more case-specific results are expected. This is because the analysis depends on how one value the gain in SIP effectiveness with respect to the various health end-points avoided. The analysis presented in this dissertation will evaluate adverse health effects at one severity level only, as it is defined by the toxic load limit.

4.3 Results and Discussion

Results from the base-case simulation agree with the main findings from Chapter 2 where a simple Gaussian plume was used to model the outdoor concentrations. Figure 4.7 shows the predicted potential casualties if people were exposed to the outdoor or indoor concentrations for the entire 4-h simulation duration. The indoor estimates assumed that people successfully implemented SIP (closed doors and windows, and shut off heaters and exhaust fans) before the plume arrived. It is further assumed in this case that the

chemical is conserved and nonsorbing indoors. In all three release durations modeled, SIP is consistently more effective as *m* becomes increasingly greater than 1. While the release is on going, the estimated number of potential casualties is similar regardless of the toxic load. A subsequent loss in effectiveness is mainly caused by accumulating exposure to the residual contaminant left indoors. With a high toxic load exponent, the health effects are largely caused by exposure to peak concentrations. Thus, post-event exposures to indoor residuals do not contribute very much to the overall adverse health effects suffered by the population in such a case. As a result, casualty estimates indoors cease to increase after the release has stopped when the toxic load exponent is high.

In these simulations, the earliest time when outdoor concentrations no longer cause additional health effects is about 0.5 h after the release has stopped. At this time, the casualty reduction factor (CRF) is similar in all cases (Table 4.9). The resulting CRF ranges from a low of 0.65 (2-h release, linear dose-response) to a high of 0.82 (0.5-h release, toxic load exponent $m = 3$). After this time, if people did not exit from their shelters, CRF would decrease due to the adverse health effects caused by exposure to the residuals indoors. The CRF would decrease by 40–50% in the case of a linear dose-response. When $m = 3$, the CRF is insensitive to the SIP termination time. These observations are consistent with the findings reported in Chapter 2.

In Chapter 2, an alternative measure of SIP effectiveness was also considered, referred to as the toxic load reduction factor (TLRF). This measure has the characteristic of being independent of the release scale, which in turn depends on the amount released, the

toxicity of the chemical, and the extent of dispersion. Figure 4.8 shows the population cumulative toxic load predictions assuming that people were exposed to the outdoor or to indoor concentrations for the entire 4-h simulation duration. In many of the cases considered, SIP is more effective when measured in terms of the toxic load reduction instead of the casualty reduction. This is because the release amounts modeled are large enough to cause potential casualties even among those who shelter-in-place. While the casualty reduction factor counts SIP as being ineffective in these residences, the toxic load reduction in these residences remains the same regardless of whether the residents are predicted to exceed the toxic load limit or not.

A disadvantage of using the toxic load reduction factor alone to measure SIP effectiveness is that it is insensitive to differences in the leakiness of dwellings that are most at risk of exposure. Based on the air leakage analysis detailed in Chapter 3 (see Figure 3.26), residences that are located closest to the release site are estimated to be the most leaky. When the release scale is small, only occupants of relatively leaky homes are affected by the release. As a result, the casualty reduction factor is smaller in the event of a smaller release. Figure 4.9 shows the normalized predicted casualties if the release amount were to scale by a factor of 0.04, 0.4, and 4, from the base-case simulations considered earlier in Figure 4.7. Depending on the release amount modeled, residential neighborhoods with different air leakage characteristics might become severely affected by the toxic plume. In this Albuquerque case study, the effect of release amount on the casualty reduction estimate is nonlinear. SIP is determined to be the least effective in reducing casualties when the release amount is scaled to 0.4 of the base case value. This

is because at that release scale, the highest fraction of the affected residences are relatively leaky. The population-weighted median air infiltration rate is 0.75 h^{-1}, which is 25% higher than predicted in the base case. In terms of the toxic load reduction, since the measure includes all residences in the model domain, the predicted values are the same regardless of the release amount. Scaling the outdoor concentration uniformly over the entire model domain does not change the ratio of the indoor-outdoor cumulative toxic load (see Eqn 2.6 and Eqn 2.8 in Chapter 2). In future analysis, the computation of the SIP toxic load reduction can be altered to overcome this limitation by considering only the residences that are the most affected by the toxic plume. This example also illustrates that determination of appropriate metrics for characterizing SIP effectiveness is challenging and merits further study.

In the remainder of this chapter, SIP effectiveness is only measured in terms of casualty reduction if people take shelter in buildings, normalized to the case if people were exposed outdoors. It is by chance that the release amount chosen in the base case simulation, which is also used in the rest of the analysis, included some neighborhoods with relatively tighter dwellings. The SIP casualty reduction estimates are generally 10% to 30% lower than most of the other estimates obtained using the different release amounts considered in Figure 4.9. The air infiltration rates of residences in the most affected areas modeled using the base case release amount are between 0.25 and 1.5 h^{-1} (10th and 90th percentile estimates of the population-weighted distribution), with 0.6 h^{-1} being the median value.

4.3.1 Effects of Air Leakage Variability Among Residences

Results shown in Figure 4.7 included modeling of the air leakage variability of houses estimated from data on their year-built, floor-area, household income, and local meteorology. As illustrated in Chapter 3, a factor of 10 variation in the air leakage of houses is not uncommon in a community of houses. Figure 4.10 shows the difference in potential casualty predictions if all houses were assumed to have the same air leakage equal to the median value in the census tract. Relative to an analysis with the broad distribution of leakage, underpredictions (10–20%) are observed in all simulations with constant leakage. This is a result of ignoring houses that are at the tail end of the air leakage distribution, which are much more leaky than the median value. The difference is small while the release is on going because in regions of high concentrations, most houses are not protective enough to eliminate adverse health effects. The difference is also small at times long after the release has stopped. This is expected because the eventual time-integrated indoor concentration is independent of the air-exchange rate, if the air-exchange rate is essentially time invariant. In these simulations, it is predicted that those who take shelter in tighter houses can avoid adverse health effects, while others who take shelter in leakier homes might not. This difference is most distinct in the more downwind areas where the outdoor concentrations are not as high.

Despite only modest dependency of the total casualty estimates on the air leakage distribution, valuable information can be extracted from an analysis that incorporates such a distribution. For example, if all houses were assumed to have the same air-leakage values, only binary results can be obtained. Areas would be classified as either in

exceedance of the safe level or not. In actuality, one would expect a gradient of effectiveness offered by SIP. In areas that are closest to the source, indoor concentrations in most residences are likely to be in exceedance of the safe level. In areas that are further downwind of the sources, fewer residences are likely to be in exceedance of the safe level. Figure 4.11 shows such a gradient in areas that are affected by the plume. Given such information, emergency responders can better allocate resources to attend to areas where people who took shelter are most likely to need assistance. When evaluating whether SIP can provide sufficient protection in a release scenario, emergency responders need to consider not only the typical dwelling, but also the safety of those who reside in the most leaky homes. Based on the analysis in Chapter 3, these homes are likely to be relatively older, smaller, and occupied by low-income households. As part of the pre-planning effort, emergency responders should pay special attention to dwellings that fit the above description and are also vulnerable because they are located close to a potential release source (e.g. an industrial sites that handle toxic chemicals).

Another way to visualize the influence of the air leakage variability on SIP effectiveness is to estimate how long residents can take shelter without suffering health consequences. Because of the temporary safety that buildings offer, large-scale immediate evacuation is not needed for the general population who live more downwind of the release source. People can stay in their homes until after the outdoor plume has sufficiently dispersed, and avoid the risks of being exposed to concentrated chemicals outdoors during a hasty evacuation. Figure 4.12 shows that many of the occupants taking shelter in houses that are among the tightest 10% in the census tract can safely shelter for the entire 4-h

duration. Even in houses that are considerably more leaky, safe conditions can be ensured in more than half of the affected areas until after the release has stopped. If emergency responders can safely relocate these people quickly after the release has stopped to minimize their post-event exposure, it might be possible for them to avoid health consequences too.

4.3.2 Effects of Sorption on Indoor Surfaces

The indoor concentrations predicted with various sorption rates for houses close to the release source (few hundred meters) are presented in Figure 4.13 for a 1-h event. Using rates from the NH_3 experiments (Table 4.4), sorption to indoor surfaces is predicted to lower the peak indoor concentrations by 15 to 35% relative to the nonreactive case. A slightly larger reduction in the peak indoor concentration is observed when the air infiltration rate of the house is low. When the air infiltration rate is high, loss of the chemical through air exfiltration competes with the rates at which chemicals sorb on indoor surfaces. The reduction in peak indoor concentrations reaches 35–65% when the set of faster sorption rates, modeled after DMMP experiments in residences, are used. In most cases, the indoor concentrations cease to change but are sustained at a low-level after the toxic plume has passed. This is particularly true when the two-sink model is used. In very leaky residences where a larger amount of toxic chemicals is brought indoors through air infiltration, the amount of chemicals sorbed onto surfaces can be substantial. After the toxic plume has dispersed, fast exfiltration to the outdoors can drive much of the sorbed chemicals to desorb from surfaces and reenter room air. Thus, the

highest residual concentrations are predicted for these residences after the plume has dispersed.

Interaction with indoor surfaces introduces yet another source of variability to the indoor concentrations expected in a community. Consider a mix of residences where some are heavily decorated with materials to which chemicals sorb favorably, and others are much less so. Modeled results suggest that the peak indoor concentrations can vary by almost a factor of ten. Here, variability is computed by taking the ratio of peak indoor concentration of the tightest and leakiest 10% of the houses with sorption rates modeled after the upper and lower rate coefficients of DMMP as shown in Table 4.4. Under the no-sorption case, the variability in the peak indoor concentration of the tightest and leakiest 10% of the houses is only a factor of four.

The effects of sorption on potential casualty estimates are shown in Figure 4.14 for the same 1-h release at different toxic load exponents. The most dramatic reduction in the number of potential casualties attributable to the loss of chemicals to indoor surfaces occurs when the toxic load exponent is 1. At the end of the 4-h simulation, the estimated number of potential casualties is reduced by a factor of two or more relative to the no-sorption case. Sorption of chemicals to surfaces eliminates the need for prompt SIP termination. This is because the amount of chemicals that desorb is relatively small over the course of a few hours after the release has stopped. Sorption reduces the sensitivity of the estimated number of potential casualties to the toxic load exponent. In most cases, over 80–90% or more of the population is predicted to be protected from adverse health

effects if they took shelter before the plume arrived. With sorption, the predicted number of potential casualties essentially remains the same even long after the release has stopped.

4.3.3 Effects of Shelter-in-Place Initiation Delay

The analysis so far has assumed that all houses implemented SIP before the plume arrives, such that air infiltration is the only air-exchange mechanism. However, under most acute release situations, it is unrealistic to expect advance notice of the release. SIP will not start until after officials have identified the hazard and informed the community to take shelter, and until after people have received the advice and acted accordingly. Figure 4.15 shows the modeled changes in the distribution of air-exchange rates before and after SIP is implemented. Two cases are simulated: (1) summertime conditions where some people have windows open, and (2) wintertime conditions where most people have heaters on. In case (1), the change is more profound (+1 h^{-1}) because window opening is expected to raise the air-exchange rate quite significantly. However, because fewer houses are assumed to have windows opened, the air-exchange rates for the lower percentiles are not affected in case (1). On the other hand, in the winter almost all houses are expected to have additional air exchange induced by operating heaters or exhaust fans. Consequently, almost the entire air-exchange rate distribution is shifted to higher values in case (2).

For each of these two pre-sheltering conditions, three SIP initiation time delays are considered: 0.25 h, 0.5 h and 1 h. Shown in Figure 4.16 are the indoor concentrations predicted at two locations close to the release source. Despite their proximity, the outdoor concentration time profile differs significantly at the two locations, as shown in the top row of Figure 4.16. This vast difference in the plume arrival time at these two locations is because of the shift in wind direction during the simulation. At the location that is closer to the release source (left column), the outdoor concentration rises rapidly and reaches its peak concentration halfway into the 1-h release. The other location (right column) is unaffected by the release until the wind changes and brings the toxic plume with it. Consequently, delaying SIP by up to 0.5-h does not change the indoor concentration predictions at all. However, if SIP is delayed for an hour after the release has started, then the indoor concentration is predicted to be much higher. At locations where the plume arrives sooner, every unit of time delay causes the indoor concentration to reach more toxic levels. Consequently, prompt SIP initiation is more critical in these locations. This is especially true when the pre-sheltering air-exchange rates are generally higher, as it is in the case of summertime conditions where 40% of the residences are modeled to have +1 h^{-1} owing to open windows. Slightly lower indoor concentrations are predicted when the pre-sheltering conditions are modeled under wintertime conditions.

At these two locations, the maximum increases in peak indoor concentration relative to the no-delay case are 1.3× under wintertime pre-sheltering conditions and 1.6× under summertime pre-sheltering conditions. These results are specific to the downwind distance of these locations from the release source. They are also specific to the air-

exchange rates of the houses modeled. Since only a fraction of the houses are affected by pre-sheltering conditions, predictions made using air-exchange rate evaluated at the tightest percentiles are hardly affected by SIP delay since these residences would already have windows closed. Figure 4.17 show that the changes in peak indoor concentration caused by SIP delay are less than 20% among tightly built houses. At the other extreme are houses that are very leaky and have their windows opened initially. The increase in peak indoor concentration in these residences can exceed a factor of 2 relative to the case of SIP starting without delay. Figure 4.17 also illustrates that houses located closest to the release source, and thus where the peak outdoor concentration appear soonest, are the ones that have to implement SIP most quickly to avoid high indoor concentrations. Houses that are located far enough downwind such that the outdoor concentrations do not peak until after the release has already stopped are much less affected by an initiation time delay.

Besides competing with the plume arrival time, the importance of SIP initiation time delay is also affected by the duration of the release. The longer the release duration, the longer the toxic load is accumulated. As a result, the penalty of having an initial period of fast air exchange with the outdoors becomes less significant to the overall exposure for longer release durations. On the other hand, for shorter releases, the penalty of not starting SIP quickly enough can be quite significant. Figure 4.18 shows the number of casualties predicted for all three release durations (0.5-h, 1-h, and 2-h) modeled for the case of linear dose-response. In all cases, there is some benefit of SIP in terms of reducing potential casualties as long as SIP is started before the release ends. For the 2-h

release, since the SIP initiation time delays considered (0.25 h, 0.5 h, and 1 h) are all considerably shorter than the release duration, the predicted number of potential casualties is essentially unaffected. For the 1-h release, starting SIP 0.25 h or even 0.5 h late is expected to have little effect. However, if no one can implement SIP before the release ends, then the ability of SIP to reduce casualties can be significantly compromised.

Finally, a worst-case scenario is modeled using a 0.5-h release for which SIP was not implemented until the release had already stopped. In this case, toxic chemicals that had infiltrated the indoors at high concentration can be trapped indoor because people shut their windows or stopped operating fans that induce air exchange. This reduction in air-exchange rate when people should instead be ventilating their homes to remove toxic chemicals from indoors can lead to severe adverse health effects. If people were to be continuously exposed to such elevated indoor concentration for 2 or 3 hours, more casualties could result as compared to the case of not implementing SIP. Judging from survey data on past chemical releases as discussed in Section 4.2.3, the assumption that no one in a community would implement SIP until after the release has stopped might be too pessimistic. However, it seems likely that some fraction of the population will not implement SIP at the times instructed by emergency responders. Consequently, the danger of trapping toxic chemicals in residences is a valid concern, especially when the community is not prepared to carry out protective actions expeditiously.

Yet, even in the case of short releases, there are three aspects of SIP that can help counteract this risk of doing more harm than good. First is the effect of nonlinear dose-response with $m > 1$. Figures 4.19 and 4.20 show the potential casualty estimates of the same three releases, but the health effects are evaluated using higher toxic load exponents ($m = 2$ and 3, respectively). The results show that SIP initiation time delay has little effect on the effectiveness of buildings to reduce potential casualties. This is because even the leakiest buildings with windows opened (air exchange exceeding 1.5 h^{-1}) can ensure a lower peak concentration indoors than outdoors. Referring to Figure 4.16, the ratio of the peak outdoor to indoor concentration is almost a factor of five if SIP is started with no delay. In the case of a significant delay, the reduction in peak outdoor to indoor concentration can still be sustained at a factor of three. Since a high toxic load exponent amplifies the reduction in adverse health effects relative to a reduction in peak concentration, effectiveness of SIP is ensured.

Terminating SIP soon after it is safe to do so can be another effective method to counteract the loss in effectiveness caused by a delay in initiation time. The potential casualty curves shown in Figure 4.18 start off being quite similar to one another for the 0.5-h release, regardless of the SIP initiation time delay. As long as SIP is terminated within an hour after the plume has dispersed and it is safe to go outdoors, the penalty of a delayed start is modest. By quickly terminating SIP, people are no longer being exposed to high levels of toxic chemicals trapped indoors. Consequently, the additional amount of chemicals infiltrating indoors at higher air-exchange rates would not cause as much adverse health effects to the occupants as otherwise.

Table 4.10 shows the estimated casualty reduction factor (CRF) evaluated at different SIP termination times for the case $m = 1$. If SIP were terminated within a half hour, CRF can be sustained at 0.61 even under the worst-case scenario. However, if SIP were allowed to extend for 2 h after the release has stopped, then the effectiveness of SIP can drop to as low as 0.07. At higher toxic load exponents (Tables 4.11 and 4.12), sensitivity to SIP termination time is much smaller for reasons discussed before.

Sorption to indoor surfaces is the third factor that can potentially counteract the loss in effectiveness caused by initiation time delay. As shown in Figure 4.14, sorption to indoor surfaces can be effective at eliminating the danger posed by exposure to residual contaminants left in the indoor air after the release has stopped. This effect is most significant when the dose-response relationship is linear. Not coincidentally, SIP effectiveness is also the most sensitive to initiation time delay when the dose-response relationship is linear. As a result, only under the cases when the dose-response is linear would the combined influences of sorption to indoor surfaces and SIP initiation time delay be of practical interest. When the dose response is nonlinear with $m > 1$, analyses so far have suggested that neither sorption to indoor surfaces (Figure 4.14) nor SIP initiation time delay (Figures 4.19 and 4.20) alter the effectiveness significantly.

Is sorption on indoor surfaces sufficient to offset the loss in SIP effectiveness caused by a time delay in SIP initiation? To exaggerate the loss in effectiveness caused by initiation delay, summertime pre-sheltering conditions are used because they have been shown to lead to slightly lower SIP effectiveness (Figure 4.18) than wintertime conditions. Only

linear dose-response conditions are considered. Figure 4.21 shows the predicted potential casualties if people were to shelter in-place with and without time delay under three sorption cases: no sorption, moderate sorption (modeled after NH_3 experiments), and strong sorption (modeled after DMMP experiments). Under all release durations and SIP initiation time delays considered, sorption to indoor surfaces even at the slowest rate modeled is sufficient to sustain SIP effectiveness. There seems to be little difference in the model results obtained between the cases where people were to start SIP with a 0.5-h or 1-h delay. Even in the worst-case scenario where SIP was not implemented until after the release has already stopped (i.e. 0.5-h release with 1-h SIP initiation time delay), SIP is expected to do more good than harm for the community. As observed before, sorption to indoor surfaces eliminates the urgency to terminate SIP. Regardless of whether the release is relatively short (0.5-h) or long (2-h), a casualty reduction factor (CRF) ranging between 0.6 and 0.9 is expected. In shorter releases, CRF is expected to be somewhat more sensitive to the rates at which sorption to indoor surfaces take place. This sensitivity can translate into model uncertainty when only one set of sorption rates is used to model a process that is expected to vary among residences.

4.3.4 Model Limitations

The case study presented here considers a large-scale release in a populated urban neighborhood. The release amount, meteorology, population density, and housing characteristics are all specific to the scenario modeled. In situations where these parameters deviate far from the set of conditions modeled here, SIP effectiveness can

differ. Consequently, interpretation of the results should focus on the functional influences of the various parameters on SIP effectiveness, and not on the numerical values of the potential casualty estimates predicted. In any emergency situation, there are inevitably specificities that demand predictions to be tailored to the release event. Real-time model predictions are therefore valuable in providing emergency responders with the expected SIP protectiveness for the exposed community in that specific situation. The insights distilled from the analysis presented here can guide such modeling efforts by prioritizing the significance of each parameter.

Among the parameters that affect indoor concentration predictions, the air infiltration rate distribution is the best characterized. While careful assessment of this parameter is justified as it is the entry pathway of toxic chemicals into the indoors under SIP conditions (windows closed, mechanical ventilation shut off), there are other aspects of this analysis that warrant more detailed consideration. It is foreseeable that other chemicals not yet studied will react differently with the indoor materials under some environmental conditions. Some chemicals can also have other important reactions or removal pathways, potentially leading to hazardous secondary chemicals being produced. Any adverse health effects associated with dermal exposure to contaminated indoor surfaces are also not considered in this analysis. Findings from this analysis are therefore limited to chemicals for which the dominant mode of exposure is inhalation, and for which adverse health effects from acute exposure to the primary chemicals is the foremost concern.

The preliminary treatment of time delay before SIP is implemented is relatively simplistic in this analysis. Given the very limited data on how people respond to emergency situations, the influence of this parameter on SIP effectiveness has been modeled by assuming that the entire community reacts similarly. In situations where the initiation time delay holds the key to SIP effectiveness (e.g. linear dose-response under releases of short duration), the distribution of initiation time in a community should be explicitly modeled in future analysis. Also not considered in this analysis is people's instinct to avoid chemical exposure if detected by its odor or visual clues (e.g. cloud of visible gas surrounding the neighborhood). It is possible that these factors might cause those who are closest to the release source, and thus are most at risk, to react more quickly than others who are further downwind. By implementing SIP sooner, their exposures can be reduced. On the other hand, this analysis assumed that the entire community was already indoors at the time of the release. Further, it assumed that after the initiation time delay, all would follow the instruction to shelter-in-place without exception. The validity of these two assumptions might vary depending on the time or day of the release, and the emergency preparedness of the community. The current state of knowledge on issues concerning human behavior in acute airborne release emergencies remains limited. More detailed assessment from past events is needed before these complications can be realistically modeled.

In this analysis, potential casualties are quantified in terms of the number of people with cumulative toxic load exceeding a certain limit. More sophisticated assessment of adverse health effects could also capture the variability in human susceptibility to the toxic

chemicals. Sensitive sub-populations (e.g. children, elderly, and the health compromised) might experience health effects at lower doses than the rest of the community. The method used here to assess the number of potential casualties does not include the distribution of susceptibility in a population. Distributional analysis of the health effects suffered by general populations acutely exposed to toxic industrial chemicals and chemical warfare agents is limited (Griffiths and Megson, 1984; Sommerville 2003). A few studies have considered the implications of such distributions of human susceptibility on the health consequences from hypothetical chemical releases (Hilderman et al., 1999). Studies by Ride (1995), Lewis (1997), and Yee (1999) examined one aspect of the interaction between fluctuating outdoor concentrations and adverse health effects. The combined effects of the distribution of human susceptibility, residential air-exchange rates, and SIP initiation and termination time as implemented by the residents can potentially alter SIP effectiveness from the model results presented here. Some high-risk subgroups of the population might be identified from such analysis, which could provide a basis for considering issues like environmental justice (Derezinkski et al., 2003; Stretesky and Lynch, 1999; Elliott et al., 2004) and risk management (Sorensen and Carnes, 1992) for chemical accidents.

Finally, the modeling approach in this analysis incrementally varies each parameter independently and observes the change in the results. This brute-force method is reasonable for this stage of investigation. However, more systematic uncertainty analysis can shed light on, for example, the contribution of each parameter to the overall uncertainty estimate of SIP effectiveness. The current state of knowledge can provide

reasonable estimates of the uncertainties associated with the air-exchange rate distribution in residences and the range of sorption rates on indoor surfaces. The uncertainty bounds that remain are expected to be narrower from these variables in comparison to parameters associated with chemical toxicity and human susceptibility, as well as parameters that affect the outdoor concentrations (e.g. local meteorology, release amount, and chemical species involved). Depending on the metric of SIP effectiveness used, the relative contribution from each of these factors to the overall uncertainty estimate can also vary. For example, instead of normalizing the potential casualty estimates with respect to the outdoor values, emergency responders are likely interested in knowing also the absolute casualty estimates for those who take shelter. Unlike normalized casualty estimates, absolute casualty estimates are highly dependent on parameters that affect the outdoor concentrations.

4.4 Conclusions

Results from the base-case simulations agree with the main findings from Chapter 2 where a simple Gaussian plume model was used to simulate hypothetical releases of various amount and duration. Shelter-in-place (SIP) is consistently more effective when the dose-response used to evaluate adverse health effects is increasingly nonlinear with toxic load exponent exceeding 1. For release durations of a few hours or less, loss in effectiveness is mainly caused by accumulating exposure to the residual contamination that remains indoors. With a high toxic load exponent, CRF is insensitive to the SIP termination time. The analysis presented here made use of the distributions of air

infiltration rates of houses as estimated in Chapter 3. The value of modeling such distributions when assessing the SIP effectiveness in a community lies in capturing the small fraction of houses that are most leaky, and where residents are the most at risk. Ignoring them will lead to underpredictions of the casualty estimates for those who shelter in their residences. Valuable information can also be extracted from modeling these distributions to help emergency responders better allocate resources to areas where people who took shelter are most likely to need assistance.

Sorption to indoor surfaces can significantly lower the peak indoor concentrations and reduce the amount of residual contamination left in the indoor air after the plume has passed. The most dramatic effect on SIP effectiveness is for chemicals that exhibit a linear dose-response relationship. Even at rates where chemicals sorb only moderately to indoor surfaces, this process is sufficient to offset the need for timely termination of SIP. To the extent that the range of sorption rates modeled represents the variability in real residences, this interaction with indoor surfaces might introduce yet another source of variability to SIP effectiveness among households in a community.

Sorption to indoor surfaces is also sufficiently fast enough to counteract the loss in effectiveness caused by SIP initiation time delay. Two pre-sheltering conditions were modeled to represent the prevalence and extent to which the air-exchange rate is in excess of the air infiltration rate in a community of houses. Analysis shows that as long as the SIP initiation time delay is less lengthy than the release duration, SIP effectiveness measured in terms of the casualty reduction factor will not be substantially degraded. In

cases where the dose-response is linear and sorption onto indoor surfaces is negligible, prompt SIP termination is important to retain SIP effectiveness as a protective action. Of course, this is not to claim that SIP initiation time delay does not matter at all in other situations. In fact, the increase in peak indoor concentrations in houses caused by the time delay can be as much as a factor of 3. The increase in exposure can lead to lesser degree of protection that is not fully quantified in this analysis by the measure of SIP effectiveness used.

In emergency situations, a purpose of model predictions is to provide officials with expectations about the effectiveness of a response. As an initial response, the decision is either to evacuate the community, or to shelter in-place. The analysis here identified the various factors that can affect SIP effectiveness, and presented estimates of their influence on model results. In practice, the decision-making process needs to consider also the feasibility of evacuation versus SIP in a given situation (Sorensen et al., 2004). Conceptually, the alternatives should be weighted by their effectiveness in protecting the public against exposure to the toxic chemical. It is based on this idea that the notion of casualty reduction factor is used as the metric of comparison in this analysis. In practice, however, decision makers and the public must be willing to accept certain risks associated with SIP, especially in cases where it does not completely eliminate casualties for those who shelter. In other words, all parties in a community must value each unit of injury avoidance as being equal, regardless of the protective action taken. In emergencies where liability and lawsuit could follow, SIP, being viewed as the inactive alternative to evacuation, might be at a disadvantage. All these issues must be addressed before a

model can be put into practice to aid the decision-making process. For now, the analyses presented here only assessed SIP effectiveness in isolation from other alternative protective actions.

The analyses presented here only assessed SIP effectiveness of single-family detached dwellings. Other forms of residences, such as town houses and apartment buildings, and other buildings, such as offices and schools, can have air leakage characteristics that are significantly different from one another. Furthermore, the airflow in these buildings tends to be more complex due to their larger sizes and due to the flow resistance of internal partitions. These types of buildings constitute a large fraction of the building stock, especially in urban areas. Depending on the time of release, a large fraction of people might be at schools and workplaces rather than at their homes. For these reasons, knowing the characteristics of these buildings is also essential to evaluating SIP as a protective strategy. In the following two chapters, I will assess the air leakage characteristics of non-residential buildings and model their effectiveness in protecting building occupants against large-scale outdoor releases.

4.5 References

Blewett, W.K., Arca ,V.J., 1999. Experiments in sheltering in place: how filtering affects protection against sarin and mustard vapor. Edgewood Chemical Biological Center, ECBC-TR-034, Aberdeen Proving Ground, MD.

Deaves, D.M., Gilham, S., Mitchell, B.H., Woodburn, P., Shepherd, A.M., 2001. Modeling of catastrophic flashing releases. Journal of Hazardous Materials A88, 1–32.

Derezinkski D.D., Lacy, M.G., Stretesky, P.B., 2003. Chemical accidents in the United States, 1990–1996. Social Science Quarterly 84 (1), 122–143.

Dunn, J.E., Tichenor, B.A., 1988. Compensating for sink effects in emissions test chambers by mathematical modeling. Atmospheric Environment 22, 885–894.

Elliott, M.R., Wang, Y., Lowe, R.A., Kleindorfer, P.R., 2004. Environmental justice: frequency and severity of US chemical industry accidents and the socioeconomic status of surrounding communities. Journal of Epidemiology & Community Health 58, 24–27.

Engelmann, R.J., Pendergrass, W.R., White, J.R., Hall, M.E., 1992. The effectiveness of stationary automobiles as shelters in accidental releases of toxic materials. Atmospheric Environment 26A, 3119–3125.

Ermak, D.L., Nasstrom, J.S., 2000. A Lagrangian stochastic diffusion method for inhomogeneous turbulence. Atmospheric Environment 34, 1059–1068.

Griffiths, R.F., Megson, L.C., 1984. The effect of uncertainties in human toxic response on hazard range estimation for ammonia and chlorine. Atmospheric Environment 18, 1195–1206.

Grøntoft, T., Raychaudhuri, M.R., 2004. Compilation of tables of surface deposition velocities for O_3, NO_2 and SO_2 to a range of indoor surfaces. Atmospheric Environment 38, 533–544.

Hilderman, T.L., Hurdey, S.E., Wilson, D.J., 1999. A model for effective toxic load from fluctuating gas concentrations. Journal of Hazardous Materials A64, 115–134.

Jetter, J.J., Whitfield, C., 2005. Effectiveness of expedient sheltering in place in a residence. Journal of Hazardous Materials A119, 31–40.

Jonson, L., Karlsson, E., Thaning, L., 2005. Toxic gas clouds: effects and implications of dry deposition on concentration. Journal of Hazardous Materials A124, 1–18.

Jørgensen, R.B., Dokka, T.H., Bjørseth, O., 2000. Introduction of a sink-diffusion model to describe the interaction between volatile organic compounds (VOCs) and material surfaces. Indoor Air 10, 27–38.

Karlsson, E., Berglund, T., Rittfeldt, L., 1992. Leakage of vapor clouds into ordinary buildings and sealed rooms, and their protective capacity. Proceedings, Chemical Protection, Ylöjärvi, Finland.

Karlsson, E.,1994. Indoor deposition reducing the effect of toxic gas clouds in ordinary buildings. Journal of Hazardous Materials 38, 313–327.

Karlsson E., Huber U., 1996. Influence of desorption on the indoor concentration of toxic gases. Journal of Hazardous Materials 49, 15–27.

Lasker, R.D., 2004. Redefining readiness: terrorism planning through the eyes of the public. Center for the Advancement of Collaborative Strategies in Health, The New York Academy of Medicine, New York, NY. www.cacsh.org

Lewis, D.M., 1997. Monte Carlo estimates of dosages of gases dispersing in the atmosphere. Environmetrics 8, 629–650.

Morrison, G.C., Nazaroff, W.W., 2002. The rate of ozone uptake on carpet: mathematical modeling. Atmospheric Environment 36, 1749–1756.

Murray, V., Goodfellow, F., 2002. Mass casualty chemical incidents – towards guidance for public health management. Public Health 116, 2–14.

Nazaroff, W.W., Gadgil, A.J., Weschler, C.J., 1993. Critique of the use of deposition velocity in modeling indoor air quality. In: Modeling Indoor Air Quality and Exposure, ASTM STP 1205, Nagda, N.L., Ed., American Society for Testing and Materials, Philadelphia, PA, 81–104.

NICS, 2001. Sheltering in place as a public protection action. National Institute for Chemical Studies, Charleston, WV.

NRC, 2003. Acute exposure guideline levels for selected airborne chemicals: volume 3. Subcommitte on Acute Exposure Guideline Levels, Committee on Toxicology, National Research Council, The National Academies Press, Washington DC.

Renard, J.J., Calidonna, S.E., Henley, M.V., 2004. Fate of ammonia in the atmosphere – a review for applicability to hazardous releases. Journal of Hazardous Materials B108, 29–60.

Ride, D.J., 1995. A practical method of estimating toxic loads in the presence of concentration fluctuations. Environmetrics 6, 643–650.

Rogers, G.O., Sorensen, J.H., 1989. Warning and response in two hazardous materials transportation accidents in the US. Journal of Hazardous Materials 22, 57–74.

Rogers, G.O., Watson, A.P., Sorensen, J.H., Sharp, R.D., Carnes, S.A., 1990. Evaluating protective actions for chemical agent emergencies. ORNL-6615, Oak Ridge National Laboratory, Oak Ridge, TN.

Rogers, G.O., Sorensen, J.H., 1991. Diffusion of emergency warning: comparing empirical and simulation results. Risk Analysis Prospects and Opportunities, Zerros, C., et al. (Eds.), Plenum Press, New York, NY, 117–134.

Rogers, G.O., 1994. The timing of emergency decisions: modeling decisions by community officials during chemical accidents. Journal of Hazardous Materials 37, 353–373.

Routley, J.G., 1991. Massive leak of liquified chlorine gas, Henderson, Nevada. Technical Report Series, National Fire Data Center, US Fire Administration, Federal Emergency Management Agency, Washington, DC.

Singer, B.C., Hodgson, A.T., Guevarra, K.S., Hawley, E.L., Nazaroff, W.W., 2002. Gas-phase organics in environmental tobacco smoke. 1. Effects of smoking rate, ventilation, and furnishing level on emission factors. Environmental Science & Technology 36, 846–853.

Singer, B.C., Revzan, K.L., Hotchi, T., Hodgson, A.T., Brown, N.J., 2004. Sorption of organic gases in a furnished room. Atmospheric Environment 38, 2483–2494.

Singer, B.C., Hodgson, A.T., Destaillats, H., Hotchi, T., Revzan, K.L., Sextro, R.G., 2005a. Indoor sorption of surrogates for sarin and related nerve agents. Environmental Science & Technology 39, 3203–3214.

Singer, B.C., Hodgson, A.T., Hotchi, H., Ming, K.Y., Sextro, R.G., Wood, E.E., Brown, N.J., 2005b. Sorption of organic gases in residential bedrooms and bathrooms. Proceedings, Indoor Air: 10th International Conference on Indoor Air Quality and Climate, Beijing, China.

Sommerville, D.R., 2003. Relationship between the dose-response for lethality and severe effects for chemical warfare nerve agents. Proceedings, 8th Annual US Army Conference on Applied Statistics, Raleigh, NC.

Sorensen, J.H., Carnes, S.A., 1992, An approach for deriving emergency planning zones for chemical munitions emergencies, Journal of Hazardous Materials 30, 223-242.

Sorensen, J.H., Vogt, B.M., 2001. Will duct tape and plastic really work? Issues related to expedient shelter-in-place. ORNL/TM-13742, Oak Ridge National Laboratory, TN.

Sorensen, J.H., Shumpert, B.L., Vogt, B.M., 2004. Planning for protective action decision making: evacuate or shelter-in-place. Journal of Hazardous Materials A109, 1–11.

Stretesky, P., Lynch, M.J., 1999. Corporate environmental violence and racism. Crime, Law & Social Change 30, 163–184.

Vogt, B.M., Sorensen, J.H., 1999. Description of survey data regarding the chemical repackaging plant accident West Helena, Arkansas. ORNL-13722, Oak Ridge National Laboratory, Oak Ridge, TN.

Ward, M., Siegel, J.A., Corsi, R.L., 2005. The effectiveness of stand alone air cleaners for shelter-in-place. Indoor Air 15, 127–134.

Yee, E., 1999. An impact-effect mathematical model incorporating the influence of exposures to fluctuating concentrations in a dispersing plume of pollutant in the atmosphere. Journal of Exposure Analysis and Environmental Epidemiology 9, 300–311.

4.6 Tables

Table 4.1 Measured deposition velocity to indoor materials of some toxic industrial chemicals and a chemical warfare agent simulant.

Chemical	v_d (m/s)	Surface Materials	Source
SO_2	1.2 to 1.6×10^{-3}	e.g. Concrete; untreated gypsum wallboard; plaster (all at 50% RH)	Grøntoft and Raychaudhuri (2004)
	1.6 to 7.6×10^{-4}	e.g. Brick; wood work; surface treated gypsum wallboard; carpet; wallpaper; cloth (50% RH)	
Cl_2	0.9 to 1.0×10^{-4}	Painted walls, roof, and synthetic carpet	Karlsson (1994)
NH_3	3.0 to 5.0×10^{-5}		
Trialkyl-Phosphono-acetate (VX simulant)	$(2.6 \pm 1.6)\times10^{-4}$		

Table 4.2 Measured one-sink sorption and desorption rate coefficients (Eqn 4.2 and Eqn 4.3) of some toxic industrial chemicals and chemical warfare agents.

Chemical	k_a (m/s)	k_d (s^{-1})	Surface Materials	Source
Cl_2	$(1.4 \pm 0.6)\times10^{-4}$	$(4.6 \pm 2.6)\times10^{-5}$	Painted walls, roof, and synthetic carpet	Karlsson (1994)
NH_3	$(1.1 \pm 0.4)\times10^{-4}$	$(5.5 \pm 2.3)\times10^{-6}$		
Trialkyl-phosphono-acetate (VX simulant)	$(2.5 \pm 1.2)\times10^{-4}$	$(1.8 \pm 1.1)\times10^{-6}$		
Sarin	1.8×10^{-4}	1.6×10^{-6}	Old chalking paint on concrete	Karlsson and Huber (1996)

Table 4.3 Measured sorption rate coefficients of three surrogates of G-series chemical warfare agents obtained from two sets of experiments.

			Sorption Rate Coefficients			
Chemicals	Test Room/ Source		k'_a (h^{-1}) [#]	k_d (h^{-1})	k_1 (h^{-1}) or k_{diff} (h^{-1})	k_2 (h^{-1})
DMMP	Rooms in Residences[‡]	(1)[*]	3.2 ± 1.4	0.09 ± 0.03		
		(2)[†]	3.5 ± 1.5	0.17 ± 0.06	0.21 ± 0.01	
		(3)[§]	5.0 ± 1.5	0.86 ± 0.40	0.72 ± 0.16	0.12 ± 0.04
	Experimental Chamber[◊]	(1)	1.4	0.04		
		(2)	1.5	0.08	0.05	
		(3)	2.1	0.40	0.20	0.03
DEEP	Rooms in Residences	(1)	3.3 ± 1.3	0.12 ± 0.03		
	Experimental Chamber	(1)	1.6	0.04		
		(2)	1.7	0.08	0.05	
		(3)	2.4	0.39	0.21	0.03
TEP	Experimental Chamber	(1)	1.8	0.04		
		(2)	1.9	0.09	0.05	
		(3)	2.5	0.37	0.21	0.04

[#] The sorption rate coefficients k'_a (h^{-1}) presented here have units that differ from that used in Eqn 4.2 to 4.7, due to slight difference in model formulation. Instead of modeling the mass sorbed to surface normalized to the surface area g/m^2, here the mass sorbed to surfaces is normalized to the room volume g/m^3. Conversion between the two formulations is through $k'_a = \frac{k_a}{S/V}$, where S/V (m^2/m^3) is the surface-to-volume ratio.

[‡] Source: Singer et al. (2005b).

[◊] Source: Singer et al. (2005a).

[*] (1) One-sink model, formulation shown in Eqn 4.2 and 4.3.

[†] (2) Two-sink diffusion model, formulation shown in Eqn 4.4 to 4.7, with the exception that k_a is replaced with k'_a.

[§] (3) Two-sink four-parameter model, formulation same as (2), with the exception that k_{diff} is replaced by two rate coefficients, k_1 and k_2, in a manner illustrated in Figure 4.2.

Table 4.4 List of sorption/desorption models and rate coefficients used to assess SIP effectiveness.

Sorption Level	Governing Equations of Indoor Concentration	Sorption Rate Coefficients		
No Sorption	$\frac{dC(t)}{dt} = \frac{Q}{V} \cdot \left(C_{out} - C(t)\right)$ where $\frac{Q}{V}$ = Air - exchange rate [s^{-1}] C_{out} = Outdoor concentration [g/m^3] $C(t)$ = Indoor concentration [g/m^3]			
Sorption with Surface Sink	$\frac{dC(t)}{dt} = \frac{Q}{V} \cdot \left(C_{out} - C(t)\right) - \frac{S}{V} \cdot \left(k_a \cdot C(t) + k_d \cdot M(t)\right)$ $\frac{dM(t)}{dt} = k_a \cdot C(t) - k_d \cdot M(t)$ where $\frac{S}{V}$ = Surface - to - volume ratio [m^2/m^3] $M(t)$ = Sorbed - phase mass per unit surface area [g/m^2]	NH_3 (Table 4.2)		
			Set I#	Set II*
		k_a [m/s]	0.7 $\times 10^{-4}$	1.5 $\times 10^{-4}$
		k_d [s^{-1}]	7.8 $\times 10^{-6}$	3.2 $\times 10^{-6}$
Sorption with Surface and Embedded Sinks	$\frac{dC(t)}{dt} = \frac{Q}{V} \cdot \left(C_{out} - C(t)\right) - k'_a \cdot C(t) + k_d \cdot M_1(t)$ $\frac{dM_1(t)}{dt} = k'_a \cdot C(t) - k_d \cdot M_1(t) - k_1 \cdot M_1(t) + k_2 \cdot M_2(t)$ $\frac{dM_2(t)}{dt} = k_1 \cdot M_1(t) - k_2 \cdot M_2(t)$ where $M_1(t)$ = Mass sorbed on surface sink per unit indoor volume [g/m^3] $M_2(t)$ = Mass sorbed on embedded sink per unit indoor volume [g/m^3]	DMMP, GB surrogate (Table 4.3)		
			Set I#	Set II*
		k'_a [s^{-1}]	1.1 $\times 10^{-3}$	1.9 $\times 10^{-3}$
		k_d [s^{-1}]	3.5 $\times 10^{-4}$	1.3 $\times 10^{-4}$
		k_1 [s^{-1}]	1.6 $\times 10^{-4}$	2.4 $\times 10^{-4}$
		k_2 [s^{-1}]	4.4 $\times 10^{-5}$	2.2 $\times 10^{-5}$

Two sets of rate coefficients are used: "Set I" refers to the set of rate coefficients that will give the *upper* indoor concentration estimates in residences.
* "Set II" refers to the set that will give the *lower* indoor concentration estimates.

Table 4.5 Approximate SIP initiation time delays estimated for a community.

	Action	Time Required (minutes)			Data Source
		Fast	Typical	Slow	
(1)	Officials to Identify Hazard	5	15	45	Rogers (1994); NICS (2001)
(2)	Population to Receive Warning	5	10	30	Rogers and Sorensen (1991)
(3)	Population to Implement Shelter-in-Place	5	10	20	Rogers and Sorensen (1989); Rogers et al. (1990)

Table 4.6 Summary of model parameters used to assess SIP effectiveness.

Parameters	Values Modeled		
Release Duration	0.5 h	1 h	2 h
Toxic Load Exponent	1	2	3
Sorption Rate[#]	0 h^{-1}	$k'_a \sim 0.9\ h^{-1}$	$k'_a \sim 5\ h^{-1}$
Pre-Sheltering Air-Exchange Rate	+ 0 h^{-1} (air infiltration only)	+0.3 h^{-1} in 80% of households (wintertime)	+ 1 h^{-1} in 40% of households (summertime)
Shelter-in-Place Initiation Time Delay[†]	0.25 h	0.5 h	1 h
Shelter-in-Place Termination Time[§]	0.5 h	1 h	2 h

[#] See Table 4.4 for details of the model formulations and parameters used.
[†] Initiation time delay measured from the start time of the release.
[§] Termination time measured from stop time of the release.

Table 4.7 List of simulations and their assigned codes[#].

Simulation Code	Toxic Load Exponent[§]	Release Duration (h)	Release Amount	Sorption on Indoor Surfaces	Air Leakage of Dwellings	Pre-SIP Air-Exchange Rate (h^{-1})	SIP Initiation Time Delay (h)
4Ai, ii, iii	1, 2, 3	0.5	1×	No	Distribution	NA	0
4Bi, ii, iii	1, 2, 3	1	1×	No	Distribution	NA	0
4Ci, ii, iii	1, 2, 3	2	1×	No	Distribution	NA	0
4Di, iii	1, 3	0.5	0.04×	No	Distribution	NA	0
4Ei, iii	1, 3	1	0.04×	No	Distribution	NA	0
4Fi, iii	1, 3	2	0.04×	No	Distribution	NA	0
4Gi, iii	1, 3	0.5	0.4×	No	Distribution	NA	0
4Hi, iii	1, 3	1	0.4×	No	Distribution	NA	0
4Ii, ii	1, 3	2	0.4×	No	Distribution	NA	0
4Ji, iii	1, 3	0.5	4×	No	Distribution	NA	0
4Ki, iii	1, 3	1	4×	No	Distribution	NA	0
4Li, iii	1, 3	2	4×	No	Distribution	NA	0
4Mi	1	0.5	1×	No	Uniform	NA	0
4Ni	1	1	1×	No	Uniform	NA	0
4Oi	1	2	1×	No	Uniform	NA	0
4Pi, ii, iii	1, 2, 3	1	1×	Moderate	Distribution	NA	0
4Qi, ii, iii	1, 2, 3	1	1×	Strong	Distribution	NA	0
4R1i, ii, iii	1, 2, 3	0.5	1×	No	Distribution	0.3 (80%)	0.25
4S1i, ii, iii	1, 2, 3	1	1×	No	Distribution	0.3 (80%)	0.25
4T1i, ii, iii	1, 2, 3	2	1×	No	Distribution	0.3 (80%)	0.25
4U1i, ii, iii	1, 2, 3	0.5	1×	No	Distribution	0.3 (80%)	0.5
4V1i, ii, iii	1, 2, 3	1	1×	No	Distribution	0.3 (80%)	0.5
4W1i, ii, iii	1, 2, 3	2	1×	No	Distribution	0.3 (80%)	0.5
4X1i, ii, iii	1, 2, 3	0.5	1×	No	Distribution	0.3 (80%)	1
4Y1i, ii, iii	1, 2, 3	1	1×	No	Distribution	0.3 (80%)	1
4Z1i, ii, iii	1, 2, 3	2	1×	No	Distribution	0.3 (80%)	1
4R2i, ii, iii	1, 2, 3	0.5	1×	No	Distribution	1.0 (40%)	0.25
4S2i, ii, iii	1, 2, 3	1	1×	No	Distribution	1.0 (40%)	0.25
4T2i, ii, iii	1, 2, 3	2	1×	No	Distribution	1.0 (40%)	0.25
4U2i, ii, iii	1, 2, 3	0.5	1×	No	Distribution	1.0 (40%)	0.5
4V2i, ii, iii	1, 2, 3	1	1×	No	Distribution	1.0 (40%)	0.5
4W2i, ii, iii	1, 2, 3	2	1×	No	Distribution	1.0 (40%)	0.5
4X2i, ii, iii	1, 2, 3	0.5	1×	No	Distribution	1.0 (40%)	1
4Y2i, ii, iii	1, 2, 3	1	1×	No	Distribution	1.0 (40%)	1
4Z2i, ii, iii	1, 2, 3	2	1×	No	Distribution	1.0 (40%)	1

Table 4.7 (continued)

Simulation Code	Toxic Load Exponent[§]	Release Duration (h)	Release Amount	Sorption on Indoor Surfaces	Air Leakage of Dwellings	Pre-SIP Air-Exchange Rate (h^{-1})	SIP Initiation Time Delay (h)
4Umi	1	0.5	1×	Moderate	Distribution	1.0 (40%)	0.5
4Vmi	1	1	1×	Moderate	Distribution	1.0 (40%)	0.5
4Wmi	1	2	1×	Moderate	Distribution	1.0 (40%)	0.5
4Usi	1	0.5	1×	Strong	Distribution	1.0 (40%)	0.5
4Vsi	1	1	1×	Strong	Distribution	1.0 (40%)	0.5
4Wsi	1	2	1×	Strong	Distribution	1.0 (40%)	0.5
4Xmi	1	0.5	1×	Moderate	Distribution	1.0 (40%)	1
4Ymi	1	1	1×	Moderate	Distribution	1.0 (40%)	1
4Zmi	1	2	1×	Moderate	Distribution	1.0 (40%)	1
4Xsi	1	0.5	1×	Strong	Distribution	1.0 (40%)	1
4Ysi	1	1	1×	Strong	Distribution	1.0 (40%)	1
4Zsi	1	2	1×	Strong	Distribution	1.0 (40%)	1

[#] Also see Table 4.6 for detail on the model parameters and values used.
[§] Toxic load exponents 1, 2, and 3 correspond to i, ii, and iii, respectively, of the simulation codes.

Table 4.8 List of simulations, as indicated by their designated codes (see Table 4.7), for which results are plotted in selected figures.

Figure	Simulation Codes	Results Presented
4.7	4Ai, ii, iii; 4Bi, ii, iii; 4Ci, ii, iii	Casualty estimates
4.8	4Ai, ii, iii; 4Bi, ii, iii; 4Ci, ii, iii	Predicted toxic load
4.9	4Ai, iii; 4Bi, iii; 4Ci, iii; 4Di, iii; 4Ei, iii; 4Fi, iii; 4Gi, iii; 4Hi, iii; 4Ii, iii; 4Ji, iii; 4Ki, iii; 4Li, iii	Casualty estimates
4.10	4Ai, 4Bi, 4Ci, 4Mi, 4Ni, 4Oi	Casualty estimates
4.11	4Bi, 4Ni	Affected areas
4.12	4Bi	Affected areas
4.13	4Bi, 4Pi, 4Qi	Predicted concentrations
4.14	4Bi, ii, iii; 4Pi, ii, iii; 4Qi, ii, iii	Casualty estimates
4.15	4S1i, 4S2i	Air-exchange rates
4.16	4Bi, 4S1i, 4V1i, 4Y1i, 4S2i, 4V2i, 4Y2i	Predicted concentrations
4.17	4Bi, 4S2i, 4V2i, 4Y2i	Predicted concentrations
4.18	4Ai, 4Bi, 4Ci, 4R1i, 4S1i, 4T1i, 4U1i, 4V1i, 4W1i, 4X1i, 4Y1i, 4Z1i, 4R2i, 4S2i, 4T2i, 4U2i, 4V2i, 4W2i, 4X2i, 4Y2i, 4Z2i	Casualty estimates
4.19	4Aii, 4Bii, 4Cii, 4R1ii, 4S1ii, 4T1ii, 4U1ii, 4V1ii, 4W1ii, 4X1ii, 4Y1ii, 4Z1ii, 4R2ii, 4S2ii, 4T2ii, 4U2ii, 4V2ii, 4W2ii, 4X2ii, 4Y2ii, 4Z2ii	Casualty estimates
4.20	4Aiii, 4Biii, 4Ciii, 4R1iii, 4S1iii, 4T1iii, 4U1iii, 4V1iii, 4W1iii, 4X1iii, 4Y1iii, 4Z1iii, 4R2iii, 4S2iii, 4T2iii, 4U2iii, 4V2iii, 4W2iii, 4X2iii, 4Y2iii, 4Z2iii	Casualty estimates
4.21	4U2i, 4V2i, 4W2i, 4Umi, 4Vmi, 4Wmi, 4Usi, 4Vsi, 4Wsi, 4X2i, 4Y2i, 4Z2i, 4Xmi, 4Ymi, 4Zmi, 4Xsi, 4Ysi, 4Zsi	Casualty estimates

Table 4.9 Casualty reduction factor[#] (CRF) for SIP under base-case simulation[*] conditions, without sorption.

Toxic Load Exp.	Release Duration			Release Duration			Release Duration		
	0.5-h	1-h	2-h	0.5-h	1-h	2-h	0.5-h	1-h	2-h
	CRF evaluated at 0.5 h after stop of release			CRF evaluated at 1 h after stop of release			CRF evaluated at 2 h after stop of release		
1	0.75	0.72	0.65	0.60	0.62	0.51	0.39	0.42	0.31
2	0.80	0.77	0.67	0.78	0.75	0.60	0.76	0.74	0.56
3	0.82	0.79	0.68	0.81	0.78	0.64	0.81	0.78	0.63

[#] Definition of casualty reduction factor (Chapter 2):

$$\text{CRF} = 1 - \frac{\text{Population (Toxic Load}_{\text{indoors}} > \text{Toxic Load Limit)}}{\text{Population (Toxic Load}_{\text{outdoors}} > \text{Toxic Load Limit)}}$$

[*] Simulation 4Ai, ii, iii; 4Bi, ii, iii; 4Ci, ii, iii.

Table 4.10 Casualty reduction factor (CRF) when toxic load exponent = 1 under various pre-sheltering air exchange distributions and shelter-in-place initiation time, without sorption.

SIP Start Delay (h)		Release Duration			Release Duration			Release Duration		
		0.5-h	1-h	2-h	0.5-h	1-h	2-h	0.5-h	1-h	2-h
		CRF evaluated at 0.5 h after stop of release			CRF evaluated at 1 h after stop of release			CRF evaluated at 2 h after stop of release		
0 h		0.75	0.71	0.65	0.60	0.62	0.51	0.39	0.42	0.31
Winter	0.25	0.73	0.72	0.64	0.58	0.61	0.50	0.37	0.41	0.31
	0.5	0.71	0.71	0.64	0.52	0.60	0.50	0.27	0.40	0.30
	1.0	0.70	0.68	0.62	0.48	0.55	0.48	0.19	0.28	0.27
Summer	0.25	0.72	0.71	0.64	0.57	0.61	0.50	0.36	0.41	0.31
	0.5	0.68	0.70	0.63	0.47	0.60	0.49	0.25	0.39	0.30
	1.0	0.66	0.66	0.61	0.43	0.50	0.46	0.07	0.21	0.26

Table 4.11 Casualty reduction factor (CRF) when toxic load exponent = 2 under various pre-sheltering air exchange distributions and shelter-in-place initiation time, without sorption.

SIP Start Delay (h)		Release Duration			Release Duration			Release Duration		
		0.5-h	1-h	2-h	0.5-h	1-h	2-h	0.5-h	1-h	2-h
		CRF evaluated at 0.5 h after stop of release			CRF evaluated at 1 h after stop of release			CRF evaluated at 2 h after stop of release		
0 h		0.80	0.77	0.67	0.78	0.75	0.60	0.76	0.74	0.56
Winter	0.25	0.79	0.77	0.66	0.77	0.74	0.60	0.75	0.73	0.56
	0.5	0.77	0.76	0.65	0.74	0.74	0.59	0.73	0.72	0.55
	1.0	0.77	0.74	0.64	0.74	0.72	0.58	0.71	0.70	0.53
Summer	0.25	0.79	0.76	0.66	0.76	0.74	0.60	0.75	0.73	0.55
	0.5	0.76	0.76	0.65	0.73	0.73	0.59	0.70	0.72	0.55
	1.0	0.74	0.73	0.63	0.70	0.69	0.57	0.68	0.66	0.52

Table 4.12 Casualty reduction factor (CRF) when toxic load exponent = 3 under various pre-sheltering air exchange distributions and shelter-in-place initiation time, without sorption.

SIP Start Delay (h)		Release Duration			Release Duration			Release Duration		
		0.5-h	1-h	2-h	0.5-h	1-h	2-h	0.5-h	1-h	2-h
		CRF evaluated at 0.5 h after stop of release			CRF evaluated at 1 h after stop of release			CRF evaluated at 2 h after stop of release		
0 h		0.82	0.79	0.68	0.81	0.78	0.64	0.81	0.78	0.63
Winter	0.25	0.81	0.78	0.67	0.80	0.78	0.64	0.80	0.77	0.62
	0.5	0.80	0.78	0.67	0.78	0.77	0.63	0.78	0.77	0.62
	1.0	0.79	0.76	0.65	0.78	0.75	0.62	0.78	0.75	0.60
Summer	0.25	0.81	0.78	0.67	0.80	0.77	0.63	0.79	0.77	0.62
	0.5	0.78	0.78	0.66	0.77	0.77	0.63	0.77	0.76	0.61
	1.0	0.77	0.75	0.65	0.76	0.74	0.61	0.75	0.74	0.59

4.7 Figures

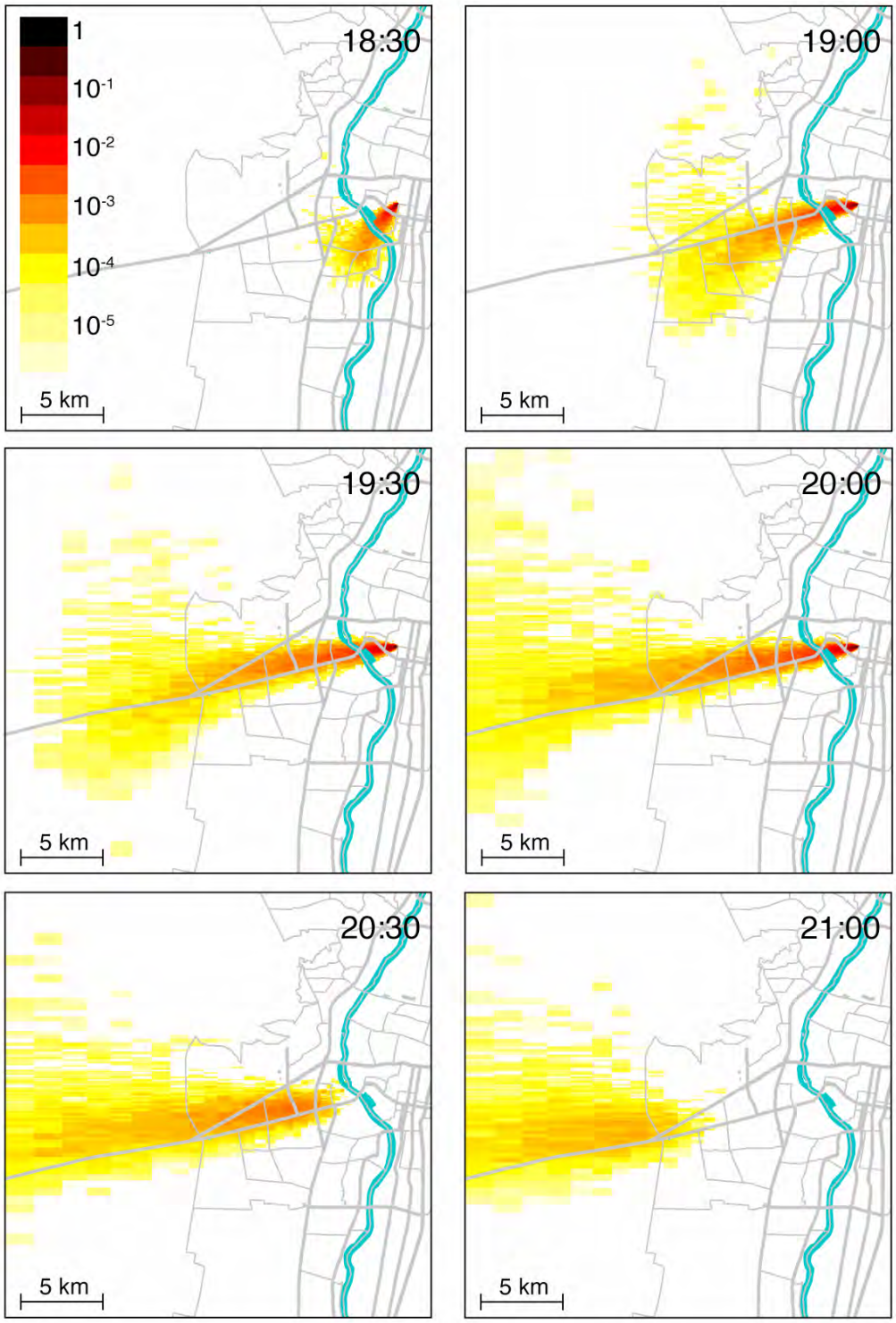

Figure 4.1 Outdoor concentrations of the 2-h contaminant release in Albuquerque (start time at 18:00). The concentrations plotted are 5-minute averages and are normalized to the highest ground level concentration.

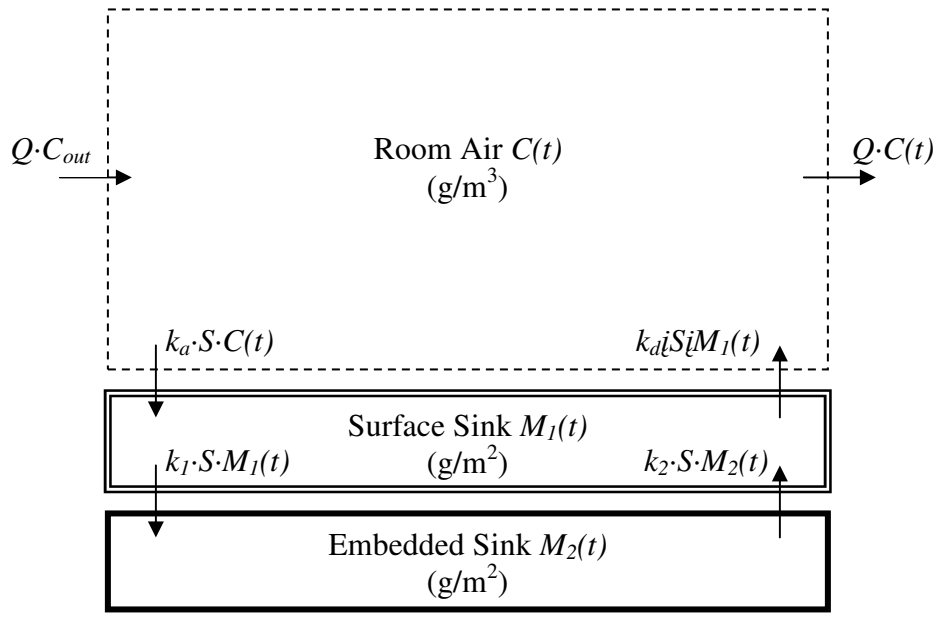

Figure 4.2 Schematic of a two-sink sorption model. Each arrow indicates the mass flow (g/s) from one compartment of the model to another. In the two-sink diffusion model, the interaction between the surface and embedded sink is simplified by setting $k_1 = k_2 = k_{diff}$ (Eqn 4.5). All rate constants have units of inverse time, except for k_a, which has units of m/s.

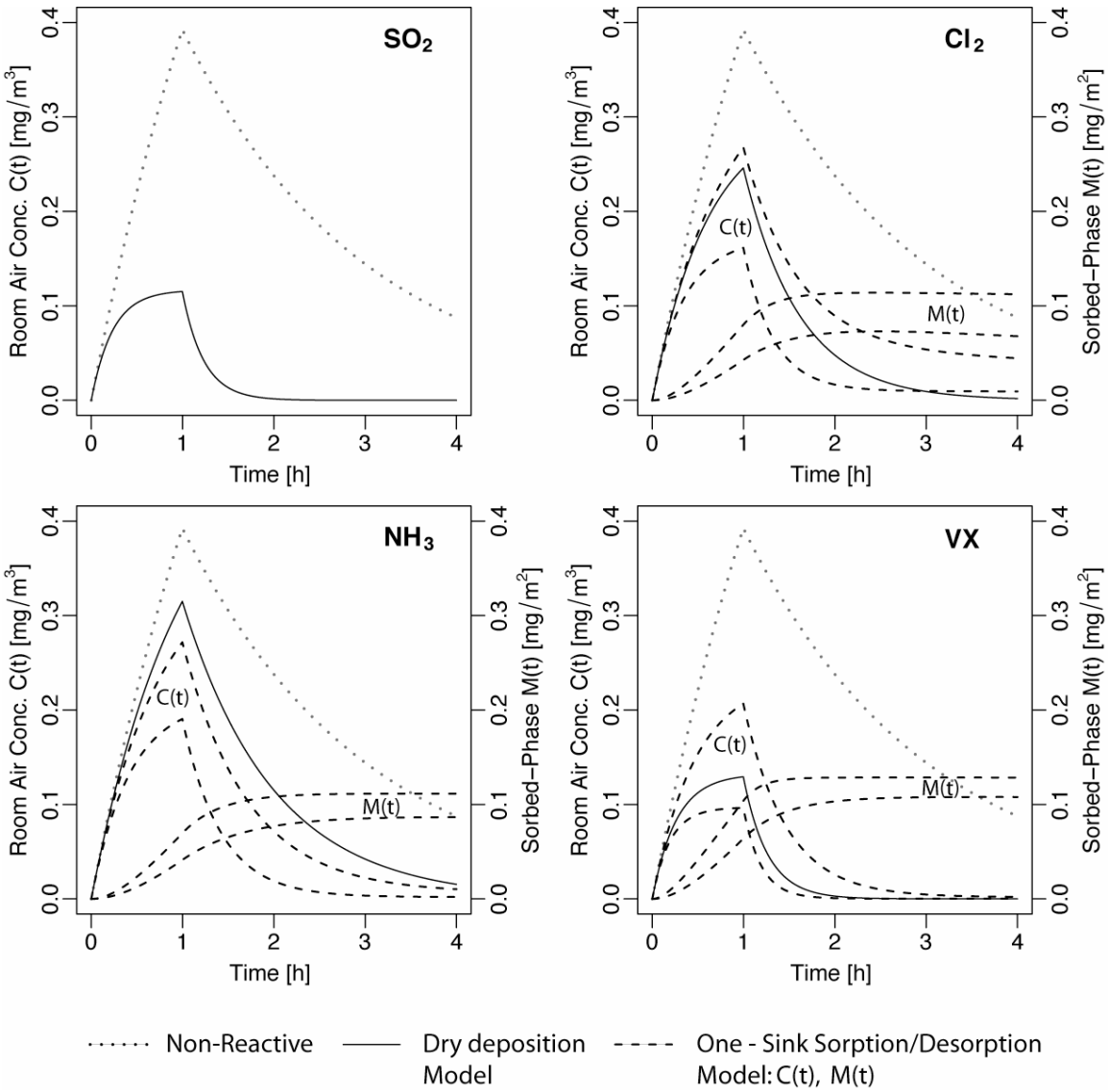

Figure 4.3 Predicted indoor concentrations for a well-mixed space exposed to constant outdoor concentration of 1 mg/m^3 for 1 h. The air-exchange rate is 0.5 h^{-1}. The light dotted line is the indoor concentration if the chemical does not sorb to surfaces. The solid line represents the indoor concentration predicted using dry deposition rates shown in Table 4.1. The dashed lines represent the range of the indoor concentrations predicted using one-sink sorption parameters shown in Table 4.2. The second set of the curves labeled *M(t)* are the predicted mass density in the sorbed-phase for the one-sink model. All concentrations and sorbed masses are normalized to the outdoor concentration.

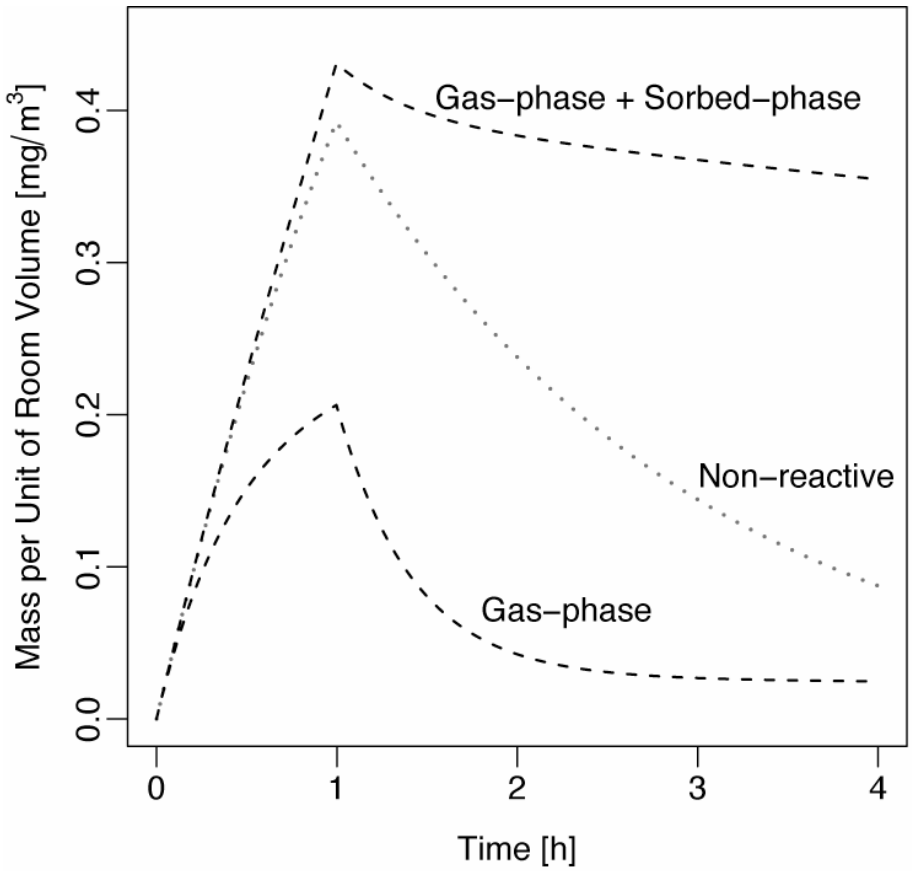

Figure 4.4 The predicted total mass in a room when subjected to ambient Cl_2 at a constant concentration of 1 mg/m^3 for 1-h. Mass of Cl_2 predicted in each compartment is normalized to the room volume. The non-reactive case is the same as the indoor concentration shown in Table 4.4. The Cl_2 sorption and desorption rate coefficients used are as shown in Table 4.2. The one-sink sorption model, as described in Eqn 4.2 and Eqn 4.3, gives mass density in the sorbed-phase M(t) in unit of mg/m^2. To convert this to mass per unit volume of the room, M(t) is multiplied by the surface-to-volume ratio, which is assumed to be 3.5 m^2/m^3 in this case.

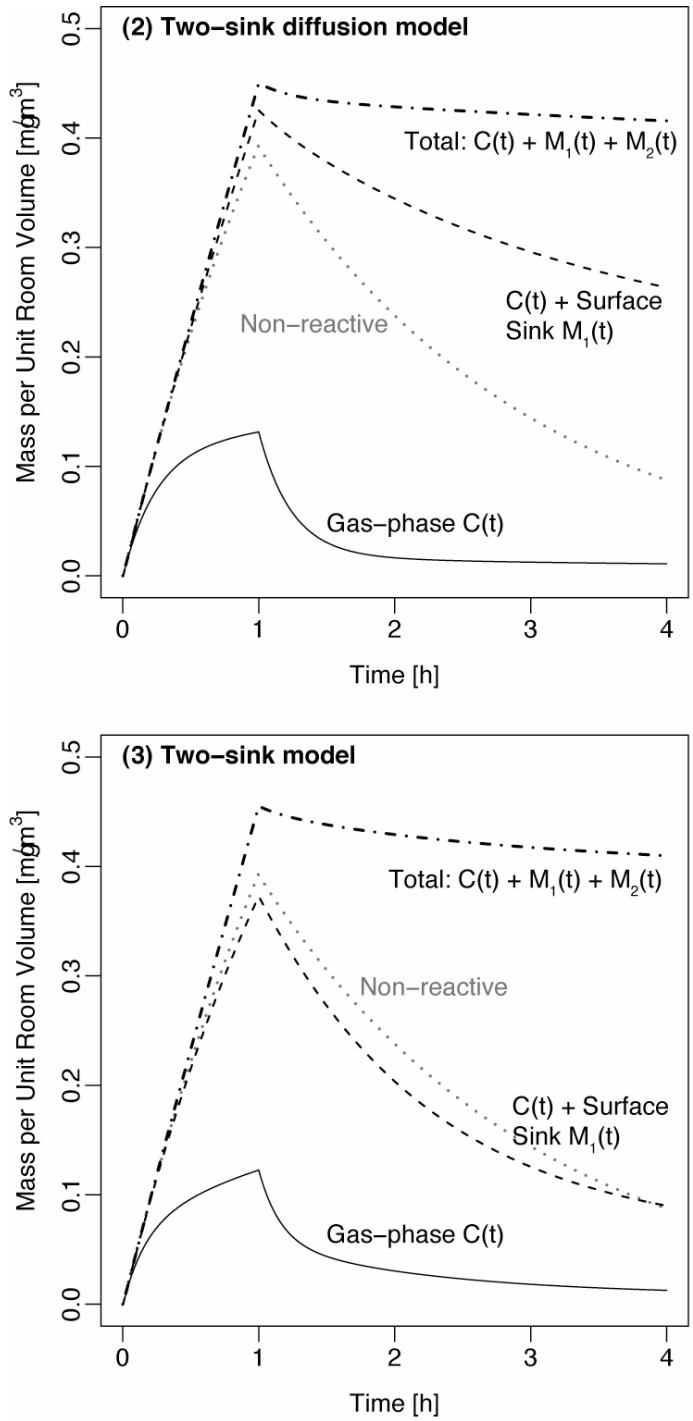

Figure 4.5 Predicted mass in a room when subjected to sarin at constant ambient concentration of 1 mg/m^3 for 1-h. Mass of sarin predicted is normalized to the room volume. Models (2) and (3) are two variants of the two-sink model, as detailed in Table 4.3. $M_1(t)$ is the mass sorbed in the surface sink, and $M_2(t)$ is the mass sorbed in the embedded sink. The sorption/desorption rate coefficients used are from the DMMP experiments carried out in rooms of residences. The air-exchange rate is 0.5 h^{-1}. The light dotted line is the indoor concentration if the chemical does not sorb to surfaces. The two models give similar C(t) and total mass contained indoors.

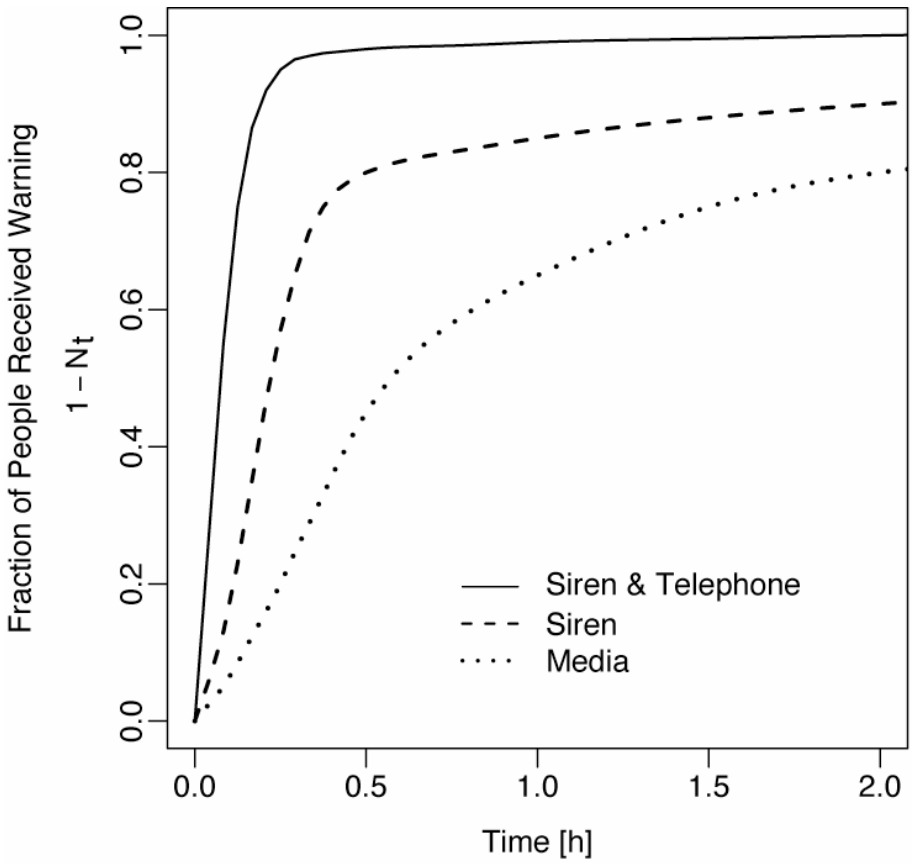

Figure 4.6 Three emergency warning diffusion curves are reproduced from Rogers and Sorensen (1991) to show the expected time needed to inform the community about an emergency using different warning methods. Predictions of these curves are based on the mathematical formulations detailed in Eqn 4.8. Adjustment to warning systems effectiveness by location and activity of population, and their time activity pattern, are also included to predict these curves.

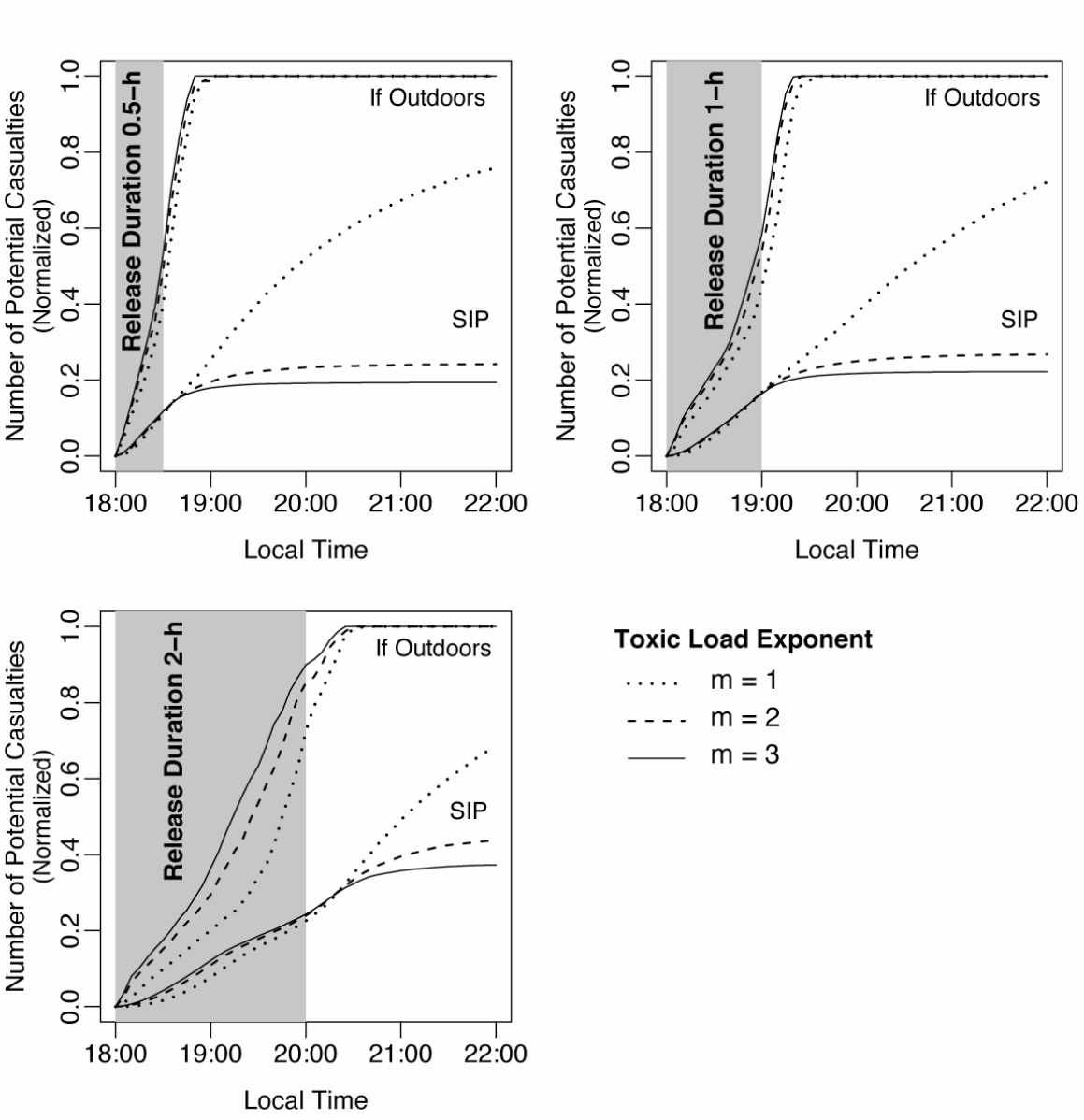

Figure 4.7 Predicted number of potential casualties in three releases of various durations (0.5-h, 1-h, and 2-h) if people were outdoors, and if people were to take shelter in buildings. Casualty estimates are normalized to the maximum outdoor values in each case. People were assumed to have implemented SIP at the start of the release. No sorption to indoor surfaces is included. For details on the parameters used in the simulation, see 4A–4C (i, ii, iii) in Table 4.7.

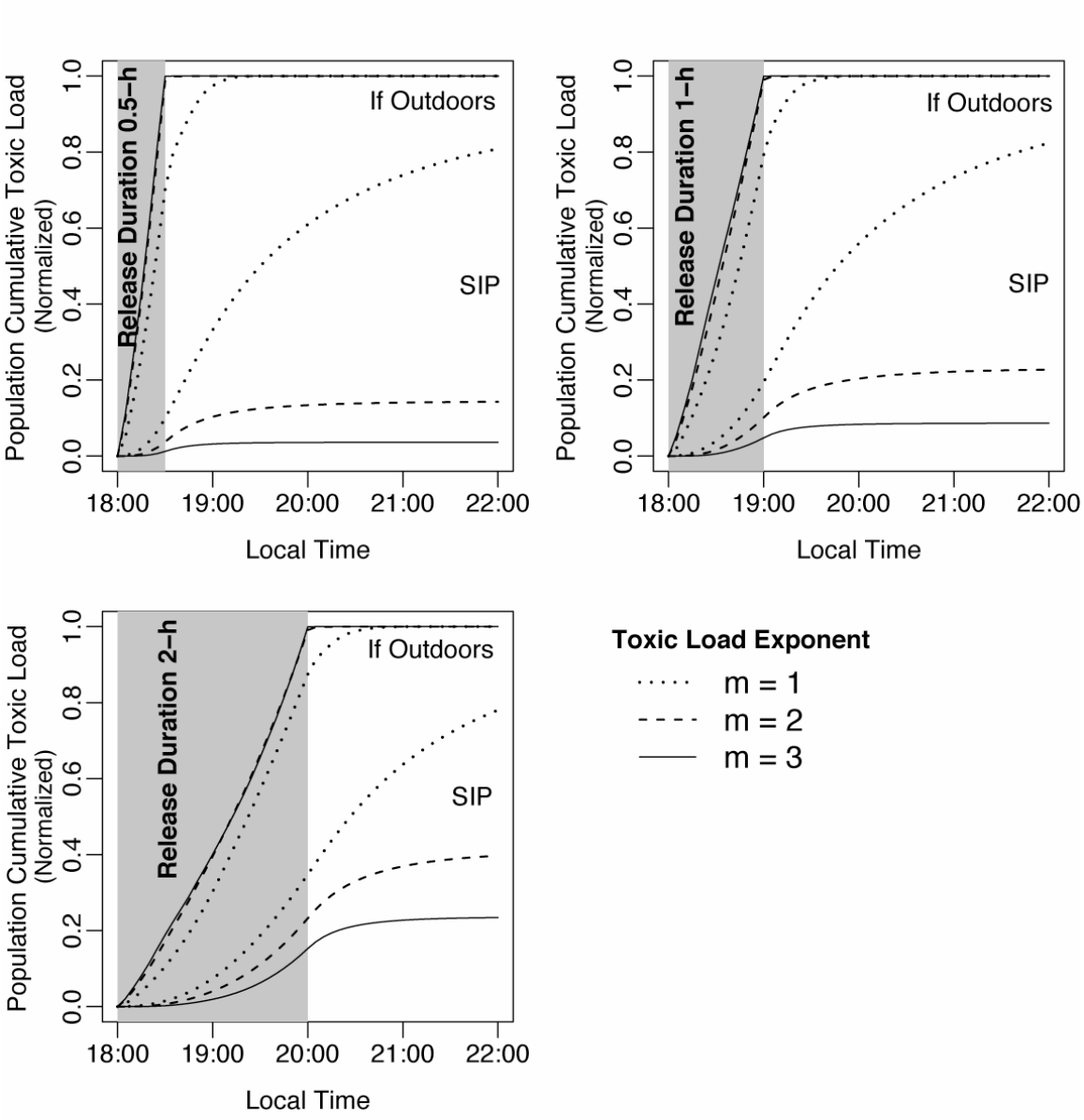

Figure 4.8 Predicted cumulative toxic load in three releases of various durations (0.5-h, 1-h, and 2-h) if people were outdoors, and if people were to take shelter in buildings. The population toxic load (Eqn 2.6, Chapter 2) is summed over all grid cells weighted by the number of people represented in each grid cell. The indoor estimates are normalized to the maximum outdoor values in each case. People were assumed to have implemented SIP at the start of the release. No sorption to indoor surfaces is included. For details on the parameters used in the simulation, see 4A–4C (i, ii, iii) in Table 4.7.

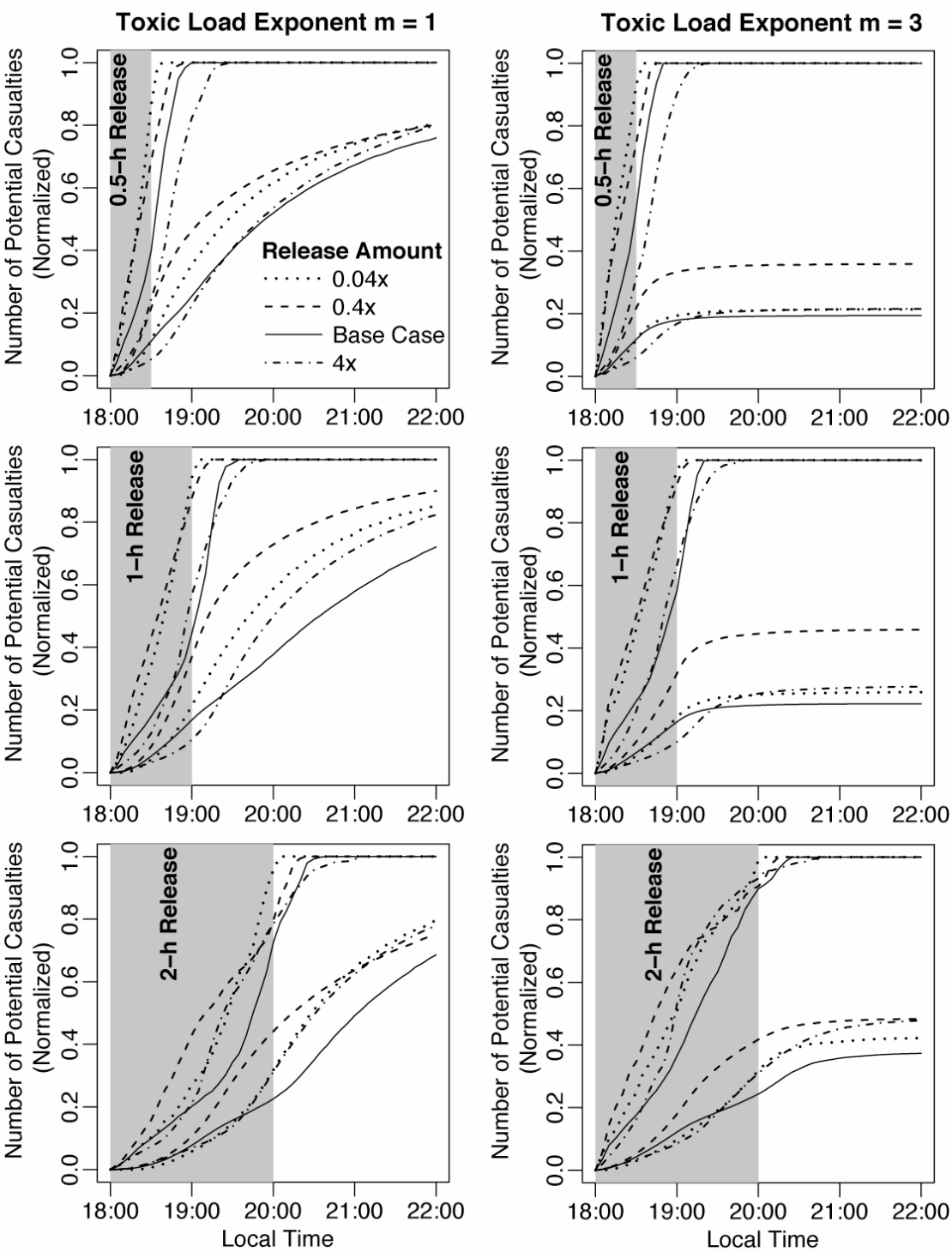

Figure 4.9 The normalized number of potential casualties estimated for 4 release amounts: base case (same as shown in Figure 4.7), 0.04×, 0.4×, and 4× of the base case amount. The variability observed here is caused by the toxic plume passing over residential neighborhoods of different air leakage characteristics. If the toxic plume principally engulfs a high fraction of leaky homes, as is in the case for the 0.4× release amount, lower SIP effectiveness is expected. For details on the parameters used in the simulation, see 4A–4L (i and iii) in Table 4.7.

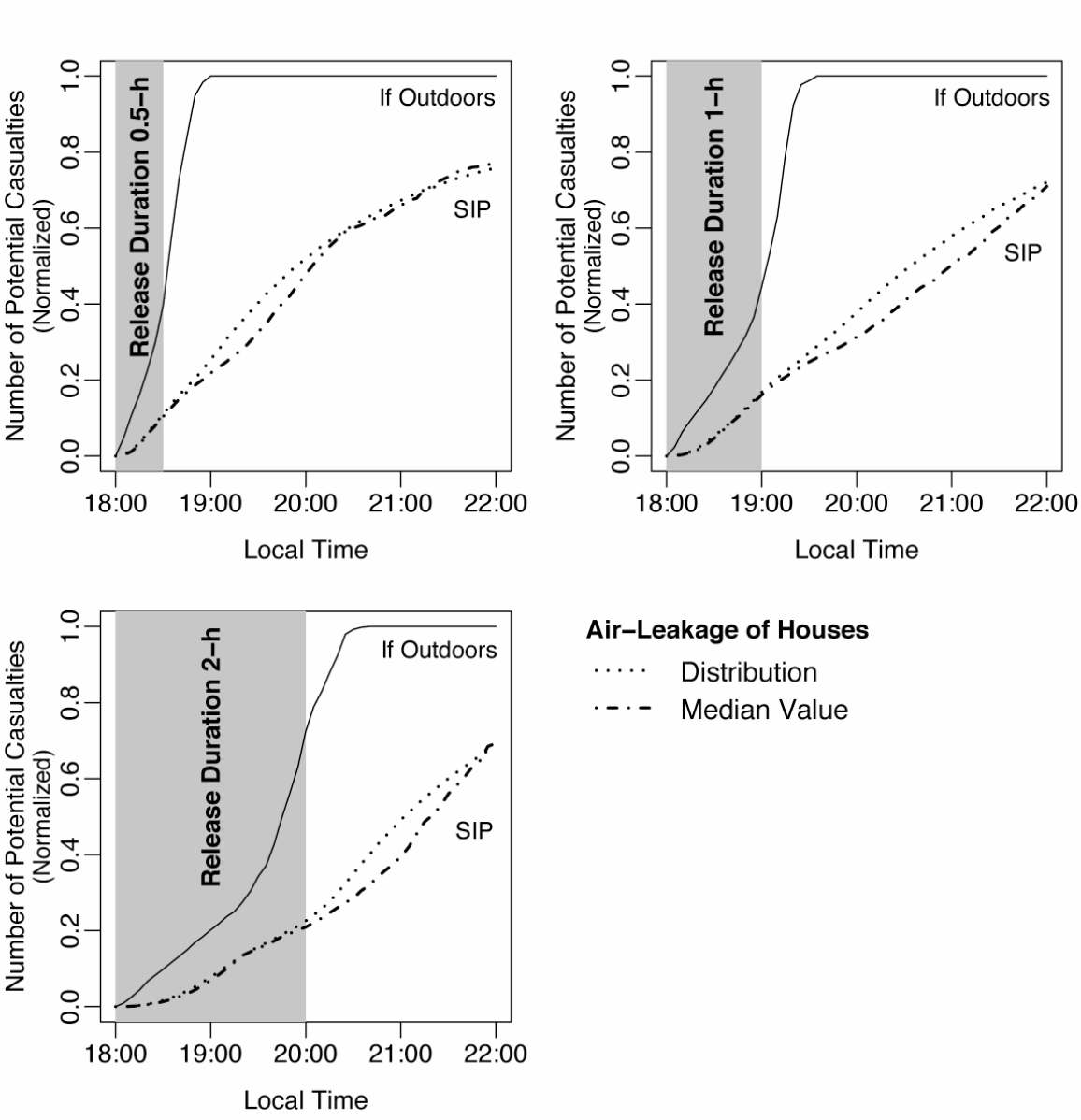

Figure 4.10 Differences in the potential casualty estimates if the distribution of air-exchange rate is captured, or if all houses in a census tract are assumed to have the median normalized air-leakage value. Normalized air-leakage describes how leaky the building envelope is, which is needed to compute the air infiltration rate of houses. Only cases of linear dose-response (i.e. toxic load exponent = 1) are presented. No sorption to indoor surfaces is considered. For details on the parameters used in the simulation, see 4Ai–4Ci, and 4Mi–4Li in Table 4.7.

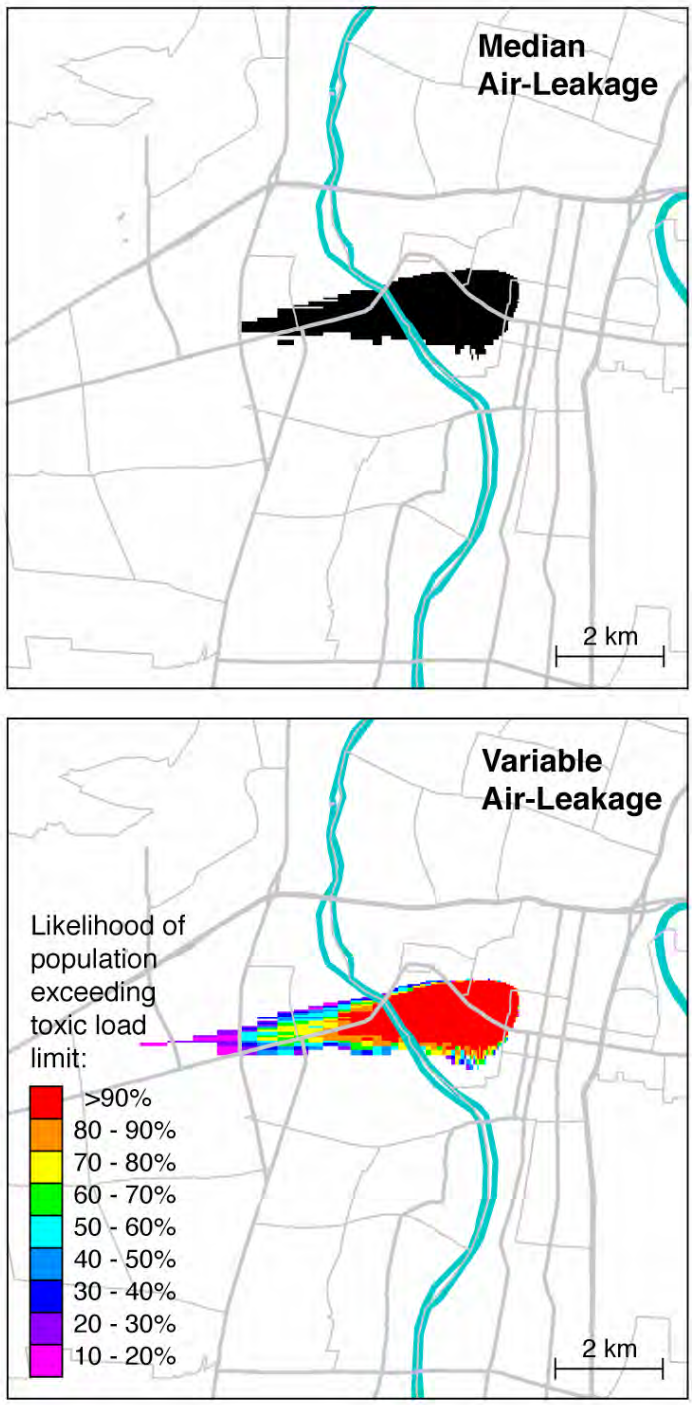

Figure 4.11 Predicted areas where indoor exposure is expected to exceed the toxic load limit for a 1-h release under linear dose-response conditions (see simulation 4Bi and 4Ni in Table 4.7). Assuming all houses have the same air leakage (top figure) gives only binary results, i.e. an exceedance or not. The bottom figure shows predictions using the distribution of air-leakage in houses. In this case, it is possible to differentiate areas according to their degree of SIP effectiveness.

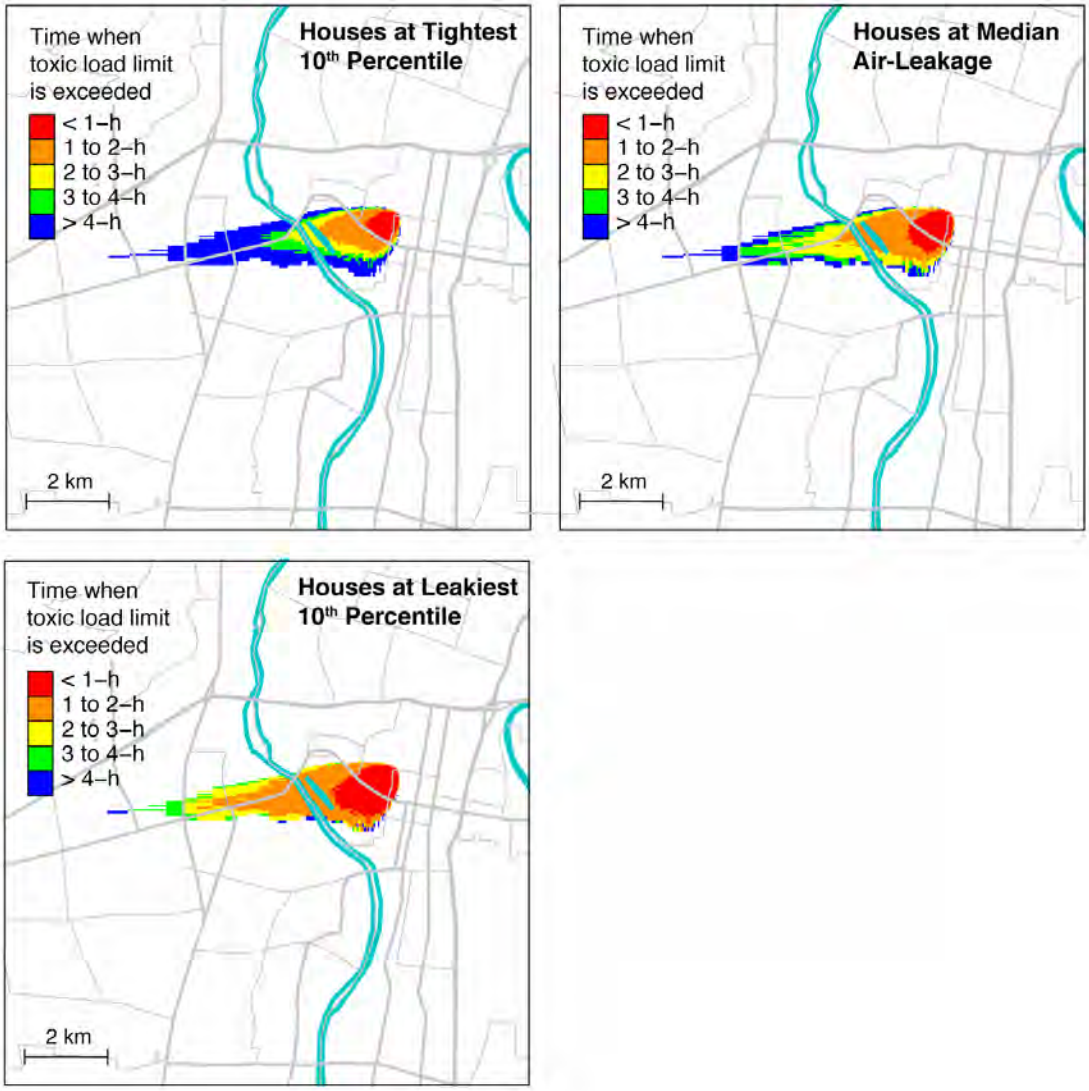

Figure 4.12 Predicted time when the toxic load limit is exceeded for houses at the tightest and leakiest 10th percentiles, and houses that are at the median of the air-leakage distribution. The scenario modeled is the same in each case: 1-h release under linear dose-response and without sorption to surfaces (see simulation 4Bi Table 4.7). People in areas colored blue are expected to suffer health effects if they were exposed to outdoor concentrations, but are expected to be safe if they took shelter during the entire 4-h simulation. People in areas colored red to green are expected to suffer health effects even if they took shelter indoors. The time indicates approximately how long people can be exposed to indoor concentrations without suffering health consequences.

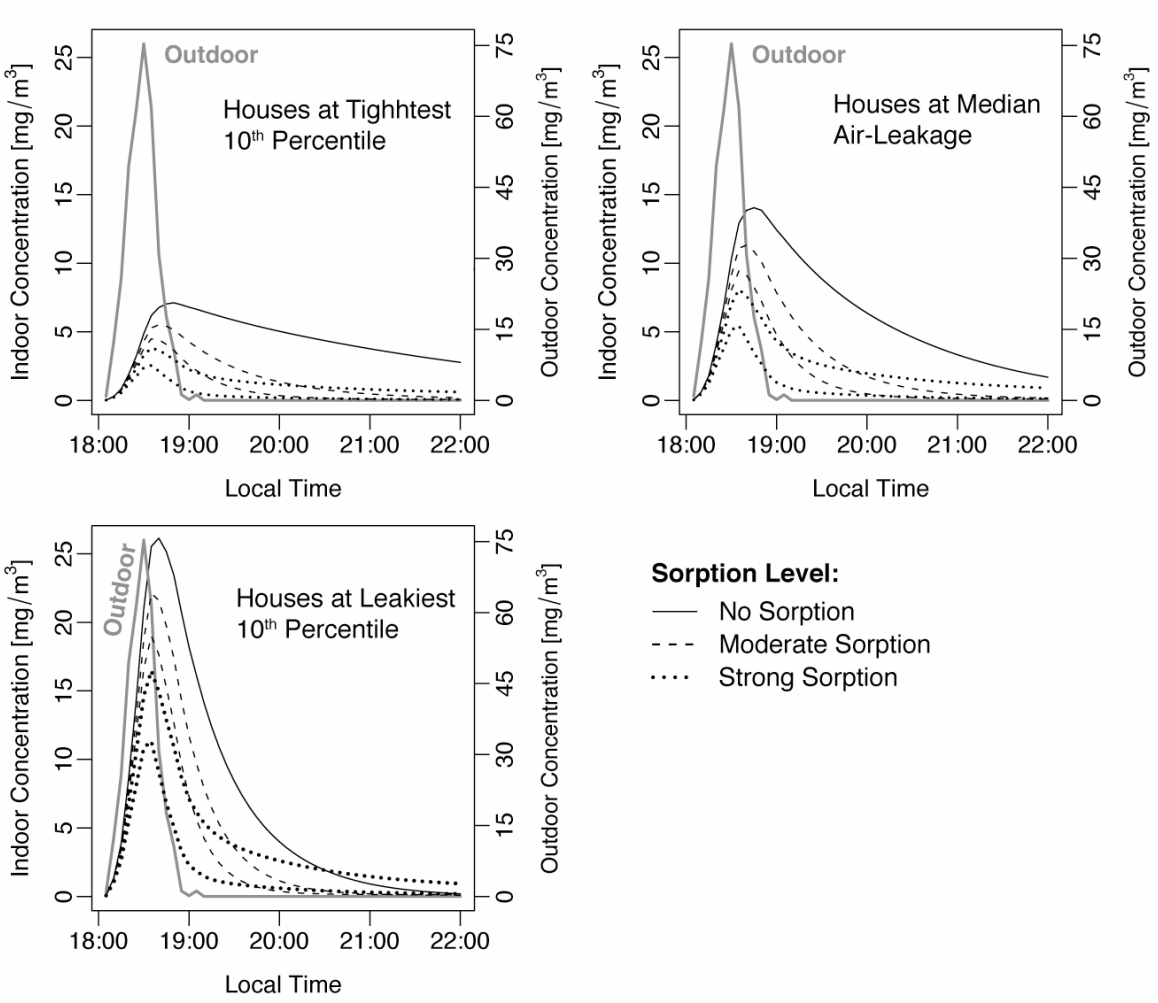

Figure 4.13 Indoor concentration predictions at a nearby location to the release site under various sorption rates. All results are from the 1-h release simulation with linear dose-response relationship (see simulation 4Bi, 4Pi, and 4Qi in Table 4.7). Predictions for houses with air-leakage at the 10th (tight), 50th (median), and 90th (leaky) percentiles of the distribution are presented. Two sets of sorption rates, moderate and fast, are modeled to illustrate the variability observed in sorption experiments of different chemicals (Table 4.4). Two indoor concentration predictions are performed using each set of sorption rates to represent the experimental variability observed for that chemical.

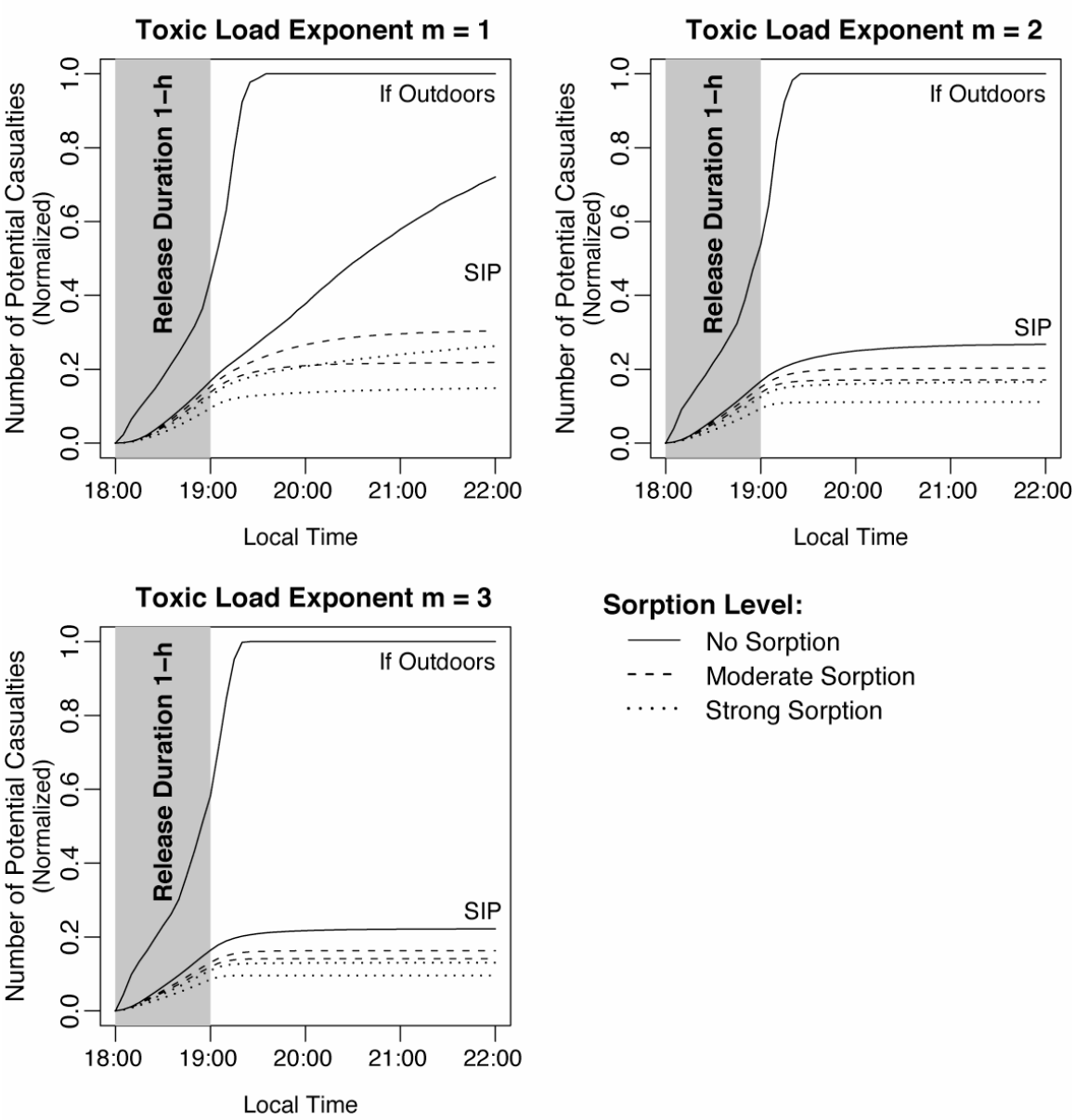

Figure 4.14 Predicted number of potential casualties if people were to take shelter indoors under various sorption conditions. Two sets of sorption rates, moderate and strong, are modeled to illustrate the variability observed in sorption experiments using different chemicals (Table 4.4). The upper and lower estimates of each set of sorption rates are presented. For details on the parameters used in the simulation, see 4B, 4P, and 4Q (i, ii, iii) in Table 4.7.

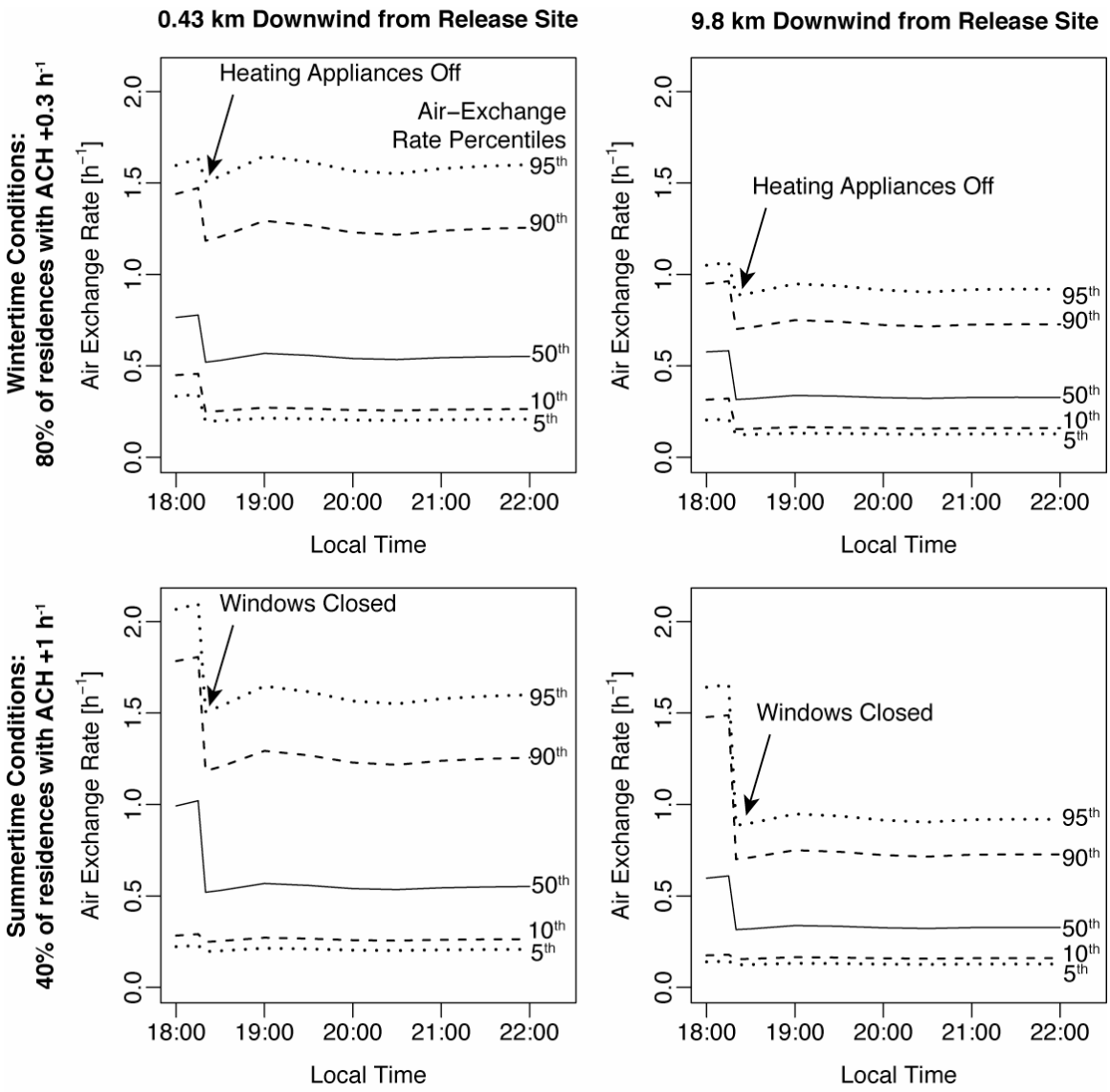

Figure 4.15 Air-exchange rate distribution of houses at two locations downwind of the release site before and after SIP is implemented. In the top figures, 80% of the houses are assumed to have their heating appliances on, leading to +0.3 h^{-1} in these houses. In the bottom figures, 40% of the houses are assumed to have their windows opened, leading to +1 h^{-1} in these houses. SIP is assumed to be initiated 15 minutes after the release started at 18:00. From that point onwards, all houses are assumed to fully comply with the instruction to take shelter, meaning that air infiltration is the sole means of air exchange.

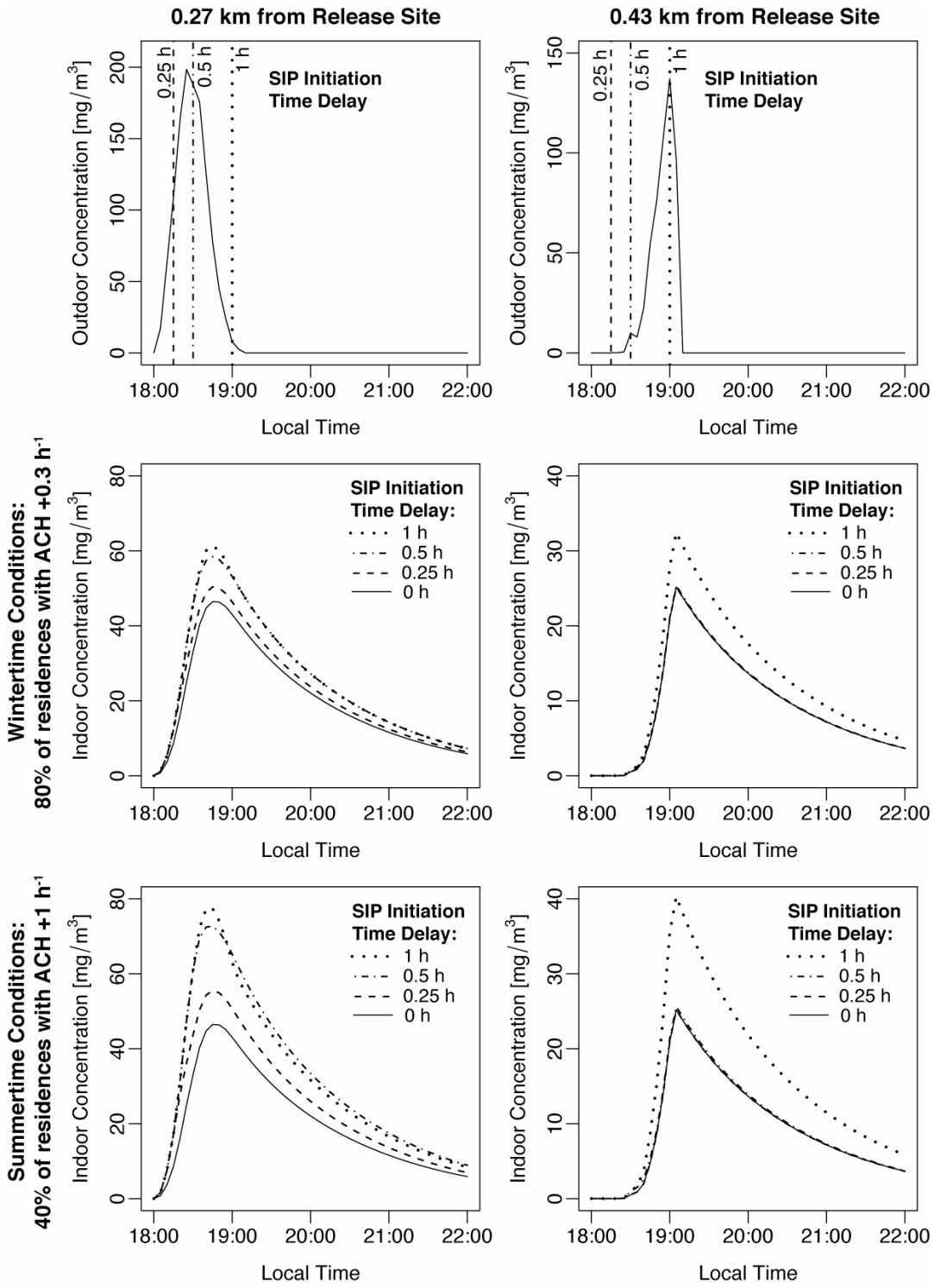

Figure 4.16 Indoor concentrations predicted at two locations close to the release source under various SIP initiation time delays: 1, 0.5, and 0.25 h. The no delay case (0 h) is also presented for comparison. The top figures illustrate the outdoor concentration profiles at the respective location, which allow for easy comparison of the plume arrival time with the modeled SIP delay time. The indoor concentrations are predicted using the median air-exchange rates, which are similar to these shown in Figure 4.15 (left column).

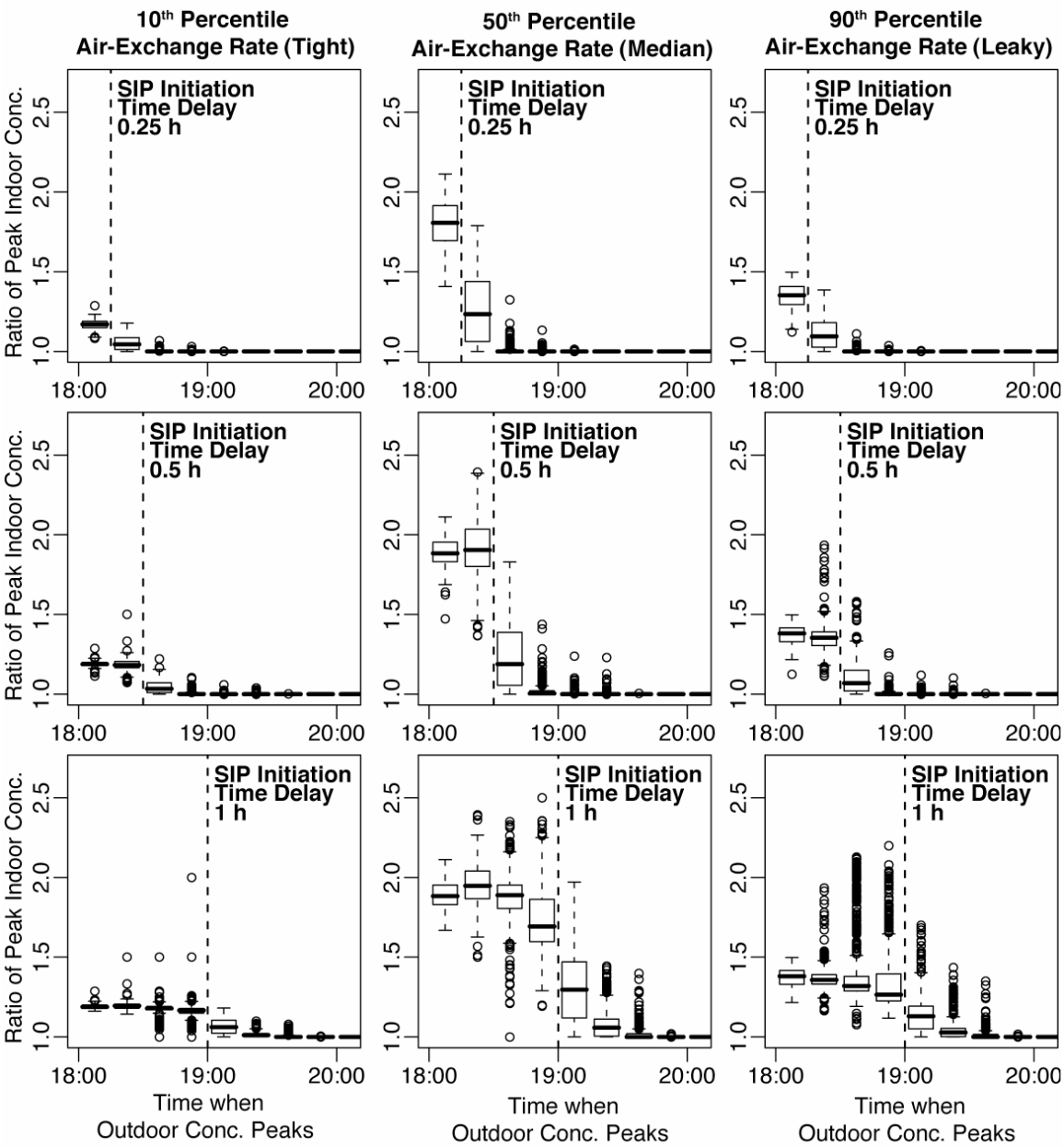

Figure 4.17 Ratio of peak indoor concentrations modeled under various SIP initiation time delay (0.25, 0.5, and 1 h) relative to the no-delay case. All predictions are obtained using the 1-h release simulation assuming summertime pre-sheltering conditions (i.e. 40% of residences with air-exchange rate +1 h^{-1} before sheltering). The box-and-whisker plots show the distributions of peak indoor concentration ratio evaluated at grid cells where the outdoor concentration reaches its peak value at a time that is indicated on the y-axis. A ratio of 1.0 plotted on the y-axis means that delaying SIP by the specified time does not cause the indoor peak concentration to change relative to the case where SIP started before the release. A ratio of 2.0 means that delaying SIP by the specified time causes the indoor peak concentration to double relative to the no-delay case. The ratios of peak indoor concentration are plotted against the time when the outdoor concentration reaches its peak at the grid cell (x-axis).

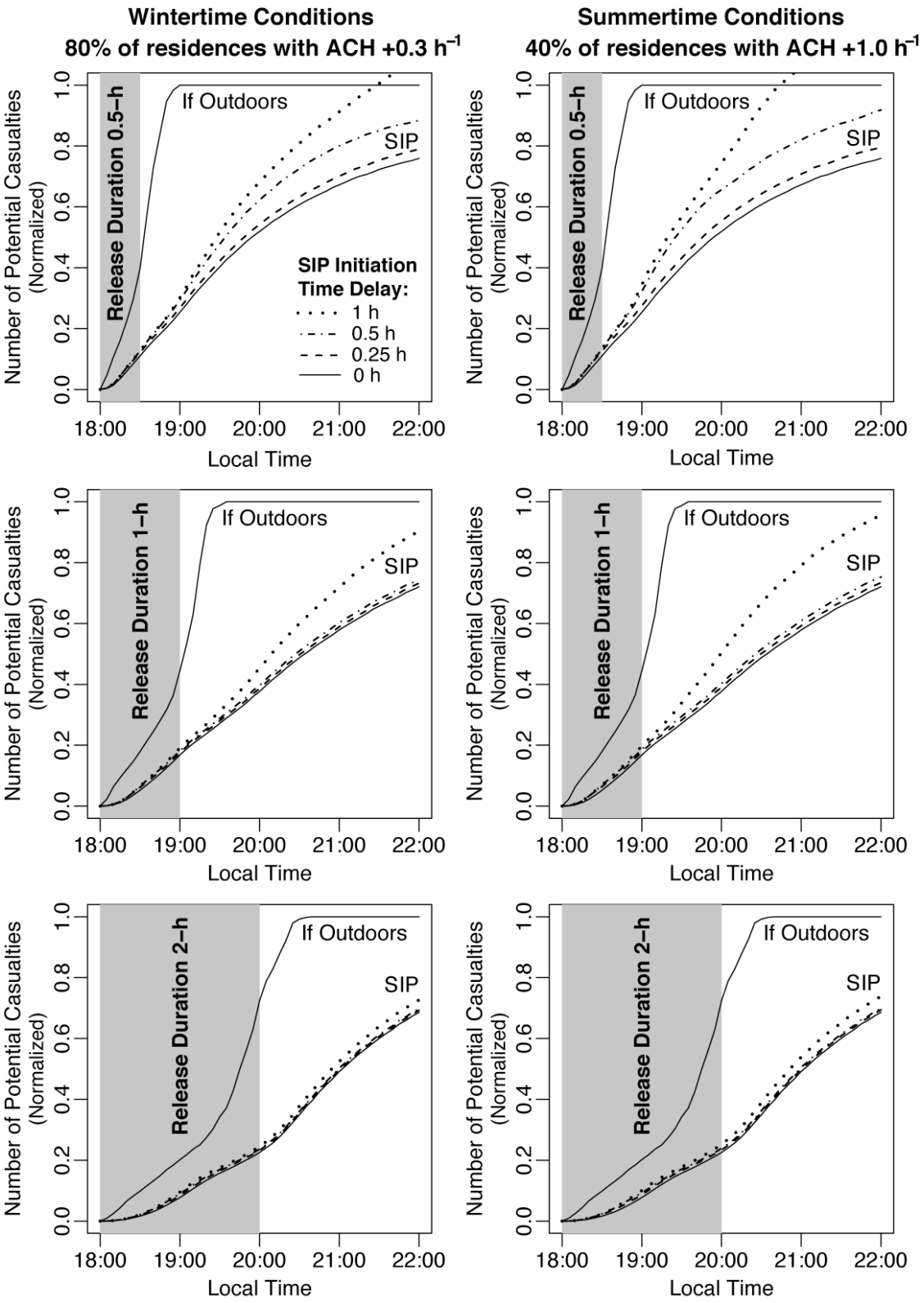

Figure 4.18 Change in estimates of potential casualties subject to the pre-sheltering air-exchange rate distributions and the time delay in initiating shelter-in-place. All simulations assumed linear dose-response (i.e. toxic load exponent = 1) and no sorption.

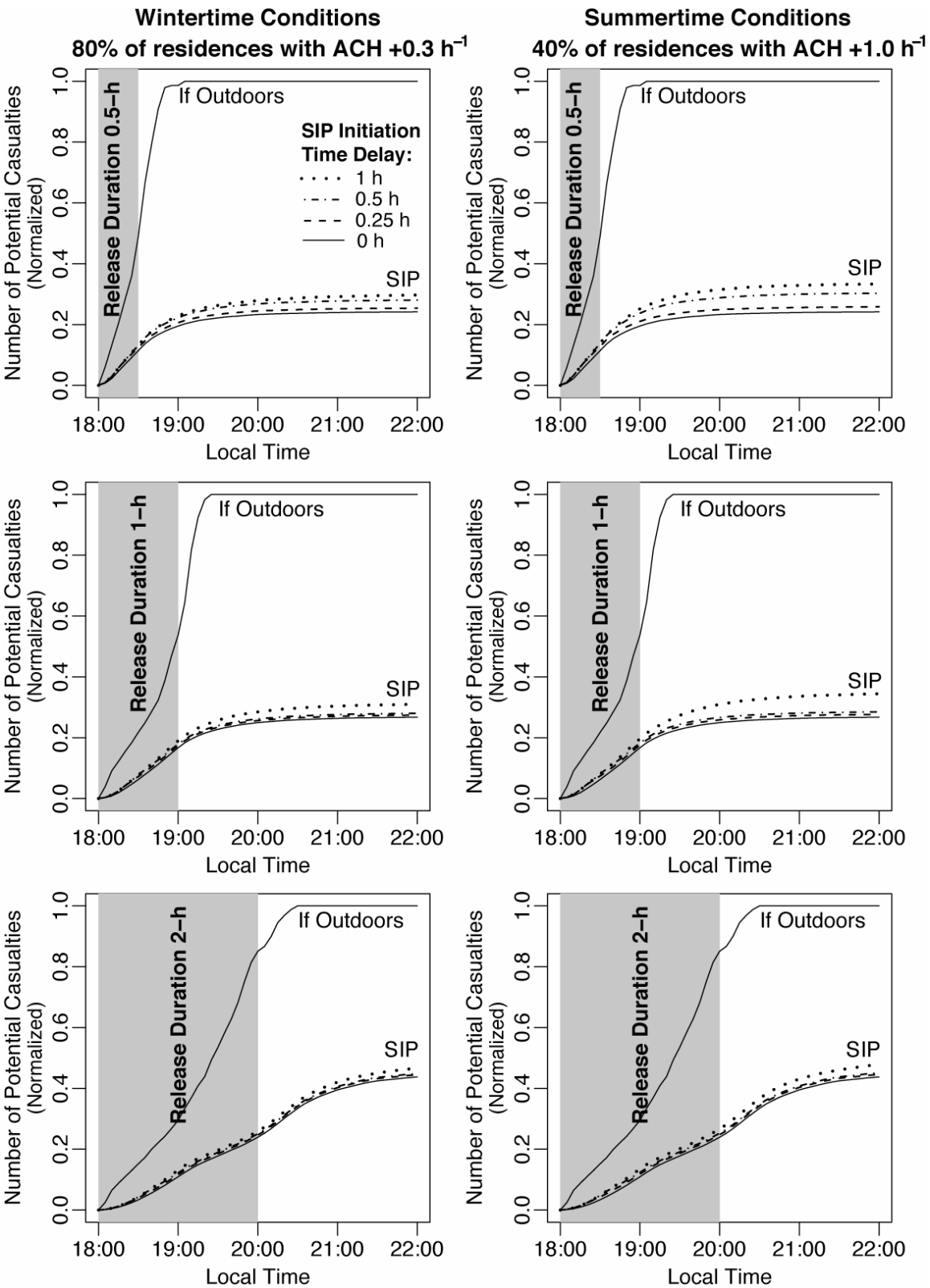

Figure 4.19 Change in estimates of potential casualties subject to the pre-sheltering air-exchange rate distributions and the time delay in initiating shelter-in-place. All simulations assumed toxic load exponent = 2 and no sorption.

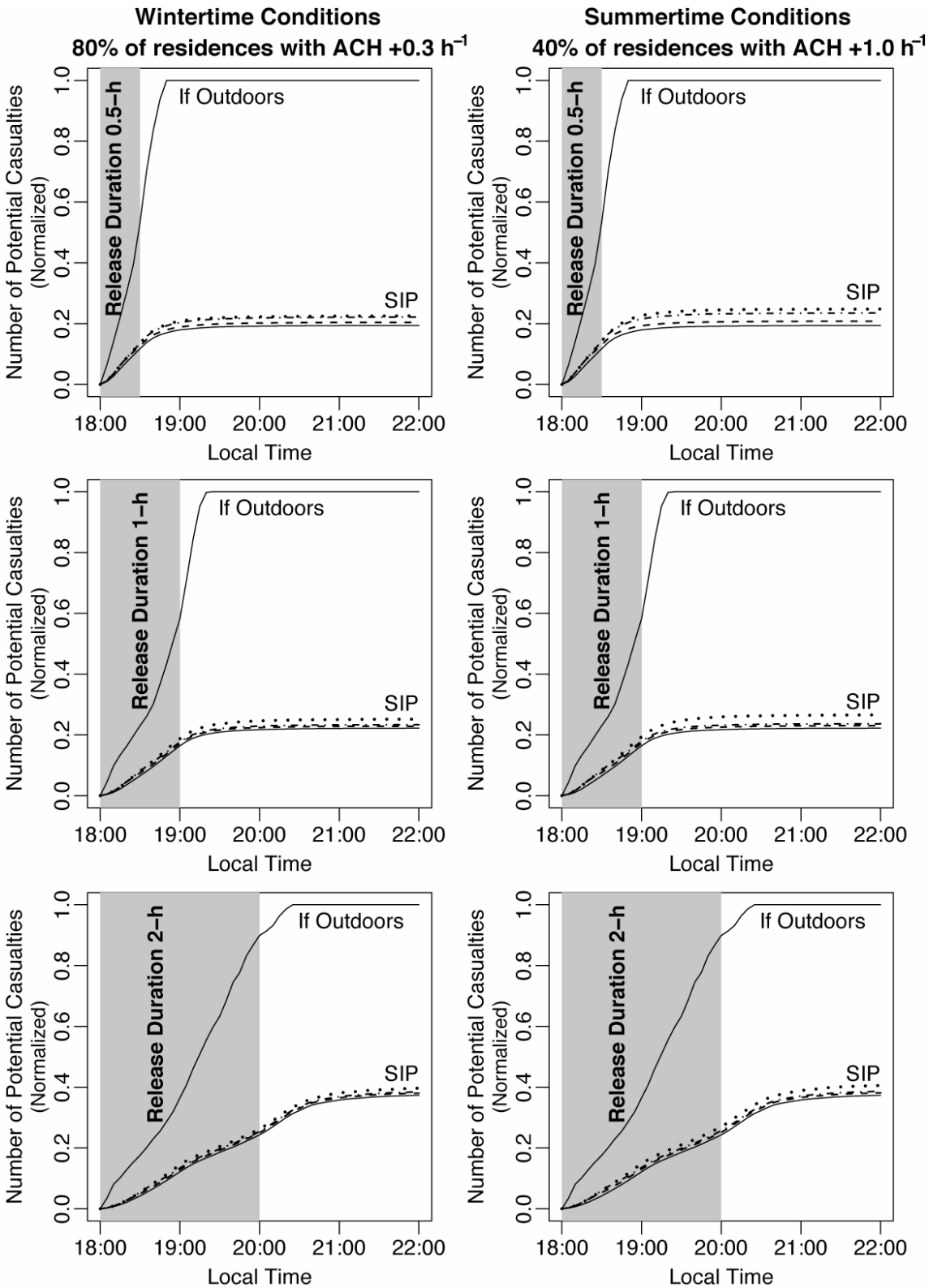

Figure 4.20 Change in estimates of potential casualties subject to the pre-sheltering air-exchange rate distributions and the time delay in initiating shelter-in-place. All simulations assumed toxic load exponent = 3 and no sorption.

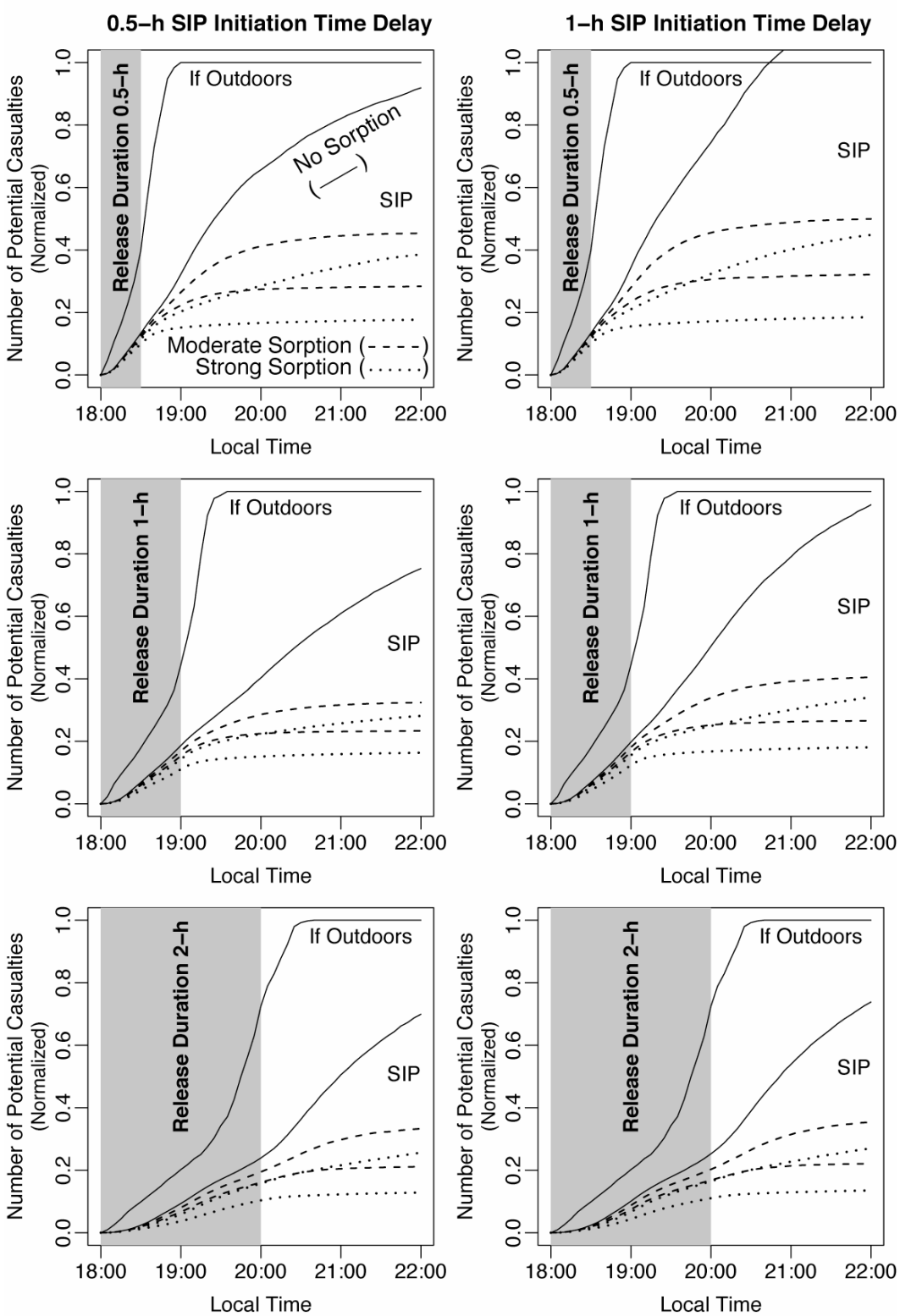

Figure 4.21 Potential casualty estimates subject to various sorption rates to indoor surfaces, and delay in SIP initiation time. All simulations assumed linear dose response (toxic load exponent = 1) and summertime pre-sheltering conditions (i.e. 40% of residences air-exchange rate increased by 1 h^{-1} before sheltering).

5 Air Infiltration and Ventilation in Commercial Buildings

5.1 Introduction

Commercial buildings, a term used here to describe buildings that are non-residential in nature, are integral parts of the building stock in urban areas. If a large-scale outdoor release were to occur during daytime, many people would likely to take shelter in these buildings instead of at their residences. The shelter-in-place (SIP) assessment presented in Chapter 4 only considered the characteristics of single-family detached dwellings. The method used to estimate air infiltration rates in the housing stock, as described in Chapter 3, is not applicable to commercial buildings. Commercial buildings are very different from houses not only in size, but also in their construction and ventilation system design. The airflow in commercial buildings is typically much more complex than in houses. There are also significant differences in the air leakage and air infiltration characteristics (Sherman and Chan, 2004). Unlike residential buildings, air exchange in commercial buildings is largely driven by mechanical ventilation system when the system is operating. All these factors can cause the SIP effectiveness of commercial buildings to differ from that of residential buildings.

"Commercial" buildings include both privately and publicly owned buildings. They can range from high-rise office buildings to single-story buildings such as small retail outlets and restaurants. Commercial buildings also include industrial facilities and warehouses.

Air leakage measurements are available only on selected types of commercial buildings. A review by Persily (1999) of such measurements found that some buildings are quite leaky per unit surface area of the building envelope. However, that review only generated descriptive statistics using part of the available data. A more detailed analysis of the air leakage data is warranted to characterize the leakage distribution in the commercial building stock. As in residential buildings, uncontrolled airflow can lead to excessive energy consumption, which can represent a serious cost burden for operating commercial buildings. Earlier studies by Briggs et al. (1992) and VanBronkhorst et al. (1995) specified 25 typical office buildings to represent the building stock in the US for estimating energy consumption. They then assigned air infiltration rates to each type of building by using a simplified building energy model. There are also data on air infiltration rates for other types of buildings (Lagus and Grot, 1995; Cummings et al., 1996) developed with a concern for indoor air quality impacts of inadequate ventilation. In this chapter, existing studies on the air leakage and air infiltration rates of commercial buildings are analyzed to quantify the central tendency and variability in the building stock for assessing their SIP effectiveness.

After analyzing building air leakage, an appropriate air infiltration model and its parameters for commercial buildings are described. Then, the air infiltration model is used to predict the amount of airflow that crosses the building envelope in a small number of buildings that have been studied. Model predictions are compared with experimental measurements to evaluate the performance of the model. The air infiltration model is also used to estimate the distribution of infiltration rates in the US commercial

building stock. Finally, the predicted air infiltration rate distribution is compared with typical air-exchange rates measured in buildings. This comparison will later serve as a basis for assessing of the benefit for SIP of turning off the mechanical ventilation system to minimize the exposure of occupants to contaminants from outdoor releases. The information developed in this chapter is used in Chapter 6 to evaluate how effective commercial buildings are in protecting building occupants against a hypothetical release in Oklahoma City, OK.

5.2 Analysis of the Commercial Building Air Leakage Database

5.2.1 Data Description

The goal of this analysis is to derive a distribution that describes the air leakage characteristics of commercial buildings in the US. Data from whole-building pressurization tests, which measure the airflow needed to pressurize a building, are compiled into a database. The underlying principle of the pressurization test is the same as described in Chapter 3 for residential buildings, and will not be repeated here. The key difference between measuring the air leakage of houses and commercial buildings is in the experimental equipment needed. To pressurize larger buildings requires fans that are capable of producing large volumetric flows (Potter and Jones, 1992; Litvak et al., 2001). Monitoring the pressure difference on the building envelope with respect to the outdoors also requires a more extensive monitoring system. In buildings that are mechanically ventilated, some researchers have used the air-handling system to produce this airflow

(Persily and Grot, 1986). Data contained in the database are summarized in Table 5.1. Most of the data compiled here have also been reviewed by Persily (1999) and Proskiw and Phillips (2001). However, these earlier studies have only generated descriptive statistics using part of the data presented here. Consequently, a more detailed analysis of the data will be performed.

Out of the 192 measurements in the database, 89 are US buildings. Other countries represented in the database include Canada, UK, Sweden, and France. Tested buildings are mostly offices (26%), industrial facilities, including warehouses (18%), and schools (18%), followed by small retail buildings (9%) and strip malls (8%). The remaining 21% of the buildings tested include supermarkets, public buildings, restaurants, lodging facilities, recreational buildings/auditoriums, health care facilities, shopping malls, and others. Close to half of the buildings are classified as masonry built. Metal frame/metal panel and concrete panel/tilt-up are also common among the offices and warehouse/industrial buildings tested. Other building construction types in the database are listed in Table 5.2. Most of the buildings were built between 1960 and 2000 (Figure 5.1). Half of the buildings are small with floor areas <1000 m^2. Close to three-quarters of the buildings are 1-story only, but there are also 12 buildings that are 10-story or more.

Pressurization tests measured the airflow Q (m^3/s) needed to pressurize the building to a pressure difference of ΔP (Pa) with respect to the outdoor. The air-leakage coefficient, C [$m^3/(s \cdot m^2 \cdot Pa^n)$], is related to these two measurable parameters as follows:

$$Q = C \cdot A \cdot \Delta P^n$$

Eqn 5.1

where A (m^2) is the surface area of the building envelope, and n (-) is the flow exponent. Typically, A includes the total surface area of the exterior vertical walls and roof of the building. With pairs of Q and ΔP measurements, C and n are estimated by curve fitting. Figure 5.2 shows the distribution of C and n obtained from the air leakage measurements in the database. The distribution of C is roughly lognormal. This observation is similar to the normalized air leakage (NL) measured in single-family detached dwellings. If these air leakage measurements were to convert to units of NL as defined in Chapter 3, then the distribution would have a geometric mean (GM) of 0.75 and a geometric standard deviation (GSD) of 2.8. Relative to the residential data (GM = 0.93, GSD = 2.2), the variability in the air leakage of commercial buildings is higher.

According to the orifice flow equation, the theoretical limit of n is between 0.5 and 1. When a building is leaky, resistance from inertia opposes the large airflow through the building envelope, thus n approaches 0.5. On the other hand, when a building is tight and there is little airflow through the building envelope, flow resistance is dominated by viscosity and n approaches 1. As a result, a negative correlation between C and n is expected. In this dataset, the correlation coefficient between C and n is -0.44 with the 95% confidence intervals between -0.55 and -0.32. Others have also found similar correlation using residential air leakage data (Orme et al., 1994), where the correlation coefficient determined is roughly -0.36. The distribution of n is also consistent with earlier studies, which is roughly normally distributed with a mean at 0.62 (Figure 5.2).

The following analysis uses the air-leakage coefficient C solely to characterize the leakiness of commercial buildings. In general, the flow exponent n should also be included when describing building air leakage. This is because different pairs of C and n can imply the same amount of air infiltration when subject to a certain pressure difference across the buiding envelope. Especially when substantial measurement errors occured during the pressurization test, uncertainty in n can influence the apparent leakiness of the building if measured in terms of C alone. An alternative method is to characterize the leakiness of buildings by a parameter that incorporates both C and n. For example, a new parameter C' can be defined as the effective air leakage coefficient that would give the same air infiltration rate when subject to a reference pressure difference ΔP_r and at a prescribed flow exponent constant $\bar{n}$. From Eqn 5.1, C' can be computed as follows:

$$Q = C \cdot A \cdot \Delta P_r^{\,n} = C' \cdot A \cdot \Delta P_r^{\,\bar{n}}$$
$$C' = C \cdot \Delta P_r^{\,(n-\bar{n})}$$

Eqn 5.2

By choosing $\bar{n}$ to equal the observed mean of 0.62 (see Figure 5.2), buildings in the commercial building air leakage database would have a distribution of C' that is roughly lognormal with a geometric mean of 3.26×10^{-4} [$m^3/(s\cdot m^2\cdot Pa^{0.62-n})$] and a geometric standard deivation of 2.5. These estimates are evaluated at a reference pressure difference of 4 Pa, which represents the weather-induced pressure across building envelopes. Relative to the distribution of C as shown in Figure 5.2, estimates of C' are similar in the central tendency but have slightly reduced variability. This suggests that the value of the flow exponent can influence the apparent air leakage coefficient of buildings, but only to a limited extent. For the purpose of quantifying the air leakage of buildings in the database, the parameter C alone is sufficient in this case. However, under conditions

where the pressure differernce across the building envelope is much higher, the influence of the flow exponent can become more significant. It is therefore important to capture the dependency of C and n when modeling the air infiltration rates in buildings.

5.2.2 Exploratory Analysis

As described in Chapter 3, residential air leakage is correlated with house year built and floor area, as well as the poverty status of the household. Following a similar approach, the correlations between commercial building characteristics and their measured air-leakage coefficients are identified. There are two types of explanatory variables contained in the dataset: continuous and categorical. Continuous explanatory variables include the year built, floor area, and height of the building. Categorical explanatory variables include the usage and construction type (predominantly exterior wall material) of the building. Owing to the sparseness of the data, advanced statistical analysis is needed to fully investigate the correlations of the different categorical parameters on the air-leakage coefficients measured. Here, only the continuous variables listed above are examined using a simple regression method. There are other factors that might influence the air leakage of a building but these will not be considered here. For example, differences in the building codes and practices among countries due to climatic reasons can affect how airtight buildings are designed. Construction workmanship and building maintenance can also affect the air leakage of the building. In the present analysis, the relationships between the measured air-leakage coefficients and the corresponding categorical

variables are examined only briefly. Quantification of these relationships is left for future investigation.

Figure 5.3 shows the measured air-leakage coefficients *C* plotted against the continuous explanatory variables. A weak negative dependence of *C* on building floor area is observed, but neither year built nor the height of the building appears to be correlated with *C*. Of course, building height is correlated with the floor area of the building to some extent: buildings that are small in floor area cannot have too many floors. Consequently, the dependence of *C* on floor area and building height must be analyzed simultaneously. There are relatively few tall buildings (height >10 m) in the database. This means that unless the correlation of *C* with height is very strong, a clear trend on a scatter plot is unlikely. Unlike residential buildings, year built[10] appears only weakly associated with the air leakage of commercial buildings.

Figure 5.4 shows the dependence of *C* on building usage and construction types, and the countries of the buildings tested. Due to the small sample size, relationships between the measured air-leakage coefficients and the categorical explanatory variables are not easy to interpret. Buildings tested in Sweden and Canada appear to be the least leaky, whereas buildings tested in the UK are the most leaky. While it is possible to explain this trend by the difference in climate among these countries, the types of buildings tested in each country might also play a role in affecting the results. For example, close to two-thirds of

[10] Some of the year built data had to be inferred from the test-date and the general description of building age in the original study, but the inference is expected to be accurate to within 5 years.

the buildings tested in Canada are schools and supermarkets, which appear to be quite airtight relative to other building types. On the other hand, 40% of the buildings tested in the UK are industrial or warehouses, which tend to be rather leaky compared to other building types. In the US, all building types but supermarkets and shopping malls were tested. This is the most complete dataset among the different countries. The US data is dominated by schools and offices (21% each), followed by strip malls (18%) and small retail units (16%). The fact that US data on air-leakage coefficients lies in the middle of all countries and that the variability in *C* is the largest can probably be explained by the inclusiveness of the dataset in terms of building usage and construction types. The only construction type that is missing from the US dataset is curtain-wall. Since US data do not appear to be out of line with data from other countries, all data are included in the regression analysis to follow.

Inevitably, there is some ambiguity in the classification of building usage and construction types. The classifications used here are based on the best information provided in the original studies, but some entries required interpretation. Many of the classifications follow the definitions used in the Commercial Building Energy Consumption Survey (CBECS) (EIA, 2003). CBECS is a national survey that collects energy-related building characteristics and energy consumption data for commercial buildings in the US. Relative to this survey, educational and office buildings are over sampled in the air leakage database (Figure 5.5). These two types of buildings are studied more frequently probably because of the indoor air quality concerns that may impact learning performance and productivity of students and office workers (Mendell and

Heath, 2005; Seppänen, et al., 2006). On the other hand, service-type buildings (e.g. vehicle service, dry cleaner, gas station, etc.) included in the "others" category and public buildings (e.g. public assembly, public order and safety, religious worship, etc.) are underrepresented in the database. It is clear that the data contained in the air leakage database are not statistically representative of the building stock in US. Consequently, interpretation of the data is required to estimate leakage characteristics of the US commercial building stock.

In the US, roughly two-thirds of commercial buildings have exterior walls that are built of masonry (EIA, 1995). The majority of the remaining buildings have siding or shingles that are made with various types of materials as the exterior walls, or are built with metal panels. Buildings that are built with concrete panels and window glass are less common. Limited by the information published in the original studies, the classification used in Figure 5.4 is slightly different from the ones used in the 1995 CBECS report. In general, the representations of the various wall types are roughly comparable to the CBECS dataset: masonry exterior walls are the most common, followed by wood and metal panels, and finally concrete panels and curtain-wall.

5.2.3 Regression Analysis

The goal of the regression analysis is to examine whether building characteristics can explain some of the air leakage variability measured. Log-transformation of the air-leakage coefficient C is performed to give approximately normally distributed

parameters. Similarly, the physical building parameters are also log-transformed, namely the volume, surface area, floor area, footprint area, height, and perimeter. When the air-leakage coefficient is regressed against each of these parameters, all but building height are negatively correlated with air-leakage coefficient (Table 5.3). The R^2 values are modest, in the range of 0.12 to 0.20, but the regression coefficients are all significantly different from zero statistically. Even though building height by itself is not correlated with ln(C), when all the explanatory parameters are analyzed together, building height and floor area are the two variables most strongly correlated with ln(C). Without considering the interaction terms between the explanatory variables, the maximum R^2 achievable by a simple linear model is 0.27. In other words, the physical dimensions of buildings can explain roughly 27% of the variability observed in the air-leakage coefficient. While a more complex model might possibly produce a higher R^2, it is unlikely that the improvement would be substantial using the same explanatory variables. This inference is based on the limited explanatory power of each of the parameters, and the highly correlated relationship of some of the parameters (e.g. building surface area and volume). Considering the simplicity of using just the building floor area and height as explanatory variables, the performance of the model is judged acceptable.

It is found that including year built does not improve the fit of the regression model. This is not to say that changes in building practices or building envelope deterioration over time do not affect the airtightness of buildings. Rather, given the limited dataset, the effect of year built is imperceptible in comparison with other explanatory variables and random variability. Data clustering is a common problem with small datasets. As

illustrated in Figure 5.6, with the exception of masonry buildings, the range of year built of the buildings measured is quite narrow within each construction type. If a construction type is associated with particularly airtight or leaky buildings, then the effect of year built will not be easily observed because its influence can be masked by the effect of construction type.

The air-leakage coefficient is negatively correlated with the building floor area, meaning that larger buildings tend to have lower air-leakage coefficients than smaller ones. This might be because of more attention paid to constructional details in larger buildings. The negative correlation implies that larger buildings have fewer leaks and cracks per envelope surface area, since the air-leakage coefficient C [$m^3/(s \cdot m^2 \cdot Pa^n)$] is normalized to the envelope surface area. It is also plausible that leaks and cracks are not uniformly distributed on the building envelope surfaces, but are rather associated with specific building elements, e.g. joints, ventilation ducts and dampers, etc. If the number of these building elements per unit of envelope surface area decreases with increasing building size, then larger buildings will appear to be tighter in terms of C. The same negative correlation has been observed in the air leakage of single-family detached units: larger houses tend to have lower normalized air leakage area.

The air-leakage coefficient is positively associated with building height in the multiple regression model. This might appear surprising, since air leakage is not correlated with building height when it is used as the only explanatory variable. Further, floor area and height are correlated parameters. One can argue that building height is picked out by the

regression model to adjust for the underpredictions among smaller buildings after using floor area as the predictor. This is perhaps the case. However, it is also possible that taller buildings are more likely to have elevator shafts, which are commonly open to the outdoors (Potter et al., 1995; Bahnfleth et al., 1999; Edwards, 1999). These building elements add to the overall air leakage of the building. Furthermore, the proportion of external surface associated with vertical walls increases with building height. In the case that most of the leakage area is associated with vertical walls, taller buildings will tend to have higher air-leakage coefficients. Closer examination reveals that the contribution to air leakage from increasing building height diminishes when the building height exceeds 15 m. Figure 5.7 shows the residuals from these two regression model fits:

(1) $\ln(C) = \beta_0 + \beta_1 \cdot \ln(\text{Floor Area}) + \varepsilon$

(2) $\ln(C) = \beta_0 + \beta_1 \cdot \ln(\text{Floor Area}) + \beta_2 \cdot \text{Height}^{-1} + \varepsilon$

Eqn 5.3

The regression results are summarized in Table 5.4. Model residuals are plotted against the floor areas and heights of buildings. The residuals of model (1) appear to be fairly independent of the floor area of the buildings. However, in terms of the height of the buildings, model (1) tends to underpredict the air-leakage coefficient for the smaller buildings. For buildings exceeding 15 m, regression residuals are no longer dependent on height, indicating that the dependence of air-leakage coefficient on height is only significant among the shorter buildings. This prompts the addition of a Height^{-1} term to the regression model (2), which not only removes the dependence of residuals on height, but also increases the explanatory power of the model, as measured by the R^2, from 0.15 to 0.30. Furthermore, the residuals of model (2) are checked against all the other physical building parameters listed in Table 5.4 as well as the year built for independence. Simple

correlation tests show that none of these parameters are strongly correlated with the residuals of the regression model.

5.2.4 Regression Model Assessment

Prediction uncertainties that arise from the standard errors of the regression coefficients is likely to be small relative to the inherent uncertainty of using this non-representative sample to make predictions for commercial building stock in the US. The 95% confidence levels of predictions based on the regression model are shown in Figure 5.8. The lower bound of the 95% conference level ranges from -11% to -37% of the best-fit estimates, and the upper bound ranges from +13% to +58%. The model only explains roughly half of the variability observed in the air-leakage coefficient of buildings. The predicted *C* has a GSD = 1.7, which is 63% of the measured GSD. The model tends to underpredict when the observed *C* is low, and overpredict when the observed *C* is high. This suggests that the predictive power of the model for determining the air-leakage coefficient for any particular building is limited.

On the other hand, the model is more reliable in predicting the air leakage distribution of a commercial building stock. Here, the underlying assumption is that the model residual, as characterized by the error term ε, is a good representation of the inherent variability found in a building stock. While this assumption cannot be tested directly, the fact that there is a good mix of building types in the dataset and that their proportions are not too far from what is observed nationally in the US is reassuring. However, when the

commercial building stock for which the air-leakage coefficient distribution is being estimated is small, or when their composition deviates far from the characteristics of the samples, then there can be significant uncertainty with the predictions. Ongoing analysis[11] of the same air leakage data using a statistical technique called BUGS (Bayesian inference Using Gibbs Sampling) suggests that educational buildings are tighter than other building types, whereas industrial/warehouses and strip malls tend to be leakier. The method also identifies buildings that are built using curtain-wall or concrete panels as somewhat tighter than other construction types. In cases where the proportions of these buildings types are over or under-represented in a building stock, the predicted air-leakage coefficient distribution could be biased.

5.3 Air Infiltration Model of Large Buildings

5.3.1 Driving Forces for Air Infiltration

Before showing predictions from the regression model, an air infiltration model designed for commercial buildings is presented. Under an SIP scenario with the mechanical ventilation system turned off, air infiltration is the key mechanism that carries toxic materials indoors. The driving forces of air infiltration remain the same as used in the LBL Infiltration Model for single-family residences (Chapter 3): wind, which exerts pressure on walls; and indoor-outdoor temperature difference, which induces buoyant flow through leakage paths. However, larger buildings tend to have more internal

[11] Ongoing work led by P.N. Price at Lawrence Berkeley National Laboratory. Findings mentioned here are preliminary, and were obtained through personal communication.

partitioning inhibiting the full development of the stack effect. On the other hand, structures like ventilation ducts, elevator shafts and stairwells tend to enhance stack flow and connectivity in buildings. Larger buildings also respond somewhat differently than low-rise buildings to wind-driven air infiltration. The vertical distribution of pressure differences can vary significantly for tall buildings. The interaction between stack and wind driven flow can also be different. All these factors make estimation of air infiltration rates in commercial buildings more complex than in single-family residences.

Multizone models are commonly used to predict airflow in large indoor spaces. In such models, a building is represented as a collection of well-mixed spaces linked by flow paths (Lorenzetti, 2002). These models can calculate the zone-to-zone flows, as well as estimate infiltration and exfiltration rates across the building envelope. However, multizone models are very data intensive to apply (Persily and Ivy, 2001; Price et al., 2004). Not only are the air leakage characteristics of the building envelope needed, but the air leakage characteristics of internal flow paths also need to be known. This requires more detailed knowledge than just the floor plan and ventilation duct configuration of the building. Furthermore, the wind-pressure coefficients on all building façades as a function of the wind direction must also be specified. Because of the demanding data requirements, it is impractical to use a multizone model to predict the air infiltration rates for a large ensemble of buildings in an urban area.

5.3.2 Shaw-Tamura Infiltration Model

An alternative approach to multizone modeling is to focus on the building envelope across which infiltration occurs, and to conceptualize the internal partitioning and connectivity of a building as adjustment factors. Tamura and Shaw (1976) and Shaw and Tamura (1977) developed a method for calculating infiltration rates of tall buildings caused by wind and stack effects separately, based on the physics of fluid flow. Data from wind tunnel experiments were used to combine the two effects to give the overall air infiltration rates. Their model is outlined here.

5.3.2.1 Stack Effect

The driving force for air infiltration due to indoor-outdoor temperature difference is fundamentally the same as described in the LBL Infiltration Model (Chapter 3). In the case that the outdoor air is cooler than the indoor air, air infiltrates from the lower part of the building, and exfiltrates at the top part of the building. The stack effect can be reversed in the summer time when the indoor temperature, T_i, is lower than the outdoor temperature, T_o. The pressure difference caused by the stack effect (ΔP_s) is as follows (see Eqn 3.15 for derivation):

$$\Delta P_s = \rho_o \cdot g \cdot \left(\frac{T_i - T_o}{T_i} \right) \cdot \left(H'' - h \right)$$

Eqn 5.4

where ρ_o (kg/m^3) is the outdoor air density, and g = 9.8 m/s^2. H'' (m) is the height where the indoor and outdoor pressure are equal, which is referred to as the "neutral pressure

height". When the indoor temperature is higher than that outdoors, infiltration occurs from ground level (h [m] = 0) up to H''. When the stack effect is reversed, infiltration occurs from the top of the building H (m) down to H''. In large buildings, many factors can affect the location of the neutral pressure level. These include internal partitions, stairwells, elevator shafts, utility ducts, chimneys, vents, operable windows, and mechanical supply and exhaust systems. An opening with a large area relative to the total building leakage can cause the neutral pressure level to be pulled towards the height of that leakage element.

Large buildings also tend to have many internal partitions that can cause significant internal airflow resistance. In a building with airtight separations at each floor, each story will act independently such that the stack effect is discontinuous from floor to floor. In this case, stack effect induced infiltration for the building can be much less than that which would result from the theoretical stack effect as defined in Eqn 5.4. Furthermore, the location of the neutral pressure height can also be affected. To quantify this effect, the thermal draft coefficient, γ (-), is defined as the sum of the pressure differences across the exterior wall at the bottom and at the top of the building, divided by the total theoretical draft for the building. For a building without internal partitions, the total theoretical draft is achieved, and thus $\gamma = 1$. Conversely, when the air leakage of the internal partitions is much tighter than the exterior envelope, γ approaches 0.

The Shaw-Tamura Infiltration Model estimates the air infiltration rates driven by the stack effect, Q_s (m^3/s), by considering the amount of airflow on an incremental surface

area dA (m^2) on the vertical walls of the building envelope. By assuming that the building has a uniform building perimeter with height, the incremental surface area can be expressed as the product of the building perimeter S (m) and the incremental height of the building dh (m). Starting with the power-law relationship between air-leakage coefficient and air infiltration rate stated in Eqn 5.1, the total air infiltration rate driven by stack effect is the integral of dQ_s over the portion of the building envelope where infiltration occurs, or, by airflow continuity, over the portion where exfiltration occurs.

$$
\begin{aligned}
dQ_s &= C \cdot dA \cdot \left(\Delta P_s\right)^n \\
&= C \cdot S \cdot dh \cdot \gamma \cdot \left(\rho_o \cdot g \cdot \left(\frac{T_i - T_o}{T_i}\right) \cdot \left(H'' - h\right)\right)^n \\
Q_s &= C \cdot S \cdot \gamma \cdot \left(\rho_o \cdot g \cdot \left(\frac{T_i - T_o}{T_i}\right)\right)^n \cdot \int_0^{H''} h^n \cdot dh \\
&= C \cdot S \cdot \gamma \cdot \left(\rho_o \cdot g \cdot \left(\frac{T_i - T_o}{T_i}\right)\right)^n \cdot \frac{\left(\beta \cdot H\right)^{n+1}}{n+1}
\end{aligned}
$$

Eqn 5.5

where β [-] = H''/H. For example, $\beta = 0.5$ means that the neutral pressure level is at the mid-height of the building. The derivation in Eqn 5.5 assumes that air leakage is evenly distributed on the building envelope with respect to height. In other words, the air leakage coefficient C is assumed constant, and not a function of h.

5.3.2.2 Wind Effect

The pressure difference caused by the kinetic energy of wind impinging on the building envelope at speed U (m/s) is described by:

$$\Delta P_w = C_p \cdot \frac{1}{2} \cdot \rho_o \cdot U^2$$

Eqn 5.6

where C_p (-) is known as the wind-pressure coefficient. As wind blows around a building, it generates areas of positive and negative pressure on the building envelope. Typically, the windward wall(s) are pressurized with respect to indoors, and the adjacent wall(s) may be depressurized. To reflect this, the value of C_p is different at each façade of the building. C_p can be measured using pressure taps on a model building in wind tunnel experiments or on real buildings in full-scale tests. Detailed airflow models would also require C_p as a function of position on the different building façades to permit reliable predictions. For simplicity, the Shaw-Tamura Infiltration Model reduces these to one mean wind-pressure coefficient per façade, $C_p^{'}$, which is determined as the weighted mean of the pressure differences measured in wind tunnel experiments (Shaw and Tamura, 1977).

The wind-pressure coefficient, $C_p^{'}$, is a function of wind angle, shielding from surrounding structures, and terrain effects. The maximum pressure difference is observed on a building wall when the wind is approaching normal to it. The remaining three walls are typically depressurized when this happens. For a 45° wind-wall angle, two windward walls are likely to be pressurized at the same time, but the $C_p^{'}$ is lower in value. To account for this effect, a wind-angle correction factor, α, is defined as follows.

$$\alpha = \left(\frac{C_p^{'}{}_{\theta,1}}{C_p^{'}{}_{0,1}} \right)^n + \frac{W}{L} \cdot \left(\frac{C_p^{'}{}_{\theta,2}}{C_p^{'}{}_{0,1}} \right)^n$$

Eqn 5.7

The subscript θ is the wind angle impinging at the longer wall of the building, with $\theta = 0^{o}$ being normal to the wall. The next subscript is the wall number. Wall 1 is defined to be the longer wall. Eqn 5.7 assumes a rectangular-shaped building, and thus only wall 1 and wall 2 are considered explicitly. When the wind angle is 0°, the maximum wind-pressure coefficient $C_{p\,0,1}^{'}$ occurs on the longer wall. In wind tunnel experiments, the ratios of mean wind-pressure coefficients are measured by the ratios of mean pressure difference on the envelope of the model building. L (m) and W (m) are the length and width of the building footprint. The ratio of these two lengths is needed to account for the wall area where infiltration occurs on the shorter wall (wall 2). The total air infiltration rate driven by wind effect on the building envelope is as follows:

$$\begin{aligned} Q_w &= C \cdot A \cdot \left(\Delta P_w\right)^n \\ &= C \cdot \left(L \cdot H\right) \cdot \alpha \cdot \left(C_{p\,0,1}^{'} \cdot \frac{1}{2} \cdot \rho \cdot U^2\right)^n \end{aligned}$$

Eqn 5.8

Similar to the LBL Infiltration Model, estimates for the shielding and terrain effects are needed. In the Shaw-Tamura Infiltration Model, shielding is accounted for by direct adjustment to the mean wind-pressure coefficient. Conceptually, two factors are important in determining the appropriate mean wind-pressure coefficient. One is the plan area density (Grosso, 1992), which is the ratio of built area to total area within a certain radius from the considered building. The other is the relative building height, which is the ratio of the height of the considered building to the height of the surrounding buildings. Wind-pressure coefficients decrease with increasing plan area density, as more buildings can shield wind from impinging on the considered building. For a similar reason, wind-pressure coefficients decrease as the heights of the surrounding buildings exceed that of

the considered building. Grosso (1992) presented a literature review on available wind tunnel data from which these observations are made.

Terrain roughness affects the vertical wind profile and the level of incident turbulence intensity on building walls. The power-law exponent of the wind profile, which describes how wind velocity changes as a function of vertical distance from a reference height, increases with increasing roughness of the surface. Wind-pressure coefficients are inversely related to the power-law coefficient as shown from wind tunnel experiments (Grosso, 1992). In a downtown urban area with enhanced surface roughness, the overall mean wind-pressure coefficients of buildings are expected to be lower than for buildings that are located in suburban areas. These findings are consistent with the terrain parameters used in the LBL Infiltration Model.

5.3.2.3 Combined Stack and Wind Effects

The relative importance of the wind and stack driven air infiltration in buildings depends on a number of factors besides the strength of the respective driving forces, including building height, internal resistance to vertical airflow, location and flow resistance characteristics of envelope openings, local terrain, and the immediate shielding of the building. Tall, narrow buildings with little internal resistance to airflow are likely to have a strong stack effect. Unshielded buildings on a relatively smooth terrain are more susceptible to wind effects. For any building, there will be ranges of wind speed and

temperature difference for which the amount of air infiltration is dominated by the wind effect, stack effect, or neither.

Shaw and Tamura carried out a few experimental studies to determine how the stack and wind effects combine to give the total air infiltration rate. Referring to Eqn 5.9, method (i) by Shaw and Tamura (1977) and method (ii) by Shaw (1979) are the empirical formulations resulting from wind tunnel experiments using a tall building model. Method (ii) includes the shielding effect from lower structures of uniform height that surround the tall building being studied. This study also investigated the influence of wind angle on the adjustment factor. Overall, the results obtained are within 20% of the predictions by method (i). Method (i) did not include shielding from surrounding structures, nor the wind angle effect.

$$\text{(i)} \quad Q_{\text{total}} = Q_{\text{large}} \cdot \left(1 + 0.24 \cdot \left(\frac{Q_{\text{small}}}{Q_{\text{large}}} \right)^{3.3} \right)$$

$$\text{(ii)} \quad Q_{\text{total}} = \begin{cases} Q_{\text{large}} \cdot \left(1 + \left(-0.0074 \cdot \theta + 0.39 \right) \cdot \left(\frac{Q_{\text{small}}}{Q_{\text{large}}} \right)^{3.6} \right) & \text{for } 0^o \le \theta \le 45^o \\ Q_{\text{large}} \cdot \left(1 + \left(0.01 \cdot \theta - 0.48 \right) \cdot \left(\frac{Q_{\text{small}}}{Q_{\text{large}}} \right)^{2.5} \right) & \text{for } 45^o \le \theta \le 90^o \end{cases}$$

$$\text{where:} \quad Q_{\text{small}} = \min\left(Q_s, Q_w\right); \; Q_{\text{large}} = \max\left(Q_s, Q_w\right)$$

and θ is in units of degrees (^{o})

Eqn 5.9

Though different in form from the relationship used in the LBL Infiltration Model (where Q_s and Q_w are added in quadrature), these relationships also suggest that the total air infiltration rate is largely driven by either the stack or wind effect, whichever is higher.

Only in the cases when both effects are similar in magnitude do the lesser terms also contribute significantly to the total air infiltration rate.

Shaw (1980) measured air infiltration rates at two school buildings in Canada, where the pressure differences were measured across the exterior walls at 7 locations continuously for 8 months. The stack and wind induced pressure difference were also computed using the Shaw-Tamura Infiltration Model, as described earlier. The computed sums of the wind and stack driven pressure differences were found to be good approximations of the overall pressure difference measured. According to this study, the relationship to obtain Q_{total} from Q_s and Q_w is:

$$\begin{aligned} Q_{\text{total}} &= C \cdot \left(\Delta P_s + \Delta P_w\right)^n \\ &= C \cdot \left(\left(\frac{Q_s}{C}\right)^{1/n} + \left(\frac{Q_w}{C}\right)^{1/n}\right)^n \\ &= \left(Q_s^{1/n} + Q_w^{1/n}\right)^n \end{aligned}$$

Eqn 5.10

Eqn 5.10 is also the form used in the LBL Infiltration Model where the flow exponent n is assumed to be 0.5.

Other studies have suggested relationships other than those presented in Eqn 5.9 and Eqn 5.10. For example, Fletcher and Johnson (1992) found that simple linear combination of wind speed and the square root of indoor-outdoor temperature difference is sufficient to explain the air infiltration rate variability observed in a small factory unit. This would imply adding Q_s and Q_w linearly to obtain Q_{total}. Experiments by Tanaka and Lee (1986)

on a high-rise building found that the linear sum of pressure differentials owing to stack, wind, and forced ventilation is not the same as the overall pressure differentials measured. In practice, it is likely that no single empirical relationship would fit all buildings. Fortunately, differences in formulations are significant only when the stack and wind driven air infiltration rates nearly equal to one another (Figure 5.9). When either Q_s or Q_w is one half of the other or less, the different formulations give total air infiltration rates that agree to within 20% of each other.

5.3.3 Air Infiltration Model Parameters and Uncertainties

Performance of air infiltration models often depends on whether site-specific information of the building being modeled is available. The Shaw-Tamura Infiltration Model has a number of adjustable parameters, namely the neutral pressure level (β), the thermal draft coefficient (γ), the wind angle factor (α), and the wind-pressure coefficient ($C_p^{'}$). A range of values is expected for each of these parameters in a group of buildings, which will contribute to the overall variability of the air infiltration rate predictions. If their distributions are known, their influences on the air infiltration rate predictions can be modeled. However, data on these input parameters are limited. Input parameters can also be time variant depending on the building operating conditions and the local meteorology. Discussed below are studies where these parameters have been measured. Even though the available data are insufficient to derive a representative distribution for each of the parameters, they do provide some indication of the range of values expected in real buildings.

5.3.3.1 Neutral Pressure Level and Thermal Draft Coefficient

Table 5.5 lists the experiments where pressure differential measurements have been made in various high-rise buildings. The range of β observed is from 0.3 to 0.76, with a mean of 0.48. These data are insufficient to derive a particular distribution for the parameter. However, a reasonable representation is to consider a possible range of β from 0.2 to 0.8, with a central tendency of 0.5. It is found from these experiments that sealing the air intake and exhaust dampers can lower the neutral pressure level. However, β is largely unaffected by operating the mechanical ventilation system. The two 1-story schools measured by Shaw (1980) both had $\beta = 0.7$. It appears that there is no significant difference in terms of the vertical pressure difference distribution between high-rise and low-rise buildings.

The resistance to flow in the vertical direction is not high even in the tall buildings measured. Measured values of the thermal draft coefficient (γ) are in the range of 0.63 to 0.82 (Table 5.5). Both studies by Tamura and Wilson (1966, 1976) found that γ is lower when the ventilation system is on, indicating higher flow resistance from floor to floor. Based on these very few data points, a reasonable range to consider for γ is from 0.6 to 0.9, with a central tendency of 0.8.

5.3.3.2 Wind Angle Correction Factor and Wind-Pressure Coefficient

Pressure differential data from wind tunnel experiments and full-scale tests on buildings are more abundant. A review by Grosso (1992) summarizes the existing literature, models that compute wind-pressure coefficient distributions, and presents a regression analysis of the wind-pressure coefficients measurements. Measured mean wind-pressure coefficients for adjacent sides of a building are out of phase by 90° with respect to wind angle (Shaw and Tamura, 1977; Shaw, 1979; Akins et al., 1979; Shaw, 1980). That is, wall 2 (shorter wall) has a mean wind-pressure coefficient at 90° wind angle that is roughly the same as wall 1 (longer wall) at 0°. At 45°, the two adjacent walls have roughly equal mean wind-pressure coefficients that sum to the same total as when wind is approaching normal to a wall.

Mathematical models of the dependence of wind-pressure coefficients on wind angle are available (Grosso, 1992). However, to apply this dependence for a population of buildings would require detailed local wind data as well as information on the location and orientation of each building. The uncertainties associated with such inputs would be large. Favoring a simple model that can provide reasonable results without excessive input data demands, the analysis to follow assumes that the wind always approaches normal to the long wall. In other words, α in Eqn 5.7 is assumed to be 1. This assumption tends to cause a slight overprediction of air infiltration rate when the building footprint has a very large aspect ratio. When the building footprint is close to square, the orientation of the building with respect to wind direction is unimportant. This is true, however, only if air leakage is uniformly distributed on all walls of a building. The

modeling approach here also assumes that all buildings have simple rectangular geometry.

Mean wind-pressure coefficients are also subject to local shielding and terrain effects. A review by Orme et al. (1994) summarizes the dependence of wind-pressure coefficient on the height of surrounding structures relative to the building being modeled. The mean wind-pressure coefficient under heavy shielding, which occurs when the building is surrounded on all sides by obstructions of similar height, can be one-third the value when there is little obstruction surrounding the building. Wind-pressure coefficients are also subject to the overall building density in the vicinity of the modeled building: surrounding buildings can only affect the mean wind-pressure coefficients of the modeled building when they are in close proximity. Increasing the plan area density[12] to 10 from the no-shielding case can reduce the wind-pressure coefficients to half their unshielded value (Grosso, 1992).

Judging from existing wind tunnel and full-scale experiments (Akins et al., 1979; Grosso, 1992; Orme et al., 1994; Persily and Ivy, 2001), mean wind-pressure coefficients for the windward wall are typically in the range of 0.3 to 0.9. The range of mean wind-pressure coefficients chosen for this analysis is from 0.5 to 0.9, with a central tendency at 0.7. In a building stock, a range of values is expected. The variability considered here is

[12] Plan area density = 10 means that the footprint area of the building is 10 times the effective area to its nearest adjacent building. The effective area is measured by the product of the closest two distances between the modeled building and the nearest adjacent building.

reasonable to account for different shielding and terrain effect on the mean wind-pressure coefficient of buildings.

5.4 Air Infiltration Model Predictions and Measurements

To gain a sense of how the air infiltration model performs when compared against measurements, two sets of analyses are presented here. The first analysis compares Shaw-Tamura Infiltration Model predictions with existing air infiltration rate measurements in commercial buildings. Such data must be accompanied by air-leakage measurements from pressurization tests for use as inputs to the model. Part of the challenge here is to gather appropriate meteorology data to run the Shaw-Tamura Model, since the meteorological conditions are only qualitatively described in the original studies. The second analysis aims to estimate a representative air infiltration rate distribution for the entire US commercial building stock. Currently, there is no representative sample of air infiltration rate measurements that addresses this task. This analysis will provide an estimate of the central tendency as well as the expected variability of the distribution. Results from this analysis will be compared against previous estimates of air infiltration and ventilation rates in US buildings.

5.4.1 Model Comparisons against Existing Air Infiltration Rate Measurements

5.4.1.1 Office Building Measurements

Grot and Persily (1986) measured air infiltration and ventilation rates during the fall, winter, and spring season in eight federal office buildings using an automated measurement system. In total, 200 hours of measurements were made in each building. The sampling system injected the tracer gas SF_6 into the fan inlets of the building supply ducts at 3-h intervals in 5 locations. Subsequent decay in tracer gas concentration at 10 locations was monitored every 10 minutes for the next 3 hours. Air infiltration measurements were made during periods when the building was not occupied. To keep the tracer gas well mixed, the air handler fans were run throughout but with air intake dampers closed. Seven of the eight buildings also had a pressurization test performed to determine the air-leakage coefficient of the building envelope (Persily and Grot, 1986). Air leakage of the building envelope was measured using the building air-handling system to pressurize the building. The supply fans were operated while all return and exhaust fans were turned off. All return dampers were closed with the intention that the supply air flowing into the building only could leave the interior through leaks in the building envelope. The airflow through the supply fans was measured using a constant-flow, tracer gas injection/decay method. Table 5.6 gives a brief description of the seven buildings tested.

In their analysis, Persily and Grot (1986) also used the Shaw-Tamura Infiltration Model to predict air infiltration rates. They found significant underpredictions when compared to measurements (Figure 5.10). There are several possible reasons for the discrepancy. The model does not account for the potentially large stack effect developed in the open elevator shafts of buildings. More importantly, with the air-handling system running, the

air exhaust and return dampers could have leaked, thus adding to the apparent air infiltration rates. Localized pressure changes within the building caused by the air-handling system could also have induced airflow through the building envelope. Third, ceiling plenums are used as return ducts in all the buildings tested. The air leakage from this plenum space can lead to additional intake of air into the building not accounted for by the model. Finally, the seven buildings tested are much shorter than the 40-story building for which the Shaw-Tamura Infiltration Model was originally developed. This leads to a question about whether the model is appropriate for medium-rise buildings.

The above comparison is made using a very narrow set of air infiltration rate measurements. The input parameters used to model air infiltration rate are similar to those used by Shaw and Tamura (1977), which might not be appropriate for the particular buildings tested. Aside from the comparison shown in Figure 5.10, measurements of air infiltration rates in each building are plotted against the outdoor temperatures at the time of the experiments. Grot and Persily (1986) fitted empirical regression models to these data in an attempt to describe the dependence of air infiltration rate on meteorology in the buildings they studied. Instead of their empirical approach, the goal of the present analysis is to test if the Shaw-Tamura Infiltration Model captures the functional dependency of air infiltration rate on meteorology. If the model is capable of describing the functional dependence of air infiltration rates on outdoor temperature and the variability in the measurements caused by wind, then the discrepancies observed could be experimental artifacts, rather than inadequacy of the model. Such comparisons can also

reveal if the input parameters used are appropriate. Finally, the method used to combine stack and wind effects can be tested to see how much it affects the model fit.

Only general descriptions of the meteorology at the time of the experiments are mentioned in Persily and Grot (1986). Since measurements were carried out in fall, winter, and spring, outdoor temperature and wind data from September through April seem reasonable. For this purpose, daily averaged climatic data from the National Climatic Data Center, known as the NCDC Global Surface Summary of Day Data (NCDC, 2005), are used. This dataset is only available from 1994 to date, and so it was not possible to model the air infiltration rates using data from the year when the experiments were performed. Instead, the years 1994 and 2004 were selected to capture some variability in the meteorological conditions at the sites. Many of the meteorological stations are located at the respective city airport. Roughly 560 days of predictions were performed for each building. The wind speed measurements taken at 10 m were adjusted to the building height using 0.3 as the power-law coefficient, appropriate for urban landscape under neutral to stable atmospheric conditions (US EPA, 1995).

The indoor temperature is assumed to be 20 ^{o}C in all buildings. Persily and Grot (1986) used the suggested neutral pressure level ($\beta = 0.5$) and thermal draft coefficient ($\gamma = 0.8$) by Shaw and Tamura (1977). The exceptions are the thermal draft coefficients of the buildings at Anchorage ($\gamma = 0.95$) and Springfield ($\gamma = 0.87$), where the open architecture led to highly interconnected buildings. It is unclear whether Persily and Grot (1986) used the mean wind-pressure coefficient ($C_p^{'} = 2.0$) suggested by Shaw and Tamura (1977),

since this value is probably too high for the shorter buildings tested. In this analysis, instead of using fixed values of β, γ, and $C_p^{'}$ for each building, an assumed distribution is defined for each of the parameters. The range and central tendency of the parameters sampled are as defined in Sections 5.3.3.1 and 5.3.3.2 (see also Table 5.7). A triangular distribution is used, meaning that the probability distribution peaks at the central tendency value, and decreases linearly from the peak to the upper and lower range limits. Each simulation samples from these distributions. In reality, these parameters might not change significantly over time in a building. This sampling approach aims to mimic the uncertainties associated with these parameters for any particular building in a given stock.

Air infiltration predictions are shown in Figure 5.11. In general, the amount of underprediction is similar to the level observed by Persily and Grot (1986), with the model predictions typically only about one-third of the measured values (Figure 5.12). A weak dependence of the air infiltration rates on the outdoor temperature is observed across all buildings. Variability in wind speed causes air infiltration rates to vary by about a factor of two at most buildings. Since the wind speeds used in the modeling are daily averages that are not affected by short-term fluctuations, it is possible that momentarily high wind speeds could lead to higher air infiltration rates. The Rayleigh distribution is commonly used to describe the distribution of wind speed given its mean value. This distribution is skewed such that moderate wind is the most common, and strong wind is relatively rare. By using the Rayleigh distribution to model the hourly wind speed at the seven office buildings while keeping all other modeling parameters the same, slightly

different air infiltration rates are predicted. Typically, the predicted 90th percentile air infiltration rate at each building is 5 to 30% higher if the distribution of wind speed is included when computing wind-effect driven air infiltration. On the other hand, the predicted 10th percentile air infiltration rate at each building would be lowered by roughly the same percentages if the distribution of wind speed is included. The median air infiltration rate predictions are affected only very slightly (-3 to 10%). These comparisons show that the predicted air infiltration rates are not systemically biased due to the use of the daily mean wind speed reported by the NCDC. However, more scatter in the predictions than those shown in Figure 5.11 is expected if more time-resolved wind speeds were to be used in the simulations instead of the daily averages.

The total air infiltration rate is estimated by combining the stack and wind effect using the relationship from method (i) in Eqn 5.9. Of the various forms suggested, this method of combining the stack and wind effect gives the lowest total air infiltration rate (Figure 5.9). Two alternative forms of combining the stack and wind effect were tested to see if they improved agreement with measurements.

$$\text{Alternative (a)}: \quad Q_{total} = \sqrt{Q_s^2 + Q_w^2}$$
$$\text{Alternative (b)}: \quad Q_{total} = Q_s + Q_w$$

Eqn 5.11

Alternative (a) is the method used in the LBL Infiltration Model, which assumes that the pressure differences sum to give the total air infiltration rate. Alternative (b) is not physically based, but rather a hypothetical way to obtain total air infiltration rates that are higher than all other alternatives shown in Figure 5.9. When these alternatives are used to compute the total air infiltration rates, alternative (a) gives results that are at most 15%

higher, and alternative (b) gives air infiltration rates that are up to 62% higher relative to the base case calculations. It is however clear that neither method is sufficient to offset the large underprediction of the model with respect to the measurements.

This analysis shows that model predictions produce temperature and wind dependencies that agree with observations qualitatively. The large offset between measurements and predictions may be caused by the difference in the operating condition of the buildings when measurements were made relative to the way they are being modeled. In the case where the air handling system of a building is kept running even with inlet and exhaust dampers shut off, the model underpredicts the air infiltration rate by approximately a factor of three. During SIP, some buildings might operate in this manner. Significant underpredictions of air infiltration rates would be likely in such buildings if the Shaw-Tamura Infiltration Model is used without adjustment.

5.4.1.2 Small Commercial Buildings

Cummings et al. (1996) studied the nature and extent of uncontrolled airflow in 70 small commercial buildings of various types (Table 5.1), all located in the state of Florida. The floor area of the buildings tested ranged from 65 to 2100 m^2 (700 to 22000 ft^2). Blower door tests were carried out on 69 buildings with the air handling system turned off and dampers sealed. In 56 buildings, air infiltration rates were measured using a tracer-gas decay method with the mechanical ventilation system turned off. A summary of the measurements is presented in Figure 5.13. As expected, there are some associations

between the air infiltration rate measured and the air-leakage coefficient. The correlation coefficient (R^2 value) between these two parameters is 0.36. A new analysis was conducted to test if the air infiltration model is capable of explaining the additional variability observed. If so, then the model would be deemed useful in explaining the air infiltration rate measurements.

Unfortunately, the outdoor temperature and wind speed at the time of measurement are not reported with the data. Following a similar method used in the analysis of office buildings, two years (1994 and 2004) of daily averaged meteorology data were used to model the air infiltration rates. It is reported that the majority of buildings were located in Brevard County on the east coast of Florida, with the remaining seven located in Orlando and one in Polk County. Each day of the two years was modeled using the outdoor temperature and wind speed of the city of Cocoa, FL, which is located in Brevard County.

Many of the buildings modeled are not much bigger than residential buildings. It is therefore possible that the LBL Infiltration Model is more appropriate for these types of buildings. Similar triangular distributions of model parameters are assumed for applying the LBL Infiltration Model (Table 5.7), where the central tendency represents the peak of the probability distribution, and the range represents the upper and lower bounds. These estimates are based on discussion presented in Chapter 3 of the LBL Infiltration Model.

Predictions of air infiltration rates using the Shaw-Tamura Infiltration Model and the LBL Infiltration Model are shown in Figure 5.14. The overall agreement between predictions and measurements are roughly within a factor of three without strong bias. This is quite different from the previous analysis where predictions were systematically less than the measurements. Relatively speaking, the Shaw-Tamura Infiltration Model still tends to under predict when compared to measurements. Sampling of input parameters (β, γ, and $C_p^{'}$) used in the Shaw-Tamura model leads to a factor of three variability in the predicted air infiltration rates. When the LBL model is used, sampling of input parameters leads to a factor of two variability in the predictions.

The Shaw-Tamura Infiltration Model performs slightly better than the LBL Infiltration Model in larger buildings. There are 20 buildings with floor area exceeding 5000 ft^2 (465 m^2), which is the approximate upper size limit for houses. Of these 20 buildings, the residual standard error after fitting the measurements with model predictions is 0.28 for the LBL model, and 0.14 for the Shaw-Tamura model. The Shaw-Tamura model is better at capturing the variability in the measurements also. In smaller buildings, however, the predictions from the LBL model are better at explaining the variability in the air infiltration rates measured. The Shaw-Tamura model tends to predict lower air infiltration rates than the LBL model (Figure 5.15). This is to be expected, since the Shaw-Tamura model assumes certain levels of discontinuity between floors, as represented by the thermal draft coefficient. In smaller buildings, however, less extensive internal partitioning means that the airflow is probably less disrupted than in larger buildings. The wind-pressure coefficients chosen for the Shaw-Tamura model are also not suited for

very small buildings. For these reasons, the LBL Infiltration model should probably be used for small commercial buildings.

The use of general climatic data instead of site and time specific data to model the air infiltration rate is a key source of uncertainty in this analysis. Assuming that the outdoor temperatures and wind speeds used to model the air infiltration rates are not biased with respect to the experimental conditions, this analysis shows that the Shaw-Tamura Infiltration Model does not systematically under predict air infiltration rates. Unlike in the previous analysis on office buildings, the air-handling systems remained off during the measurements in these buildings. This difference in experimental procedure might explain why substantial underpredictions are observed among office buildings, but not here. It is based on these findings that the Shaw-Tamura Infiltration Model will be used to predict the air infiltration rates of large commercial buildings while the LBL Infiltration Model will be used for smaller commercial buildings in addition to single-family residences.

5.4.2 Air Infiltration Rate Distribution of the US Commercial Building Stock

Currently, there exist no well-sampled measurements of the air infiltration rates in US commercial buildings. In SIP scenarios, knowing such a distribution is necessary to estimate the expected amount of toxic chemicals that can infiltrate indoors from an outdoor release. Comparing this distribution with measurements of ventilation rates can also provide important information about the benefit of SIP action for commercial

buildings, in which mechanical ventilation fans would be turned off as an emergency response. To characterize the ventilation rate distribution experimentally would require extensive effort and cooperation from a large number of building owners nationwide. Aside from the study by Cummings et al. (1996), one of the more complete datasets is from Lagus and Grot (1995), who tested the air infiltration rates of 40 buildings from different climate zones in California by means of the tracer-gas decay method. Their results are shown in Figure 5.16, which appear to be roughly lognormally distributed with geometric mean (GM) = 0.38 h^{-1} and geometric standard deviation (GSD) = 2.7. A similar distribution (GM = 0.34 h^{-1}, GSD = 2.0) is inferred from the measurements in the small Florida commercial buildings, as shown in Figure 5.13. Given such a wide variability in the air infiltration rate measured, a large number of measurements would be needed to accurately characterize the distribution.

An alternative method is to model the air infiltration rate distribution of the building stock by taking into account variability in air leakage of the building envelope and the driving forces for air infiltration. Briggs et al. (1992) and VanBronkhorst et al. (1995) designed 25 typical office buildings to represent the building stock in the US. They then assigned air infiltration rates to each type of building. The infiltration rates were generated using a simplified building energy model (Etheridge and Alexander, 1980), which accounts for stack and wind effects, building age and the presence of operable windows. The simulated range (Figure 5.16) is narrower than the 40 measured air infiltration rates by Lagus and Grot (1995). This difference may be due to the reduced number and limited types of buildings being considered.

Perhaps not by coincidence, the variability measured in air infiltration rates is similar to the variability observed in the air-leakage coefficient of buildings (Figure 5.2). This seems to suggest that the modeling approach should generate a reasonable air infiltration rate distribution. The analysis presented here uses both the Shaw-Tamura Infiltration Model and the LBL Infiltration Model to estimate the air infiltration rate distribution of the US commercial building stock. The method used is similar to that described in Section 5.4.1, and therefore is not repeated in detail here.

5.4.2.1 Characteristics of US Commercial Buildings

The 1999 Commercial Building Energy Consumption Survey (CBECS) sampled 5430 buildings in the US. The survey sample was designed such that responses can be used to estimate characteristics of the entire commercial building stock. Building floor area, number of floors, number of employees and building occupancy limit are among the data reported. Building floor area and height are used from these data to estimate the distribution of air-leakage coefficients according to the regression model detailed in Table 5.4. The predicted distributions are shown in Figure 5.17.

Building heights are estimated from the number of stories reported. To protect the identity of some of the larger buildings being surveyed, the exact number of stories of buildings exceeding 15-story in height are not reported. A method is therefore needed to assign an actual number of stories to the 124 buildings that are between 15 and 25-story,

and the 120 buildings that exceed 25-story. To do so, the relationship between building floor area and number of stories is quantified. For example, among buildings that have a certain floor area, the distribution of the number of stories of these buildings is curve fitted using standard regression technique. These probability density functions are obtained using buildings with known floor area and number of stories in the CBECS. Then, these probability density functions are used to estimate the number of stories of buildings that are taller than 15-story, based on their floor area. The building heights obtained are shown in Figure 5.18. The tallest buildings are estimated to be about 60-story.

As discussed earlier, the flow exponent (n) and air-leakage coefficient (C) are negatively correlated. Figure 5.19 shows a roughly linear relationship between ln(C) and n using the 192 measurements in the commercial air leakage database. The flow exponent decreases from 0.7 to 0.5 as the air-leakage coefficient decreases from 5×10^{-5} to 2×10^{-3} $m^3/(s\cdot m^2\cdot Pa^n)$. Least-square linear regression between ln(C) and n gives:

$$n = 0.232 - 0.0482 \times \ln(C) + \varepsilon \quad , \quad \varepsilon \sim N(\mu = 0,\ \sigma = 0.0862)$$

Eqn 5.12

where the residual standard error, ε, is roughly normally distributed with mean (μ) and standard deviation (σ) as indicated. The regression model fit yields $R^2 = 0.2$. There is still significant variability in the regression residuals, as shown in Figure 5.19 (lower plot). However, because the model residuals are independent of the air-leakage coefficients, modeling of the flow exponent is straightforward. Using Eqn 5.12 and the predicted air-leakage coefficient distribution of US commercial building stock, the corresponding

distribution of flow exponents spans the range from 0.4 to 0.9 (Figure 5.17), with a median at 0.65.

Aside from the basic building characteristics detailed above, both the Shaw-Tamura and the LBL Infiltartion Model require the geometry of the building to be known. Building footprint area, perimeter, and surface area of the long wall are needed. To estimate these, some simplifying assumptions are made. All buildings are assumed to be rectangular and all floors of the building are assumed to have the same floor area. Under such cases, the building footprint area is obtained by equally dividing the total floor area (given in CBECS) by the number of floors. To estimate the building perimeter and the long wall area, however, requires knowing the aspect ratio of buildings, which is not available from CBECS. To estimate the aspect ratio, the geometry of buildings in downtown Oklahoma City, OK was analyzed. These data constitute a test case of a larger dataset made available by the National Atmospheric Release Advisory Center at Lawrence Livermore National Laboratory. At the time of this analysis, however, only a very limited set of cities has been characterized. The choice of Oklahoma City is based on convenience, since this is also the case study used in Chapter 6 to assess SIP effectiveness in commercial buildings.

The outlines of the footprint areas and heights of 6334 buildings in and near downtown Oklahoma City were coded geographically by their latitude and longitude. Judging from the size of these buildings, most of them are single-family homes. Details on these data are discussed in the next chapter. For now, the analysis will focus on quantifying the

distribution of aspect ratio of commercial buildings. Only buildings with estimated floor area greater than 460 m^2 (5000 ft^2) are considered, which is about 25% of the buildings. The aspect ratio of these buildings is estimated by the distance between the most north corner or side of the building to the most south, and the distance between of the most west to the most east. This simple method works for buildings in Oklahoma City because most of them are oriented parallel to the northing and easting coordinate system. The estimated aspect ratios of these larger buildings are shown in Figure 5.20. The majority of buildings have a footprint with length that is less than twice the width. The most probable aspect ratio is 1, i.e. buildings have square-like footprint. A follow up analysis shows that the smaller buildings in Oklahoma City tend to be slightly more square-like, relative to larger buildings. The distribution of aspect ratio can be described well by an exponential density function: $f(x) = \lambda \exp(-\lambda x)$, where the best-fit rate, λ, is 1.3. This function is used to predict the aspect ratio of the buildings in CBECS, which is needed to estimate the perimeter length and the long wall surface area of buildings.

5.4.2.2 Modeling of Air Infiltration Rates of US Commercial Buildings

Out of the 4,657,000 commercial buildings estimated to exist in US according to CBECS, 50% are smaller than 460 m^2 in floor area, and 87% are only 1 or 2-story tall. These statistics show that the majority of commercial buildings are similar in size to single-family homes. Even though these small buildings have different air leakage characteristics than houses, the way they respond to air infiltration driving forces is more similar to houses than large commercial buildings. Only the large commercial buildings are modeled using the Shaw-Tamura Infiltration Model. Of the 5430 buildings surveyed

in the CBECS, 23% of them are less than or equal to 1000 m^2 in floor area and 3-story in height. These buildings, however, represent close to 75% of the US commercial building stock[13]. They will be modeled using the LBL Infiltration Model. The input parameters used in the air infiltration models are the same as described in previous analyses (Table 5.7). The effective leakage area (ELA) needed by the LBL Model Infiltration is computed from the air-leakage coefficient *C* as follows:

$$\text{ELA} = \frac{Q_{4\ \text{Pa}}}{\sqrt{\frac{2 \cdot 4\ \text{Pa}}{\rho}}} = \frac{C \cdot A \cdot (4\ \text{Pa})^n}{\sqrt{\frac{2 \cdot 4\ \text{Pa}}{\rho}}}$$

Eqn 5.13

where A [m^2] is the envelope area of the building including walls and roof. In computing the ELA, the convention of the LBL Infiltration Model is to use the total air leakage of the building envelope. This is different from the Shaw-Tamura approach, where only air leakage on the walls is generally considered. This difference between the two models becomes an issue when modeling a continuum of building sizes. Buildings that are slightly bigger than the cut-off for the Shaw-Tamura model have significantly lower air infiltration rates than buildings that are slightly smaller and were modeled using the LBL model. To resolve this, the air-leakage coefficients of buildings modeled by the Shaw-Tamura Infiltration Model were adjusted as follows:

$$C_{adj} = C \cdot \frac{\text{Wall + Roof Area}}{\text{Wall Area}}$$

Eqn 5.14

The adjusted air-leakage coefficient, C_{adj}, is always higher than the original definition of this parameter used in the Shaw-Tamura Infiltration Model. This adjustment is most

[13] Each building surveyed in CBECS is assigned a weight, which is the number of buildings in the US that the particular sample building represents.

important for buildings that are large in footprint area, but short in height, and so have a large roof area relative to vertical wall area. Of the buildings surveyed in the CBECS, the median ratio of C_{adj}/C is 1.3 for buildings that exceed 5-story in height. For buildings that are less than or equal to 5-story but have floor area that exceeds the cut-off for the Shaw-Tamura Infiltration Model, the median ratio of C_{adj}/C is 3.5. Even though this adjustment departs from the original definition of the air-leakage coefficient used in the Shaw-Tamura model, it is needed in order to obtain sensible predictions in the types of buildings that differ significantly in shape from the 40-story building the model was originally developed for. Without this adjustment step, the predicted air infiltration rates in large but short buildings would be much smaller than the expected range based on measurements.

To model air infiltration rates that represent the commercial building stock, climatic data from the mostly populated 45 cities in the US are used. Roughly 15% of the US population lives in one of these 45 cities. The buildings modeled are each randomly assigned to a city. The allocation is proportional to the population of the cities. For example, there are 8.1 million people living in the New York City area, which constitutes 19% of the total population living in the 45 cities. Consequently, 19% of the buildings were modeled using New York City's climatic data. Los Angeles, Chicago, Houston and Philadelphia are the next four most populous cities, which together made up another 24% of the population. The monthly normals for outdoor temperatures and wind speeds

(Figure 5.21) of each city were obtained from the National Climatic Data Center[14] (NCDC, 2004). The indoor temperature was assumed to be 20 ^{o}C at all times.

The air infiltration rates of each of the 5430 buildings surveyed were modeled using the 12 pairs of outdoor temperature and wind speed assigned to it. The method to combine stack and wind effects is the one originally recommended by Shaw and Tamura (1977) when the infiltration model was first developed (i.e method (i) in Eqn 5.9). The resulting air infiltration rate predictions are shown in Figure 5.22.

Most buildings are predicted to have air infiltration rate ranges from 0.05 to 2 h^{-1}, with 80% of them in the range 0.1 to 1 h^{-1}. Air infiltration rates are lowest in summer and early fall, when the indoor-outdoor temperature difference and wind speed for most cities are at their minimums. Air infiltration rates are highest in the winter months. The predicted median air infiltration rate of the building stock in the winter months is twice that in the summer months (Figure 5.22). However, this seasonal variability is small relative to the variability within the building stock. The composite distribution, obtained by considering all 12 months of simulations and weighted to give a national estimate, is approximately lognormal with GM = 0.35 h^{-1} and GSD = 2.1. This distribution agrees well with the air infiltration rates measured in buildings (Figures 5.13 and 5.16). In fact, the predicted GM and GSD are very close to the measured values, which are 0.34, 0.35, and 0.38 h^{-1}, and 1.7, 2.0, and 2.7 respectively. The predicted distribution therefore conforms with expectation as suggested by measurements in small populations of commercial buildings.

[14] Normals of average monthly data are the arithmetic mean of a climatological element computed over three consecutive decades, which is from 1971 to 2000 in this case.

Among the buildings modeled, both stack and wind effects are important. Considering all simulations, the number of cases in which stack-driven air infiltration rates dominate over wind-driven infiltration equals the reverse (Figure 5.23). The stack effect tends to dominate in wintertime when the indoor-outdoor temperature difference is large. In milder climate conditions, high winds can drive large air infiltration rates that dominate stack-induced flow by up to 2 orders of magnitude. Much of the scatter in the Q_s / Q_w ratio is caused by the building parameters used to run the Shaw-Tamura and LBL models. Some of these parameters are not likely to vary strongly over time in a building. Nonetheless, the sampling approach generated results that appear to reasonably describe the behavior of the building stock as a whole.

5.4.2.3 Implications for Shelter-in-Place in Commercial Buildings

The amount of air exchange with the outdoors is one of the key factors that determines the SIP effectiveness of buildings. The above analyses considered the amount of unavoidable air infiltration that would likely take place without pre-event hardening of the building envelope. Without timely warning of an outdoor release, however, many buildings are likely to have their mechanical ventilation system running, and therefore have higher air-exchange rate with the outdoors. The analysis of seven office buildings by Persily and Grot (1986) (see Section 5.4.1.1) suggests that even with the air exhaust and intake dampers shut, leaving the air handling system running can induce significant air exchange.

Concerning indoor air quality, ASHRAE 62 (1999) is a ventilation standard that recommends 20 cfm/person, or 0.0094 $m^3/(s \cdot person)$, in most indoor environments. Grot and Persily (1986) found that many of the eight office buildings measured operated very close to or below the recommended ventilation rates. The measured monthly average ventilation rates ranged from 0.3 to 1.0 h^{-1} during the winter months, and were typically well over 1 h^{-1} in most buildings in spring and fall. When the outdoor temperature is mild, higher ventilation rates occur because outdoor air is used to cool the buildings. Lagus and Grot (1995) measured the air-exchange rates of 22 office buildings and 13 retail buildings in California and found the median to be 1.1 and 1.8 h^{-1} respectively. Assuming a conversion factor of 20 cfm/person = 0.8 h^{-1}, the authors concluded that the measured ventilation rates are higher than the ASHRAE ventilation rate recommendations, which would be 0.8 h^{-1} for office buildings, and 1.2 h^{-1} for retail buildings. This study also found that schools tend to have higher air-exchange rates on average (median = 2.2 h^{-1}), but still not high enough to satisfy the ventilation standard recommended for schools. Among the full set of 49 buildings tested by Lagus and Grot (1995), the typical air-exchange rates under normal operating conditions were in the range of 1 to 3 h^{-1}, with a minimum at roughly 0.5 h^{-1}.

Ludwig et al. (2002) reported the ventilation rates of 100 office buildings determined as part of the US EPA Building Assessment Survey and Evaluation (BASE) Study. These buildings were randomly selected in 37 cities located in 25 states. The ventilation rates were determined using occupant-generated CO_2 as tracer gas. Ideally, the steady-state

CO_2 level would be obtained and used to compute the air-exchange rate based on mass balance. In practice, however, factors like building occupancy level, and the fresh-air intake rate of the ventilation system all vary with time. Thus, the indoor CO_2 concentrations measured are also time varying. To overcome these problems, the authors chose the 90th percentile CO_2 concentration measurement to estimate the air-exchange rates. Justification of this choice is detailed in their paper. They found that 80% of the ventilation rates estimated are in the range between 20 and 65 cfm per person. Assuming that the same conversion factor of 20 cfm/person = 0.8 h^{-1} (Lagus and Grot, 1995) also applies here, then the air-exchange rate of the 100 BASE buildings ranges from 0.8 to 2.6 h^{-1}.

As would be expected, this evidence indicates that relative to air infiltration rates, which mostly range between 0.1 and 1 h^{-1} (Figure 5.22), operating the mechanical ventilation system can cause the air-exchange rate in buildings to increase substantially. In two of the studies (Cummings et al., 1996; Lagus and Grot, 1995) where both the air infiltration rate and air-exchange rate with the mechanical ventilation system running were measured in buildings, the observed ratios of these two rates were mostly in the range of 0.1 to 0.8 (Figure 5.24). Similar expectations for this ratio are implied by the difference between the range of air infiltration rates (0.1 and 1 h^{-1}) obtained in this analysis, and the range of air-exchange rates measured in buildings (1 to 3 h^{-1}). The variability in this ratio means that the reduction in the amount of outdoor air brought into the building by turning off the mechanical ventilation systems can be very significant in some buildings, but only modest in others. The amount of fresh outdoor air intake that the mechanical ventilation

systems supply also tend to vary seasonally. As observed by Grot and Persily (1986), ventilation systems tend to operate with minimum outdoor air intake in the wintertime. Air infiltration rate predictions yield higher values in the winter because of stronger driving forces. As a result, the amount of outdoor air leaking into the building by uncontrolled air infiltration can approach that provided by mechanical ventilation. In such cases, the added protection by shutting down the mechanical ventilation system during SIP might be small. On the other hand, when the climate is mild and many buildings have their ventilation systems operating at high rate of outdoor air intake, then the added protection by shutting down the system is potentially very large.

5.5 Conclusions

Data on the air leakage of commercial buildings in the existing literature have been compiled and analyzed. The air-leakage coefficient of commercial buildings was found to correlate with building floor area and height. Smaller commercial buildings tend to have more leaky building envelopes per unit surface area. On the other hand, taller buildings tend to have additional air leakage associated with their height, but only to a certain extent. The fit of the regression model using floor area and height to predict air leakage is reasonable and convenient to use, but the explanatory power of the model is limited. Plots of air-leakage coefficients grouped by building usage and construction type show that these two parameters can potentially explain more of the variability observed. However, analysis of these categorical parameters, including country of origin of the measured

buildings, would require advanced statistical techniques because of the small dataset size. Extension from the simple regression method presented here is left for future work.

For large commercial buildings, the air infiltration model described in Chapter 3 is inappropriate because of greater size and major structural differences from that of single-family dwellings. An alternative model, known as the Shaw-Tamura Infiltration Model, is described in this chapter for the purpose of predicting the air infiltration rates of large buildings. The model formulation and input parameters have been discussed. Predictions are compared with existing air infiltration rate measurements. In general, the Shaw-Tamura model captures the functional dependence of air infiltration rate on the two driving forces: indoor-outdoor temperature difference and wind. Comparison with measurements also indicates that the mechanical ventilation system, when operating, can have a large effect on the air infiltration rates of buildings even when dampers are closed. It is also evident that the LBL Infiltration Model performs somewhat better than the Shaw-Tamura model for small commercial buildings.

Using both the Shaw-Tamura and the LBL Infiltration Models, the air infiltration rate distribution of the US commercial building stock has been estimated. Data from the Commercial Building Energy Consumption Survey and the National Climatic Data Center are used to estimate the building characteristics and the driving forces for air infiltration, respectively. A factor of ten variability between the tightest 10% and leakiest 10% of the buildings is predicted. Relative to the predicted air infiltration rates (0.1 to 1 h^{-1}), air-exchange rate measurements in buildings under normal operating conditions are

substantially higher. In accidental releases, advance warning may not occur. Many buildings would still have their ventilation systems running, leading to air-exchange rates in the range of 1 to 3 h^{-1}. This is expected to significantly and adversely influence the overall effectiveness of an SIP strategy in some scenarios.

In the following chapter, the effectiveness of shelter-in-place in commercial buildings is modeled for a simulated release at Oklahoma City, OK. The air leakage distribution of commercial buildings in the city is estimated based on the regression model developed here. Then, the air infiltration rates of the buildings are estimated using the appropriate air infiltration model. SIP effectiveness is assessed using similar metrics as before. Estimates of SIP effectiveness in nearby residential buildings are also computed using the same method outlined in Chapter 3 and 4. Unlike in residential buildings where window opening is the main concern before SIP is initiated, analysis for commercial buildings should also consider protectiveness of buildings with the mechanical ventilation system running. The air-exchange rate measurements reviewed in this chapter will be used to guide parameter selection when modeling the additional air-exchange rate induced by the ventilation system.

5.6 References

Akins, R.E., Peterka, J.A., Cermak, J.E., 1979. Averaged pressure coefficients for rectangular buildings. Proceedings: 5th International Conference on Wind Engineering, July 8-14, Fort Collins, CO.

ASHRAE, 1999. ANSI/ASHRAE Standard 62-1999. Ventilation for acceptable indoor air quality. American Society of Heating, Refrigerating, and Air-Conditioning Engineers, Atlanta, GA.

Bahnfleth, W.P., Yuill, G.K., Lee, B.W., 1999. Protocol for field testing of tall buildings to determine envelope air leakage rate. ASHRAE Transactions 105 (2), 27–38.

Brennan, T., Turner, W., Fisher, G., Thompson, B., Ligman, B., 1992. Fan pressurization of school buildings. Proceedings: Thermal Performance of the Exterior Envelopes of Buildings V, December 7-10, Clearwater Beach, FL.

Briggs, R.S., Crawley, D.B., Schliesing, J.S., 1992. Topical report: energy requirements for office buildings, volume 1, existing buildings. GRI-90/0236.1, Gas Research Institute, Portland, OR.

Cummings, J.B., Withers, C.R., Moyer, N., Fairey, P., McKendry B., 1996. Final report: uncontrolled air flow in non-residential buildings. FSEC-CR-878-96, Florida Solar Energy Center, Cocoa, FL.

Edwards, C., 1999. Report: modeling of ventilation and infiltration energy impacts in mid and high-rise apartment buildings. Sheltair Scientific Limited, Vancouver, Canada.

EIA, 1995. A look at commercial buildings in 1995: characteristics, energy consumption, and energy expenditures. DOE/EIA-0625(95), Energy Information Administration, US Department of Energy, Washington, DC.

EIA, 2002. Manufacturing buildings energy consumption survey. Energy Information Administration, US Department of Energy, Washington, DC.

EIA, 2003. Commercial buildings energy consumption survey, public use files. Energy Information Administration, US Department of Energy, Washington, DC. http://www.eia.doe.gov/emeu/cbecs/cbecs2003/public_use_2003/2003microdat.html

Etheridge, D.W., Alexander, D.K., 1980. The British gas multi-cell model for calculating ventilation. ASHRAE Transactions 86 (2), 808–821.

Fletcher, B., Johnson, A.E., 1992. Ventilation of small factory units. Journal of Wind Engineering and Industrial Aerodynamics 40, 293–305.

Fleury, E., Millet, J.R., Villenave, J.G., Veyrat, O., Morisseau, C., 1998. Theoretical and field study of air change in industrial buildings. Proceedings: 19th Air Infiltration and Ventilation Centre Conference, September 28-30, Oslo, Norway.

Grosso, M., 1992. Wind pressure distribution around buildings: a parametrical model. Energy and Buildings 18, 101–131.

Grot, R.A., Persily, A.K., 1986. Measured air infiltration and ventilation rates in eight large office buildings. In: Measured Air Leakage of Buildings, ASTM STP 904, Trechsel, H.R., Lagus, P.L., Eds., American Society for Testing and Materials, Philadelphia, PA, 151–183.

Hayakawa, S., Togari, S., 1990. Simple test method for evaluating exterior wall airtightness of tall office buildings. In: Air Change and Airtightness in Buildings, ASTM STP 1067, Sherman, M.H., Ed., American Society for Testing and Materials, Philadelphia, PA, 231–245.

Jones, P.J., Powell, G., 1994. Reducing air infiltration losses in naturally ventilated industrial buildings. Proceedings: 15th Air Infiltration and Ventilation Centre Conference, September 27-30, Buxton, UK.

Lagus, P.L., Grot, R.A., 1995. Consultant report: air change rates in non-residential buildings in California. Lagus Applied Technology, Inc., P400-91-034BCN, California Energy Commission, Sacramento, CA.

Litvak, A., Boze, D., Kilberger, M., 2001. Airtightness of 12 non residential large buildings results from field measurement studies. Proceedings: 22nd Air Infiltration and Ventilation Centre Conference, September 11-14, Bath, UK.

Lorenzetti, D.M., 2002. Assessing multizone airflow simulation software. Proceedings: 9th International Conference on Indoor Air Quality and Climate, June 30-July 5, Monterey, CA.

Ludwig, J.F., Baker, B.J., McCarthy, J.F., 2002. Analysis of ventilation rates for the base study: assessment of measurement uncertainty and comparison with ASHRAE 62-1999. Proceedings: 9th International Conference on Indoor Air Quality and Climate, June 30-July 5, Monterey, CA.

Lundin, L.I., 1986. Air leakage in industrial buildings – description of equipment. In: Measured Air Leakage of Buildings, ASTM STP 904, Trechsel, H.R., Lagus, P.L., Eds., American Society for Testing and Materials, Philadelphia, PA, 101–105.

Mendell, M.J., Heath, G.A., 2005. Do indoor pollutants and thermal conditions in schools influence student performance? A critical review of the literature. Indoor Air 15, 27–52.

NCDC, 2004. US climate normals 1971–2001, climatography of the US No. 81. National Climatic Data Center, Asheville, NC. http://www.ncdc.noaa.gov/oa/climate/normals/usnormalsprods.html#CLIM81

NCDC, 2005. Federal climate complex global surface summary of day data, version 6. National Climatic Data Center, Asheville, NC. http://www.ncdc.noaa.gov/cgi-bin/res40.pl.

Orme, M., Liddament, M., Wilson, A., 1994. An analysis and data summary of the AIVC's numerical database. Technical Note 44, Air Infiltration and Ventilation Centre, Coventry, UK.

Perera, M., Tull, R.G., 1989. Envelope leakiness of large, naturally ventilated buildings. Proceedings: 10th Air Infiltration and Ventilation Centre Conference, September 25-28, Dipoli, Finland.

Perera, M., Henderson, J., Webb, B.C., 1997. Predicting envelope air leakage in large commercial buildings before construction. Proceedings: 18th Air Infiltration and Ventilation Centre Conference, September 23-26, Athens, Greece.

Persily, A.K., Grot, R.A., 1986. Pressurization testing of federal buildings. In: Measured Air Leakage of Buildings, ASTM STP 904, Trechsel, H.R., Lagus, P.L., Eds., American Society for Testing and Materials, Philadelphia, PA, 184–200.

Persily, A.K., 1999. Myths about building envelopes. ASHRAE Journal, March, 39–47.

Persily, A.K., Ivy, E.M., 2001. Input data for multizone airflow and IAQ analysis. NISTIR 6585. National Institute of Standards and Technology, Gaithersburg, MD.

Potter, I.N., Jones, T.J., 1992. Ventilation heat loss in factories and warehouses. Technical Note TN 7/92, Building Services Research and Information Association, Berkshire, UK.

Potter, I.N., Jones, T.J., Booth, W.B., 1995. Air leakage of office buildings. Technical Note TN 8/95, Building Services Research and Information Association, Berkshire, UK.

Price, P.N., Chang, S.C., Sohn, M.D., 2004. Characterizing buildings for airflow models: what should we measure? LBNL-55321, Lawrence Berkeley National Laboratory, Berkeley, CA.

Proskiw, G., Phillips, B., 2001. Air leakage characteristics, test methods, and specifications for large buildings. Report, Canada Mortgage and Housing Corporation, Ottawa, Canada.

Seppänen, O., Fisk, W.J., Lei, Q.H., 2006. Ventilation and performance in office work. Indoor Air 16, 28–36.

Shaw, C.Y., Tamura, G.T., 1977. The calculation of air infiltration rates caused by wind and stack action for tall buildings. ASHRAE Transactions 83 (2), 145–158.

Shaw, C.Y., 1979. A method for predicting air infiltration rates for a tall building surrounded by lower structures of uniform height. ASHRAE Transactions 85 (1), 72–84.

Shaw, C.Y., Jones, L., 1979. Air tightness and air infiltration of school buildings. ASHRAE Transactions 85 (1), 85–95.

Shaw, C.Y., 1980. Wind and temperature induced pressure differentials and an equivalent pressure difference model for predicting air infiltration in schools. ASHRAE Transactions 86 (1), 268–279.

Shaw, C.Y., 1981. Air tightness: supermarkets and shopping malls. ASHRAE Journal, March, 44–46.

Shaw, C.Y., Reardon, J.T., 1995. Changes in airtightness levels of six office buildings. In: Airflow Performance of Building Envelopes, Components, and Systems, ASTM STP 1255, Modera, M.P., Persily, A.K., Eds., American Society for Testing and Materials, Philadelphia, PA, 47–57.

Sherman, M.H., Chan, W.R., 2004. Building airtightness: research and practice. LBNL-53356, Lawrence Berkeley National Laboratory, Berkeley, CA.

Tamura, G.T., Wilson, A.G., 1966. Pressure differences for a nine-story building as a result of chimney effect and ventilation system operation. ASHRAE Transactions 72 (1), 180–189.

Tamura, G.T., Shaw, C.Y., 1976. Studies on exterior wall air tightness and air infiltration of tall buildings. ASHRAE Transactions 82 (1), 122–134.

Tamura, G.T., Wilson, A.G., 1976. Pressure differences caused by chimney effect in three high buildings. ASHRAE Transactions 73 (2), 1.1–1.10.

Tanaka, H., Lee, Y., 1986. Scale model verification of pressure differentials and infiltration induced across the walls of a high-rise building. Journal of Wind Engineering and Industrial Aerodynamics 25, 1–14.

US EPA, 1995. User's guide for the industrial source complex (ISC3) dispersion models, volume II – description of model algorithms. EPA-454/B-95/003b, US Environmental Protection Agency, Research Triangle Park, NC.

VanBronkhorst, D.A., Persily, A.K., Emmerich, S.J., 1995. Energy impacts of air leakage in US office buildings. Proceedings: 16th Air Infiltration and Ventilation Centre Conference, September 19-22, Palm Springs, CA.

5.7 Tables

Table 5.1 Types of data in the commercial building air leakage database.

Country	Data Source	Buildings Measured
Canada	Proskiw and Phillips (2001)	8 Assembly/Public buildings
	Shaw and Reardon (1995)	6 Office buildings
	Shaw (1981)	9 Supermarkets 1 Shopping mall
	Shaw and Jones (1979)	11 Schools
France	Litvak et al. (2001)	4 Hotels 4 Educational buildings 2 Office buildings 2 Multi-use halls
	Fleury et al. (1998)	4 Industrial buildings
Sweden	Lundin (1986)	9 Industrial buildings
UK	Perera et al. (1997)	10 Office buildings
	Potter et al. (1995)	12 Office buildings
	Jones and Powell (1994)	3 Industrial buildings
	Potter and Jones (1992)	14 Factories/Warehouses
	Perera and Tull (1989)	4 Office buildings
US	Cummings et al. (1996)	69 Buildings, including: Small offices Small retail buildings Educational buildings Restaurants Assembly/Recreational Light industrial Medical Lodging Medium offices
	Brennan et al. (1992)	13 Schools
	Persily and Grot (1986)	7 Office buildings

Table 5.2 Buildings in the commercial air leakage database categorized by their usage and construction types.

	Construction Type							
Building Type	Masonry	Metal frame/ Metal panel	Concrete panel/ Tilt-up	Frame/ Masonry	Wood frame	Manufactured	Curtain-wall	Other
Office	20	9	13		1	4	2	
Warehouse/Industrial	6	20	6					3
Educational	31	1			1	1		
Small retail	10	2		1	1			4
Strip mall				12				
Supermarket	7		2					
Public building	4			1				2
Restaurant	4			1		2		
Lodging	4					2		
Recreational/Auditorium	4					1		
Health care	3							
Mall	1							
Others								2

Table 5.3 Regression results of log-transformed air-leakage coefficient C [$m^3/(s \cdot m^2 \cdot Pa^n)$] using the physical dimensions of the building as explanatory parameters[#].

Model I[‡] : $\ln(C) = \beta_0 + \beta_i \cdot \ln(\text{Parameter}_i) + \varepsilon$

β_0	Explanatory Parameter: β_i						Adjusted R^2	Residual Std. Error ε
	Volume (m^3)	Floor Area (m^2)	Surface Area (m^2)	Footprint Area (m^2)	Height (m)	Perimeter (m)		
-6.00 (0.401) ***	-0.237 (0.0464) ***						0.116	0.932
-5.99 (0.350) ***		-0.287 (0.0484) ***					0.152	0.913
-5.25 (0.455) ***			-0.371 (0.0602) ***				0.162	0.908
-5.40 (0.384) ***				-0.392 (0.0566) ***			0.198	0.888
-8.06 (0.178) ***					0.0191 (0.0890)		-0.00502	0.994
-4.82 (0.465) ***						-0.781 (0.112) ***	0.200	0.887
Model II[§] : $\ln(C) = \beta_0 + \Sigma\, \beta_i \cdot \ln(\text{Parameter}_i) + \varepsilon$								
-6.06 (0.751) ***	-0.388 (0.611)	-0.679 (0.237) **	-0.459 (0.386)	0.611 (0.557)	1.41 (0.629) *	0.708 (0.593)	0.268	0.848

[#] The three entries in each cell (in order) are the regression coefficient β_i, its standard error, and its confidence level. The adjusted R^2 and the residual standard error ε of the model fit are also included. Confidence level codes: >99.9% ***, >99% **, >95% *. No symbol means the regression coefficient is not statistically significant at 95% confidence level. Adjusted R^2 is very similar to standard R^2 in definition, but it imposes a penalty for each additional explanatory parameter used in the regression model (this explains the small negative R^2 value in one of the model fits).

[‡] Model I: each parameter is regressed with $\ln(C)$ individually (first 6 rows).

[§] Model II: all parameters are used in the regression.

Table 5.4 Regression results of log-transformed air-leakage coefficient C [$m^3/(s \cdot m^2 \cdot Pa^n)$] using the building floor area (m^2) and height (m) as the explanatory variables.

(1) $\ln(C) = \beta_0 + \beta_1 \cdot \ln(\text{Floor Area}) + \varepsilon$

	Estimate	Std. Error	t value	Pr(>|t|)	Conf. level
β_0	-5.99	0.350	-17.1	$< 2\times10^{-16}$	> 99.9%
β_1	-0.287	0.0484	-5.93	1.42×10^{-8}	> 99.9%

$\varepsilon \sim N(0, 0.913)$, Adjusted $R^2 = 0.152$

(2) $\ln(C) = \beta_0 + \beta_1 \cdot \ln(\text{Floor Area}) + \beta_2 \cdot \text{Height}^{-1} + \varepsilon$

	Estimate	Std. Error	t value	Pr(>|t|)	Conf. level
β_0	-3.65	0.485	-7.53	2.01×10^{-12}	> 99.9%
β_1	-0.487	0.0541	-9.01	2.31×10^{-16}	> 99.9%
β_2	-4.53	0.710	-6.37	1.38×10^{-9}	> 99.9%

$\varepsilon \sim N(0, 0.831)$, Adjusted $R^2 = 0.298$

Table 5.5 Neutral pressure level (β) and thermal draft coefficient (γ) from pressure differential measurements on various high-rise buildings.

Data Source	Building Tested	Location	Exterior Walls	Damper Position	β	γ
Tamura and Wilson (1966)	9-story office building	Ottawa, Canada	Brick-faced, reinforced concrete	Closed	0.72	0.80
				Sealed	0.62	
Tamura and Wilson (1976)	44-story office building	Montreal, Canada	Reinforced concrete spandrel faced with green slate and backed with rigid insulation	Closed	0.40	0.63 to 0.82
	34-story office building	Montreal, Canada	Aluminum spandrel panel with fiberglass insulation backed with rigid insulation	Closed	0.35	0.82
	17-story office building	Ottawa, Canada	Pre-cast concrete panel backed with rigid insulation	Sealed	0.52	0.77
Hayakawa and Togari (1990)	9-story office building	Sendai City, Japan	Cast-in-place reinforced concrete	Unknown	0.76	
	17-story office building	Tokyo, Japan	Steel-frame with pre-cast concrete panels	Unknown	0.30	
	55-story office building	Tokyo, Japan	Aluminum curtain wall with fixed glazing	Unknown	0.36	

Table 5.6 Descriptions of seven US federal office buildings pressure tested by Persily and Grot (1986) for their air leakage characteristics.

Building Location	Floor Area	Number of Floors	Air-leakage coefficient *C*	Flow Exponent *n*	Average Air Infiltration Rate
	[m^2]		[$m^3/(s \cdot m^2 \cdot Pa^n)$]	[-]	[h^{-1}]
Anchorage, AK	45500	2 to 6 stories[#]	2.61×10^{-4}	0.61	0.28
Ann Arbor, MI	4900	4 stories	1.32×10^{-4}	0.67	0.70
Columbia, SC	24700	15 stories	3.67×10^{-4}	0.47	0.40
Huron, SD	6420	4 stories	6.72×10^{-4}	0.64	0.20
Norfolk, VA	17300	8 stories	1.85×10^{-4}	0.74	0.52
Pittsfield, MA	1730	2 stories	3.06×10^{-4}	0.36	0.32
Springfield, MA	13500	5 stories	3.15×10^{-4}	0.65[†]	0.52

[#] The building in Anchorage has six connected modules with heights varying from 2 to 6-stories.

[†] Following suggestion of the authors, the flow exponent of the Springfield building has been replaced by 0.65 because the fitted value, $n = 2.09$, seemed too high to be reasonable. The air-leakage coefficient shown above has already been modified using $n = 0.65$ such that the predicted airflow at 25 Pa matches the value measured from pressurization test.

Table 5.7 Assumed input parameter distributions of Shaw-Tamura and LBL Infiltration Models used in this analysis to predict distributions of air infiltration rates.

Air Infiltration Model	Parameter	Central Tendency	Range
Shaw-Tamura	Neutral pressure level (β)	0.5	0.2 – 0.8
	Thermal draft coefficient (γ)	0.8	0.6 – 0.9
	Mean wind-pressure coefficient (C_p')	0.7	0.5 – 0.9
LBL[#]	Proportion of air leakage from ceiling and flooring (R)	0.5	0.3 – 0.7
	Difference in proportion of air leakage between ceiling and flooring (X)	0	0 – 0.2
	Terrain	Urban (class 4)	Rural (class 3) to downtown of a large city (class 5)
	Shielding	Obstructions around most of perimeter (class 4)	Some obstructions (class 3) to large obstructions (class 5)

[#] See Section 3.3.1 for a more detailed description of the LBL Infiltration Model and its input parameters.

5.8 Figures

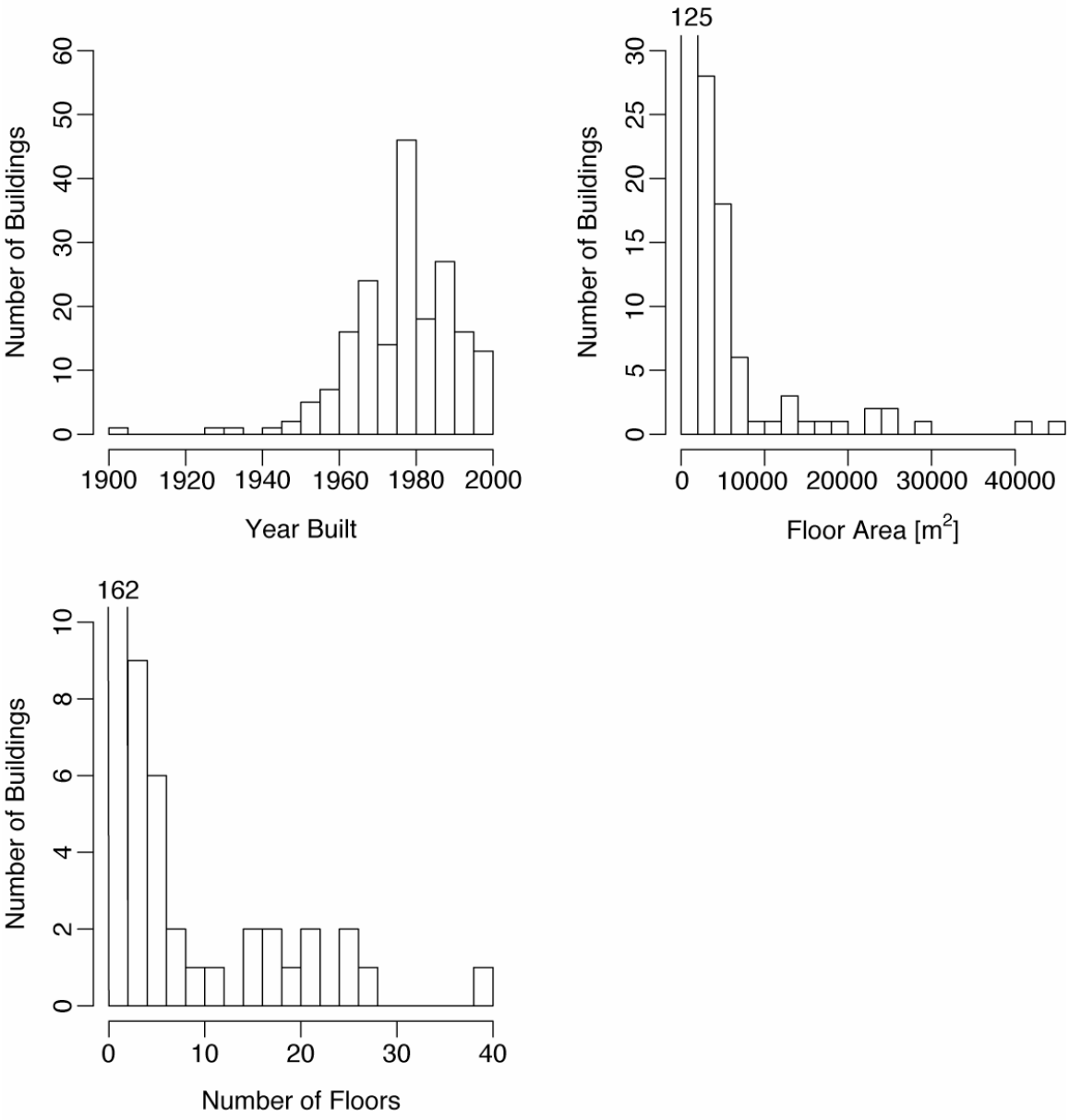

Figure 5.1 Number of buildings in the commercial building air leakage database as a function of year built, floor area, and number of floors. There are a total of 192 buildings in the database.

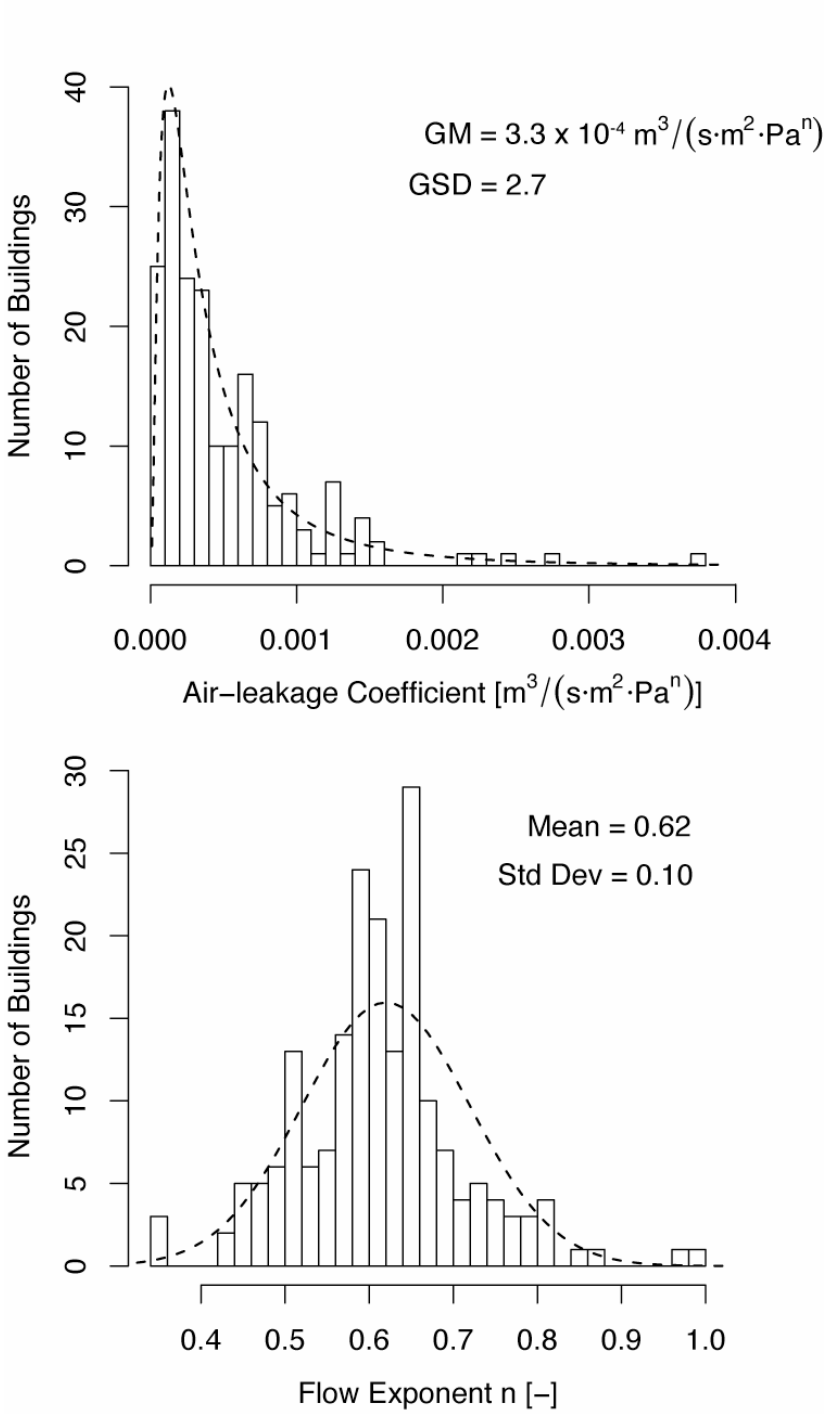

Figure 5.2 Histogram of the air-leakage coefficient *C* and flow exponent *n* in the commercial building air leakage database. Since *C* is roughly lognormally distributed, the geometric mean (GM) and geometric standard deviation (GSD) are shown. For *n*, which is roughly normally distributed, the arithmetic mean and standard deviation are shown.

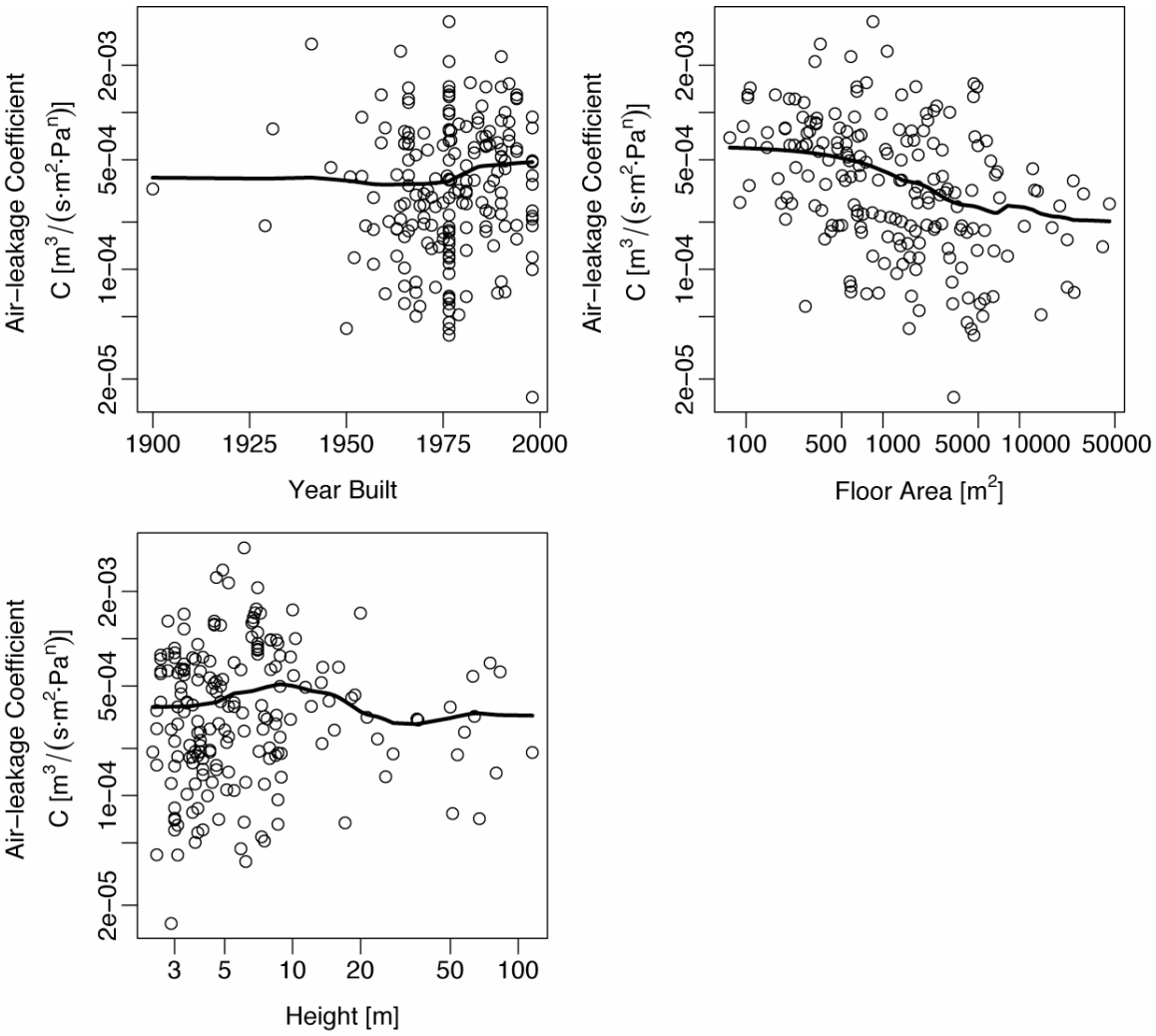

Figure 5.3 Scatter plots of air-leakage coefficients of buildings in the commercial air leakage database against building year built, floor area, and height. The solid line highlights the trend implied by the scatter plot, and is obtained by localized averaging of neighboring data points. The air-leakage coefficients are plotted on a log-scale (y-axis).

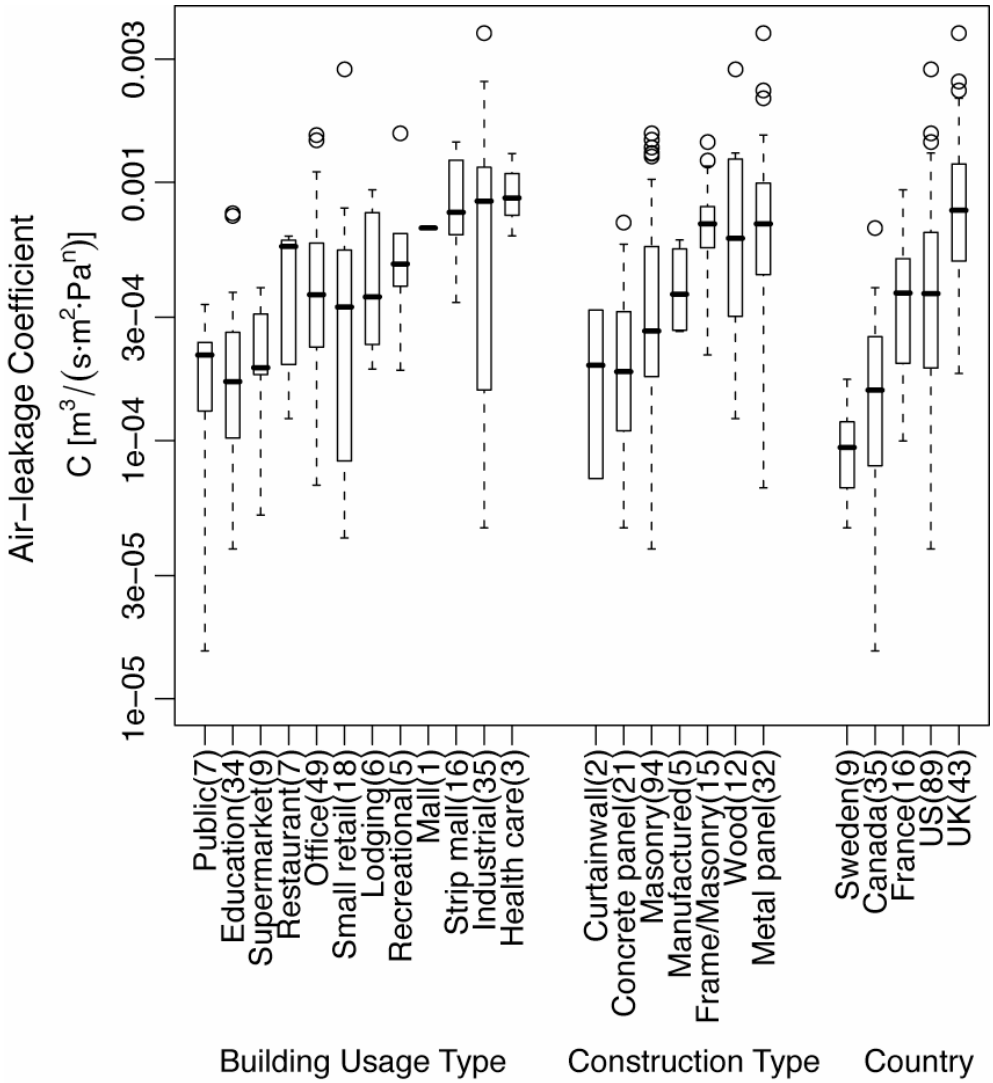

Figure 5.4 Boxplots of air-leakage coefficients *C* of buildings in the commercial air leakage database grouped by their usage and construction types, and country where measurements were made. In parentheses are the numbers of data points in each group. The groups are sorted such that the mean *C* of each group is in ascending order. The air-leakage coefficients are plotted on a log-scale (y-axis).

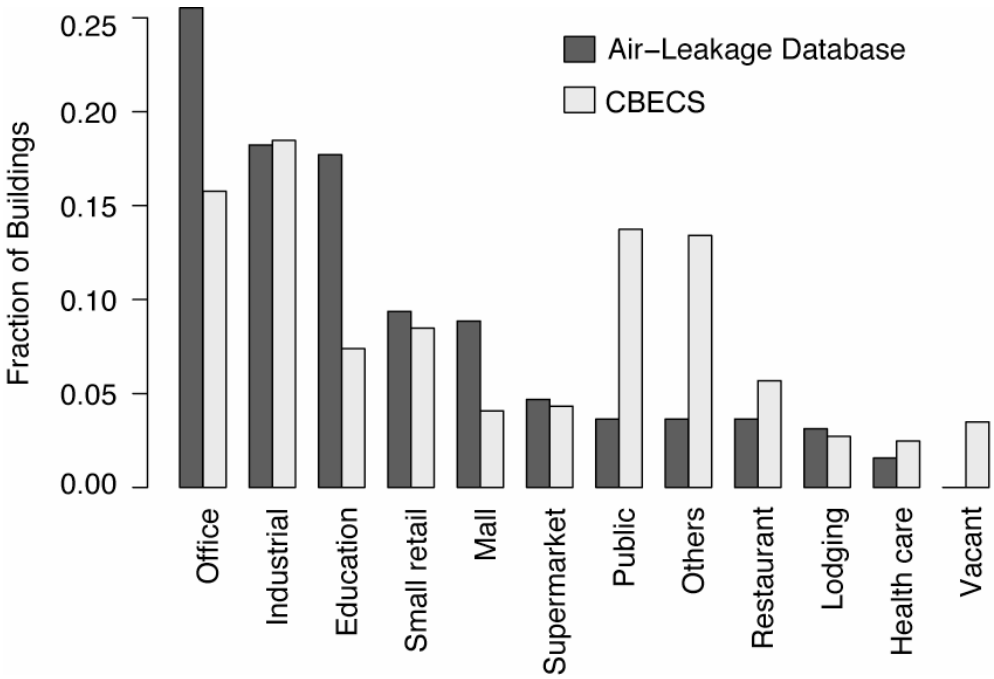

Figure 5.5 Comparison of the prevalence of various building types in the commercial air leakage database and the US national estimates from CBECS. CBECS refers to Commercial Building Energy Consumption Survey (EIA, 2003), which is a national survey of commercial buildings in the US. Category "Industrial" includes warehouses, storages, and manufacturing facilities, for which statistics are partly based on the Manufacturing Energy Consumption Survey (EIA, 2002).

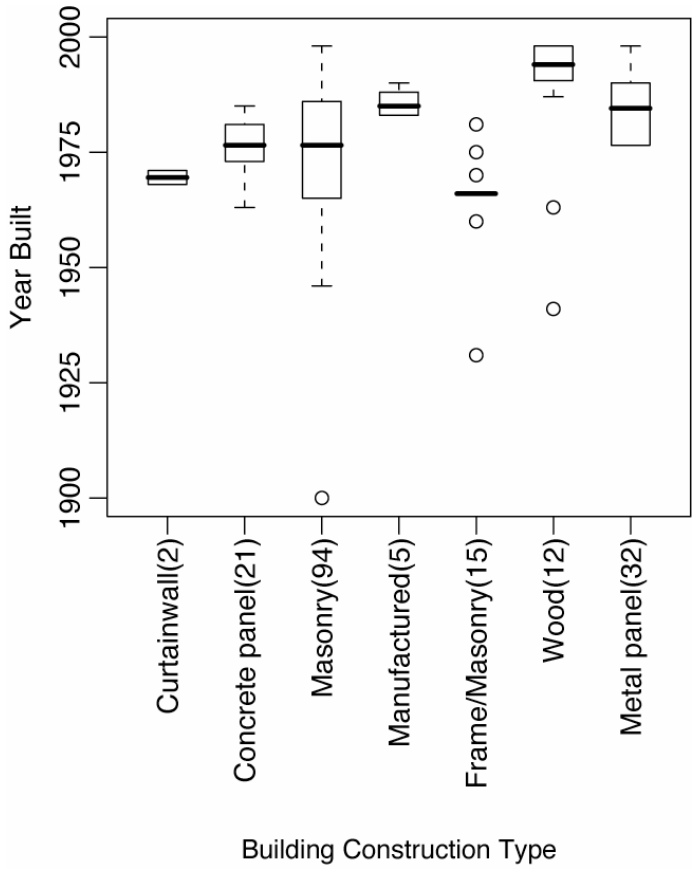

Figure 5.6 Year built of the buildings in the commercial air leakage database sorted by their construction types.

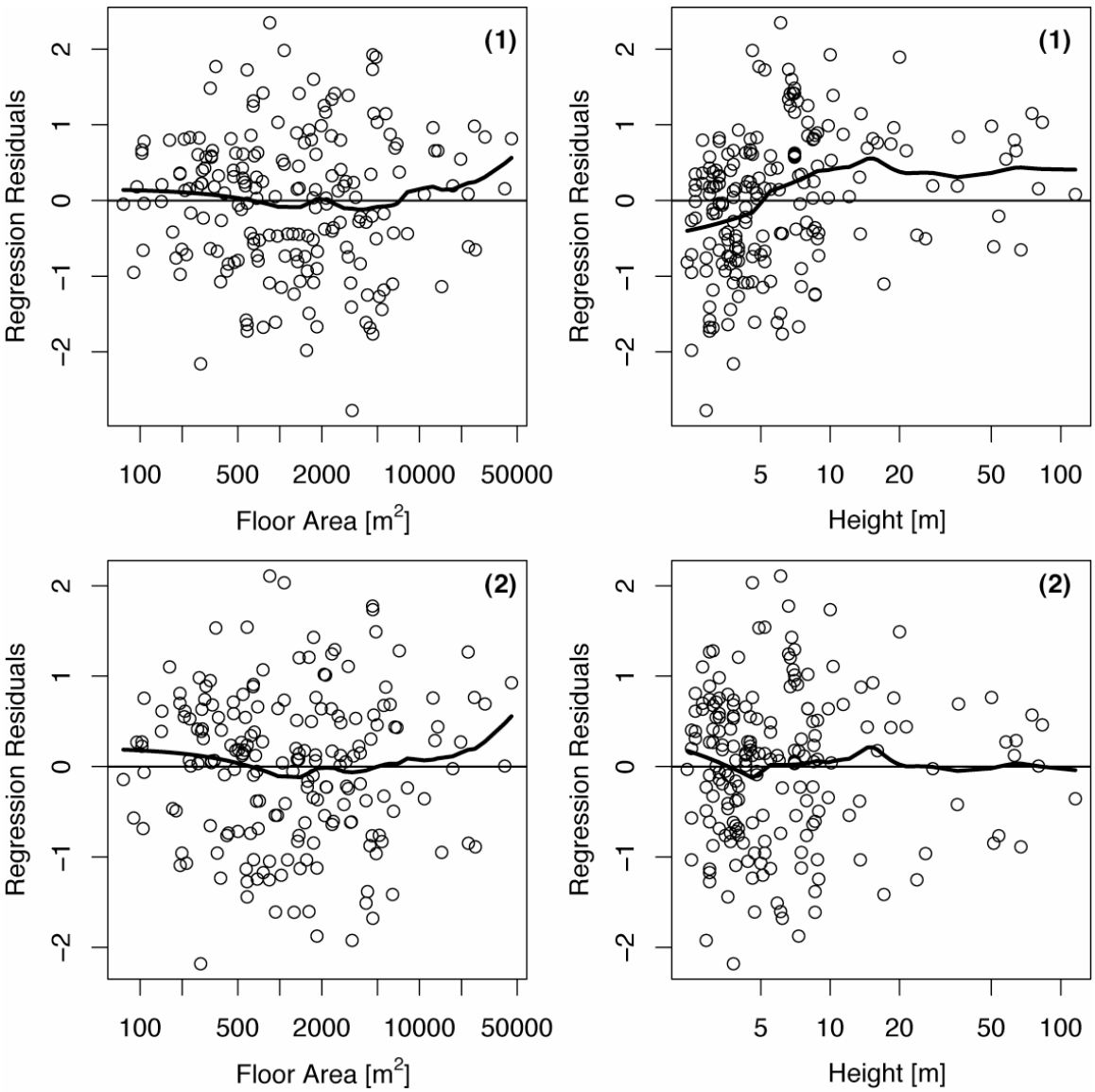

Figure 5.7 Regression results of the two models detailed in Table 5.4, where model (1) refers to only using floor area against which to regress the air-leakage coefficient, and model (2) refers to using both floor area and height. Regression residuals are computed as $\ln(C_{\text{predicted}}) - \ln(C_{\text{observed}})$, so that regression residual of 0 means that the prediction is the same as the observation. The range of regression residuals is approximately from -2 to 2, which corresponds about 0.8 to 1.3 in terms of the ratio $C_{\text{predicted}}/C_{\text{observed}}$. The solid line represents the trend implied by the scatter plot, and is obtained by localized averaging of neighboring data points. The key difference between the two sets of plots is that model (2) is able to resolve the dependence of regression residuals on building height such that the residuals are reasonably independent of the explanatory variables.

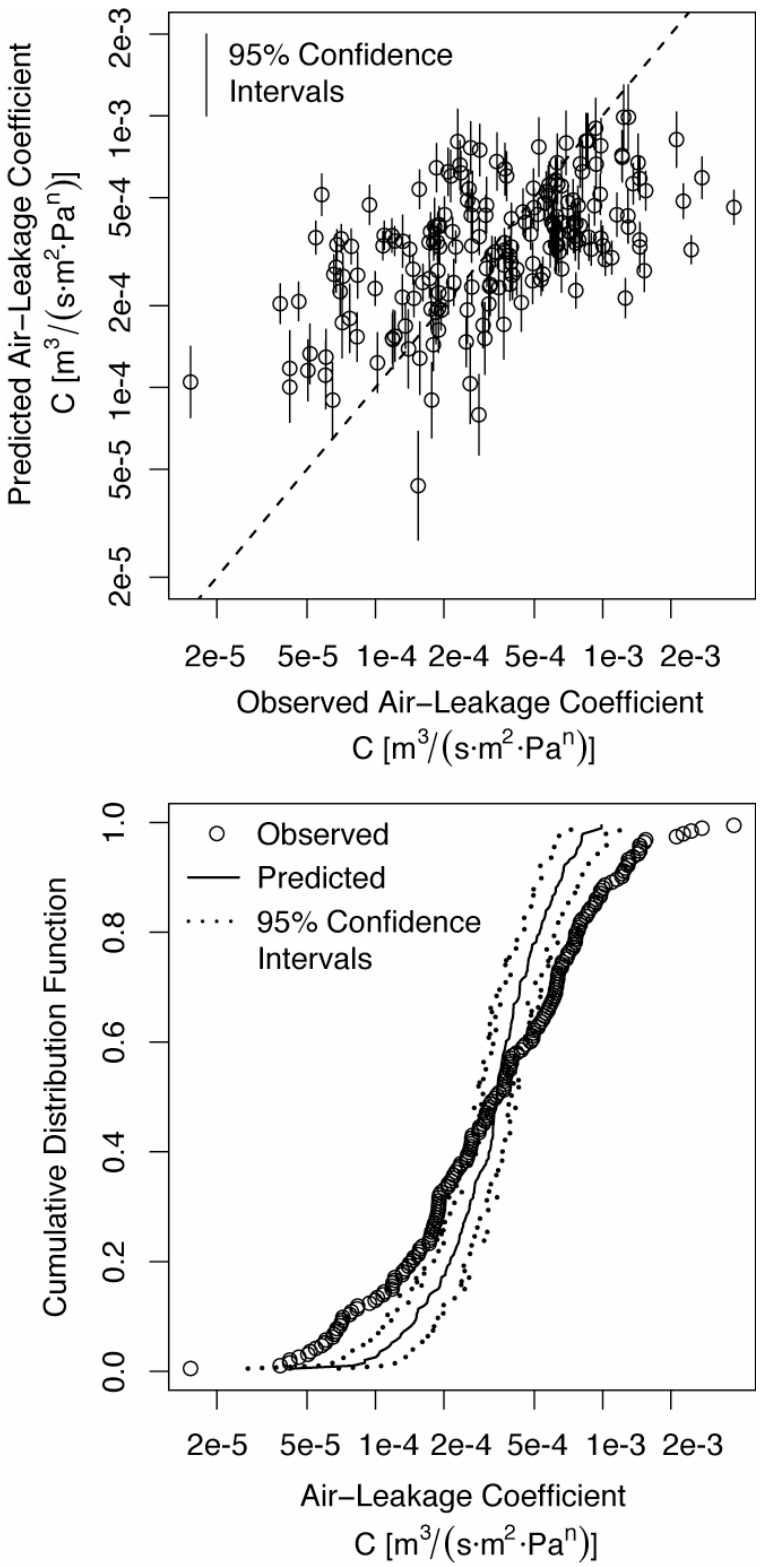

Figure 5.8 Comparison of observed and predicted air-leakage coefficients *C* presented in 1-to-1 scatter plot (top), and in terms of their cumulative distribution (bottom). The 95% confidence levels on the predictions are indicated in both plots. The air-leakage coefficients are plotted on a log-scale.

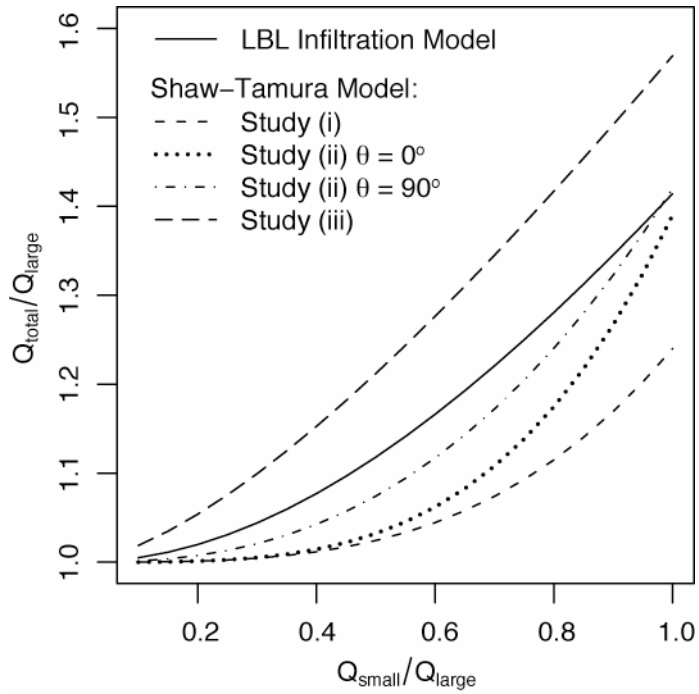

Figure 5.9 Various methods to combine stack and wind induced air infiltration rates to give the total air infiltration rate (Q_{total}) proposed for the Shaw-Tamura Infiltration Model. The different formulations are described in Eqn 5.9 (method (i) and (ii)) and Eqn 5.10 (method (iii)). Q_{small} is the lesser air infiltration rate driven by either one of the two effects, and Q_{large} is greater of the two. Therefore $Q_{small} / Q_{large} = 1$ means that stack-effect and wind-effect driven air infiltration rates are the same. The estimate suggested by method (ii) is subject to wind angle impinging on the building, where $\theta = 0^o$ means the wind is normal to the long wall of the building. In method (iii), the flow exponent n used to compute the curve is 0.62, which is the mean value found in the commercial air leakage database (Figure 5.2). The method used in the LBL Infiltration Model is included for comparison.

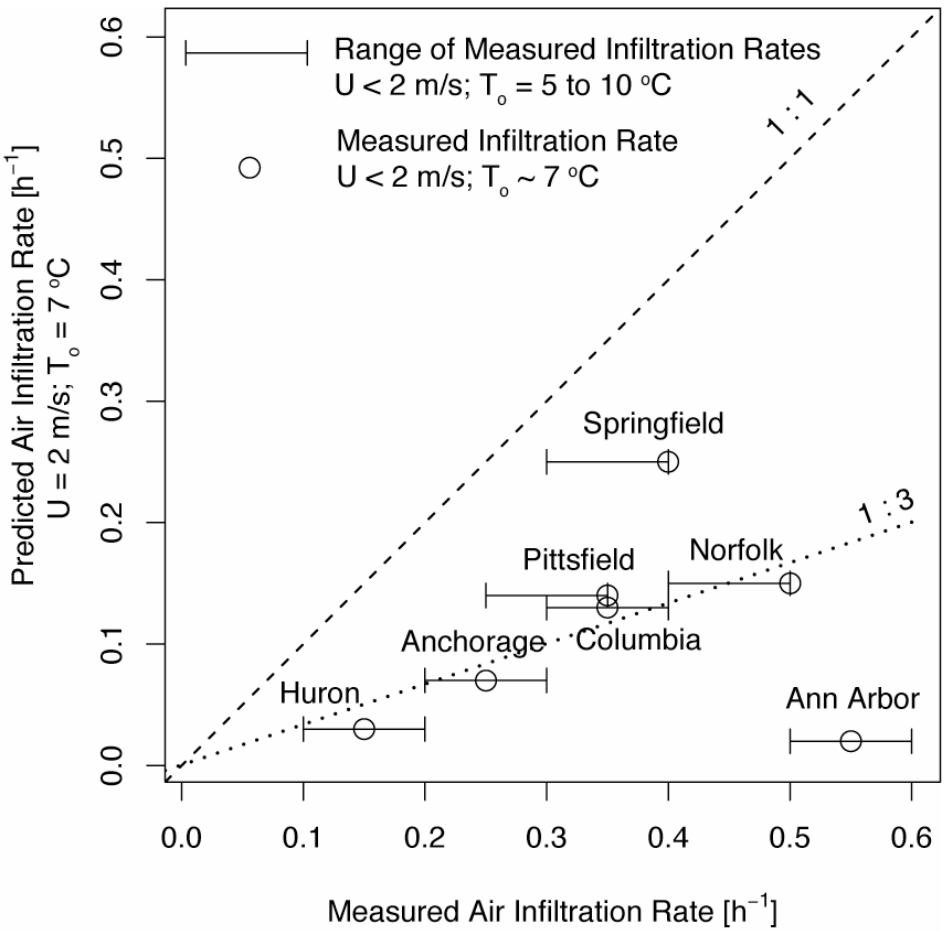

Figure 5.10 Comparison of measured and predicted air infiltration rates (Persily and Grot, 1986) under meteorology conditions with wind speed < 2 m/s measured at 5 m above ground, and the outdoor temperature ~ 7 °C. Predictions were obtained using the Shaw-Tamura Infiltration Model (U = 2 m/s, T_o = 7 °C). Except for the buildings at Springfield and Ann Arbor, the model predictions are about one-third of the measured values.

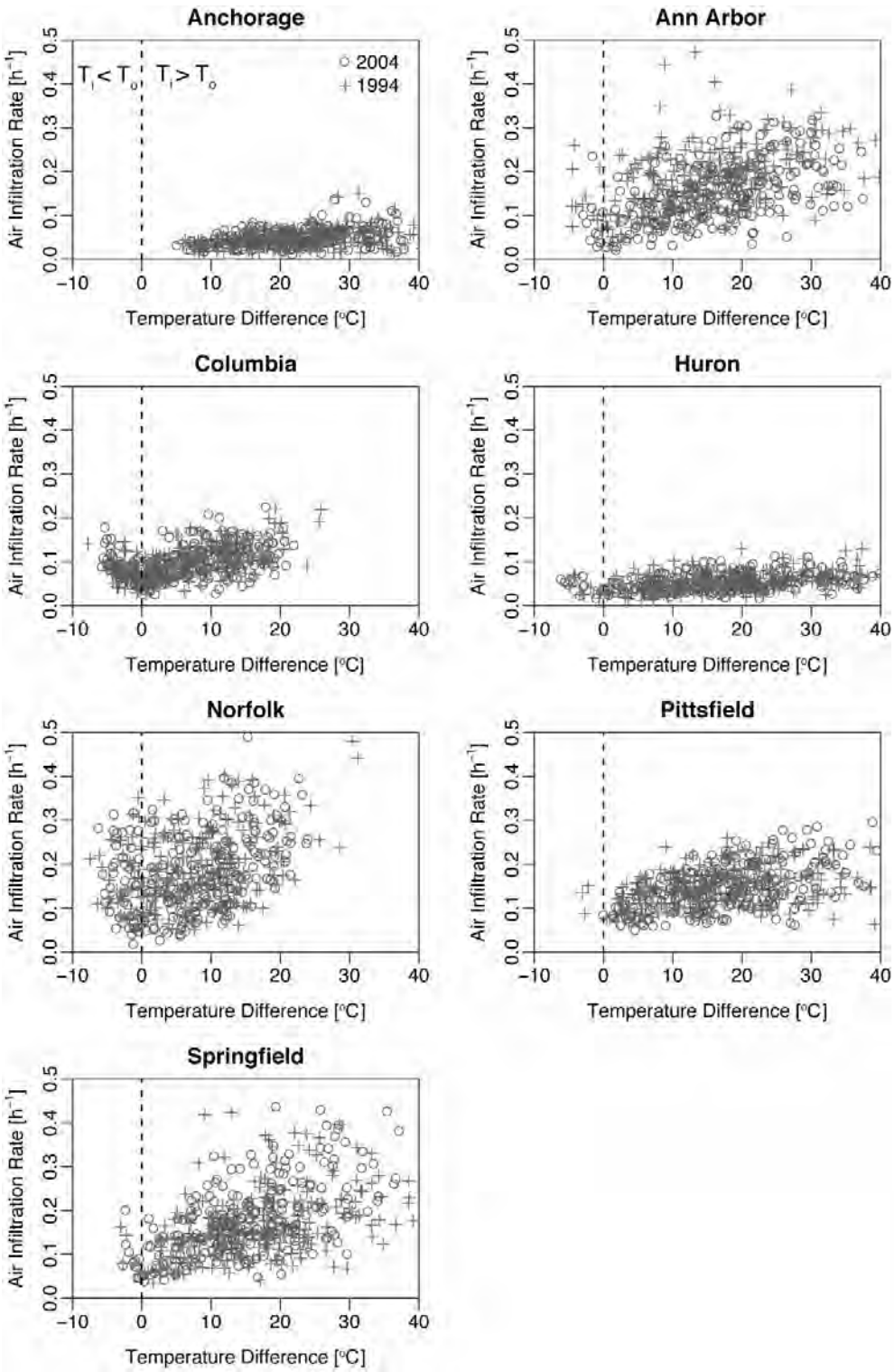

Figure 5.11 Predicted air infiltration rates of the seven US federal buildings measured by Persily and Grot (1986). Air infiltration rates are predicted using the Shaw and Tamura model and 1994 and 2004 monthly normals for outdoor temperatures (T_o) and wind speeds for the 45 largest cities in the US. The indoor temperature (T_i) is assumed to be 20 ^oC in all simulations.

(1)

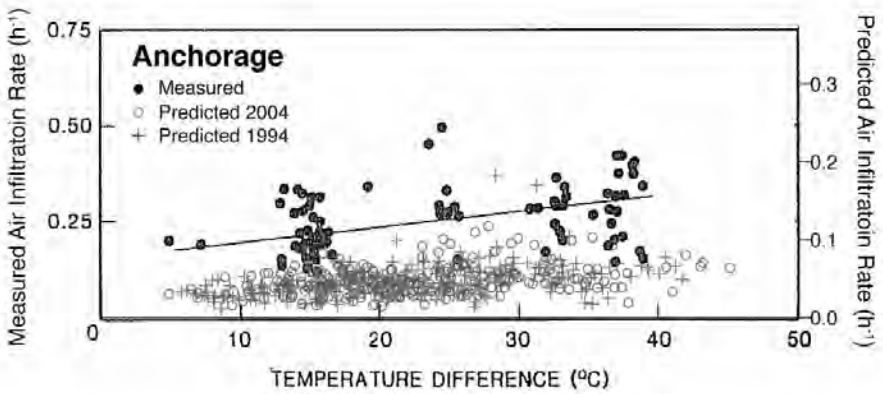
Anchorage
Measured
Predicted 2004
Predicted 1994
Measured Air Infiltratoin Rate (h⁻¹)
Predicted Air Infiltratoin Rate (h⁻¹)
TEMPERATURE DIFFERENCE (°C)

(2)

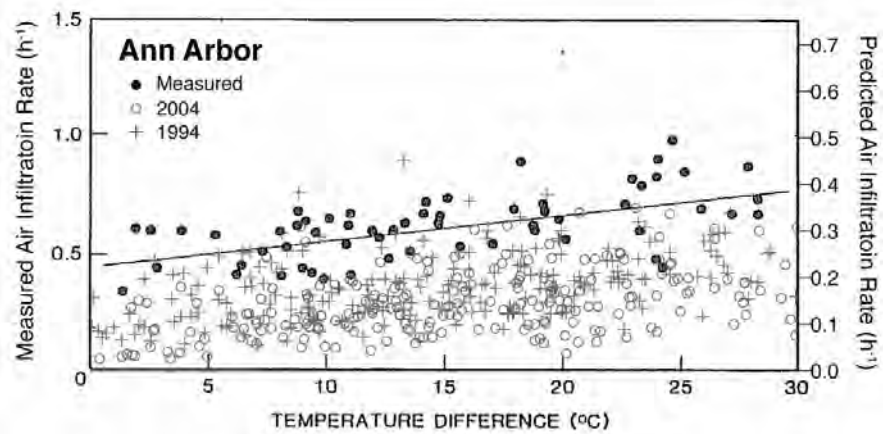
Ann Arbor
Measured
2004
1994
Measured Air Infiltratoin Rate (h⁻¹)
Predicted Air Infiltratoin Rate (h⁻¹)
TEMPERATURE DIFFERENCE (°C)

(3)

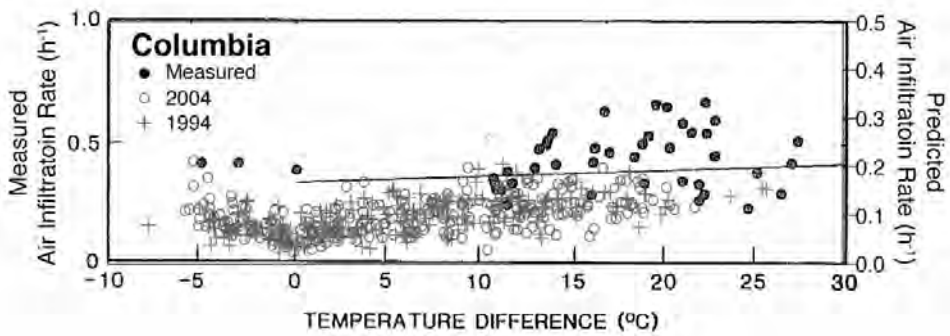
Columbia
Measured
2004
1994
Measured Air Infiltratoin Rate (h⁻¹)
Predicted Air Infiltratoin Rate (h⁻¹)
TEMPERATURE DIFFERENCE (°C)

(4)

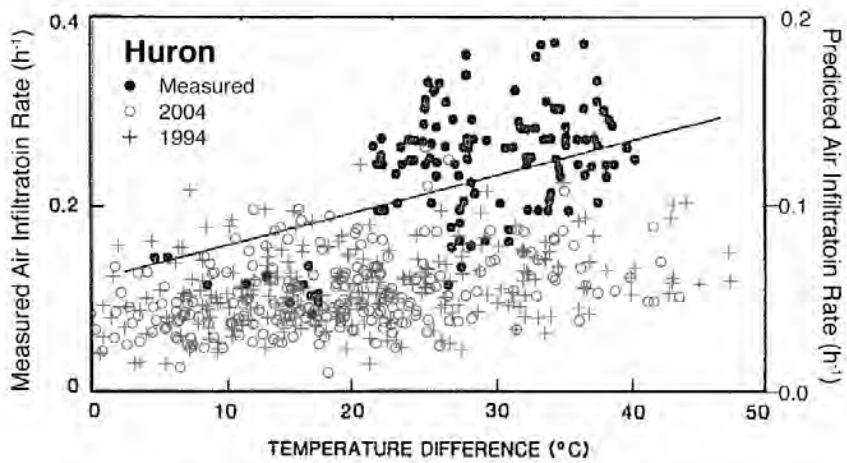
Huron
Measured
2004
1994
Measured Air Infiltratoin Rate (h⁻¹)
Predicted Air Infiltratoin Rate (h⁻¹)
TEMPERATURE DIFFERENCE (°C)

(5)

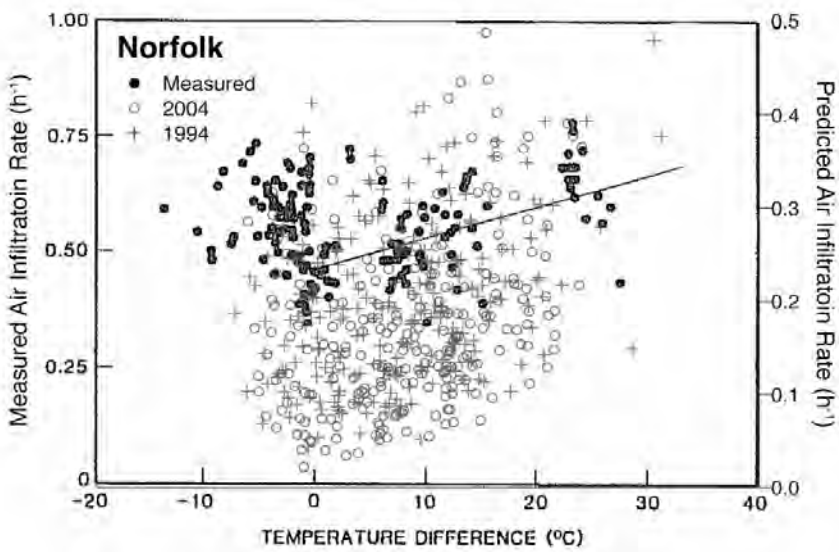

(6)

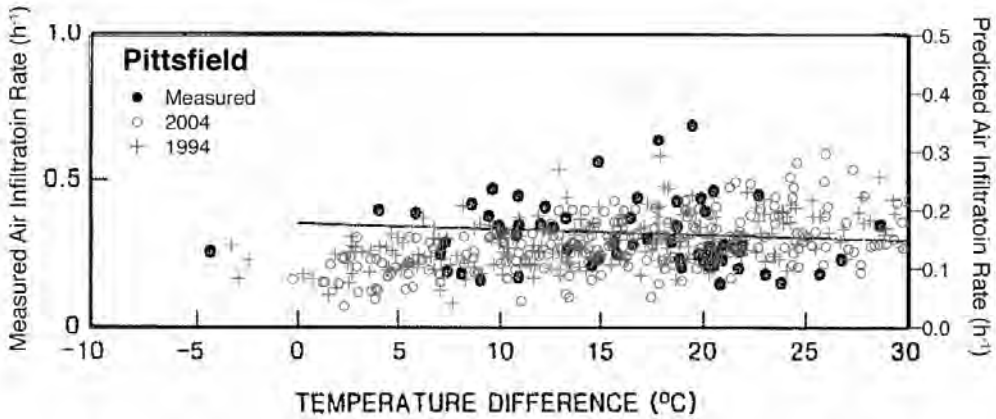

(7)

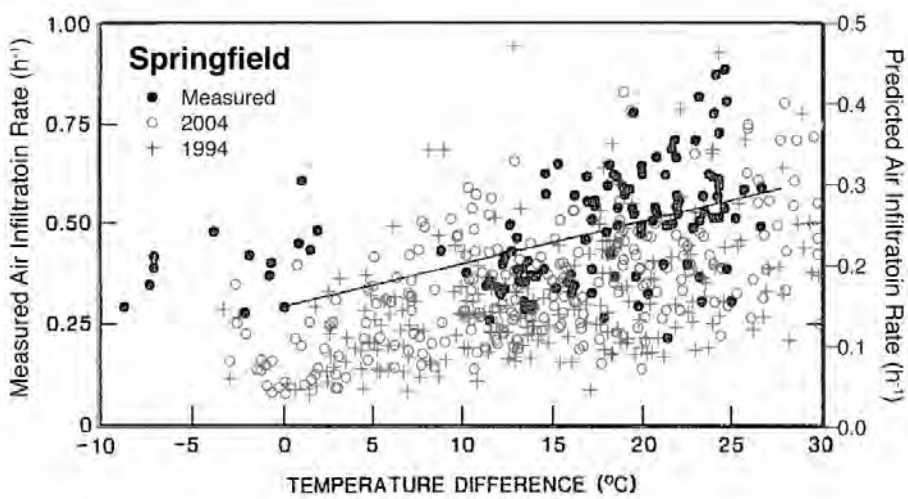

Figure 5.12 Measured and predicted air infiltration rates of seven US federal office buildings studied by Persily and Grot (1986). Air infiltration rates are predicted using the Shaw and Tamura model and 1994 and 2004 monthly normals for temperatures and wind speeds, and are the same as shown in Figure 5.11. Predictions are plotted on a scale that is 1/2 of the measurements.

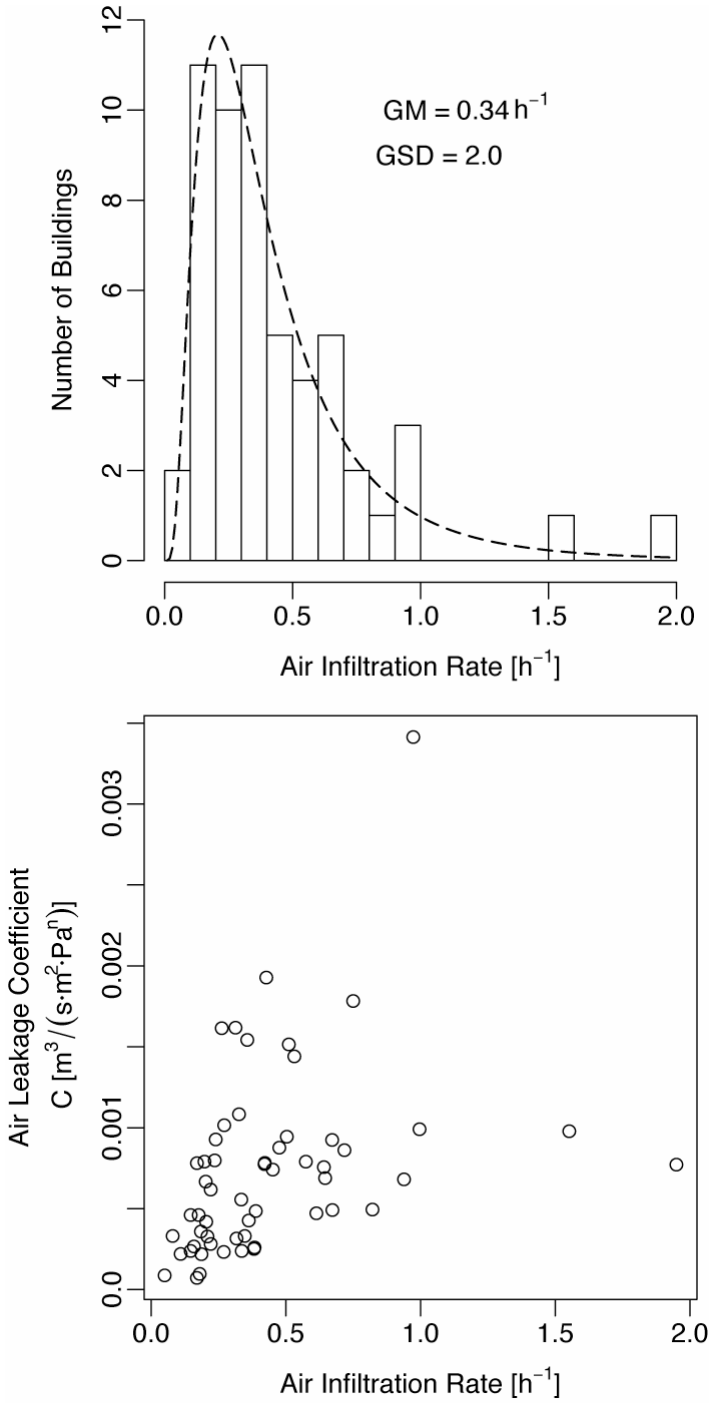

Figure 5.13 Air infiltration rates measured in 56 small commercial buildings by Cummings et al. (1996). In the bottom plot, the air-leakage coefficient of these buildings measured using a blower door test are plotted against their respective air infiltration rates. The air-leakage coefficients are plotted on a linear scale.

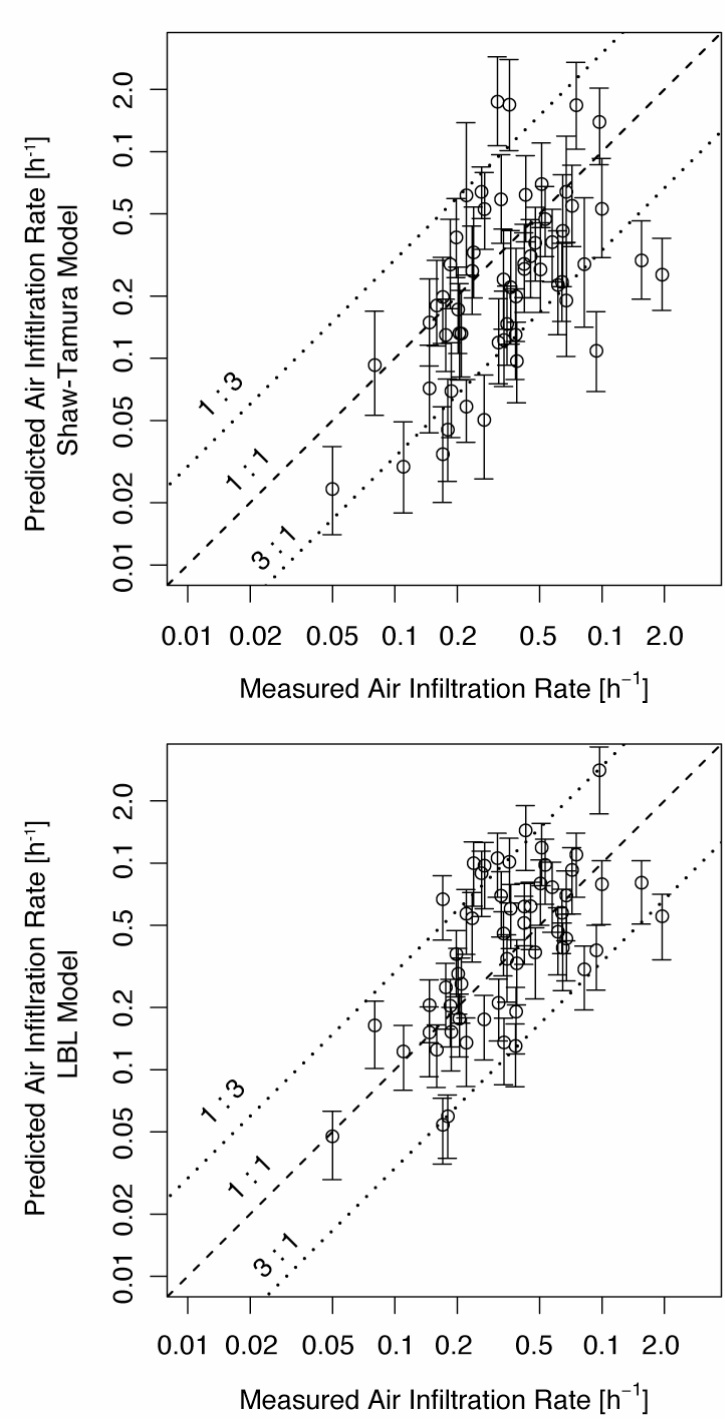

Figure 5.14 Comparison of air infiltration rate model predictions and observed values for the 56 small commercial buildings tested by Cummings et al. (1996). In general, model predictions using the LBL Infiltration Model (bottom) agree with measurements better than the Shaw-Tamura Infiltration Model (top). The three lines represent 3:1, 1:1, and 1:3 agreement. The bars on each data point represent the 10th and 90th percentiles of the predictions for that building, subject to the variation in meteorology.

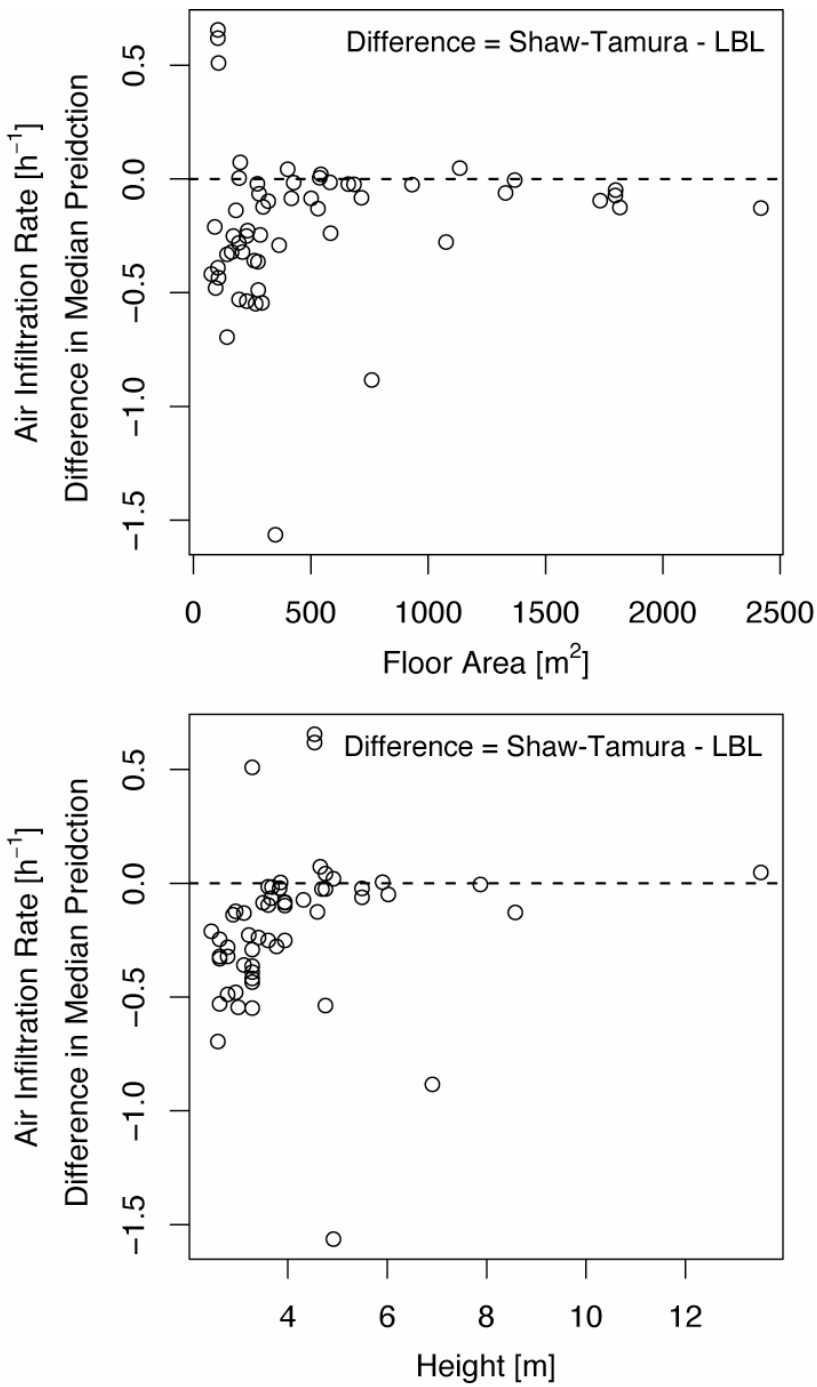

Figure 5.15 Differences in the median air infiltration rate for each of the 56 small commercial buildings in Floridapredicted using the Shaw-Tamura Infiltration Model and the LBL Infiltration Model (see Figure 5.14). Most of the differences among smaller commercial buildings are negative, meaning that the Shaw-Tamura model tends to predict lower air infiltration rates than the LBL model.

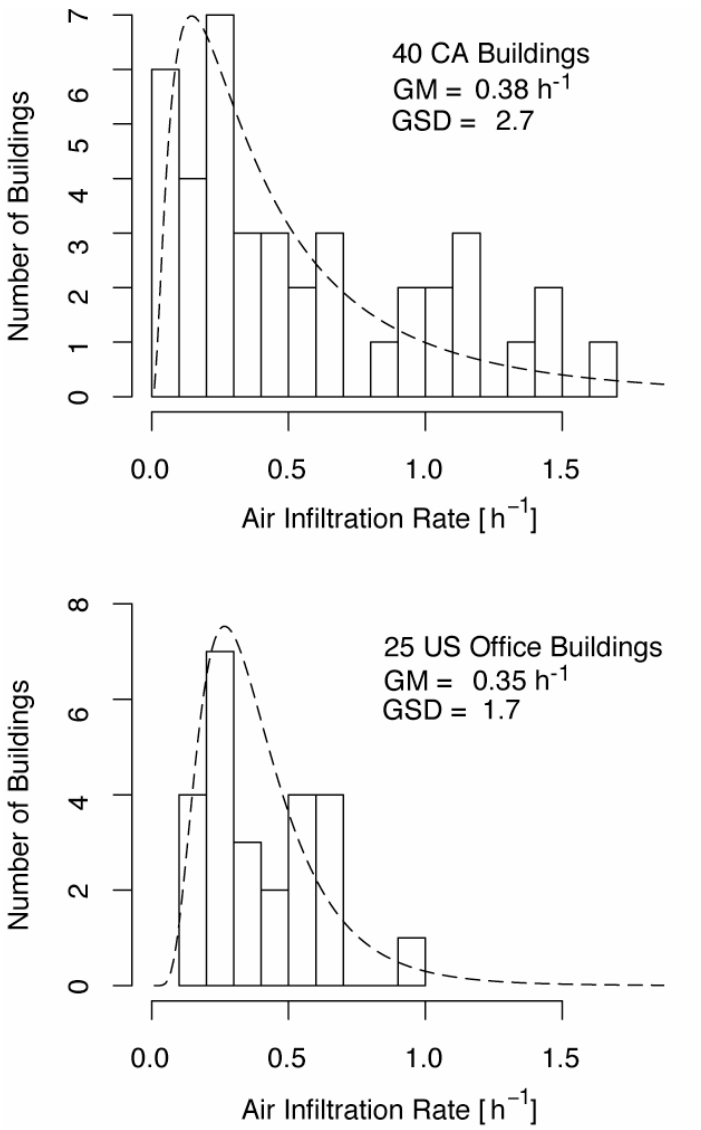

Figure 5.16 Air infiltration rates measured in 40 California buildings including schools, retail buildings, and offices (top) by Lagus and Grot (1995). The bottom figure is the predicted air infiltration rate of 25 US office buildings (Briggs et al., 1992; VanBronkhorst et al., 1995). Both distributions peak at an air infiltration rate of about 0.2 h^{-1}, with most values falling between 0.1 and 1.0 h^{-1}.

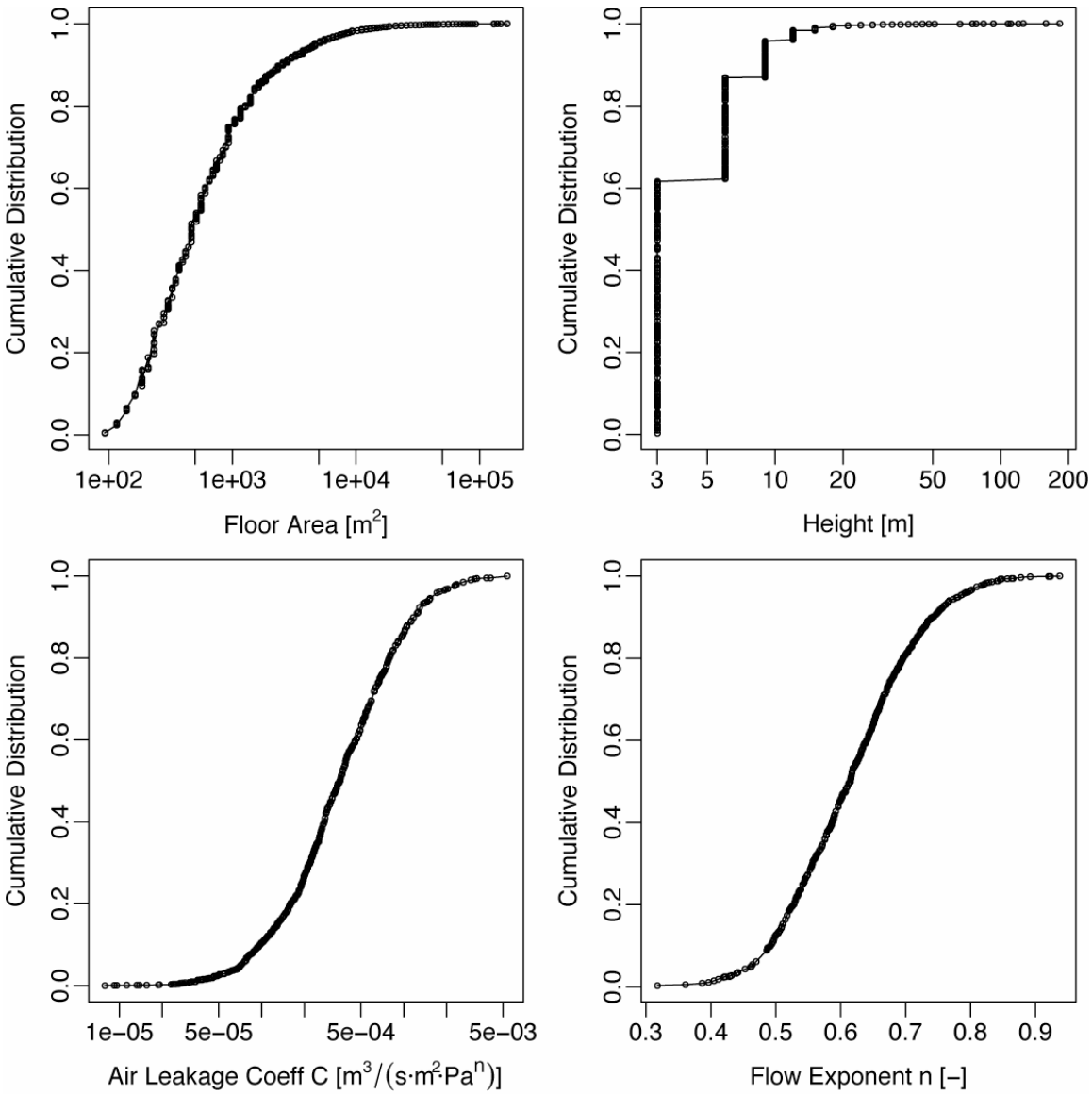

Figure 5.17 Building floor area of US commercial buildings surveyed in CBECS. Building height distribution is estimated from the number of floors, which is reported in the CBECS. The piecewise form of the cumulative distribution function arises from the assumption that each story is 3 m in all the buildings. Distributions of building floor area and height are used to estimate the air-leakage coefficient according to model (2) in Table 5.4. Finally, the flow exponent of the buildings is estimated using Eqn 5.12.

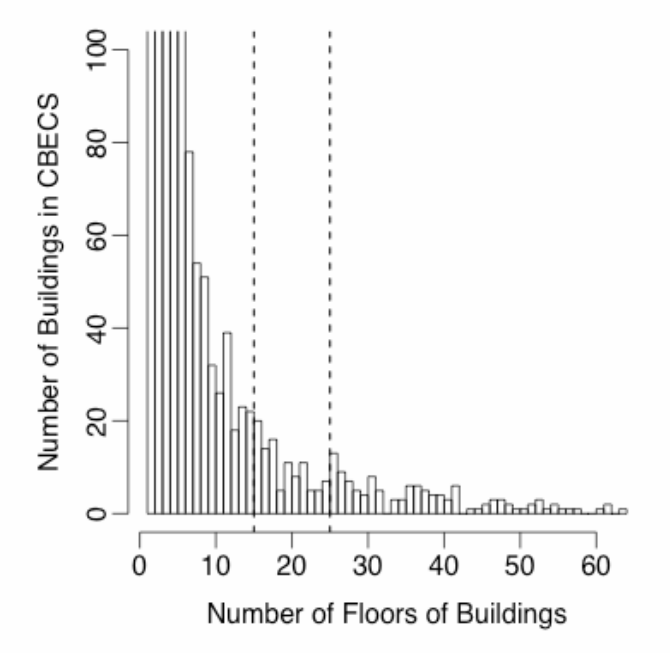

Figure 5.18 Histogram of the estimated number of stories of buildings surveyed in CBECS. The two dotted lines highlight buildings between 15 and 25-stories, and above 25-stories. The number of stories of these buildings are estimated based on their floor areas. The number of stories of buildings <15-stories are directly reported in CBECS.

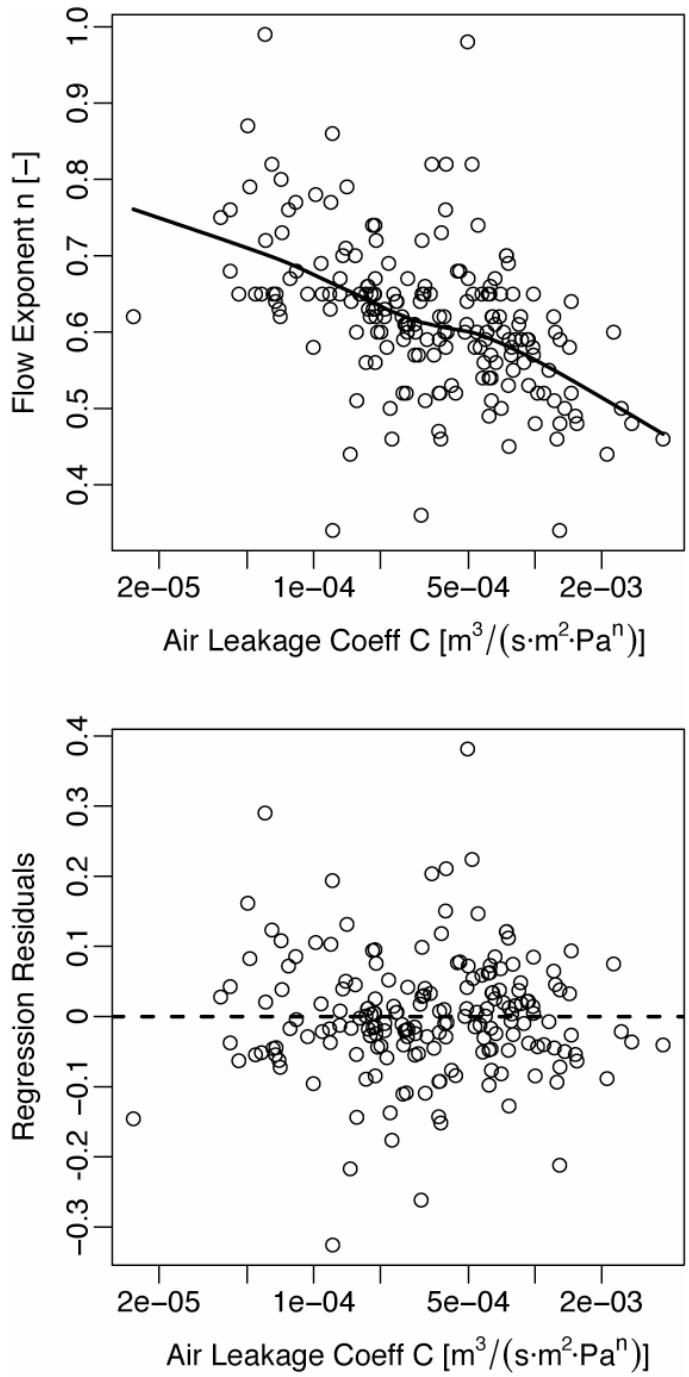

Figure 5.19 Scatter plot of flow exponent and air-leakage coefficient (x-axis plotted on a log-scale). The solid line in the upper figure highlights the trend implied by the scatter plot, which is obtained using local averaging of the data points. Eqn 5.12 shows the regression model used to predict the flow exponent using air-leakage coefficient as the explanatory variable. The regression residuals are computed by subtracting the observed flow exponent of buildings in the commercial air leakage database from the predicted values. The bottom figure shows no specific trend between the regression residuals and air-leakage coefficient, which suggests that the regression model captures most of the relationship between *C* and *n*.

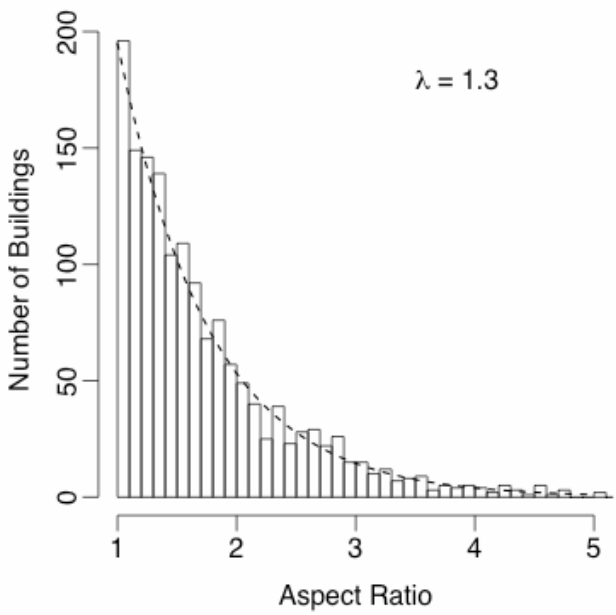

Figure 5.20 Distribution of building aspect ratio, defined as the ratio of the length to width of the footprint area, of 1552 buildings in Oklahoma City. This dataset of geo-coded building footprint area and height is made available by the National Atmospheric Release Advisory Center at Lawrence Livermore National Laboratory on selected US cities. The dotted line is an exponential probability density function $f(x) = \lambda \exp(-\lambda \cdot x)$, for which $\lambda = 1.3$ is found to give the best fit to the aspect ratio observed.

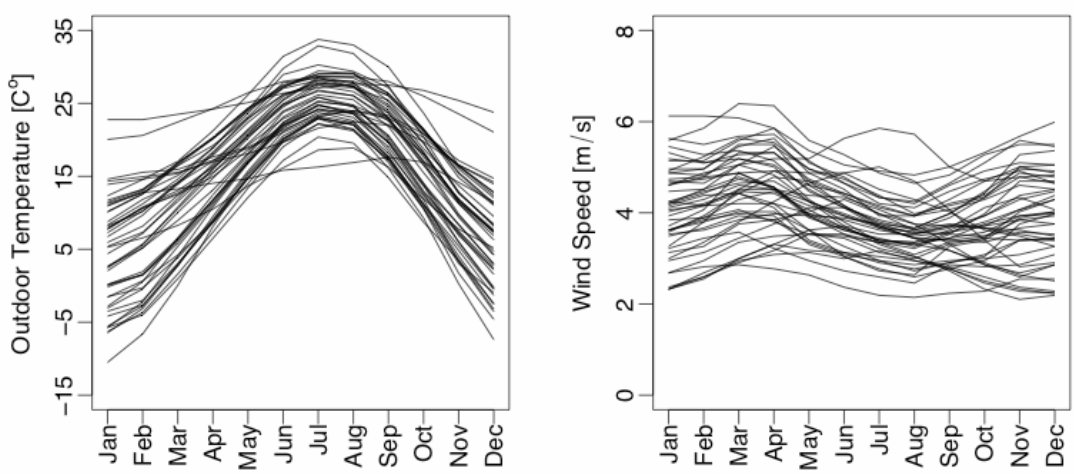

Figure 5.21 The monthly average temperature and wind speed in the 45 most populous cities in the US (NCDC, 2004). These data are used to predict the air infiltration rate distribution of the US commercial building stock.

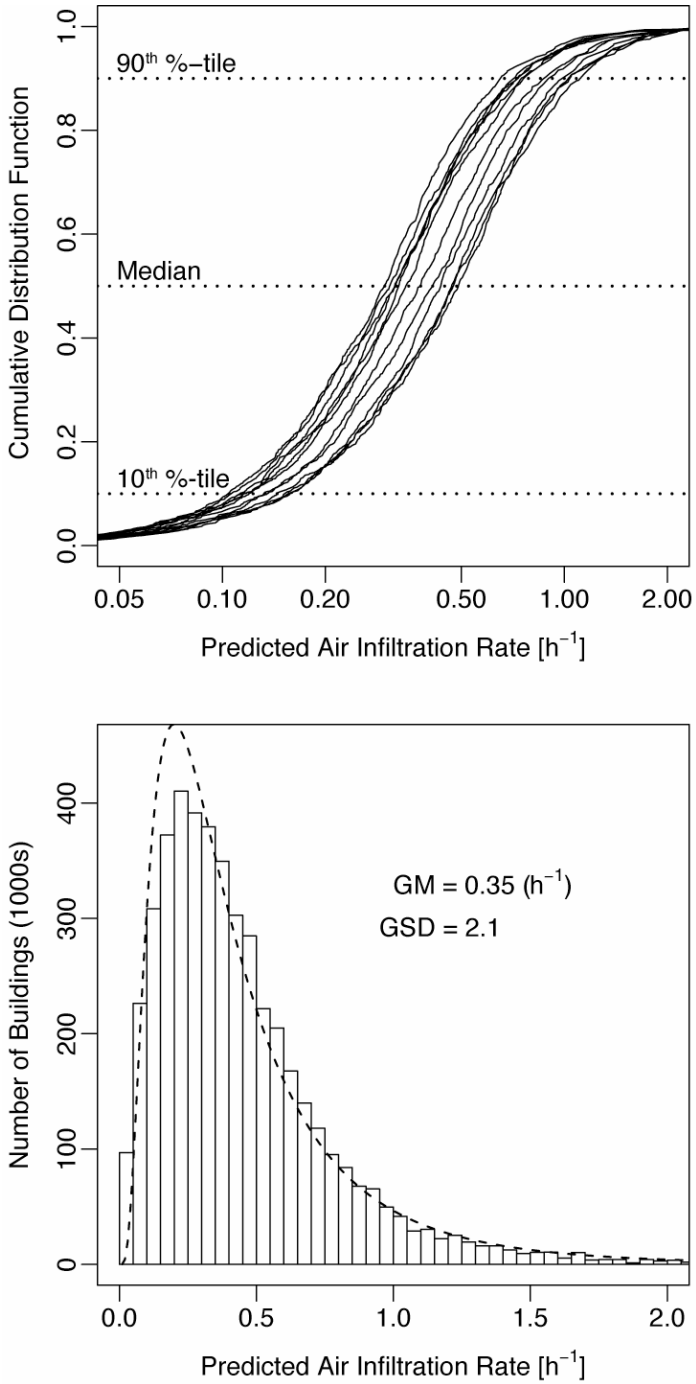

Figure 5.22 Predicted air infiltration rates of US commercial buildings. The top figure shows the cumulative distributions predicted using monthly averaged climatic data in the 45 most populous US cities (Figure 5.21). The overall distributions, one for each of the 12 months, are plotted on the top figure. The overall distribution, including all 12 months of predictions, is roughly lognormal (bottom figure). The dotted line shows the density function of a lognormal distribution with geometric mean and geometric standard deviation as indicated on the plot.

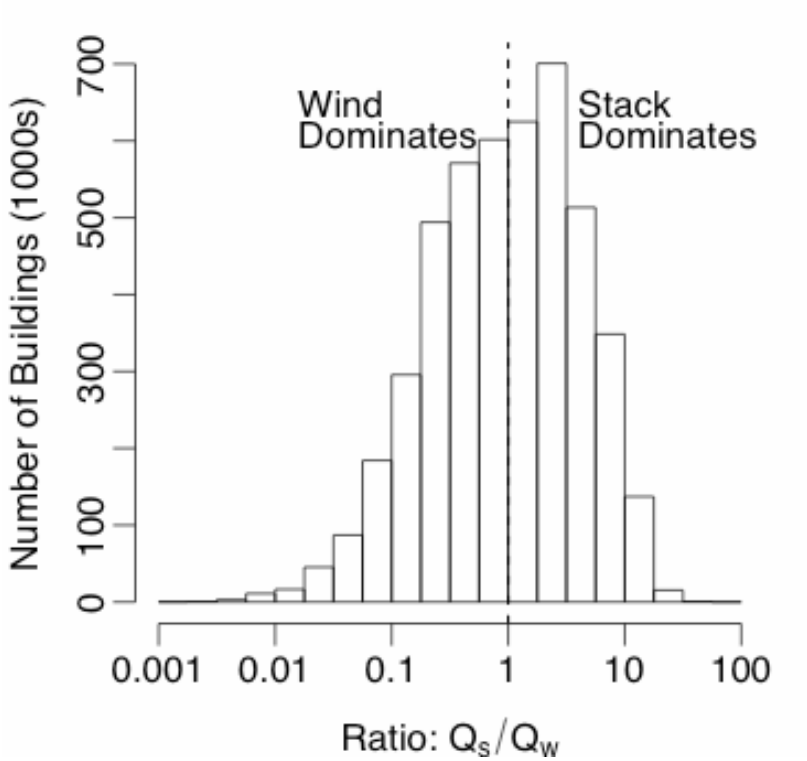

Figure 5.23 Ratio of monthly averaged stack-effect driven air infiltration rate (Q_s) to wind-effect driven air infiltration rate (Q_w) predicted in the US commercial building stock.

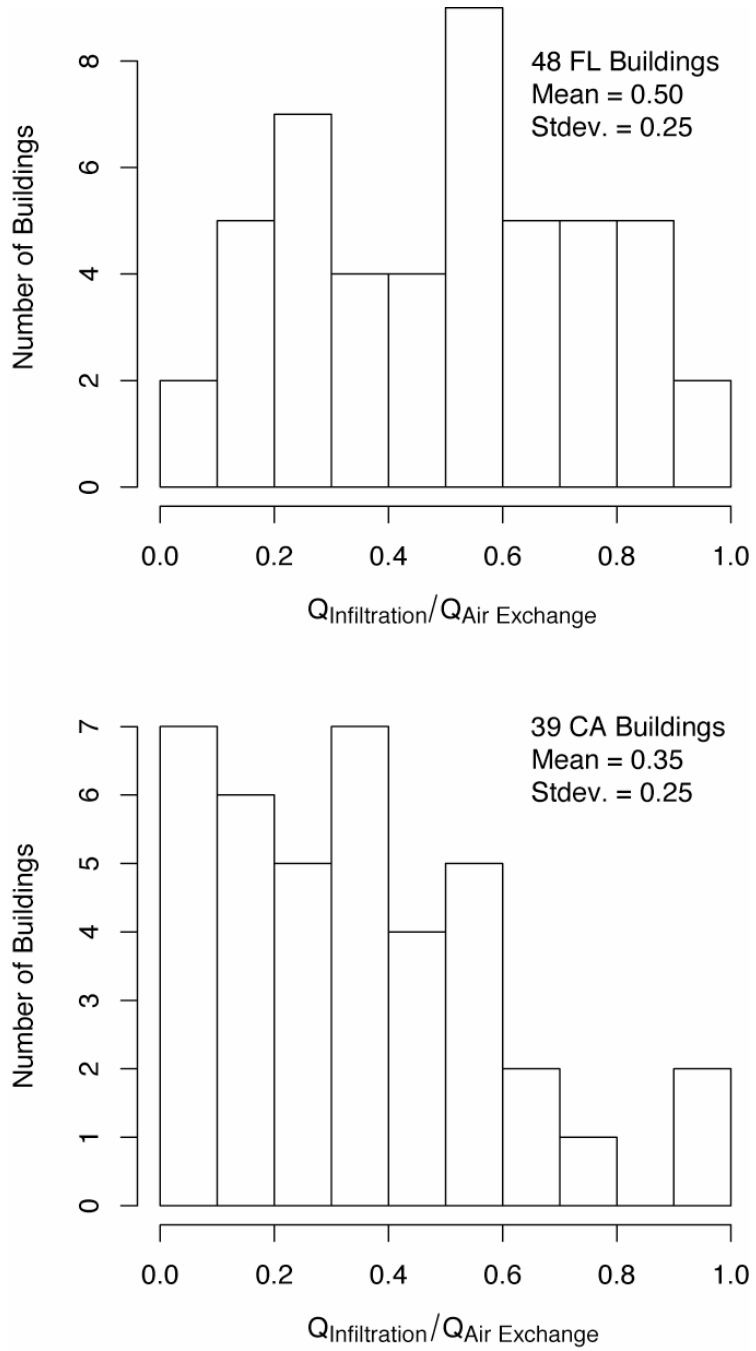

Figure 5.24 Ratio of measured air infiltration rate and air-exchange rate from two datasets. $Q_{Air\ Exchange}$ represents measurements made by tracer-gas decay method with mechanical ventilation on, and $Q_{Infiltration}$ are measurements made with mechanical ventilation off. The upper plot shows data from relatively small commercial buildings in Florida, measured by Cummings et al. (1996). The bottom plot includes office buildings, retail buildings, and schools measured by Lagus and Grot (1995) in California.

6 Shelter-in-Place Effectiveness in Commercial Buildings

6.1 Introduction

Commercial buildings dominate the downtown core of most cities. They are also numerous in residential areas where people live, in the form of schools, retail stores, restaurants, etc. Occupants of commercial buildings are at risk of exposure in the event of sudden releases of toxic chemicals that might occur at nearby industrial facilities or while chemicals are in transit. Certain types of commercial buildings, e.g. port terminals and warehouses, might be associated with additional risks because of the high flow of potentially hazardous materials. Some high-value buildings or popular sites might be targeted in the case of intentional releases. In these scenarios, shelter-in-place (SIP) in commercial buildings might be a viable option to protect occupants from exposure to the toxic chemicals released outdoors.

Similar to the approach used in Chapter 4, in which SIP effectiveness in single-family dwellings was assessed, a hypothetical release simulation is used to model the SIP effectiveness of the commercial building stock in an urban area. Results from the analysis in Chapter 5 are used to estimate the distribution of air infiltration rates of the commercial buildings. Results for nearby residential buildings that are also affected by the release are presented. Since most commercial buildings are equipped with a mechanical ventilation system, the implications of leaving the system running during SIP

are explored. Topics addressed in Chapter 4, such as the influence of chemical sorption on indoor surfaces, and the effect of SIP initiation time delay are also covered in this chapter.

Commercial buildings are predicted to have lower air infiltration rates than single-family dwellings on average. However, a small fraction of the commercial building stock is expected to have quite high air infiltration rates, and might not provide much protection to occupants during SIP. No previous study has examined the variability among commercial buildings in their SIP protectiveness. Community-based assessment of SIP in this class of the building stock is also lacking. General SIP guidelines in certain types of commercial buildings exist, e.g. schools (SWT, 2000; Sabiha et al., 2001), workplaces (NICS, 2003), and large apartment buildings (Damian, 2003), but they tend to focus on the practicality of SIP, such as preparedness and advised actions during an event. Expert advice on how to prepare and operate mechanical ventilation systems to the advantage of enhancing SIP effectiveness is also available (Price et al., 2003; Aumann et al., 2004; Persily, 2004; Edwards et al., 2005). It is the goal of this analysis to assess the SIP effectiveness in a commercial building stock, considering variability in air infiltration among buildings and the importance of the operating state of the mechanical ventilation system.

6.2 Description of the Case Study

The hypothetical release used to assess SIP effectiveness of commercial building is a 0.5-h outdoor release at the southern edge of the downtown business district in Oklahoma

City, OK (Figure 6.1). The outdoor concentrations were predicted by the National Atmospheric Release Advisory Center at Lawrence Livermore National Laboratory using the same atmospheric dispersion model as described in Chapter 4 for the residential analysis. Outdoor concentration predictions were reported as 1-minute averages. The simulation lasted for 2 hours from the start of the hypothetical release. The model domain is 2 km × 2 km at a constant grid resolution of 50 m by 50 m (Figure 6.1). The release source is modeled at 2 m above ground. Predicted outdoor concentrations are given at the 5-m plane.

The date and time of the release run is July 13, 2003 at 9:00 am local time. During the 2-h simulation, the outdoor temperature increased from 26 to 29 ^{o}C. It is assumed that the temperature is spatially uniform. Spatially varying wind speeds were available but only at one point in time (corresponding to the start time). Consequently, it is assumed that the wind speed is temporally constant for the 2-h simulation. Wind was blowing from the southwest fairly uniformly across all grid cells. The wind speed at 10 m above ground is roughly 2.2 m/s. The plume takes roughly 10 minutes to travel 1 km, which carries it out of the model domain. The grid resolution of the wind field is different from the concentration grid. The meteorology grid is 19 km × 19 km in the horizontal plane, evenly divided into 60 × 60 grid cells. The vertical grid resolution is variable with height. A much finer grid (few meters) is used near the ground compared to aloft.

Figure 6.2 shows the concentration grid in relation to the buildings in Oklahoma City and the surrounding census tract boundaries. The building geometry plotted is also made available by the National Atmospheric Release Advisory Center. Oklahoma City is

among the first cities for which this dataset of geo-coded footprint area and height of buildings has been released. In Chapter 5, these data were used to estimate the aspect ratio of commercial buildings. In this chapter, this dataset will be used to estimate the air infiltration rates and occupancy of commercial buildings in Oklahoma City. These are needed to compute indoor concentrations and to assess the SIP effectiveness of commercial buildings. As shown in Figure 6.2, the concentration grid is centered at the downtown core of the city. It crosses the boundaries of 10 census tracts. Of the 677 buildings located within the concentration grid, the vast majority has been classified as commercial buildings.

Oklahoma City is also selected as the case study site because an extensive set of experiments was conducted in 2003 to study the transport of outdoor contaminants in urban areas (Allwine et al., 2004). A series of tracer gas releases were preformed in the downtown core of the city to track air movement in street canyons. Many wind sensors and tracer samples were deployed to study atmospheric dispersion from a point source. Further, to understand how outdoor contaminants enter buildings, experiments were carried out in three large commercial buildings in conjunction with the outdoor tracer gas release (Black et al., 2004). The airflows within buildings were also characterized by additional tracer gas releases indoors. Analysis of these measurements is ongoing. It is the intention that findings from these experiments will complement the information revealed from the modeling work developed here.

The following analysis can be divided into three parts. First, description and manipulation of the geo-coded building geometry data are detailed for the purpose of predicting the air infiltration rates in commercial buildings. Then, the method used to predict the distribution of air infiltration rates and indoor concentrations in the commercial building stock is described. Finally, assessments of the SIP effectiveness of commercial buildings that encounter the plume are presented for different release scenarios.

6.3 Commercial Building Characteristics in Oklahoma City

6.3.1 Description of Buildings

Oklahoma City is a mid-size city with a population of half a million and a well-defined urban core. It has a flat terrain and fairly well characterized climatology. The physical dimensions of buildings in and around the city have been provided by the National Atmospheric Release Advisory Center, a participating agency in the atmospheric dispersion study in 2003. A total of 6334 buildings were captured within a 5.4×5.4 km domain (Figure 6.2). Building footprint area and height were geo-coded using images that are processed by a geographical information system. The majority of buildings in Oklahoma City, including residential buildings, have heights that correspond to a single story building (Figure 6.3). The distribution of building heights is bimodal. There is a peak at 3.5 m (1-story), and another at 7 m (2-story). Only a small fraction of the buildings are taller than 2 stories. Fewer than 2% of the buildings have heights exceeding 15 m. The tallest 3 buildings in Oklahoma City are 114, 107, and 75 m in height, and are located in the downtown core. The tallest building estimated from the geo-coded data is

about 38-story, which is a good representation of the 36-story Chase (Bank One) Tower in downtown Oklahoma City. By assuming that each floor is 3 m in height, the fraction of buildings that are 1, 2, and 3-story are 58%, 29%, and 9% respectively.

Even in this downtown part of the city, a significant number of the buildings are residential units. Clusters of houses characteristic of residential neighborhoods are observed in the top part of the aerial map shown in Figure 6.2. Since residential and commercial buildings have different air leakage characteristics, it is necessary to differentiate between the two building types when modeling their air infiltration rates. Floor area is a convenient parameter to use because it incorporates both the footprint area and the height of the building. The US Census Survey and the American Housing Survey (AHS, 1996) carried out in the Oklahoma City metropolitan area together provide estimates of the floor area distribution of houses at a census-tract level. These distributions can be used to compare against the floor area distribution of buildings contained in the aerial map. Ideally, the differences between these two distributions would define the distribution of commercial buildings. However, there are considerable uncertainties in both sets of floor area distributions. For example, the house floor area distribution in a census tract is estimated from the number of rooms in the housing unit. The floor area of buildings contained in the aerial map (Figure 6.3) is estimated using the footprint area and the estimated number of stories, which in turn is estimated from the building height by assuming 3 m per floor. Some adjustments must be made when using these distributions to distinguish commercial buildings from single-family dwellings.

6.3.2 Identifying Commercial Buildings by Floor Area Distribution

There are 34 census tracts in Oklahoma City whose boundaries lie at least partially within the 5.4 × 5.4 km model domain. To make use of the US Census data, all the residential buildings in a census tract must be contained within the domain. Twelve census tracts fit this criterion. Roughly 60% of the buildings are located in one of these census tracts. If no houses are reported in a census tract, then all buildings are assumed to be commercial by default. In this way, 171 buildings in 3 census tracts are classified as commercial buildings. In census tracts where the total number of houses in the census tract is greater than the number of buildings captured in the aerial maps, then it is assumed that there are no commercial buildings in the census tract. By this criterion, 1050 buildings in 2 census tracts are classified as houses. Other residential units that are not single-family detached houses, such as apartment buildings, will be misclassified as commercial buildings, which is a shortcoming of this method.

A majority of the census tracts contain a mix of residential and commercial buildings (Figure 6.4). The apportionment of buildings by size into these two building classes is done using the following procedure. The numbers of houses with floor area <46 m^2 (500 ft^2), 46 to 93 m^2 (500 to 1000 ft^2), …, and >232 m^2 (2500 ft^2) are determined using data from the US Census Survey and the American Housing Survey[15]. The total number of buildings in these same size categories is obtained from the geo-coded data. Then, the differences in the floor area distribution of houses and that of all buildings are computed. To distinguish between houses and commercial buildings, it is assumed that there are no

[15] See Chapter 3 for the method used to obtain this floor area distribution.

commercial buildings until the number of all buildings exceeds that of houses alone. Any deficiency in the number of buildings to account for the presence of houses is carried forward. When there is a surplus in the number of buildings after the number of houses is accounted for, this surplus, after subtracting any accumulated deficiency, is assumed to represent the number of commercial buildings. Table 6.1 illustrates how this method works using one of the census tracts as an example. There are 200 buildings in this census tract, of which 76 are houses according to the US Census Survey. Figure 6.5 shows the floor area distributions of the two classes of buildings in this census tract.

Using this method, 42% of the 2745 buildings in 12 census tracts are identified as commercial buildings. The floor area distributions of these commercial buildings and their residential counterparts are shown in Figure 6.6. In general, the prevalence of commercial buildings having floor area less than 230 m^2 (2500 ft^2) is low. However, the method outlined is still useful to ensure that the presence of small commercial buildings is not overlooked.

In census tracts with boundaries that lie partially outside of the 5.4×5.4 km domain, the above method cannot be used because the US Census Survey house counts include all units in the census tract. Instead, a national distribution of the fraction of buildings being commercial as function of floor area is used (Table 6.2). This distribution is based on building counts of commercial buildings from the CBECS Commercial Building Energy Consumption Survey (EIA, 2003), and building counts of single-family detached units from the American Housing Survey national data, as functions of their floor area.

The methods described so far estimate the total number of commercial buildings in each census tract. However, to characterize the air leakage and subsequently the indoor concentration distribution in commercial buildings, it is necessary to quantify the other building parameters also, including building height, footprint area, and volume. One way to achieve this is to first classify each individual building as either residential or commercial using the floor area distributions obtained above. Then, each building that has been classified as commercial is modeled for its air leakage and indoor concentration according to its height, footprint area, etc. Finally, the composite distribution is obtained by appropriately weighting all the predictions performed in the census tract. For buildings with floor area less than 560 m^2 (6000 ft^2), certain numbers of buildings are classified as commercial according to the floor area distributions obtained above. Classification is based on their floor area: the larger buildings are systemically assigned to be commercial, leaving the smaller ones as residential. For buildings larger than 560 m^2 in floor area or 3-story in height, all are assumed to be commercial.

Of the 6334 buildings included in the 5.4×5.4 km sector of Oklahoma City, 1997 (32%) are assigned through these procedures to be commercial. The remaining buildings are assumed to be single-family detached houses. The floor area and height distributions of these two groups of buildings are shown in Figure 6.7. The house height distribution is bimodal, with most houses being 1-story and roughly 23% being 2-story. The method estimates that 6% of the houses are 3-story, which appears to be a small overestimate compared to statistics from the American Housing Survey. It is possible that some of these houses have taller ceiling heights or an attic, and are only 2-story instead.

The method outlined generates a floor area and height distribution of commercial buildings that is separate from those of the residential buildings (Figure 6.7). The peak of the floor area distribution is at 500 m^2 instead of 120 m^2 in the case of houses. As expected, the range in floor area is also wider for commercial buildings. The height distribution appears to have a single peak instead of being bimodal because the fraction of 1- and 2-story commercial buildings are comparable (33% and 41% respectively). The fraction of 3-story commercial buildings is about 15%, which is more than twice the fraction of houses that are determined to be 3-story.

6.3.3 Building Occupancy Estimates

Unlike in single-family dwellings, the number of occupants in commercial buildings can vary greatly within a building stock. For SIP analysis, to give indoor concentration predictions that represent the exposure of occupants in buildings, more weight should be given to buildings with more occupants. Building size, type, and time of day are some of the factors that affect the number of people in a given building. The simplified approach taken here is to estimate building occupancy by floor area, and ignore the other factors. Since building occupancy estimates are used only to give the relative weights when estimating the overall indoor concentration distribution, the actual numerical values are less important than their relative magnitudes. Even so, not capturing the type of building and the time of day means that the estimates can be unreliable in certain types of buildings with occupancy-time patterns that differ from most others.

Data from the CBECS are analyzed to characterize the relationship between building occupancy and other building parameters, such as the floor area. CBECS gives the number of employees at most buildings surveyed and the occupant capacity for 7 types of buildings: religious worship seating capacity, public assembly seating capacity, total seats in classrooms, food service seating capacity, inpatient licensed bed capacity, skilled care licensed bed capacity, and number of guest/occupant rooms. If building occupancy is assumed to equal the sum of the number of employees and the occupant capacity, then the distribution of building occupancy is approximately lognormal with a geometric mean of 0.018 persons/m^2 and a geometric standard deviation of 3.5. Comparison of the estimated building occupancy with the theoretical lognormal distribution suggests that the building occupancy estimates might be overpopulated with high values (Figure 6.8). If instead the building occupancy is estimated by the sum of the number of employees and 25% of the occupant capacity, the estimates follow the theoretical distribution very closely.

Figure 6.9 shows the building occupancy as estimated by the sum of employees and 100% of the occupant capacity for the different types of buildings surveyed by CBECS. Most buildings have occupancy per floor area in the range of 0.002 to 0.2 person/m^2. Occupancy estimates that include occupant capacity data are higher than most other types, especially among classrooms, restaurants, and buildings for religious worship. In general, the variability of occupant density within a building type outweighs the variability between building types. For example, the median occupant density in office buildings is 0.022 persons/m^2, which is roughly 3× the value in warehouses (0.0075

persons/m^2). On the other hand, the variability between the highest and lowest 5% occupant density within both building groups is 10× or more.

Besides building type, occupancy per floor area can also be a function of a building's physical dimensions. For example, buildings that tend to have very large floor area, such as enclosed malls and warehouses, have relatively low building occupant densities (Figure 6.9). On the other hand, high-rise buildings, which are commonly office buildings, have higher building occupant densities. Assuming that the number of occupants in a building can be reasonably estimated by the sum of the number of employees and 25% of the occupant capacity, the relationship between building occupancy and the physical dimension of buildings can be quantified by regression analysis as follows:

$$\text{(i)}\quad \ln\left(\frac{\text{Number of Occupants}}{\text{Floor Area}[\text{m}^2]}\right) = -2.5 - 0.25 \cdot \ln(\text{Floor Area}[\text{m}^2]) + 0.44 \cdot \ln(\text{Number of Floors}) + \varepsilon$$

$$\text{(ii)}\quad \ln(\text{Number of Occupants}) = -2.5 + 0.75 \cdot \ln(\text{Floor Area}[\text{m}^2]) + 0.44 \cdot \ln(\text{Number of Floors}) + \varepsilon$$

Eqn 6.1

The two forms of the regression model are essentially the same, but their R^2 values are very different. Model (ii) has an R^2 of 0.62, whereas model (i) has an R^2 of only 0.096. This means that most of the variability in the estimated number of occupants can be explained by building floor area alone. However, the added explanatory power by including the dependence on the physical dimension of buildings is statistically significant. The regression coefficients suggest that larger buildings tend to have lower

occupant density, but building height tends to be positively correlated with occupant density. See Table 6.3 for detailed regression results.

Using this regression model, the estimated occupancy in the commercial buildings in the 5.4×5.4 km study area of Oklahoma City range from a few persons to a few thousands (Figure 6.10), with a median of 17 persons in a building. The central 90% of the buildings is estimated to have 0.012 to 0.027 persons/m^2 of floor area. Most of the variability in estimated number of occupants arises from variability in building floor area. Thus, the distribution of the building occupancy resembles the distribution of commercial building floor area, as shown in Figure 6.7.

The estimated building occupancy is used in the analysis two ways. First, it is used as a weighting factor to obtain the air infiltration rate distribution for commercial buildings in a census tract. Larger buildings are systemically predicted to have more occupants, and more weight is given to the predictions for such buildings. Second, the estimated building occupancy of all commercial buildings in a census tract is summed to estimate the total number of potentially exposed people in that census tract. Then, it is assumed that all grid cells that lie within the census tract have the same occupant density. In both steps, the error term ε in Eqn 6.1 is not modeled such that larger buildings are systematically predicted to have more occupants.

The preliminary estimates of building occupancy can be integrated with other datasets, such as the Los Alamos National Laboratory's Day and Night Population Database

(McPherson and Brown, 2003), to improve its reliability. The Day and Night Population Database was developed to estimate the daytime and nighttime population for the entire US at a 250 m grid resolution. The daytime population estimates account for the spatial allocation of the workforce by making use of US census data on residents' journey to work between counties, and the State Business Directory for business locations. However, one limitation of this database is the lack of an indoor/outdoor component to estimate the number of people in buildings. A direct overlay of the building map on the daytime estimate for Oklahoma City reveals that there are some grid cells where buildings are present but the population estimate is zero (Figure 6.11). Even so, when the building occupancy estimates obtained from the regression model (Eqn 6.1) are allocated onto the same 250 m grid (Figure 6.12), reasonable spatial agreement is observed in grid cells that are densely populated in the daytime.

While many factors could contribute to differences between building occupancy and the LANL daytime population estimates, the inherent large variability in the number of people in specific buildings at any given time suggests that a deterministic approach might not be sufficient. Instead, one should characterize and properly account for the probability distribution of the number of persons in a building as a function of time. To do this, survey data on building occupancy, building types, and a number of other time-dependent parameters are needed. In future analyses, integration with the Day and Night Population Dataset and with suitable human activity pattern data (Klepeis et al., 2001) should be considered to improve the estimates of occupancy in commercial buildings. In this dissertation, the LANL dataset is not utilized.

6.3.4 Grouping Small Commercial Buildings to Reduce Model Runs

In this section, the method developed to predict the air leakage distribution of the 1997 commercial buildings in the Oklahoma City study area is outlined. As discussed in Chapter 5, the air infiltration rates of smaller commercial buildings, those that are equal to or less than 1000 m^2 in floor area and 3-story, are modeled using the LBL Infiltration Model. Roughly half of the 1997 commercial buildings are modeled this way. The remaining buildings are modeled using the Shaw-Tamura Infiltration Model. However, in terms of the estimated building occupancy, close to 90% of the total population in the Oklahoma City study area are predicted to be in these larger buildings. Even though the computational requirement to model the air infiltration rate and subsequently the indoor concentration of each commercial building in the Oklahoma City study area is not tremendous, there are certainly situations where it can become much more demanding. For example, a large-scale outdoor release in a densely populated major city might impact tens of thousands of buildings. Furthermore, a release that continues for many hours might require the model to be rerun with updated meteorology. Especially in emergency situations, modeling strategies that can substantially reduce computation demands without sacrificing necessary detail in the model results should be exploited. One such opportunity is to group smaller buildings together to reduce the number of individual building cases in the model runs.

A desirable grouping method should limit the number of model runs while leaving larger buildings with high occupancy ungrouped. Furthermore, buildings that are grouped should have similar air leakage characteristics, leading to similar indoor concentration

distributions. If the necessary information in a city is available, it might be useful to group buildings of similar functional or construction type together. In this analysis, however, because of limitations in available data, the grouping can only be based on the physical dimensions of the buildings. Recall that the air leakage coefficient of buildings is found to depend on both the floor area and the height of the building. Therefore, by grouping together buildings of similar floor area and height, the variance in their air leakage coefficients will be reduced.

In the previous chapter, the air-leakage coefficients of buildings surveyed in CBECS were predicted using a regression model that includes the dependence on both building floor area and height. These surveyed buildings can also be used as a sample to test if groups of buildings with similar predicted air-leakage coefficient can be identified by their floor area and height. The objective is to minimize the variance in the air leakage coefficient within each group of buildings. The reason for using the simulated CBECS data is because it is a relatively well-sampled set of buildings. The original air leakage measurements on which the regression analysis is based are not suitable for this task because the data are sparse. Of course, this method still relies on the assumption that the predicted air leakage characteristics of buildings surveyed in CBECS have been well characterized by the regression model. See Chapter 5 for a discussion on the model limitations.

The classification or regression tree method recursively partitions the response, i.e. the air leakage coefficients, by splitting the sample by the predictor variables, i.e. the building

floor area and height. To obtain more intuitive cutoffs, the number of floors replaces building height as one of the predictor variables in the present analysis. Using all 5430 buildings surveyed in CBECS, the classification tree method grouped buildings by those that are 1-story, and those that have more than 1 story (Figure 6.13). The floor area cutoffs for 1-story buildings are 530 m^2, 2700 m^2, and 11000 m^2. For the taller buildings, the floor area cutoffs are 810 m^2, 2700 m^2, and 16000 m^2. These groups are selected such that the variances in air leakage coefficients within the groups are minimized. The analysis is performed after taking the log-transformation of air leakage coefficients to avoid having the analysis dominated by the few high leakage cases.

When the same method is reapplied to 1-story buildings only, more floor area cutoffs are identified: 220 m^2, 530 m^2, 1900 m^2, 9100 m^2, and 38000 m^2 (Figure 6.14). The next step is to sequentially identify if the taller buildings can be grouped further by their floor areas and number of floors. Note that a split is only meaningful when it reduces the variability of the air leakage coefficient within a group of buildings. After removing 1-story buildings from the sample, the regression tree method identifies 2-story buildings as a subgroup. Among 2-story buildings, the floor area cutoffs identified are 910 m^2, 2400 m^2, 14000 m^2, and 41000 m^2 (Figure 6.15). These cutoffs are systemically larger than those for the 1-story buildings, but similar in magnitude and in their spacing. The remaining buildings, those that are 3-story and above, can be further grouped by their floor area, but not by number of stories. To ensure that larger buildings are modeled individually, buildings with more than five floors are left ungrouped. Among buildings that are 3 to 5-

story, the floor area cutoffs are largely the same as when buildings >5-story were included: 1300 m^2, 3600 m^2, 7200 m^2, 17000 m^2 and 58000 m^2 (Figure 6.16).

To further reduce the number of groups of buildings to model, only three of the most significant splits are used. The length of the forks displayed in Figures 6.14 to 6.16 represents the significance of the split. For 1-story buildings, the three most significant splits are at 530 m^2, 1900 m^2, and 9100 m^2. One-story buildings with floor area larger than 9100 m^2 are modeled individually. For 2-story buildings, the splits are at 910 m^2, 2400 m^2, and 14000 m^2. For 3 to 5-story buildings, the splits are at 1300 m^2, 3600 m^2, and 17000 m^2. The geometric mean and geometric standard deviation of the predicted air leakage coefficients for each of the nine groups are detailed in Table 6.4. One-story buildings with floor area between 1900 and 9100 m^2 are roughly 7 times less leaky than buildings that are between 3- to 5-story but are small (<1300 m^2). Through this classification method, the within-group variability is roughly the same in all nine groups. It is reasonable to assume that each group has a common geometric standard deviation of about 2.3. The predicted air leakage coefficient distributions of the 9 groups are shown in Figure 6.17. Since the distributions have almost the same variability, the slopes of the probability distribution functions are similar. However, these distributions are distinct from one another because of the differences in their geometric means. For example, 75% of the buildings in the leakiest group (3–5 story, <1300 m^2) have predicted air leakage coefficients that exceed 5×10^{-4} [$m^3/(s\cdot m^2\cdot Pa^n)$], but only 5% of the buildings in the tightest group (1-story, 1900–9100 m^2) have a predicted air leakage coefficient that exceeds this value.

In the Oklahoma City 5.4 km × 5.4 km study area, over 93% of the commercial buildings fall into one of these nine groups. However, half of the building occupants are predicted to be in the 7% of the buildings that are modeled individually. By grouping the smaller buildings together, more computational resources can be devoted to the buildings that contain the most occupants.

6.4 Modeling Approach

For this case study, there are a few modeling approaches that are viable to give estimates of indoor concentrations. One is to predict the indoor concentration only at grid cells that fall within a building. In that case, each grid cell would be assigned to one or a few specific buildings only. The air leakage probability distribution of these few buildings would be estimated based on their size (floor area and height). Then, either the LBL or the Shaw-Tamura Infiltration Model would be used to predict the probability distribution of the air infiltration rate. Under an SIP condition that assumes there is no additional air exchange between the outdoors and the indoors besides uncontrolled air infiltration, the probability distribution of indoor concentrations could be computed. This method would give building-specific indoor concentrations, which might give a false sense of accuracy to the model predictions. Current understanding of airflow in buildings is insufficient to justify such confidence at the individual building level. To characterize building-specific air-exchange rates in a specific urban environment would require extensive on-site experiments and detailed modeling work (Haghighat and Megri, 1996; Sohn et al., 2002a;

Price et al., 2004). The analysis in this dissertation is community-based, and therefore inadequate to give building-specific predictions.

The key question then is how to sensibly collect buildings together when modeling their air infiltration rates and indoor concentrations. Lumping together buildings with similar characteristics that might affect their indoor concentrations is useful to narrow the scope of the analysis. There should be enough buildings in each group such that the predicted indoor concentration distribution describes the expected range of concentrations in buildings. Census tract was selected as the spatial unit for characterizing the air leakage characteristics of residential buildings. In that case, the choice is logical because the housing data used are also census tract based. It was also a suitable one because when first delineated, census tracts are designed to be relatively homogeneous with respect to population characteristics, economic status, and living conditions. Most census tracts also have 1500 to 8000 residents, which ensures a sizeable population of residential buildings.

Even though census tract boundaries are not drawn with commercial buildings as a focus, they do tend to separate the downtown core from the rest of the city. In Oklahoma City, the estimated number of commercial buildings ranges from 17 to 147 per census tract (mean = 44) in the 17 census tracts with boundaries that are fully contained within the study area. There are significant differences in the size of the commercial buildings located in these census tracts. Consequently, the building air leakage characteristics are also expected to differ among census tracts. The variability in building size is also reduced after buildings are grouped by census tract, suggesting that there are some

similarities among buildings in a census tract. Certainly there are other ways to group commercial buildings together, but this preliminary evidence seem to suggest that census tract boundary is a reasonable choice.

As a result of this approach, the location of the building is taken into account only when computing the census tract level air-leakage distribution. Regardless of whether there are buildings present in a grid cell or not, the air infiltration rate and indoor concentration distributions are computed. Even in grid cells where there is only one building present, the model predictions are not specific to that particular building. Instead, the expected number of potential casualties is computed probabilistically by assuming that any commercial buildings in the census tract could apply to a building located in that grid cell. This method ensures that predictions made in each grid cell generally apply to buildings that are characteristic of the area. This is deemed the most appropriate way to use the available information since data are lacking with which to specifically assess any particular building in the model domain.

6.4.1 Distributions of Air Infiltration Rate

The following method was used for determining air infiltration rates in the commercial buildings in the Oklahoma City study area. The air infiltration rates of buildings located in the 17 census tracts were predicted using the LBL Infiltration Model for buildings with floor area and height equal to or less than 1000 m^2 and 3-story, respectively. The Shaw-Tamura Infiltration Model was used for buildings that are larger than these cutoffs.

Smaller buildings are grouped into 9 groups according to their floor area and number of stories. The cutoffs and the geometric means of the air leakage coefficients of each group are the same as in Table 6.4, except for the floor area cutoffs of 1-story buildings. The floor area range for mid-size 1-story buildings have been changed from 530–1900 m^2 to 530–1000 m^2. The reason for this change is to avoid a large discontinuity in the predictions owing to a switch between the two air infiltration models among buildings that are otherwise similar in size. Consequently, the geometric mean of the air leakage coefficients were also changed slightly from 1.90×10^{-4} to 2.19×10^{-4} [$m^3/(s\cdot m^2\cdot Pa^n)$] for the 1-story buildings between 530 and 1000 m^2 in floor area, and from 1.04×10^{-4} to 1.21×10^{-4} [$m^3/(s\cdot m^2\cdot Pa^n)$] for 1-story buildings between 1000 and 9100 m^2 in floor area.

A large majority of commercial buildings in these 17 census tracts were modeled by the grouping method. Out of the 1997 commercial buildings in the Oklahoma City study area, only 130 were modeled individually. The air-leakage coefficients of buildings modeled individually are estimated using the regression model detailed in Chapter 5 (see Eqn 5.3 and Table 5.4). The remaining 1867 smaller commercial buildings are allocated into 249 different groups according to their floor area, height, and the census tract in which the building is located. At most, 88 buildings of similar size and height are combined as one group in a census tract. The typical number of building in a group is about 10. In each census tract, the air infiltration rates are predicted for all individual buildings and for each group of buildings. The grouped buildings are assumed to have a distribution of air-leakage coefficients with geometric means and geometric standard deviations determined above. The median building characteristics of the group, such as

building envelope area, height, and volume, are used as inputs to the air infiltration model. The flow exponents of buildings that are modeled using the Shaw-Tamura Infiltration Model, regardless whether they are modeled individually or as a group, are estimated using the correlation with C as detailed in Eqn 5.12. After applying the appropriate air infiltration model, all predictions are weighted by the number of occupants to give the composite air infiltration rate distribution for the census tract.

Chapter 5 describes the expected range of values of the neutral pressure level (β), the thermal draft coefficient (γ), and the wind pressure coefficient ($C_p^{'}$) used in the Shaw-Tamura Infiltration Model. Instead of sampling from these distributions as was done before, all buildings were assumed to have the same parameter values, namely $\beta = 0.5$, $\gamma = 0.8$, and $C_p^{'} = 0.7$. These values were chosen because they represent the estimated central tendency. For the smaller commercial buildings that are modeled using the LBL Infiltration Model, a similar model simplification is made. It is assumed that the ceiling of a building is as leaky as the junction between the wall and the floor ($X = 0$; see Chapter 3), and that half of the total leakage area of a building is from the walls ($R = 0.5$). Furthermore, it is assumed that the terrain is urban at locations in Oklahoma City (terrain class 4), and that there is shielding from the surrounding around most of the building perimeter (shielding class 4).

When predicting the stack-effect driven air infiltration rates, the indoor temperature is assumed to be 20 ^{o}C in all buildings, which is typical for indoor spaces. The LBL Infiltration Model uses wind speed at 10 m height, which is fairly uniform in this case

study at 2.2 m/s. The Shaw-Tamura Infiltration Model uses wind speed at the top of the building height, which was determined by a distance-weighted average of the closest available wind speeds. The estimated wind speeds at the top of the building height are in the range 1.9 to 3.8 m/s.

6.4.2 Distributions of Indoor Concentrations

Similar to the approach used in Chapter 4 to predict the indoor concentration distributions in residential buildings, each grid cell is assigned to a specific census tract according to its location. Using the corresponding census-tract based air infiltration rate distribution and the outdoor concentration time profile predicted at the grid cell, the time-dependent indoor concentrations are predicted by mass balance. The governing equations are the same as those used in Chapter 4, which assume well-mixed conditions within each building. Since the air infiltration rate distributions used are occupancy-weighted, the predicted indoor concentration distributions are also weighted more heavily towards buildings with higher numbers of occupants. The method used to compute the indoor concentration distribution in houses is the same as discussed in Chapter 3 and 4. All the residential air infiltration rates are predicted using the LBL Infiltration Model.

6.4.3 Adverse Health Effects from Exposure

In the simulations presented in this chapter, adverse health effects under a linear dose-response relationship are evaluated at a toxic load limit of 1 $(mg/m^3)\cdot h$. At higher toxic

load exponents (m = 2 and 3), the release amount is scaled such that the same number of potential casualties from outdoor exposure is expected in all simulations. The corresponding toxic load limits at m = 2 and 3 are 1 $(mg/m^3)^2 \cdot h$ and 1 $(mg/m^3)^3 \cdot h$, respectively. The selections of model parameters are comparable in scale to those used in Chapter 4. Scaling of the release amount is needed to avoid comparing simulation results at different release scale, which can affect SIP effectiveness measured in terms of the casualty reduction factor. This sensitivity with respect to the release scale has been illustrated in both Chapter 2 and Chapter 4, and therefore will not be investigated here.

The number of people with exposure exceeding the toxic load level is counted at the end of each minute for each grid cell. As explained earlier, the number of people in a grid cell is determined by dividing the total number of building occupants estimated in a census tract uniformly over the enclosed land area. The outdoor plume modeled in this case is predicted to cause adverse health effects owing to outdoor exposure that extend a distance of about 2 km from the release site. This is roughly modeled at half the scale of the test cases considered in Chapter 4. Most but not all of the adverse health effects are captured within the 2 km × 2 km model domain (Figure 6.18). While it is possible to scale back the release amount such that all health consequences are contained within the model domain, modeling a larger release is preferred such that more buildings are included in the analysis. Doing so helps to ensure that the air infiltration rates estimated for the census tracts are good representations of the expected distribution among the buildings present in a grid cell.

Tables 6.5 and 6.6 detail all the simulations performed from which SIP effectiveness of commercial buildings are evaluated and compared among the different scenarios. A unique simulation code is assigned to each model run. The resulting estimated numbers of potential casualties are shown in the indicated figures. Before analyzing the casualty estimates, the intermediate results are discussed, which include the air infiltration rates and indoor concentrations predicted in commercial buildings. In these initial discussions, the simulation used is 6Ai, which is referred to as the base-case simulation.

6.5 Results and Discussion

6.5.1 Air Infiltration Rate Predictions

The air infiltration rates of commercial buildings in the 17 census tracts that lie at least partially within the 2 km × 2 km model domain are predicted to range from 0.01 to 2 h^{-1} (Figure 6.19). The variability among census tracts spans roughly a factor of five at the median air infiltration rate. Ten of the 17 census tracts that lie entirely within the model domain have some of the tightest commercial buildings in Oklahoma City. Most buildings are predicted to have an air infiltration rate less than 1 h^{-1}. Buildings in the surrounding census tracts are smaller in size on average and are therefore predicted to be relatively more leaky.

A check is performed to quantify the differences between the air infiltration rate distributions obtained by the deterministic/group approach and the sampling approach.

The deterministic/group approach was used to give the predictions shown in Figure 6.19. The invoked assumptions and methods used are detailed in Section 6.4. In the sampling approach, instead of the smaller buildings being grouped, each building is modeled individually regardless of its size. Furthermore, probabilistic parameters are used as inputs to the air infiltration models, instead of their central tendencies being used for all buildings. It is found that the model efficiency gained by replacing stochastic variables with constants and grouping smaller buildings together outweighs the small loss in the predicted variability. Figure 6.20 shows that the differences in the predicted air infiltration rate distribution in selected census tracts are less than 20%.

The air infiltration rate distribution predicted for the census tract is the sum for all buildings weighted by their respective estimated occupancy. Since larger buildings with higher occupancy tend to have lower air infiltration rates, the weighting tends to shift the air infiltration rate distributions to lower values (Figure 6.21). In the most extreme case, the median air infiltration rate decreases by more than 80%. This occurs in a residential census tract with mostly small commercial buildings but also a few large commercial buildings, which dominate the occupancy-weighted distribution. The median air infiltration rate in most census tracts weighted by building occupancy ranges from 0.04 to 0.5 h^{-1}, which is roughly 30% to 60% lower than the unweighted values.

In general, the predicted air infiltration rates are quite low in the downtown core of Oklahoma City, which is dominated by large commercial buildings. There are three main factors that contribute to these low values. First, large buildings are predicted to be less leaky than small buildings per unit of building envelope surface area. This has been

observed in their lower air leakage coefficient values relative to smaller buildings. Second, large buildings have smaller ratios of exterior surface area to volume ratio than small buildings. As air infiltration scales largely with the surface area of the building envelope, its rate after normalizing by the volume of the building is expected to be lower in large buildings as compared with small ones. Finally, the use of building occupancy to weight the distribution causes the median value to shift towards estimates for the larger buildings. If the air infiltration rate distributions were to be weighted by number of buildings, and not by occupancy, then the median air infiltration rates at these two grid cells would be 0.1 and 0.2 h^{-1} respectively. Air infiltration rates of such magnitude have certainly been measured in buildings experimentally (Chapter 5).

Figure 6.22 compares the predicted air infiltration rates among houses to that of commercial buildings in the study area. The comparison reveals that most houses, but not all, have higher infiltration rates than commercial buildings. Yet, there are certainly some commercial buildings that are expected to be leakier than houses, especially in census tracts that have mostly small commercial buildings. The range of air infiltration rates predicted in single-family detached units is also considerably narrower than the variability among commercial buildings.

6.5.2 Indoor Concentration Predictions

As the plume moves across the model domain, it first encounters large commercial buildings in the downtown area. It takes the plume 5 to 10 minutes to reach the

neighboring census tracts where some houses might be located. From the outline of the buildings shown on the concentration maps (Figure 6.1), there are only a few small buildings in the pathway of the plume until further downwind and outside of the model domain. For the sake of comparison, however, residential predictions are still performed in census tracts that have some reported houses.

The predicted median indoor concentrations in both residential and commercial buildings are summarized in Figure 6.23. Initially, the differences between the indoor and outdoor concentrations at most grid cells are more than two orders of magnitude. As the release event progresses, indoor concentration increases as more contaminants infiltrate the building envelope. At the end of the 0.5-h release, the median indoor concentrations at most grid cells have reached 10% of the outdoor values. At this time, buildings that are closest to the release source have been exposed to the release the longest, and therefore have the highest indoor concentration. Shortly after the end of the release, the indoor concentrations in some buildings exceed the outdoor levels. This can happen because once contaminants infiltrate into a building, the removal from that environment is slower than outdoors. In addition, in some grid cells, the indoor concentrations exceed the outdoor levels even before the release has stopped. These buildings are located in grid cells that are on the fringe of the plume where the outdoor concentrations fluctuate more in time. As a result of these fluctuations, the relationship between the instantaneous indoor and outdoor concentration weakens, which explains the scatter among the lower concentrations shown in Figure 6.23.

As a result of the large variability in the air infiltration rates of commercial buildings, the predicted distributions of indoor concentration also vary greatly. Figure 6.24 shows the indoor concentrations predicted at two locations not far from the release location. One grid cell is located in census tract 103102, which is in the direct pathway of the moving plume. As a result, the outdoor concentration is maintained an elevated level that is a relatively constant over the entire release duration. The peak indoor concentration expected in the leakiest 5% of commercial buildings is roughly 10% of the time-average concentration outdoors during the release. The other grid cell in census tract 103601 is slightly further away, located about 500 m from the source. Buildings in this grid cell tend to be leakier, as is reflected in the faster decay in the indoor concentration after the plume has passed. This grid cell only encounters the fringe of the plume, which explains the more intermittent outdoor concentration time profile. As a result, the peak indoor concentration only reach 4% of the peak outdoor value, even though the commercial buildings located in this grid cell are predicted to be twice as leaky as those in the other grid cell. As the release continues, the differences among buildings narrow. The reason for decreasing indoor concentration variability with time is because buildings with higher air infiltration rates also facilitate faster exfiltration. While the lower indoor concentrations in tighter buildings remain relatively stable with time after the plume has passed, the concentrations in leaky buildings quickly decrease, thus reducing the difference.

As the plume traverses the model domain and encounters areas with potential residential buildings, a comparison between the two types of buildings reveals that the indoor

concentrations in commercial buildings are on average lower than their residential counterparts (Figure 6.25). Depending on the types of buildings present in the census tract, the peak indoor concentrations are predicted to be two to three times lower in commercial buildings than in residential buildings. However, not all commercial buildings are predicted to have lower indoor concentrations than houses. In some census tracts, such as tract 102600, the leakiest 5% of the commercial buildings are expected to have higher indoor concentrations than in most houses. On the other hand, there are also areas where the predicted peak indoor concentrations in commercial buildings are all lower than in residential buildings (e.g. tract 103101). After the release has stopped, tighter buildings can trap the infiltrated gas for a longer period of time. As a result, indoor concentrations in commercial buildings that are quite low early in an event can still lead to substantial exposure. This shifts the important period of exposure towards times after the plume has passed in commercial buildings, perhaps even more so than in residential buildings. In turn, this feature might increase the potential importance of punctual termination of shelter-in-place in commercial buildings, relative to its importance in the residential sector.

6.5.3 Shelter-in-Place Characteristics of Commercial Buildings

Much of the discussion about SIP effectiveness of residential buildings also applies to commercial buildings because of the similarity in indoor concentration time-profiles relative to the outdoors. Lowering the peak indoor concentration means that buildings are most effective at protecting occupants if the chemical dose-response relationship is

nonlinear with toxic load exponent $m > 1$. Prompt termination after the plume has passed is especially important to limit exposure in cases where the dose-response relationship to the chemical is linear. Sorption of the toxic chemicals to indoor surfaces can significantly improve SIP effectiveness, especially in the case of a linear dose-response. Even though the sorbed chemical may be released back into the room air through desorption, this is expected to occur at rates slow enough that it is unlikely to pose serious acute health effects. SIP effectiveness, measured in terms of the casualty reduction factor, is expected to be the highest when the release duration is short, provided that SIP is initiated promptly. In catastrophic-scale events, however, some casualties can be expected even among those who take shelter. These events can be caused by large amount of very toxic chemicals being released into the atmosphere, or when the meteorology suppresses dispersion and the toxic plume lingers in the same area for a long period.

Nonetheless, certain characteristics of the commercial building stock can lead to differences under SIP scenarios relative to their residential counterparts. Commercial buildings tend to have air infiltration rates that are lower than those of residential buildings, which lead to lower indoor concentrations during the early stages of an event. However, there is also more variability in the air infiltration rates in the commercial building stock. Some of the leakiest commercial buildings in Oklahoma City are expected to be more leaky than residential buildings. In an acute release event, the indoor concentration in this small portion of the building stock might reach levels that are dangerous for the occupants taking shelter. Even though the majority of the commercial buildings are likely to have relatively lower indoor concentrations, the number of

potential casualties among those who take shelter in commercial buildings might still be significant, relative to the number estimated for residential buildings.

Figure 6.26 shows the estimated fraction of the population with indoor exposures high enough to exceed the toxic load limit in commercial and residential buildings. There are two census tracts that do not contain any single-family detached units. Thus, no indoor predictions for residential buildings are made in those grid cells. In areas where both commercial and residential predictions are made, it is clear that lower proportions of the sheltering population are expected to exceed the toxic load limit for those who take shelter in commercial buildings as compared with residences. However, in the outer edges of the plume, there are some areas where almost all who shelter in residential buildings are predicted to be free of potential adverse health effects, whereas a small fraction (10 to 20%) of those who shelter in commercial buildings might have exposures that exceed the toxic load limit. This is because the most leaky commercial buildings in these areas are predicted to have higher air infiltration rates than most residential buildings, as illustrated earlier in Figure 6.25.

Figure 6.27 shows the predicted number of people with exposures exceeding the toxic load limits as the release progresses. As expected, SIP in commercial buildings is more effective than single-family homes when $m = 1$. However, the method of scaling simulations for different toxic load exponents in order to give the same number of potential casualties from outdoor exposures affects the casualty estimates for residential buildings in an unusual manner. At high values of the toxic load exponent, adverse health

effects only occur in areas of high concentrations. Since there are no single-family detached units in the two census tracts adjacent to the release location, the predicted number of potential casualties for residential SIP drops to zero when the toxic load exponent is 2 or 3. On the other hand, this method of scaling among simulations with different toxic load exponents affects the assessment for commercial buildings in a more predictable way.

At a toxic load exponent of $m = 1$, a lesser fraction of people sheltering in commercial buildings are expected to suffer from adverse health effects compared to those in residential buildings (Figure 6.27). However, the difference between the two building classes in terms of casualty reduction is small. Part of the reason is because residential buildings are not present near the release source. The outdoor concentrations faced by most residential buildings are therefore more benign than those faced by commercial buildings. If the effect of spatial population distribution is removed from the simulation by assigning equal numbers of people to each grid cell both in the commercial and residential buildings[16], then the difference in their SIP effectiveness is larger (Figure 6.28). For the case $m = 1$, owing to the lower air infiltration rates in commercial buildings, roughly 72% of the people taking shelter in buildings for the entire 2 h can avoid acute adverse health effects. In residential buildings, only 40% of the population would be free of adverse health effects under these conditions. When the influence of the

[16] For the two census tracts that do not have any houses present, the air leakage distribution from a neighboring census tract is used to compute the air infiltration rates for this simulation.

spatial population distribution is included, these fractions become 66% and 58% in commercial buildings and residential buildings, respectively, as illustrated in Figure 6.27.

Table 6.7 shows the predicted fraction of people that can avoid adverse health effects by means of shelter-in-place, as evaluated at different toxic load exponents. These fractions correspond exactly to the casualty reduction factor (CRF) as defined in Chapter 2. The CRF is also evaluated at two specific times in the simulation: 0.5 and 1.5 h after the end of the 0.5-h release. The former time represents SIP effectiveness that could be achieved by prompt termination soon after the release has stopped. The latter time represents a case where there is more time lag between when SIP could safely be terminated (roughly 15 minutes after the end of the release) to when SIP is actually terminated. As observed earlier in the analysis of residential buildings, for contaminants with a high toxic load exponent, prompt termination of SIP becomes relatively unimportant, as compared with contaminants for which $m = 1$.

6.5.4 Normal Operating Conditions

Operation of mechanical ventilation systems can greatly increase the air-exchange rate of commercial buildings. During daytime hours, most buildings would be operating under such conditions unless advance notification to shelter-in-place has been effectively communicated to the building managers and the guidance has been effectively implemented. As discussed in Chapter 5, the air-exchange rates measured in commercial buildings are in the range of 1 to 3 h^{-1} and are much higher than air infiltration rates.

Consequently, an erosion of SIP effectiveness is expected if the mechanical ventilation systems of commercial buildings remain in operation during a release event. Unlike the case of residential buildings for which only a moderate fraction is expected to have open windows under favorable weather conditions, the majority of commercial buildings, especially those that are large, are likely to be mechanically ventilated whenever they are substantially occupied. To properly model the added air-exchange rates of building would require knowledge about the fraction of outdoor air the system utilizes, which can vary according to several factors. Here, it is assumed that all mechanical ventilation systems introduce an additional level of 0.5 h^{-1} or 1 h^{-1} on top of the air infiltration rates modeled. Consequently, the air-exchange rates of buildings are in the range of 0.5 to 2 h^{-1} in one case, and 1 to 2.5 h^{-1} in the other before SIP is initiated. It is also assumed in this analysis that there is no loss of chemicals to the filters and ductwork in the ventilation system. For a conventional mechanical ventilation system exposed to a gaseous contaminant, this modeling assumption is reasonable. Note though that properly designed, installed and maintained air-filtration and air-cleaning systems could be effective at removing certain types of contaminants from a building's air supply and thereby provide improved SIP effectiveness (NIOSH, 2003).

Keeping all other input parameters the same, the SIP effectiveness of commercial buildings can be affected adversely and substantially by the additional air exchange (Figure 6.29 and Table 6.8). Erosion of effectiveness is most severe when the toxic load exponent is 1. By the time the outdoor plume has moved out of the model domain, 70% to 80% of the population with outdoor exposure exceeding the toxic load limit is also at

risk of acute health consequences if sheltered in commercial buildings. This analysis indicates that for commercial buildings to provide reasonable protection for occupants against outdoor releases, the mechanical ventilation system must be shut off during and after the release event. Otherwise, large amounts of outdoor air are drawn into the buildings, carrying with it the high levels of toxic chemicals from outdoors. At high toxic load exponents, this effect is dampened somewhat. However, relative to the effect of natural ventilation in residences (Chapter 4), the loss in SIP effectiveness is even more pronounced in commercial buildings. This is because the added air-exchange rate is much larger than the baseline air infiltration rate predicted in most of the commercial building stock. By shifting the entire air-exchange rate distribution to higher values, much of the potential benefit of shelter-in-place fades throughout the exposed region. This loss in effectiveness is amplified in this case study by the relatively short release duration.

6.5.5 Sorption to Indoor Surfaces

As in residential buildings, sorption of toxic chemicals onto indoor surfaces would tend to improve the SIP effectiveness of commercial buildings. However, depending on the types of commercial buildings, the amount and types of indoor surfaces can be very different from those found in residential settings. For example, an empty warehouse or a large indoor stadium is likely to have a small surface-to-volume ratio (S/V [=] m^2/m^3) of mostly hard surfaces, whereas retail stores and offices can have much higher S/V, commonly including carpets and other plush furnishings that may exhibit higher degrees of sorption. The sorption studies reviewed in Chapter 4 were mostly conducted to

represent generic indoor environments that are not specific to either residential or commercial buildings. Among commercial buildings, however, larger variability in sorption characteristics is expected because of the wider range in the building types present. Despite these expectations, lacking detailed data on which to base a refined analysis, the same sorption rates presented in Table 4.4 of Chapter 4 are used here.

Figure 6.30 shows the effect of sorption to indoor surfaces on the SIP effectiveness of commercial buildings. In these simulations, all commercial buildings are assumed to have implemented SIP measures at the start of the release, specifically turning off mechanical ventilation systems. At the low air infiltration rates characteristics of commercial buildings, sorption is quite effective at removing chemicals from the indoor air. At the end of the 2-h simulation, as much as 44 to 88% of the potential casualties for those who took shelter indoors could be avoided if sorption is in effect for the $m = 1$ case. As observed in residential buildings, strong sorption of chemicals on indoor surfaces combined with slow desorption rate constants means that post-release exposure to indoor residual contaminant may be relatively unimportant. Most potential casualty estimates cease to increase shortly after the release has stopped.

However, if mechanical ventilation systems continue to operate, the large rate of induced air exchange will supply contaminants that competes with sorption in removing chemicals from the indoor air. Figure 6.31 shows the effect of sorption to SIP effectiveness when 0.5 h^{-1} is added to the air infiltration rate of all commercial buildings. For the case $m = 1$, the reduction in casualties from the no sorption case to the moderate

or strong sorption cases is only 15 to 43%. At higher toxic load exponents, the estimated reduction in potential casualties caused by sorption is also less than if the mechanical ventilation system was not running, but the differences between the two cases are not as large. In residential buildings, sorption to indoor surfaces is sufficient to ensure satisfactory SIP effectiveness even in cases in which the windows were left opened. The reason is partly because there, it is assumed that only 40% of the residences have their windows opened before SIP, and the remaining 60% of the residences are not affected by the pre-sheltering conditions. For commercial buildings, since the large majority is likely to be mechanically ventilated, all are modeled to have elevated air exchange before SIP. The other reason that sorption is less capable of counterbalancing the loss in SIP effectiveness in commercial buildings is because the additional 0.5 h^{-1}air exchange is high relative to the air infiltration rate distribution. Roughly 65 to 85% of the commercial buildings are predicted to have air infiltration rates lower than 0.5 h^{-1} (Figure 6.22). Compare this to the cases modeled in Chapter 4 where in one case, 80% of the residences were assumed to have +0.3 h^{-1} before SIP; only about 10 to 20% or so of the residences have air infiltration rates lower than this value. To reiterate, punctual shut down of mechanical ventilation systems is very important for maximizing SIP effectiveness in commercial buildings.

6.5.6 Shelter-in-Place Initiation Time Delay

As discussed in Chapter 4, significant time delay may occur between the moment when a release event starts to when SIP is fully implemented in a community. The response time

for officials to identify and decide to instruct the community to shelter-in-place might be different if the release were to occur in the downtown part of a city. One would hope that an expedited response might be possible given the potentially large number of people at risk of exposure. On the other hand, while shutting down the mechanical ventilation system might be simple in small buildings, the process can be complex and time consuming in larger buildings. The time needed to advise building managers to shut down their buildings can also be substantial. The survey data reviewed in Chapter 4 do not address these issues in a manner that is specific to commercial buildings in a downtown area. In the present analysis, 10- and 30-minute SIP initiation time delays are modeled to examine how they might affect SIP effectiveness. Even though these time delays are not supported by empirical data, they seem reasonable for scenarios where informed and well-prepared building managers are in place.

Figures 6.32 to 6.34 show the effect of initiating SIP with different initiation time delays on the predicted effectiveness (see also Table 6.9). As observed in the analysis of residential buildings, SIP initiation time delay affects effectiveness the most in the case of a linear dose-response relationship ($m = 1$) and for non-sorbing contaminants. If either the dose-response relationship is nonlinear with $m > 1$ or the chemical sorbs moderately or strongly onto indoor surfaces, then a casualty reduction of at least 50% relative to the outdoors can be expected. However, as explained earlier, sorption alone is not sufficient to offset the large loss in effectiveness when the air-exchange rates in commercial buildings are high. If the chemical is only moderately sorptive on indoor surfaces, then as

little as a 20 to 30% reduction in potential casualties relative to the outdoors can be expected.

Significant improvement in SIP effectiveness is observed by reducing the initiation time delay from 30 to10 minutes. Shortening the response time in this way can cut casualty estimates indoors by half for the higher toxic load exponents. Even with a linear dose-response, a similar level of improvement can be expected if sorption is effective in removing some chemicals from the indoor air. The only case for which even a 10-minute SIP initiation delay cannot be tolerated without significant loss in SIP effectiveness is when $m = 1$ and there is negligible sorption on indoor surfaces. Many toxic chemicals would sorb and nonlinear dose response with $m > 1$ is common for acute exposures. If, however, SIP cannot be successfully initiated until after the release has already stopped, then little can be gained by instructing building managers to shut off ventilation systems. This is illustrated in Figures 6.34 to 6.36 by comparing the casualty estimates from the 30-minute delay simulations with the results from the case where SIP is not initiated at all (i.e. mechanical ventilation systems remain on during the entire 2-h simulation).

6.5.7 Summary

Even though the analysis has only been performed on one test location and for one release condition, it illustrates the key similarities and differences between commercial and residential buildings in their SIP effectiveness that are expected to be generally true. Commercial buildings are tighter than houses on average, but there is also a wider

variability in the distribution. A fraction of commercial buildings is therefore likely to be more leaky than typical residences. However, depending on the scale of the release and the spatial distribution of commercial and residential buildings in relation to the release location, the overall casualty estimates for those who shelter might not differ markedly from one building class to another. Spatially, a wider area of commercial buildings may be adversely affected by the plume, due to more leaky buildings in the tail of the distribution.

Turning off the mechanical ventilation system is essential for commercial buildings to provide a high degree of protection to the occupants. At high air-exchange rates, even removal of chemicals by sorption to indoor surfaces might be insufficient to make up for the loss in effectiveness. For a short release such as the 0.5-h event modeled here, it is important to implement SIP soon after the start of the release. Otherwise, little is gained if buildings managers are unable to shut off ventilation systems until after the release has already stopped. Longer releases, like those simulated in Chapter 4, are less constrained by the tight time requirement shown here.

6.6 Model Evaluation and Limitations

In this section, a qualitative critique is presented on some key limitations of the model. Key model uncertainties are also discussed, with the focus on the relative importance among contributing sources of uncertainty. Finally, some selected aspects of model limitations will be evaluated here in greater detail.

One method of validating model predictions would be to conduct experiments in which the outdoor and indoor concentrations were measured simultaneously. Measurements would need to be made in multiple buildings and at various distances from the release source. The outdoor concentrations would need to be monitored outside of these buildings. Inside the buildings, measurements would need to be made at various locations, because indoor concentrations would likely not be uniform. Time-resolved measurements would be needed to characterize the temporal profile of the measured indoor concentrations, which further increases the experimental effort. Ideally, meteorology would be monitored at all key building sites. Full cooperation from building owners and managers would be essential, as control and monitoring of the mechanical ventilation system is required to distinguish between air infiltration and ventilation. The air leakage characteristics of each of the monitored buildings would need to be quantified beforehand, meaning that both pressurization and tracer gas tests would need to be carried out.

The time and effort required to perform such experiments can be quite extensive. The atmospheric dispersion study carried out in Oklahoma City, 2003 (briefly described in Section 6.2) measured the indoor concentrations in four buildings located 0.3 to 0.7 km from the source of the release. Twelve tracer gas (SF_6) releases were performed outdoors with concurrent measurements indoors. When the analysis of this set of measurements becomes available, it can be used to compare experimental results with model predictions. However, such comparison alone cannot explain the disagreements without first evaluating the possible sources of uncertainty from each modeling step. With only

four buildings measured, the comparison would be insufficient to directly address most of the between-building variability predicted by the model. Furthermore, there are important intermediate steps in obtaining the model predictions that cannot be verified by the measurements alone, such as building occupancy estimates. A step-by-step evaluation of the key sources of model uncertainty and limitation is therefore warranted and is discussed below.

6.6.1 Air Leakage Characterization of Commercial Buildings

The largest uncertainty in characterizing the air leakage of buildings is the lack measurements in a statistically representative sample of buildings. Of the 192 buildings measured using pressurization tests, there are considerable clusters in terms of building types and sizes. Differences in building practices between countries can also mean that the distribution obtained might not be applicable to buildings in the US. For example, many buildings in the UK are naturally ventilated, more commonly so than in the US. If these buildings are built intentionally more leaky, then including them in the air leakage database can cause bias in the estimated distribution relative to a population of mechanically ventilated buildings. The lack of a large sample size makes identifying such dependencies challenging whether using straightforward regression analysis or more sophisticated statistical techniques. A non-representative sample can also affect the characterization of variability among buildings. By undersampling certain types of buildings, the variability estimate of the distribution might be biased low.

Relative to the issue of potential error introduced by non-representative sampling of buildings for air leakage measurements, the error estimates in the regression parameters are expected to be small. On the other hand, the most significant limitation of the regression model is likely to be the use of building floor area and height alone to describe variability in the air leakage coefficients of buildings. More advanced Bayesian analysis has identified certain types of buildings as more leaky or more tight than the rest of the sample. However, the lack of spatially resolved data on the composition of the building stock in US cities limits the utility of such findings. The relationship identified by the regression model between air leakage and building floor area and height is convenient to apply, but these explanatory parameters are merely correlated with the real reasons why some buildings are more leaky than others. Understanding the fundamental characteristics of buildings could serve to improve the reliability of the regression model. Careful building inspections could reveal key sources of air leakage in a building, but translating such individualized information about a building to modeling of the air leakage distribution of a building stock requires extensive data collection and analysis. Ultimately, a balance should be struck between the amount of detail captured by an air leakage model and the input data needed to apply the model.

6.6.2 Air Infiltration Rate Predictions

Air infiltration through the building envelope is known to be non-uniform across the different façades. Internal partitions of buildings as well as the locations of dampers, vents, air supply ducts, and other building elements can also affect where and how much

infiltration takes place. By opting for a simple model, these details are reduced to a few key input parameters in the Shaw-Tamura Infiltration Model. Uncertainty is introduced through the use of this simplified model. Uncertainty also arises in model application owing to the limited data with which to characterize the distributions of input data in a building stock. However, a comparison between the estimated air infiltration rates by sampling from the possible distributions and by assigning constants to these input parameters shows little difference between the two. Relative to the variability in air leakage coefficient, these input parameters can effectively be treated as constants when modeling a building stock. In other words, the distribution of air infiltration rates in a building stock is not highly sensitive to these input parameters.

More difficult to quantify is whether the model accurately captures certain air infiltration pathways that might be important in some types of buildings. For example, the presence of a large opening can dominate the overall air infiltration rate of the building. The air infiltration patterns in some buildings can also deviate far from the idealized case for which the Shaw-Tamura Infiltration Model was developed. Interactions between stack-driven and wind-driven air infiltration are likely to vary among buildings and also with local meteorology. Inevitably, only more complex multi-compartment air infiltration models could address these details. When modeling the air infiltration rate of an individual building, often the input parameters are used as tuning parameters to best fit the measured data. When predicting the distribution of infiltration rates across a building stock, it becomes more difficult to separate model and measurement differences into mischaracterization of the input parameters versus inherent limitations of the model.

Comparison has proven to be especially difficult when additional causes for air infiltration are present in buildings during the experiments, such as the continuous operation of system fans to promote mixing of the tracer gases.

When applying the air infiltration model, additional uncertainty is introduced by not accounting for the variability in wind speed and ground level temperature. The operating conditions of buildings can also have a large effect on the air infiltration rate. Any induced airflow within buildings by occupants can interact with air infiltration patterns. In all likelihood, the air infiltration rates in occupied buildings will be higher than the predicted values. Buildings with their mechanical ventilation system running at full recirculation will alter the distribution of indoor air pressures and thereby influence the rate of airflow across the building envelope, even when no outdoor air is intentionally drawn in by the ventilation system. The difference between the amount of air infiltration in a quiescent building and an occupied building with certain heat load and induced airflow can be substantial, especially when the driving forces for air infiltration are small.

Finally, an undesirable side effect of the modeling approach used here is that it incorporates multi-family residential buildings as part of the commercial building stock when predicting the air infiltration rate distributions in a city. This occurs because many multi-family residential buildings are likely to be misclassified as commercial buildings based on the size of their footprint area and height. This shortcoming can potentially compromise the estimation for commercial buildings, especially in areas where there are a large number of multi-family residential buildings. Nationwide, about one-fourth of the

US population lives in multi-family dwellings. In future work, the US Census Survey can help identify these potentially problematic regions. While some multi-family dwellings, such as high-rise apartment buildings, might look physically similar to some types of commercial buildings, such dwellings can have quite different air leakage characteristics because of their different structural and ventilation designs (Sherman and Chan, 2004). Further analysis of the air leakage characteristics of multi-family residential buildings is also needed to properly estimate the SIP effectiveness of that portion of the housing stock.

6.6.3 Indoor Concentration Predictions

The calculation of indoor concentrations assumes that air within the building is well mixed. While this assumption is reasonable in small spaces like houses, it likely fails in many commercial buildings especially those that are larger in size. Internal partitions in buildings can isolate certain areas from the rest of the building. For example, enclosed rooms in the interior of the building can be more shielded from the infiltrating air than the peripheral areas. On the other hand, stairwells and elevator shafts can enhance air exchange between floors. When the ventilation system is left running, air within the building will tend to be more well-mixed. In this case, the interconnectivity among the different parts of the building is largely determined by the design and operation of the air-handling units.

In the simplest case beyond a single well-mixed zone, the building can be modeled as having two well-mixed zones. See Figure 6.35 for a schematic of a two-zone configuration. Two key parameters determine the difference between the indoor concentrations in these two zones. The first is the relative volume of the two zones, denoted by V_p (m^3) and V_c (m^3), where p and c stand for perimeter zone and the core zone respectively. The second is the airflow rate between the two zones, denoted by Q_c (m^3/s), relative to the airflow rate between the perimeter zone and the outdoors, denoted by Q_p (m^3/s). It is further assumed that there is no direct airflow between the core zone and the outdoors. The governing equations for the indoor contaminant concentration in these two zones owing to an outdoor release event are as follows:

$$\frac{dC_p(t)}{dt} = \frac{Q_p}{V_p} C_{out}(t) - \frac{Q_p}{V_p} C_p(t) - \left[\frac{Q_c}{V_p} C_p(t) - \frac{Q_c}{V_p} C_c(t) \right]$$
$$\frac{dC_c(t)}{dt} = \frac{Q_c}{V_c} C_p(t) - \frac{Q_c}{V_c} C_c(t)$$

Eqn 6.2

where $C_p(t)$ and $C_c(t)$ are the indoor concentrations in the respective zones, $C_{out}(t)$ is the time-varying outdoor concentration. This coupled set of first-order differential equations can be solved analytically when $C_{out}(t)$ is represented by a simple linear relationship. A more general representation of a two-zone indoor environment is described in work by Miller and Nazaroff (2001).

To illustrate how the concentrations in this two-zone system may differ from the concentration in a single well-mixed zone, two simple cases are simulated at the same locations analyzed and presented earlier in Figure 6.24. In one, 80% of the building volume is assigned to the core zone ($V_c = 0.8V$), and the remaining 20% is assumed to be

in the perimeter zone ($V_p = 0.2V$). The second case is the reverse, where the core zone constitutes only 20% of the total building volume. In both cases, the volumetric airflow rate caused by air infiltration between the perimeter zone and the outdoors is assumed to be unchanged from the one-zone, well-mixed case (i.e. $Q_p = Q$). Furthermore, it is assumed that the volumetric airflow rate between the core zone and the perimeter zone is the same as that between the perimeter zone and the outdoor ((i.e. $Q_c = Q_p$). Consequently, the volume normalized airflow rates in the two zones, k_c and k_p (h^{-1}), are related as follows:

$$\text{Core Zone}: \; k_c = \frac{Q_c}{V_c} = \frac{Q}{f \cdot V} = \frac{1}{f} \cdot k$$

$$\text{Perimeter Zone}: \; k_p = \frac{Q_p}{V_p} = \frac{Q}{(1-f) \cdot V} = \frac{1}{(1-f)} \cdot k$$

Eqn 6.3

where f (-) is the fraction of the building volume assigned to the core zone, and is k (h^{-1}) the air-exchange rate of the one-zone, well-mixed building. Table 6.10 shows the values of k_p and k_c modeled at the two study locations. When 80% of the building volume is assigned to the core zone, this modeling scheme gives k_p that is four times the value of k_c. When only 20% of the building volume is assigned to the core zone, then k_c is higher than k_p by the same factor.

Figure 6.36 shows the predicted concentration time-profile at the two studied locations. By modeling the building volume as two zones, the infiltrated contaminants are partitioned into areas of high and low concentration. The perimeter zone of the building is subject to a higher concentration than in the one-zone case, owing to a decrease in volume of indoor air within which the chemical is diluted. The difference between the

two simulated cases, as parameterized by the value *f*, are mostly in the perimeter zone concentrations. The predicted concentrations in the core zone of the building are much less sensitive to the value of *f* chosen. In all cases considered, the rise of the indoor concentration in the core zone is more gradual relative to the single well-mixed building. The peak concentration reached in the core zone is also lowered. If people were to shelter in this inner zone of the building, their exposure to the toxic contaminants can be reduced compare to the one-zone case given that SIP is terminated soon after it is safe to do so. Depending on the specifics of the release scenarios, this can be an effective strategy to further enhance the effectivenss of SIP. Aside from adjusting the value of *f*, another method to ensure low concentration in the core zone is by reducing the amount of air exchange with the perimeter zone. For example, if Q_c is restricted to only one-half the value of Q_p while keeping all other parameters the same, the resulted C_c will only reach two-third of their values shown in Figure 6.36.

In practice, most large buildings would be expected to have more interconnected zones that are not necessarily partitioned and coupled in the same perimeter-core manner as described here. There will be multiple connections between adjacent zones and the outdoors. The outdoor concentration presented to each zone of the building can also vary. Tall buildings can experience a vertical gradient of the outdoor concentration. Large buildings might even affect the dispersion of the outdoor plume, causing areas of high and low concentrations on different façades. In the event of imperfect internal mixing, it is likely that the one-zone, well-mixed concentrations underestimate the exposure that would occur for some building occupants. On the other hand, the variability in indoor

concentrations from incomplete mixing provides an opportunity for occupants to reduce their exposures simply by entering the inner zone of the building. In that case, the one-zone, well-mixed indoor concentration predictions would be overestimates of the population exposure in buildings.

6.6.4 Exposure Assessment

With substantial variability in indoor concentrations both among and within buildings, population exposures can depend on where people are at the time of the release. Currently, the model weighs results towards buildings that are predicted to have higher occupancy based on floor area. In the case that the building occupancy estimates are biased towards certain types of buildings that are particularly tight or leaky, over- or underprediction of the population exposure can result. For example, warehouses are large buildings but contain few people. Workplaces and recreational venues will have different occupancies at different times. Spatially resolved population time-activity patterns could help to identify whether this issue is important to specifically address in future assessments of SIP effectiveness. Preferably, the data should include a building component, which gives estimated numbers of occupants in different types of buildings.

The analysis conducted so far excludes other possible routes of exposure besides inhalation. It also does not consider the benefit of SIP in reducing the severity of adverse health effects, even if it cannot be completely eliminated in some portion of the population. More detailed modeling of adverse health effects in a population should

account for the distribution of susceptibility among individuals. Better mechanistic analysis of the relationship between exposure and acute adverse health effects would facilitate such an effort.

6.7 Conclusions

The shelter-in-place (SIP) effectiveness of a building stock against a short-term, hypothetical toxic release in an urban area is modeled. Both residential and commercial buildings are included in this assessment. The air infiltration rate distributions of commercial buildings are estimated. Relative to single-family dwellings, commercial buildings tend to have lower air infiltration rates on average. However, a small fraction of the commercial building stock is predicted to have air infiltration rates higher than residential buildings. The overall SIP effectiveness of commercial buildings, measured in terms of casualty reduction relative to outdoor exposure conditions, is higher than in residential buildings. However, the difference between the two is not large because of the presence of some leaky commercial buildings with high air infiltration rates.

Significant erosion of SIP effectiveness can result if the mechanical ventilation systems remain in operation during and after the release. If mechanical ventilation systems are not turned off, the additional air exchange can limit the effectiveness of possible removal of toxic chemicals from indoor air by sorption on indoor surfaces. In some circumstances, mechanical ventilation systems can be manipulated in ways that are beneficial for SIP (Price et al., 2003). However, the general advice for operators of buildings that have not undergone careful testing and possible equipment retrofits is still to shut off their

ventilation systems. In the case of a short-duration outdoor release as is simulated here, buildings operating in normal conditions are expected to provide modest to moderate levels of protection. It is nonetheless wise to take advantage of the large effectiveness gain by minimizing the air exchange with the outdoors during an outdoor release emergency.

Key aspects of model uncertainty and model limitations have been identified. The method developed here is suitable for community-based assessment. When more detailed predictions are desired, building and site-specific models and input parameters must be used. Assessment of within-building indoor concentration variability by modeling or by literature review of existing measurements can address one of the shortcomings of this analysis. Potentially, taking shelter in the interior of a building can be a simple intervention to further reduce exposure of occupants to toxic chemicals released outdoors. However, the effectiveness and practicality of this strategy remains to be proven.

The approach used here treats all non-residential buildings as a single class. In certain areas with large distinct building types, such as airport terminals and large convention venues, more detailed simulation tools can be used to address specific SIP concerns and opportunities. For example, Edwards et al. (2005) recommend guidelines to improve airport preparedness against chemical and biological terrorism. In such large indoor environments, more advanced tools, such as multizone airflow models and computational fluid dynamics software, can be developed to describe internal airflow and pollutant transport. Even there, a community-based analysis of the type presented here can

complement the exposure assessment where clusters of buildings might also be exposed in the surrounding area.

It can be anticipated that technological advances would enhance SIP effectiveness in some high-valued buildings. For example, with the advancement of chemical sensors and algorithms to interpret their signals (Weetall, 1999; Sohn et al., 2002b), quick identification of releases near buildings could reduce response times. Implementing SIP with shorter delay could greatly enhance its protectiveness especially in commercial buildings. Using the framework of community-based analysis detailed here, it would be possible to assess different strategies to improve SIP effectiveness in a community with different types of buildings. Pre-event planning utilizing the model predictions could also help emergency responders to identify under what release scenarios SIP is most effective for the specific types of incidents most likely to occur in their community.

6.8 References

AHS, 1996. American Housing Survey for the Oklahoma City Metropolitan Area: 1996. Current Housing Reports, Series H170/96-54, US Department of Housing and Urban Development and US Census Bureau, Washington, DC.

Allwine, K.J., Leach, M.J., Stockham, L.W., Shinn, J.S., Hosker, R.P., Bowers, J.F., Pace, J.C., 2004. Overview of the Joint Urban 2003 – An atmospheric dispersion study in Oklahoma City. Proceedings, 84th Annual Meeting, American Meteorology Society, January 11-15, Seattle, WA.

Aumann, D., Sextro, R., Thatcher, T., 2004. Building vulnerability assessment & mitigation program. California Energy Commission, Sacramento, CA, and Lawrence Berkeley National Laboratory, Berkeley, CA. http://securebuildings.lbl.gov/BVAMP.html

Black D., Sextro, R., Thatcher, T., Delp, W., Chang, S.C., Wood, E., Deputy, J., Hotchi, T., Sippola, M., Sullivan, D., Gressel, M., Mead, K., Earnest, S., Blade, L., Valladares, R., Martin, S., Hammond, D., 2004. Joint Urban 2003: Indoor measurements final data report. Lawrence Berkeley National Laboratory, Berkeley, CA.

Damian, J.G., 2003. Evacuation and shelter instructions for residents of large apartment buildings. Wayne Township Fire Department, Indianapolis, IN.

Edwards, D.M., Price, P.N., Gordon, S.P., Gadgil, A.J., 2005. Guidelines to improve airport preparedness against chemical and biological terrorism (unlimited release version). SAND2005-3237, Sandia National Laboratories, Albuquerque, NM, and LBNL-54973, Lawrence Berkeley National Laboratory, Berkeley, CA.

EIA, 2003. Commercial buildings energy consumption survey, public use files. Energy Information Administration, US Department of Energy, Washington, DC. http://www.eia.doe.gov/emeu/cbecs/cbecs2003/public_use_2003/2003microdat.html

Haghighat, F., Megri, A.C., 1996. A comprehensive validation of two airflow models – COMIS and CONTAM. Indoor Air 6 (4), 278–288.

Klepeis, N.E., Nelson, W.C., Ott, W.R., Robinson, J.P., Tsang, A.M., Switzer, P., Behar, J.V., Hern, S.C., Engelmann, W.H., 2001. The National Human Activity Pattern Survey (NHAPS): a resource for assessing exposure to environmental pollutants. Journal of Exposure Analysis and Environmental Epidemiology 11, 231–252.

McPherson, T.N., Brown, M.J., 2003. U.S. day and night population database (revision 2.0) – description of methodology. LA-UR-03-8399, Los Alamos National Laboratory, Los Alamos, NM.

Miller, S.L., Nazaroff, W.W., 2001. Environmental tobacco smoke particles in multizone indoor environments. Atmospheric Environment 35, 2053–2067.

NICS, 2003. Shelter in place at your office – a general guide for preparing a shelter in place plan in the workplace. National Institute for Chemical Studies, Charleston, WV.

NIOSH, 2003. Guidance for filtration and air-cleaning systems to protect building environments. National Institute for Occupational Safety and Health, Centers for Disease Control and Prevention, US Department of Health and Human Services, Washington, DC.

Persily, A., 2004. Building ventilation and pressurization as a security tool. ASHRAE Journal, September, 18–24.

Price, P.N., Sohn, M.D., Gadgil, A.J., Delp, W.W., Lorenzetti, D.M., Finlayson, E.U., Thatcher, T.L., Sextro, R.G., Derby, E.A., Jarvis, S.A., 2003. Protecting buildings from a biological or chemical attack: Actions to take before or during a release. LBNL-51959, Lawrence Berkeley National Laboratory, Berkeley, CA.

Price, P.N., Chang, S.C., Sohn, M.D., 2004. Characterizing buildings for airflow models: what should we measure? LBNL-55321, Lawrence Berkeley National Laboratory, Berkeley, CA.

Sabiha, A.G., Devaull, J., Salmi, D., Biagi, A., Grek, K., Nelson, T., 2001. Model emergency plan for schools. Contra Costa County Community Awareness & Emergency Response (CAER) Group, Martinez, CA.

Sherman, M.H., Chan, W.R., 2004. Building airtightness: Research and practice. LBNL-53356, Lawrence Berkeley National Laboratory, Berkeley, CA.

Sohn, M.D., Sextro, R.G., Gadgil, A.J., Daisey, J.M., 2002a. Responding to sudden pollutant release in office buildings: 1. Framework and analysis tools. Indoor Air 13 (3), 267–276.

Sohn, M.D., Reynolds, P., Singh, N., Gadgil, A.J., 2002b. Rapidly locating and characterizing pollutant releases in buildings. Journal of the Air and Waste Management Association 52 (12), 1422–1432.

SWT, 2000. Texas school safety center planning manual for safe schools. Texas School Safety Center, Southwest Texas State University, San Marcos, TX, and Criminal Justice Division, Office of the Governor, Austin, TX.

Weetall, H.H., 1999. Chemical sensors and biosensors, update, what, where, when and how. Biosensors & Bioelectronics 14, 237–242.

6.9 Tables

Table 6.1 Two-step[#] method to estimate the floor area distribution of commercial buildings in census tract 102600 in Oklahoma City.

		Building Floor Area					
		<46.5 m^2	46.5 to 93.0 m^2	93.0 to 139 m^2	139 to 186 m^2	186 to 232 m^2	>232 m^2
Data (i)	All Buildings	0	7	19	35	27	112
Data (ii)	Residential Buildings	5	10	22	23	10	6
Step (I)	Difference (i) - (ii)	-5	-3	-3	12	17	106
Step (II)	Commercial Buildings	0	0	0	12 - (5+ 3+3) = 1	17	106

[#] Step (I): direct subtraction of the two floor area distributions. It compares the difference between the floor area distribution of all buildings in the census tract (i), with the floor area distribution of residential buildings in the census tract (ii). Step (II): accounts for the deficient number of buildings from previous floor area categories, and gives the final commercial building estimates. It assumes there are no commercial buildings until the difference is sufficient to account for the deficiency from all previous categories.

Table 6.2 Fraction of commercial buildings as a function of building floor area as estimated from US national data[#].

Building Floor Area	Fraction of all buildings of indicated size that are commercial buildings
<139 m^2	0.016
139 to 186 m^2	0.019
186 to 232 m^2	0.036
232 to 279 m^2	0.035
279 to 372 m^2	0.088
372 to 465 m^2	0.33
>465 m^2	0.53

[#] Based on the floor area distribution of commercial buildings from CBECS, and the floor area distribution of single-family detached units from the American Housing Survey.

Table 6.3 Building occupancy regression model results, estimated by summing number of employees and 25% of the building capacity.

Model (Eqn 6.1):
$\ln(\text{Occupancy}) = \beta_o + \beta_1 \times \ln(\text{Floor Area } [m^2]) + \beta_2 \times \ln(\text{Number of Floors}) + \varepsilon$

	Estimate	Standard Error	t-value	Significance Level
β_o	-2.53	0.0897	-28.2	>99.9%
β_1	0.748	0.0117	63.8	>99.9%
β_2	0.438	0.0222	19.7	>99.9%

Residual standard error = 1.16
Adjusted R-squared = 0.619

Table 6.4 Statistics of the predicted air leakage coefficient of buildings surveyed by the CBECS[#].

		Building Floor Area Category		
1-Story Building		< 530 m^2	530 to 1900 m^2	1900 to 9100 m^2
	Air Leakage Coefficient $[m^3/(s \cdot m^2 \cdot Pa^n)]$	GM = 3.81×10^{-4} GSD = 2.34	GM = 1.90×10^{-4} GSD = 2.28	GM = 1.04×10^{-4} GSD = 2.41
		Building Floor Area Category		
2-Story Building		<910 m^2	910 to 2400 m^2	2400 to 14000 m^2
	Air Leakage Coefficient $[m^3/(s \cdot m^2 \cdot Pa^n)]$	GM = 6.28×10^{-4} GSD = 2.25	GM = 3.51×10^{-4} GSD = 2.31	GM = 1.80×10^{-4} GSD = 2.32
		Building Floor Area Category		
3 to 5-Story Building		<1300 m^2	1300 to 3600 m^2	3600 to 17000 m^2
	Air Leakage Coefficient $[m^3/(s \cdot m^2 \cdot Pa^n)]$	GM = 6.77×10^{-4} GSD = 2.53	GM = 4.04×10^{-4} GSD = 2.36	GM = 2.28×10^{-4} GSD = 2.34

[#] Buildings are grouped into nine categories according to their floor area and number of stories when modeling the air infiltration rate distribution. Buildings with floor area above the upper limit for the largest group are modeled individually, as are all buildings that are taller than 5-story.

Table 6.5 List of simulations and their assigned codes.

Simulation Code	Toxic Load Exponent[§]	Level of Sorption on Indoor Surfaces	Additional Ventilation[#] (h^{-1})	SIP Initiation Time Delay (minutes)	Population Density[*]
6Ai, ii, iii	1, 2, 3	No	NA	0	Spatial
6Bi, ii, iii	1, 2, 3	No	NA	0	Uniform
6Ci, ii, iii	1, 2, 3	No	0.5	≥120	Spatial
6Di, ii, iii	1, 2, 3	No	1.0	≥120	Spatial
6Ei, ii, iii	1, 2, 3	Moderate	NA	0	Spatial
6Fi, ii, iii	1, 2, 3	Strong	NA	0	Spatial
6Gi, ii, iii	1, 2, 3	Moderate	0.5	≥120	Spatial
6Hi, ii, iii	1, 2, 3	Strong	0.5	≥120	Spatial
6Ii, ii, iii	1, 2, 3	No	0.5	10	Spatial
6Ji, ii, iii	1, 2, 3	Moderate	0.5	10	Spatial
6Ki, ii, iii	1, 2, 3	Strong	0.5	10	Spatial
6Li, ii, iii	1, 2, 3	No	0.5	30	Spatial
6Mi, ii, iii	1, 2, 3	Moderate	0.5	30	Spatial
6Ni, ii, iii	1, 2, 3	Strong	0.5	30	Spatial

[§] Toxic load exponent 1, 2, and 3 correspond to i, ii, and iii of the simulation codes.
[#] Additional ventilation refers to the air-exchange rate added on top of the predicted air infiltration rates in commercial buildings to simulate the effect of operating the mechanical ventilation systems. This parameter only affects the indoor concentration predictions when SIP initiation time delay is modeled.
[*] In most simulations, spatially varying population density is included in the model by using US census residential population count, and predicted occupancy in commercial buildings.

Table 6.6 List of simulations, as indicated by their designated codes (see Table 6.5), for which the estimated number of casualties are plotted in selected figures.

Figure	Simulation Codes[#]	Building Class Evaluated
6.27	6Ai, ii, iii	Commercial and Residential
6.28	6Bi, ii, iii	Commercial and Residential
6.29	6Ai, ii, iii; 6Ci, ii, iii; 6Di, ii, iii	Commercial
6.30	6Ai, ii, iii; 6Ei, ii, iii; 6Fi, ii, iii	Commercial
6.31	6Ci, ii, iii; 6Gi, ii, iii; 6Hi, ii, iii	Commercial
6.32	6Ai, 6Ei, 6Fi, 6Ci, 6Gi, 6Hi, 6Ii, 6Ji, 6Ki, 6Li, 6Mi, 6Ni	Commercial
6.33	6Aii, 6Eii, 6Fii, 6Cii, 6Gii, 6Hii, 6Iii, 6Jii, 6Kii, 6Lii, 6Mii, 6Nii	Commercial
6.34	6Aiii, 6Eiii, 6Fiii, 6Ciii, 6Giii, 6Hiii, 6Iiii, 6Jiii, 6Kiii, 6Liii, 6Miii, 6Niii	Commercial

Table 6.7 SIP effectiveness of commercial buildings estimated in the 0.5-h release simulation in terms of casualty reduction factor[#].

Toxic Load Exponent	Casualty Reduction Factor (CRF)	
	CRF evaluated at 0.5 h after end of release	CRF evaluated at 1.5 h after end of release
$m = 1$	0.84	0.66
$m = 2$	0.92	0.88
$m = 3$	0.94	0.92

[#] Definition of casualty reduction factor.

$$\text{CRF} = 1 - \frac{\text{Population (Toxic Load}_{\text{indoors}} > \text{Limit)}}{\text{Population (Toxic Load}_{\text{outdoors}} > \text{Limit)}}$$

Table 6.8 SIP effectiveness of commercial buildings estimated in the 0.5-h release in terms of casualty reduction factor, with additional air exchange to represent the mechanical ventilation system running in all buildings during the entire simulation.

Toxic Load Exponent	Casualty Reduction Factor (CRF)			
	CRF evaluated at 0.5 h after end of release		CRF evaluated at 1.5 h after end of release	
	Additional Air-Exchange Rate			
	$+0.5\ h^{-1}$	$+1\ h^{-1}$	$+0.5\ h^{-1}$	$+1\ h^{-1}$
$m = 1$	0.26	0.13	0.08	0.03
$m = 2$	0.50	0.30	0.34	0.26
$m = 3$	0.62	0.39	0.57	0.35

Table 6.9 SIP effectiveness of commercial buildings measured in terms of casualty reduction factor in the 0.5-h release, including effects of sorption[#] and initiation delay[§].

SIP Initiation Time Delay	Toxic Load Exponent (m)	Casualty Reduction Factor (CRF)					
		CRF evaluated at 0.5 h after stop of release			CRF evaluated at 1.5 h after stop of release		
		Sorption Rates					
		No Sorption	Moderate	Strong	No Sorption	Moderate	Strong
No Delay	$m = 1$	0.84	0.88 – 0.91	0.93 – 0.96	0.66	0.81 – 0.88	0.92 – 0.96
	$m = 2$	0.92	0.94 – 0.96	0.96 – 0.98	0.88	0.93 – 0.95	0.96 – 0.98
	$m = 3$	0.94	0.96 – 0.97	0.97 – 0.98	0.92	0.95 – 0.97	0.97 – 0.98
10 minute	$m = 1$	0.58	0.67 – 0.76	0.79 – 0.88	0.29	0.54 – 0.70	0.77 – 0.88
	$m = 2$	0.76	0.82 – 0.87	0.88 – 0.92	0.67	0.80 – 0.86	0.88 – 0.92
	$m = 3$	0.82	0.87 – 0.90	0.90 – 0.94	0.77	0.86 – 0.90	0.90 – 0.94
30 minute	$m = 1$	0.26	0.33 – 0.47	0.54 – 0.72	0.05	0.20 – 0.33	0.49 – 0.71
	$m = 2$	0.51	0.62 – 0.70	0.73 – 0.83	0.31	0.56 – 0.69	0.72 – 0.83
	$m = 3$	0.61	0.71 – 0.78	0.79 – 0.87	0.50	0.69 – 0.77	0.79 – 0.87
No SIP	$m = 1$	0.26	0.32 – 0.45	0.52 – 0.70	0.08	0.22 – 0.33	0.33 – 0.48
	$m = 2$	0.50	0.61 – 0.70	0.72 – 0.83	0.34	0.58 – 0.69	0.71 – 0.83
	$m = 3$	0.62	0.70 – 0.77	0.78 – 0.87	0.57	0.69 – 0.77	0.78 – 0.87

[#] Simulations are performed under various toxic load exponents and sorption rates (see Table 4.4 in Chapter 4).

[§] An additional air-exchange rate of 0.5 h^{-1} is added to all buildings to represent the effect of leaving the mechanical ventilation systems running before SIP is initiated.

Table 6.10 Modeling parameters for the two-zone analysis of the commercial buildings[#] in two grid cells in the simulation.

Ratio of Core Volume (V_c) to Total Building Volume (V)	Volume normalized airflow rate in the two zones[§]: k_p (h^{-1}) = Q_p/V_p and k_c (h^{-1}) = Q_c/V_c			
	Census Tract 103102		Census Tract 103601	
	Perimeter to Outdoor Zone (k_p)	Core to Perimeter Zone (k_c)	Perimeter to Outdoor Zone (k_p)	Core to Perimeter Zone (k_c)
$V_c = 0.8\times V$	1.30	0.325	2.28	0.57
$V_c = 0.2\times V$	0.325	1.30	0.57	2.28

[#] For the purpose of clearly illustrating the differences between the indoor concentrations predicted in the two-zone system, the building modeled has fairly high air leakage that corresponds to the 95th percentile of the distribution in the census tract.

[§] It is assumed in this simple analysis that $Q_c = Q_p$.

6.10 Figures

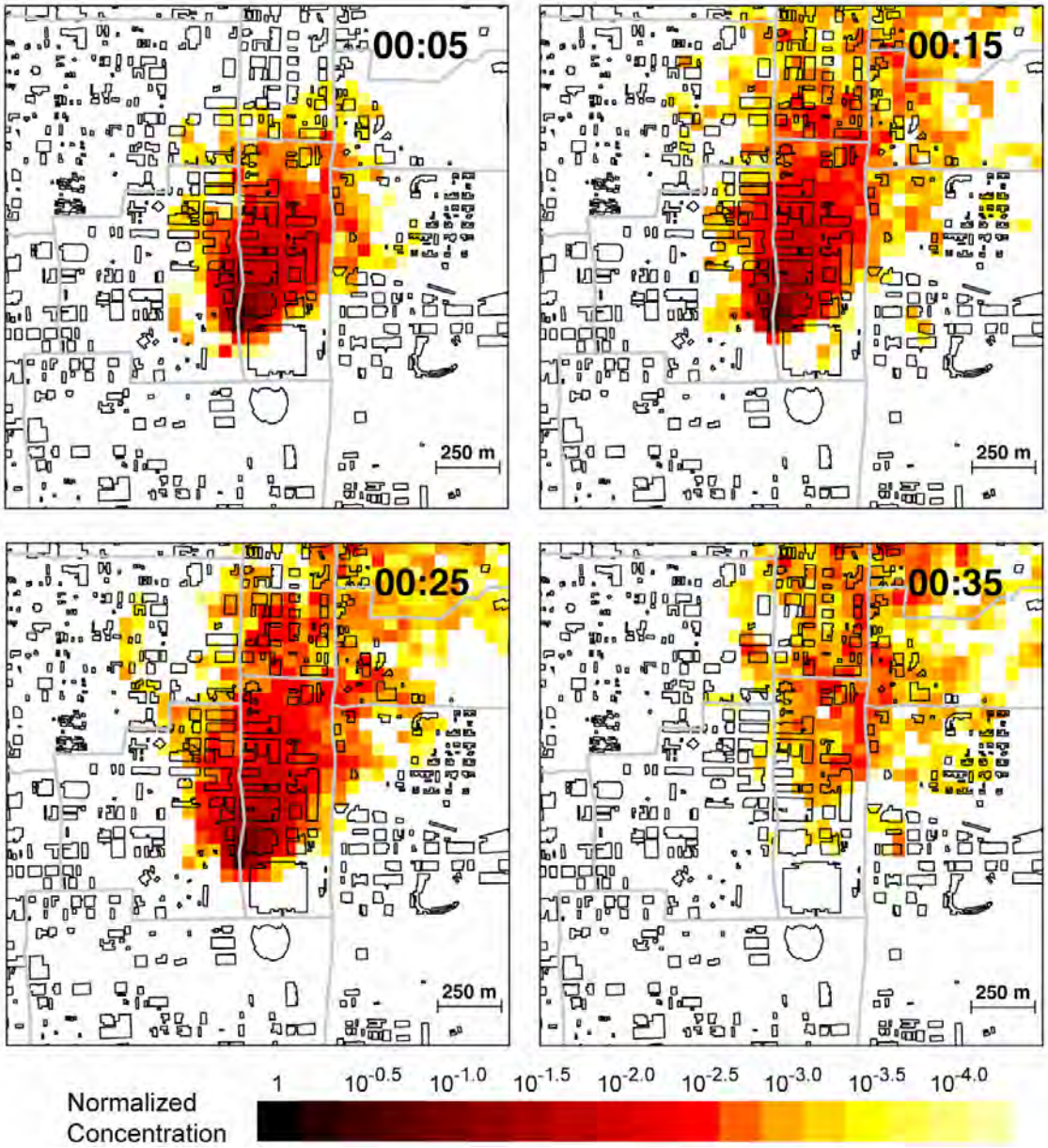

Figure 6.1 Outdoor concentrations predicted at 5, 15, 25, and 35 minutes from the onset of a 0.5-h release. Dispersion of the plume was modeled using meteorological conditions dated July 13, 2003 from 9:00 to 11:00 am. The concentrations are 1-minute averages for the 2-m plane above ground. The model domain is 2 km × 2 km. Each grid cell is 50 m × 50 m in dimension. Outlined are the building footprint areas. The census tract boundaries are shown in light gray. All outdoor concentrations are normalized to the highest value observed at the 2 m plane.

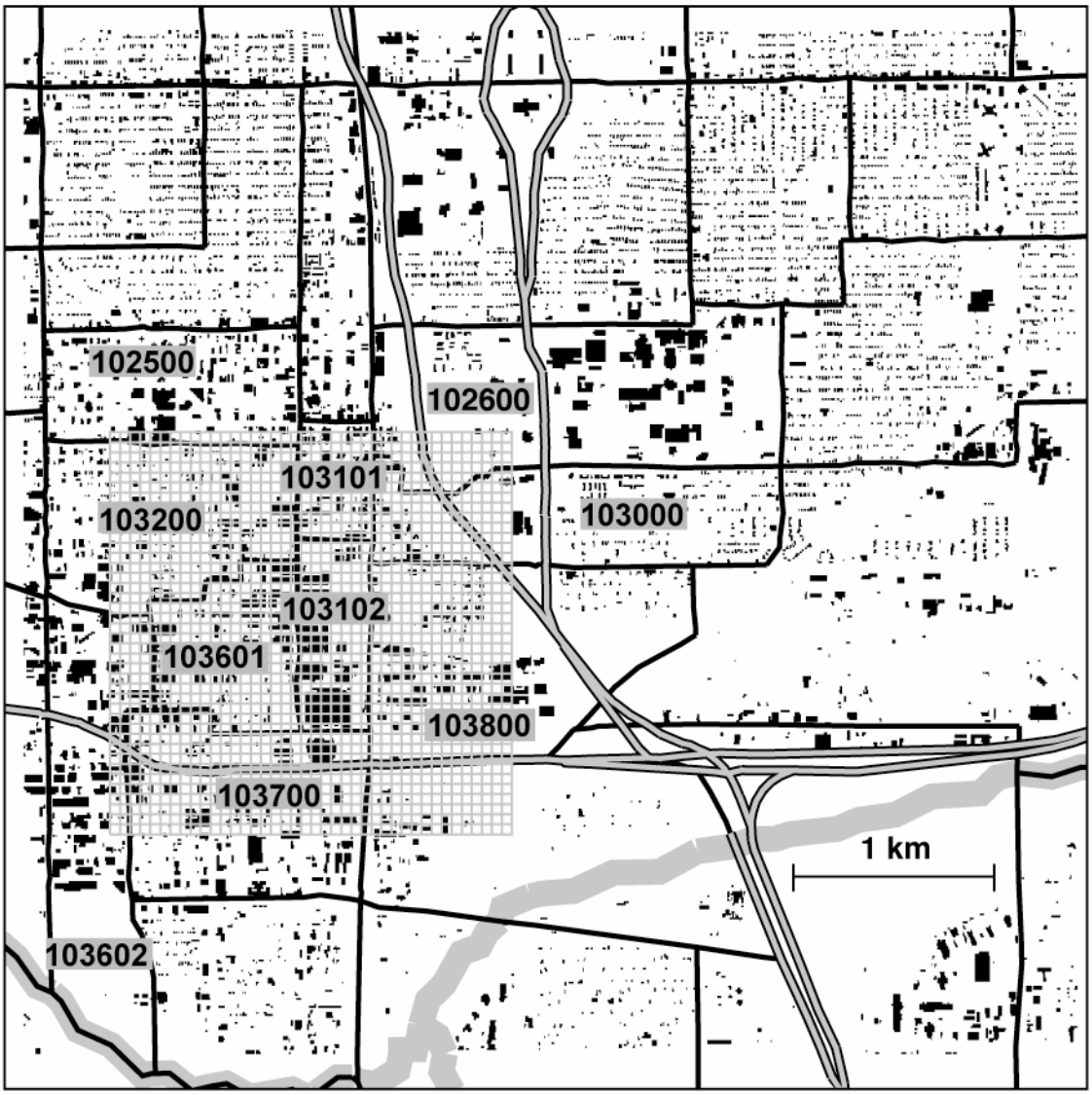

Figure 6.2 Outdoor concentration grid (gray) on the footprint of 6334 buildings in Oklahoma City contained within a 5.4 km × 5.4 km area. Census tract boundaries are outlined in black solid lines. The 10 census tracts where the concentration grid crosses are labeled with their unique tract ID number. Major interstate highways and the Oklahoma River are also shown.

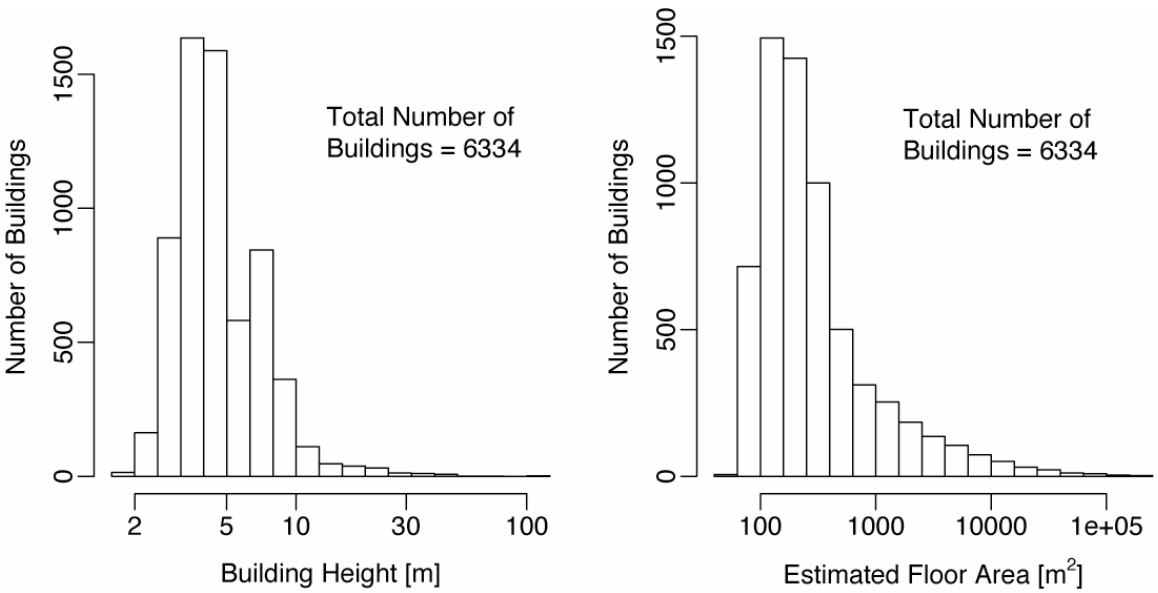

Figure 6.3 Distribution of height (left) and floor area (right) of all buildings contained in the Oklahoma City 5.4 km × 5.4 km study area. Floor area was estimated by multiplying the footprint area with the number of floors of each building. Each floor is assumed to be 3 m in height. Building heights and footprint areas were obtained from aerial images of the city analyzed using a Geographical Information System by National Atmospheric Release Advisory Center at Lawrence Livermore National Laboratory. The estimated building heights range from 1.7 to 114 m, with a median at 4.2 m. The estimated building floor areas range from 44 to 2.1×10^5 m^2, with a median at 210 m^2.

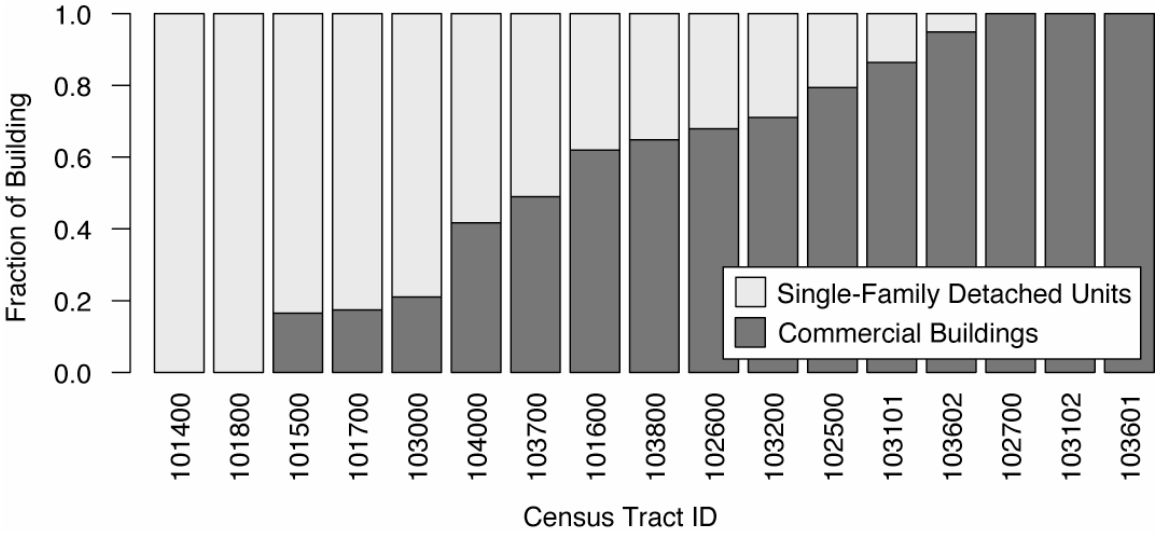

Figure 6.4 Estimated fraction of residential and commercial buildings in 17 census tracts in Oklahoma City. Two census tracts are exclusively residential, and three census tracts are exclusively commercial.

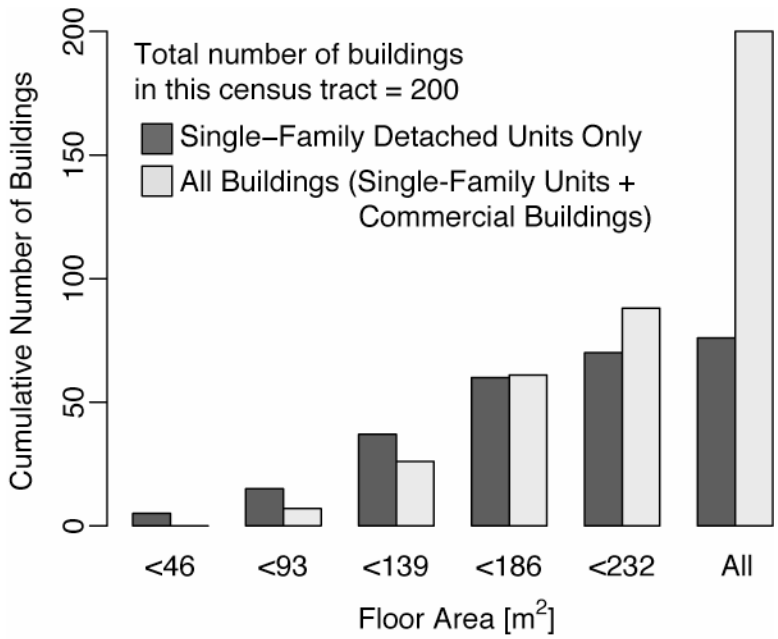

Figure 6.5 Cumulative floor area distribution of single-family detached units in census tract 101600 in Oklahoma County, and the combined distribution that includes commercial buildings. Altogether, the allocation method predicts that there are 124 commercial buildings in this census tract, most of them with floor area exceeding 232 m^2.

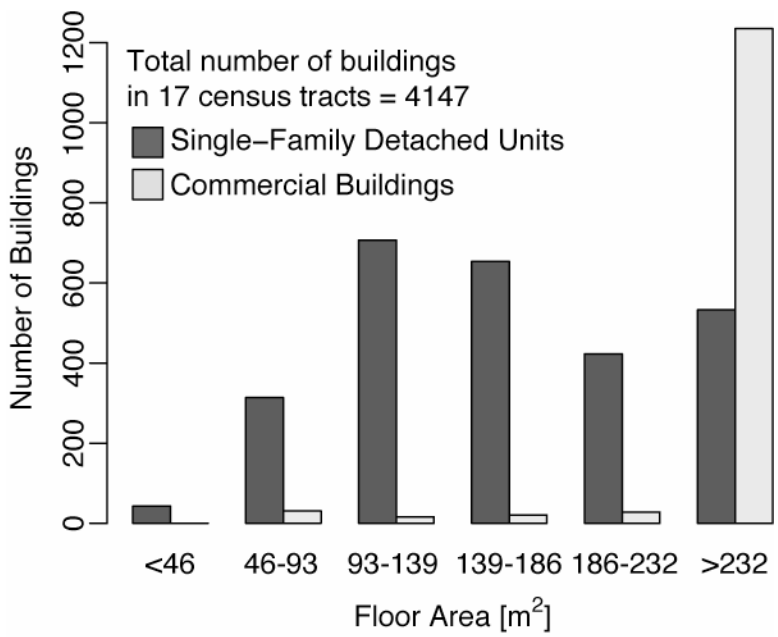

Figure 6.6 Estimated number of residential and commercial buildings as a function of floor area. These buildings are located in census tracts with boundaries that lie entirely within the 5.4 km × 5.4 km study area of Oklahoma City, as shown in Figure 6.2.

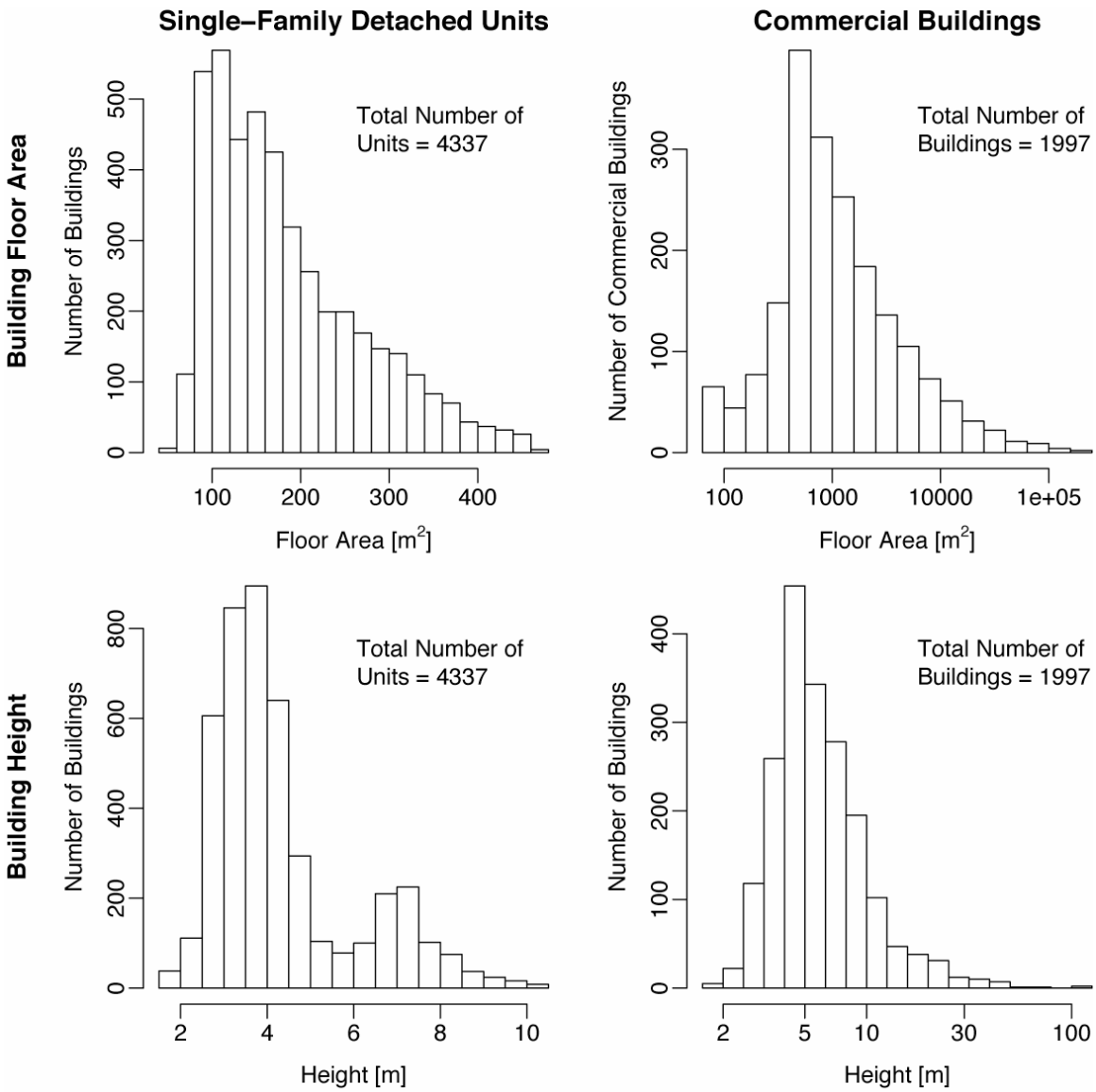

Figure 6.7 Estimated floor area and height of single-family detached units and commercial buildings in the 5.4 km × 5.4 km study area of Oklahoma City. Allocation between the two types of buildings is based on a comparison of their respective floor area distributions.

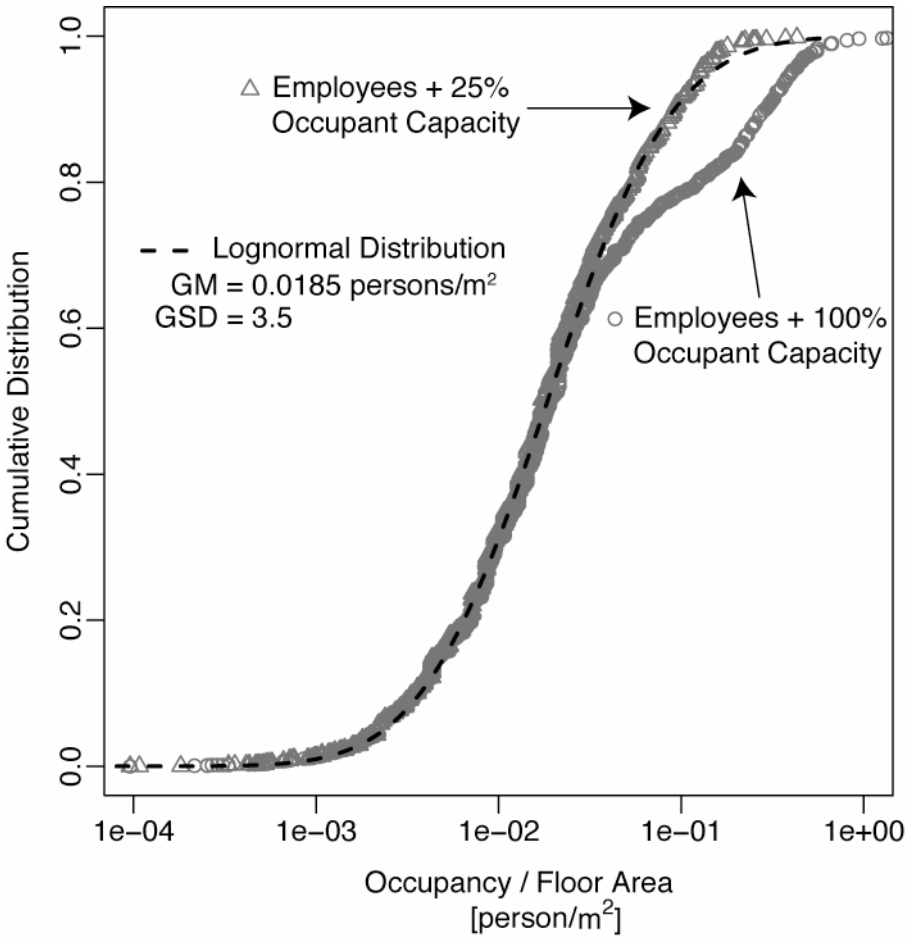

Figure 6.8 Cumulative distribution of building occupancy per floor area estimated by two methods, which differ by whether the occupant capacity reported in CBECS is counted at 100% or at 25% when computing the building occupancy per floor area. The resulting distributions are compared with a lognormal distribution with the best-fit geometric mean (GM) and geometric standard deviation (GSD) for the 25% case.

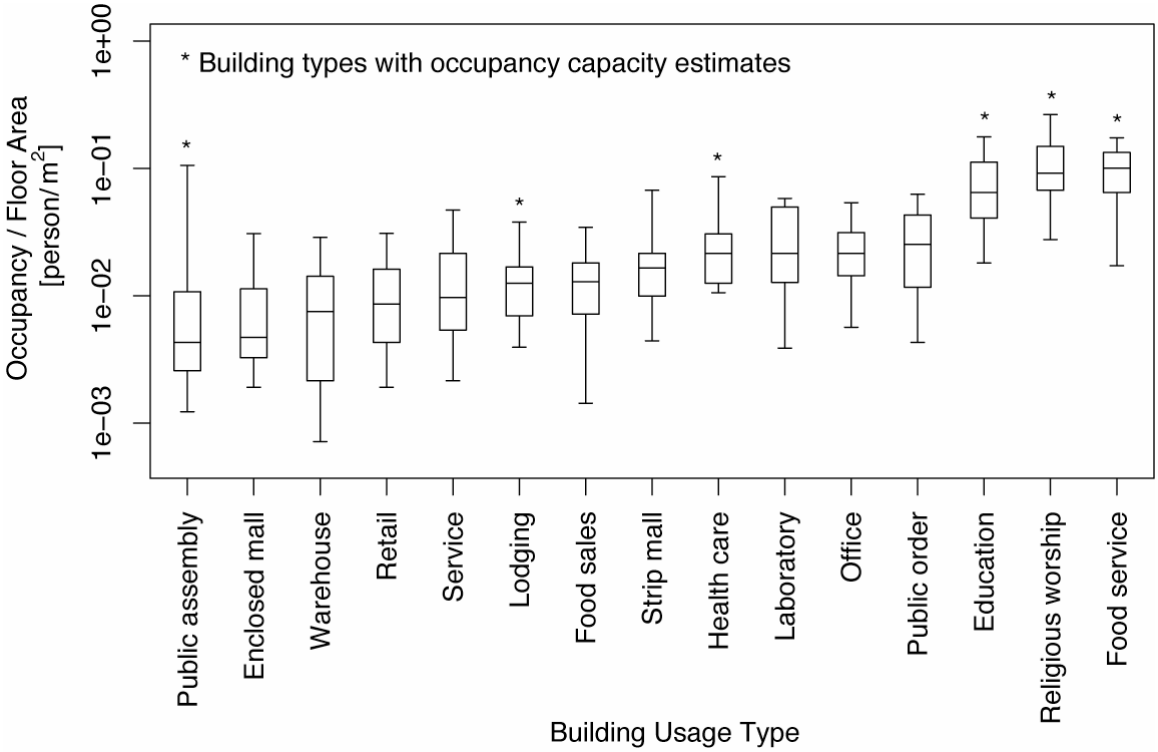

Figure 6.9 Estimated occupancy per building floor area in buildings that were surveyed by the CBECS. Building occupancy is estimated by the sum of the number of employees and the occupant capacity. Number of employees data are available for all types of buildings, whereas occupant capacity are only available for the types of buildings indicated by the symbol *, which include public assembly, health care, lodging, education, food service, and religious worship. Each lower and upper hinge signifies the 25th and 75th percentiles of the distribution. The middle bar is the median. The two whiskers represent the 5th and 95th percentiles.

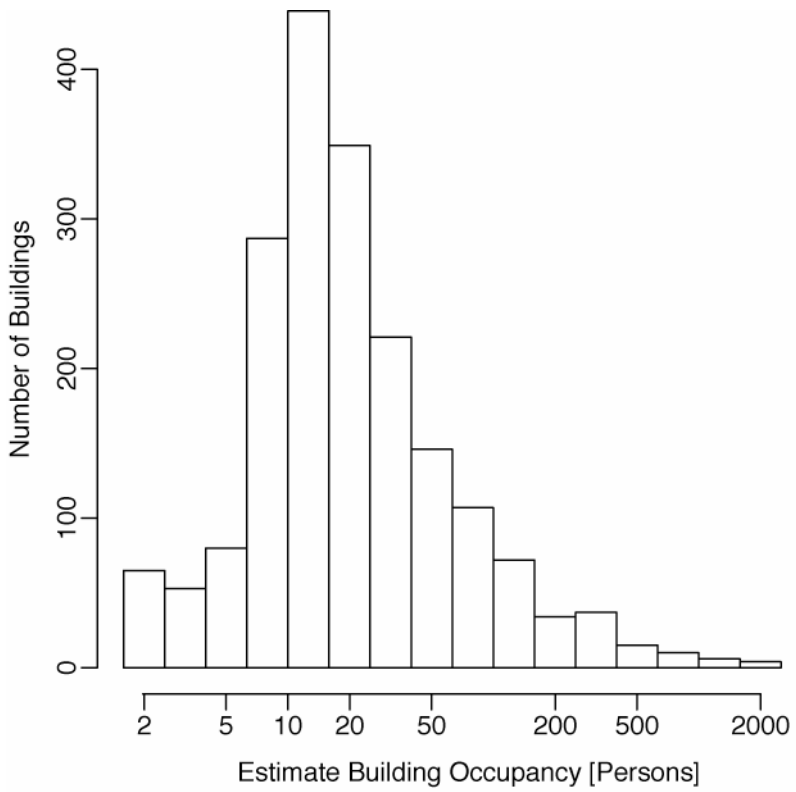

Figure 6.10 Estimated building occupancy in 1997 commercial buildings that are located in the 5.4 km × 5.4 km study area of Oklahoma City. Occupancy estimates are obtained using the regression model shown in Eqn 6.1 (error term ε not included).

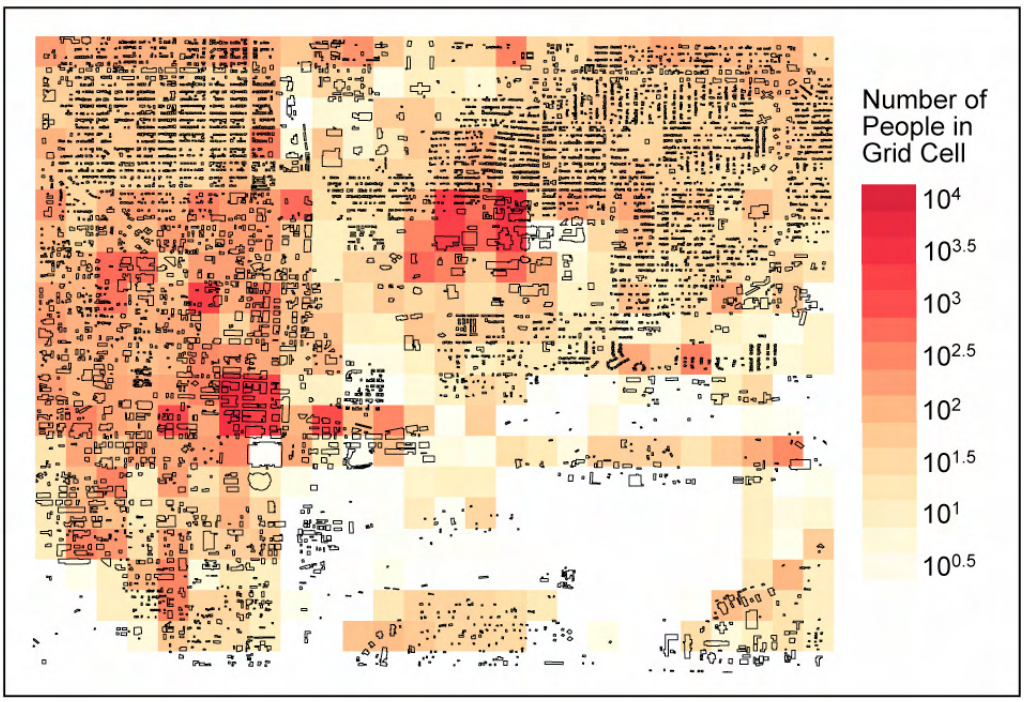

Figure 6.11 LANL daytime population estimates in Oklahoma City on a 250 m grid. Also shown are outlines of buildings located in the 5.4 km by 5.4 km study area. The figure appears to be stretched in the horizontal direction because of the change in projection system from UTM to latitude-longitude to match that used in the LANL database.

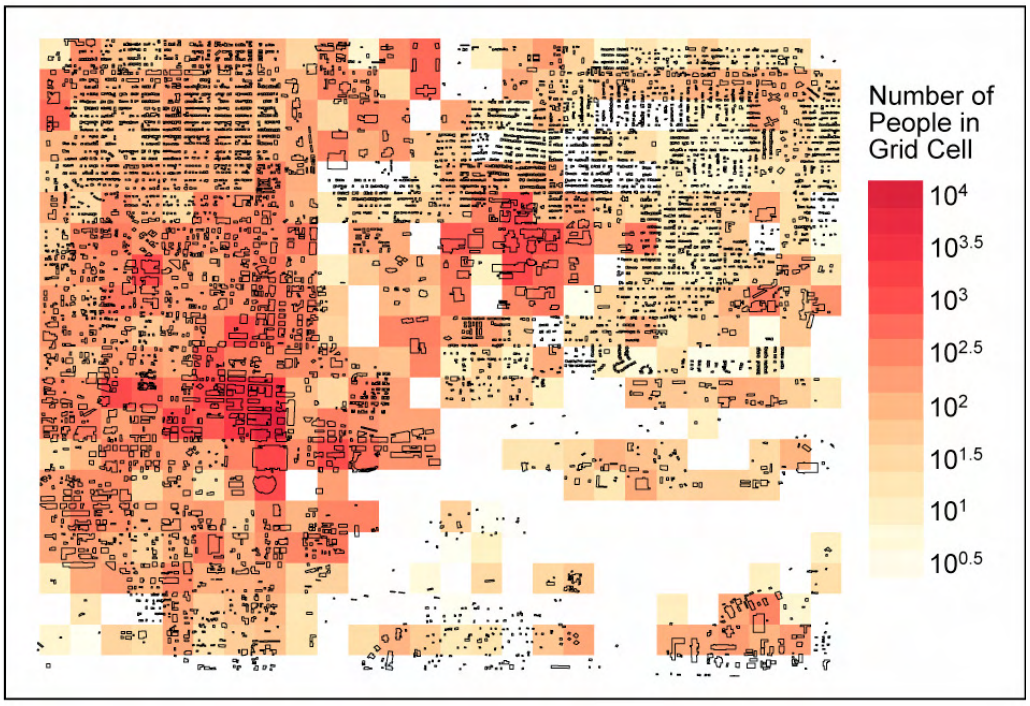

Figure 6.12 Estimated commercial building occupancy in Oklahoma City projected on the same grid used in the LANL database.

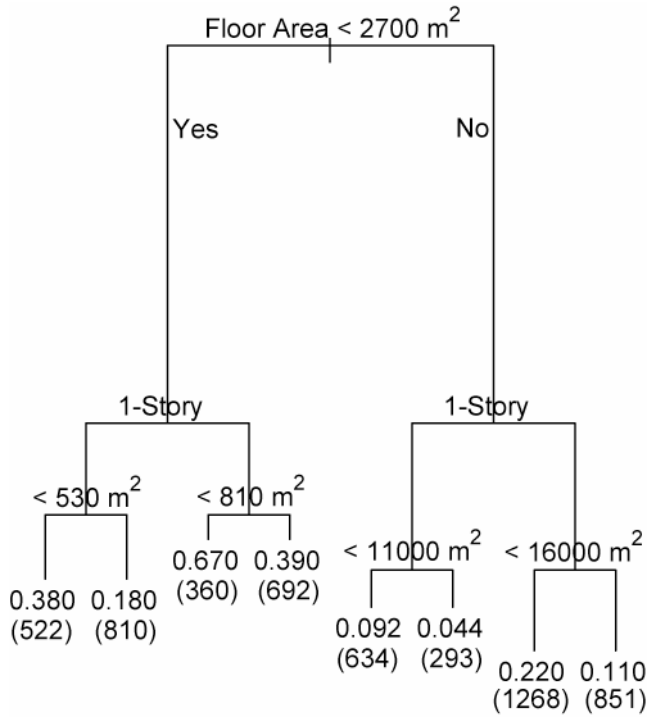

Figure 6.13 Building floor area and number of story splits identified by the classification tree method to minimize the variance of air leakage coefficient estimated for buildings in the CBECS. Each number in parenthesis represents the number of buildings that belongs to the respective group. Above these numbers are the air leakage coefficients [$L/(s \cdot m^2 \cdot Pa^n)$] that best describe the group. The length of each fork represents the amount of reduction in variance resulting from the split. A longer fork represents a more significant reduction in variance, and is therefore more important.

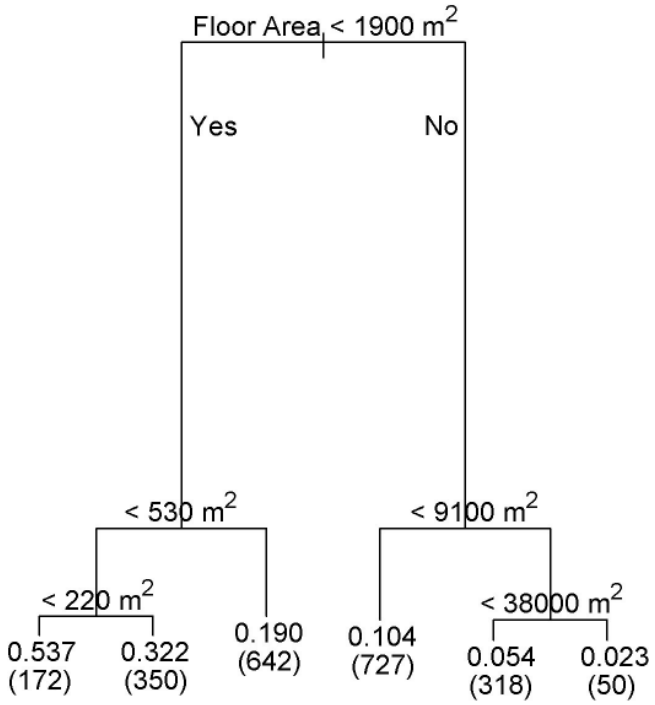

Figure 6.14 Classification tree analysis for 1-story commercial buildings surveyed in the CBECS. Only building floor area is used as the predictor variable. The two lines of results at the end of each fork are the air leakage coefficients [$L/(s \cdot m^2 \cdot Pa^n)$] that can best describe the group, and the number of 1-story buildings that have the indicated floor areas. See Figure 6.13 for additional details.

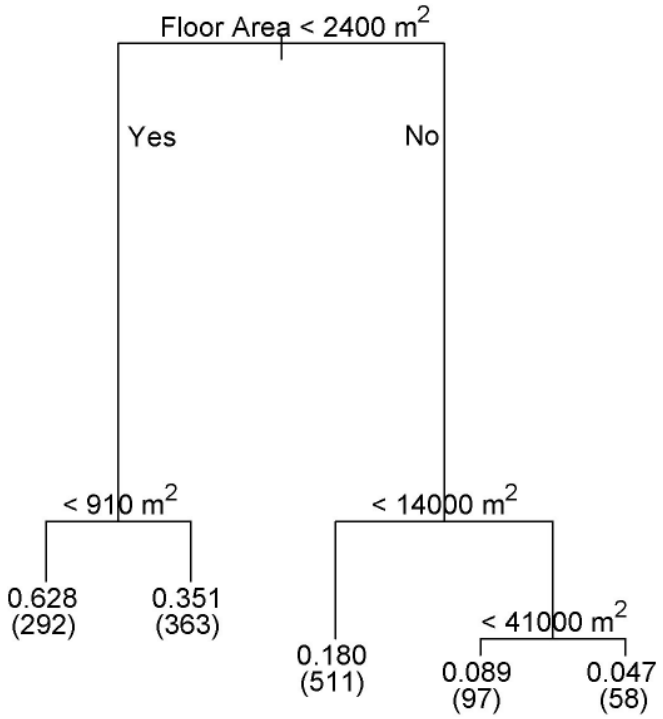

Figure 6.15 Classification tree analysis for 2-story buildings surveyed in the CBECS. See Figure 6.14 for additional details.

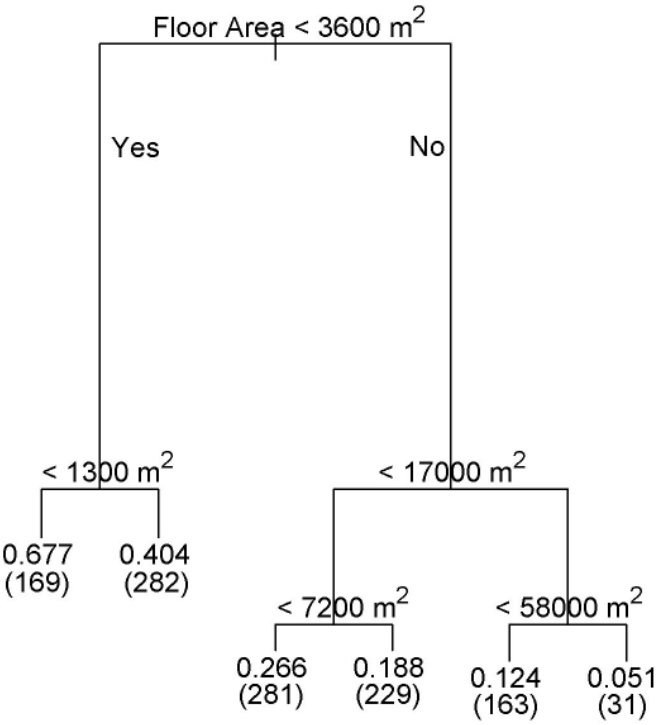

Figure 6.16 Classification tree analysis for 3 to 5-story buildings surveyed in the CBECS. See Figure 6.14 for additional details.

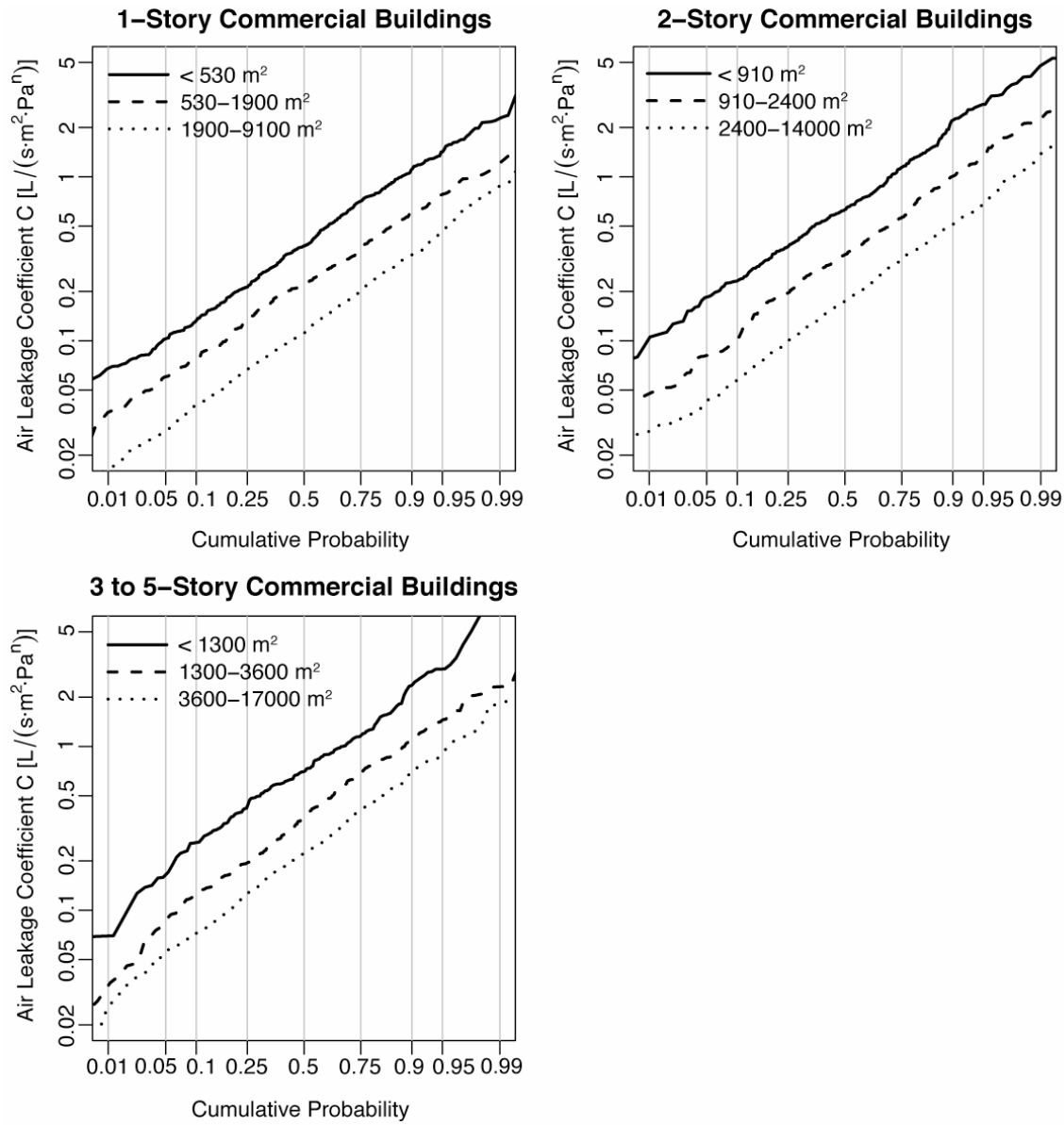

Figure 6.17 Predicted air leakage coefficient distributions of buildings surveyed in CBECS partitioned into 9 groups by their number of floors and floor area. Table 6.4 presents the summary statistics for each distribution.

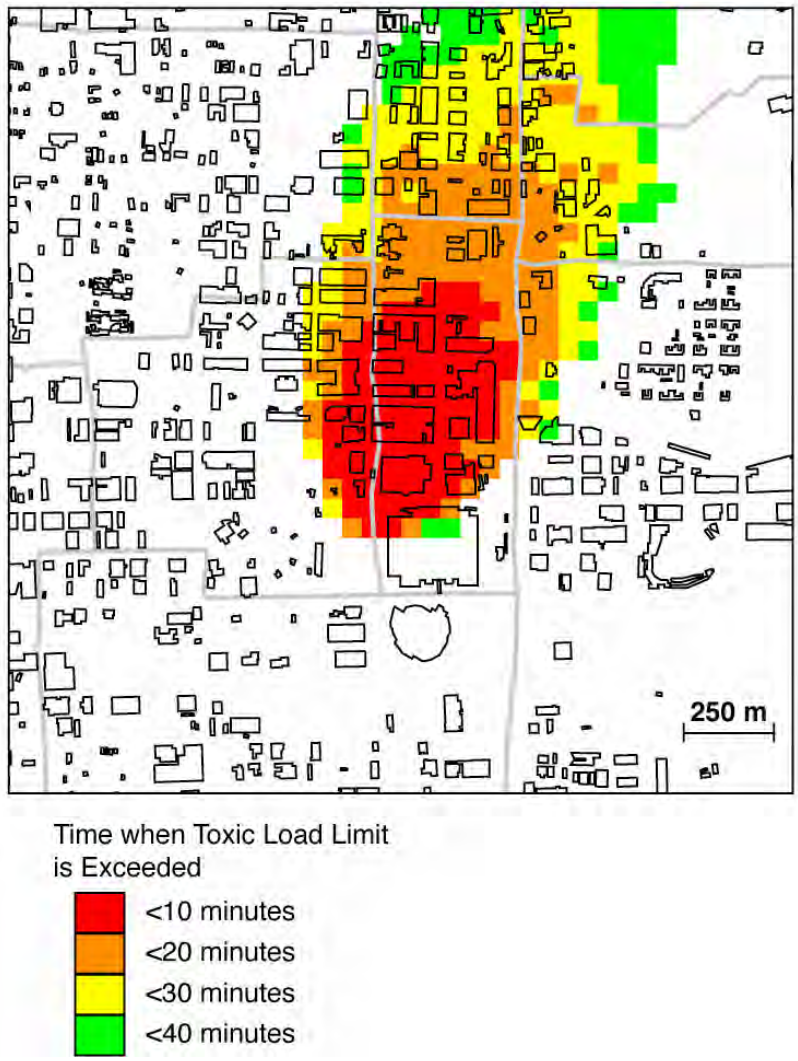

Figure 6.18 Predicted areas where exposure to the outdoor concentrations are expected to exceed the toxic load limit for the modeled 0.5-h release event. The population cumulative toxic loads are evaluated at the end of the 2-h simulation. The extent of the toxic plume that is concentrated enough to cause health concern is roughly 2 km in the windward direction. For details on the parameters used in the simulation, see 6Ai in Table 6.5.

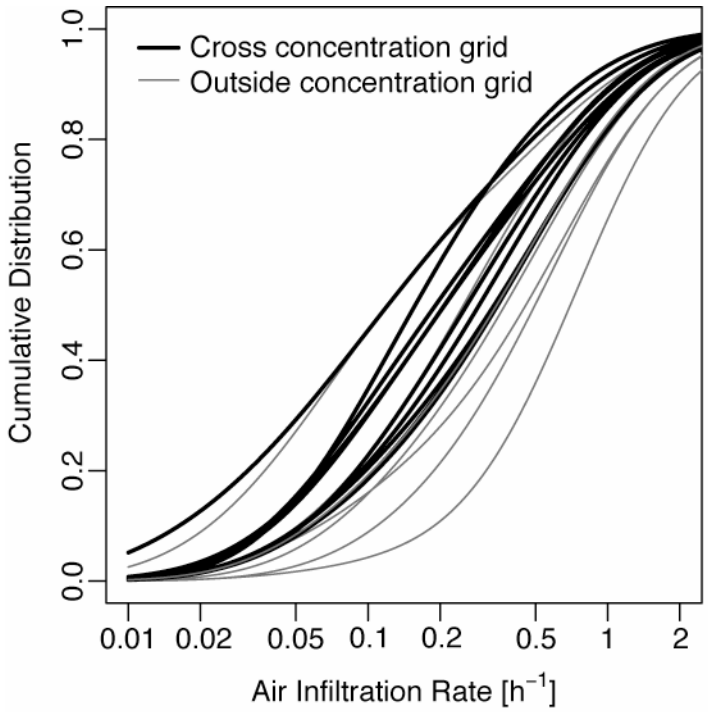

Figure 6.19 Predicted air infiltration rates of commercial buildings in 17 census tracts selected from the 5.4 km × 5.4 km study area in Oklahoma City. Highlighted are the 10 census tracts with boundaries that cross the concentration grid (see Figure 6.2). Large commercial buildings are modeled individually using the Shaw-Tamura Infiltration Model. Smaller commercial buildings are first partitioned into 9 groups according to their floor area and number of stories, and then either the Shaw-Tamura or the LBL Infiltration Model is used to predict their air infiltration rates. The cumulative distributions represent the predicted number of buildings having certain air infiltration rate or less in a census tract.

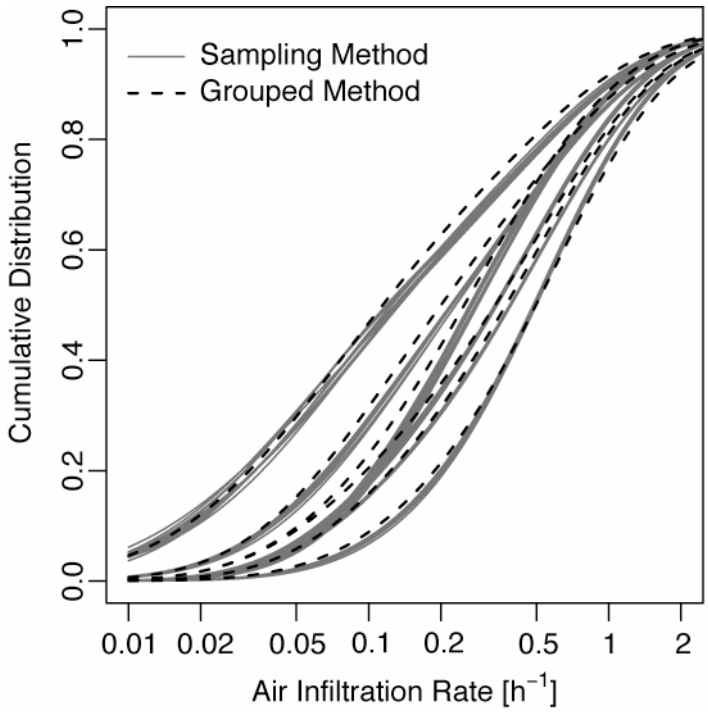

Figure 6.20 Comparison of two methods used to predict the air infiltration rate distribution of commercial buildings in 5 randomly selected census tracts in Oklahoma City. "Sampling method" refers to predicting distributions by modeling each individual building while sampling from distributions of LBL and Shaw-Tamura Infiltration Model input parameters. The composite distributions from 10 separate model runs are plotted for each census tract. "Grouped method" refers to predicting the air infiltration rate distribution by first grouping smaller commercial buildings into 9 groups by their sizes. Also, the model input parameters are assumed to be constants instead of sampling from their respective distributions. The cumulative distributions represent the predicted numbers of buildings having a certain air infiltration rate or less in a census tract.

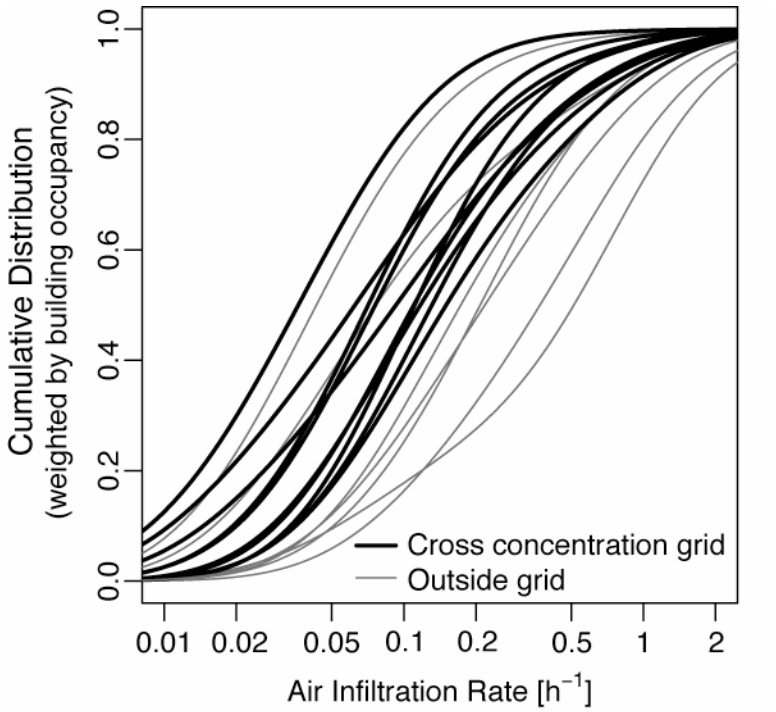

Figure 6.21 Predicted air infiltration rate distributions of commercial buildings in 17 census tracts selected from the 5.4 km × 5.4 km study area in Oklahoma City. Highlighted are the 10 census tracts with boundaries that cross the concentration grid (see Figure 6.2). These distributions are weighted by the estimated occupancy in buildings.

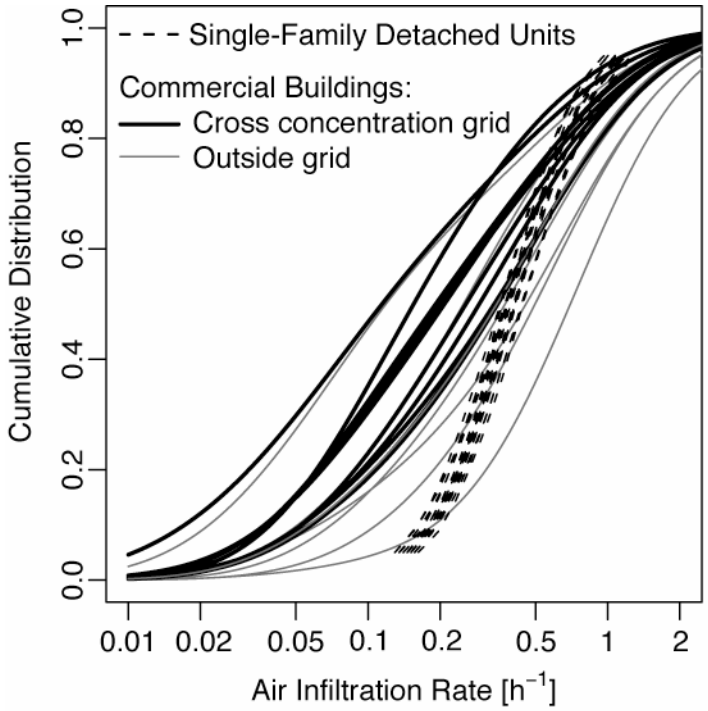

Figure 6.22 Air infiltration rates predicted for single-family detached units and commercial buildings in the 17 census tracts in the Oklahoma City study area. All distributions are weighted by the number of buildings.

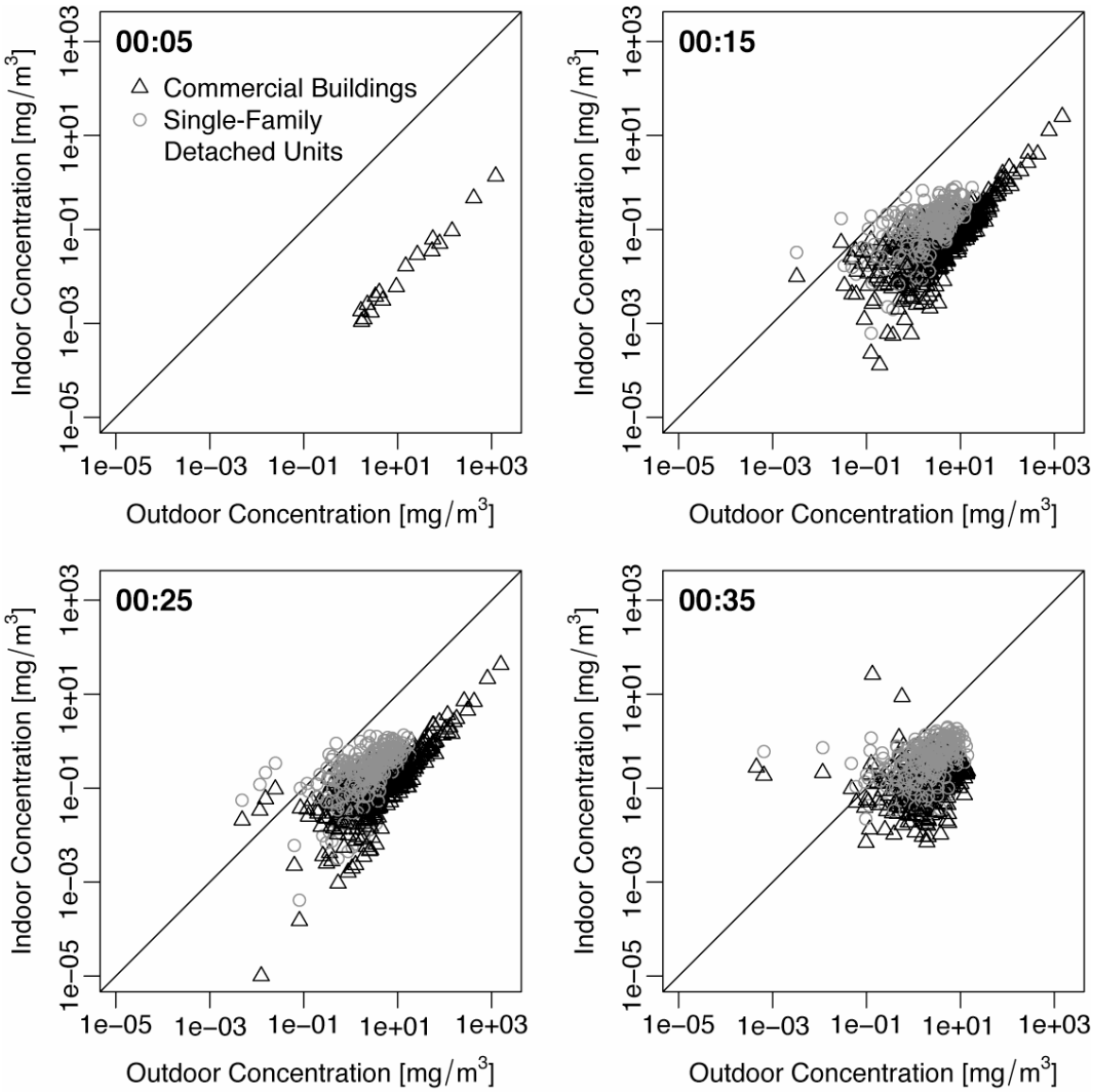

Figure 6.23 Median indoor concentrations (y-axis) predicted at each grid cell in the two classes of buildings: commercial and residential. Predictions are plotted against the outdoor concentration (x-axis) at that grid cell. In the first 5 minutes, no predictions were computed for residential buildings because there are no houses next to the release source. For details on the parameters used in the simulation, see 6Ai in Table 6.5.

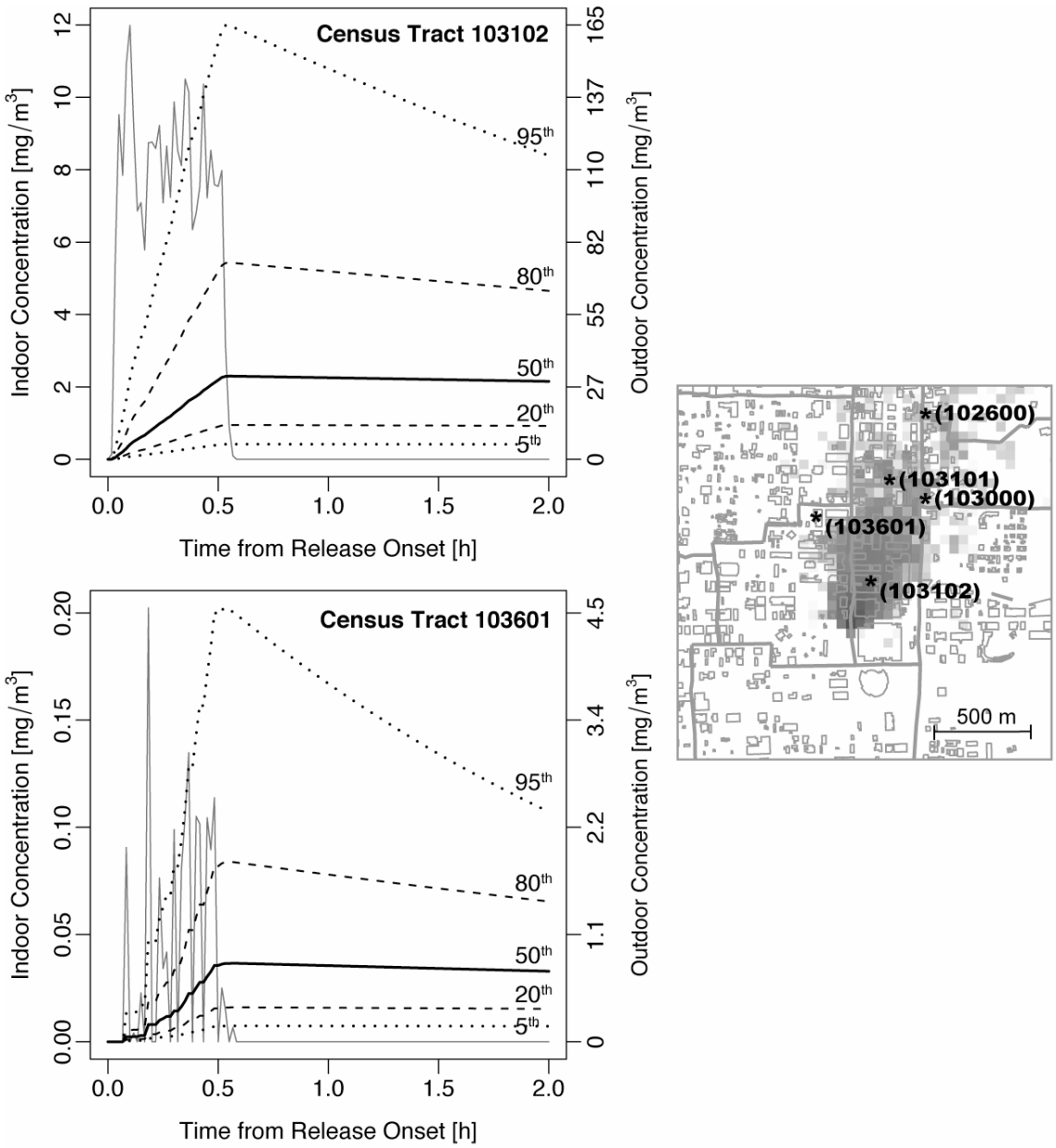

Figure 6.24 Predicted indoor concentrations in commercial buildings at two locations as indicated on the side map by their respective census tract ID (note that the remaining three locations are *not* analyzed in this figure; see Figure 6.25 instead). The dark solid line represents the indoor concentration predicted for buildings having the median air infiltration rate. The dotted lines represent the different indoor concentration predicted using an air infiltration rate at the 5th, 20th, 80th, and 95th-percentiles. The modeled outdoor concentration is shown as the trace line that fluctuates for $0 < t < 0.5$-h, and then is ~0 for $t > 0.5$ h. For details on the parameters used in the simulation, see 6Ai in Table 6.5.

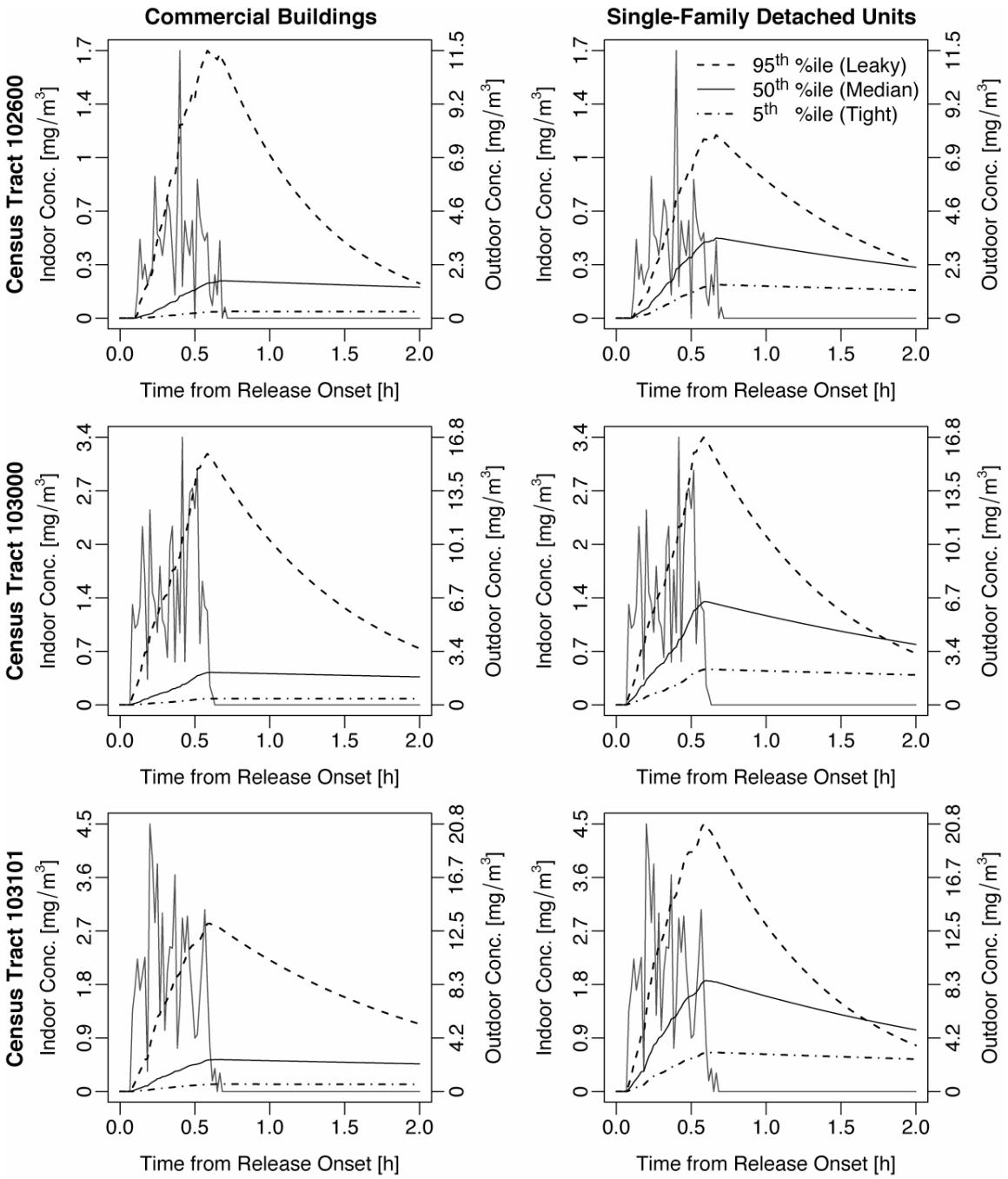

Figure 6.25 Predicted indoor concentration distributions in commercial and residential buildings at 3 locations in Oklahoma City (see the map in Figure 6.24 for the locations of these sites, which are referenced by their respective census tract ID). The black solid lines represent the median indoor concentration predicted for buildings located in that grid cell. The dotted lines represent the 5th and 95th percentile indoor concentrations. The census tracts where each grid cell is located are indicated on the left margin. The modeled outdoor concentration is shown as the trace that fluctuates for $0 < t < 0.5$-h, and then is ~0 for $t > 0.5$ h. For details on the parameters used in the simulation, see 6Ai in Table 6.5.

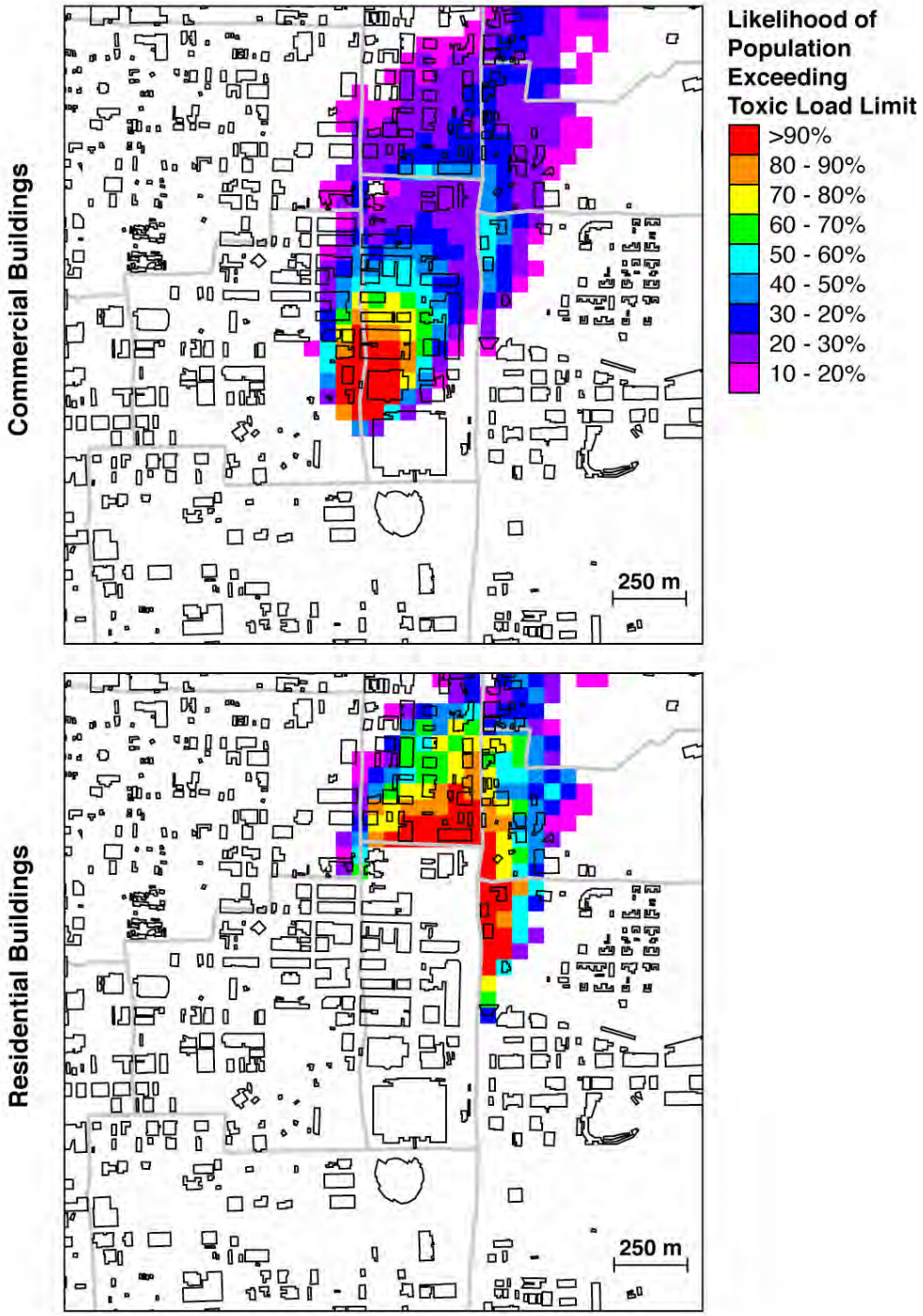

Figure 6.26 Predicted areas with various fractions of buildings having indoor concentrations toxic enough to exceed the toxic load limit for the modeled 0.5-h release event. The top figure shows predictions using indoor concentration estimates in commercial buildings. The bottom figure shows predictions in residential buildings (single-family detached units only). The population cumulative toxic loads from indoor exposure are evaluated at the end of the 2-h simulation. For details on the parameters used in the simulation, see 6Ai in Table 6.5.

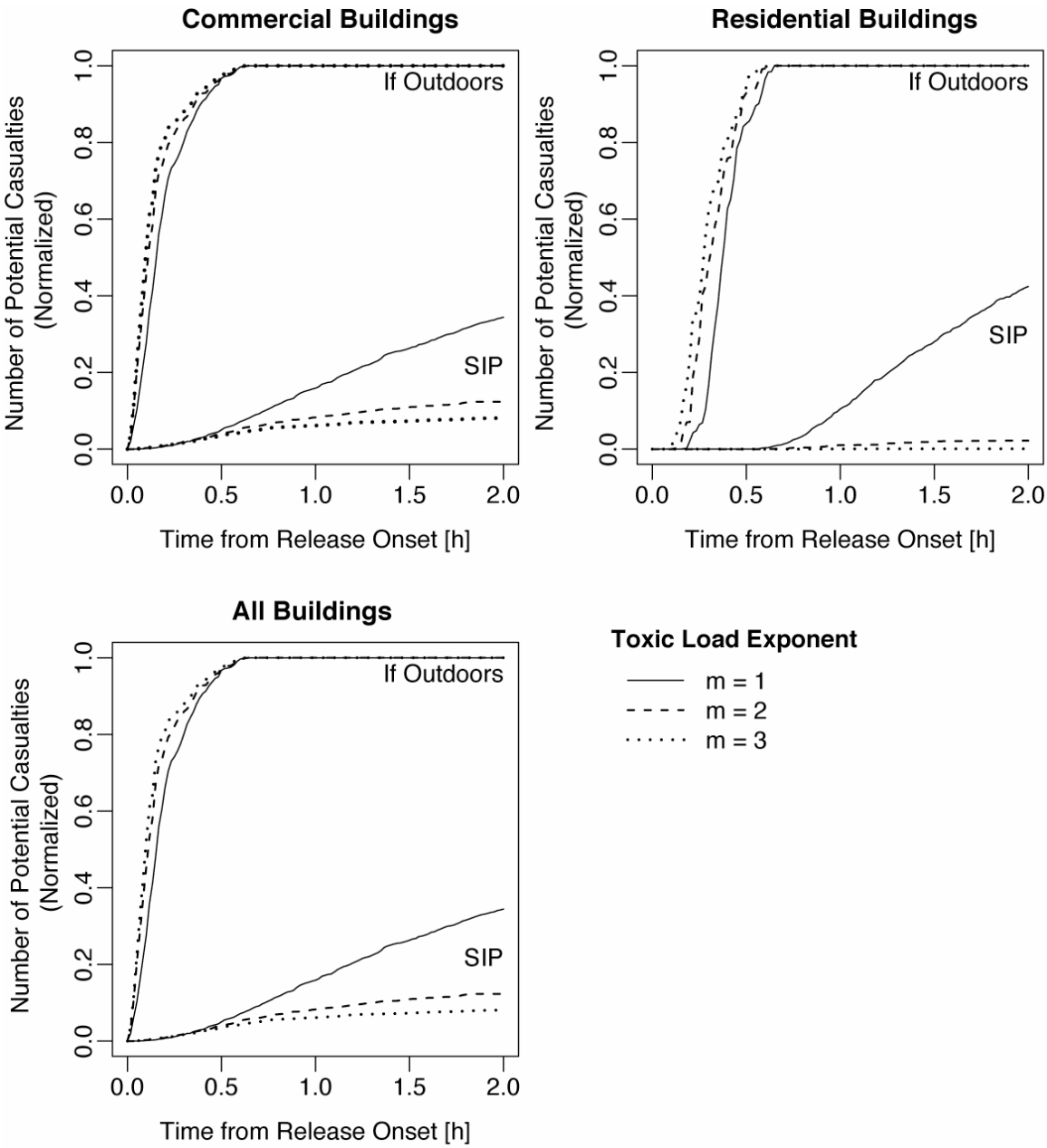

Figure 6.27 Predicted population for which toxic load exceeds the toxic load limit for the simulated 0.5-h release event in Oklahoma City. The outdoor curves represent the estimated population that if exposed to the outdoor concentrations, would have toxic loads that exceed the toxic load limit. The indoor estimates are normalized to the corresponding outdoor maximum prediction. Since the exposed downtown area is dominated by the number of occupants in commercial buildings, the overall casualty estimates (bottom figure) resemble the prediction for commercial buildings.

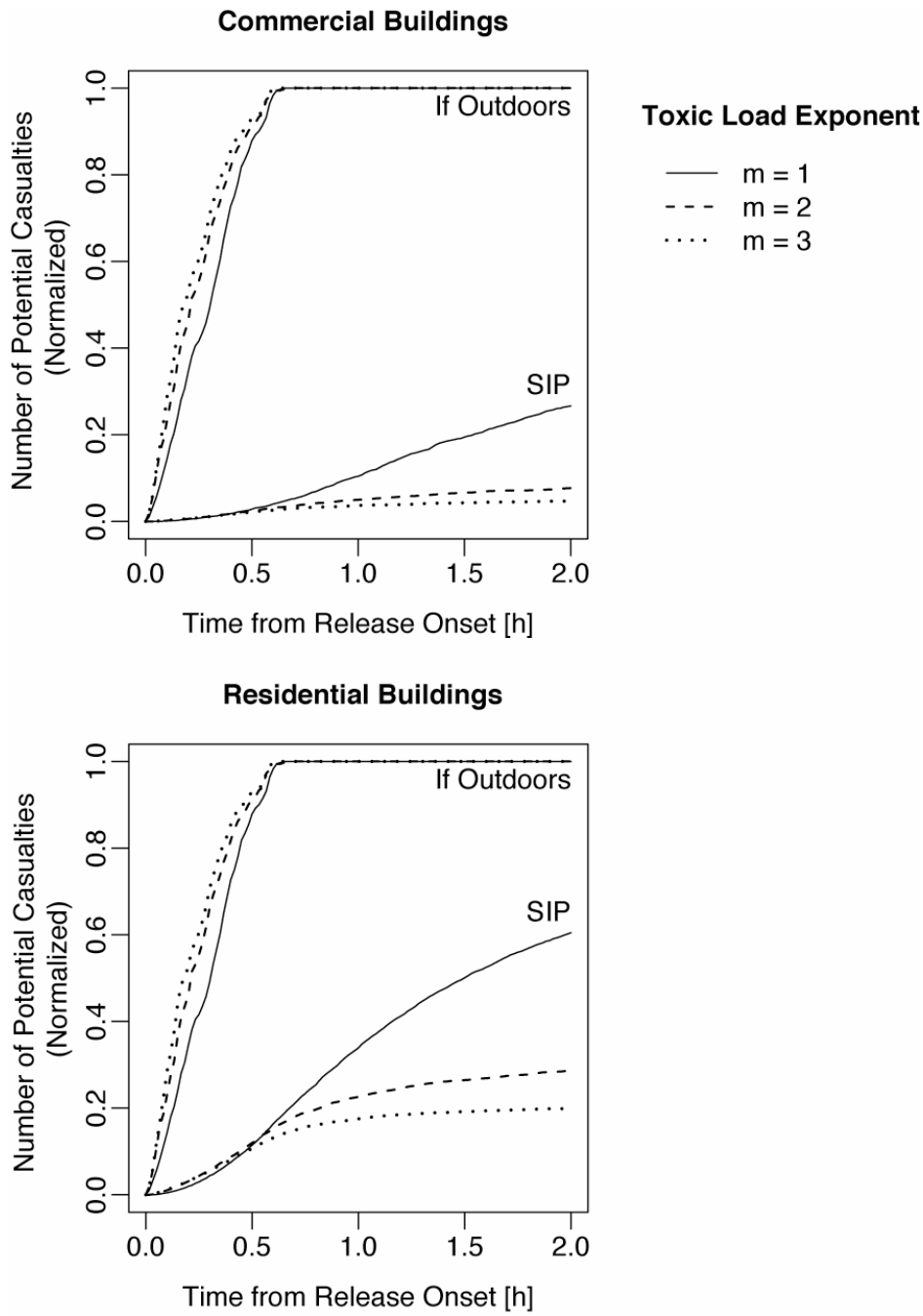

Figure 6.28 Predicted potential casualties if people were to shelter in commercial buildings and in residences (single-family detached units). These simulations differ from the ones shown in Figure 6.27 in that each grid cell is assumed to have the same number of people in both residential and commercial buildings. By assuming uniform population density, the population that is exposed to levels in exceedance of the toxic load limit is weighted evenly across the model domain instead of towards heavily populated areas.

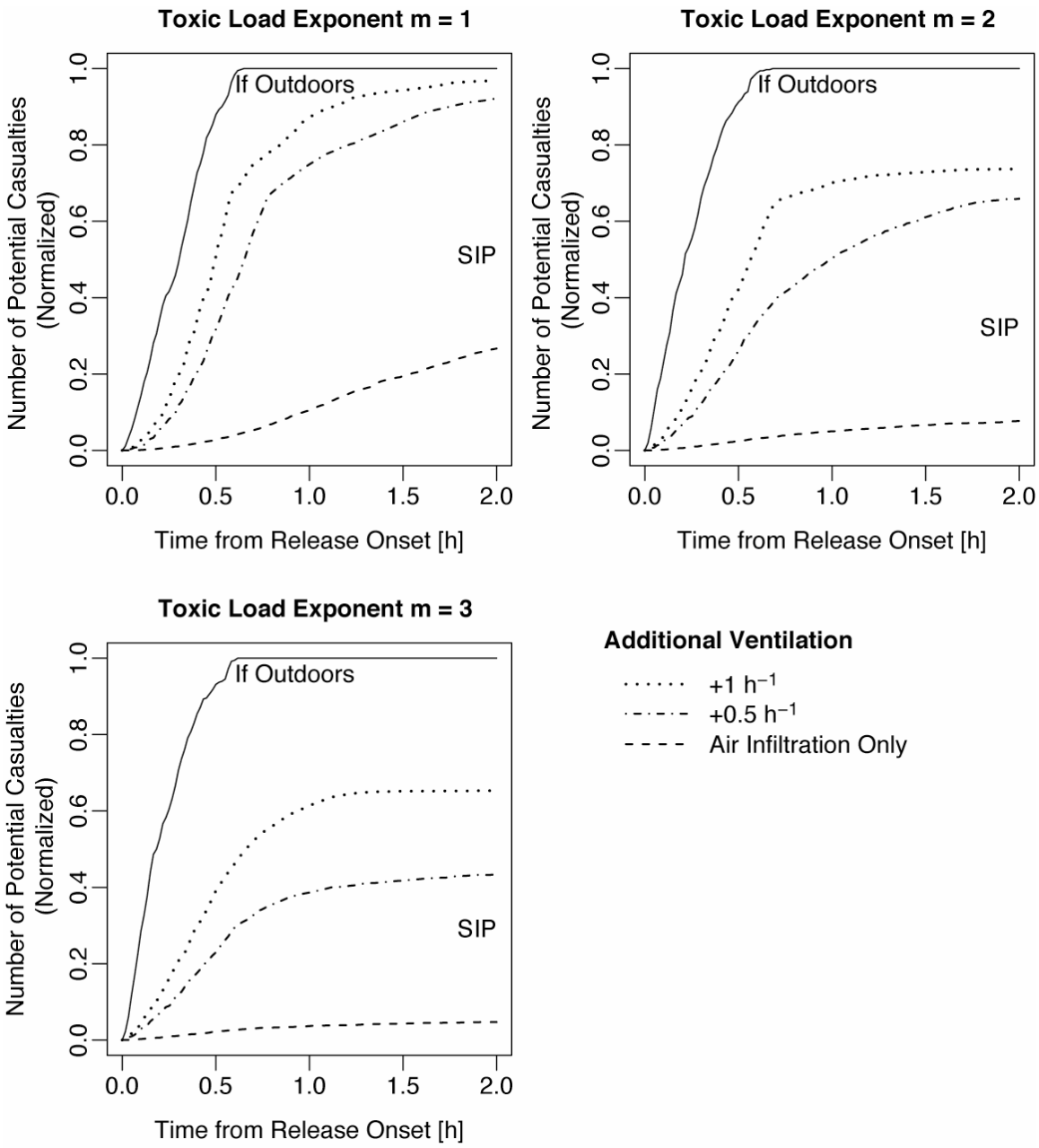

Figure 6.29 Effect of additional air exchange induced by mechanical ventilation systems on SIP effectiveness of commercial buildings. For the entire 2-h simulation, 1 h^{-1} or 0.5 h^{-1} is added to the air infiltration rate of each commercial building to obtain its total air-exchange rate. For comparison, results from the cases 6Ai, ii, and iii (see Table 6.5) where air infiltration is the only source of air exchange are also plotted.

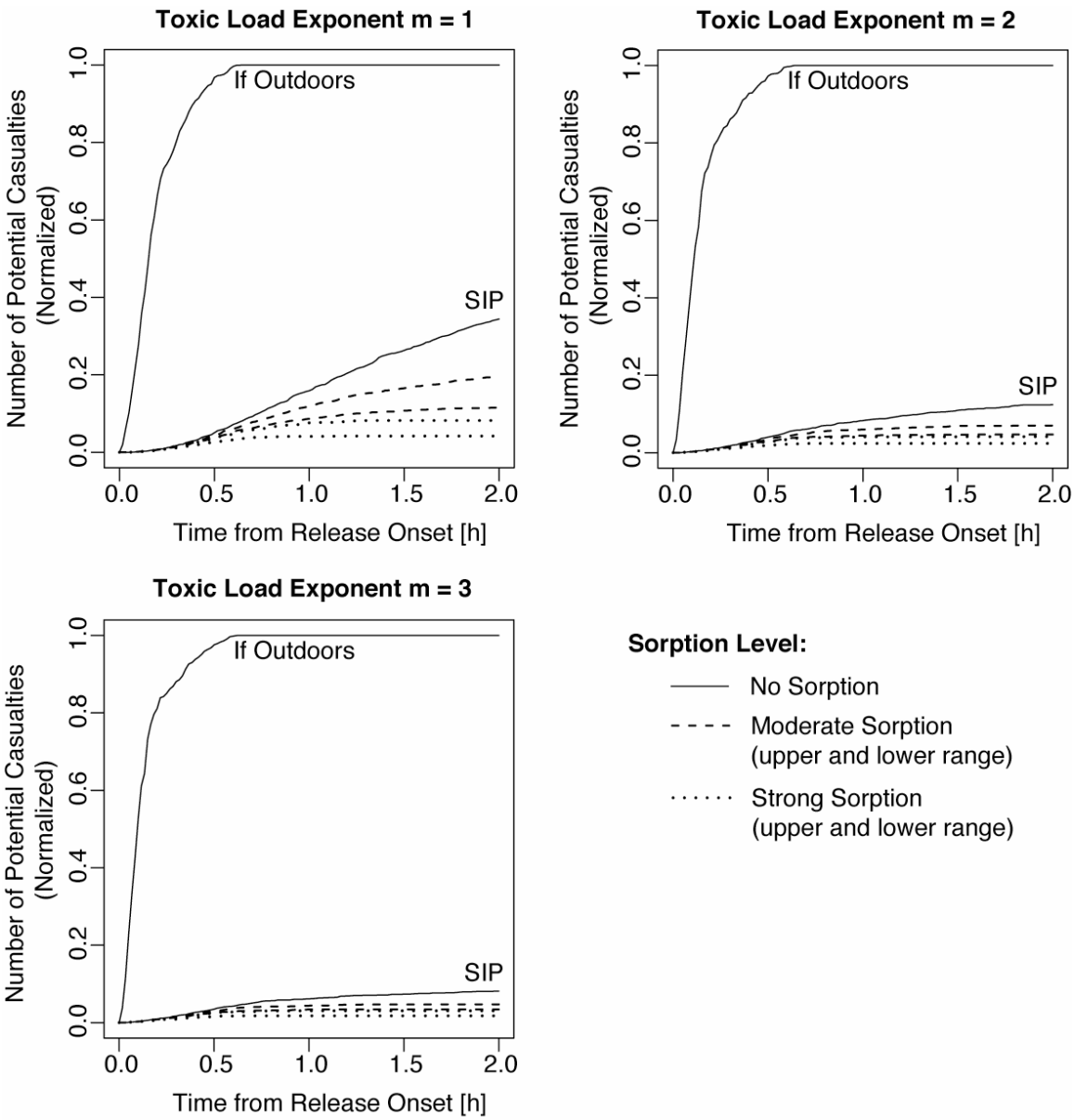

Figure 6.30 Effect of chemical sorption on indoor surfaces on the SIP effectiveness of commercial buildings. The range of sorption rates used is based on values observed in experiments. NH_3 is the chemical from which moderate sorption rates are modeled. DMMP, a surrogate for G-series chemical warfare agent, is the chemical from which strong sorption rates are modeled. (See Table 4.4 for details about the sorption model and parameters used.) The upper and lower limits of the sorption rates observed are used to give the range of potential casualty estimates. For the entire 2-h simulation, all commercial buildings are modeled in SIP conditions (i.e. mechanical ventilation systems turned off, air infiltration only).

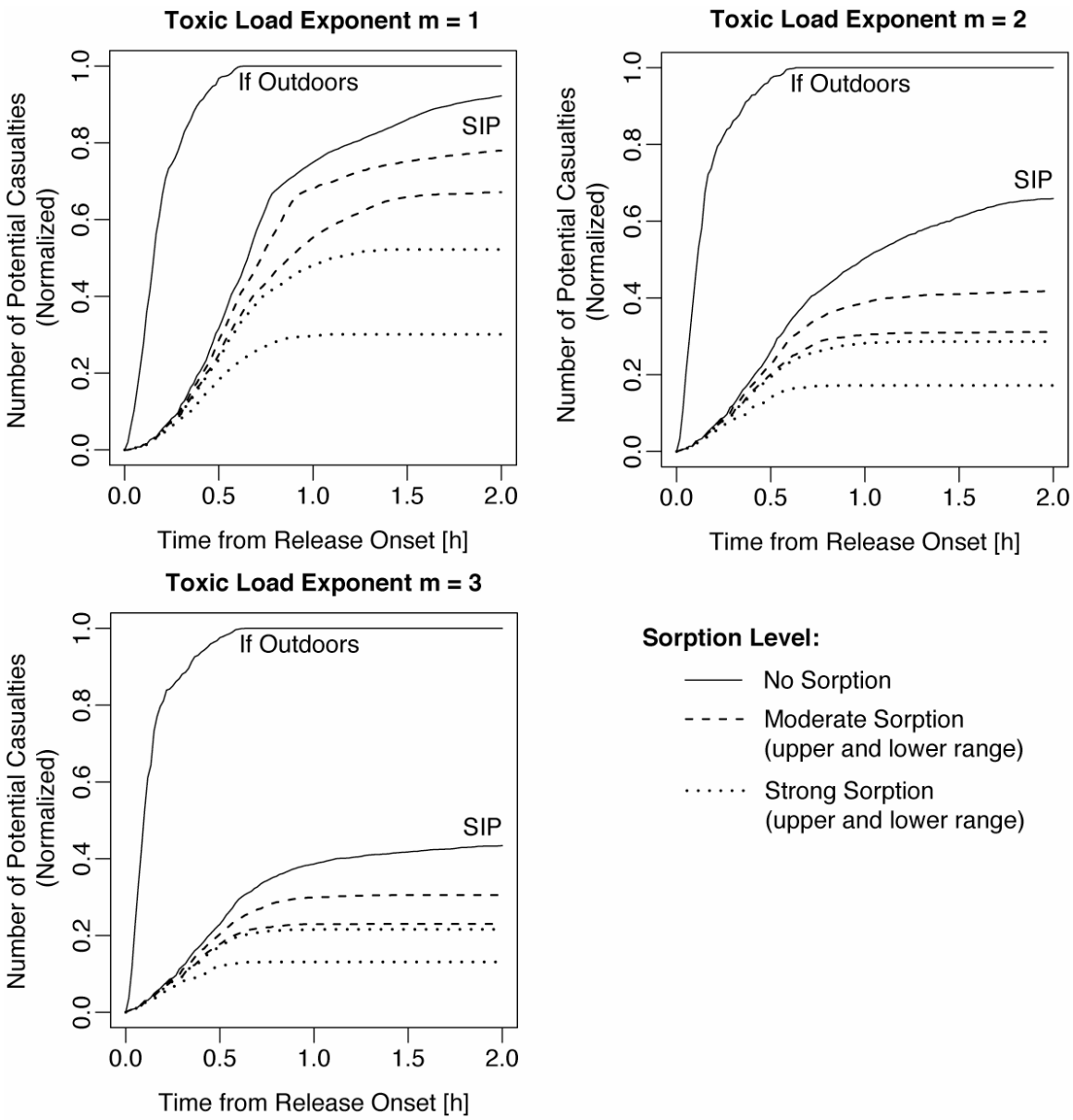

Figure 6.31 Effect of chemical sorption on indoor surfaces on the SIP effectiveness of commercial buildings under normal operating conditions. For the entire 2-h simulation, 0.5 h^{-1} is added to the air infiltration rate in buildings to represent the additional air exchange from mechanical ventilation. Sorption rates modeled are the same as in Figure 6.30.

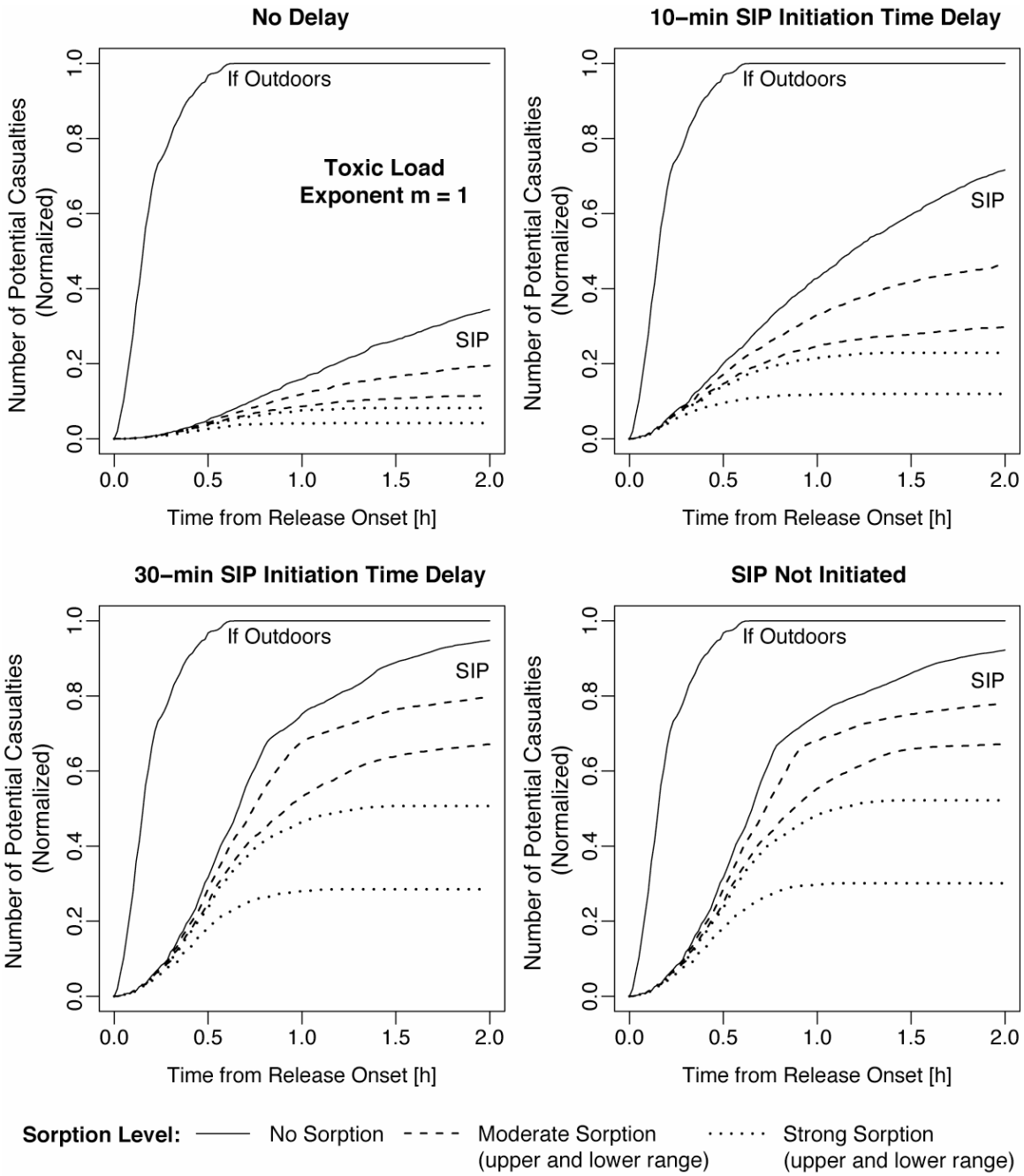

Figure 6.32 Effects of initiation delay on the SIP effectiveness of commercial buildings in reducing potential casualties among the exposed population. Besides the 10-minute and 30-minute time delay measured from the start of the release, two other cases are also modeled: SIP begins immediately at the start of the release (top left), and SIP is not practiced (bottom right). In all cases other than "no delay", 0.5 h^{-1} is added to the air infiltration rates before SIP is initiated. Adverse health effects are assessed using toxic load exponent $m = 1$ in all simulations.

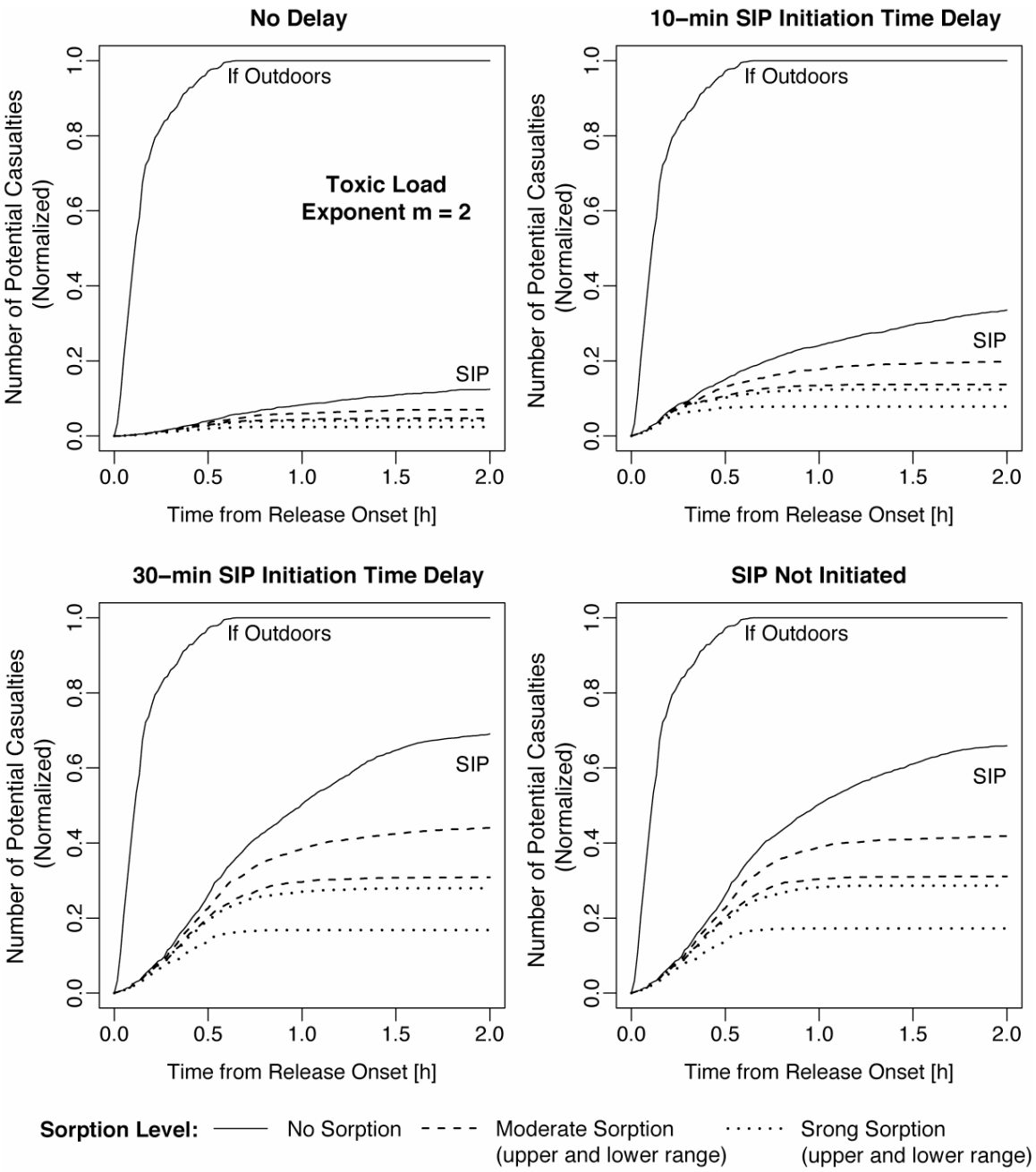

Figure 6.33 Effects of delay in initiating SIP on the effectiveness of commercial buildings in reducing potential casualties among the exposed population. Adverse health effects are assessed using toxic load exponent $m = 2$ in all simulations. Otherwise, conditions are the same as in Figure 6.32.

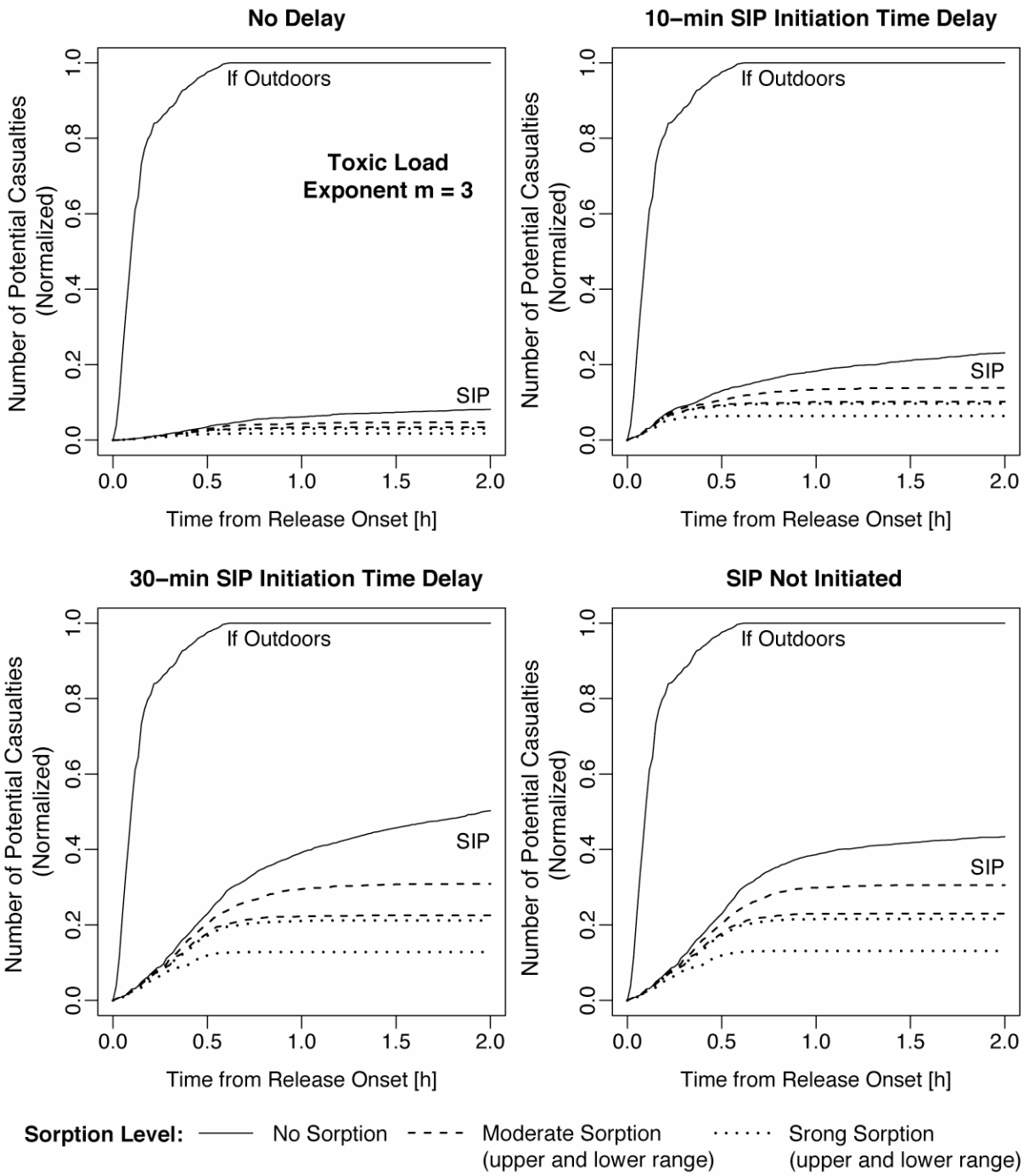

Figure 6.34 Effects of delay in initiating SIP on the effectiveness of commercial buildings in reducing potential casualties among the exposed population. Adverse health effects are assessed using toxic load exponent $m = 3$ in all simulations. Otherwise, conditions are the same as in Figure 6.32.

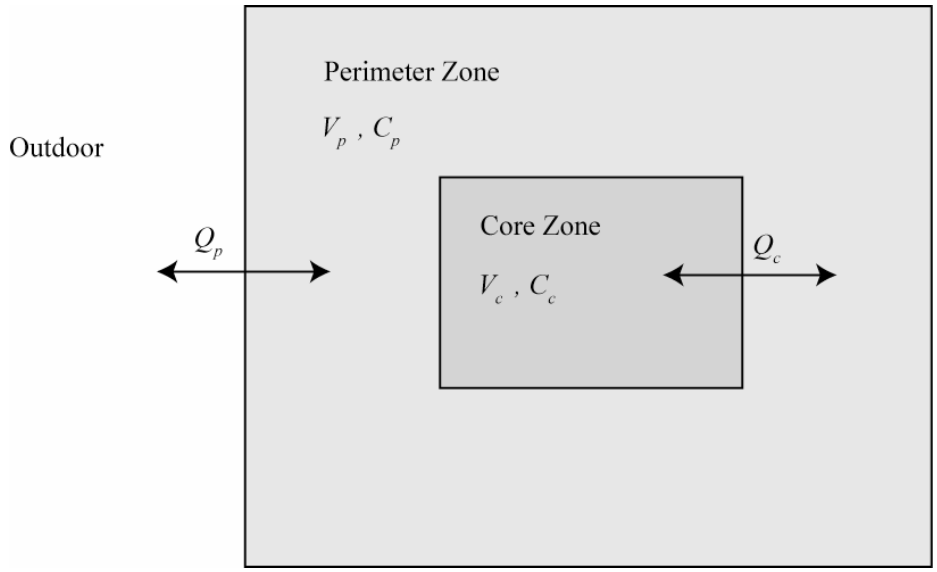

Figure 6.35 Plan view of a building illustrating the two-zone configuration used to model the indoor concentrations in the perimeter (C_p) and core zone (C_c). The height of the building is coming out of the page. The corresponding volumes of the perimeter and core zone are V_p and V_c respectively. Q_p is the airflow rate between the perimeter zone and the outdoors. In the core zone, airflow is assumed to occur with the perimeter zone only, and not directly with the outdoors.

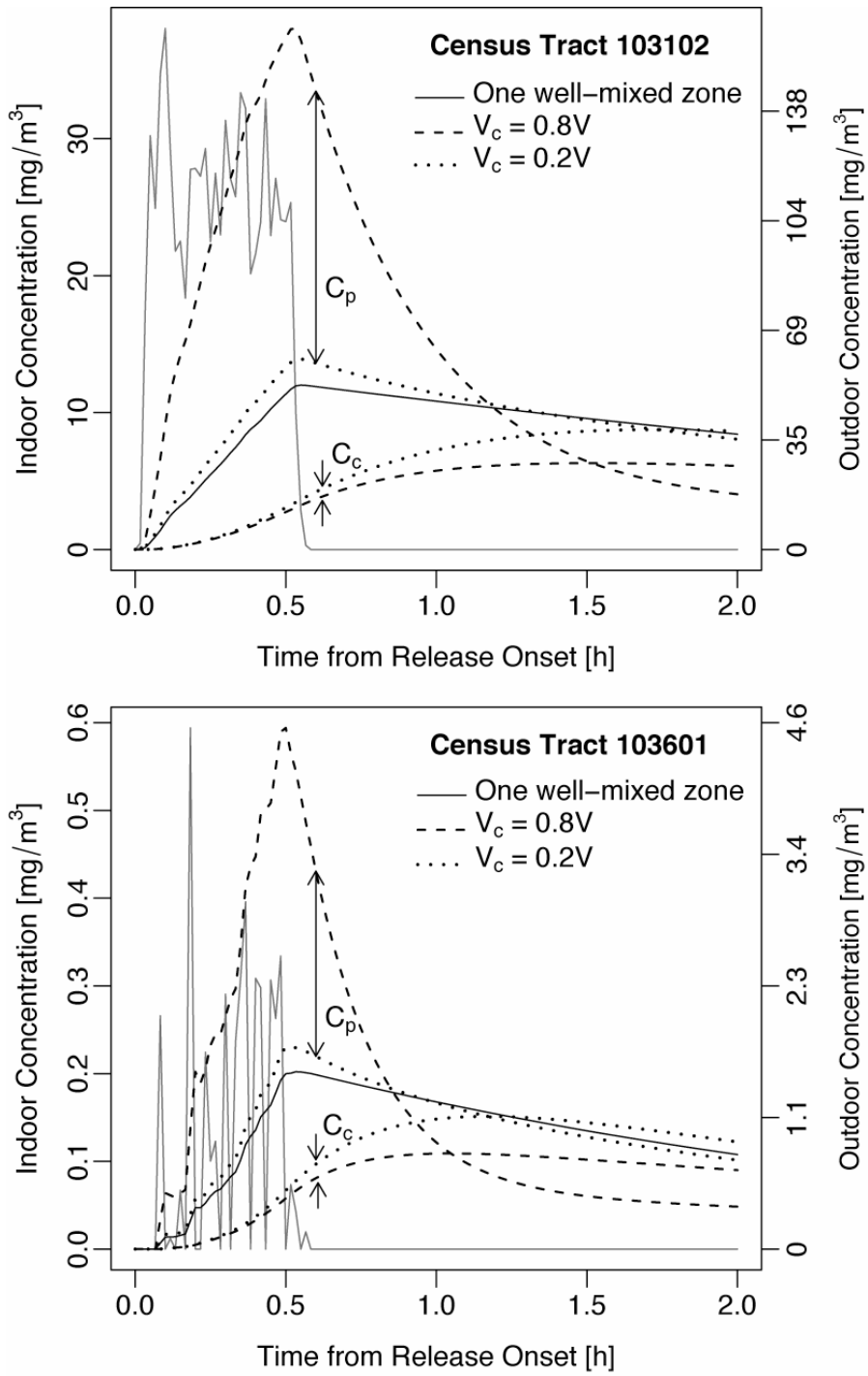

Figure 6.36 Predicted two-zone indoor concentrations in commercial buildings in two census tracts. Here, C_p represents the concentration in the perimeter zone of the building and C_c represents the concentration in the core zone of the building. The well-mixed single-zone results, plotted for comparison, are predicted using air leakage at the 95th percentile. Two core zone volumes are simulated: one comprising 80% of the total volume of the building, the other comprising 20%. The perimeter zone makes up the remaining volume of the building. Sorption effects are not included.

7 Summary and Conclusions

7.1 Summary of Results

Community shelter-in-place (SIP) effectiveness in residential and commercial buildings has been explored by means of data analysis, information synthesis, and modeling. To prioritize the types of input parameters that most affect SIP effectiveness, a systematic exploration has been performed using simplified models. The air leakage distributions of single-family dwellings and various types of commercial buildings were thoroughly analyzed. Methods were developed to predict air infiltration rates that are spatially and temporally specific to a community exposed to a release. Two sets of hypothetical large-scale outdoor releases were used as test cases to evaluate SIP effectiveness for realistic scenarios. The resulting distributions of indoor concentrations were evaluated to estimate potential health consequences in the exposed community. SIP effectiveness was then quantified in terms of the degree of potential casualty reduction if the community were to take shelter indoors, relative to exposure to outdoor conditions. Practical aspects of SIP, including the initiation and termination time during implementation, and if the community is caught unaware of the release and does not take protective measures, were also considered.

7.1.1 Community-Based Modeling of Shelter-in-Place

Shelter-in-place is an emergency response strategy where the community at risk of exposure to an acute, short-term release of toxic chemicals outdoors is advised to take shelter indoors for protection. Because of the variability among shelters in the community, it is important to consider the differences in characteristics among residences and other types of buildings when assessing SIP effectiveness. Furthermore, the effectiveness of SIP should not be measured simply by the degree of reduction in indoor concentrations. The ultimate goal of this emergency response strategy is to minimize the acute harm caused to the exposed population. Reduction in health endpoints is therefore the purpose of SIP, and its effectiveness should be evaluated using appropriate metrics. Results from this work can clearly and directly communicate the anticipated reduction in adverse health outcomes if the community were to shelter-in-place under a given release scenario.

In this dissertation, a method has been presented to model the health consequences caused by a large-scale outdoor release if people were to take shelter under different scenarios. A major difference of the approach taken here relative to past assessments of SIP effectiveness is to capture in detail the variability among buildings with fidelity to the underlying data. This is made possible by thoroughly considering the differences in the leakiness of building envelopes, and by the appropriately modeling the driving forces of air infiltration. The tools used in each component of the research, for example, multivariate regression to analyze air leakage measurements, and air infiltration models to predict infiltration rates, are commonly used in research and application. However, the

intermediate steps required to link the two together, as well as the selection and preparation of spatially resolved data, are tailored to the specific needs for assessing SIP effectiveness. Much thought has gone into ensuring that the method developed here can be easily applied in other locations and release scenarios, as long as some localized building characteristics data are available.

The other key feature of this analysis is the introduction of an SIP effectiveness metric that is consistent with the goal of the emergency response strategy. The metric "casualty reduction" is the expected outcome if a community were to shelter-in-place in response to an emergency release event. It has taken into consideration that people would be exposed to a range of indoor concentrations, thus leading to some disparity in the resulting health consequences. The need for a community-based metric arises not only because a population of individuals is at risk of exposure, but also because there is significant variability among buildings in the level of protection provided. A measure of SIP effectiveness in one building does not apply in general to other buildings. More importantly, the precise indoor concentration in a given building at a specific time cannot be deterministically modeled. This is an inherently probabilistic parameter, for which only the distribution is reliably predictable in a community-based assessment.

7.1.2 Key Factors Affecting Shelter-in-Place Effectiveness

Large-scale, airborne toxic chemical releases outdoors can devastate lives and the surrounding environment. Most industrial accidents could be avoided, yet they are

recurring. As more toxic chemicals are being transported in large quantities over long distances, evidence suggests that the potential risks may even be increasing with time. In the event of an accidental release, there are many aspects that cannot be controlled: the amount and toxicity of the chemicals, the location and duration of the release, and the local meteorology. All these factors can affect SIP effectiveness, to various degrees. Using simplified but well-established models and input parameters, a systematic exploration in Chapter 2 found that parameters that affect the scale or extent of the release, namely the release amount, the toxic load limit of the chemical, and the dispersion of the toxic plume, only affect SIP effectiveness slightly. This is because all these factors affect the casualty estimates for exposure both indoors and outdoors. Thus, in terms of the casualty reduction effectiveness of SIP, these factors are less influential than factors that affect mostly the potential casualty estimates for those who shelter indoors. The release duration and, to a lesser extent, the speed of plume dispersion, are the factors that affect casualty reduction quite strongly. The degree of nonlinearity of the dose-response relationship is also a determining factor that influences the effectiveness of SIP. This common characteristic of acute exposure to a toxic chemical, which is defined by a toxic load exponent greater than 1, amplifies the importance of the differences between the indoor and outdoor concentrations.

There are some controllable factors that can influence SIP effectiveness. Understanding these factors and utilizing this knowledge wisely in practice can maximize the degree of protection offered by buildings. Of foremost importance is the amount of air exchange with the outdoors. For the present purpose, one can distinguish between the two

components of air exchange in buildings. One is the uncontrollable airflow (air infiltration), which can only be minimized by tightening the building envelope or by enhanced SIP procedures that are not considered in this dissertation. The other component is natural or forced ventilation, which can be induced by opening windows or by running mechanical ventilation systems. Analysis of air leakage measurements in Chapters 3 and 5 revealed considerable variability in both single-family dwellings and commercial (non-residential) buildings. Some basic building characteristics are found to be correlated with the building envelope air leakage when the measure is normalized to either the floor area of a house or the building envelope surface area of a commercial building. Older and smaller houses, and those occupied by low-income households, tend to be leakier than other houses. Commercial buildings with smaller floor area tend to be leakier than larger commercial buildings. Additional air leakage is also associated with buildings with more stories, but only up to a certain limit. Air infiltration modeling performed in these chapters revealed that more uncontrollable airflow, measured in terms of air changes per hour, tends to occur in single-family dwellings relative to commercial buildings. However, a small fraction of the commercial building stock is also quite leaky, even in comparison with residences. Furthermore, it is expected that the amount of airflow induced by mechanical ventilation systems in commercial buildings yields higher overall air-exchange rates than the common natural ventilation practices (open windows) adopted in residences. While most commercial buildings in the US are mechanically ventilated, only a fraction of households would have open windows at a given time. Differences such as these in the air infiltration and ventilation rates between residential

and commercial buildings, as well as the respective variability within each building class, have important implications for SIP effectiveness.

Two basic decisions required in SIP are when to start sheltering, and when to stop sheltering. Although simple, such choices can strongly influence SIP effectiveness in a community. Chapters 4 and 6 used two hypothetical simulations to explore the consequences of initiating SIP after the release had already started. Also explored were the consequences of exposure to indoor residuals if SIP was not terminated punctually when it first became safe to do so. For almost all circumstances, SIP is a no-regrets option, meaning that no more harm is caused than the worst-case condition of all people being exposed to the outdoor concentrations, provided that the community can implement SIP before the release ends. After the plume has dispersed, SIP should be terminated by exiting or deliberating ventilating the indoors. Analyses show that a short delay in terminating SIP will not significantly reduce the overall effectiveness of the strategy. Of course, there are exceptions. Many toxic industrial chemicals and other hazardous agents are sorptive on indoor surfaces such that SIP effectiveness is greatly increased and sustained without loss over time. However, in a case in which the toxic chemicals are essentially inert in the indoor environment, then SIP effectiveness can be significantly reduced by delays in initiation and termination. Chemicals that exhibit a nonlinear dose-response relationship for acute effects with toxic load exponent exceeding 1 are immune from this weakness of SIP. The analysis presented in this dissertation shows that as long as either the toxic chemical sorbs at least moderately to indoor surfaces, or that the dose-response relationship is nonlinear, then simply staying indoors under normal operating

conditions can provide reasonably effective protection. The estimated reduction in potential casualties in such cases is at least one-half in reference to conditions in which the entire community is exposed outdoors.

On the other hand, a potentially large enhancement of SIP effectiveness can be realized by reducing the time delay for SIP initiation. The analyses in Chapter 4 and 6 have quantified the effectiveness gain by shortening SIP response time. In the event that commercial buildings are in a plume path, the urgency of turning off mechanical ventilation systems in commercial buildings appears to be more important than eliminating natural ventilation in a residential neighborhood. There are two reasons for this. First, as suggested by ventilation studies in residences, a substantial proportion of single-family dwellings is likely to be already in SIP-mode (windows closed, no additional induced air exchange besides infiltration). Second, the amount of airflow introduced by mechanical ventilation is far greater than the air infiltration rate predicted in the majority of commercial buildings. As a result, SIP effectiveness in commercial buildings is more affected by initiation time delay than in residential dwellings. If SIP is started immediately in all buildings, however, the casualty reduction achieved by taking shelter in the commercial building stock is expected to be higher than in single-family dwellings.

Limited survey data on past emergencies show substantial time delays in each step of the response process. In case of a short-duration release, exposure to the residual contaminants indoors after the plume has passed can contribute a large fraction of the

total toxic load that is accumulated during the SIP period. If significant time passes before SIP is implemented in the community, and if neither of the two factors that favor SIP effectiveness apply (sorption on indoor surfaces and nonlinear dose-response with toxic load exponent exceeding 1), then emergency responders must face the challenge of ordering SIP termination as soon as it is safe to do so. Delays in SIP termination can cause the casualty estimates for indoor exposure to double or even triple within a few hours after the release has stopped. In some situations, it is even plausible that keeping the natural and mechanical ventilation rates constant throughout the event is better than to risk trapping toxic chemicals indoors that have already entered some buildings. The work here has identified some exceptional conditions where the effectiveness of SIP might be limited. In response to any real emergency, however, only model predictions that are tailored to the situation can give the specific advice needed to inform the decisions at hand.

7.2 Recommendations for Future Research

7.2.1 Model Refinements

In this dissertation, a large part of the effort has gone into characterizing the air infiltration rate distribution. This is justifiable, as the amount of toxic chemicals brought indoors by uncontrolled airflow constitutes the baseline for SIP effectiveness. However, other factors that influence SIP effectiveness have been determined to be important as well. For example, the natural and mechanical ventilation rates in various types of

buildings determine their protectiveness under normal operating conditions. The response times of people in initiating SIP strongly influences the effectiveness of the strategy in a community as a whole. The susceptibilities of exposed individuals determine the health effects that can result from exposure to the toxic chemicals. Each of these aspects in the model, namely the added air exchange from ventilation, the SIP initiation time delay, and the toxic load limit, are treated as constant parameters in all simulations in which they were considered. In reality, however, a certain level of variability is expected for each of these parameters. Together with the air infiltration rate distribution already modeled, the combined effect of these distributional parameters can affect the expected estimates of SIP effectiveness. Throughout this work, pieces of data and past research reviewed have suggested that assessing the distributions of these parameters should be a manageable task, although additional research to expand the body of relevant empirical evidence is also warranted.

There are two underlying assumptions in this dissertation that can lead to systematic overestimates of SIP effectiveness. First, it is assumed that all buildings successfully comply with the instruction to shelter in-place after the modeled initiation time delay. Second, it is assumed that the entire population is already indoors at the time of the release. In many scenarios, neither of these assumptions is likely to be valid. Adverse consequences can result in commercial buildings that failed to turn off the mechanical ventilation system in time, or in residences that are caught unaware of the release and kept their windows open. Depending on the time of day and location of the release event, many people may be outdoors or in transit, where they can be exposed to substantial

levels of toxics. Such factors might significantly influence the overall effectiveness of the community response in protecting public health. However, to properly model these factors would require the assessment of knowledge about human behavior and decision-making in emergencies. Substantial new research efforts are likely needed to obtain detailed, distributional estimates for these parameters. Results from existing survey studies on the response of a community in emergencies (Vogt and Sorensen, 1999; Lasker, 2004) might help inform estimates of parameters like the expected fraction of non-compliance to SIP instruction. Data on human time-activity patterns (Jenkins et al., 1992; Klepeis et al., 2001) might also help to infer the fraction of the population outside an enclosed building at a given time. A comprehensive SIP emergency response strategy should consider how to advise those who happen to be outdoors or who are in transit to best protect themselves.

7.2.2 Model Uncertainty Assessment

Three types of models were used in this dissertation to evaluate SIP effectiveness: an atmospheric dispersion model to predict outdoor concentrations resulting from a release; a building model to predict air infiltration rates and indoor concentrations that result; and a dose-response model to estimate acute health consequences of exposure. Each of these models has uncertainties. As these models are applied sequentially, model uncertainties can compound to influence the estimates of SIP effectiveness. For example, in an accidental release, it is often a challenge to quickly identify which chemicals are being released and in what amount. The start and stop time of the release can also be difficult to

determine or ill defined. Local meteorology can be difficult to predict without on-the-ground verification from nearby weather stations. Mischaracterizing the outdoor concentration fields as a result of these uncertainties will mean that the predicted indoor concentrations and the subsequent health consequences would be inaccurate also. To quantify the relative importance of various sources of uncertainties on the estimates of SIP effectiveness, a system-wide analysis is required.

In this dissertation, SIP effectiveness is measured almost exclusively in terms of the casualty reduction factor. When evaluating the model uncertainties, the analysis should consider the impact on other metrics that might also affect emergency planning and response. For example, when the direction of the advecting plume deviates from the model prediction, entirely different neighborhoods can be exposed. While it is possible that the two neighboring communities have similar SIP effectiveness measured in terms of the casualty reduction factor, it does not mean that uncertainty in the advecting direction of the toxic plume is unimportant. Instead, emergency response can greatly benefit from predictions that consider this source of uncertainty to ensure that the instruction to shelter-in-place is communicated to all those who might be at risk of exposure.

Finally, the decision to terminate SIP will also benefit from this kind of uncertainty analysis. There is a potentially a large penalty of terminating SIP too soon because a few individuals can be exposed to lingering toxics in the outdoor air when exiting from their shelter. On the other hand, the risk of staying in shelter for slightly longer after the plume

has passed to avoid potential exposure to the lingering toxics outdoors can be quite small. Consequently, the appropriate strategy for the community in such a case would be to delay the all-clear signal somewhat. Analysis that considers the relative magnitude of the uncertainties associated with the outdoor and indoor predictions is therefore needed to determine the optimal SIP strategy that maximizes the protection offered by buildings.

7.2.3 Characterize Variability in Model Predictions

This dissertation has only considered the expected number of casualties if people were to shelter in-place and if they were exposed to outdoor levels. As described in the above section, such measures of SIP effectiveness can be uncertain owing to the limited knowledge about input parameters, and the assumptions used in models to arrive at the result. In a given release scenario, the exact casualty estimates are also inherently probabilistic because of the distributional aspects of some of the input parameters. For example, each exposed building has a certain set of characteristics at a given time as described by the distributions of air infiltration rate, ventilation rate, etc. Each exposed individual will decide to take shelter indoors and complete the necessary actions at a time that is described by the distribution of response times. Even though the distributions of these input parameters have been quantified based on measurements or survey data, the exact attribute of any particular exposed person or building remains a probabilistic variable in an event.

The probabilistic nature of the casualty estimates can be characterized by sampling from distributions of input parameters to obtain a number of realizations of the model outcomes. Certain combinations of input parameters can greatly influence the effectiveness of SIP, relative to the expected value. This will become important when results of the model are used to guide decisions such as whether to order SIP, and when to give the all-clear signal, etc. It is expected that such probabilistic analysis can also pinpoint worst-case scenarios when SIP might not provide adequate protection to the public, and identify certain subgroups of the population that are most at risk from exposure to toxic releases. Such knowledge can be utilized to improve the community emergency action plan to best protect the public. This kind of analysis can also be used to characterize the full range of scenarios with probabilistic consequences, which is important in risk management for such events.

7.2.4 Other Opportunities for Shelter-in-Place Modeling

The modeling framework developed here can be used to analyze the SIP effectiveness of specific types of indoor enclosures in a community. For example, evaluation of the SIP effectiveness in multi-family dwellings is a logical extension to the single-family dwellings analysis presented in this dissertation. In some urban areas, multi-family dwellings might even constitute the majority of housing units. The challenge there would be to model the in-unit indoor concentrations while properly accounting for the interconnectivity between units using an appropriately simple model. Data on the air leakage of the whole building and the airflow connectivity of the living unit would be

needed. Another opportunity to build on the present work is to consider the degree of protection offered by vehicles. In the event of a large-scale outdoor release event, is likely that some would encounter the advecting plume while in their vehicles. This is especially a concern for releases caused by on-road accidents where nearby traffic can be directly engulfed in the toxic plume. After properly characterizing the in-vehicle air exchange and important pollutant dynamics, it would be possible to include them as part of the community-based SIP assessment.

In commercial buildings, the within-building indoor concentration variability is worthy of more careful consideration. Not only does such variability affect the casualty estimates as model output, it can also be utilized as a proactive strategy to minimize exposure. To assess such variability will require multizone airflow simulations, preferably complemented by measurements of the interzonal transport of pollutants of outdoor origin within buildings. The analysis would need to consider cases when the mechanical ventilation system is running and when it is off, since its operation affects the airflow and rate of mixing within buildings.

The efficacy of proactive strategies to enhance SIP effectiveness can be usefully assessed, especially for communities that are most at-risk to exposure from outdoor releases. It should be fairly straightforward to incorporate the effect of reduced air-exchange rate achieved by means of duct tape and plastic sheets, or the effect of active filtration of chemicals from the indoor air, to the community-based analysis of SIP effectiveness. It is possible that some communities located close to potential release

sources (e.g. industrial facilities, hazardous materials storage sites) might even benefit from deliberate structural tightening or other aggressive measures to prepare for uncontrolled releases of toxic chemicals. These proactive strategies vary in cost, effectiveness, and public acceptability. In addition to simulations of the effect on SIP effectiveness of such proactive measures, cost-benefit analysis and decision analysis can be used to help select specific measures that are most appropriate for the community.

Even in chemical releases, particles and droplets can be formed. Other types of emergencies, such as explosions, can cause toxic fumes with a mix of particulate matter that can also pose serious health concerns. In such cases, modeling of SIP effectiveness needs to take into account mixtures of pollutants of different types, which can have important dynamics and removal pathways indoors not considered in this dissertation. Similar cautions apply to the single-pathway (inhalation) assessment of health effects, which may also be too simplistic. It is possible that post-event dermal exposure to contaminated indoor surfaces also constitutes a health concern. In such a case, the methods and results of this dissertation could be expanded to assess the amount of toxic materials that had entered indoors and sorbed or deposited onto surfaces. Such estimates could also help guide post-event cleanup efforts in buildings.

7.2.5 Emergency Response Tools

The modeling framework presented in this dissertation can be used in both pre-event planning and real-time emergency response. In the planning mode, the model can be

exercised to identify scenarios where SIP is sufficient to eliminate all adverse health effects, and scenarios where quick relocation of occupants following the release will be necessary to help protect their safety. In response mode, the model can give an assessment of SIP effectiveness and the number of potential casualties using input parameters that are tailored to the release event. Results can also be used to identify areas where most residences or building occupants might need health assistance. Finally, advice on the timeliness of SIP termination can also be obtained from the model predictions.

For the purpose of assisting emergency responders to make the decision between shelter-in-place and evacuation, the criteria for selecting between the two alternatives must be first decided upon. Casualty reduction estimates for each strategy, while quantifiable, might not be the only consideration because of the large variability and uncertainty associated with the predictions. Logistical limitations and public compliance with the recommended action are a few of the reasons that one alternative might be favored over the other. Combining the two approaches, first shelter-in-place and then gradually relocate those that are most in need of medical assistance, can also be a viable option. The value of realistic models that can capture the essence of the different protective strategies is to present emergency responders and others involved in the decision process a logical way to evaluate the alternatives. To facilitate a well thought out response plan, communication of model assumptions and limitations must be made explicit. The modeling approach described in this dissertation can be used to illustrate the benefit of fast response and community cooperation, achievable by pre-event planning efforts and

public education, in maximizing the effectiveness of protective response actions in emergencies.

7.3 References

Jenkins, P.L., Phillips, T.J., Mulberg, E.J., Hui, S.P., 1992. Activity patterns of Californians: use of and proximity to indoor pollutant sources. Atmospheric Environment 26, 2141–2148.

Klepeis, N.E., Nelson, W.C., Ott, W.R., Robinson, J.P., Tsang, A.M., Switzer, P., Behar, J.V., Hern, S.C., Engelmann, W.H., 2001. The National Human Activity Pattern Survey (NHAPS): a resource for assessing exposure to environmental pollutants. Journal of Exposure Analysis and Environmental Epidemiology 11, 231–252.

Lasker, R.D., 2004. Redefining readiness: terrorism planning through the eyes of the public. Center for the Advancement of Collaborative Strategies in Health, The New York Academy of Medicine, New York, NY. www.cacsh.org

Vogt, B.M., Sorensen, J.H., 1999. Description of survey data regarding the chemical repackaging plant accident West Helena, Arkansas. ORNL-13722, Oak Ridge National Laboratory, Oak Ridge, TN.